

Air Force Institute of Technology

AFIT Scholar

Theses and Dissertations

Student Graduate Works

3-26-2020

Wideband Metasurface Antenna

Thomas A. Lepley

Follow this and additional works at: <https://scholar.afit.edu/etd>



Part of the [Materials Science and Engineering Commons](#), and the [Signal Processing Commons](#)

Recommended Citation

Lepley, Thomas A., "Wideband Metasurface Antenna" (2020). *Theses and Dissertations*. 3177.
<https://scholar.afit.edu/etd/3177>

This Thesis is brought to you for free and open access by the Student Graduate Works at AFIT Scholar. It has been accepted for inclusion in Theses and Dissertations by an authorized administrator of AFIT Scholar. For more information, please contact richard.mansfield@afit.edu.



**METASURFACE ANTENNA FOR
WIDEBAND APPLICATIONS**

THESIS

Thomas A Lepley, Capt, USAF
AFIT-ENG-MS-20-M-036

**DEPARTMENT OF THE AIR FORCE
AIR UNIVERSITY**

AIR FORCE INSTITUTE OF TECHNOLOGY

Wright-Patterson Air Force Base, Ohio

DISTRIBUTION STATEMENT A
APPROVED FOR PUBLIC RELEASE; DISTRIBUTION UNLIMITED.

The views expressed in this document are those of the author and do not reflect the official policy or position of the United States Air Force, the United States Department of Defense or the United States Government. This material is declared a work of the U.S. Government and is not subject to copyright protection in the United States.

AFIT-ENG-MS-20-M-036

WIDEBAND METASURFACE ANTENNA

THESIS

Presented to the Faculty
Department of Electrical and Computer Engineering
Graduate School of Engineering and Management
Air Force Institute of Technology
Air University
Air Education and Training Command
in Partial Fulfillment of the Requirements for the
Degree of Master of Science in Electrical Engineering

Thomas A Lepley, B.S.E.E.

Capt, USAF

March 26, 2020

DISTRIBUTION STATEMENT A
APPROVED FOR PUBLIC RELEASE; DISTRIBUTION UNLIMITED.

AFIT-ENG-MS-20-M-036

WIDEBAND METASURFACE ANTENNA

THESIS

Thomas A Lepley, B.S.E.E.
Capt, USAF

Committee Membership:

Peter J Collins, Ph.D
Chair

Michael J Havrilla, Ph.D
Member

Andrew J Terzuoli, Ph.D
Member

Abstract

This research effort explored a methodology for design of metasurface antennas and evaluated their suitability for ultra-wideband applications (2 to 18 GHz). Six unit cell types were characterized. Eigenmode simulations produced frequency vs. phase data for the unit cells, from which impedance vs. gap size data was computed. The antenna design was generated using holographic interferometry to manipulate wave equations, producing the required impedance profile. A method for metasurface antenna pattern simulation in Computer Simulation Technology (CST), was explored, but further effort is required to produce valid results. The unit cell simulations revealed that the assumption of single mode operation is not valid in all cases, and is a factor to consider for wideband designs. The mode 2 activation frequency varies with dielectric constant, cell size, gap size, and other parameters. A 16" by 10" metasurface antenna using square unit cells, a Duroid 5880 dielectric, and a design frequency of 17 GHz was fabricated and tested. This antenna has a peak measured gain of 18 dBi, a beamwidth of 5° , and an elevation beam angle of $\theta_L = 38^\circ$. These results matched Sievenpiper's published results for an identical antenna with the exception of θ_L , which was $\approx 5^\circ$ higher than Sievenpiper's measured results. The accuracy of these results validates the design methodology as a whole. An 8" by 8" metasurface antenna using square unit cells with a Rogers 3010 dielectric and a design frequency of 10 GHz was fabricated and tested. It had a 1.5:1 Standing Wave Ratio (SWR) bandwidth of 8.06 GHz (6.47 to 14.53 GHz) and a 2:1 SWR bandwidth of 12.09 GHz (5.91 to 18 GHz). The main beam was 30° wide and had a peak measured gain of 1.8 dBi at 10 GHz. The center of the main beam was $\theta_L = 0^\circ$ (+Z direction), which resulted in weaker gain as this is the endfire direction from the driven element.

Despite that challenge, this antenna demonstrated that metasurfaces show promise for ultra-wideband applications when high gain is not a requirement.

Acknowledgments

I would like to thank Dr. Collins for his guidance through the research process and for doing the chemical etching for the antennas. Thank you to Dr. Teruzoli and Dr. Havrilla for your instruction and assistance, with both coursework and research. Thank you to Jeffrey Massman and Carl Pfeiffer for the help getting the eigenmode CST simulations running correctly, which were the foundation for this research. Thank you to Captain Marc Chale for the help with linear regression techniques. Thank you to John Glett for doing the anechoic chamber antenna measurements which provided critical results.

Thomas A. Lepley

Table of Contents

	Page
Abstract	iv
List of Figures	ix
List of Tables	xv
I. Introduction	1
1.1 Problem Background	1
1.2 Research Objectives	3
1.3 Investigative Questions	3
1.4 Research Significance	4
1.5 Document Overview	4
II. Background and Literature Review	6
2.1 Metamaterials	6
2.2 Metasurfaces	7
2.3 Metasurface Antennas	8
III. Methodology	12
3.1 Introduction	12
3.2 Design Process Overview	12
3.3 Unit Cell Impedance	15
3.3.1 Simulation Setup	15
3.3.2 Impedance Calculation	19
3.3.3 Postprocessing and Linear Regression	19
3.4 Antenna Design	29
3.5 Antenna Modeling and Simulation	36
3.5.1 Supercell Generation	37
3.5.2 CST Model Construction	39
3.6 Antenna Fabrication	41
IV. Results and Analysis	46
4.1 Introduction	46
4.2 Unit Cell Impedance	47
4.2.1 Square Duroid 5880 Unit Cell	47
4.2.2 Circular Duroid 5880 Unit Cell	53
4.2.3 Fractal Duroid 5880 Unit Cell	56
4.2.4 Square FR4 Unit Cell	63
4.2.5 Circular Rogers 3010 Unit Cell	66

	Page
4.2.6 Fractal Rogers 3010 Unit Cell	71
4.3 Antenna Measurements	74
4.3.1 Duroid 5880 Antenna	74
4.3.2 FR4 Antenna	88
4.3.3 Rogers 3010 Antenna	94
V. Conclusions	110
5.1 Conclusions	110
5.1.1 Cell Analysis Conclusions	110
5.1.2 Design Conclusions	111
5.2 Future Work	112
5.2.1 Error Characterization of Eigenmode Unit Cell Simulations	112
5.2.2 Additional Unit Cell Research	114
5.2.3 Additional Antenna Design Research	115
5.2.4 Improvement of the 8" by 8" Receive Probe Antenna	115
Appendix A. Square Duroid 5880 Unit Cell	117
Appendix B. Circular Duroid 5880 Unit Cell	170
Appendix C. Fractal Duroid 5880 Unit Cell	223
Appendix D. Square FR4 Unit Cell	276
Appendix E. Circular Rogers 3010 Unit Cell	329
Appendix F. Fractal Rogers 3010 Unit Cell	382
Appendix G. 10" by 16" 17 GHz Duroid 5880 Antenna	398
Appendix H. 10" by 16" FR4 Antenna	423
Appendix I. 8" by 8" 10 GHz Rogers 3010 Antenna	444
Bibliography	473
Acronyms	476

List of Figures

Figure		Page
1	Octocopter Bistatic RCS Measurement System	2
2	Metamaterial Cell	7
3	Example Metamaterial Topology.....	7
4	Example of Pixel Designs	9
5	Metasurface Antenna Structure	9
6	Design Methodology	14
7	The CST Environment	15
8	Square Unit Cell Layout	16
9	Square Unit Cell Geometry Parameters	16
10	Simulation Boundary Conditions.....	17
11	Impedance Z vs. Gap Size g , 17 GHz (Sievenpiper).....	20
12	Impedance Z vs. Gap Size g , 17 GHz.....	21
13	Model Residuals	23
14	Histogram of Model Residuals	24
15	Data and Model Comparison	25
16	Difference between Models	26
17	Comparison of Simulated Data	27
18	Calculated Impedance Profile.....	33
19	Sievenpiper's Impedance Profile	33
20	Gap Size Profile	34
21	MATLAB Generated Design Image (partial).....	36
22	Supercell Impedance Model, 17 GHz	38

Figure	Page
23	Supercell Impedance Model, 12 GHz 38
24	Supercell Impedance Model, 19 GHz 39
25	CST Tabulated Surface Impedance Antenna Model..... 40
26	CST S Parameter Port 40
27	Laser Etcher: EPILOG Fibermark 30 42
28	Antenna after Laser Etching 43
29	Drilling the hole for the driven element after chemical etching 44
30	Cutting the driven element 44
31	Installed driven element 45
32	Completed 17 GHz Antenna 45
33	Square Unit Cell Dimensions 47
34	Square D5880 Cell: Dispersion Diagram, Mode 1 48
35	Square D5880 Cell: Impedance vs. Frequency, Mode 1 48
36	Square D5880 Cell: Dispersion Diagram, $g = 0.2$ mm 49
37	Square D5880 Cell: Impedance vs. Frequency, $g = 0.2$ mm 50
38	Square D5880 Cell: Dispersion Diagram, Mode 2 51
39	Square D5880 Cell: Impedance vs. Gap, 1-19 GHz 51
40	Square D5880 Cell: Impedance vs. Gap, 1-9 GHz 52
41	Circular Unit Cell Dimensions 53
42	Circle D5880 Cell: Dispersion Diagram, Mode 1 54
43	Circle D5880 Cell: Impedance vs. Gap, 1-19 GHz 55
44	Circle D5880 Cell: Impedance vs. Frequency, $g = 0.2$ mm 55
45	Fractal Unit Cell Dimensions 56

Figure	Page
46	Fractal D5880 Cell: Dispersion Diagram, Mode 1 57
47	Fractal D5880 Cell: Impedance vs. Frequency, Mode 1 58
48	Fractal D5880 Cell: Impedance vs. Frequency, $g = 0.2$ mm 58
49	Fractal D5880 Cell: Impedance vs. Gap, 17 GHz 59
50	Fractal D5880 Cell: Impedance vs. Frequency, $g = 0.4$ mm 60
51	Fractal Unit Cell: Mode 1 E Field 61
52	Fractal Unit Cell: Mode 4 E Field 61
53	Fractal D5880 Cell: Impedance vs. Gap, 1-19 GHz 62
54	Square FR4 Cell: Dispersion Diagram, Mode 1 63
55	Square FR4 Cell: Impedance vs. Gap, 1-19 GHz 64
56	Square FR4 Cell: Impedance vs. Frequency, Mode 1 65
57	Circular RO3010 Cell: Dispersion Diagram, Mode 1 66
58	Circular RO3010 Cell: Impedance vs. Gap, 1-19 GHz 67
59	Circular RO3010 Cell: Impedance vs. Frequency, Mode 1 68
60	Circular RO3010 Cell: Impedance vs. Gap, 18 GHz 68
61	Circular RO3010 Cell: Dispersion Diagram, $g = 0.2$ mm 69
62	Measured vs. Theoretical Dispersion Diagram of a Frequency-Selective Metasurface 70
63	Fractal RO3010 Cell: Dispersion Diagram, Mode 1 71
64	Fractal RO3010 Cell: Impedance vs. Frequency, $g = 0.2$ mm 72
65	Fractal RO3010 Cell: Impedance vs. Frequency, $g = 1.0$ mm 73
66	D5880 Antenna S11: 74

Figure	Page
67	D5880 Antenna: Reflection Coefficient, Γ 75
68	D5880 Antenna: SWR 76
69	D5880 Antenna: Elevation Pattern, Co-Polarized, 3 GHz 77
70	D5880 Antenna: 3D Pattern Plot, 3 GHz 78
71	D5880 Antenna: Elevation Pattern, Co-Polarized, 9 GHz 79
72	D5880 Antenna: Measured Elevation Pattern, Co-Polarized, 15.36 GHz 80
73	D5880 Antenna: Measured Elevation Pattern, Co-Polarized, 17 GHz 81
74	Measured Antenna Elevation Pattern from Sievenpiper, 17 GHz 82
75	D5880 Antenna: 3D Pattern Plot, 17 GHz 83
76	D5880 Antenna: Elevation Pattern, Co-Polarized, 18 GHz 84
77	Square D5880 Cell: Impedance vs. Frequency, $g = 0.2$ mm 84
78	D5880 Antenna: Azimuth Pattern, Co-Polarized, 5 GHz 85
79	D5880 Antenna: Azimuth Pattern, Co-Polarized, 17 GHz 85
80	D5880 Antenna: Elevation Waterfall Gain Plot 86
81	D5880 Antenna: Azimuth Waterfall Gain Plot 87
82	FR4 Antenna: Elevation Pattern, Co-Polarized, 13 GHz 89
83	FR4 Antenna: Elevation Pattern, Co-Polarized, 15 GHz 89
84	FR4 Antenna: Elevation Pattern, Co-Polarized, 16 GHz 90
85	FR4 Antenna: Elevation Pattern, Co-Polarized, 17 GHz 90
86	FR4 Antenna: 3D Measured Gain Plot, Co-Polarized, 17 GHz 91
87	Square FR4 Cell: Impedance vs. Frequency, $g = 0.2$ mm 92

Figure	Page
88	FR4 Antenna: Elevation Pattern, Co-Polarized, 18 GHz 92
89	FR4 Antenna: Elevation Waterfall Gain Plot 93
90	Completed RO3010 Antenna 94
91	RO3010 Antenna: SWR 96
92	RO3010 Antenna: Azimuth Pattern, Co-Polarized, 2 GHz 97
93	RO3010 Antenna: S11 98
94	RO3010 Antenna: Elevation Pattern, Co-Polarized, 7.86 GHz 99
95	RO3010 Antenna: Elevation Pattern, Co-Polarized, 10 GHz 99
96	RO3010 Antenna: 3D Measured Gain Plot, 10 GHz 100
97	RO3010 Antenna: Azimuth Pattern, Co-Polarized, 10 GHz 101
98	RO3010 Antenna: Elevation Pattern, Co-Polarized, 11 GHz 101
99	RO3010 Antenna: Elevation Pattern, Co-Polarized, 15 GHz 102
100	RO3010 Antenna: 3D Measured Gain Plot, 15 GHz 103
101	RO3010 Antenna: Elevation Waterfall Gain Plot 104
102	Copper Plate: Elevation Waterfall Gain Plot 105
103	Circle RO3010 Cell: Impedance vs. Gap, 10 GHz 106
104	Circle RO3010 Cell: Impedance vs. Frequency, $g = 0.2$ mm 107
105	Circle RO3010 Cell: Impedance vs. Frequency, $g = 0.5$ mm 107
106	RO3010 Antenna: Azimuth Elevation Waterfall Gain Plot 108

Figure		Page
107	Copper Plate: Azimuth Waterfall Gain Plot	109

List of Tables

Table		Page
1	Square Duroid 5880 Unit Cell Parameters	17
2	Square Duroid 5880 Unit Cell: Model Coefficients, 17 GHz	21
3	Sievenpiper's Model of his Data vs. MATLAB-Generated Model of his Data	27
4	Antenna Design Parameters (16" by 10" Duroid 5880)	32
5	Antenna Design Parameters (8" by 8" Rogers 3010)	95

I. Introduction

1.1 Problem Background

Stealth technology has become a key part of the United States Air Force's weapons systems in the last 20 years. The F-22 Raptor, B-2 Spirit, F-35 Joint Strike Fighter, and most recently, B-21 Raider, together comprise a significant percentage of the United States Air Force (USAF) budget, and all feature technology to reduce Radar Cross Section (RCS). With that technology comes the burden of radar signature measurement and maintenance.

One of the challenges of RCS measurement is the massive size of the targets to be measured, which causes the indoor ranges to be large and expensive as well. This makes outdoor ranges an attractive alternative in some cases. Knisely developed an octocopter-mounted field probe system suitable for use as the receive probe at outdoor RCS test facilities (see fig. 1) [1].

Putting the receive probe on an octocopter means that targets of any size can be measured at an outdoor range. The octocopter flies around the target on whatever azimuth/elevation profile desired, as the interrogating signal is sent from the stationary transmit probe. The receive probe mounted on the octocopter captures the desired electromagnetic field measurements, which are later processed into an RCS profile. Knisely's design incorporated a pair of monopoles mounted at 90 degree from each other, resonant 300-700 MHz. The small bandwidth is a significant design limitation. There is a need for a compact, lightweight, ultra-broadband antenna for use as the

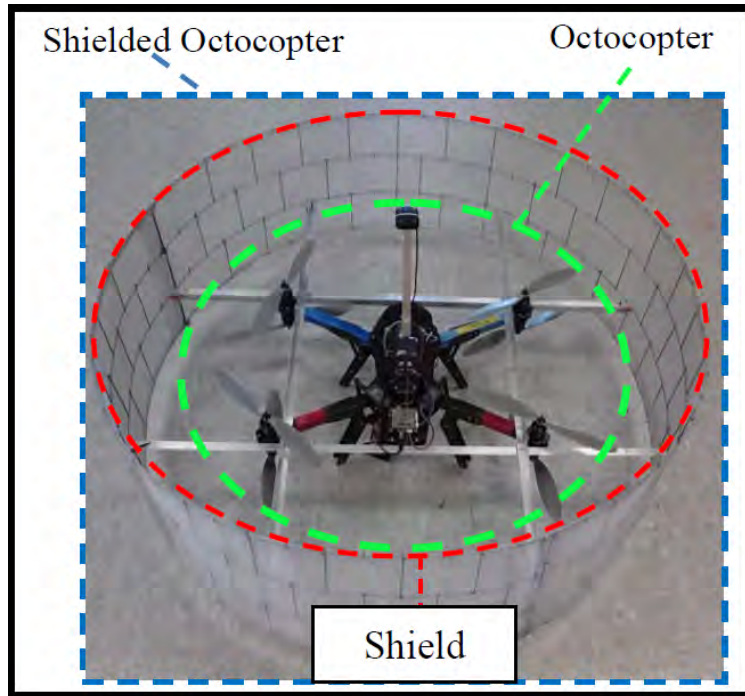


Figure 1: Octocopter-mounted Bistatic RCS Measurement Receive Probe

receive probe for this system.

1.2 Research Objectives

The main research objective is to develop a compact, light-weight, ultra-broadband antenna for use as the octocopter-mounted receive probe in a bistatic RCS measurement system. The desired bandwidth is 2-18 GHz, and the main beam is desired to be 90 to 180 degrees, so that precise sensor pointing is not a requirement, as the antenna will be mounted on a octocopter which will be flown outdoors in other than totally calm conditions. Consistent main beam gain is also desired.

A relatively new class of antennas using metasurfaces, will be explored as a potential solution for the octocopter receive probe. The lower level objectives are to generate and validate a metasurface antenna design process, evaluate the bandwidth, and explore ways to increase bandwidth. The design predicted to have the highest performance will be built and tested.

The methodology pursued will be to establish a working metasurface antenna design process: develop and validate a reliable way to simulate metasurface cell impedance and metasurface antenna patterns. Once this process is established, it will then be used to generate bandwidth predictions for antenna designs and explore various mechanisms for increasing antenna bandwidth.

1.3 Investigative Questions

This research will explore the following questions:

- 1) What is the design process for metasurface antennas?
- 2) How can the impedance of a metasurface cell be simulated?
- 3) How can antenna patterns be simulated for metasurface antennas?
- 4) What cell geometry type results in the highest antenna bandwidth?
- 5) How do the parameters in the antenna control equations affect the antenna pattern?

- 6) What antenna parameters affect the resonant frequency of the antenna?
- 7) How does each design choice affect the overall antenna bandwidth?

1.4 Research Significance

This research is sponsored by the National RCS Test Facility (NRTF), located at Holloman AFB, New Mexico. The octocopter bistatic RCS dynamic field probe currently in use has a bandwidth from 300 MHz to 700 MHz [1]. If this research is successful, the bandwidth of that system could potentially be increased from 400 MHz to as much as 16 GHz, and increase the efficiency of RCS measurement. This would eliminate one of the challenges the new system faces, bringing it a step closer towards operational use. Valid results could also lead to elimination of an antenna type as a viable alternative to the current design.

1.5 Document Overview

Chapter II gives background information on metamaterials, metasurfaces, and an explanation of the basic physical phenomena occurring inside a metasurface. Chapter III describes the technical avenues pursued towards the solution of the research goals. First, phase and frequency data is collected via simulations in Computer Simulation Technology (CST) Studio Suite by doing eigenmode simulations while sweeping geometry and phase. This data is processed and impedance models are generated as a function of the cells' geometry. A holographic control equation is used to determine the desired two-dimensional impedance profile for the antenna. The cell impedance model is used to link the impedance profile with the required geometry profile. Then, the reverse process is used to generate a wideband impedance profile based on the geometry. This wideband model is input into CST using a tabular impedance surface, with impedance values defined at all frequency values that the wideband cell model

includes. Then, CST is used to generate predicted antenna patterns and bandwidth estimates. This process will be used to optimize the bandwidth of a metasurface antenna with a design frequency of 10 GHz (the center point of 2-18 GHz). The design antenna will then be built and tested for the purpose of validating the simulated predictions. Chapter IV gives the results generated by using the process documented in Chapter III. Six different unit cell configurations were evaluated, and circular patches with Rogers RO3010 dielectric was determined to be the cell type that would permit the largest bandwidth. An antenna with a design frequency of 10 GHz was designed using the circular RO3010 cells. This antenna was evaluated at the anechoic chamber at Air Force Research Laboratory (AFRL). Chapter V briefly summarizes the results of this investigation of metasurface antennas and provides recommendations for further research.

II. Background and Literature Review

This chapter covers the relevant background subjects and related research of which an understanding is necessary for comprehension of later chapters. Section 2.1 defines the term metamaterial and Section 2.2 describes a subset of metamaterials called metasurfaces. Section 2.3 outlines the overall operation and characteristics of metasurface antennas.

2.1 Metamaterials

The term “metamaterial” was coined by Dr. Rodger Walser (University of Austin-Texas) in 1999 to describe artificially created materials which have constitutive parameters that do not occur naturally [2]. The Greek word “meta” means “beyond” or “after”, so the electromagnetic properties of these materials go beyond nature [2]. Artificial structural elements are arranged three-dimensionally (e.g. 3D printing) to give a material advantageous properties [3]. Because the elements are much smaller than wavelength, the material can be represented with bulk constitutive parameters (instead of using periodic analysis via the Floquet Theorem) [2]. According to Dr. Walser, these materials are “macroscopic composites having man-made, three-dimensional, periodic cellular architecture designed to produce an optimized combination, not available in nature, of two or more responses to specific excitation” [2]. Figure 2 below shows a single cell of a metamaterial made up of split-ring resonators. Figure 3 shows a metamaterial made from the cells like the one in figure 2. Metamaterials include engineered textured surfaces, artificial impedance surfaces, artificial magnetic conductors, electromagnetic band-gap (EBG) structures, photonic band-gap (PBG) surfaces, double negative (DNG) materials, frequency selective surfaces, and fractals or chirals [2].

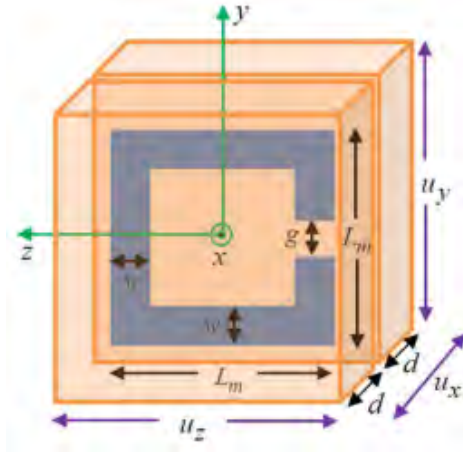


Figure 2: A single cell of a metamaterial with dimensions labeled. The grey material is a metal split-ring resonator. The orange material is dielectric. [4]

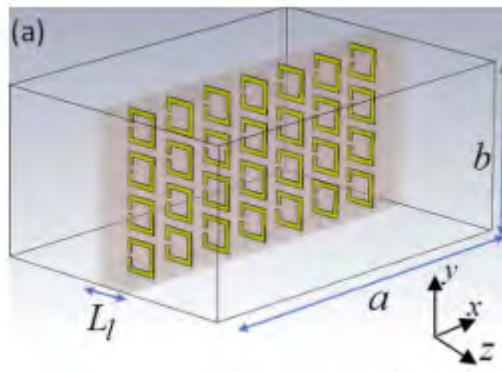


Figure 3: Diagram of a metamaterial showing only a single layer in the xy plane for illustration purposes [4].

2.2 Metasurfaces

Metasurfaces, also referred to as artificial impedance surfaces, can be thought of as the two-dimensional subset of metamaterials. A metasurface is “a composite material layer designed and optimized in order to control and transform electromagnetic fields [3]. These are metamaterials whose thickness is of negligible value (compared to wave length) [5]. Applications include use to change surface impedance, control reflection coefficient phase, manipulate propagation of surface waves, control frequency band, control edge diffractions, control radiation patterns of antennas, and create tuneable

impedance surfaces for use as steerable reflectors and leaky-wave antennas [2]. These surfaces are described by their effective surface-averaged properties on a wavelength scale [3]. They are usually constructed by varying the size and orientation of a series of metal patches on a dielectric material. The cells are much smaller than the intended wavelength. Locally, properties gradually change (capacitance, impedance, etc.) as the dimensions and orientation of the cells change. The parameters result from two-dimensional, surface averaging of microscopic currents on the wavelength scale [3].

2.3 Metasurface Antennas

A metasurface antenna is composed of a metasurface and a driven element. It would be an oversimplification to describe it as a patch antenna array because of the size (small relative to wavelength) and number of individual elements (large), as well as the specialized design processes which carefully manipulate the impedance as a function of position on the surface to control the surface wave radiation pattern and sometimes polarization [6]. The driven element could be a small patch antenna located behind the surface, or one or several of the unit cell patches could be driven, or a monopole could be used. Figure 4 below shows four examples of pixel variation schemes.

The metasurface structure (or artificially-modulated, high-impedance structure) can be thought of similarly to wave guide. As an example, fig. 5 shows a metasurface with square unit cells. The top view shows the dimensions of the cell patterning. It is typical for these surfaces to have a constant lattice size, a . The side view shows how the structure may be thought of as a wave guide. The bottom surface is solid metal (usually copper), and can be approximated as a Perfect Electric Conductor (PEC). The dielectric in the middle of the structure functions as the space inside

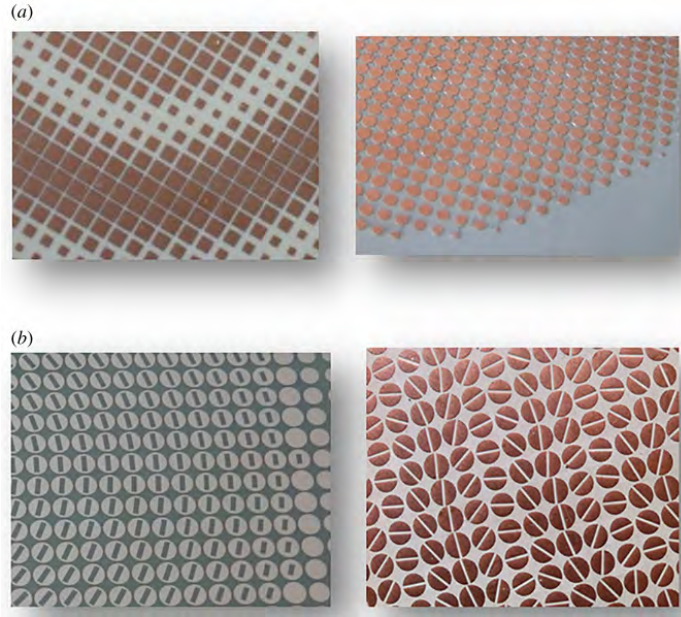


Figure 4: Examples of several pixel variation schemes [6].

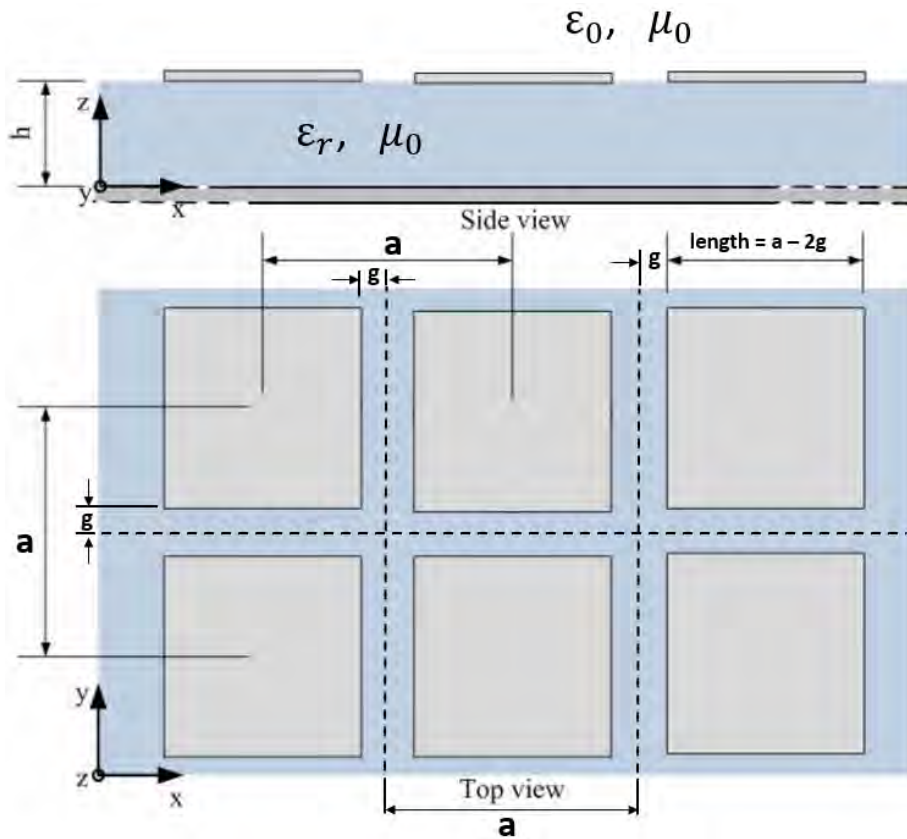


Figure 5: Metasurface Antenna Structure [7]

the “waveguide”. The impedance boundary condition along the top of the structure varies in the XY plane as a result of changes in the gap size parameter, g . These metasurfaces are designed to support surfacewave modes. A surface wave propagates in the XY plane but is evanescent in the Z direction. (By contrast, a leaky-wave mode propagates in the Z direction but is evanescent in the X and Y directions) [8]. The patterning of the metallic patches on the top of the surface causes the changing impedance, and can be designed such that the surface waves are steered, forming a beam in a desired direction, even one including a Z component (for example a beam in the XZ plane).

Some researches use effective-medium theory to describe metasurface impedance [9]. The electric and magnetic fields are averaged over a certain period, and these average field values are used to determine the effective permittivity and permeability of the surface, and therefore the refractive index of the surface. This approach is only valid when the lattice constant (size of metasurface cells) is small in comparison to wavelength. This theory provides some insight into the physical behavior of exhibited by these surfaces. A single wavelength contains many cells. These cells are a mixture of metal (reactance $\approx \infty$) and bare dielectric (reactance ≈ 0), so the wave “sees” the average impedance. As the wave moves along the surface, the wave “sees” a changing impedance because the gap size, g , changes along the surface. The metasurfaces studied are inductive, and therefore designed to support transverse magnetic (TM) waves [10]. The larger the size of the metal patch on top of the cell, the higher the inductance (positive reactance). Inductance is opposition to phase change. The magnetic field is polarized in the Z direction, and during the positive half of a wave cycle, the metal patches on top of the cells charge up, storing energy in a magnetic field, and during the negative half of the wave cycle, that energy is released, opposing the phase change of the waves. Therefore by controlling the phase, the path of the

waves can be manipulated.

III. Methodology

3.1 Introduction

The methodology used for this research largely follows the work done in "Scalar and Tensor Holographic Artificial Impedance Surfaces" by Sievenpiper et al. [11]. The first half of this article describes the development of an artificially modulated (meta) surface impedance antenna. Section 3.2 gives an overview of the design methodology as a whole. Section 3.3 describes the simulations used to generate the unit cell impedance data, as well as the statistical techniques used to model the impedance behavior of the cells based on geometry. Section 3.4 documents the control equations used to create the antenna designs as well as the major features of the MATLAB script which implements those equations. Section 3.5 describes construction of an antenna impedance model in Computer Simulation Technology (CST) Studio Suite. Although progress was made towards the construction of a wideband antenna model in CST, further efforts are required to use that model to produce valid antenna pattern predictions. Section 3.6 describes the details of the process used to fabricate the antenna designs.

3.2 Design Process Overview

The design methodology is illustrated in fig. 6. First, cell parameters (thickness, dielectric material, geometry) are selected. Then eigenmode simulations are performed in CST, sweeping 2 parameters: the phase change boundary condition and the unit cell gap size. These simulations compute the resonant frequency of the structure for each parameter case. The resulting data set is processed via a MATLAB script, which uses the phase and frequency data to generate geometry (gap size) vs. impedance models in 1 GHz increments across the frequency band of interest

(2-18 GHz). The next step is to use holographic design equations to generate a two-dimensional impedance profile at the design frequency for the metasurface antenna. Once this is known, the impedance models generated from the eigenmode simulations are used to convert the impedance profile to a gap size profile. The post processing script then converts the gap size profile into a design image for laser etching, and also uses the gap size profile along with the impedance model to determine the antenna's impedance profile across the entire band of interest. This profile is the input to a third MATLAB script which builds an antenna model in CST, so that antenna gain patterns and S11 parameters can be simulated. If the performance does not meet the specifications, the input parameters to the design equations can be changed and a new impedance profile must be generated and the process re-accomplished, ending with new antenna pattern simulations. Alternatively, a different cell type (change of thickness, size, dielectric, cell shape) could be chosen and the process restarted from the beginning. If these predictions are as desired, the process is over and the antenna can be fabricated and tested to validate the simulations and verify performance.

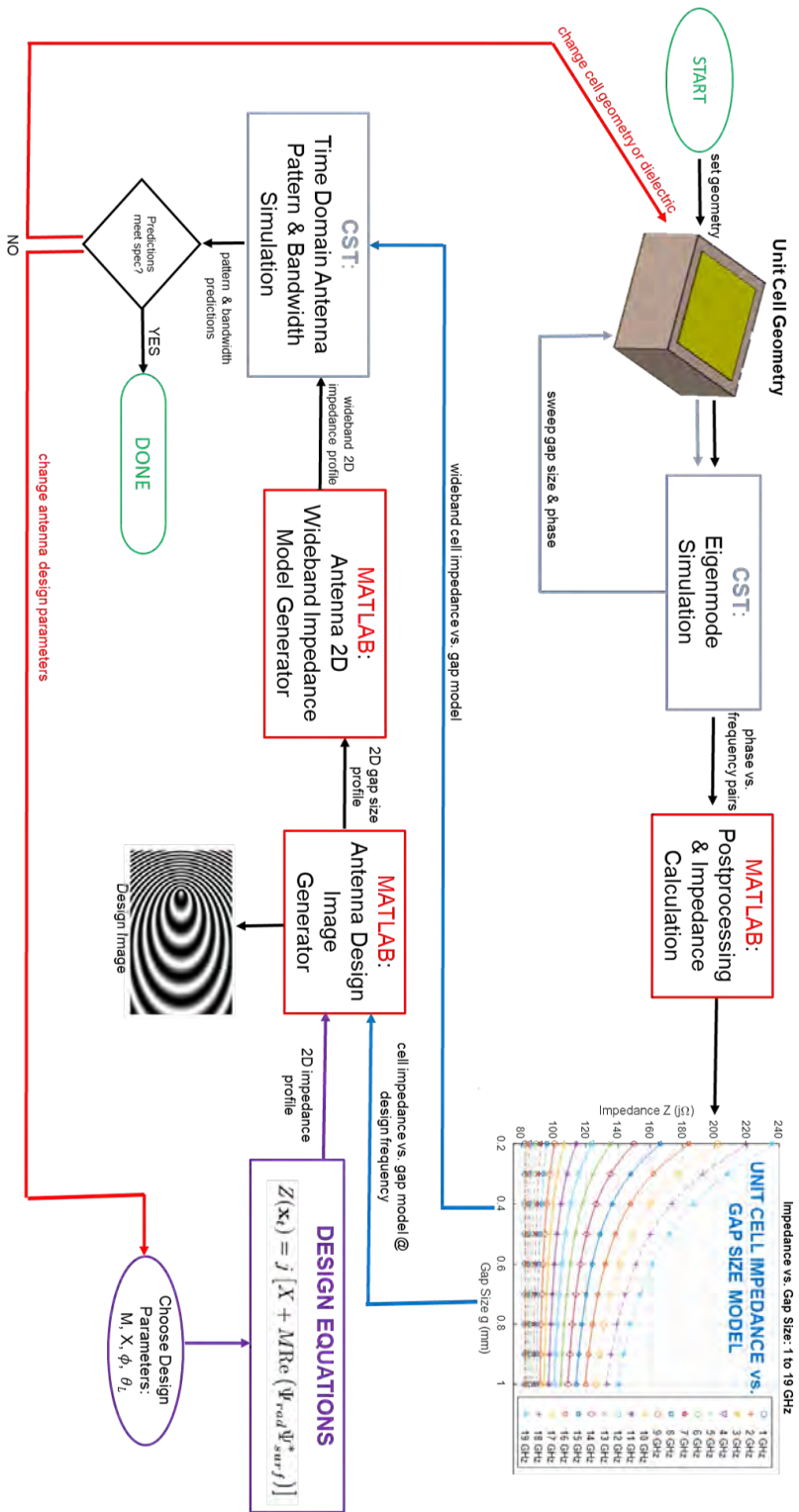


Figure 6: Design Methodology

3.3 Unit Cell Impedance

3.3.1 Simulation Setup

All simulations for this research were conducted using CST Studio Suite, 2019 edition. The CST simulation environment is shown in fig. 7.

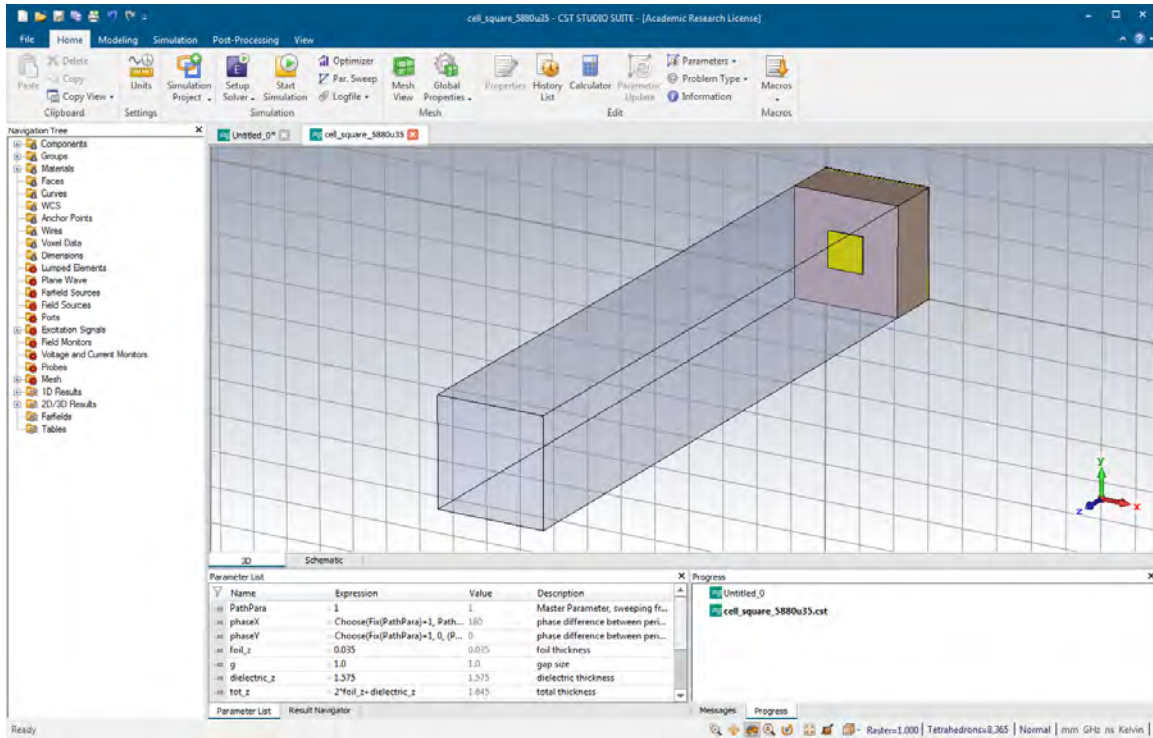


Figure 7: The CST Environment

Figure 8 shows the basic setup for the unit cell simulations. There are four layers: copper ground plane on the bottom, dielectric, copper patch on top of the dielectric, and air or vacuum in the cell above that. Figure 9 shows the square cell geometry in more detail. The geometry parameter a is the fixed cell lattice size (ie. every cell has a size of a by a , 3 mm by 3 mm in this case). Gap size, g , is a parameter that describes the distance between the edge of the cell and the copper patch on the top of the cell. The structure on top of the cell inside the gap area is exposed dielectric. The rest of the cell parameters used by Sievenpiper and this methodology validation

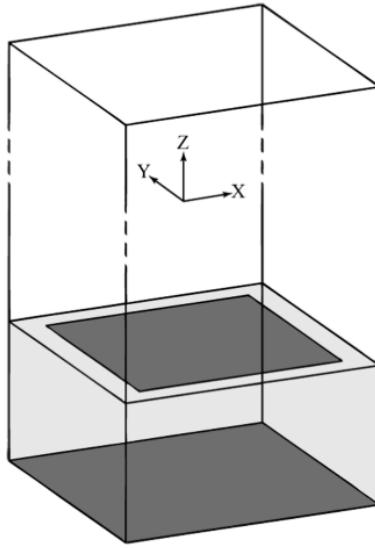


Figure 8: Square Unit Cell Layout [11]

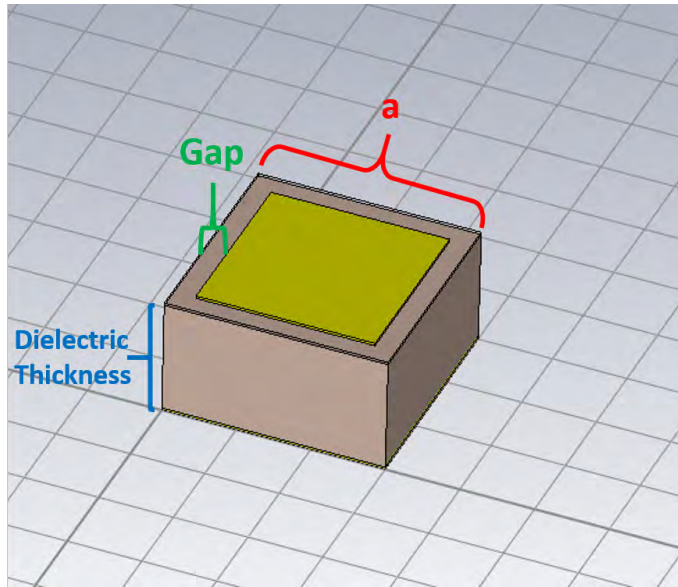


Figure 9: Square Unit Cell Geometry Parameters

are below in table 1. The area above the copper patch on top of the cell consists of either air or vacuum. The choice of air or vacuum is not significant as the relative permittivity of air is very close to 1 (see eq. (1)). Air was used for these simulations.

$$\epsilon_{air} \approx 1.000589\epsilon_0 \quad (1)$$

Unit Cell Parameters	
Parameter	Value
Dielectric:	Rogers Duroid 5880
Dielectric Constant, ϵ_r :	2.20
Dissipation Constant, $\tan \delta$:	0.0009
Shape:	square
Dielectric Thickness:	1.575 mm
Copper Thickness:	0.035 mm
Cell Size, a :	3 mm

Table 1: Square Duroid 5880 Unit Cell Parameters

The design frequency of the antenna from Sievenpiper is 17 GHz, so the space above the cell was set to be 17.635 mm, one wavelength at that frequency. The boundary conditions for the eigenmode simulations are shown in Figure 10. The top and the bottom are Perfect Electric Conductor (PEC), and the sides are periodic boundary conditions, so that the simulated structure acts as if it is many cells with identical geometry adjacent to each other endlessly in both the X and Y directions.

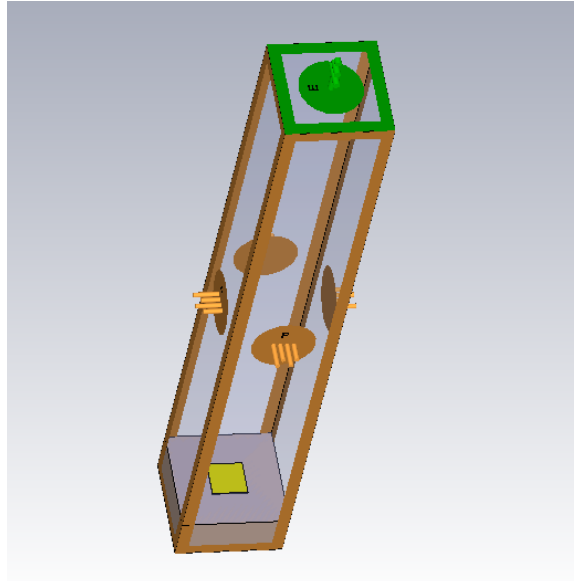


Figure 10: Simulation Boundary Conditions

The second order eigenmode solver was used ("good accuracy" vs. "very good accuracy" with the third order solver), and the maximum accuracy setting (10^{-12})

was used. The mesh accuracy was set to 10^{-10} , a reduction from the default of 10^{-12} . The solver was also set to do a minimum of two passes and a maximum of six to reach desired accuracy. These settings were decided upon after a comparison of results under various conditions (combinations of maximum and minimum gap sizes, maximum and minimum phase change boundary conditions), and various accuracy settings. The maximum difference between the results achieved using the chosen settings and the maximum accuracy settings (third order solver with 10^{-12} accuracy for both the solver and the mesh) was 2 ohms, but the typical difference was usually 0.1 to 0.5 ohms. Periodic boundary conditions require a phase change input for both horizontal axes (X and Y), which describes the phase change of the electromagnetic waves across a single cell. A phase change of 0° was chosen in the Y direction. The parameter sweep tool was used to perform simulations while sweeping the phase in the X direction (Xphase) in 10 degree increments from 10° to 180° , while also sweeping through each geometry increment (gap size of 0.2 to 1.0 mm in 0.1 mm increments). The phase change parameter was only swept through the first 180° because the results from 180 to 360 would be the mirror image of the first 180° because of the symmetry of the unit cell across both X and Y. The eigenmode simulations yield the resonant frequency of the structure with the chosen parameters and phase boundary condition. After the sweeping phase and gap size, the optimizer function was used to find the exact phase boundary condition yielding each of the chosen model frequencies (1 to 19 GHz in 1 GHz increments) within 1 Hz, for each gap size step. The resulting data was run through a postprocessing script to calculate impedance and generate gap size vs. impedance models for each discrete frequency (1-19 GHz).

3.3.2 Impedance Calculation

Impedance is calculated using the three equations. First the transverse wavenumber, k_t , is found by dividing ϕ , the phase difference, by a , cell length (eq. (2)) [11].

$$k_t = \frac{\phi}{a} \quad (2)$$

Then, k_t is used in eq. (3) to calculate n , the refractive index [11].

$$n = k_t \frac{c_0}{\omega} = k_t \frac{c_0}{2\pi f} \quad (3)$$

Finally n is used in eq. (4) to calculate Z [11].

$$Z = Z_0 \sqrt{1 - n^2} \quad (4)$$

The term Z_0 in eq. (4) is the impedance of free space, which is approximately 376.7 Ω .

3.3.3 Postprocessing and Linear Regression

The goal of linear regression analysis is to generate a model that is both statistically significant and adequate. Statistical significance is measured via significance testing, and model adequacy is examined using residual analysis. The postprocessing script implements the impedance calculation and performs other postprocessing functions, including removal of data points resulting from non-surfacewave modes (indicated by a refractive index, n , less than 1), linear regression of the gap vs. impedance data to produce models for every frequency of interest, statistical significance testing of the models, and production of data plots.

Figure 11 shows the impedance vs. gap data that Sievenpiper generated at his

antenna design frequency, 17 GHz. Figure 12 is the result of an effort to duplicate

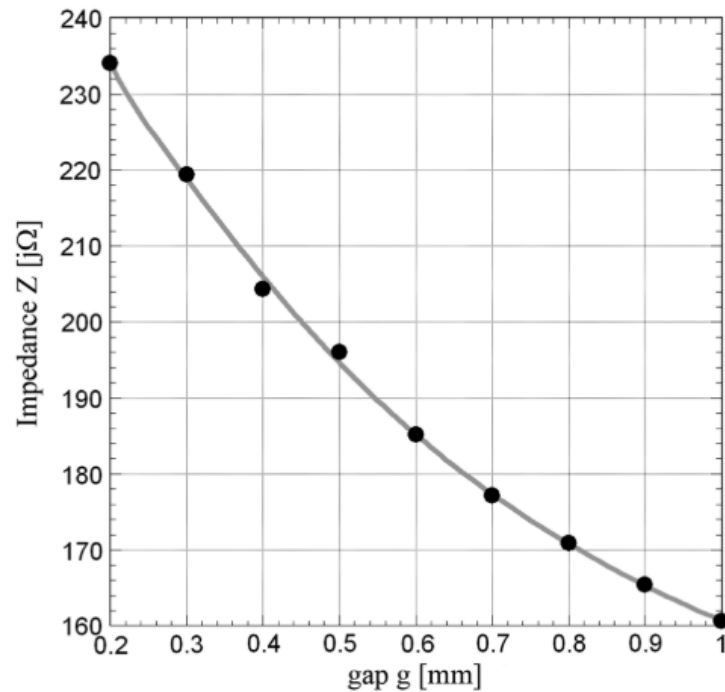


Figure 11: Impedance Z vs. Gap Size, 17 GHz (Sievenpiper) [11]

Sievenpiper's work, using CST to do the same eigenmode simulations with the same materials, geometry, and frequency.

Note that in both fig. 11 and fig. 12, a polynomial models the data. Sievenpiper did a least-squares fit to generate his polynomial model [11]. Similarly, MATLAB's `stepwiselm` function was used to generate a polynomial model via linear regression of the data from CST. This function accepts three inputs: a predictor variable, a response variable, and an initial number of terms to attempt. The function then generates a polynomial to fit the data and tests the statistical significance of each term in the polynomial, as well as the significance of the model as a whole. The function then adds or removes terms from the model until the terms and the model as a whole are determined to be statistically significant. The function outputs a polynomial modeling the data. It also automatically generates statistics which describe how well

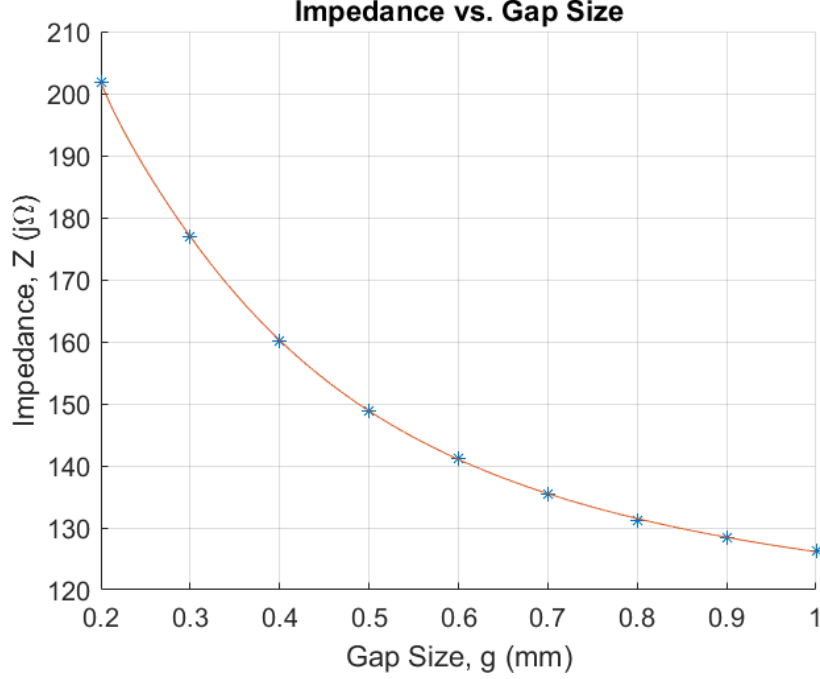


Figure 12: Impedance Z vs. Gap Size g (17 GHz)

the model fits the data. The student T distribution, along with the T test, is used for the significance testing of the terms and the F test is used for significance testing of the model as a whole. The T test is commonly used for linear regression analysis [12]. The output from `stepwiselm` for the data generated in CST is below in table 2.

	<u>Coefficient</u>	<u>SE</u>	<u>tStat</u>	<u>pValue</u>
c_0 (intercept)	104.33	1.2785	81.609	5.2349×10^{-9}
c_1	20.232	1.7143	11.802	7.6854×10^{-5}
c_2	1.7492	0.6645	2.6324	0.046398
c_3	-0.37996	0.075388	-5.0401	0.0039666

Table 2: Square Duroid 5880 Unit Cell: Model Coefficients, 17 GHz

The equation describing the data generated in CST is below (eq. (5)).

$$Z = j\left(104.3 + \frac{20.232}{g} + \frac{1.749}{g^2} - \frac{0.380}{g^3}\right) \quad (5)$$

The null hypothesis for the significance testing is that the term in question does

not describe the data in a statistically significant way. Significance is measured by comparing the chosen confidence level, α , with the p-value generated for the particular term. If the p-value is smaller than α , then the null hypothesis is rejected, meaning that the term in question is statistically significant for describing the data set [12]. The widely accepted confidence level, α , for linear regression is 0.05 [12], however MATLAB uses $\alpha = 0.10$, which allows a lower confidence for terms included in the model. This meant that occasionally the models generated by `stepwiselm` included extraneous terms. This issue was resolved by using another MATLAB function, `cftool` (curve fitting tool), to manually select the regression model order, for cases where `stepwiselm` produced mediocre results. This function allows the user to input a set of datapoints and also choose the number of terms in the model. This function was used to manually compare models with different numbers of terms and select the model that best fit the data. Note that the p-values of the model terms (table 2) are all below 0.05. The p-value of the F test was 9.42×10^{-11} , which is also below 0.05. This indicates that both the terms and the model as a whole is statistically significant.

An important concept for linear regression is parsimony. This is the idea that it is better to use the minimum number of terms (minimum polynomial order) needed to describe the data and tolerate slightly larger residuals, than it is to use a high polynomial order and have zero or minuscule residuals [12]. The later case often leads to excursions between the data points used to generate the model. These excursions do not truly represent the behaviour of the system. At four terms, (third order polynomial), eq. (5) follows the principle of parsimony, as evidence by fig. 12.

While T tests and F tests are used to determine model statistical significance, residual analysis is used to determine model adequacy. There are four assumptions of residual analysis [12], [13]:

1. Linearity: the relationship between the predictor variable and the response variable is linear, or at least approximately so.
2. Homoscedasticity: the variance of residuals is the same for any value of X.
3. Independence: observations are independent of each other.
4. Normality: for any fixed value of X, Y is normally distributed.

The assumption of linearity between the predictor variable (gap, g) and response variable (impedance, Z), can be verified using fig. 12. Although there is an obvious polynomial relationship between the variables of higher order than 1, the relationship between g and Z could in fact be roughly approximated as linear. It does not matter that such an approximation would have a negative slope. The assumption of approximate linearity is satisfied. A residual, or error term, is a deviation between the data and the fit [12], ie. the difference between the data point, and the model at that data point. The model residuals are plotted below in fig. 13. Note that the magnitude of the residuals in fig. 13 do not appear to depend on the x values (gap

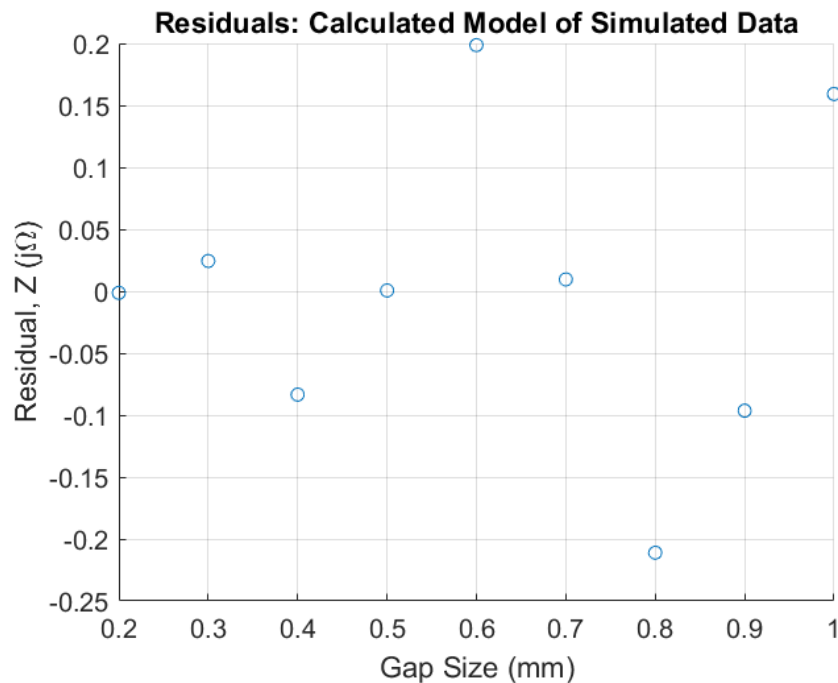


Figure 13: Model Residuals

size, g). In other words, it is seen by inspection that the variance of the residuals is constant. This satisfies the assumption of homoscedasticity. It can also be seen that in fig. 13 that the residuals also appear not to have any relationship or correlation to each other. This satisfies the assumption of independence. Figure 14 below is a histogram of the residuals from fig. 13. The assumption of normality requires that

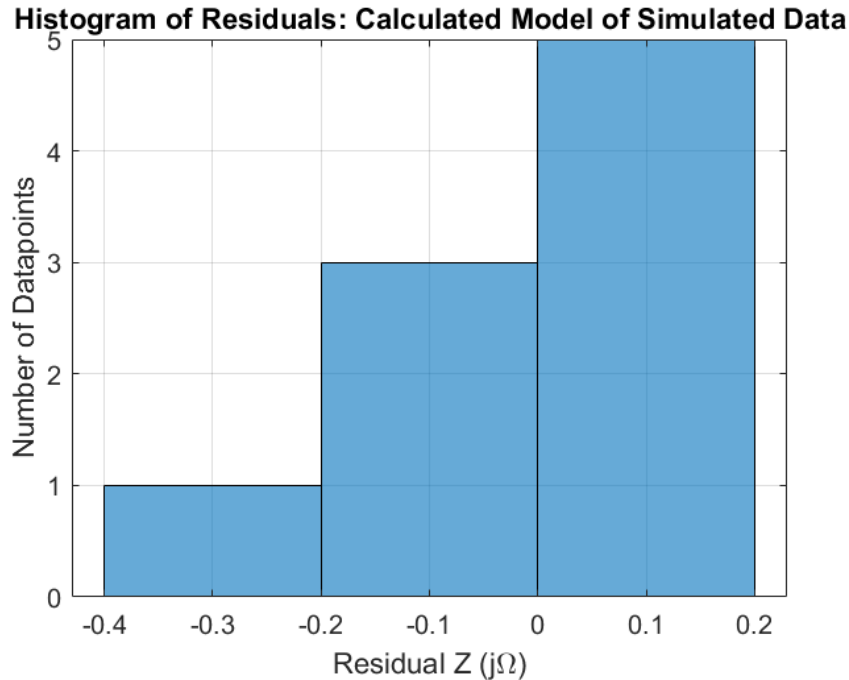


Figure 14: Histogram of Model Residuals

the residuals be normally distributed [12]. Of the nine total data points, five are above zero, and four are below, so the central tendency about zero is present. This particular histogram does not show a normal distribution. However, the number of datapoints is so small that this is not a concern. The number of bins in the histogram is small as a consequence of the low number of datapoints. It is probable that if more datapoints were added to the data set, the histogram would begin to appear to be more normally distributed. It can be concluded that the model is a statically significant descriptor of the data from the CST simulations based on the low p-value of each term (all less than 0.05), and adequate, based on the residual analysis done with

fig. 13 and fig. 14.

Sievenpiper used a polynomial, eq. (6), with inverted X-axis terms for his impedance model [11].

$$Z = j(107 + \frac{65.5}{g} - \frac{12.7}{g^2} + \frac{0.94}{g^3}) \quad (6)$$

Inverted polynomial models can be generated by inverting the predictor variable (gap, g) prior to using `stepwiselm` or `cftool` [12]. It is possible to do other transformations on the predictor variable [12], however, inversion was the only transformation used in this research effort. Some of the impedance models generated are inverse polynomials, and others are not. The option providing the better fit was selected in each case. A comparison of the data and model from Sievenpiper’s article is made with the data and model designed to duplicate his work for the same case in fig. 15 below. There are two data sets and three models present in this plot. The data sets

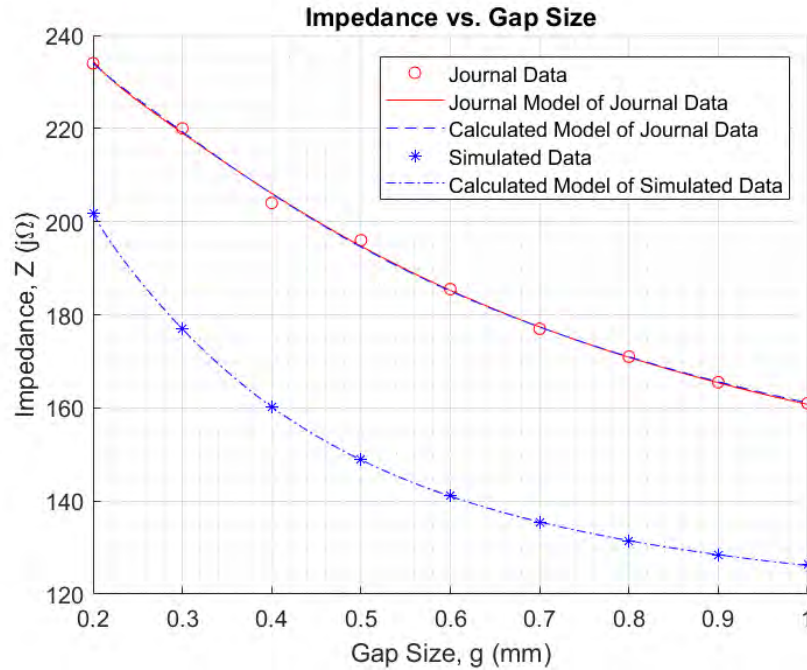


Figure 15: Data and Model Comparison

are the impedance vs. gap values from Sievenpiper and from CST. The two models

for Sievenpiper’s data are the one he gave and also one generated for his data using `stepwiselm`. The model for the CST data is as described above. This plot is an effort to accomplish two things: validate the CST simulation method used to generate the impedance data (as compared to Sievenpiper’s data) as well as validate the method for generating polynomials. Note that the MATLAB-generated polynomial is very close to Sievenpiper’s model of his data. This makes sense as the MATLAB-generated model, eq. (7), has coefficients that are very close to Sievenpiper’s polynomial.

$$Z = j\left(109.6 + \frac{62.08}{g} - \frac{11.38}{g^2} + \frac{0.789}{g^3}\right) \quad (7)$$

Figure 16 below plots the disparity between Sievenpiper’s model for his data, and the model created for his data in MATLAB. Note that the difference curve is approxi-

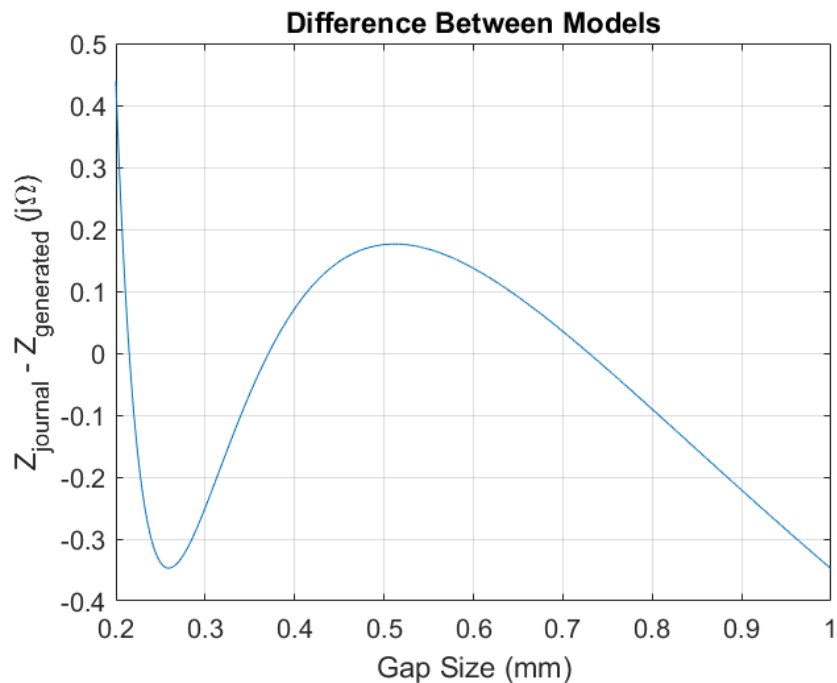


Figure 16: Difference Between Models

mately centered on zero, and that the order of magnitude is small. It is likely that the biggest contributor to the difference between the two models for Sievenpiper’s data

(see table 3) is error caused by reading the data points from the plot in the article.

Sievenpiper's Model vs. MATLAB-Generated Model ($j\Omega$)			
<u>Coefficient</u>	<u>Sievenpiper's Model</u>	<u>MATLAB Model</u>	<u>Difference</u>
c_0 (intercept)	107	109.6	2.6
c_1	65.5	62.08	3.42
c_2	-12.7	-11.38	1.32
c_3	0.94	0.789	0.151

Table 3: Sievenpiper's Model of his Data vs. MATLAB-Generated Model of his Data

It is also probable that even closer agreement between the models would occur if the precise data Sievenpiper collected was input to `stepwiselm`. It is therefore likely that the modeling process is valid.

The disparity between Sievenpiper's data, and the data from CST is somewhat more difficult to reconcile. The difference between these two data sets are plotted in fig. 17 below. The average difference is $40.4 j\Omega$ with a standard deviation of 4.9

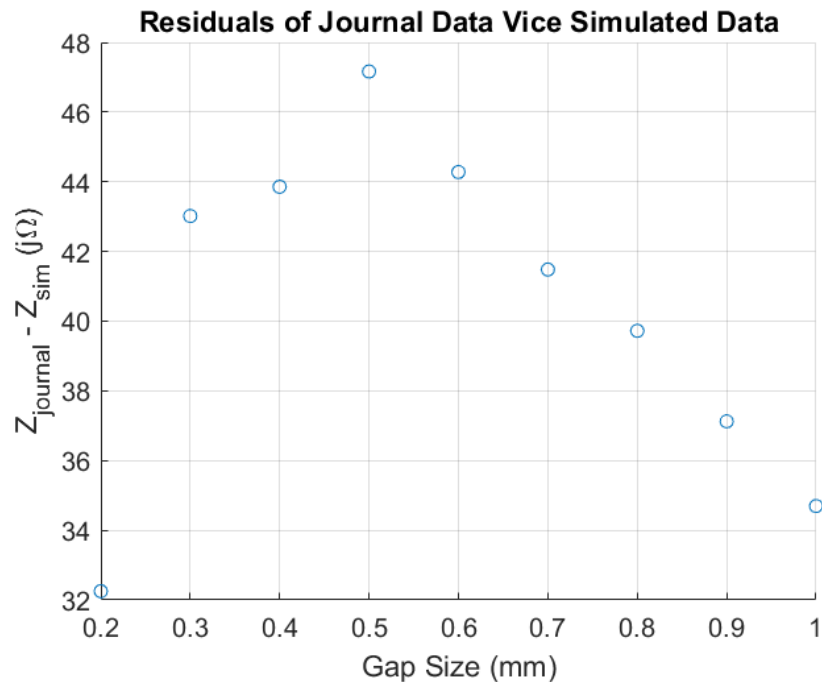


Figure 17: Comparison of Simulated Data

$j\Omega$. Figure 15 also shows that there is a curve shape difference in addition to the dis-

placement in the y-axis. The data from the CST simulations has more concavity in its curve. Sievenpiper’s simulations were performed using High Frequency Simulation Software (HFSS), which has an eigenmode solver which allows complex frequencies, which allows lossy materials to be simulated [11]. That means that HFSS eigenmode simulation data could be processed to produce complex impedances as a result. Sievenpiper’s data has purely imaginary impedance (ie. reactance), but it is unclear whether or not the HFSS eigenmode simulations were run using lossy materials, resulting in a small real impedance component which would have been discarded prior to generating the model of the resulting data. This setting could affect the results. The eigenmode solver in CST does not use complex frequencies, and therefore cannot simulate lossy materials, so the lossy annealed copper was modeled as PEC, and the lossy Duroid 5880 dielectric was modeled as lossless Duroid 5880. Another unknown is the mesh settings used by Sievenpiper. Mesh fidelity can have a large impact on simulation accuracy. It is also possible that Sievenpiper’s data points are the result of interpolation or linear regression of dispersion diagrams. He may have swept the phase boundary condition, ϕ , every 5 or 10 degrees, resulting in phase/frequency pairs for only that limited data set which were then interpolated to generate the exact phase vs. frequency pairs at 17 GHz needed for the impedance calculations. Eigenmode simulations can be very phase-sensitive, meaning that a small phase change results in a large frequency change. For example, a change of $\phi = 10^\circ$ may result in a frequency difference of 3 GHz. This could mean that fitting a polynomial to the dispersion diagram from anything other than a very finely swept data set may result in artificial linearity in the gap vs. impedance data points. The optimizer function in CST was used with accuracy set to at least within 1 Hz for all datapoints used in the impedance models generated for this research. This use of the optimizer function was very time consuming, which might have been a reason for Sievenpiper

to avoid it and use a phase-sweep method followed by interpolation of the resulting dispersion plot to generate the phase vs. frequency data at exactly 17 GHz. As an example, Sievenpiper’s data says that a cell with the previously stated parameters (table 4) has an impedance of $Z = 234 \text{ j}\Omega$ at 17 GHz [11]. Using eq. (2), eq. (3) and eq. (4), the required ϕ (phase change boundary condition) is calculated to be 72.095° . The simulations performed for this research effort for the same scenario resulted in $\phi = 69.471^\circ$ at 17 GHz. This value is 3.64% lower than Sievenpiper’s equivalent data point, and this small difference results in Sievenpiper’s impedance for the same data point being roughly $32.2 \text{ j}\Omega$ higher than the one calculated in CST. Therefore, it is plausible to suggest that the $40.4 \text{ j}\Omega$ average difference could easily be caused by any of several solver accuracy settings, mesh settings, or that the ≈ 3 percent difference could be caused by interpolation/modeling of a dispersion diagram while generating the exact phase-frequency pair desired. More investigation is necessary to gain better fidelity regarding the the cause of these differences between Sievenpiper’s data and the data collected for this effort.

3.4 Antenna Design

Despite the complexities of generating the impedance models, design of the desired impedance profile is relatively straightforward: the profile is determined using a control equation derived with holographic interferometry applied to electromagnetic waves rather than light waves. The control equation is based on two wave equations. The first models the waves from the driven element as a cylindrical wave in eq. (8) [11].

$$\Psi_{surf} = e^{-jknr} \quad (8)$$

The term k is the wavenumber, calculated with eq. (9) [11].

$$k = \frac{\omega}{c_0} = \frac{2\pi f}{c_0} \quad (9)$$

The term n is the refractive index of the metasurface. This term can be calculated directly by substituting eq. (2) into eq. (3), resulting in eq. (10):

$$n = \frac{c_0\phi}{2\pi fa} \quad (10)$$

Radius, r , is a two dimensional radius in the X-Y plane from the origin, (x_0, y_0) , the point at which the driven element is located in eq. (11):

$$r = \sqrt{(x - x_0)^2 + (y - y_0)^2} \quad (11)$$

The second wave equation, eq. (12), describes the desired radiation from the antenna:

$$\Psi_{rad} = e^{jkx\sin(\theta_L) + j\phi} \quad (12)$$

The term k is the same wavenumber described in eq. (9). θ_L is the mainbeam angle in the X-Z plane, measured from the X-Y plane (same plane as the metasurface). The x coefficient of the term $x\sin(\theta_L)$ is what causes the main beam angle to be in the X-Z plane. Phi (ϕ) is a reference phase. According to Sievenpiper, it determines how much the phase of the wave changes per cell [11]. This is not the same ϕ as the phase boundary condition used for the electromagnetic computations done in the simulations generating the impedance data. The choice for this ϕ is arbitrary.

The impedance control equation, eq. (13), uses both wave equations:

$$Z(x_t) = j[X + MRe(\Psi_{rad}\Psi_{surf}^*)] \quad (13)$$

The Re operator means the real part of the enclosed terms, and the $*$ operator is the complex conjugate (switch the real and imaginary components of a complex expression, and then multiply the new imaginary term by -1). x_t means that the impedance, Z is a function of x and y . After substitution of the the wave equations, the control equation becomes eq. (14):

$$Z(x, y) = j[X + MRe(e^{j2\pi fx \frac{1}{c_0} \sin(\theta_L) + j\phi} (e^{-j\phi \frac{1}{a} \sqrt{(x-x_0)^2 + (y-y_0)^2}})^*)] \quad (14)$$

The terms X and M are real modulation depth, and average impedance, respectively. These two terms are special, because they are calculated from the particular impedance model used. X can be described as impedance bias point, about which the wave equations cause deviations. Sievenpiper does not directly say how he calculates this quantity, however, the value he gives for that quantity can be computed exactly from his data using eq. (15):

$$X = \frac{Z_{max} + Z_{min}}{2} \quad (15)$$

Although Sievenpiper calls X the "average impedance," a more accurate term might be impedance midpoint. The term M is the real modulation depth, and describes how much the wave equations are permitted to modulate the impedance about the bias point, X (eq. (16)).

$$M = \frac{Z_{max} - Z_{min}}{2} \quad (16)$$

Sievenpiper says that M is usually set so that the range of impedances allowed by eq. (14) spans the entire range permitted by changing the gap size (ie. $Z_{max} = X + M$ and $Z_{min} = X - M$) [11]. However, radiation rate is also proportional to M , so M may be adjusted depending on the size of the surface to get the desired beam profile.

Further research is required to characterize the effects of X , M , and ϕ on the

antenna pattern. Neither Sievenpiper’s referenced paper or this research provide analytical analysis sufficient to make reliable predictions regarding the effects of these parameters.

To validate the unit cell impedance simulation data and application of impedance control equations, an antenna with identical design choices was fabricated, except that it uses the impedance model generated by the CST simulations rather than Sievenpiper’s impedance data. Both sets of antenna design parameters are below in table 4.

Antenna Design Parameters		
<u>Parameter</u>	<u>Sievenpiper’s Antenna</u>	<u>Fabricated Antenna</u>
Dimensions	16” by 10”	16” by 10”
Material	Duroid 5880	Duroid 5880
Cell Shape	square	square
Cell Size, a	3 mm	3 mm
Number of Cells	unknown	135 by 83 = 11,205
Design Frequency	17 GHz	17 GHz
Monopole Length	3 mm	3 mm
ϕ	72°	70
θ_L	60°	60
X	197.5 j Ω	164 j Ω
M	36.5 j Ω	37.7 j Ω
Z_{min}	161 j Ω	126.3 j Ω
Z_{max}	234 j Ω	201.8 j Ω

Table 4: Antenna Design Parameters (16” by 10” Duroid 5880)

A MATLAB script, `design_generator.m` was used to implement the equations above. This script calculates the center point of each impedance cell, given the unit cell size and the dimensions of the structure. It then applies eq. (13) along with the design parameters in table 4 to generate an array containing the desired impedance at each center point. Figure 18 is a plot of the resulting impedance profile generated using the scaled color image command, `imagesc`.

Sievenpiper’s impedance profile is below in fig. 19. There is excellent agreement

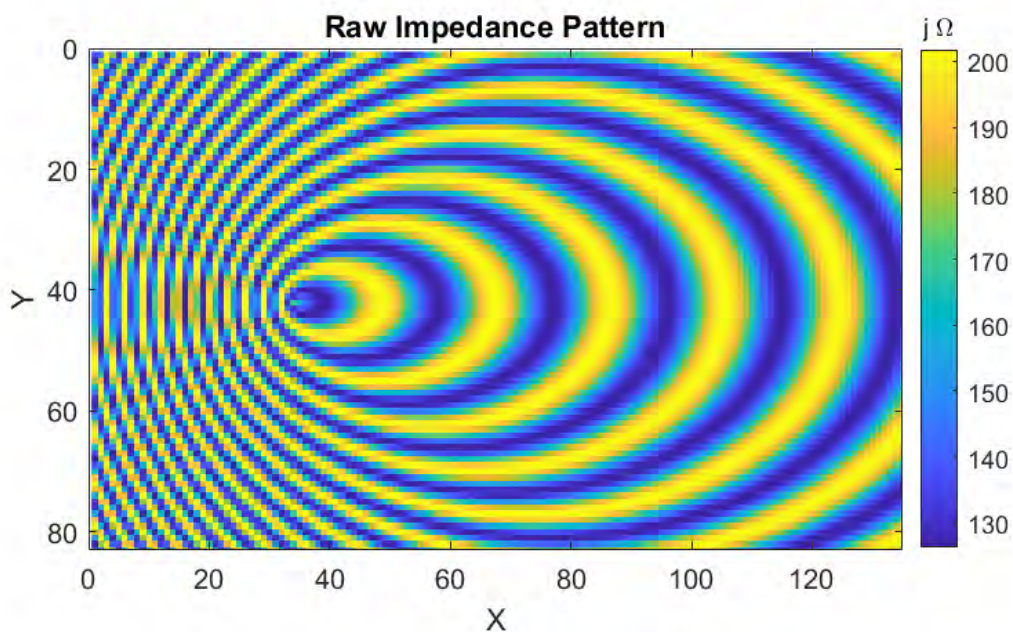


Figure 18: Calculated Impedance Profile

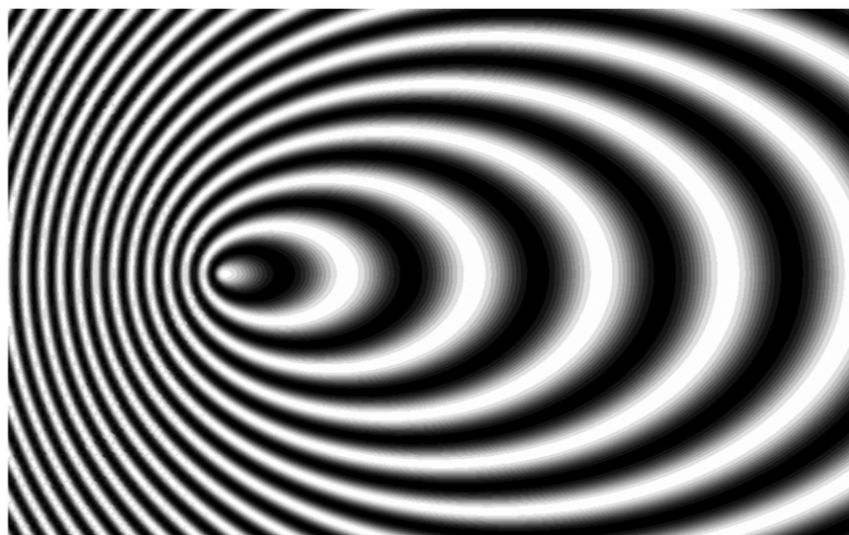


Figure 19: Sievenpiper's Impedance Profile [11]

between the calculated profile and Sievenpiper's profile. The calculated profile is noticeably more coarse as the cells correspond one to one with the cells of the antenna, whereas the resolution in Sievenpiper's impedance profile appears to be higher for illustration purposes. The impedance profile in fig. 18 is converted to gap size profile

using eq. (5): $Z = j(104.3 + \frac{20.232}{g} + \frac{1.749}{g^2} - \frac{0.380}{g^3})$. Because gap size is the independent variable in that equation, a brute force method was used to compute the gap size from the impedance: first a gap size array was generated starting at $g = 0.2$ mm and ending at $g = 1.0$ mm, with step sizes of 5.0×10^{-8} mm. Equation (5) was then used to generate a second array containing impedance values for every gap size value in the previous array. Then, for each cell impedance value, a for loop was used to find the closest impedance value in the impedance array, which was then matched to its corresponding gap size value. A scaled color image plot of the gap size profile is below in fig. 20.

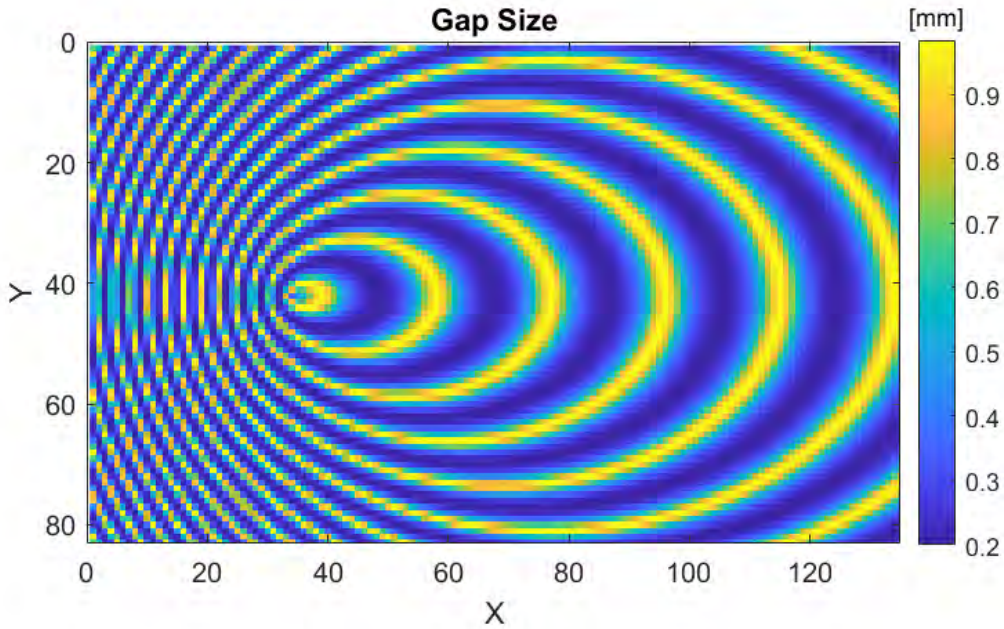


Figure 20: Gap Size Profile

There is a noticeable difference between Figure 20 and fig. 18. Less of fig. 20 is spent at the higher range of gap sizes than fig. 18 spends in the higher range impedance values. This is because of the nonlinear response of the impedance to gap size (see fig. 12). In otherwords, as gap size increases, impedance drops off rapidly at first, so most of the available impedance range can be reached using the smaller half

of the gap size range.

The next step of the design process is converting the gap size profile to a full scale design image which can then be fabricated. To calculate the size of the array needed to hold the image, the physical dimensions of the antenna are multiplied by the resolution (600 dpi). The `ones` command was used to initialize an array with the same number of pixels as the desired image (the image matrix). Then, the physical centerpoints of the pixels in the image array were calculated and stored in another array. After that the gap size array is used in combination with the cell centerpoint matrix and the pixel centerpoint matrix to write zeros over the pixels within each of the patches. This was accomplished by finding the pixel closest to the actual physical location of each patch corner, and then using those four array locations as the boundaries within which to write zeros in the image array. The array was then converted to a `.png` using `imwrite`. Figure 21 shows a section of this design image containing the origin point (focus of the ellipses in the patterning).

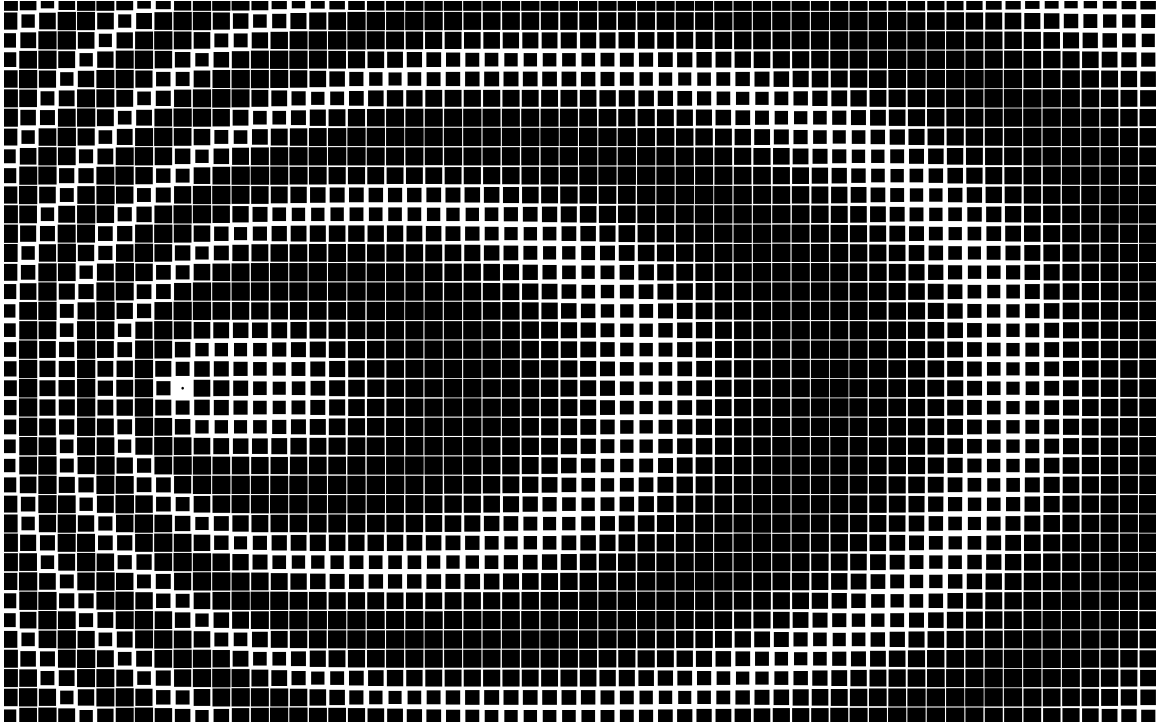


Figure 21: MATLAB Generated Design Image (partial)

3.5 Antenna Modeling and Simulation

The last function accomplished by `design_generator.m` is creation of a wideband impedance model of the antenna. This is a three dimensional array. The size of the Z dimension is 19, the number of frequencies. The X and Y dimensions are the same size as the number of cells the antennas has on those sides respectively. The impedance profile of the antenna at the design frequency has already been determined, and the impedance models for the rest of the frequencies are used to convert the antenna's gap size array into the impedance arrays contained in the wideband model. The wideband model is the input for a third script, `CST_sim_builder.m`. This script accomplishes two functions: modification of the data from the wideband impedance array to reduce the number of cells via the use of supercells, as well as construction of the simulation model by calling commands in CST.

3.5.1 Supercell Generation

The unit cells in the metasurface antenna explored thus far are much smaller than the wavelength. The cells are 3 mm by 3 mm, however wavelength at 17 GHz is ≈ 17.635 mm. This means that roughly six cells fit in one wavelength. Therefore impedance that the waves "see" is a local average of nearby cells. One consequence of this is that, for the purposes of simulation in CST, it is possible to reduce the impedance model resolution below the antenna cell resolution, and still generate valid predictions from simulations using that model. This step is advantageous, as any reduction of the number of unit cells reduces onerous meshing requirements, which in turn reduces the lengthy simulation time required for the time and frequency domain solvers need to produce antenna patterns. `CST_sim_builder.m` accomplishes this task by combining groups of cells and using the average impedance. The 10" by 16" antenna described in section 3.4 has 11,205 cells. By making each supercell from 4 by 4 unit cells (16 cells), the number of supercells drops to 660, a 94.1 percent reduction. The top two subplots in fig. 22 below show the original impedance profile. The bottom two subplots show the impedance profile of the antenna structure using 1 super cell for every 16 unit cells. The color subplots on the left are scaled such that the minimum impedance color is determined by the minimum value in the wideband model, across all frequencies. The subplots on the right are scaled using the maximum and minimum impedance values for the particular frequency. `CST_sim_builder.m` generates a similar plot for all wideband model frequencies (1 to 19 GHz in 1 GHz increments). Figure 23 below is a similar to fig. 22, however it shows the impedance profile of the antenna at 12 GHz rather than 17 GHz. Note that the subplots on the left (scaled to the wideband model) are darker than the left subplots in fig. 22 because the profile has a lower impedance at 12 GHz than it does at 17 GHz. The opposite case is found below in fig. 24. Note that the globally scaled left subplots are

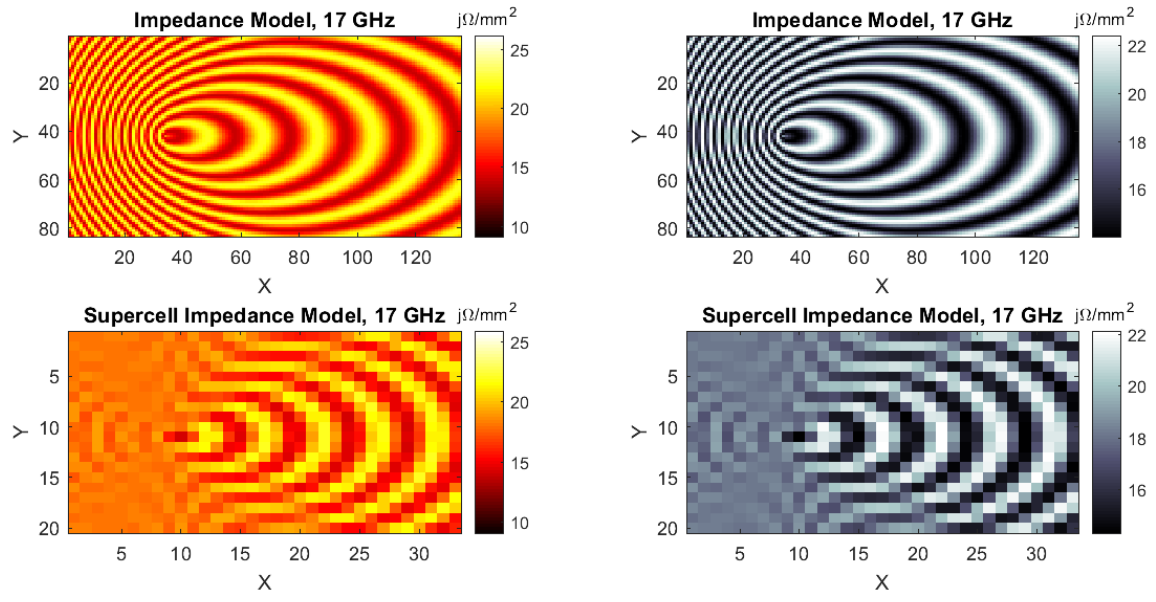


Figure 22: Supercell Impedance Model, 17 GHz

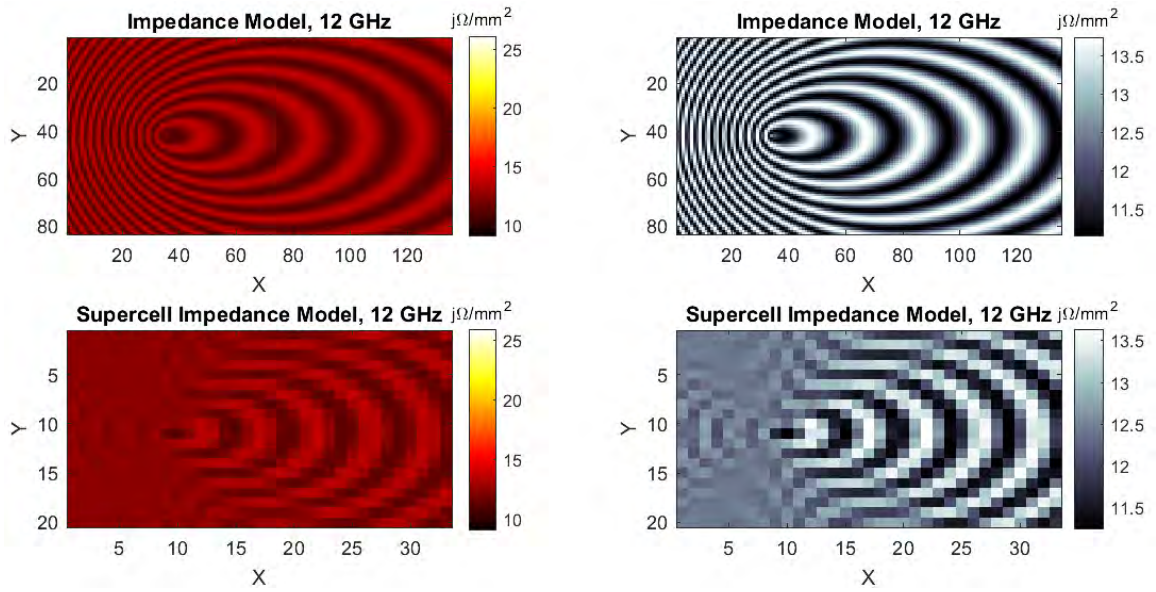


Figure 23: Supercell Impedance Model, 12 GHz

oversaturated and brighter than they are in fig. 22 because the antenna has a higher impedance at 19 GHz.

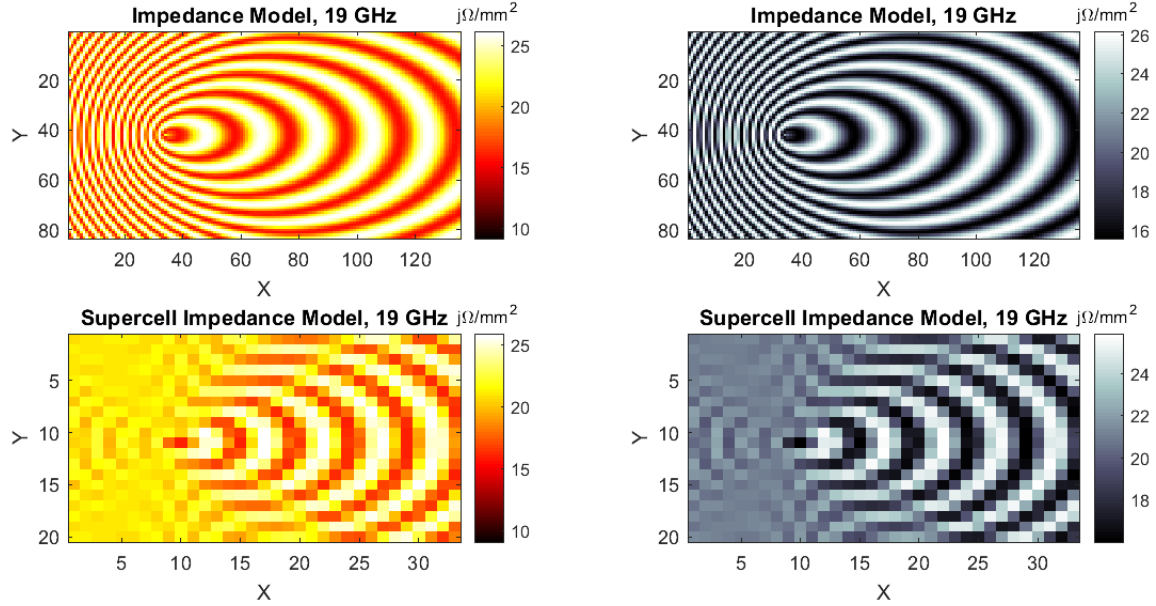


Figure 24: Supercell Impedance Model, 19 GHz

3.5.2 CST Model Construction

MATLAB scripts borrowed from Nazmul Hasan of Tensorbundle Lab were adapted to build the supercell impedance model described above [14]. Hasan’s code calls CST and creates a distinct material for each cell. His code was modified to use tabular impedance surface material type, which allows the user to define the impedance at as many frequency samples as desired [15]. `CST_sim_builder.m` defines each supercell at all 19 frequencies covered by the wideband impedance profile. Because CST defines impedances in tabular surface impedance material as a function of area, additional math must be done to correctly convert the values from the wideband profile to equivalent values for the CST supercells. The average impedance of all the unit cells within the super cell is divided by the area within the unit cell, which is 9 mm^2 in this case. The result is units of $\frac{j\Omega}{\text{mm}^2}$ so CST can automatically scale the impedance of each supercell based on its area. Much of Hasan’s code is built with heavy reliance on the commands within CST’s history list [14]. His code was modified by performing

simple modeling tasks within CST and then comparing the code in the history list with Hasan's code to determine what adaptations were required. Figure 25 below shows an 8" by 8" antenna built in the CST environment using `CST_sim_builder.m`. The red item in the middle of the antenna is a S parameter source, the same length as the driven element. Figure 26 is a closer view of the port.

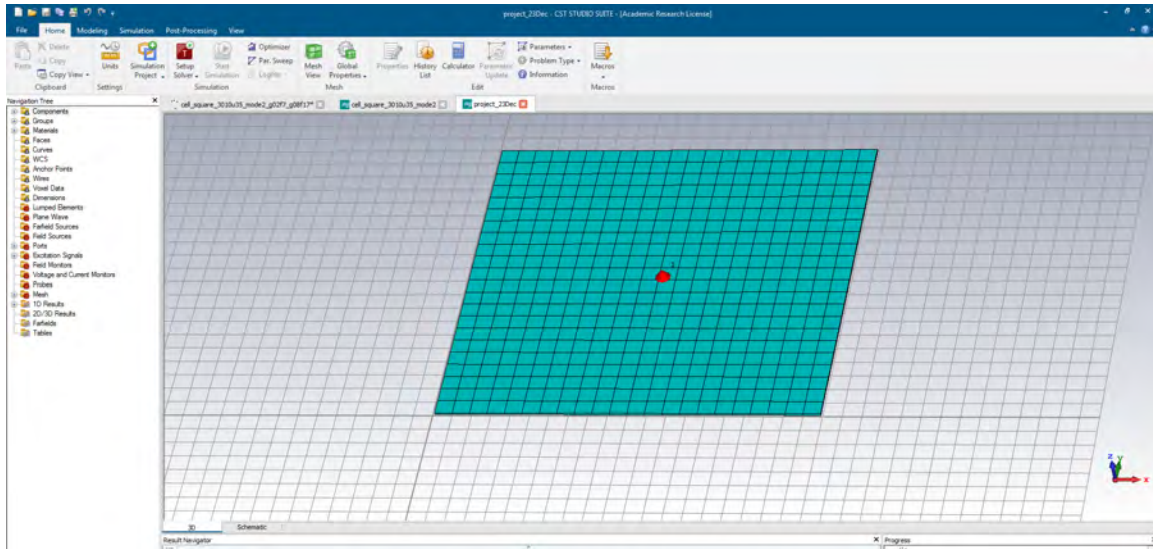


Figure 25: CST Tabulated Surface Impedance Antenna Model

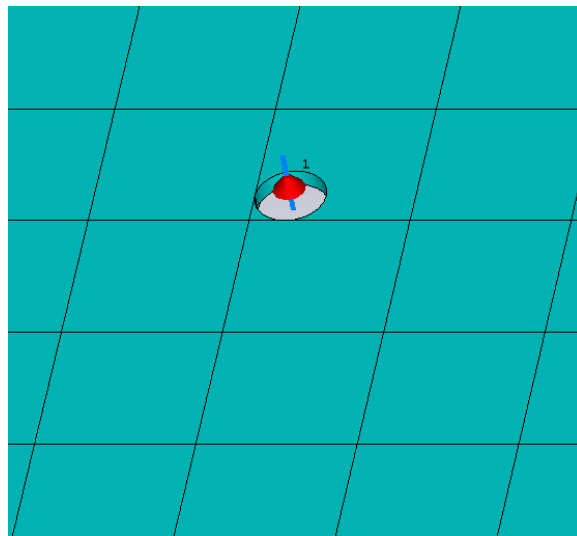


Figure 26: CST S Parameter Port

Although the modeling barrier in CST was overcome, the efforts to produce valid results were unsuccessful, although not unpromising. `CST_sim_builder.m` is a good start towards that effort. Further time and effort is required to produce valid pattern predictions. This was problematic because it prevented characterization of the control equation design parameters (X, M, ϕ) , and prevented use of the feedback loop in the design methodology (fig. 6).

3.6 Antenna Fabrication

The fabrication process was relatively straightforward. First, the copper-clad dielectric substrate was cut to the desired dimensions. Then, the surface of the copper was rouged up using steel wool. Fine grit sandpaper would probably be more effective at creating a consistently rough surface on the copper. Then the substrate was washed and dried to remove dust and fingerprint oil. After that the substrate was painted with flat black spray paint. Several thin coats produce better results than one thick coat. A minimum of 3 thin coats is recommended, with at least 3 days for drying after application of the third coat. Next, the design image described in section 3.4 was inverted so that the sections between the copper patches could be removed by “printing” the inverted image to a laser etcher with the copper-clad dielectric substrate inside. Figure 27 is a photo of the particular laser etcher used. A single etching pass takes about an hour and ten minutes for a 10” by 16” antenna. The etcher settings used are below:

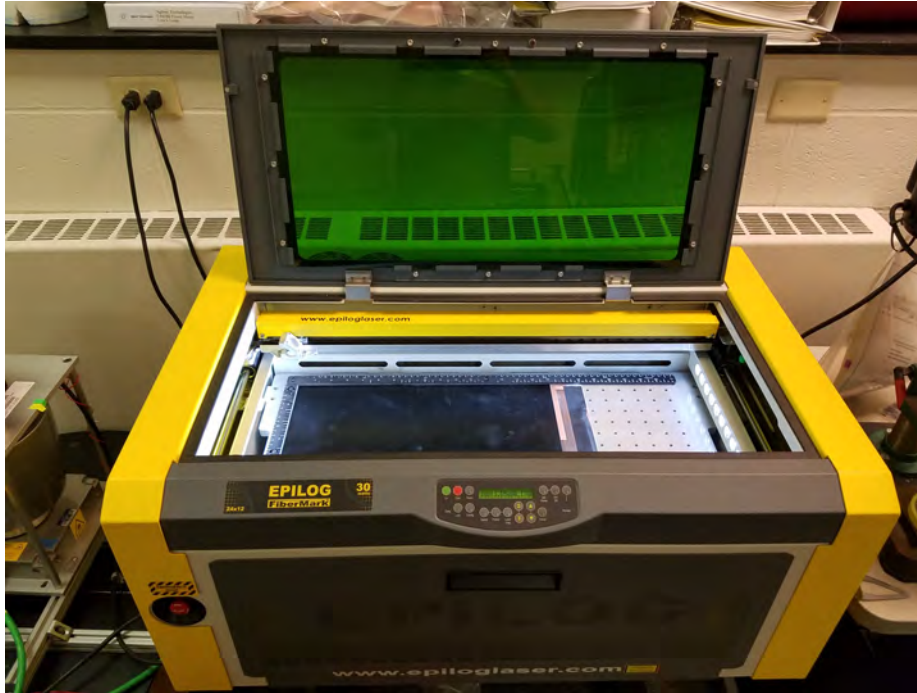


Figure 27: Laser Etcher: EPILOG Fibermark 30

Speed: 90 percent
Power: 75 percent
Frequency: 90 percent
Resolution: 1200 dpi

Two laser passes were used. The first pass removes the majority of the paint. The second pass removes paint dust left from the first pass, as well as the last bit of paint in any spots where the paint was thicker. Figure 28 shows a 10" by 16" antenna after etching. The paint left on the substrate covers the parts of the antenna that will stay copper. The paint forms a mask, so that the exposed copper can be removed via chemical etching in a bath of hydrogen peroxide and muriatic acid. Figure 29 below shows the antenna after chemical etching. The paint was left on the antenna to protect the unit cells, and jig was taped to the antenna with blue painters tape to facilitate drilling the hole for the driven element. The space between the cells is no longer shiny because the copper has been removed, exposing the Duroid 5880 dielectric, which is dark brown. Before drilling the hole, a square area on the back of



Figure 28: Antenna after Laser Etching

the antenna was taped off using painter's tape, around the origin. Then, acetone was applied to the square to remove the paint, exposing a section of the copper on the the ground plane side of the antenna. The paint is removed from this section so that the driven element can be soldered in place with a good mechanical and electrical connection. The hole is drilled from the top of the antenna, so that the lip that results from the hole is on the backside of the antenna, where it can be sanded off to provide a smooth surface for attachment of the driven element. Figure 30 shows the driven element before it is shortened and then installed on the metasurface. Figure 31 below shows back side of the antenna after installation of the driven element. The completed antenna is pictured below in fig. 32. Removal of the painter's tape on the top unitentially took some of the paint with it exposing some of the copper cells. Most of the paint was purposefully left on the antenna to protect the copper cells and groundplane. The paint is nonmetallic and has a negligible effect the electromagnetic properties of the structure.

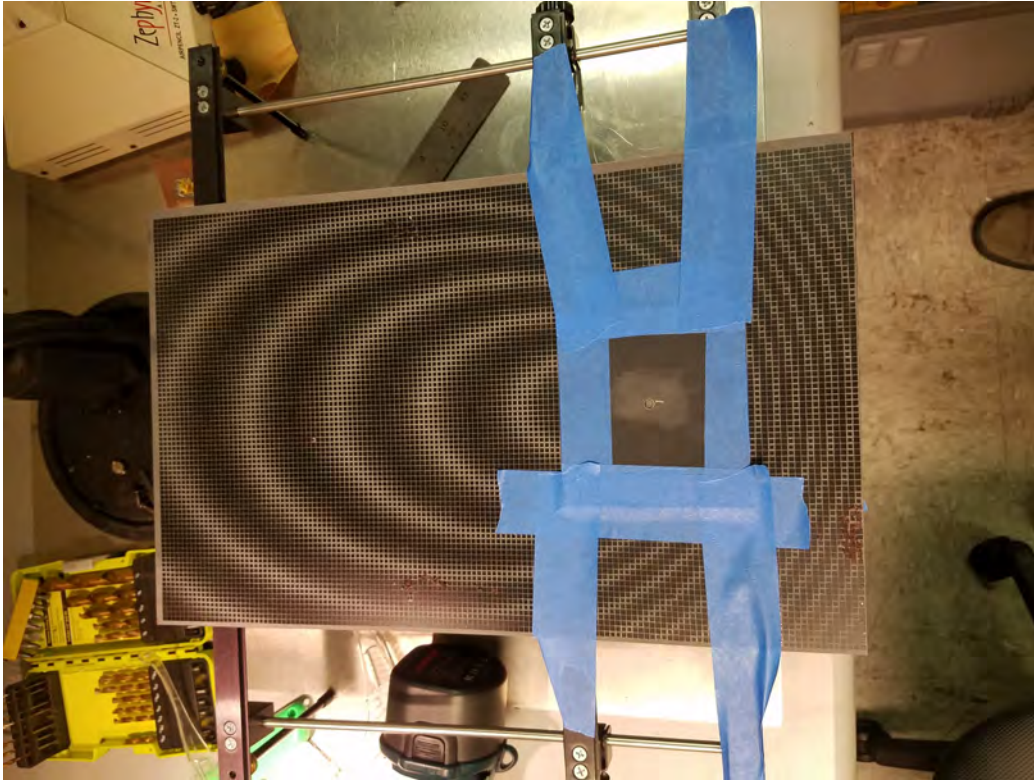


Figure 29: Drilling the hole for the driven element after chemical etching



Figure 30: Cutting the driven element



Figure 31: Installed driven element

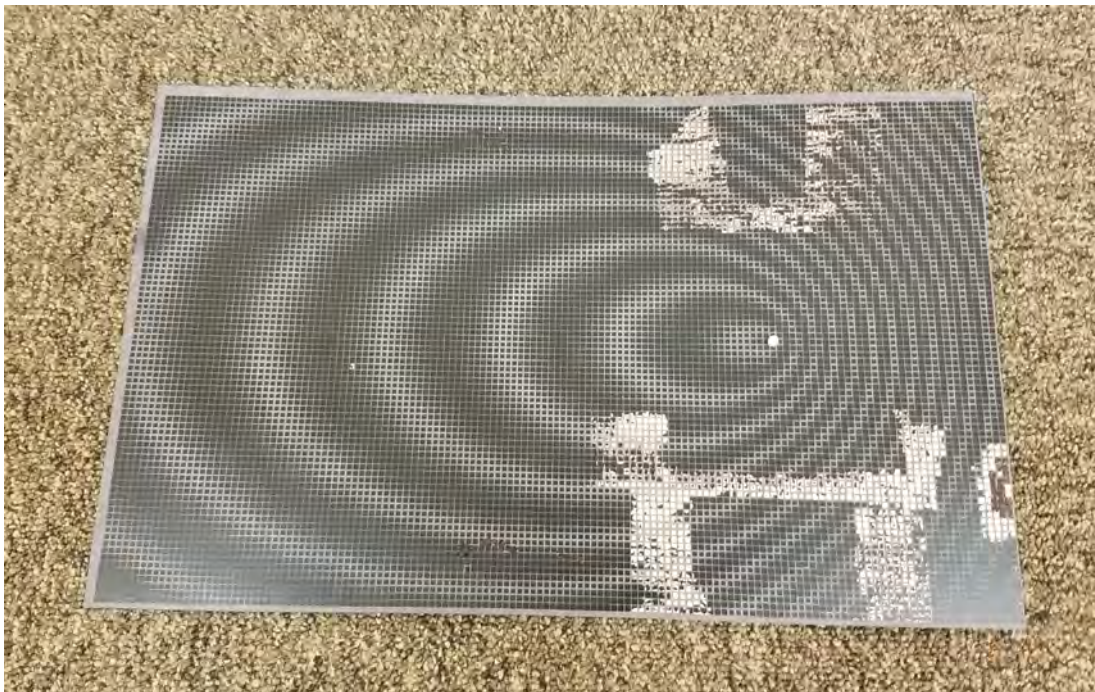


Figure 32: Completed 17 GHz Antenna

IV. Results and Analysis

4.1 Introduction

This chapter details the results generated by using the techniques described in section 3.3 to generate dispersion diagrams and impedance models for several unit cell configurations (section 4.2), as well as an analysis of antenna measurements (section 4.3) made for three antennas designed using the techniques from section 3.4. Six unit cell configurations were examined: square, circular, and fractal cells made with a D5880 dielectric, square cells made with an FR4 dielectric, and circular and fractal cells made with a RO3010 dielectric. Three antennas were fabricated, measured, and analyzed. A 16" by 10" antenna using Sievenpiper's data, impedance model, and design equation parameters was etched onto a piece of copper-clad FR4, rather than the Duroid 5880 dielectric he used, the only intentional design (section 4.3.2). A second 16" by 10" antenna was etched onto copper-clad Duroid 5880, similar to Sievenpiper's antenna, but created using a geometry vs. impedance model generated from independently performed simulations. The intent for this antenna was to provide some experimental confidence in the impedance simulation and modeling process developed in section 3.3, as well as the design process in section 3.4. A third antenna was designed and built which was 8" by 8", had circular cells and RO3010 dielectric. This design was built and tested both as a way of demonstrating successful implementation of the design methodology for an antenna different than Sievenpiper's design, as well as a prototype antenna to be used as the octocopter-mounted receive probe in a bistatic Radar Cross Section (RCS) measurement system. It was an effort to use all of the knowledge gained thus far to meet the design requirements for the receive probe.

4.2 Unit Cell Impedance

4.2.1 Square Duroid 5880 Unit Cell

The first unit cell type evaluated was the same used by Sievenpiper, a square cell with a Duroid 5880 dielectric (see fig. 33) [11]. The cell parameters are below:

Square Duroid 5880 Cell Parameters

Material: Rogers Duroid 5880

Dielectric Constant, ϵ_r : 2.20

Dissipation Constant, $\tan \delta$: 0.0009

Shape: square

Dielectric Thickness: 1.575 mm

Copper Thickness: 0.035 mm

Cell Size, a : 3 mm

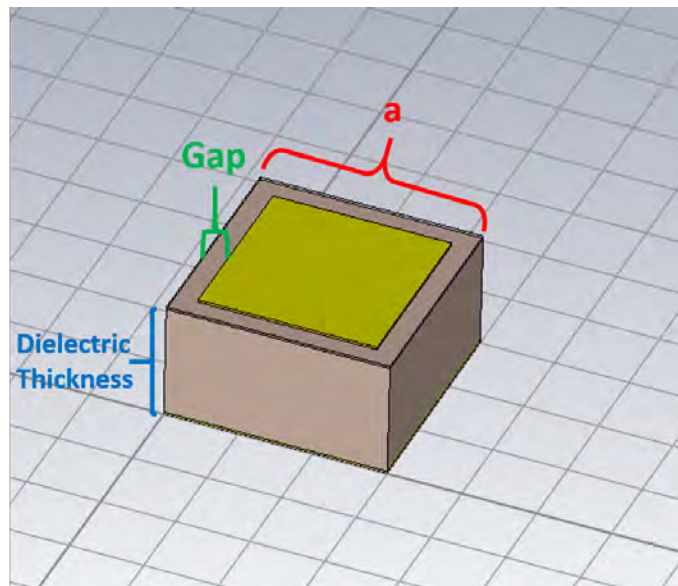


Figure 33: Square Unit Cell Dimensions

The dispersion diagram for mode 1 is below in fig. 34. Note that the frequency response of the different geometries is nearly co-linear from 0° to 50° , and the variation in frequency response starts noticeably fanning out between 60° and 80° . Figure 56 below is the impedance vs. frequency plot generated from the same mode 1 data. There is a similar point in fig. 56 as there was in fig. 34, however it is noticeable at a

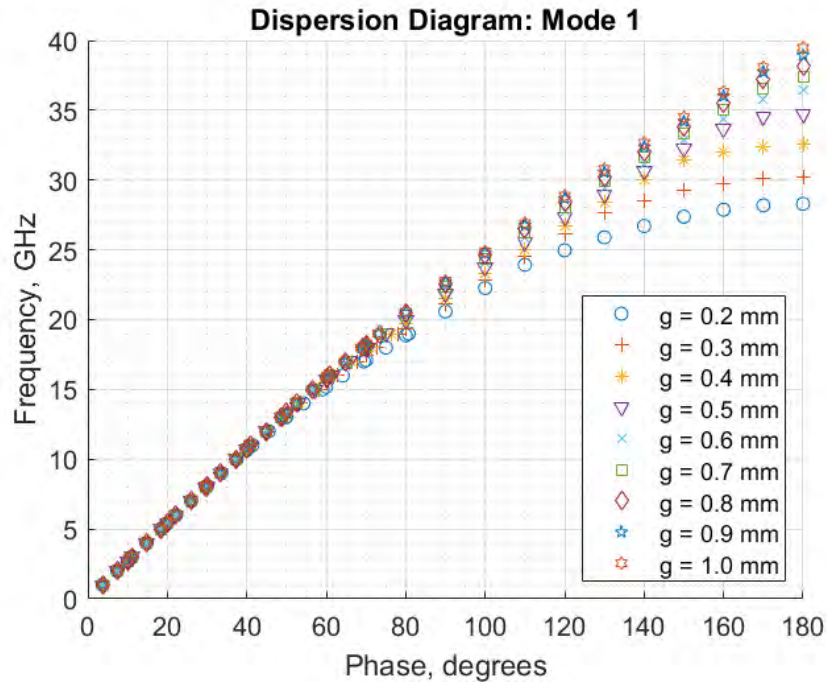


Figure 34: Square D5880 Cell: Dispersion Diagram, Mode 1

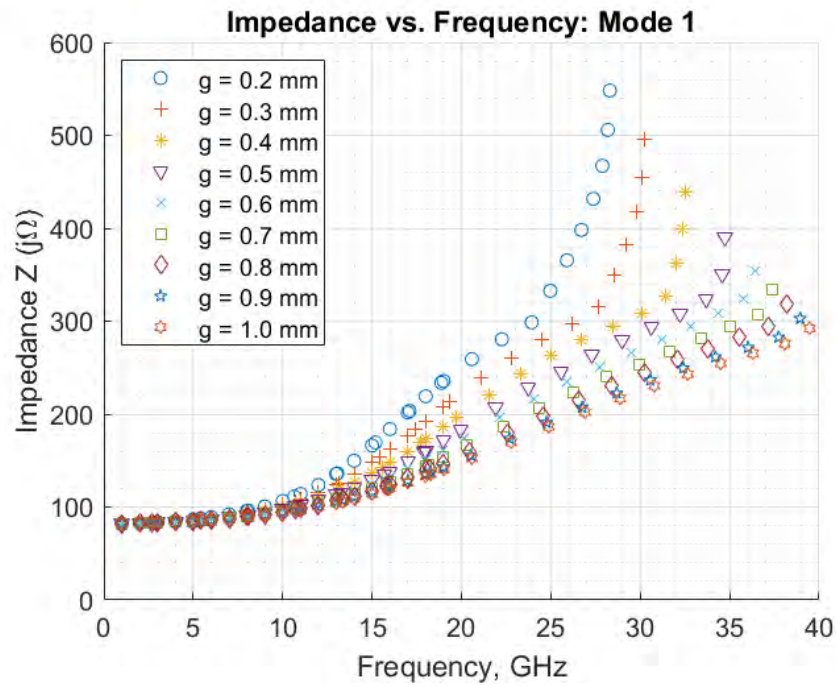


Figure 35: Square D5880 Cell: Impedance vs. Frequency, Mode 1

lower frequency, roughly 10 GHz. Below this point, the responses on the dispersion and impedance vs. frequency plots are co-linear because the wavelength is large enough that the gaps between the metal patches on the top of the top of the antenna electrically approximate zero, so electromagnetic (EM) waves see a solid metal sheet. In other words, the structure looks like dielectric sandwiched between Perfect Electric Conductor (PEC) if the wavelength is low enough. Figure 36 below is the dispersion diagram for 0.2 mm gap size case. Note that mode 2 turns on at approximately 70°,

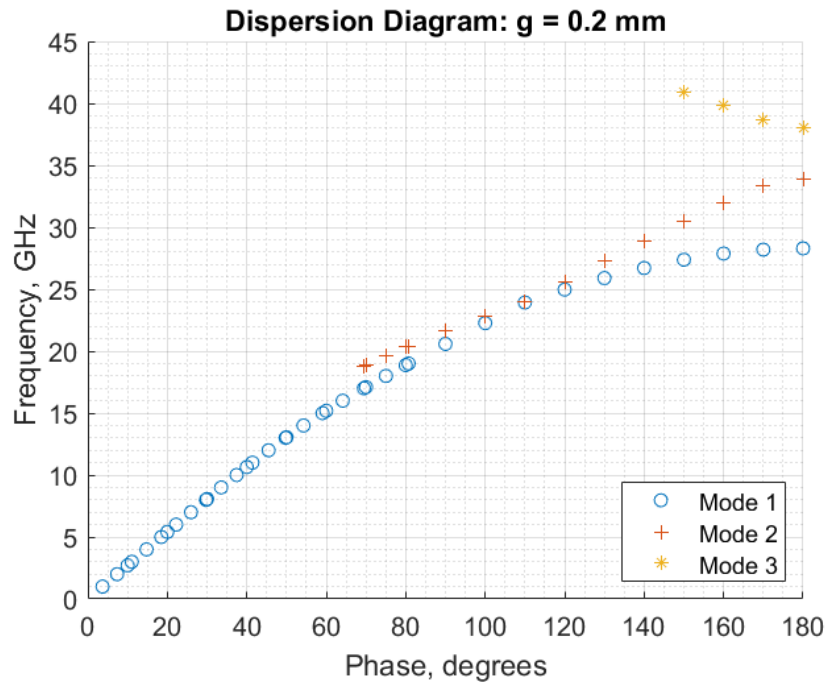


Figure 36: Square D5880 Cell: Dispersion Diagram, $g = 0.2$ mm

and mode 3 turns on at approximately 150°. As seen in fig. 37, this corresponds to roughly 19 and 38 GHz, respectively. There is some apparent interaction between the mode 1 trendline and the mode 2 trendline. Mode 2 turns on at 19 GHz and intersects the mode 1 line at 24 GHz, at which point, the mode 1 line dramatically increases slope, and the mode 2 line drastically decreases slope. It is plausible that the "steep slope line" (first half mode 2, second half mode 1) and the "medium slope line" (first half mode 1, second half mode 2) are actually two separate phenomena.

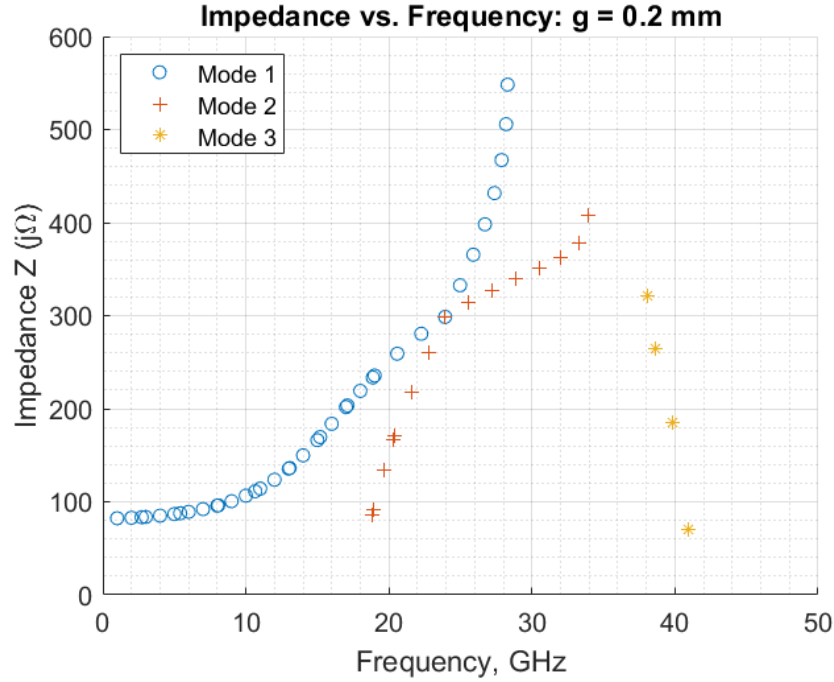


Figure 37: Square D5880 Cell: Impedance vs. Frequency, $g = 0.2 \text{ mm}$

The same intersection point is seen above in fig. 36, at 110° . Computer Simulation Technology (CST) automatically labels mode 1 as the lowest frequency, mode 2 as the second lowest, and so on. It is likely that the "medium slope line" in fig. 37 is actually composed of all the same mode, mode 1. Figure 38 below is the mode 2 dispersion diagram, which provides a different perspective on the turn on frequencies for mode 2 at the various gap sizes simulated. The larger the gap size, the later mode 2 turns on. Figure 39 below shows the impedance verses gap size data and models for the entire range of frequencies simulated. For frequencies above 9 GHz, the impedance response is nonlinear: change in gap size is greater with the smaller gaps than the larger gaps. The impedance response (to adjusting gap size) is almost completely flat below 9 GHz, which can be seen more clearly below in fig. 40

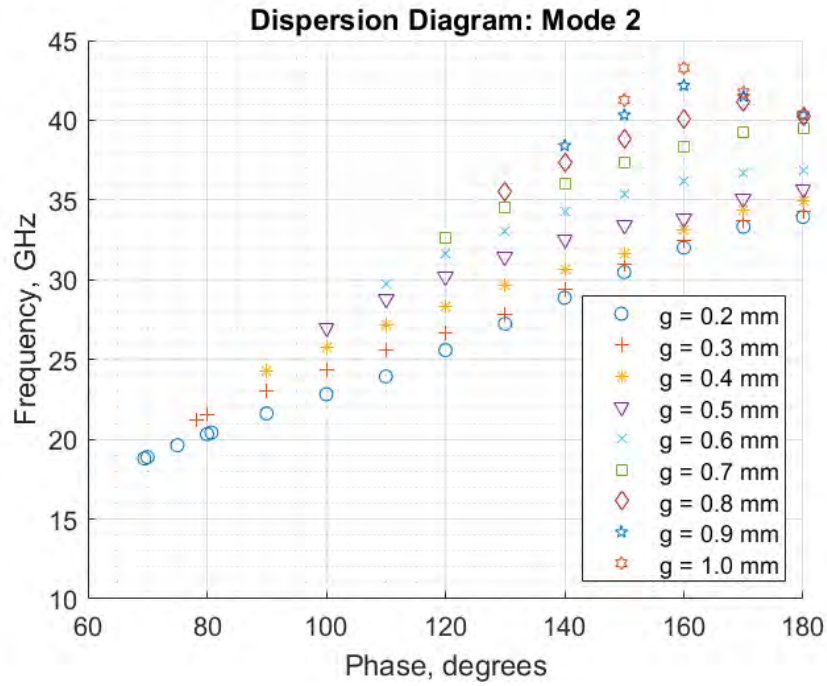


Figure 38: Square D5880 Cell: Dispersion Diagram, Mode 2

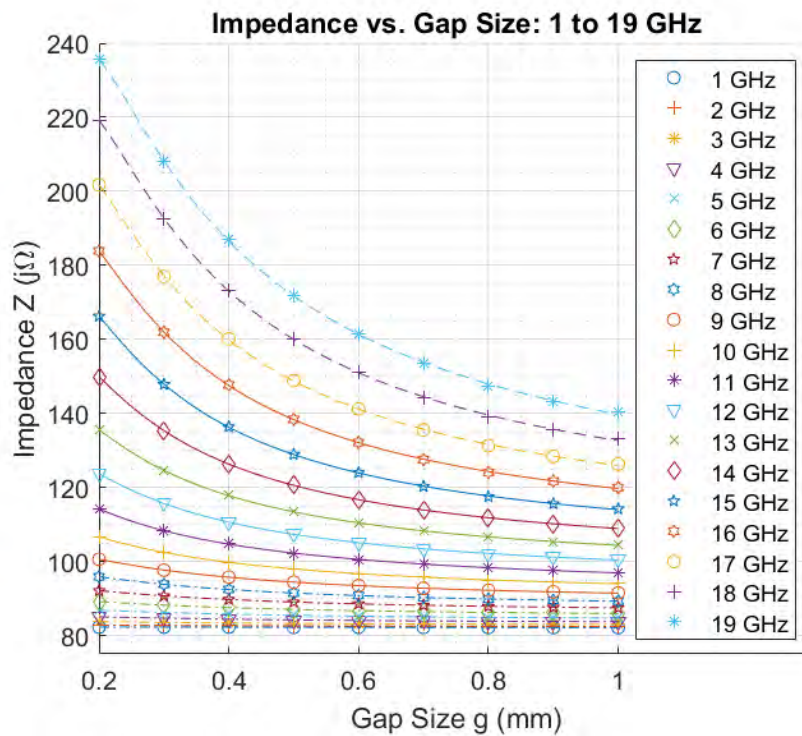


Figure 39: Square D5880 Cell: Impedance vs. Gap, 1-19 GHz

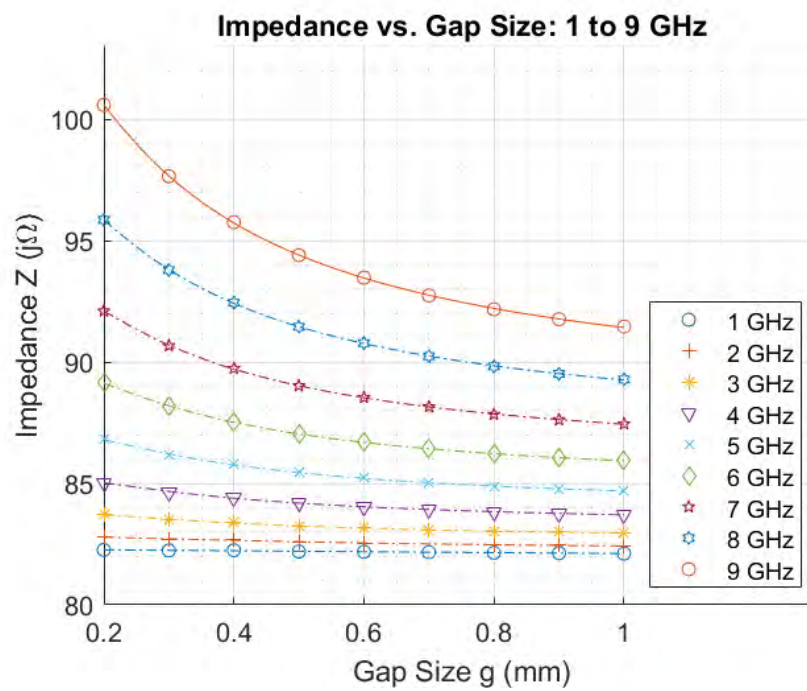


Figure 40: Square D5880 Cell: Impedance vs. Gap, 1-9 GHz

4.2.2 Circular Duroid 5880 Unit Cell

The parameters of the circular Duroid 5880 unit cell (see fig. 41) are below:

Circular Duroid 5880 Cell Parameters

Material: Rogers Duroid 5880

Dielectric Constant, ϵ_r : 2.20

Dissipation Constant, $\tan \delta$: 0.0009

Shape: circular

Dielectric Thickness: 1.575 mm

Copper Thickness: 0.035 mm

Cell Size, a : 3 mm

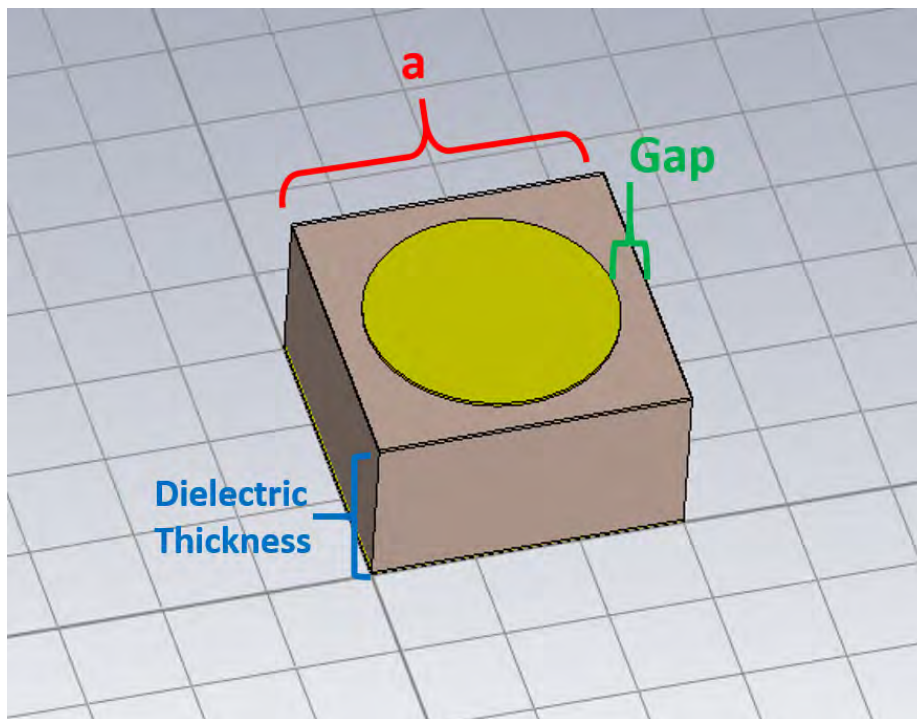


Figure 41: Circular Unit Cell Dimensions

This unit cell has the same parameters as the square Duroid 5880 cell, with the exception of the patch geometry. Note that gap size, g , is measured from the midpoint of the cell. The mode 1 dispersion diagram for the circular D5880 unit cell is below in fig. 42. Note that the "fan point" of the unit cell, the point at which the frequency response starts to depend on gap size, is later than it was for the square D5880 unit

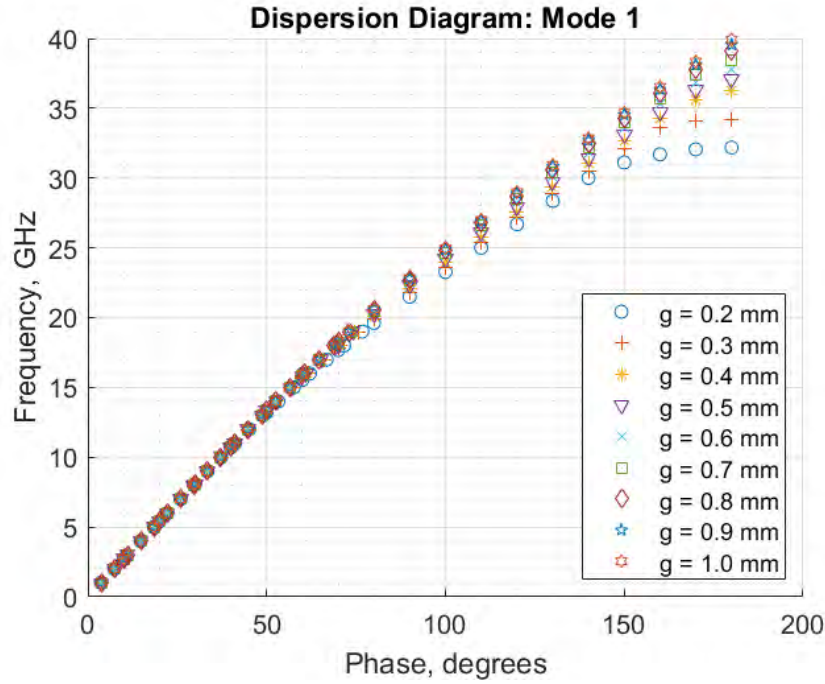


Figure 42: Circle D5880 Cell: Dispersion Diagram, Mode 1

cell, and the fanning is less pronounced. This means that there should be reduced impedance sensitivity to gap distance changes at the higher frequencies. Figure 43 confirms that this is true: The slope of the impedance models at the higher frequencies is smaller than the slopes seen on the sister models of the square D5880 cell. The circular D5880 unit cell has the same slope switching mode interactions as the square D5880 unit cell at $g = 0.2$ mm (fig. 44), but the mode 1 and 2 intersection point happens later, at 30 GHz rather than 22 GHz.

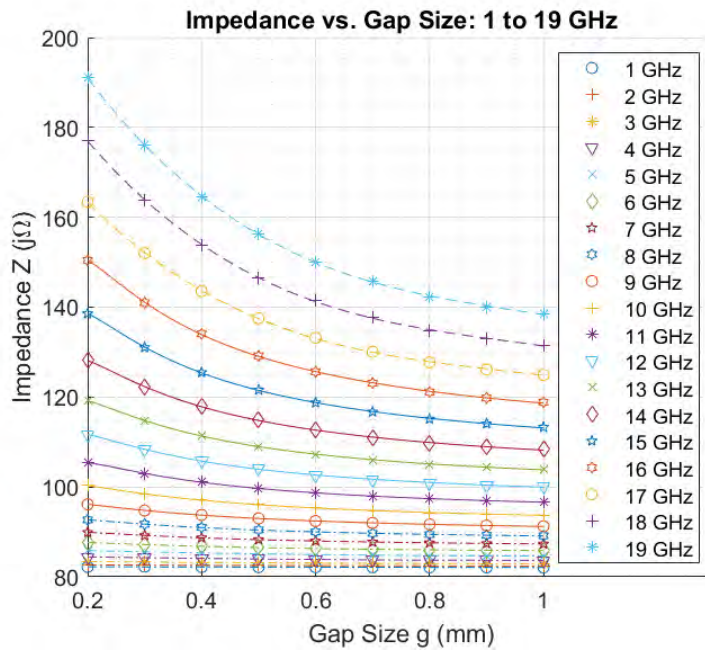


Figure 43: Circle D5880 Cell: Impedance vs. Gap, 1-19 GHz

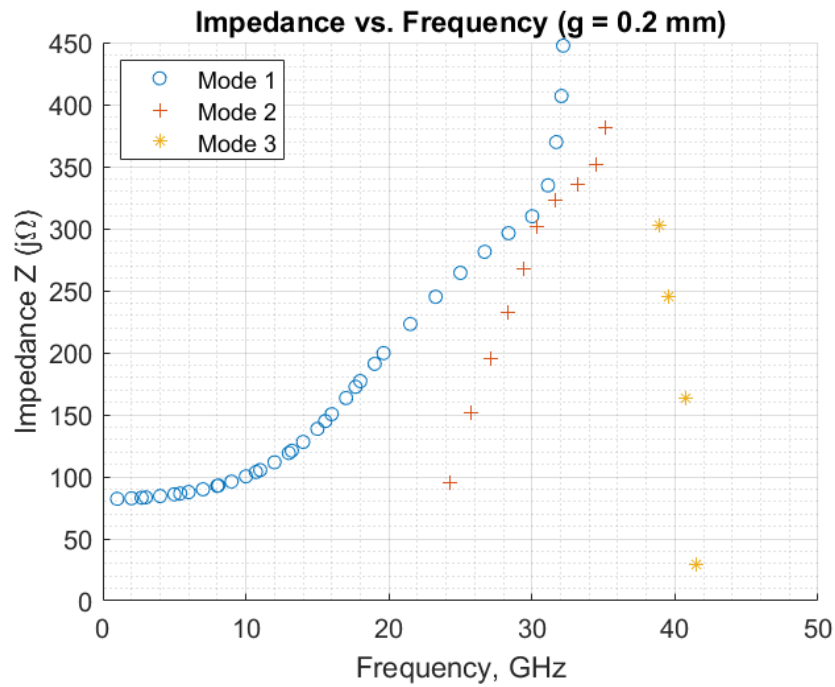


Figure 44: Circle D5880 Cell: Impedance vs. Frequency, g = 0.2 mm

4.2.3 Fractal Duroid 5880 Unit Cell

The parameters of the Duroid 5880 fractal unit cell (see fig. 45) are below:

Square Duroid 5880 Cell Parameters

Material: Rogers Duroid 5880

Dielectric Constant, ϵ_r : 2.20

Dissipation Constant, $\tan \delta$: 0.0009

Shape: square

Dielectric Thickness: 1.575 mm

Copper Thickness: 0.035 mm

Cell Size, a : 4 mm

Subcell Size, $b = \frac{a-2g}{3}$

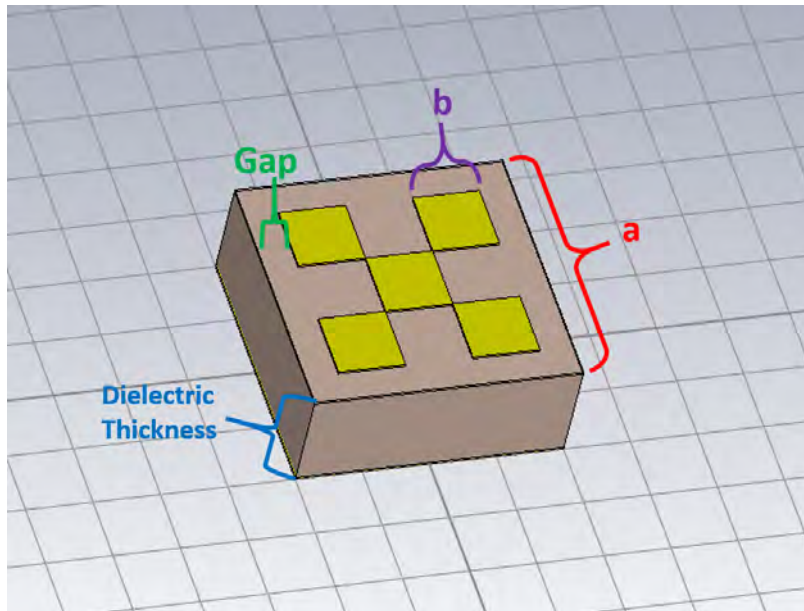


Figure 45: Fractal Unit Cell Dimensions

This is a second order, reverse-plus-sign fractal pattern. The cell size, a , was enlarged from 3 mm to 4 mm because of potential manufacturing limitations (preventing the subcells from being too small to laser etch). The mode 1 dispersion diagram for the fractal Duroid 5880 unit cell is below in fig. 46. The spread in the dispersion fan is much greater for the fractal D5880 unit cell than it was for the circular or square unit cells with the D5880 dielectric. This indicates much greater frequency sensitivity to change in gap size. The other difference is that each of the trend lines

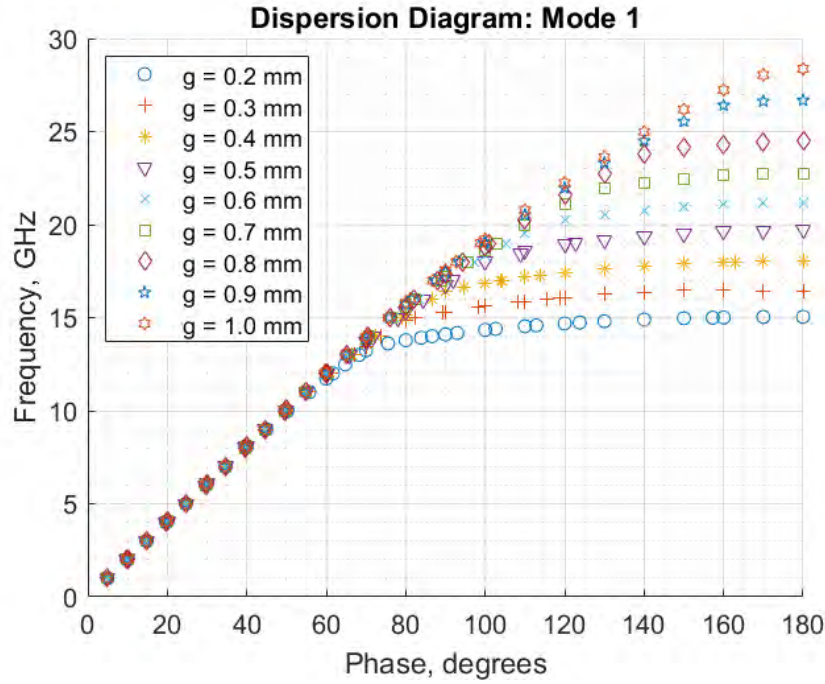


Figure 46: Fractal D5880 Cell: Dispersion Diagram, Mode 1

seems to asymptotically approach a different frequency, and the slope of the lines becomes small. This sensitivity is further illustrated by fig. 47, the impedance verses frequency plot for mode 1.

There are three regions for each of the trendlines in fig. 47: the first region is from 0 to approximately 9 GHz. In this region, the wavelengths are large enough that they see the patches on top of the cells as a solid sheet of copper, and thus are approximately co-linear, sharing the same impedance across the range of gap values. In the second region, the trendlines begin to curve and separate from each other. This region is usable for mode 1 operation. In the third region, the trendlines are nearly vertical. In this region, the impedance is highly sensitive to changes in both frequency and geometry. The first and third regions are unusable.

The impedance vs. frequency plot for $g = 0.2$ mm is below in fig. 48. The trendlines of the 3 modes intersect, similar to the mode intersections for the square D5880 unit cell (fig. 36).

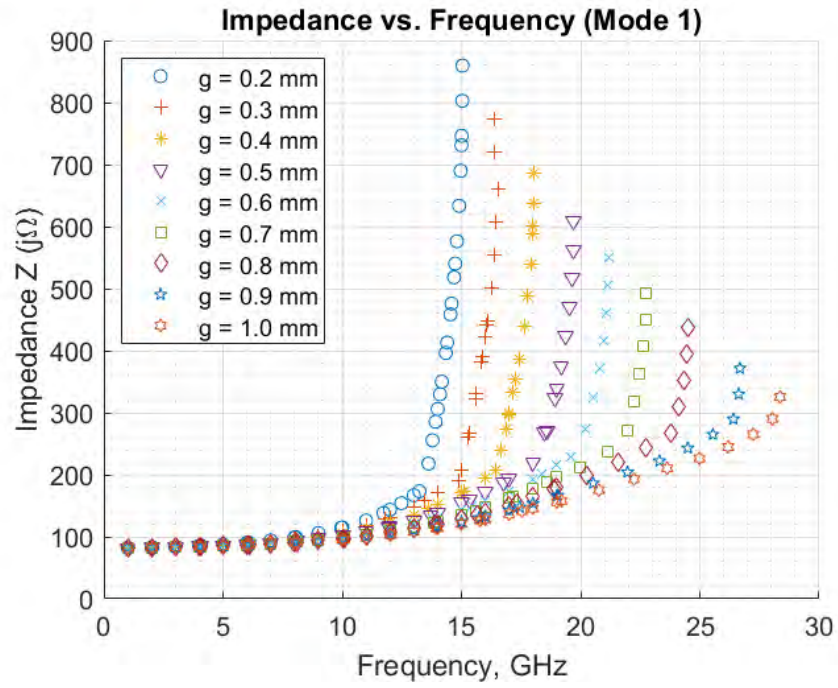


Figure 47: Fractal D5880 Cell: Impedance vs. Frequency, Mode 1

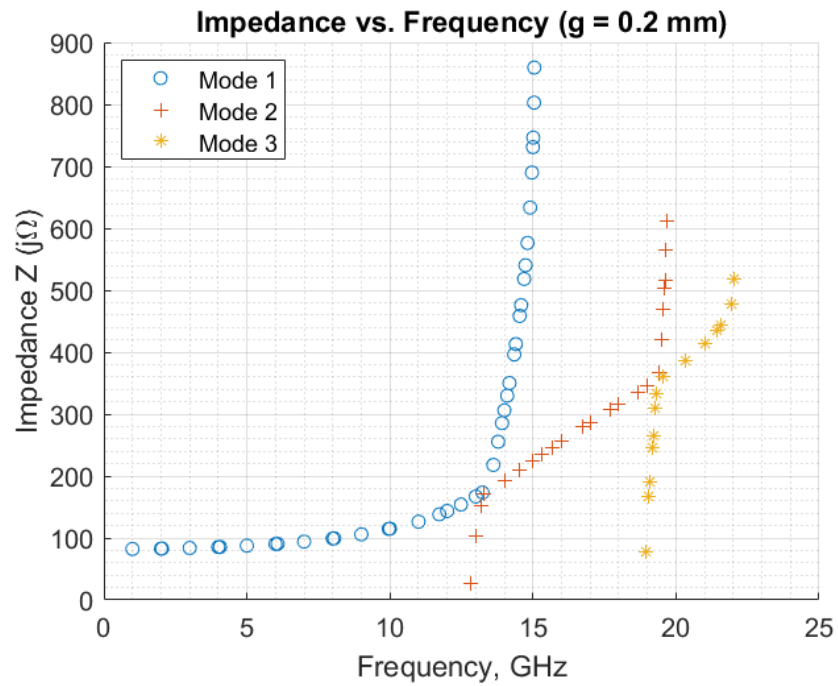


Figure 48: Fractal D5880 Cell: Impedance vs. Frequency, $g = 0.2$ mm

Again, it is possible that CST is not labeling the modes correctly. There seems to be three distinct trendlines: the first extends from 0 to 22 GHz and is made of data from modes 1, 2, and 3. This line starts at $100\ j\Omega$ and gradually curves upwards to about $500\ j\Omega$. The second trend line starts at $0\ j\Omega$, extends to approximately $900\ j\Omega$, and is comprised of mode 2 and then mode 1 data. The third trend line begins at $80\ j\Omega$ and extends almost vertically to about $600\ j\Omega$. It contains mode 3 data and then mode 2 data. It is plausible that each of these trendlines is a distinct mode, and that CST is not pairing the data points to the correct modes. It is also possible that one or both of the vertical modes in fig. 48 are non-physical, existing in simulation only. The impedance models developed for the unit cells were made with mode 1. However, there were a few cases where there the particular gap size and frequency combination did not resonate in mode 1, after data points with a refraction index less than 1 were filtered out. Figure 49 below shows the impedance model for the D5880 fractal cell at 17 GHz.

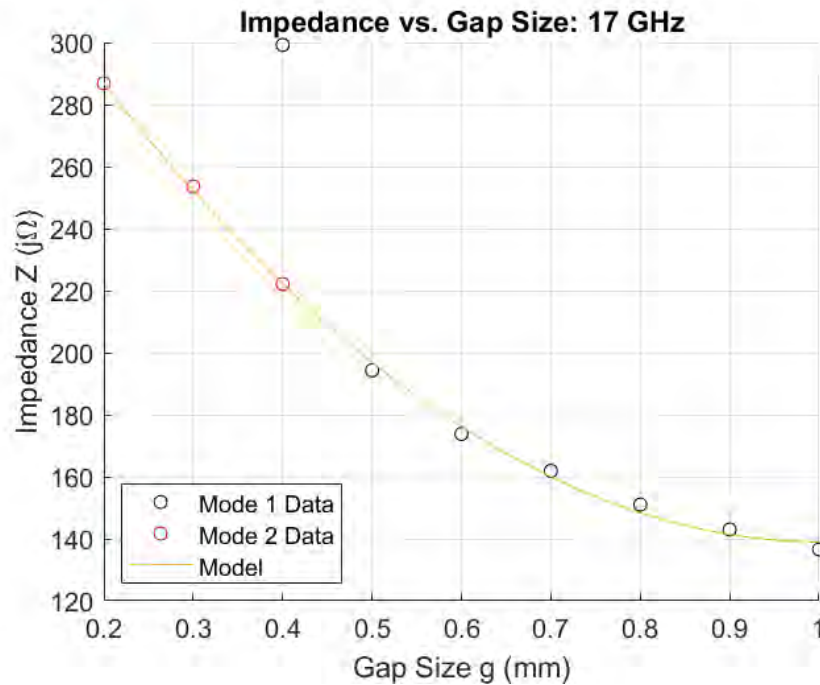


Figure 49: Fractal D5880 Cell: Impedance vs. Gap, 17 GHz

For $g = 0.2$ mm and 0.3 mm, there is no mode 1 data. Additionally, for $g = 0.4$ mm, there is data for both mode 1 and mode 2. Both of these data points have refractive indexes greater than 1. It is obvious that the mode 1 data point should not be used in the model at $g = 0.4$ mm, and that the mode 2 data appears to fit right in with mode 1 data, describing the physical behavior of the system. This suggests that CST may not be labeling modes correctly. Use of data from multiple modes in the same model assumes that one of the modes is indeed mislabeled, and that the data used is all from the same mode, because the impedance seen by waves from one mode is completely independent from the impedance seen by another mode. Figure 50 provides another perspective on the 17 GHz $g = 0.4$ mm data point.

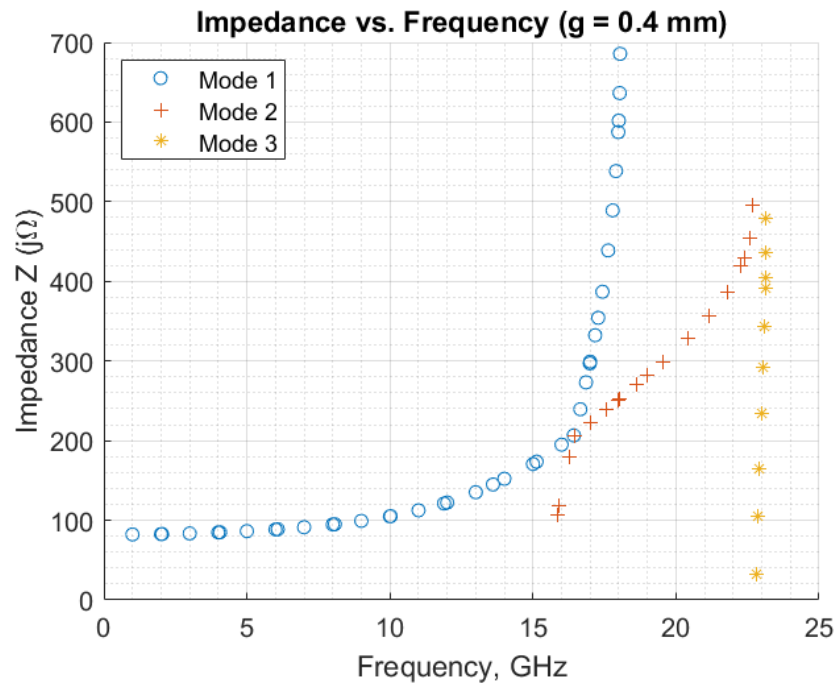


Figure 50: Fractal D5880 Cell: Impedance vs. Frequency, $g = 0.4$ mm

This plot shows that at 16 to 18 GHz, there is data for both modes 1 and 2. It also shows that the same cross-mode trendline behavior fig. 48. One of the limitations of the eigenmode solver is that the fields must be examined to see what is actually occurring. Figure 51 shows the mode 1 field for the D5880 fractal unit cell with a

gap size of 0.2 mm, and a phase boundary condition of 80° . The field is radiating



Figure 51: Fractal Unit Cell: Mode 1 E Field, $g = 0.2$ mm, $\phi = 80^\circ$

from the surface of the cell, so it is a surface wave mode. Figure 52 shows the mode 4 field for the same case. The field is not bound to the surface, so any impedance



Figure 52: Fractal Unit Cell: Mode 4 E Field, $g = 0.2$ mm, $\phi = 80^\circ$

values calculated from this field would not be valid for use in impedance modeling. Further research, including examining the EM fields, is needed to determine if CST is indeed mislabeling the modes for some of the eigenmode results. The impedance vs. gap size models of the D5880 fractal unit cell for 1-19 GHz is below in fig. 53

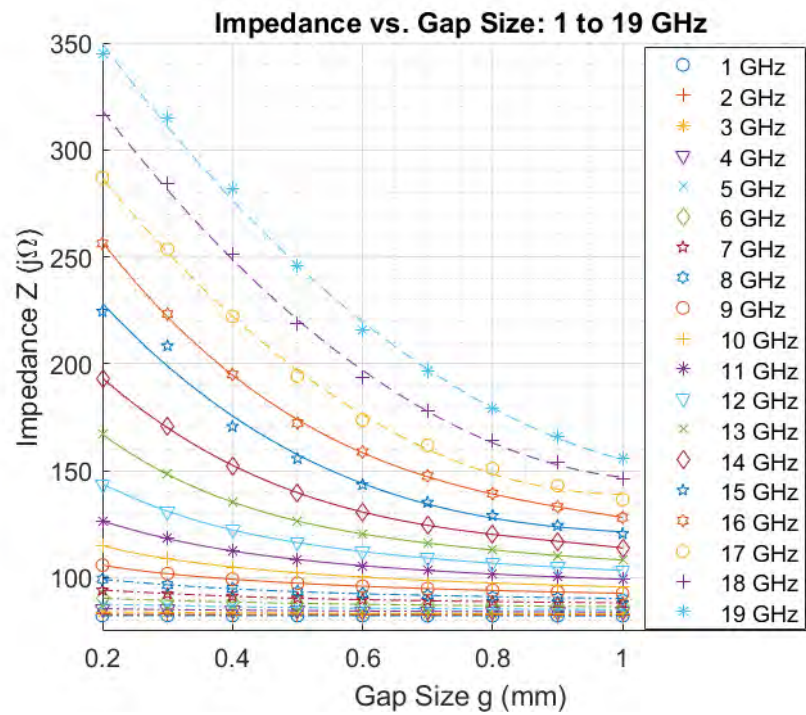


Figure 53: Fractal D5880 Cell: Impedance vs. Gap, 1-19 GHz

4.2.4 Square FR4 Unit Cell

A unit cell made with FR4 was evaluated. The parameters are below.

FR4 Cell Parameters

Material: FR4

Dielectric Constant, ϵ_r : 4.3

Dissipation Constant, $\tan \delta$: 0.025

Shape: square

Dielectric Thickness: 0.7874 mm

Copper Thickness: 0.035 mm

Cell Size, a : 3 mm

The main differences between the square FR4 cell and the square D5880 cell are the higher dielectric constant (almost double) and the thinner dielectric substrate (about half the thickness). The mode 1 dispersion diagram is below in fig. 54. The

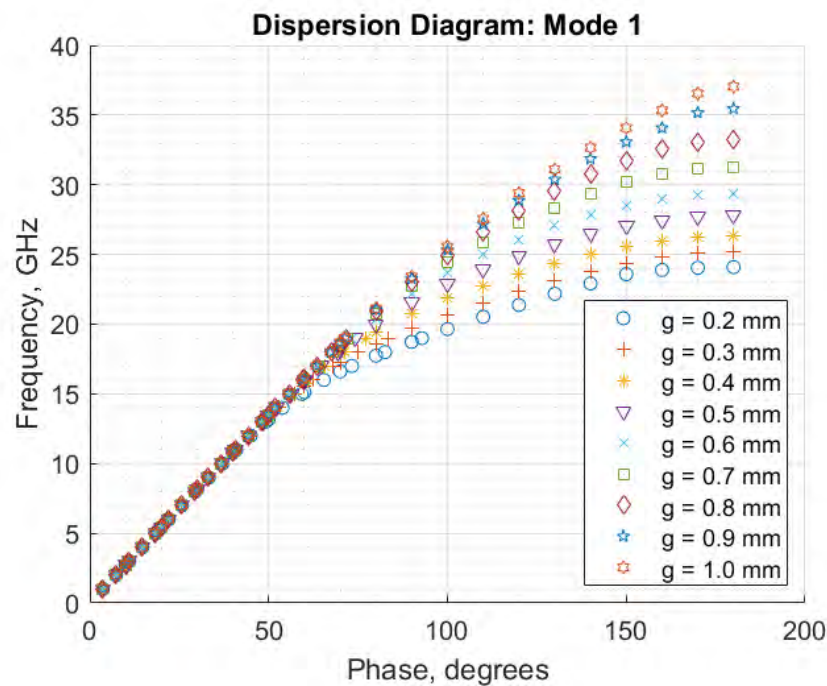


Figure 54: Square FR4 Cell: Dispersion Diagram, Mode 1

trendlines are more spread out than the square or circular D5880 cells. The FR4 dispersion trendlines are also more curved than the square or circular D5880 cells,

but less curved than the trendlines in the D5880 fractal unit cell dispersion plot. Figure 55 shows the impedance models for the entire bandwidth of interest. The

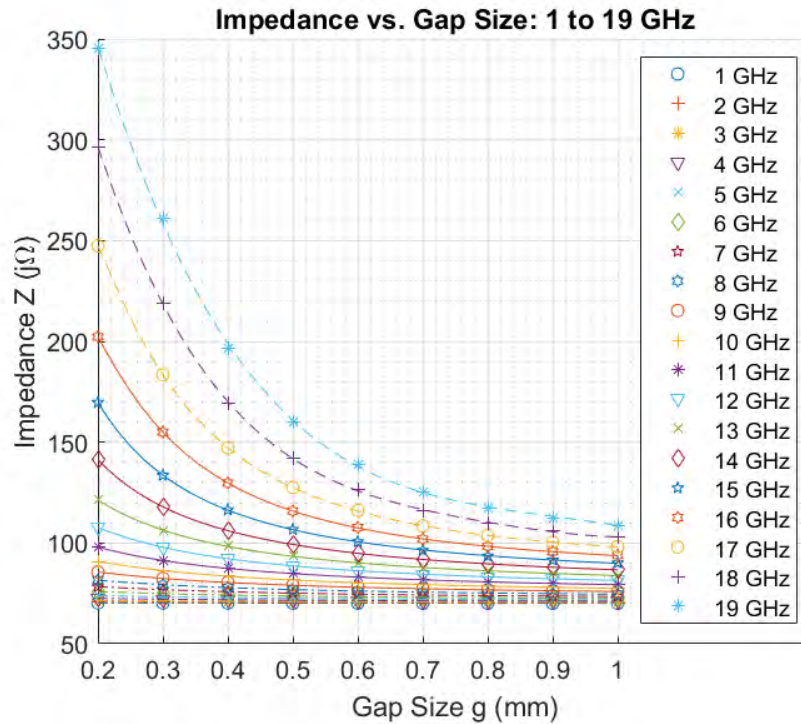


Figure 55: Square FR4 Cell: Impedance vs. Gap, 1-19 GHz

impedances tend to be higher than those of the circular or square D580 unit cells. A higher dielectric constant, thicker dielectric, or smaller gap size leads to a higher impedance [11]. The FR4 unit cell has both a smaller dielectric thickness and larger dielectric constant than the square D5880 unit cell, so it appears that in this case the larger dielectric constant trumps the thinner dielectric, because the impedances are higher. The gap-impedance relationship is more nonlinear than experienced by the other unit cells examined. This nonlinearity is undesirable because it means that the impedance is very gap size sensitive, and the majority of the impedance range available is disproportionately concentrated at the lower end of the gap size range.

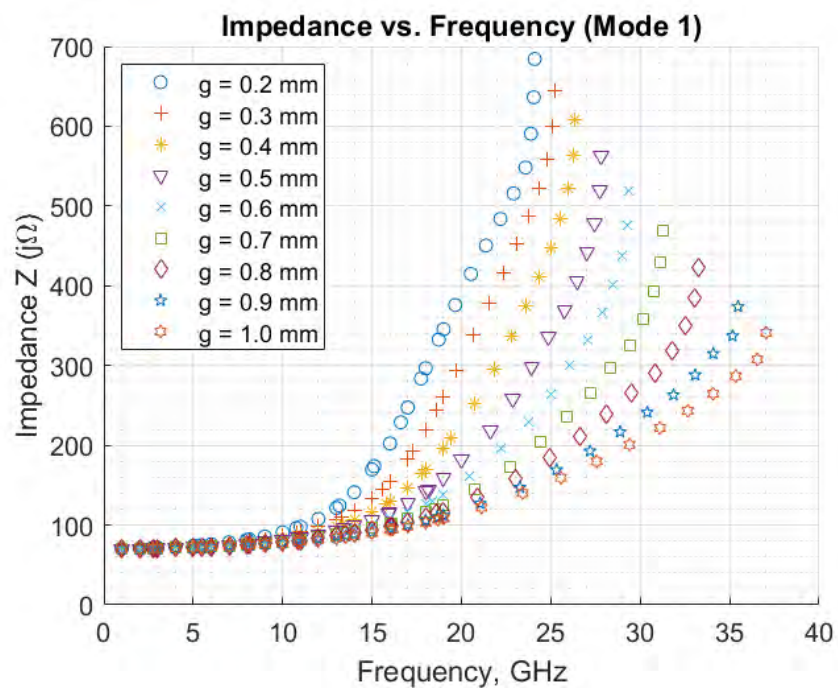


Figure 56: Square FR4 Cell:Square FR4 Cell: Impedance vs. Frequency, Mode 1

4.2.5 Circular Rogers 3010 Unit Cell

A circular unit cell made of Rogers 3010 was also evaluated. The dielectric constant is 11.2, approximately five times the dielectric constant of Duroid 5880.

Rogers 3010 Circular Cell Parameters

Material: Rogers 3010

Dielectric Constant, ϵ_r : 11.2

Dissipation Constant, $\tan \delta$: 0.022

Shape: circular

Dielectric Thickness: 1.27 mm

Copper Thickness: 0.035 mm

Cell Size, a : 3 mm

The mode 1 dispersion diagram (fig. 57) has an earlier fan point than the Duroid 5880 unit cells (roughly 9 GHz vs. 15 GHz). This means that the minimum frequency at

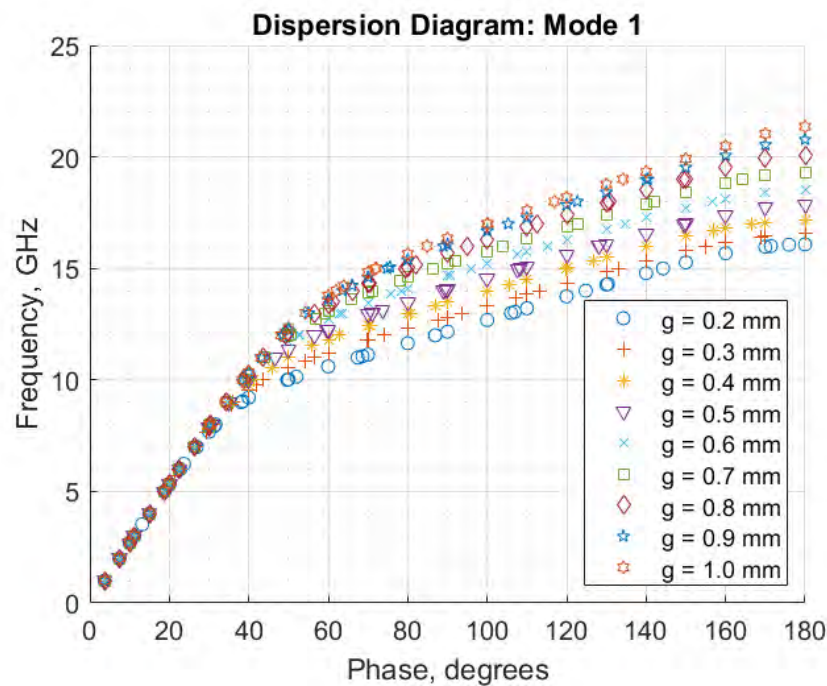


Figure 57: Circular RO3010 Cell: Dispersion Diagram, Mode 1

which this cell type has a large enough impedance range to be useable for surface wave control, is lower. Another desirable characteristic of the mode 1 impedance diagram

is that after the fan point, the impedance trendlines maintain a relatively constant spread, and do not continue to diverge from each other. This should result in better linearity of impedance response to gap size. Figure 58 confirms this. The impedance

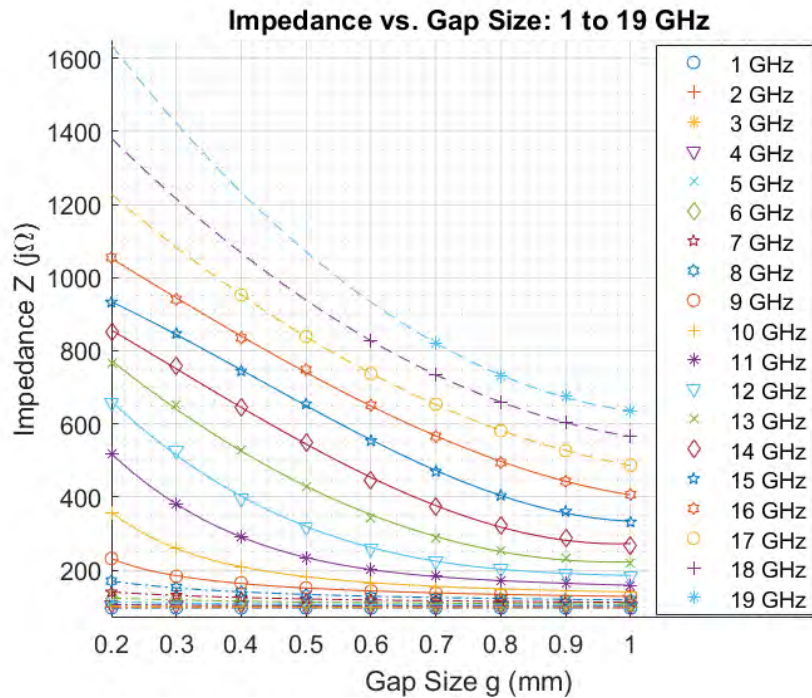


Figure 58: Circular RO3010 Cell: Impedance vs. Gap, 1-19 GHz

lines are more linear than for previous cell types, and that there is a usable impedance response across the gap size range, all the way down to 9 GHz. At the smaller gap sizes for 17, 18 and 19 GHz, there are some missing data points. No mode 1 data was found for these gap and frequency combinations. Figure 59 further illustrates this. At the top right corner of the fan, the smaller gap size trend lines do not make it all the way to 19 GHz, but instead their behavior becomes nearly vertical. Figure 60 shows the model for mode 1 at 18 GHz as well as the mode 2 data at 18 GHz. It is obvious that in this particular case, the data that CST is labeling as mode 1 vs mode 2 are actually from different modes. No data points in mode 1 or 2 were resonant at 18 GHz, $g = 0.2$ mm for this unit cell. The dispersion diagram for $g = 0.2$ mm provides

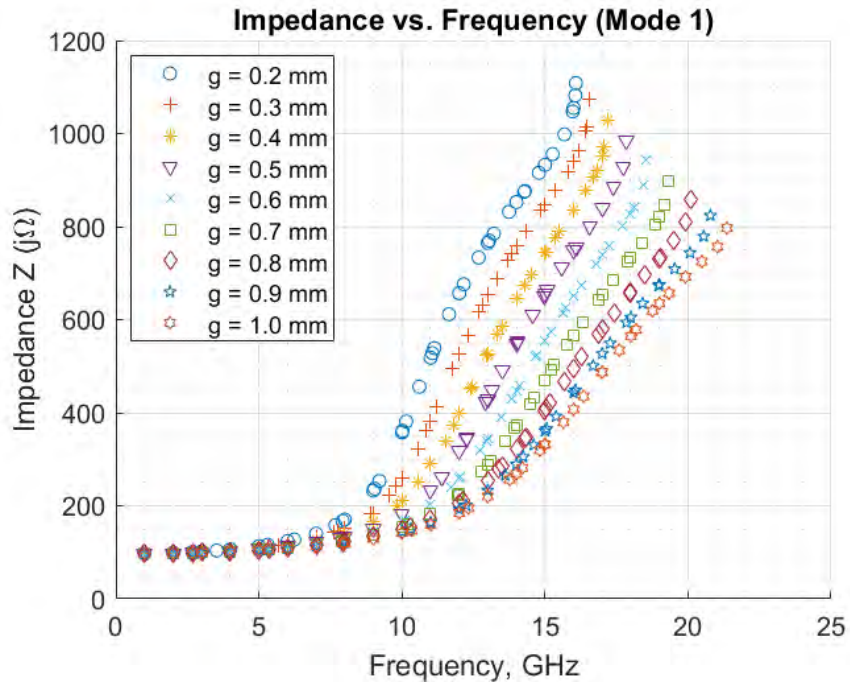


Figure 59: Circular RO3010 Cell: Impedance vs. Frequency, Mode 1

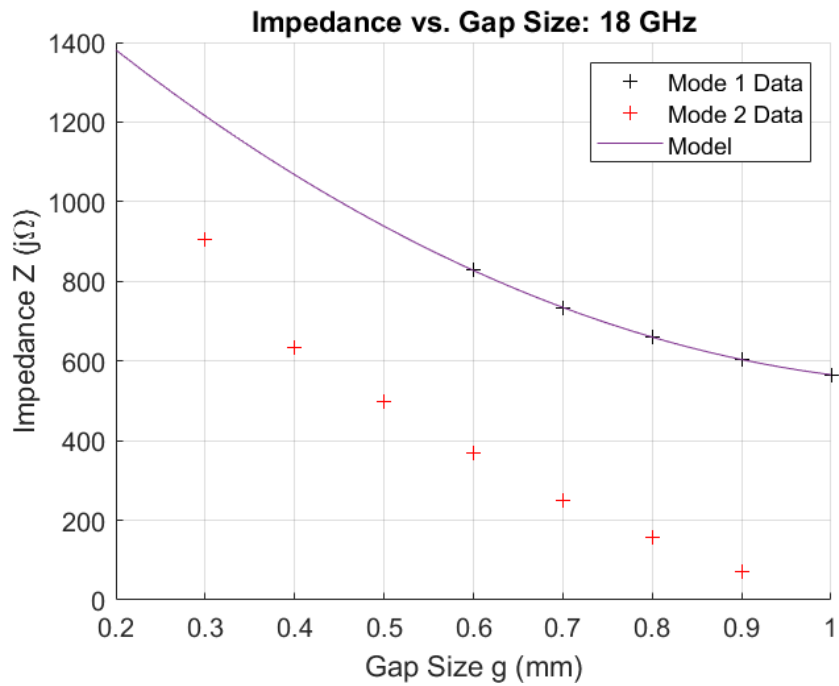


Figure 60: Circular RO3010 Cell: Impedance vs. Gap, 18 GHz

more insight (fig. 61). There appears to be a phase dependent band-gap between

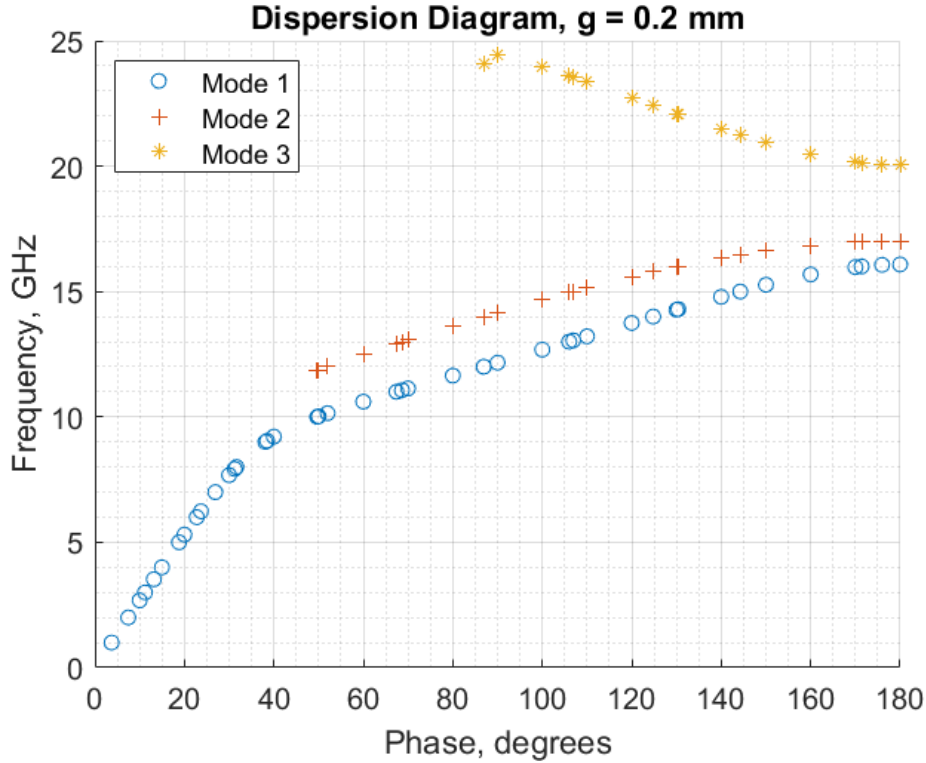


Figure 61: Circular RO3010 Cell: Dispersion Diagram, $g = 0.2$ mm

modes one and two, approximately 2 GHz wide, starting at 50° . There is also a phase dependent band-gap between mode 2 and mode 3, which starts out at roughly 10 GHz wide and narrows to 3 GHz by the time phase = 180° . This behavior is an indication that the $g = 0.2$ mm RO3010 unit cell is frequency selective. Another interesting feature of fig. 61 is the slope of the mode 3 trendline - negative. The negative slope indicates a negative index of refraction. This would mean that cylindrical waves from the driven element would be refracted downward (negative z) into the surface, rather than away from it. It is not clear in this case whether or not this phenomena genuinely represents physical reality, as CST sometimes produces eigenmode results that do not exist in the real world. An examination of the fields would be necessary to obtain better understanding. Such behavior, negative refraction and band-gap,

has been demonstrated by other research. Caloz et al. produced a similar dispersion plot for a metasurface they tested [16]. This plot is below in fig. 62. This dispersion

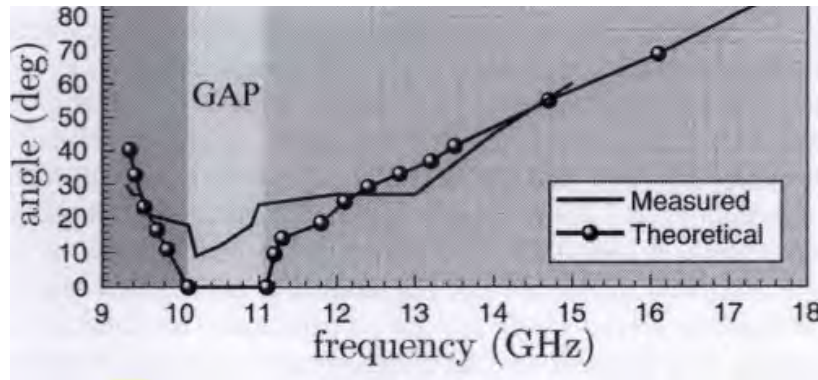


Figure 62: Measured vs. Theoretical Dispersion Diagram of a Frequency-Selective Metasurface

diagram has the same three regions as fig. 61: a region of negative refractive index, followed by a band gap, followed by a region of positive refractive index.

4.2.6 Fractal Rogers 3010 Unit Cell

The final unit cell evaluated was a fractal unit cell made from Rogers 3010. The parameters are below.

Fractal Rogers 3010 Unit Cell Parameters

Material: Rogers Duriod 5880
 Dielectric Constant, ϵ_r : 11.2
 Dissipation Constant, $\tan \delta$: 0.0022
 Shape: square
 Dielectric Thickness: 1.27 mm
 Copper Thickness: 0.035 mm
 Cell Size, a : 4 mm
 Subcell Size, $b = \frac{a-2g}{3}$

No models were produced for this type of unit cell because it became clear based on preliminary results that it exhibits an even larger band gap than the circular RO3010 unit cell, making it unusable for a wideband metasurface. The mode 1 dispersion diagram is below (fig. 63). The fan point begins at approximately 7 GHz, and the trendlines spread noticeably more than the trendlines in any of the mode 1 dispersion

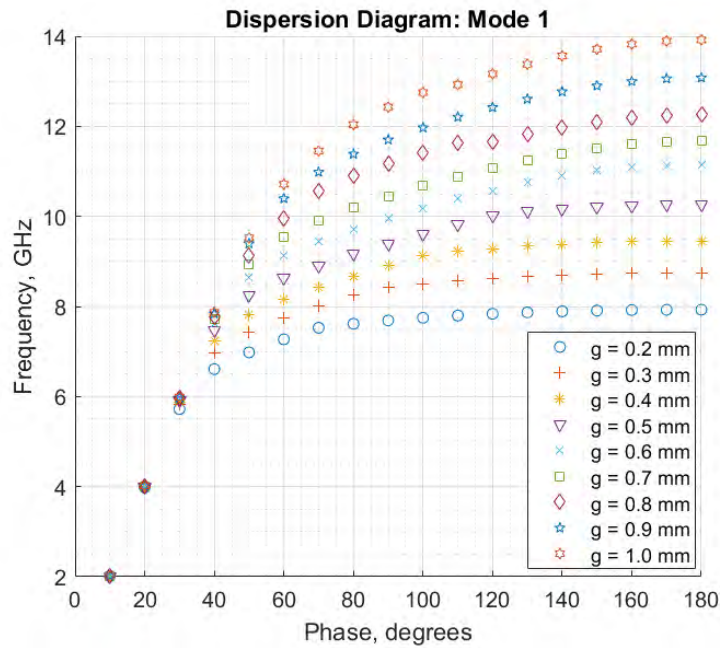


Figure 63: Fractal RO3010 Cell: Dispersion Diagram, Mode 1

plots for the other unit cells. The frequency sensitivity to gap size is also much more pronounced than it is for the other unit cells. Figure 64 below shows how dramatic the band gap is. Between modes 3 and modes 4, there is a band gap from 10 to 16

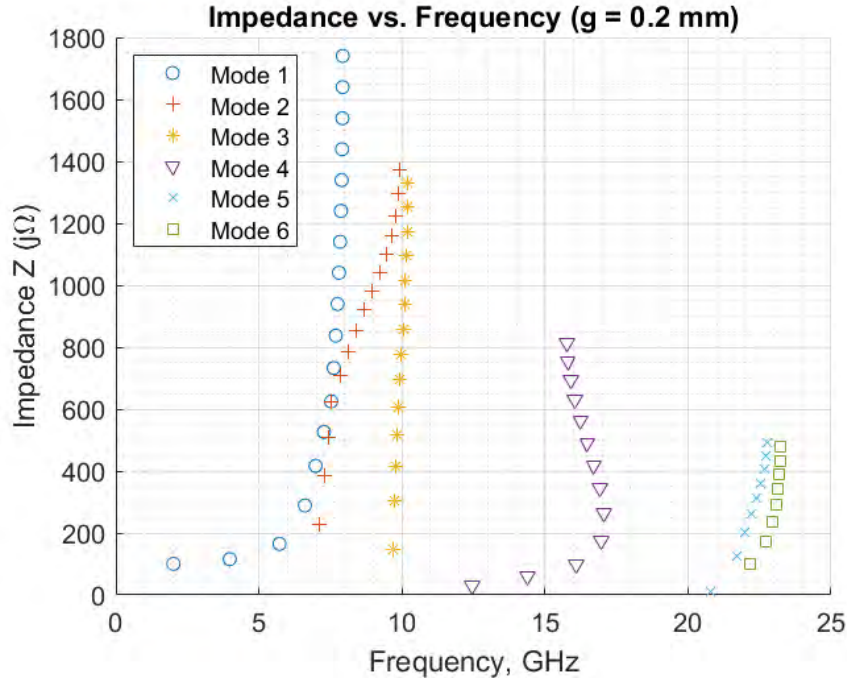


Figure 64: Fractal RO3010 Cell: Impedance vs. Frequency, $g = 0.2$ mm

GHz. Additionally there is another band gap between mode 4 and mode 5, from 16 to 22 GHz. This means that this cell type is unusable if the bandwidth desired is 2 to 18 GHz. Figure 65 below shows that the band gaps are not much less severe at $g = 1.0$ mm than they are at $g = 0.2$ mm in fig. 64. This plot shows a band gap from 15 to 19 GHz. The band-gap behavior in the fractal RO3010 cell is exacerbated as compared to the circular RO3010 cell. Other than the obvious shape difference, the other parameter difference is that the fractal cell is 4 mm by 4 mm rather than the 3 mm by 3 mm of the circular cell made from the same material. The larger surface area should tend to reduce the resonant frequencies, moving them farther into the bandwidth of interest. Another factor driving the increased band-gaps may be resonances between the subpatches. The fractal patch design seems to encourage

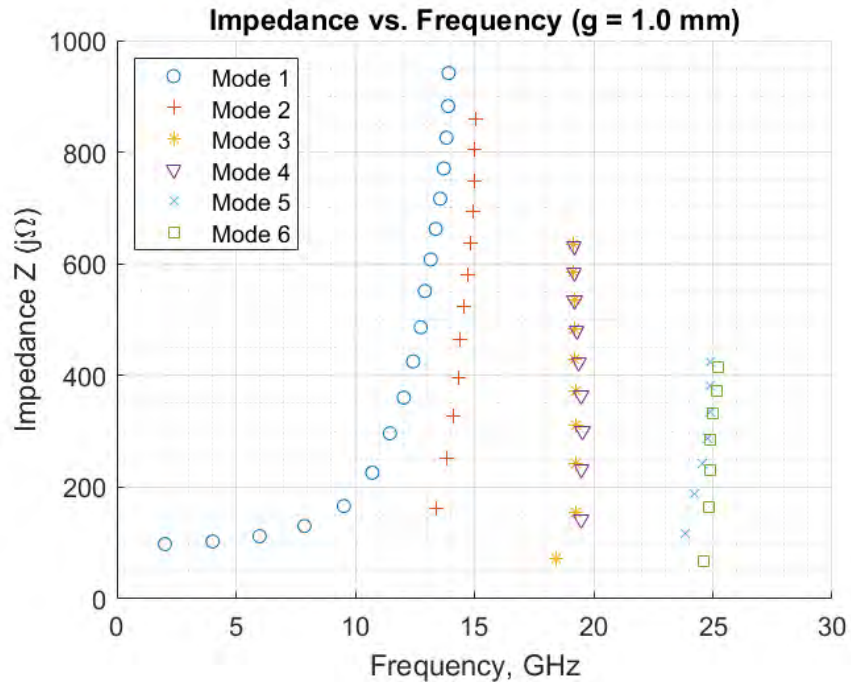


Figure 65: Fractal RO3010 Cell: $g = 1.0 \text{ mm}$

multi-modal behavior.

4.3 Antenna Measurements

4.3.1 Duroid 5880 Antenna

The antenna described in section 3.4, table 4, and section 3.6 was sent to Air Force Research Laboratory (AFRL) for measurement in their anechoic chamber. S11 parameter data (Γ , reflection coefficient), principle plane antenna patterns, and several conic antenna patterns were collected. The conic antenna patterns were used to generate 3D pattern plots. The S11 parameter plot is below in fig. 66. This plot

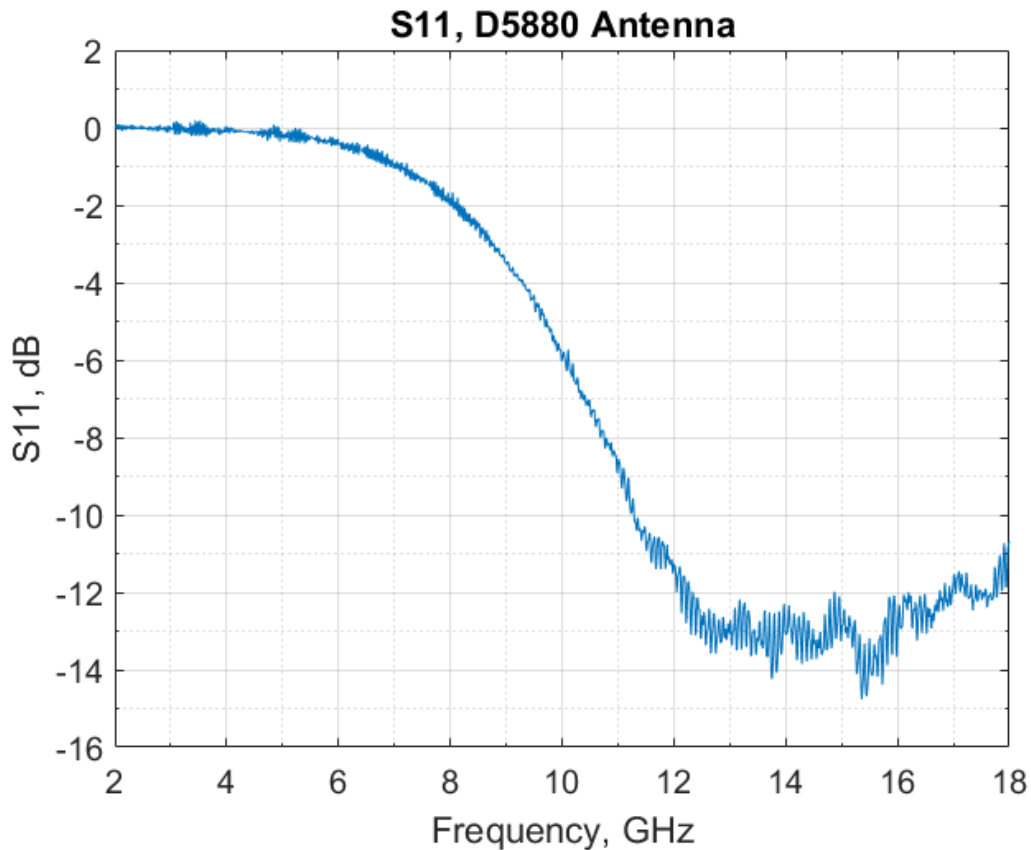


Figure 66: D5880 Antenna: S11

shows that this antenna is very poorly matched between 2 and 8 GHz, and transitions to resonance between roughly 8 and 10 GHz. The lowest point on the plot occurs at approximately 15.36 GHz. This is the frequency at which the impedance of the

antenna is best matched to the feed. This is also the resonant frequency of the antenna. Plotted on a non-logarithmic scale, S11 (or reflection coefficient, Γ), is below in fig. 67. Equation (17) was used to convert Γ to Standing Wave Ratio (SWR).

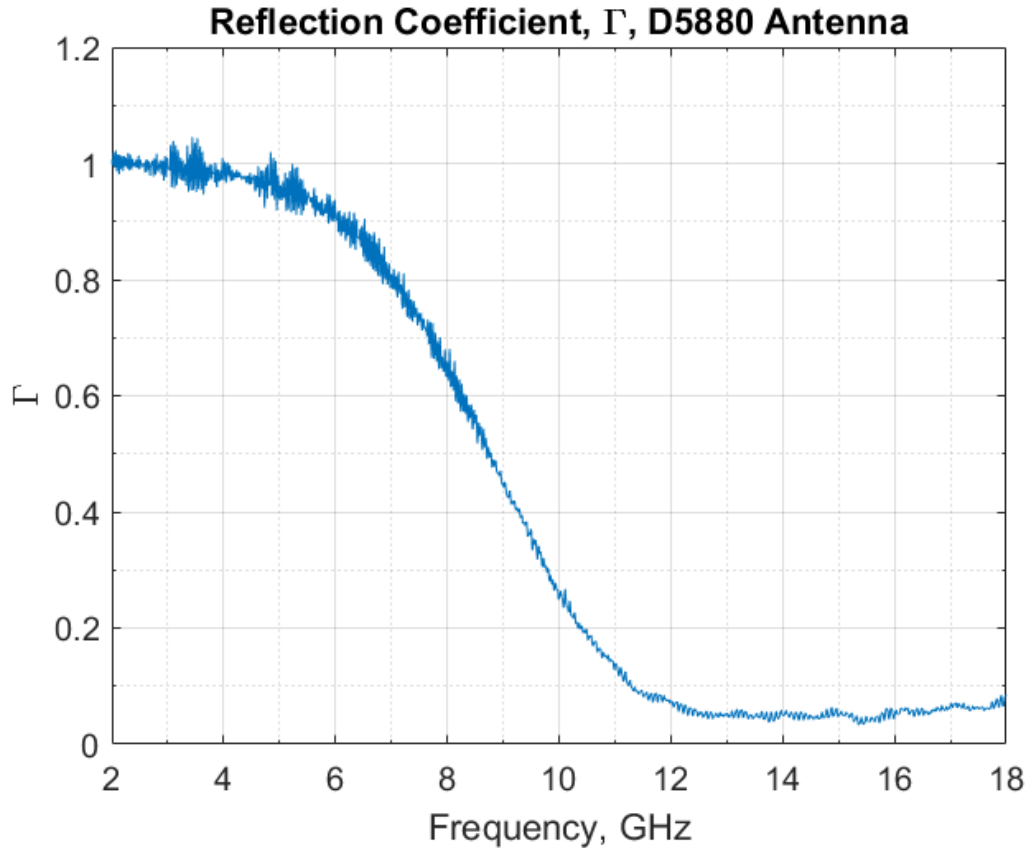


Figure 67: D5880 Antenna: Reflection Coefficient, Γ

$$SWR = \frac{1 + |\Gamma|}{1 - |\Gamma|} \quad (17)$$

The SWR of the antenna is plotted below in fig. 68. This plot shows that the 1.5:1 SWR bandwidth is 7.59 GHz: 10.41 to 18 GHz. Figure 69 below shows that at the low end of the frequency band, the antenna elevation pattern is as expected. The gain units are dBi. Note that the elevation angle is referenced at zero degrees parallel to the X-Y plane (the plane of the surface), and increases counter-clockwise. The beam

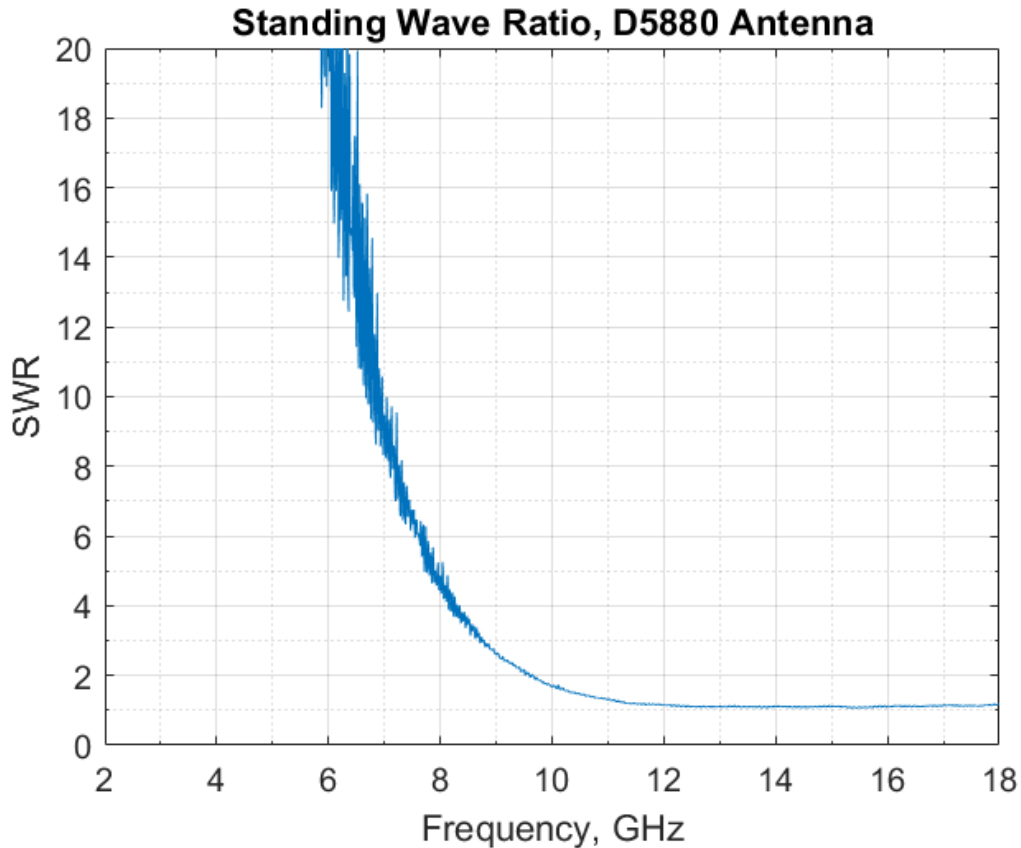


Figure 68: D5880 Antenna: SWR

angle design parameter, θ_L , is referenced at zero, normal to the metasurface plane (straight up is zero). A very poor impedance match results in a reflection coefficient of nearly 1 (almost no power transfer for radiation), and the larger wavelength sees the patterning of the unit cells as a solid copper sheet, so the pattern looks very similar to the pattern that would result from a metal plate. The three dimensional pattern plot at 3 GHz is below in fig. 70 As expected, this pattern is a poorly resonating, low-gain blob shape with no distinctive beams or wave control. By 9 GHz (fig. 71), the pattern has improved somewhat. An SWR of roughly 3:1 ($\Gamma \approx 0.55$) results in better power transfer for radiation (5.9 dBi vs -14.8 dBi peak gain). The elevation principle plane (X-Z) gain plot of the antenna at the resonant frequency, 15.36 GHz is below in fig. 72. Unless otherwise noted, the elevation angles referenced to the

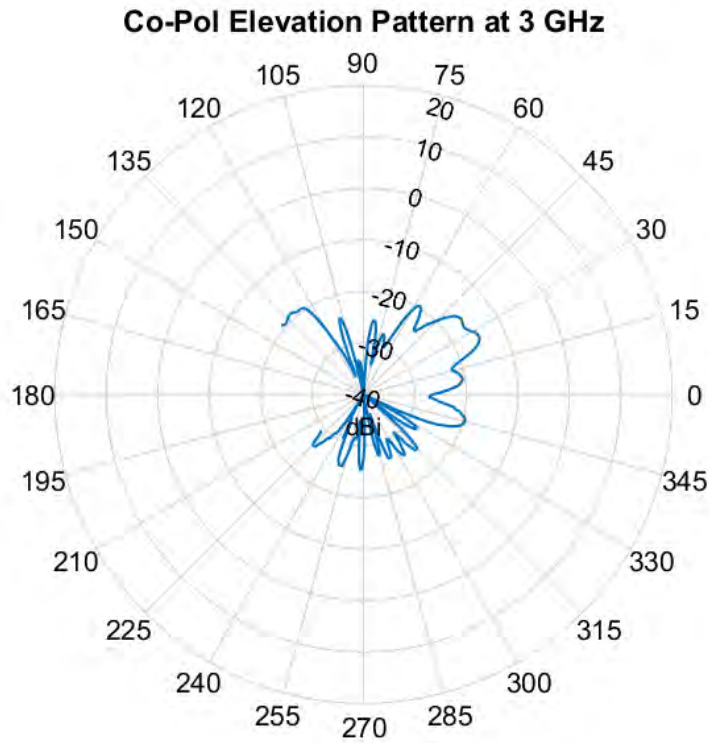


Figure 69: D5880 Antenna: Elevation Pattern, Co-Polarized, 3 GHz

system used for the measurements (0° is in the X-Y plane). The design choice of $\theta_L = 60^\circ$ corresponds to 30° for the elevation plane measurements. Data was not collected between 135° and 220° for any of the elevation plane measurements.

The main beam is a pencilbeam at roughly 45° , 5° wide, with a peak gain of 15.5 dBi. This is 15° off of the intended design, however 15.36 GHz is 1.63 GHz shy of the 17 GHz design frequency. It makes sense that the resonant frequency is lower than the design frequency, because the metasurface was designed to have a strongly inductive impedance (positive reactance, $+j\Omega$) at the design frequency. Resonance should occur at the frequency where the reactive component of the impedance is minimized.

The measured elevation gain profile at 17 GHz is below in fig. 73. The main lobe is a pencil beam and has 18.1 dBi of gain, centered at 38° , 8° more than the

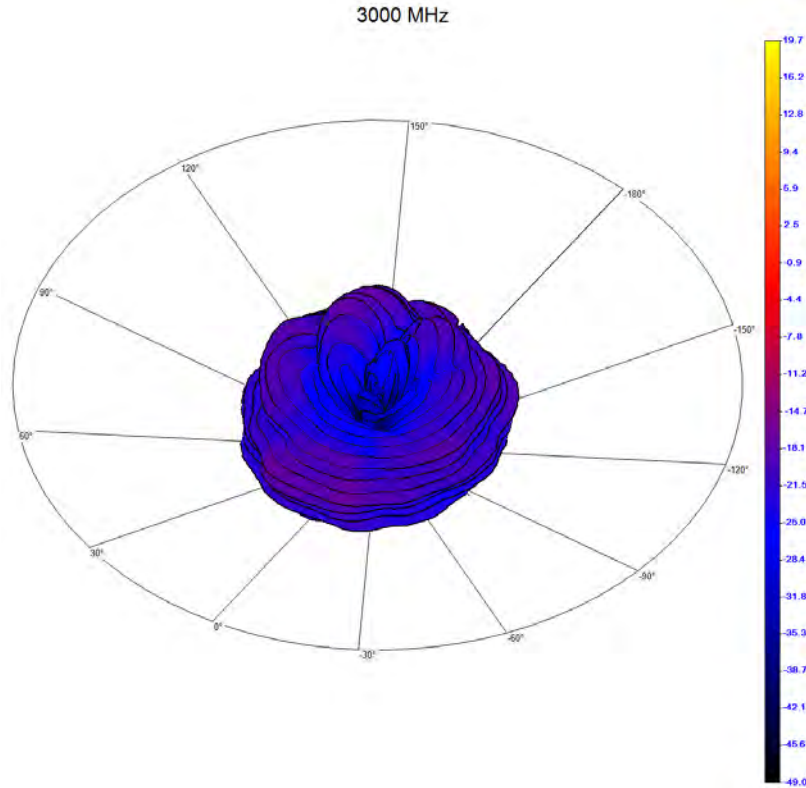


Figure 70: D5880 Antenna: 3D Pattern Plot, 3 GHz

design beam angle. Despite the 8° discrepancy, this pattern shows good agreement with the intended design as well as the measured results produced by Sievenpiper. Figure 73 also provides some measure of validation of the methodology used described in section 3.3 to produce the cell impedance models as well as the application of the design equations in section 3.4, as well as the fabrication process described in section 3.6. This is important to note, given that the antenna pattern simulations in section 3.5 require further effort to produce valid results. Figure 73 confirms successful replication of the work done in the first half of Sievenpiper's "Scalar and Tensor Holographic Artificial Impedance Surfaces" [11]. Sievenpiper's elevation pattern at 17 GHz is below in fig. 74. Figure 73 has the same beam width as Sievenpiper's: 5° . The peak gain is also close: 18.1 dBi vs. Sievenpiper's 20 dBi. The most obvious difference is that the measured main beam angle is 38° , 8° off of the designed angle,

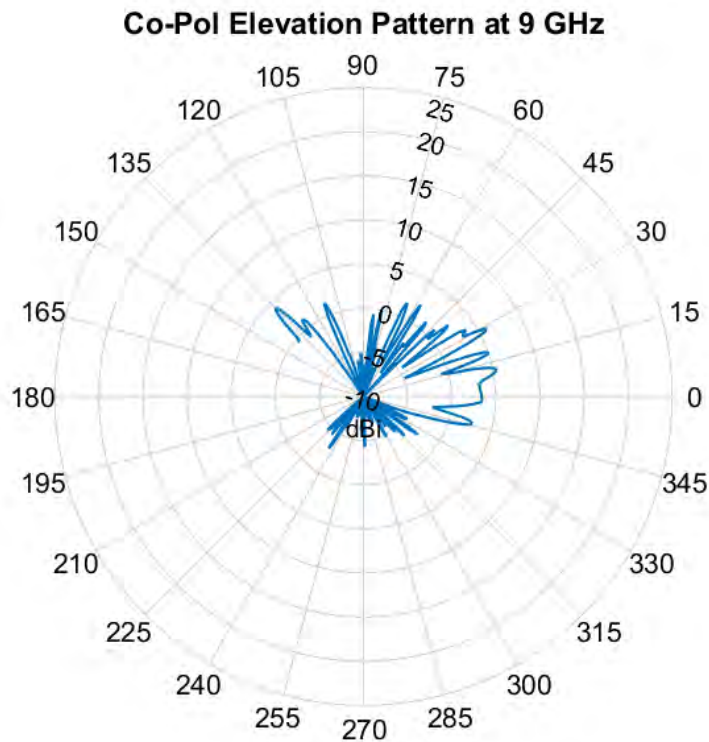


Figure 71: D5880 Antenna: Elevation Pattern, Co-Polarized, 9 GHz

$\theta_L = 30^\circ$, (equivalent to 60° in the design coordinate system). Using equivalent coordinate systems, Sievnpiiper's measured main beam is centered on $\approx 33^\circ$. The reason for this difference is not obvious, however several factors may have contributed. The fabricated D5880 antenna was $\frac{1}{16}$ of an inch longer in the X and Y directions due to precision limitations. This small excess (bare dielectric with copper ground plane underneath) may have helped bend the beam slightly further upward (+Z). There were also a few cells that were not manufactured correctly, either due to the paint flaking off of the protected area prior to chemical etching, causing the cell to be completely removed, or to uneven paint resulting in inadequate laser etching, causing several cells to remain connected after the chemical etching process. Another factor could be the soldering process. Overheating of the substrate while soldering

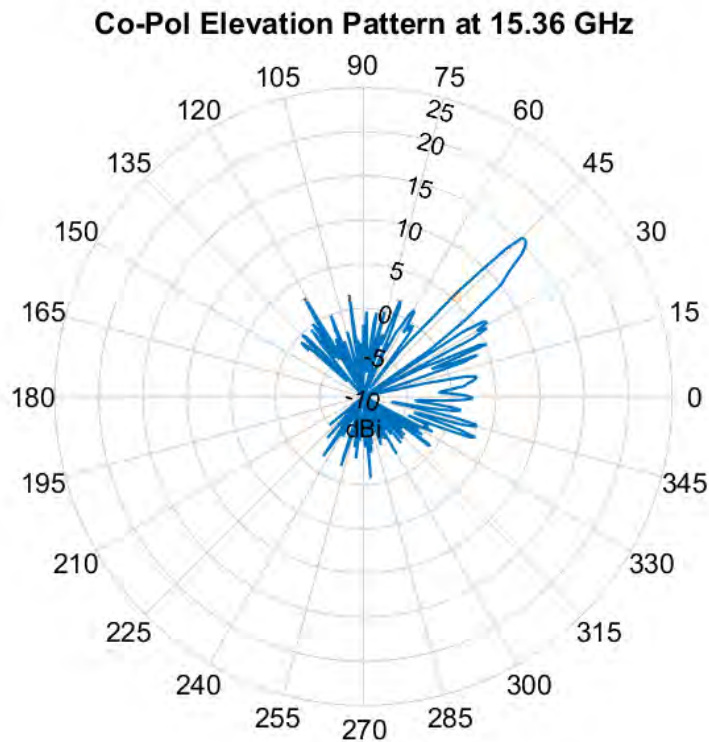


Figure 72: D5880 Antenna: Measured Elevation Pattern, Co-Polarized, 15.36 GHz

the driven element to the board may have increased the dielectric constant near the driven element. This would have made the dielectric seem to be electrically larger to the waves generated by the driven element, curving the waves from the main beam further upward than dictated by the design. It is also possible that the disparity is entirely due to calibration differences between the step motors used to position the antennas during the measurement process. Further investigation would be necessary to definitively determine the the cause of the difference.

Both the measured elevation pattern and Sievenpiper's elevation pattern at 17 GHz seem to show a side beam developing adjacent to the main beam, -10 dBi from the main beam peak. The three dimensional pattern plot at 17 GHz is below (fig. 75). Note the bright yellow spot where the main beam is located. In fig. 76, measured

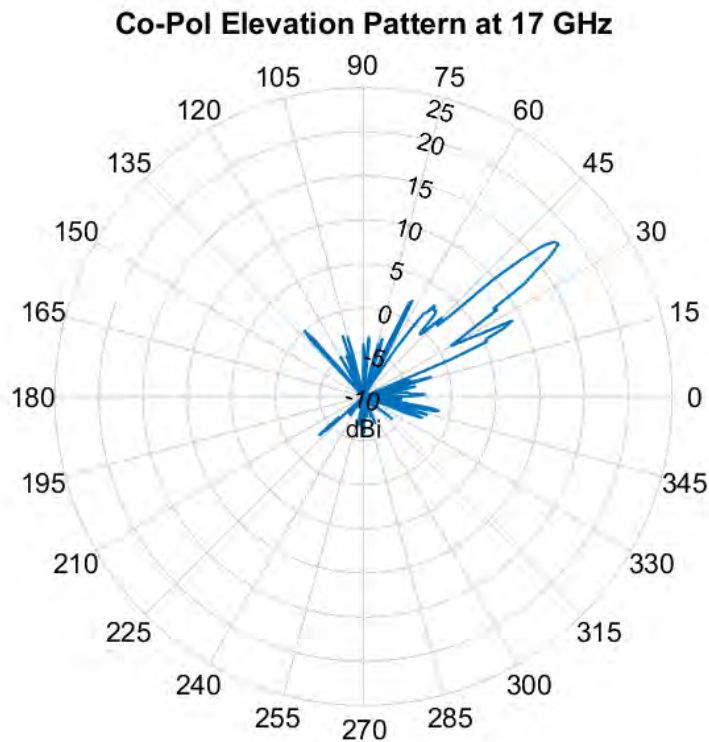


Figure 73: D5880 Antenna: Measured Elevation Pattern, Co-Polarized, 17 GHz

elevation pattern at 18 GHz, the side beam is more developed and is partially merged with the main beam which has dropped 4° to 34° . It is possible that this sidebeam is a second pencil beam starting to develop as a result of a second mode being to be excited. The eigenmode cell impedance simulations provide support for the plausibility of this hypothesis. Figure 77 is the impedance vs. frequency plot of the $g = 0.2$ mm condition for the square Duroid 5880 cells used by this antenna type. This plot shows mode 2 turning on at roughly 18.5 GHz. This is close enough to support the idea that the two strongest beams in fig. 76 may be the result of separate modes interacting independently with the metasurface.

The azimuth pattern plots behave as expected. At the lower frequencies (5 GHz in this case, see fig. 78) the high reflection coefficient results in poor radiation. Centering

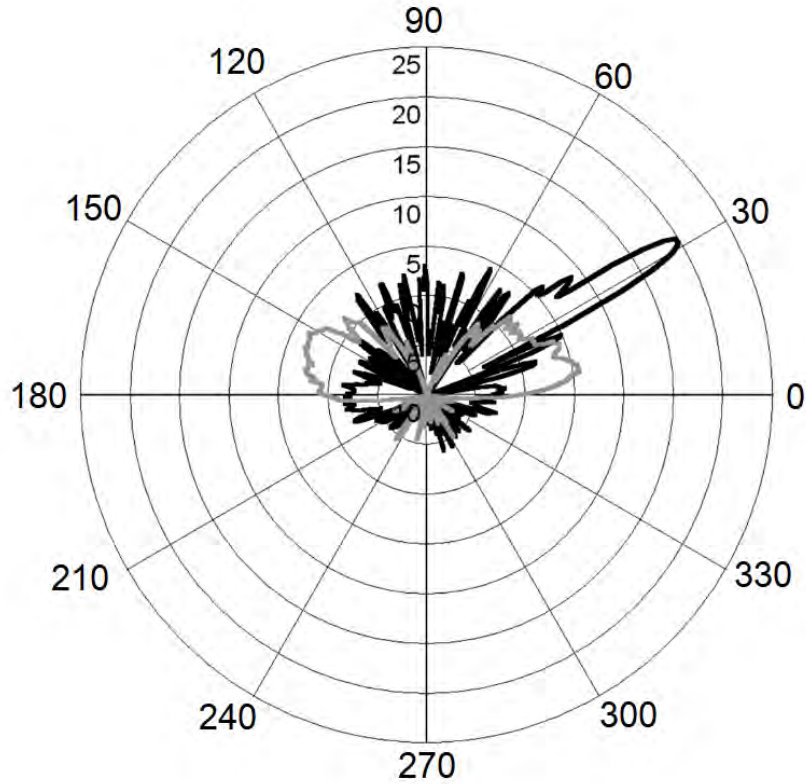


Figure 74: Measured Antenna Elevation Pattern from Sievenpiper, 17 GHz [11]. Magnitude units are in dBi. Sievenpiper plotted the pattern from a metal plate in grey overtop of his antenna pattern for comparison.

on 0° , the radiation is weaker because the copper patterning steering the conical waves from the driven element upward ($+Z$) in the direction of the main beam. The gain at 5 GHz is between roughly -15 and -10 dBi all the way around the antenna (X-Y plane). The measured azimuth pattern at 17 GHz is below in fig. 79.

By 17 GHz, the gain in the azimuth principle plane has increased dramatically to 0 dBi. Like the azimuth plane plot at 5 GHz, the similar plot at 17 GHz shows some attenuation centered on 0° , because the metasurface is steering energy away from the horizontal plane, upward in the X-Z plane where the main beam is located.

The elevation waterfall gain plot displays the gain vs. angle data across the entire bandwidth of interest in a single plot (fig. 80). The largest amounts of blue (low gain) present in the lower frequencies is evidence of the high SWR in that region.

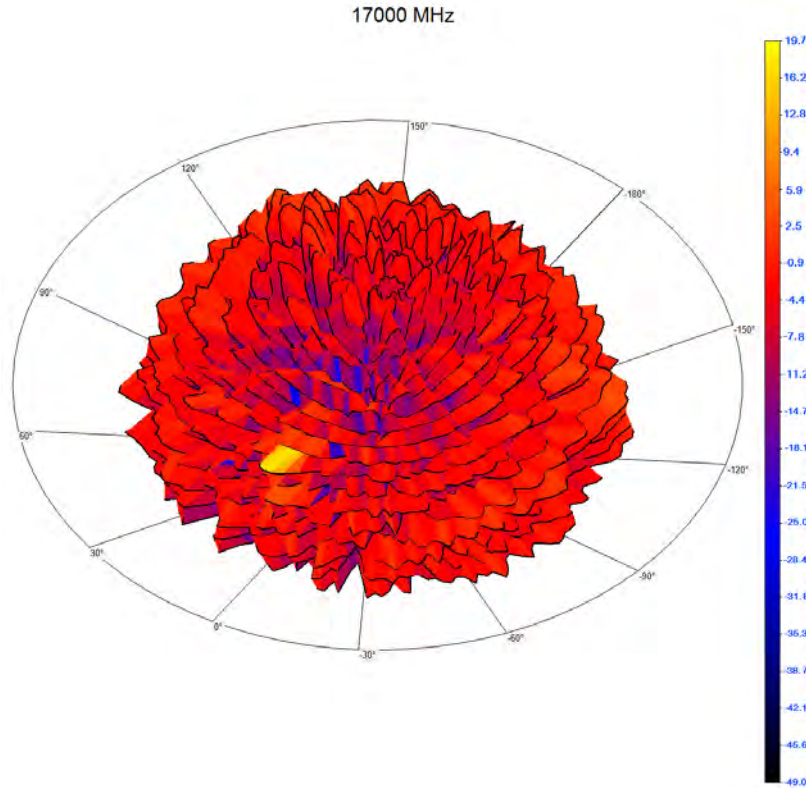


Figure 75: D5880 Antenna: 3D Pattern Plot, 17 GHz

The main beam is easily spotted - a sharp yellow line starting at roughly 13 GHz extending all the way to 18 GHz. It begins to widen between 17 and 18 GHz, which further supports the hypothesis that a second mode is becoming excited.

The azimuth waterfall gain plot also exhibits expected behavior (fig. 81). The plot gradually transitions from lower gain to relatively higher gain. At the lower frequencies (< 6 GHz) the coloring is relatively constant across the angle dimension. As the frequency increases, the angular contrast along lines of constant frequency increases as the antenna becomes resonant.

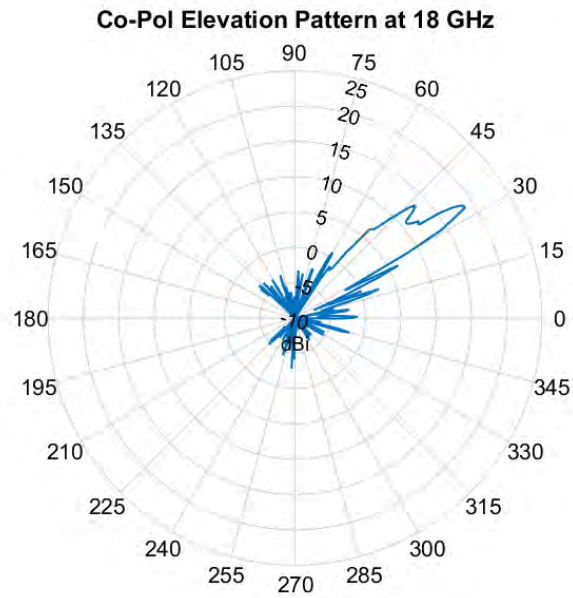


Figure 76: D5880 Antenna: Elevation Pattern, Co-Polarized, 18 GHz

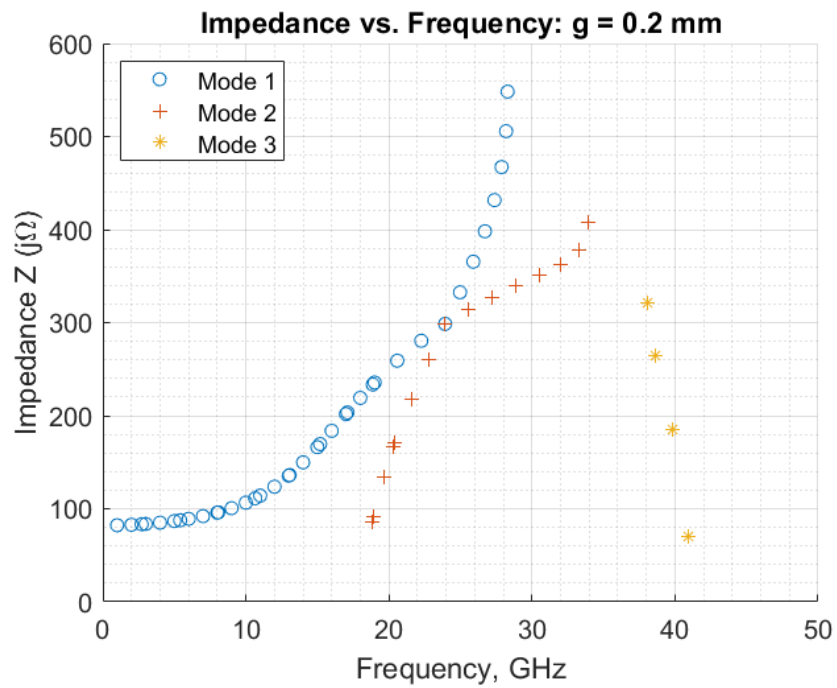


Figure 77: Square D5880 Cell: Impedance vs. Frequency, g = 0.2 mm

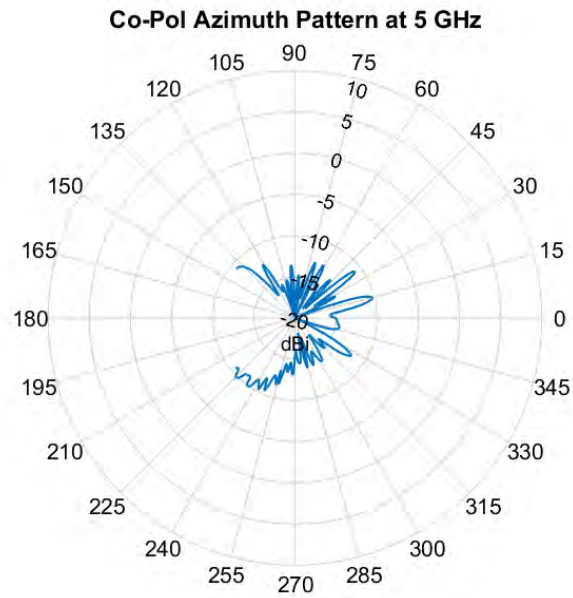


Figure 78: D5880 Antenna: Azimuth Pattern, Co-Polarized, 5 GHz

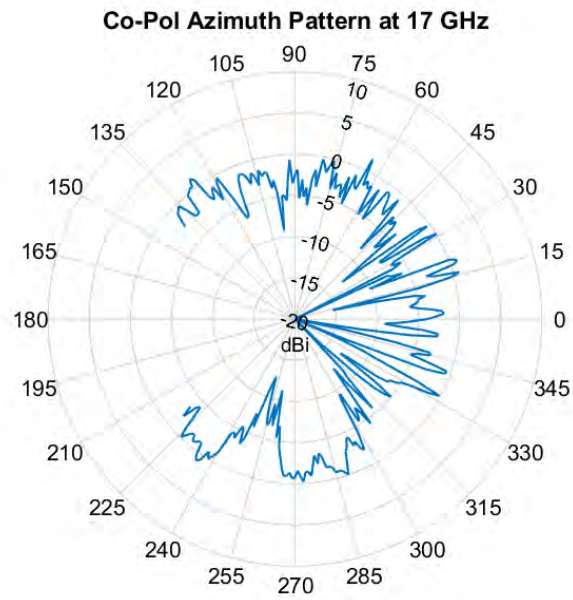


Figure 79: D5880 Antenna: Azimuth Pattern, Co-Polarized, 17 GHz

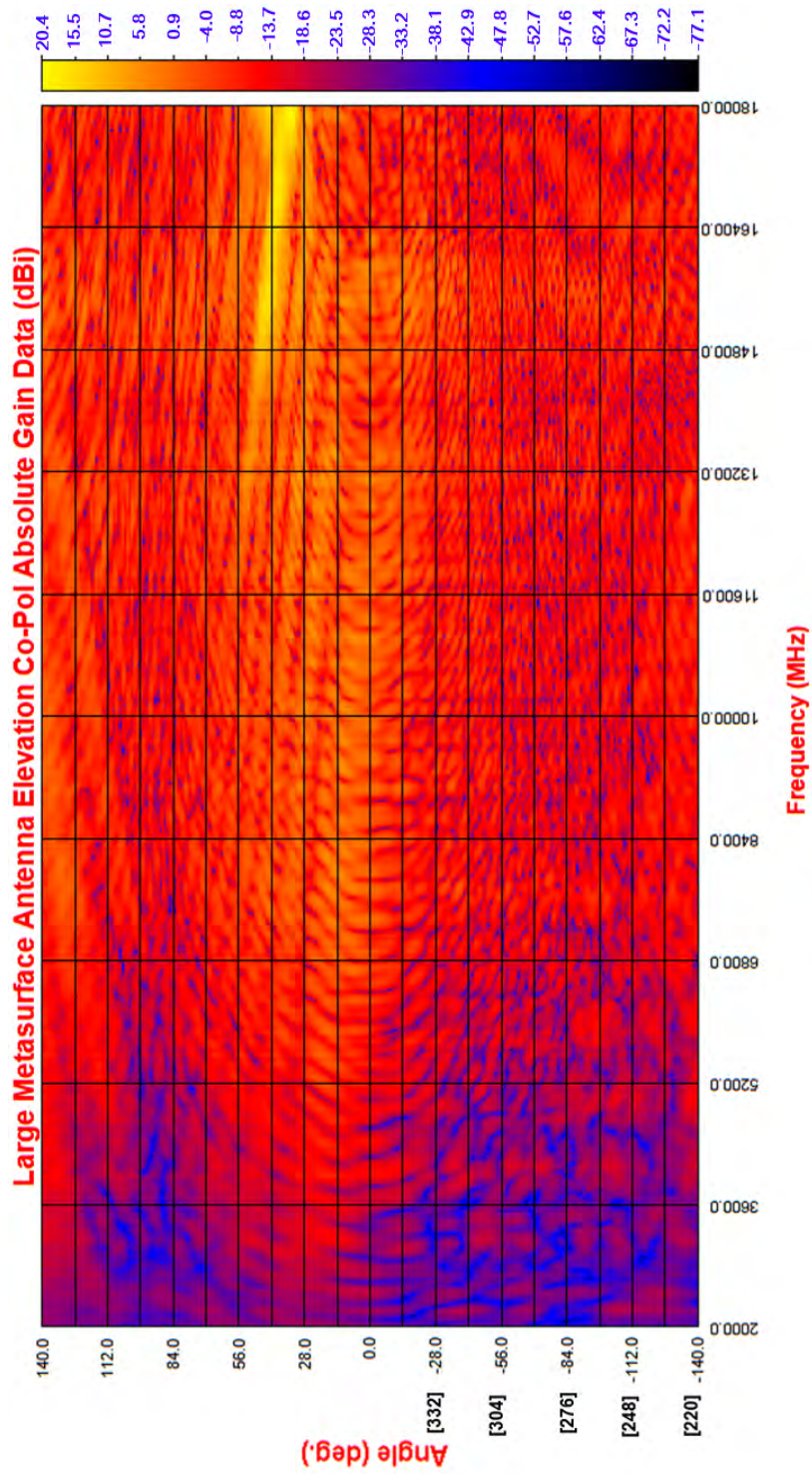


Figure 80: D5880 Antenna: Elevation Waterfall Gain Plot

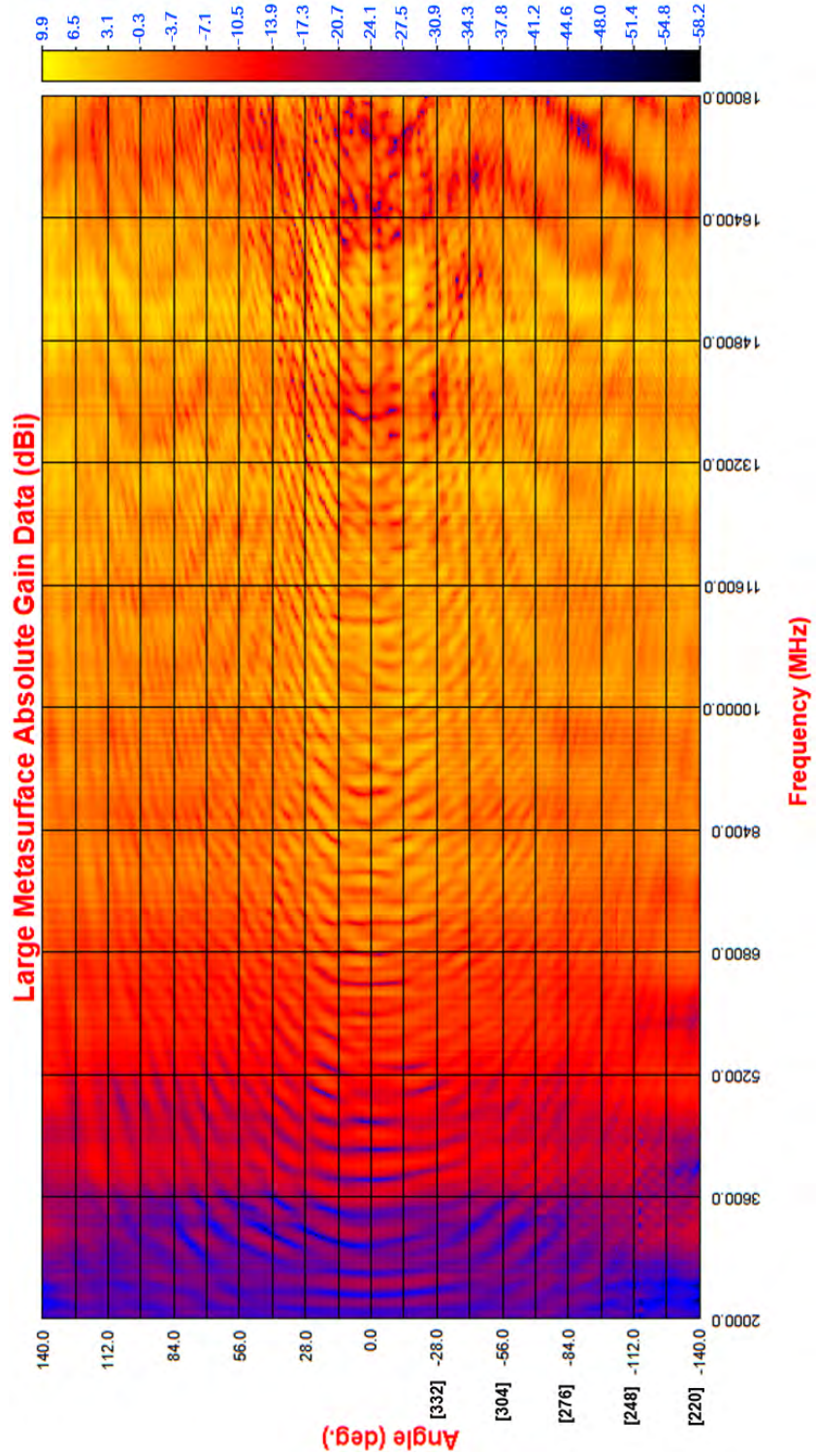


Figure 81: D5880 Antenna: Azimuth Waterfall Gain Plot

4.3.2 FR4 Antenna

Another 16" by 10" antenna was fabricated and tested: Sievenpiper's design etched into a different substrate. This antenna was created using Sievenpiper's gap vs. impedance equation (eq. (6)) and design parameters (table 4). This antenna was fabricated as a low cost way of comparing simulated antenna pattern predictions with measurements because FR4 is more economical than high performance copper clad microwave substrates. The parameter differences with this material vice Duroid 5880 are a smaller dielectric thickness (0.7874 mm verses 1.575 mm) and a higher dielectric constant (4.3 verses 2.2). The efforts to produce antenna pattern simulations in CST have not yet yielded valid results, however several interesting things can be observed in the FR4 antenna measurements. Because S11 data was not collected for this antenna, the best place to begin analyzing this antenna is the waterfall elevation pattern plot, below in fig. 89. The most noticeable feature of this plot is the main beam, the bright yellow streak, which begins at roughly 13 GHz. The elevation plot of the FR4 antenna at 13 GHz (fig. 82) reveals that by 13 GHz, a main beam with a 5 dB beamwidth of roughly 10° centered on an elevation of 51° has developed. Examination of the waterfall elevation gain plot shows that at approximately 15 GHz, the main beam reaches its widest point. Figure 83 shows that the main beam is probably 16° wide, centered on an elevation of 40°. The waterfall elevation gain plot also shows that a second main beam starts to develop at 16 GHz. The elevation gain plot at 16 GHz confirms that this is true (fig. 84). By 17 GHz, the second beam is more developed (fig. 85). The 3D gain plot of the FR4 antenna is below in fig. 86

The FR4 multi-mode unit cell impedance vs frequency plot at $g = 0.2$ mm indicates that mode 2 starts to become active as a surfacewave mode at roughly 19 GHz (fig. 87). This is close enough to suggest that it is plausible that the dual main beams are indeed a result of the metasurface refracting two separate modes. At 18 GHz, the second

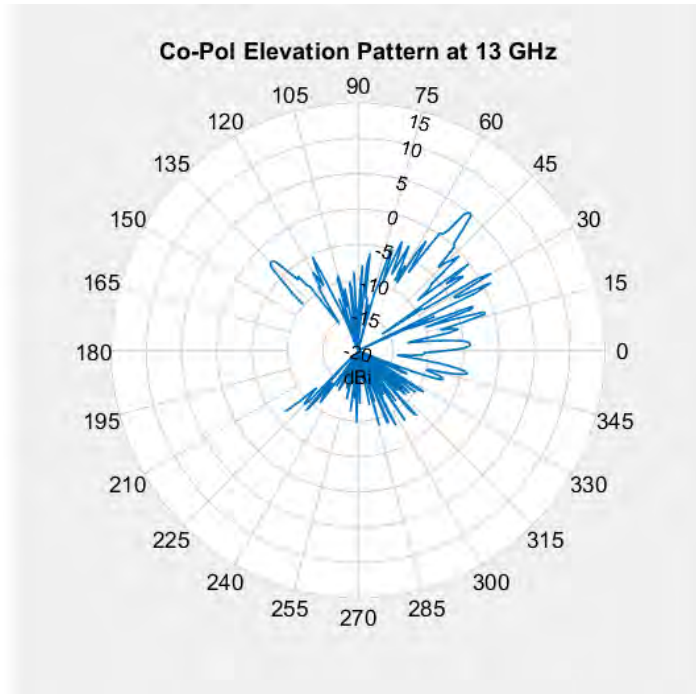


Figure 82: FR4 Antenna: Elevation Pattern, Co-Polarized, 13 GHz

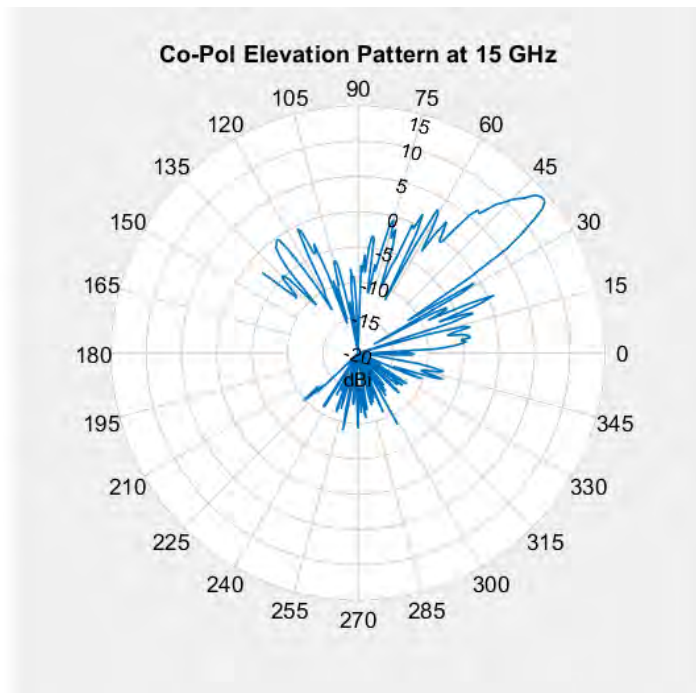


Figure 83: FR4 Antenna: Elevation Pattern, Co-Polarized, 15 GHz

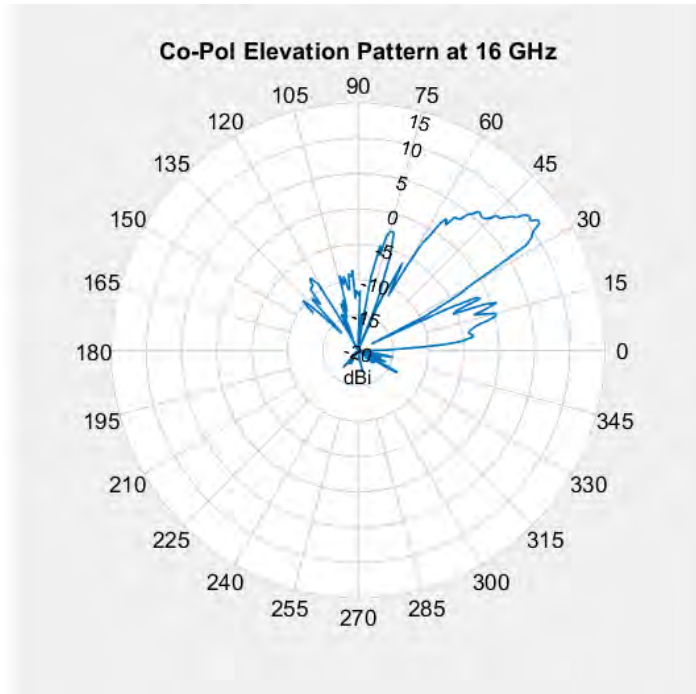


Figure 84: FR4 Antenna: Elevation Pattern, Co-Polarized, 16 GHz

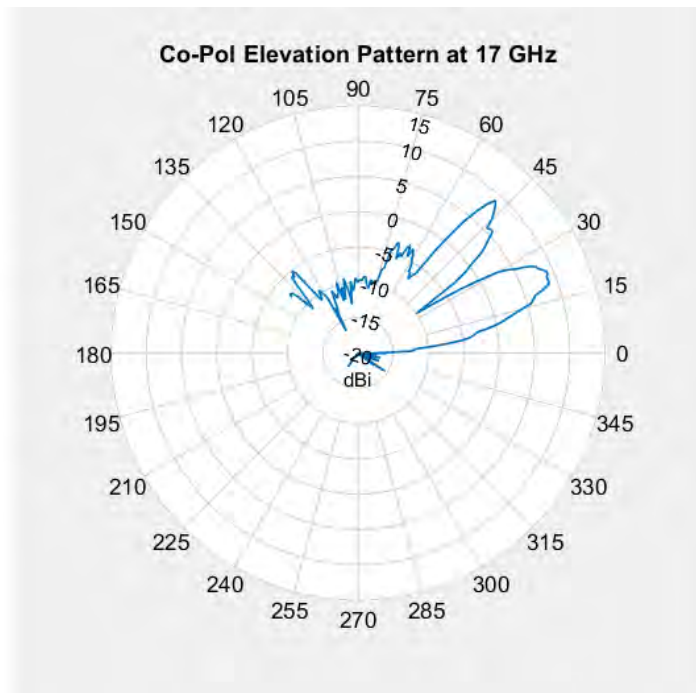


Figure 85: FR4 Antenna: Elevation Pattern, Co-Polarized, 17 GHz

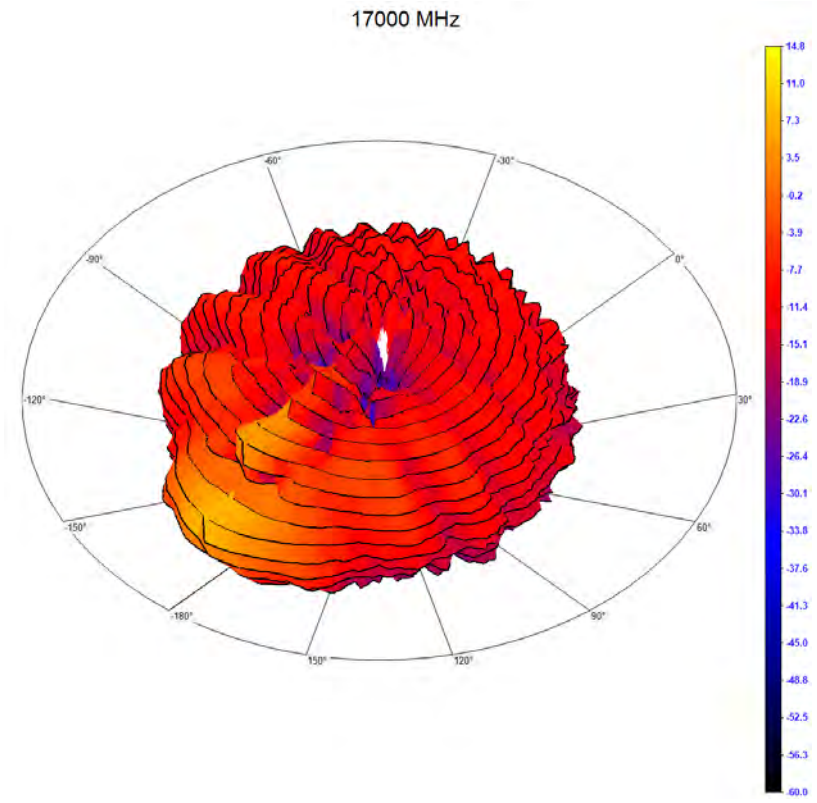


Figure 86: FR4 Antenna: 3D Measured Gain Plot, Co-Polarized, 17 GHz

beam is wider (fig. 88). This makes sense because the increase in frequency should mean that more of the energy from the driven element is activating mode 2.

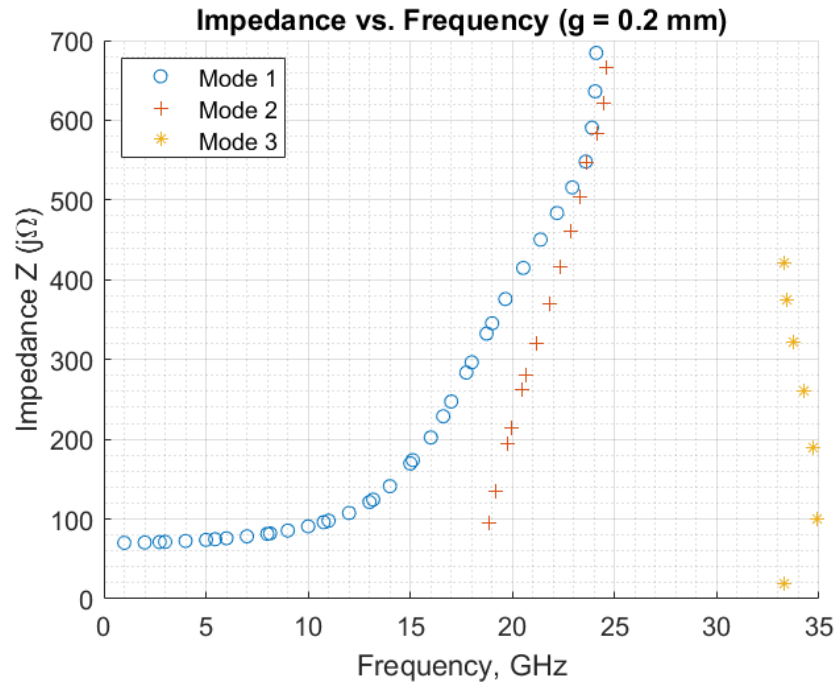


Figure 87: Square FR4 Cell: Impedance vs. Frequency, $g = 0.2$ mm

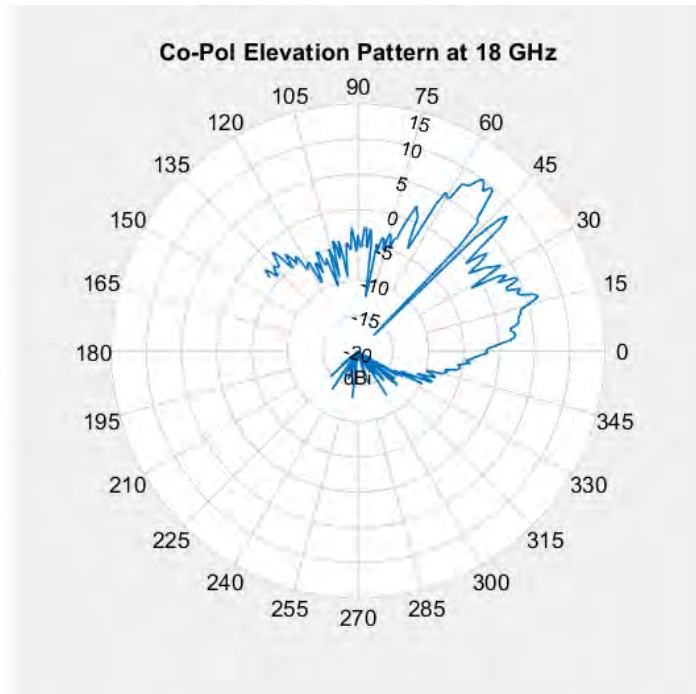


Figure 88: FR4 Antenna: Elevation Pattern, Co-Polarized, 18 GHz

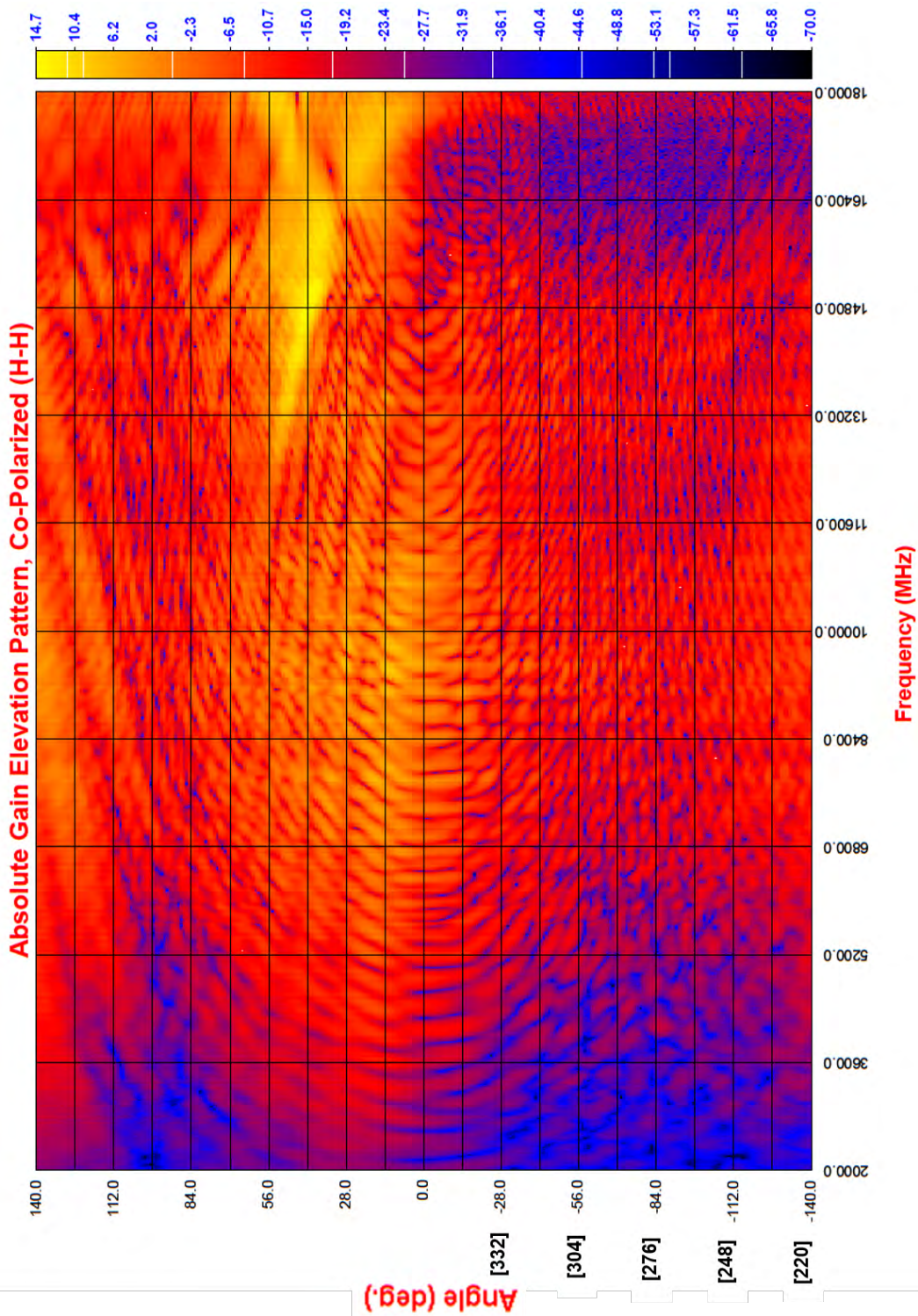


Figure 89: FR4 Antenna: Elevation Waterfall Gain Plot

4.3.3 Rogers 3010 Antenna

A third antenna was fabricated: an 8" by 8" made from Rogers 3010 with circular unit cells (fig. 90). This antenna was fabricated as way to use all of the information



Figure 90: Completed RO3010 Antenna

gathered by this research effort to construct the best possible solution. The antenna design parameters are below in table 5. This antenna was designed to radiate in the +Z direction ($\theta_L = 0^\circ$), normal to the surface. The design frequency chosen was 10 GHz, the center frequency of the desired bandwidth, 2-18 GHz. M , modulation depth, was reduced to 80 percent of the model value, as an attempt to widen the beam width because a pencil beam is not desirable for the receive probe application. Additionally, the origin and driven element were placed at the center point of the surface. An 8" by 8" copper plate was also fabricated with an identical driven element and measured along with the RO3010 antenna. The SWR plot for the RO3010 antenna and the

Antenna Design Parameters	
Dimensions	8" by 8"
Material	Rogers 3010
Cell Shape	circular
Cell Size, a	3 mm
Number of Cells	67 by 67 = 4,489
Driven Element Length	6 mm
Design Frequency	10 GHz
ϕ	40.984°
θ_L	0°
X	249.6
M	$0.8 \times 108.1 \text{ j}\Omega$ $= 86.5 \text{ j}\Omega$
Z_{min}	141.5
Z_{max}	357.8

Table 5: Antenna Design Parameters (8" by 8" Rogers 3010)

copper plate is below in fig. 91 From this plot, the 1.5:1 SWR bandwidth of the antenna is 8.06 GHz (6.47 GHz to 14.53 GHz). If the SWR requirement is reduced to 2:1, the bandwidth increases to 12.09 GHz (5.91 GHz to 18 GHz). By comparison, the 1.5:1 and 2:1 SWR bandwidths of the copper plate are 10.05 GHz (7.95 GHz to 18 GHz) and 10.69 GHz (7.31 GHz to 18 GHz), respectively.

The coordinate system in the RO3010 antenna elevation plots has the zero degree position straight above the metasurface. This is the same coordinate system as the design parameter θ_L , the design beam angle, which was chosen to be 0° for this antenna. No data was collected between 130° and 225°.

The low frequency performance of the antenna was as expected. Figure 92 below shows that the elevation pattern plots of the antenna and the copper plate have a nearly identical shape. The antenna is radiating very poorly because of the large impedance mismatch. The patterns are almost identical because at 3 GHz, the patterning of the copper circles on the top of the antenna are close enough that the waves see a solid copper layer. The cells are 3 mm wide, but the wavelength at 3 GHz is

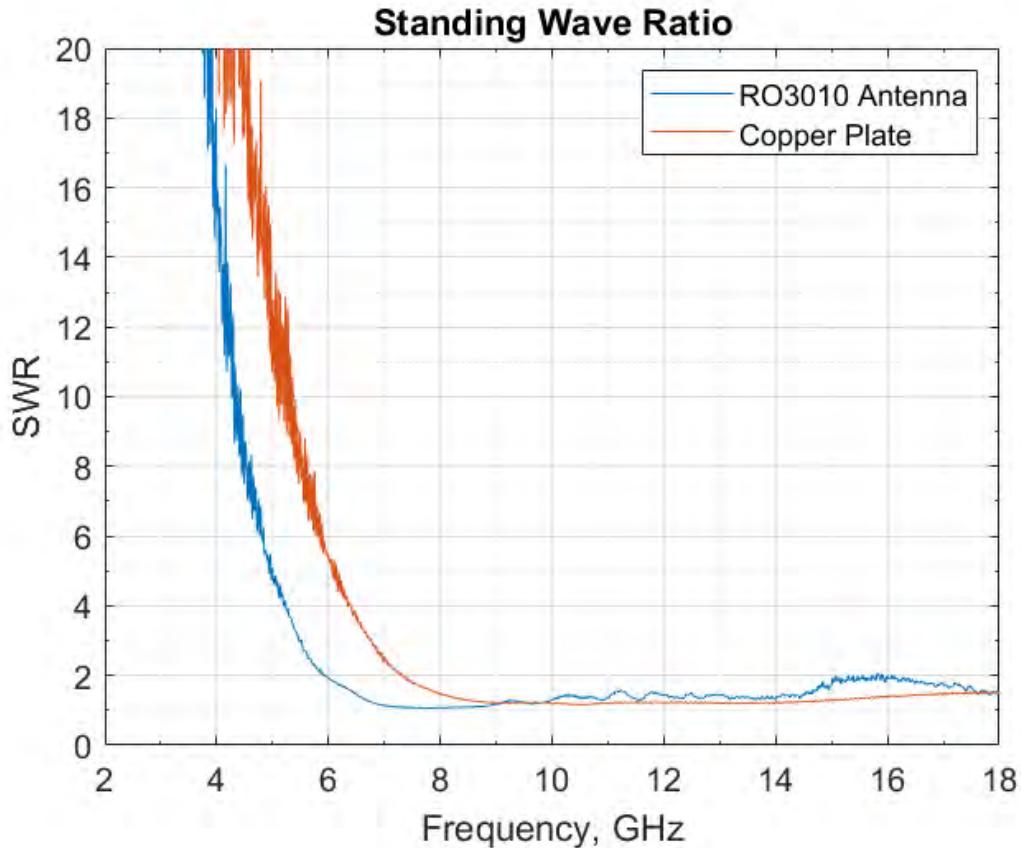


Figure 91: RO3010 Antenna: SWR

roughly 100 mm.

The S11 plot of the antenna and copper plate are below in fig. 93. This plot shows that the resonant frequencies of the antenna and the copper plate are approximately 7.86 GHz and 10.54 GHz, respectively. Like the Duroid 5880 antenna, it is not surprising that the resonant frequency of the antenna is lower than the design frequency for the reasons stated in section 4.3.1. The pattern elevation plot of the antenna at resonant frequency is below in fig. 94. The most noticeable feature of this plot is the similarity between the pattern from the copper plate and the antenna. The gain is roughly equal. Both patterns look reasonable for a monopole mounted on a groundplane. Even though this is the resonant frequency, the metasurface offers no advantage over the copper plate. The endfire null of the driven element is a major

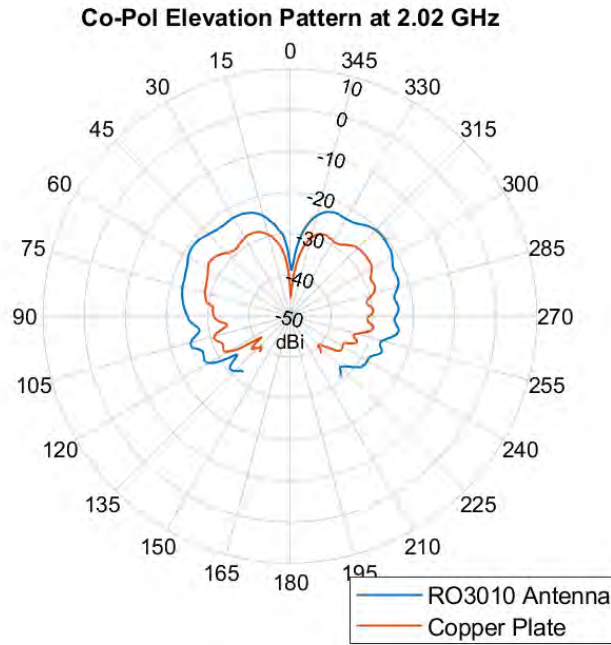


Figure 92: RO3010 Antenna: Azimuth Pattern, Co-Polarized, 2 GHz

feature of this plot, even though the design beam angle is 0° , the angle aligned with the driven element.

The elevation pattern at 10 GHz, the design frequency, is below in fig. 95. The main beam is 30° wide, centered on 0° . The main beam is probably a single beam split by a null rather than two separate beams. The metasurface was not able to totally overcome the null that the driven monopole experiences naturally along its Z axis. The copper plate pattern has a null between 15° and 345° , which shows that the all of the energy contained in that region of the RO3010 antenna's pattern is there because the waves were bent upward by the metasurface, as designed. Despite the null at 0° , the metasurface antenna is effective at directing the waves per the holographic design equations. Both the side beams and the main beam have a gain of roughly 2 dBi. A 3D plot of the antenna pattern at 10 GHz is below in fig. 96. The azimuth pattern at 10 GHz is as expected (fig. 97), having an approximately circular shape. The gain of the metasurface azimuth pattern is roughly 0 dBi all the way around the antenna,

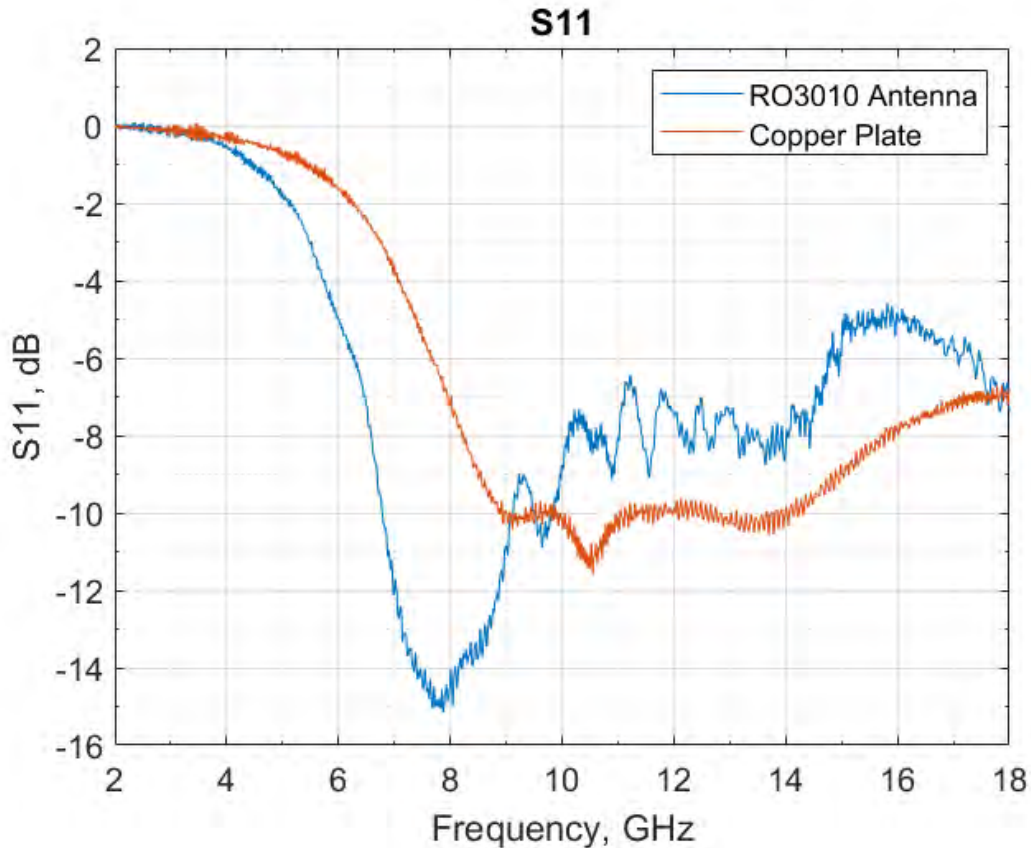


Figure 93: RO3010 Antenna: S11

because the side lobes (which have a gain of 0 dBi) have a low enough elevation to be in the azimuth principle plane. By 11 GHz, the mainbeam is stronger, increasing to 4.7 dBi, roughly 6.5 dBi stronger than the side beams (fig. 98). The metasurface antenna reaches its highest gain at roughly 15 GHz, with the mainbeam at 8.2 dBi, 4 dBi stronger than the side lobes. A 3D plot of the metasurface gain at 15 GHz is below in fig. 100.

The waterfall elevation gain plot reveals how the metasurface antenna behaves across the entire bandwidth (fig. 101). There are three regions: 2 to 10 GHz, 10 to 14 GHz, and 14 to 18 GHz. In the first region (2 to 10 GHz) the metasurface behaves almost the same as the copper plate, because the wavelengths are large relative to the copper patches, so the waves see a solid metal surface. The copper plate elevation gain

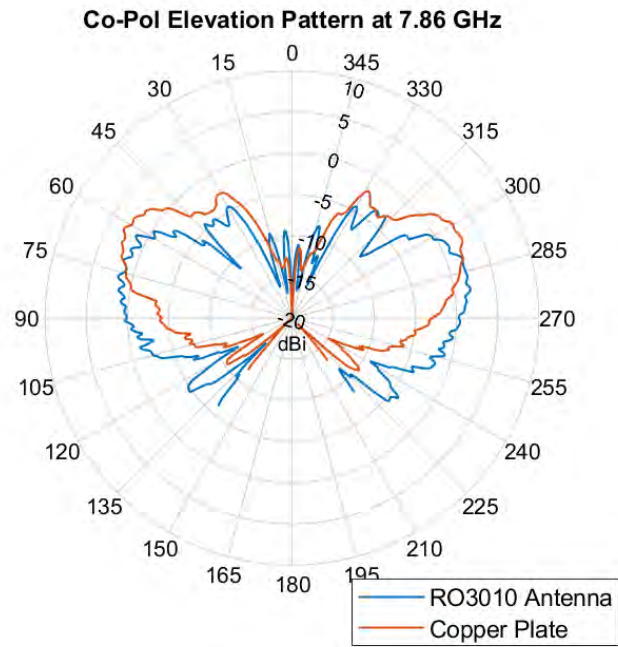


Figure 94: RO3010 Antenna: Elevation Pattern, Co-Polarized, 7.86 GHz

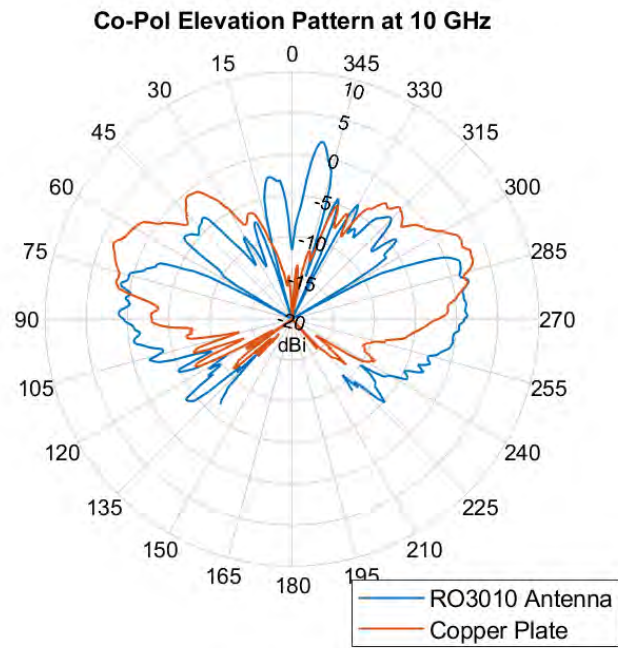


Figure 95: RO3010 Antenna: Elevation Pattern, Co-Polarized, 10 GHz

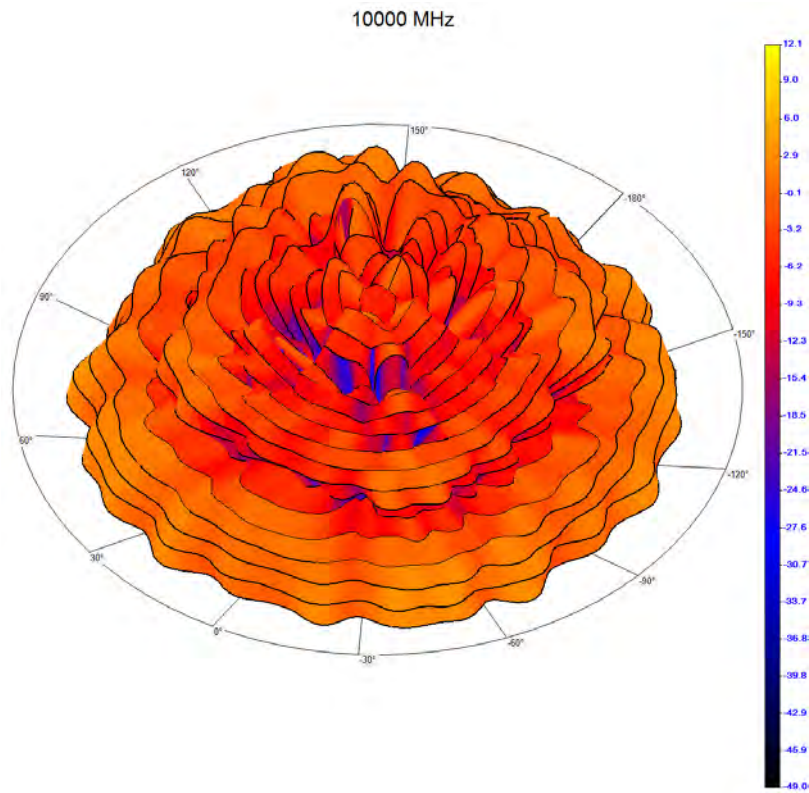


Figure 96: RO3010 Antenna: 3D Measured Gain Plot, 10 GHz

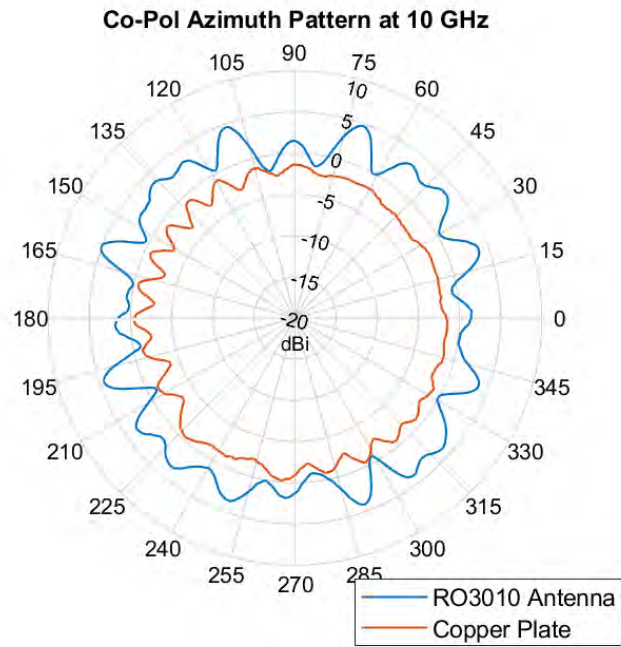


Figure 97: RO3010 Antenna: Azimuth Pattern, Co-Polarized, 10 GHz

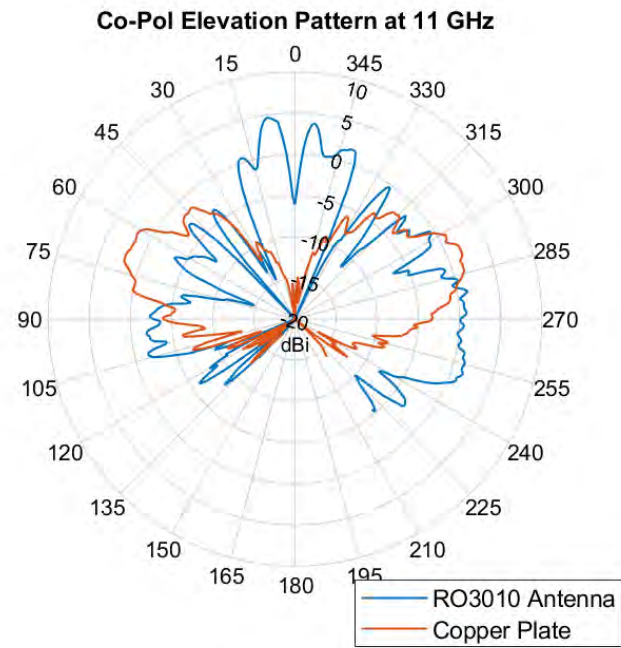


Figure 98: RO3010 Antenna: Elevation Pattern, Co-Polarized, 11 GHz

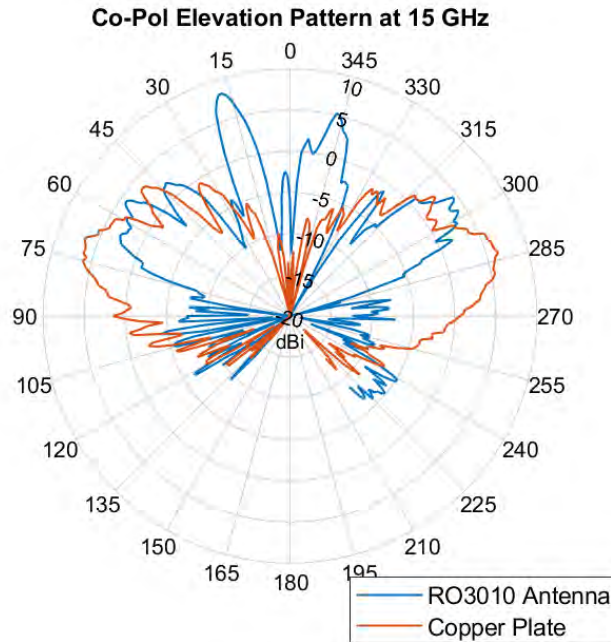


Figure 99: RO3010 Antenna: Elevation Pattern, Co-Polarized, 15 GHz

waterfall plot confirms this and looks extremely similar from 2 to 10 GHz (fig. 102). In the second region, 10 to 14 GHz, mode 1 becomes active and the metasurface redirects the EM waves, weakening the sidelobes by directing energy into the mainlobe at 0° . Note the "V" patterning, as the 0° null widens from 10 to 14 GHz. The third region is from 14 to 18 GHz. In this region, mode 2 becomes active. Another "V" pattern begins inside of the arms of the previous "V" pattern that began at 10 GHz. The arms of the mode 1 main lobe do not widen any further after 14 GHz, but the arms of the mode 2 lobe interfere with the mode 1 lobe, and affects the pattern by moving around a pair of nulls inside the mode 1 lobe. The mode 2 nulls widen with frequency (the "V" shape develops). The hypothesis that mode 2 becomes active at roughly 14 GHz is supported by the eigenmode cell simulations. The impedance vs. gap size plot at the 10 GHz design frequency (fig. 103) shows that most of the impedance range available is obtained with gap sizes from 0.2 to 0.5 mm, due to the nonlinearity of the impedance curve. This means that most cells on the metasurface antenna have a

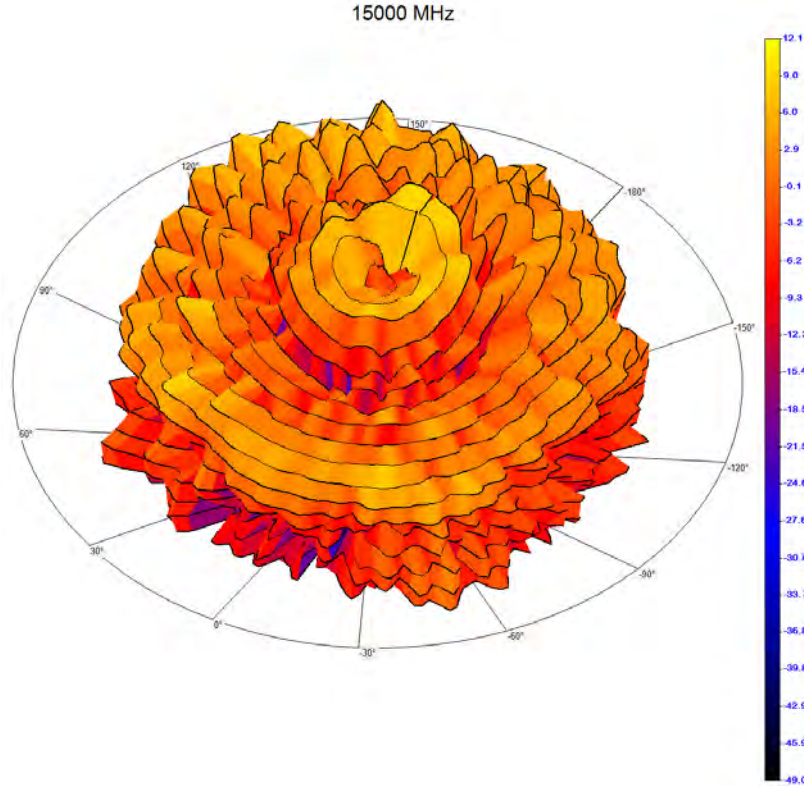


Figure 100: RO3010 Antenna: 3D Measured Gain Plot, 15 GHz

gap size of 0.2 to 0.5 mm. On the multi-mode impedance verses frequency plot for $g = 0.2$ mm (fig. 104), mode 2 turns on as a surface wave mode at 12 GHz. On the multi-mode impedance verses frequency plot for $g = 0.5$ mm (fig. 105), mode 2 turns on as a surface wave mode at roughly 14.5 GHz. Therefore, a second surface wave mode is activated by 14 GHz, which supports the hypothesis that the waterfall gain elevation plot shows the behavior of another mode between 14 and 18 GHz.

The metasurface waterfall azimuth pattern plot also has 3 distinct regions: 2 to 6.8 GHz, 6.8 to 11 GHz, and 11 to 18 GHz (fig. 106). From 2 to 6.8 GHz, the metasurface is poorly matched, but gradually becomes better matched, so as frequency increases, the antenna radiates more effectively, indicated by the transition from dark red to yellow. In this region the metasurface operates as a driven monopole on a solid metal plate so there is little to no angular variation in the pattern. From 6.8 to 11 GHz,

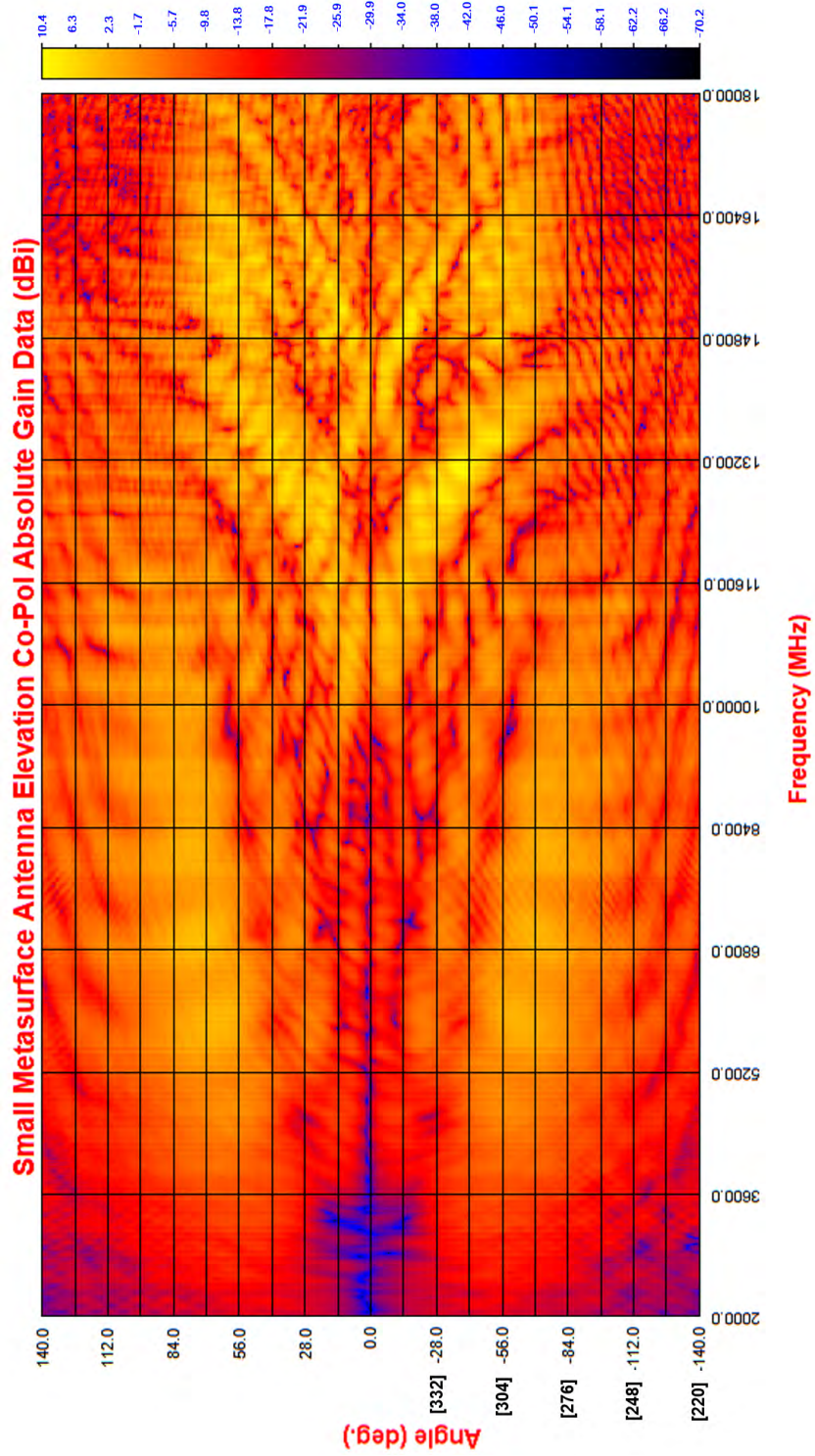


Figure 101: RO3010 Antenna: Elevation Waterfall Gain Plot

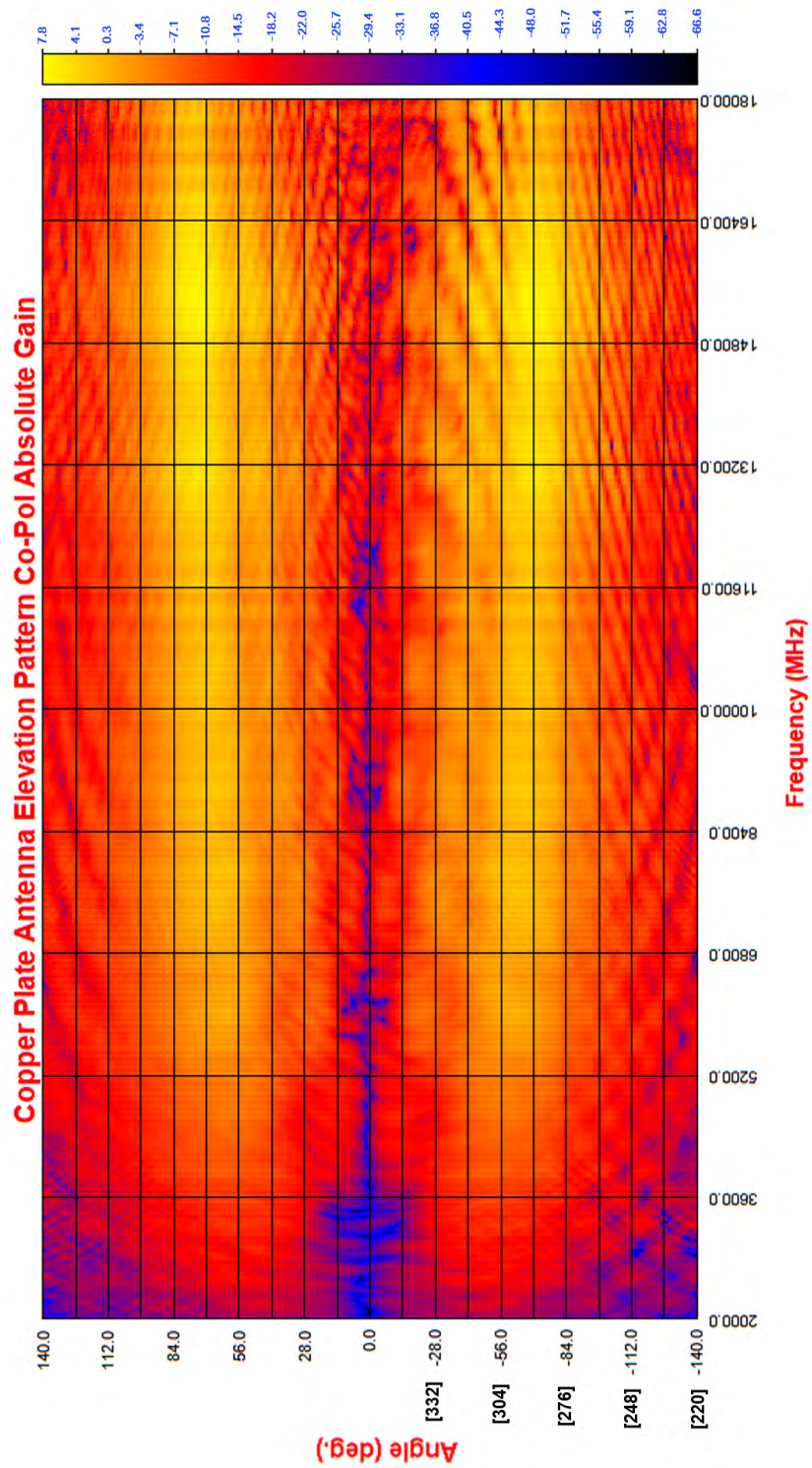


Figure 102: Copper Plate: Elevation Waterfall Gain Plot

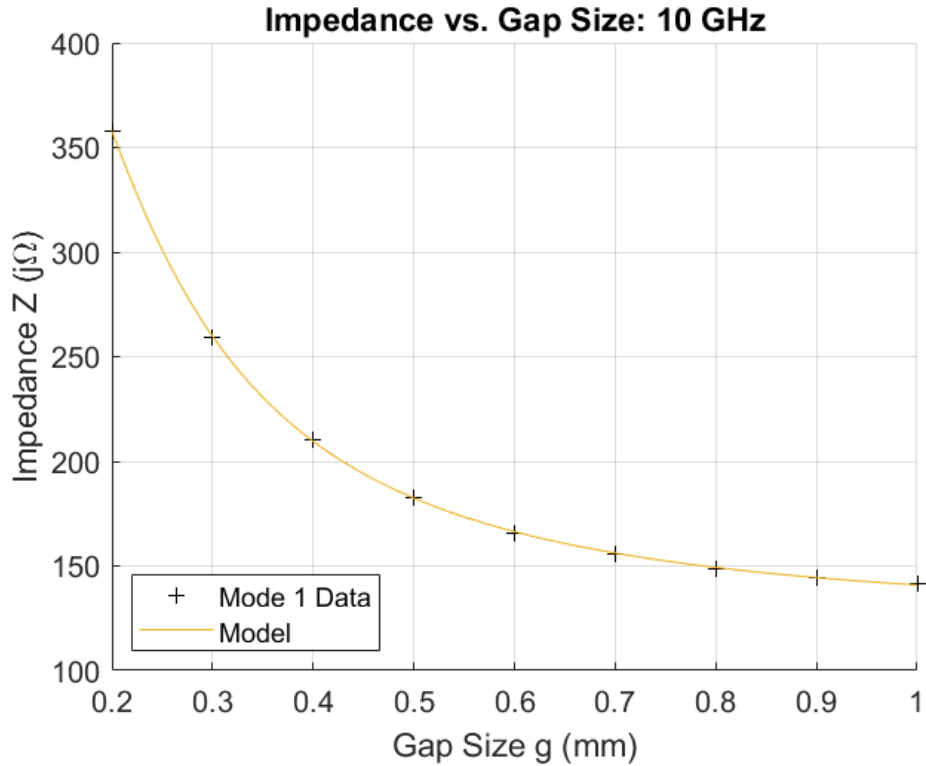


Figure 103: Circle RO3010 Cell: Impedance vs. Gap, 10 GHz

a subtle angular variation becomes more and more noticeable as the metasurface reaches the design frequency and begins to pull energy from the sidelobes naturally generated by the monopole, into the main beam (0°). Then, at 11 GHz the gain in the azimuth drops off as the metasurface becomes even more effective at redirecting the waves, resulting in reduced radiation in the azimuth plane. The copper plate's azimuth waterfall gain plot contains only one region, the same region first region experienced by the the metasurface (fig. 107) Along the frequency axis the copper plate, the gain gradually increases as the impedance match improves. Along the azimuth angle axis, there is little to no variation because the pattern resulting from a driven monopole on a ground plane is not perturbed by variations in the structure as is the case for the metasurface antenna.

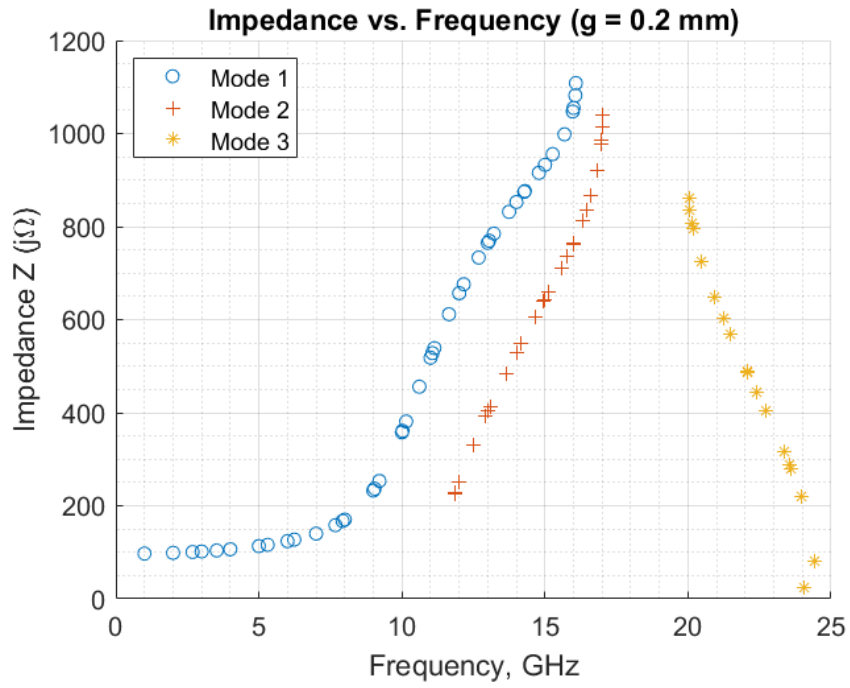


Figure 104: Circle RO3010 Cell: g = 0.2 mm

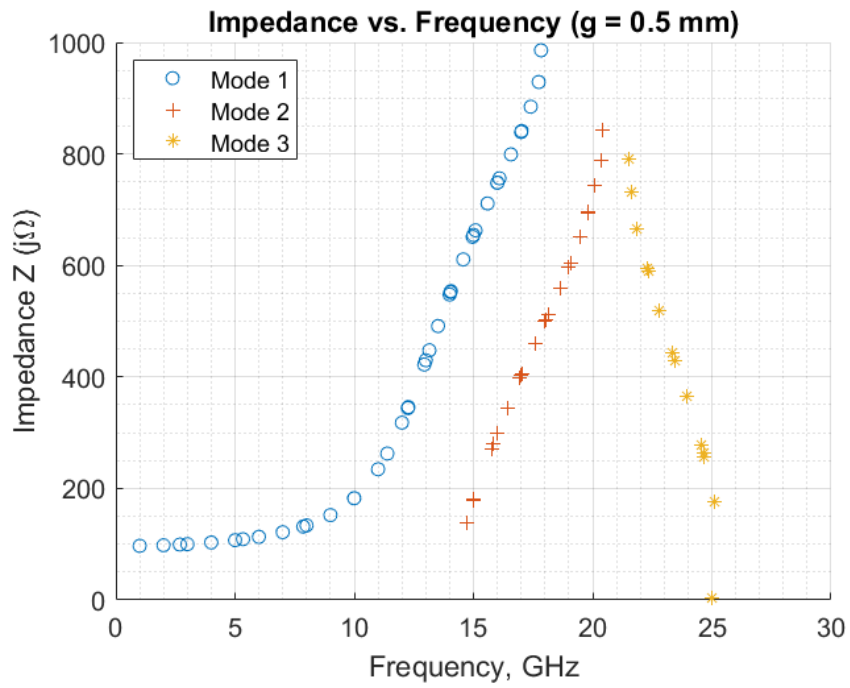


Figure 105: Circle RO3010 Cell: g = 0.5 mm

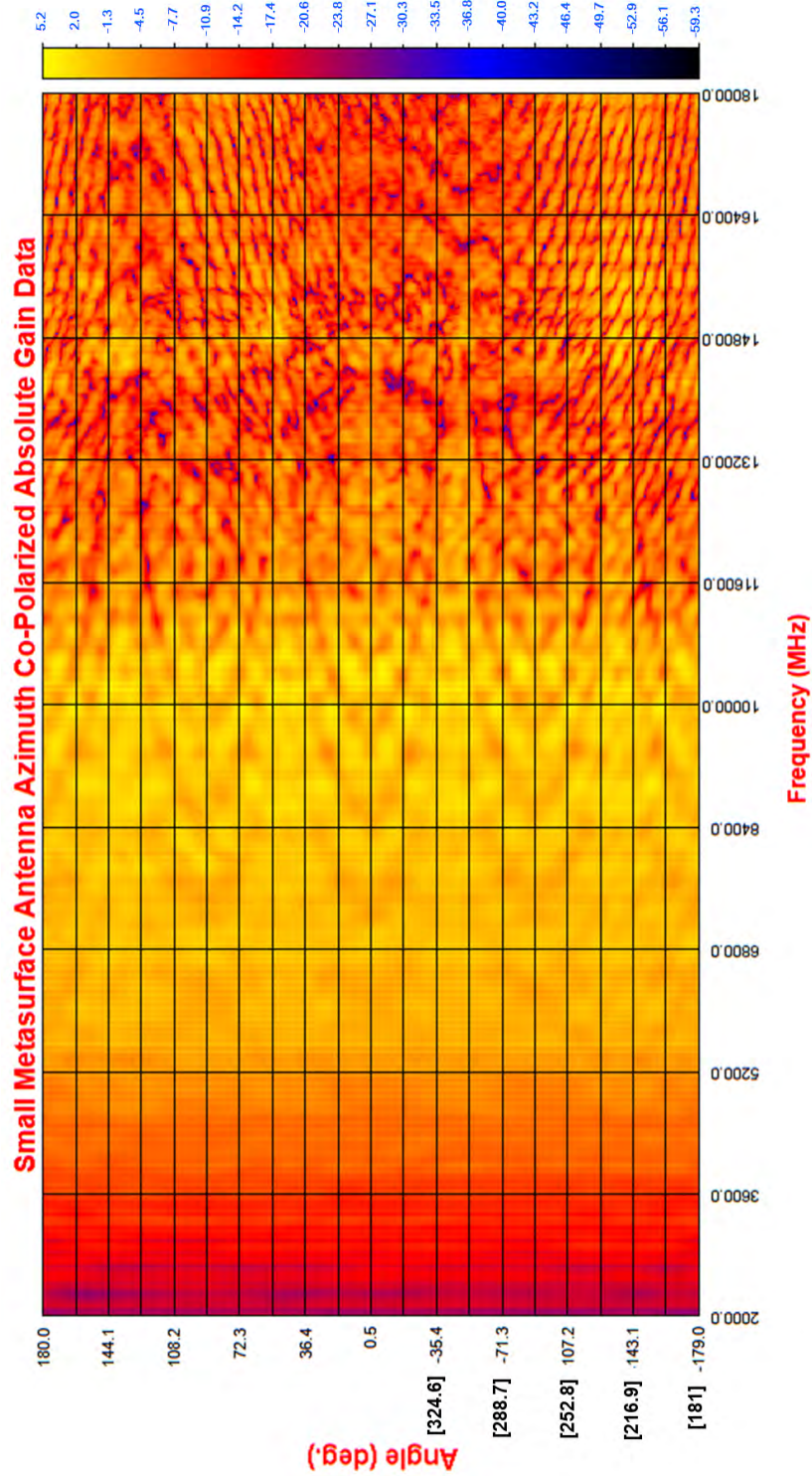


Figure 106: RO3010 Antenna: Azimuth Waterfall Gain Plot

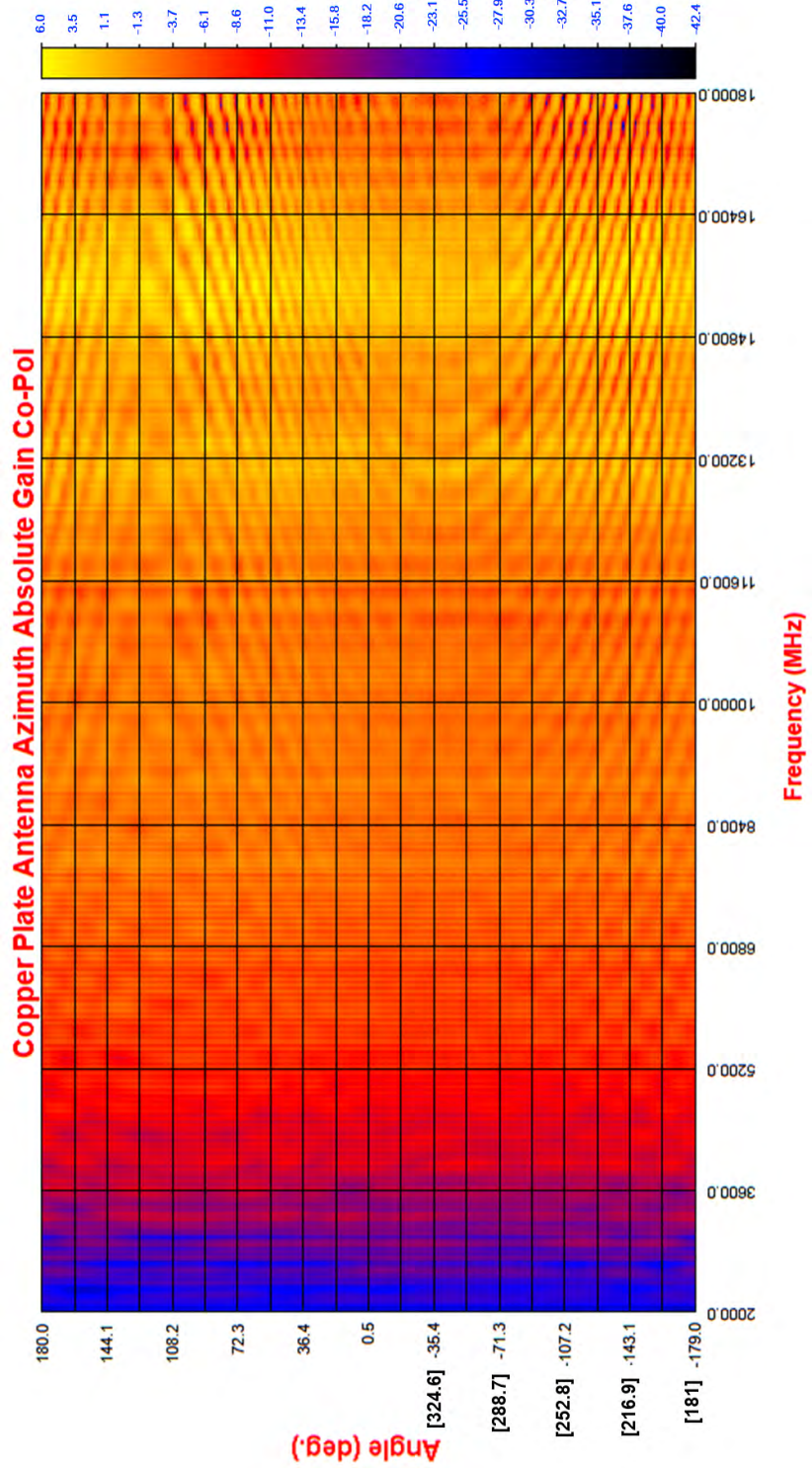


Figure 107: Copper Plate: Azimuth Waterfall Gain Plot

V. Conclusions

5.1 Conclusions

5.1.1 Cell Analysis Conclusions

The eigenmode unit cell simulation and impedance vs. gap linear regression processes successfully characterized the six cell types examined. The big picture conclusion from this effort was that the possibility of multi-mode behavior cannot be ignored, and that care must be taken if single mode operation is desired. Impedance models are only valid for the same mode the model is generated from. If a second mode does become active, its waves will behave differently than the mode 1 waves behave. Each mode sees a different impedance. A potential challenge for modeling multi-mode behavior is that it is not clear how much power for the driven element is coupled into each mode. This ratio may be frequency dependent. Even if separate pattern simulations were generated for each mode, the ratio at which to combine them would still be unknown. The same problem would occur if one were to combine the electromagnetic (EM) fields from mode specific pattern simulations - the strength ratio of the fields would be unknown.

For the circular D5880 unit cell, mode 2 doesn't turn on until after 20 GHz. For the square FR4 and square D5880 unit cells, mode 2 turns on at 19 GHz (assuming the $g = 0.2$ mm geometry). Widening g increases the mode 2 activation frequency, so for these 3 cell types, the possibility of multi-mode operation can be ignored. This is not the case for the other three cell types. The fractal Duroid 5880 and circular RO3010 unit cells experience mode 2 activation for the $g = 0.2$ mm geometry at 12 GHz. Mode 2 for the fractal RO3010 cell becomes active at 7 GHz. No impedance models were generated for the fractal RO3010 unit cell because of severe band gaps, or forbidden frequency bands, in the middle of the bandwidth of interest. It is possible

that the reason no treatment of fractal unit cells was found in available literature is that the difficulties associated with simultaneously modeling or controlling multiple modes have not yet been successfully addressed. It is also possible that Sievenpiper chose 17 GHz as the design frequency for his metasurface with square Duroid 5880 unit cells, because it is the highest frequency allowed by that unit cell type while still leaving a 2 GHz buffer before mode 2 becomes active at 19 GHz [11]. This buffer ensures the validity of the single mode operation assumption. The unit cell predictions for the mode 2 activation frequencies seemed to have a fidelity of roughly ± 1 GHz, compared with the results observed from the antenna measurements.

5.1.2 Design Conclusions

The measurement results for the 16" by 10" metasurface antenna with square Duroid 5880 unit cells (17 GHz design frequency) validates the design methodology as a whole. This antenna was made using the same processes Sievenpiper used, but with an independently simulated cell model [11]. The measured antenna had a mainbeam gain of 18 dBi (2 dBi less than Sievenpiper) and a beam width of 5° in the elevation plane (X-Z) (the same as Sievenpiper). The measured elevation beam angle, θ_L , was 38° , 8° different than the design value of 30° , and 5° different than the $\approx 33^\circ$ realized elevation beam angle presented by Sievenpiper. (θ_L is referenced at 0° in the X-Y plane.) The measured antenna had a 1.5:1 Standing Wave Ratio (SWR) bandwidth of 7.59 GHz: 10.41 to 18 GHz. This is promising, given that this antenna was not optimized for bandwidth.

The measurement results for the 16" by 10" metasurface antenna With an FR4 substrate clearly displayed multi-mode behavior, which agrees with the unit cell predictions.

The 8" by 8" Rogers 3010 antenna demonstrated a 1.5:1 SWR bandwidth of 8.06

GHz (6.47 GHz to 14.53 GHz), and a 2:1 SWR bandwidth of 12.09 GHz (5.91 GHz to 18 GHz). Although this does not cover the entire bandwidth of interest (2-18 GHz) this result is also very promising and suggests that bandwidth requirements does not necessarily preclude the metasurface class of antennas from being a viable option for the receive probe application. However, the lower frequencies present a challenge, as the spacing between the metal patches is small enough that to those frequencies, the surface is effectively solid copper.

The RO3010 antenna was designed to radiate normal to the metasurface, placing the center of the main beam in the center of the null off of the end of the driven element. Despite this challenge, the surface did a good job of redirecting energy from the broadside of the driven element towards the +Z direction. For most of the bandwidth, the mainbeam and broadside beam gain was roughly 0 dBi. Despite less than optimal gain, this antenna is a good prototype for the bistatic RCS measurement receive probe application. The three antennas fabricated and tested demonstrate that metasurfaces potentially have both the bandwidth and the beam control (width and angle) required for the application.

5.2 Future Work

5.2.1 Error Characterization of Eigenmode Unit Cell Simulations

Although the unit cell simulations produced reasonable data, further research effort is needed to obtain a better understanding of the accuracy of those simulations and characterize error. Several avenues are available for this task.

- Perform unit cell simulations with using small parameter variations (thickness, dielectric constant, etc.) to characterize the sensitivity of the results.
- Perform unit cell simulations for the high and low end of the specification values

(ex. dielectric constant) given by material manufacturer to characterize design accuracy limitations.

- Perform unit cell eigenmode simulations using High Frequency Simulation Software (HFSS) with the option for complex frequencies selected to allow simulation of lossy materials. The results should include a small real impedance. Then compare the results with those obtained from Computer Simulation Technology (CST) to compare impedances to see if the reactive impedances are significantly different.
- Perform linear regression on the dispersion data for the square Duroid 5880 unit cell. Then use that model to generate the frequency/phase pairs needed for the 17 GHz impedance model, and use the process described in section 3.3 to generate an impedance vs. gap model. Then, compare this model with Sievenpiper's to see if this yields results closer to Sievenpiper's, because it is possible that he generated his model in a similar manner.
- Do time and frequency domain simulations for meatasurface with the same exact cell patch repeated on the top (identical gap size and shape). Then perform the field integration method on the results to calculate an impedance for comparison with previous results. Also generate pattern predictions.
- Construct the impedance surface from the previous item, and do field measurements in a wave guide to validate the simulations with measured results.

The above items are a good start towards characterizing the accuracy of the cell simulations.

5.2.2 Additional Unit Cell Research

Much more research is needed to fully understand and optimize the metasurface unit cell. The mode labeling issue in CST should be further explored, to determine if the multi-mode trendlines are really made up of data from the same mode (which would mean that CST is mislabeling some of the points). This could be accomplished by examining the fields of the modes in question before and after the intersection points.

Probably the biggest assumption of the methodology is that there will only be a single active mode, the mode use to generate the impedance models. A series of simulations could be performed to gain better fidelity on the mode activation frequencies: for each cell type, simulate 2 separate geometries: one with solid copper on both top and bottom of the dielectric, and one with solid copper on the bottom of the dielectric, and nothing on the top of the dielectric. Use the parameter sweep function with the eigenmode solver to generate dispersion curves for both cases. This data will indicate the maximum and minimum frequencies supported by each mode, and can be processed to predict the maximum and minimum impedances available to the cell type for each mode.

This research effort was by no means exhaustive of the potential geometry options for unit cells. Other geometries should be explored, including multi parameter geometries. For example, an additional design could be a circular ring for which both the inner and outer radii are varying parameters.

An another additional area to explore is control of the stop bands experienced with the fractal cells. This characteristic might be useful for an application where a specific band of operation is desired, with some level of rejection of frequencies outside that band.

5.2.3 Additional Antenna Design Research

The most important area of additional research for the metasurface antenna topic is antenna pattern simulation. Valid antenna pattern simulations would complete the feedback loop needed for the overall design methodology presented in Chapter 3 to work correctly. It would allow characterization of the effects of selection of X , M , and ϕ on the antenna pattern. It would also allow characterization of the other relevant antenna design parameters: physical dimensions, driven element length, and driven element location. The driven element of the 8" by 8" metasurface antenna was increased to 6 mm (roughly 20 percent of the 10 GHz design wavelength), rather than the 3 mm used for the 16" by 10" antennas (roughly 17 percent of the 17 GHz wavelength). This may have reduced the overall efficiency of the antenna by radiating energy further away from the metasurface, rather than putting the maximum amount of energy into driving the surface waves. Antenna pattern simulations would allow optimization of both the driven element length and placement on the surface.

5.2.4 Improvement of the 8" by 8" Receive Probe Antenna

The 8" by 8" RO3010 was designed to funnel the surface waves towards the +Z direction, the same direction as the driven element null. The design might be improved substantially by, rather than fighting the natural pattern a monopole experiences, working with it. The main beam design angle could be changed to $\theta_L = 90^\circ$ (or close to it), making of main beam radiate off the side of the surface, mostly in the X-Y plane. This would reinforce the broadside radiation of the driven element, rather than attempting to force an endfire radiation pattern. This would also allow the lobes experienced on the low frequency side of the bandwidth (roughly 2 to 6 GHz) to be used. At these frequencies, the waves are long enough that they see the patterning of the copper patches on the top of the surface as a solid copper sheet. The driven

element could be moved closer to the $X = 0$ side of the board, potentially a 5th or 4th of the total X dimension away from $X = 0$. It would stay centered in the Y axis ($y = 4$ inches). This would allow more of the board to direct the waves toward of the main beam, and would in some ways mimic the Yagi-Uda antenna design. Yagi-Udas have a single reflector behind the driven element, but may have many director elements in front of the driven element in the direction of the main beam. Functional antenna pattern simulations would allow for the optimization of the driven element length, and location. The other parameters to examine for this design are M , modulation depth (which may have an effect on beam width) and ϕ . Another improvement to the design might be reduction of the dielectric constant through use of Rogers 3006 rather than 3010. This material has a dielectric constant of 6.15, which is between the 2.2 of the Duroid 5880 and the 11.2 of Rogers 3010. This would increase the frequency at which mode 2 operation is possible, making the single mode assumption valid for a larger portion of the desired bandwidth, reducing the uncertainty inherent in any impedance surface based pattern simulations.

Appendix A. Square Duroid 5880 Unit Cell

Model Summary

Cell Parameters

Material: Rogers Duroid 5880

Dielectric Constant, ϵ_r : 2.20

Dissipation Constant, $\tan \delta$: 0.0009

Shape: square

Dielectric Thickness: 1.575 mm

Copper Thickness: 0.035 mm

Cell Size, a : 3 mm

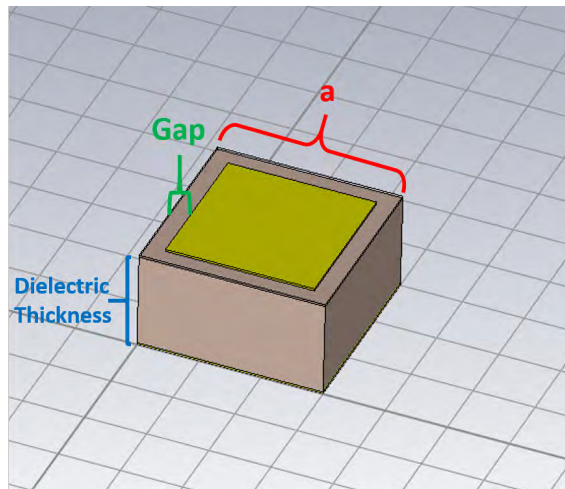


Figure 108: Square Cell Geometry

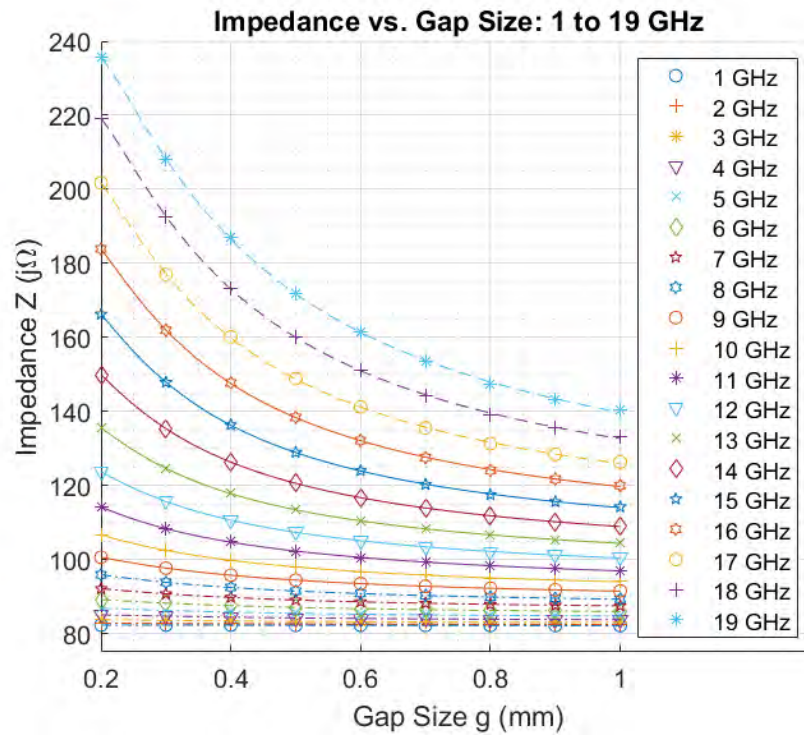


Figure 109: Square Duroid 5880: Cell Impedance vs. Gap, 1-19 GHz

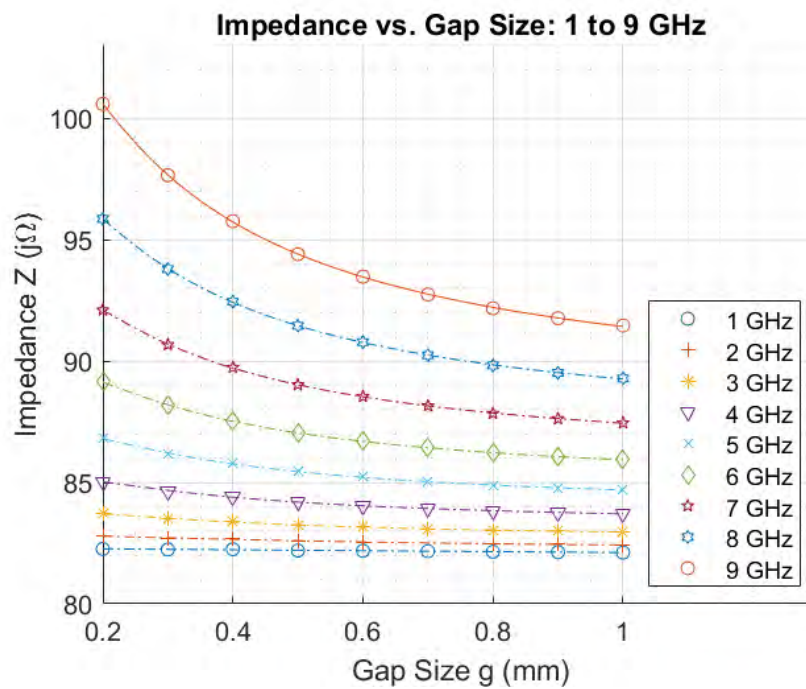


Figure 110: Square Duroid 5880: Cell Impedance vs. Gap, 1-9 GHz

Unit Cell Impedance Model: Square Duroid 5880

Frequency \rightarrow Parameter \downarrow	1 GHz	2 GHz	3 GHz	4 GHz	5 GHz	6 GHz	7 GHz	8 GHz	9 GHz	10 GHz
c_4	0	0	0	0	0	0	0	0	0	0
c_3	0	0	0	0	0	0	0	0	0	0
c_2	0	0.363907	-0.03476	-0.05186	-0.07467	-0.1037	-0.13944	-0.18205	-0.23131	-0.28634
c_1	-0.19302	-0.88959	0.393931	0.640262	0.977564	1.423304	2.000602	2.739763	3.68072	4.875227
c_0 (intercept)	82.30422	82.95324	82.59925	83.11755	83.78681	84.60791	85.58151	86.70503	87.9711	89.36434
Z_{min}	82.11108	82.4231	82.94938	83.69946	84.68713	85.93079	87.45389	89.28544	82.11108	94.01934
Z_{max}	82.25968	82.79352	83.70467	85.02726	86.81322	89.13714	92.10342	95.85631	82.25968	106.5783
X	82.18538	82.60831	83.32703	84.36336	85.75017	87.53397	89.77866	92.57087	82.18538	100.2988
M	0.0743	0.185208	0.377648	0.663902	1.063046	1.603177	2.324765	3.285433	0.0743	6.279503
ϕ_{avg}	3.687226	7.376064	11.06809	14.76528	18.46977	22.18423	25.91204	29.65758	3.687226	37.22721
Inversion Factor	1	1	-1	-1	-1	-1	-1	-1	-1	-1

Frequency \rightarrow Parameter \downarrow	11 GHz	12 GHz	13 GHz	14 GHz	15 GHz	16 GHz	17 GHz	18 GHz	19 GHz
c_4	0	0	0	0	0	0	0	0	0
c_3	0	-0.04484	-0.07947	-0.13239	-0.20691	-0.29567	-0.37996	-0.42754	-0.41965
c_2	-0.34499	-0.01277	0.221152	0.58198	1.049342	1.502334	1.749241	1.514809	0.677859
c_1	6.384699	7.295767	8.942707	10.85985	13.17573	16.18628	20.23229	25.78936	32.89857
c_0 (intercept)	90.86438	93.14538	95.26726	97.57282	99.97984	102.3009	104.3349	105.7729	106.6007
Z_{min}	97.00858	100.4775	104.475	109.0434	114.209	119.9734	126.305	133.139	140.385
Z_{max}	114.1515	123.7036	135.5805	149.8797	166.2377	183.8448	201.75	219.1726	235.6169
X	105.58	112.0905	120.0277	129.4615	140.2233	151.9091	164.0275	176.1558	188.001
M	8.571455	11.61307	15.55272	20.41817	26.01431	31.93571	37.72253	43.01683	47.61591
ϕ_{avg}	41.06999	44.96958	48.94482	53.01786	57.21087	61.54125	66.01829	70.64367	75.4127
Inversion Factor	-1	-1	-1	-1	-1	-1	-1	-1	-1

Table 6: Square Duroid 5880: Unit Cell Impedance Model

Dispersion Diagrams and Impedance vs. Frequency Plots by Mode

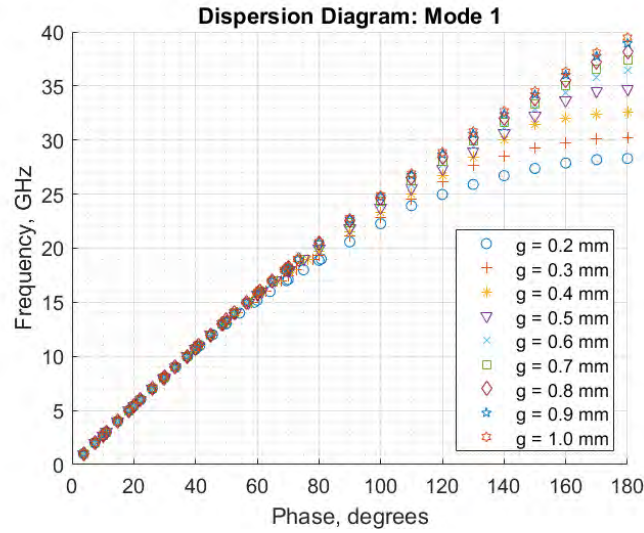


Figure 111: Square Duroid 5880: Dispersion Diagram, Mode 1

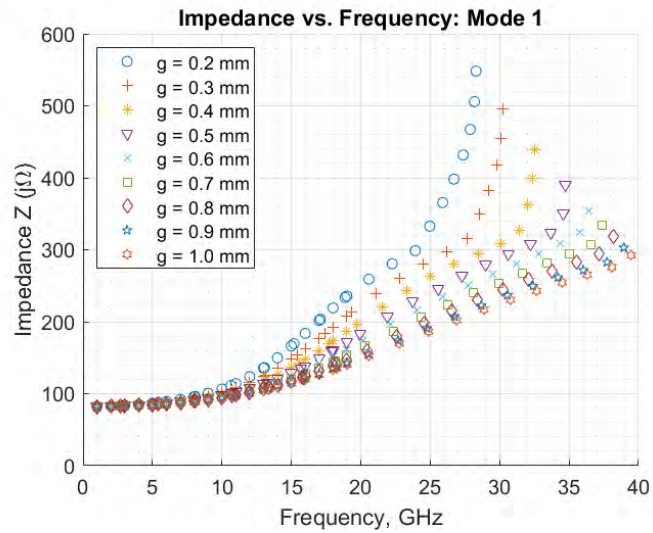


Figure 112: Square Duroid 5880: Impedance vs. Frequency, Mode 1

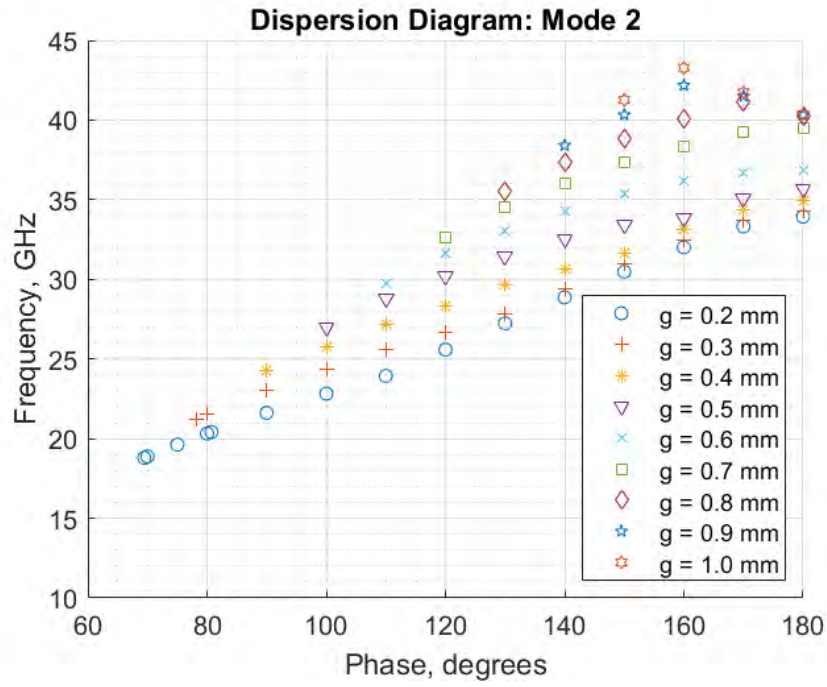


Figure 113: Square Duroid 5880: Dispersion Diagram, Mode 2

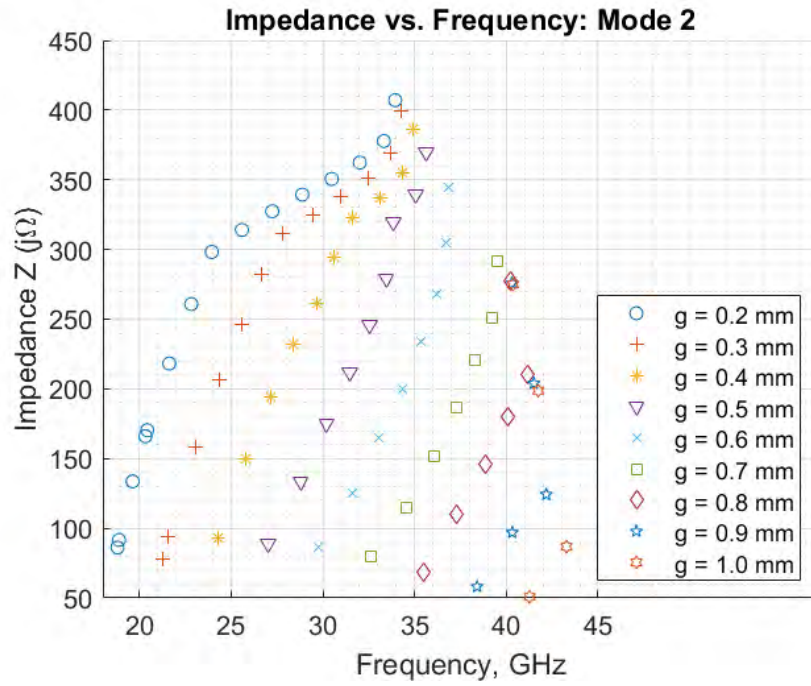


Figure 114: Square Duroid 5880: Impedance vs. Frequency, Mode 2

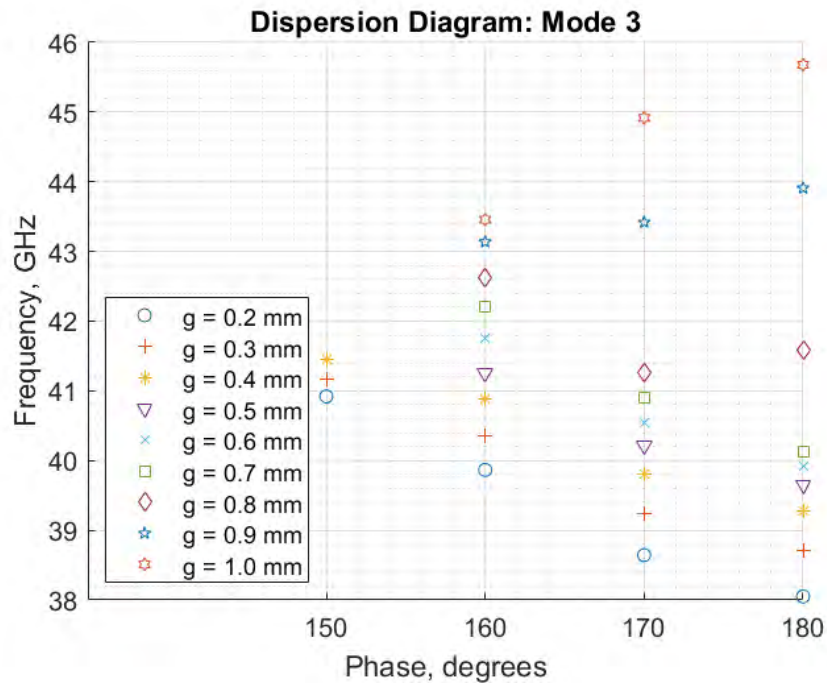


Figure 115: Square Duroid 5880: Dispersion Diagram, Mode 3

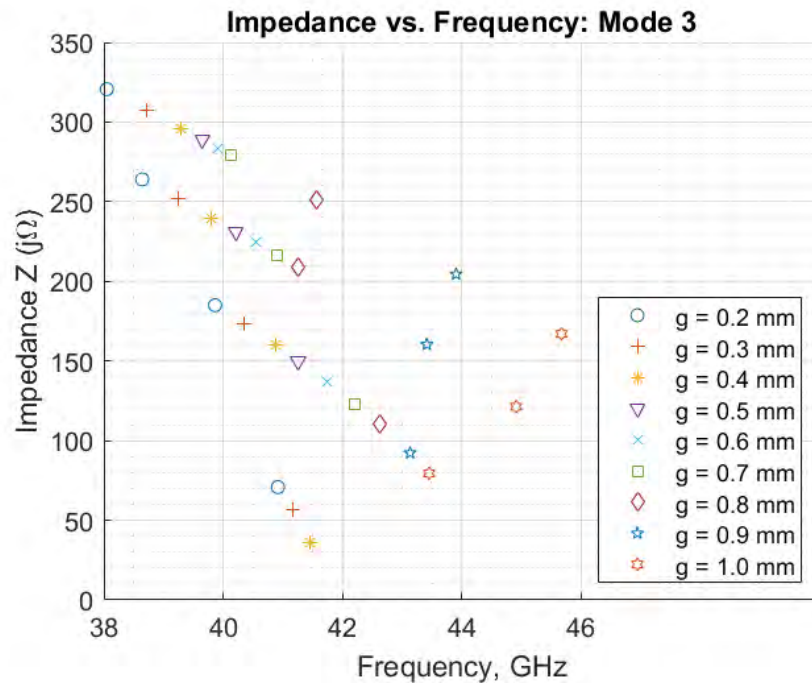


Figure 116: Square Duroid 5880: Impedance vs. Frequency, Mode 3

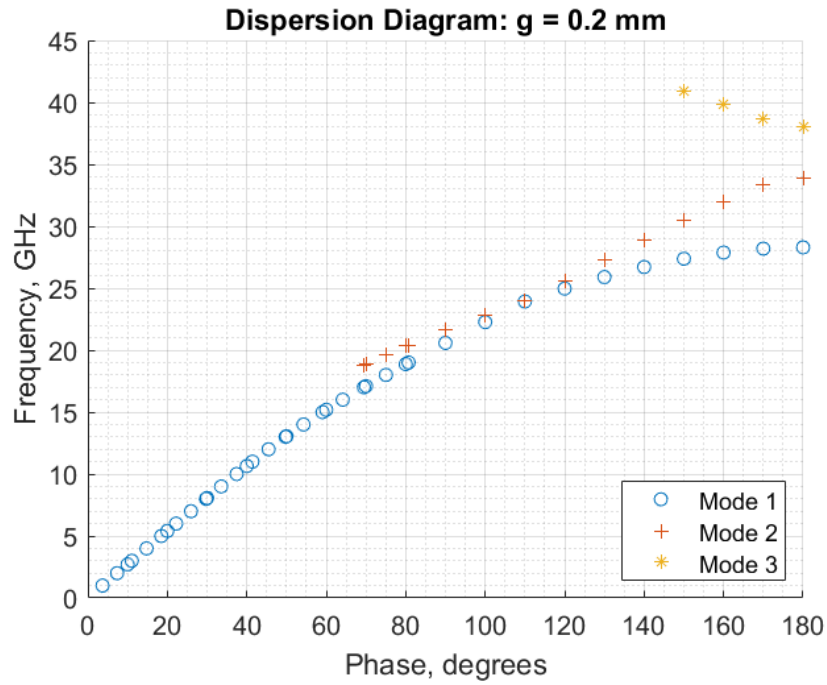


Figure 117: Square Duroid 5880: Dispersion Diagram, $g = 0.2$

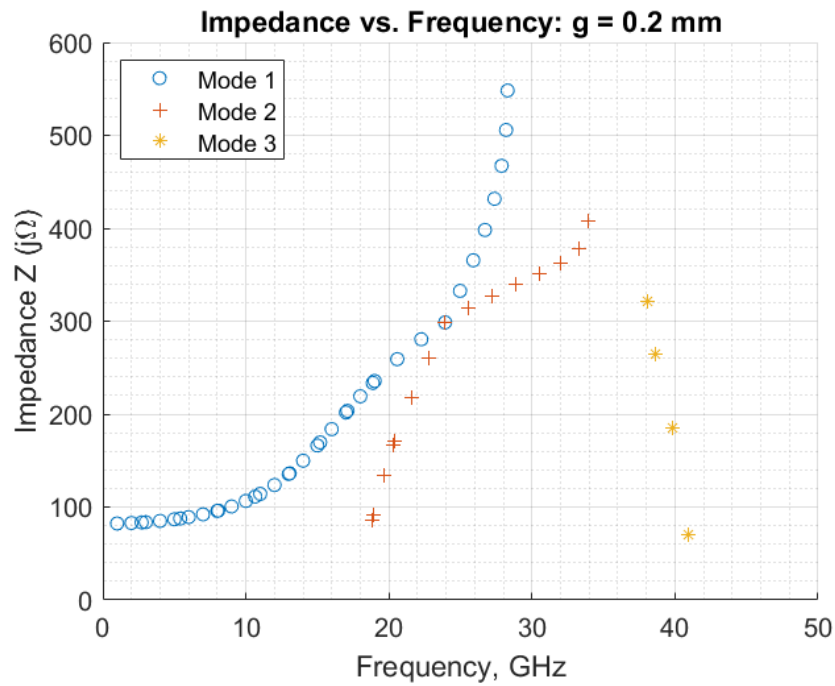


Figure 118: Square Duroid 5880: Impedance vs. Frequency, $g = 0.2$

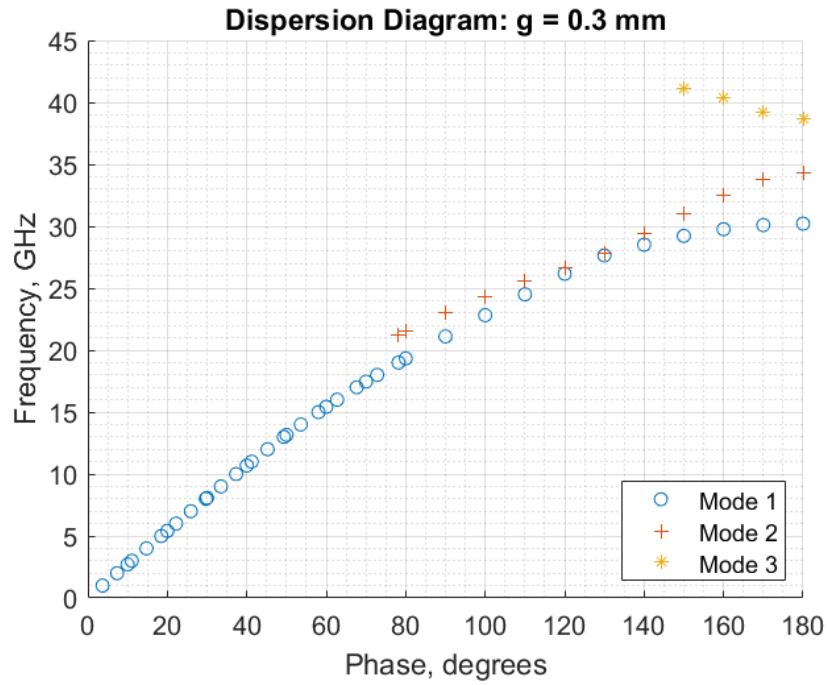


Figure 119: Square Duroid 5880: Dispersion Diagram, $g = 0.3$

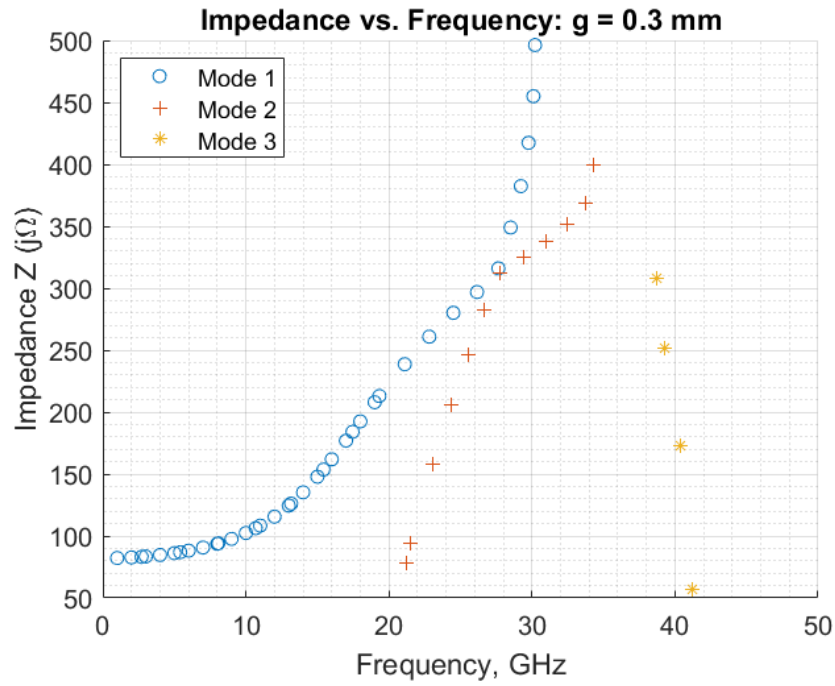


Figure 120: Square Duroid 5880: Impedance vs. Frequency, $g = 0.3$

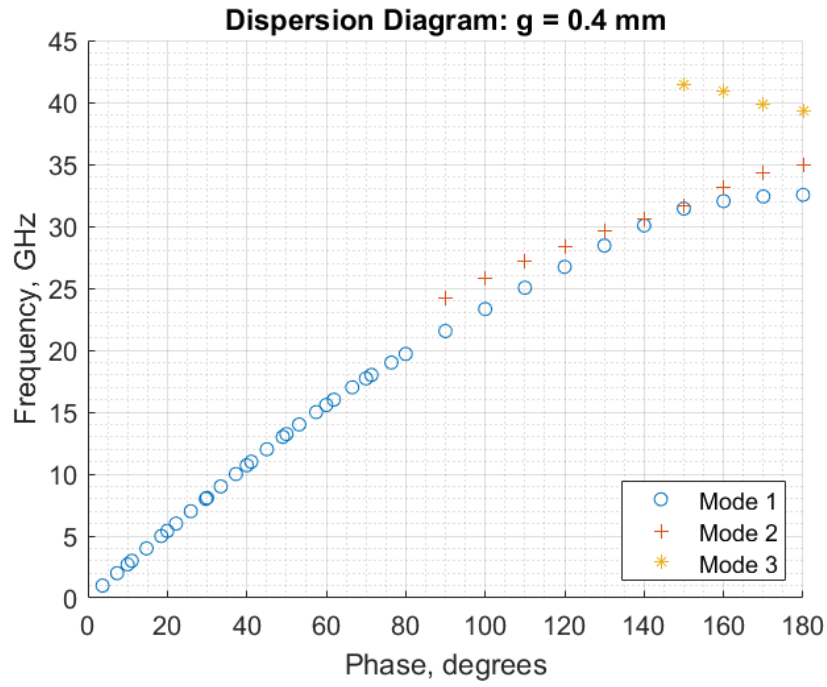


Figure 121: Square Duroid 5880: Dispersion Diagram, $g = 0.4$

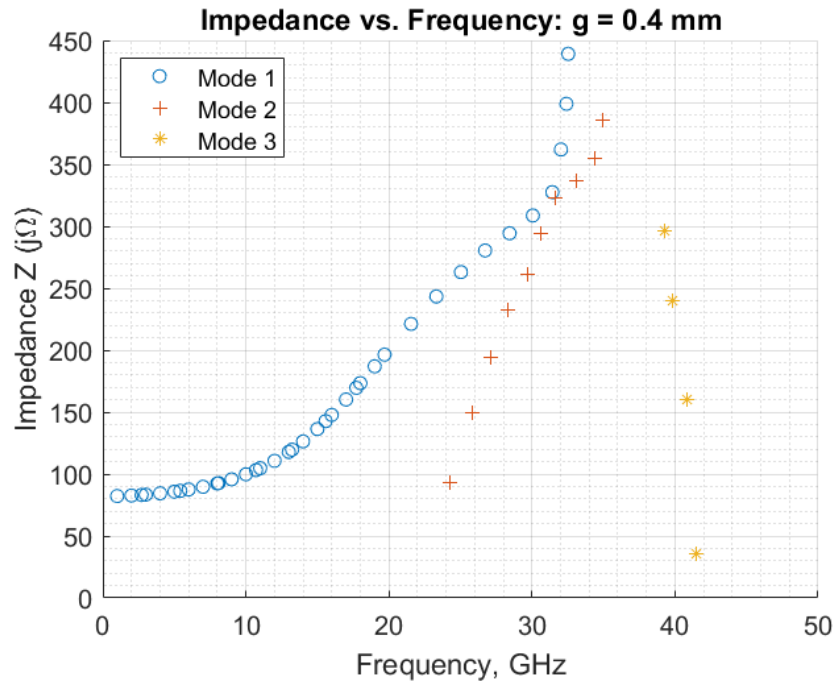


Figure 122: Square Duroid 5880: Impedance vs. Frequency, $g = 0.4$

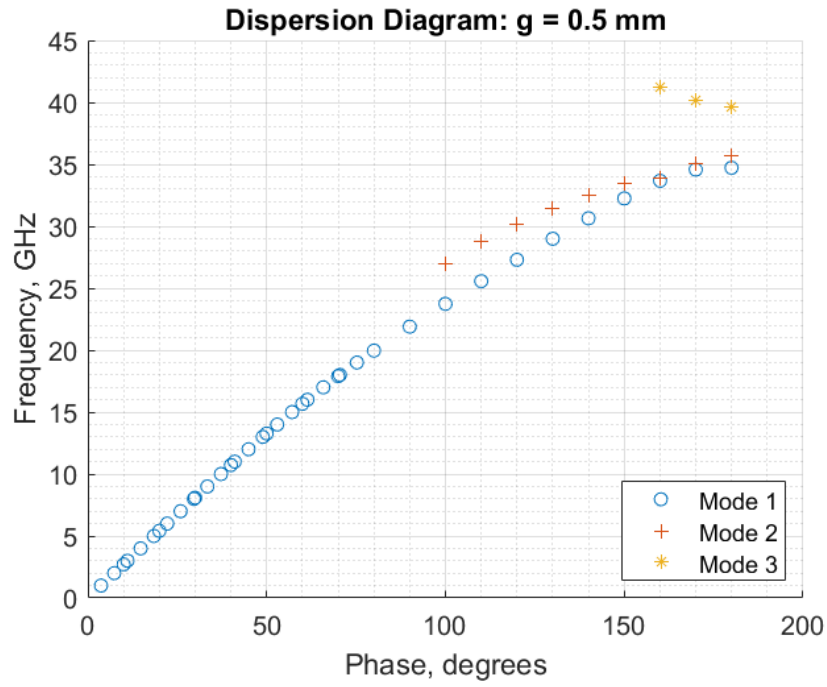


Figure 123: Square Duroid 5880: Dispersion Diagram, $g = 0.5$

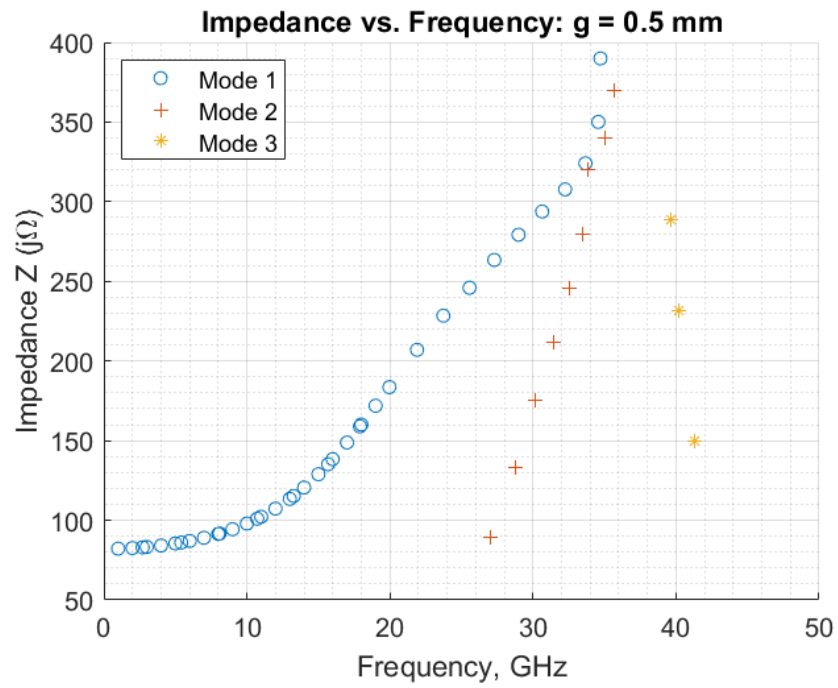


Figure 124: Square Duroid 5880: Impedance vs. Frequency, $g = 0.5$

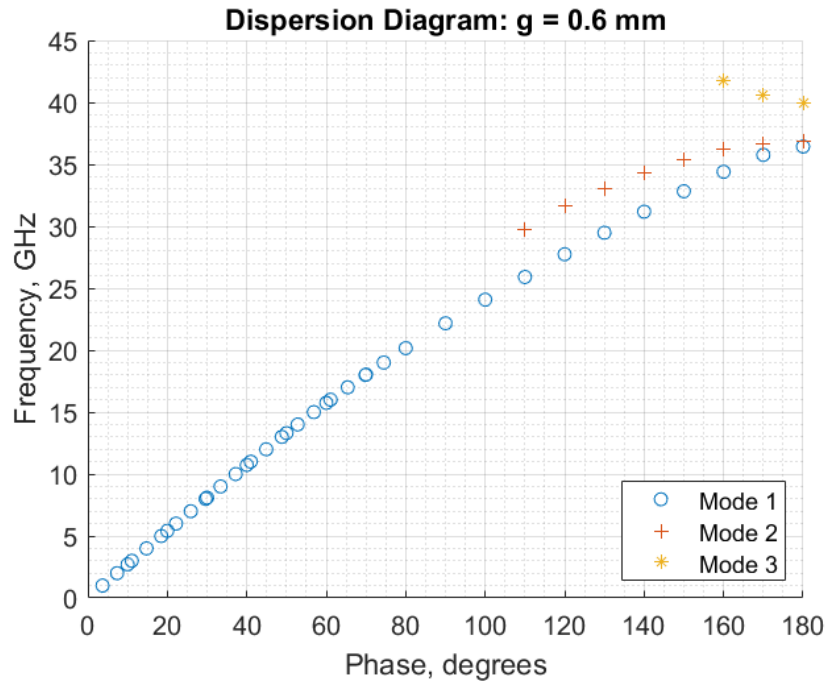


Figure 125: Square Duroid 5880: Dispersion Diagram, $g = 0.6$

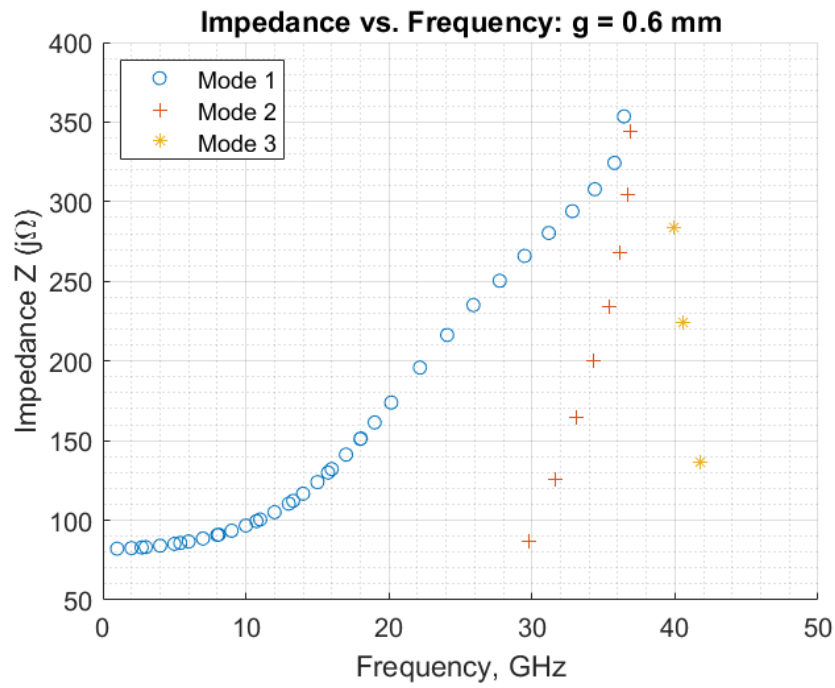


Figure 126: Square Duroid 5880: Impedance vs. Frequency, $g = 0.6$

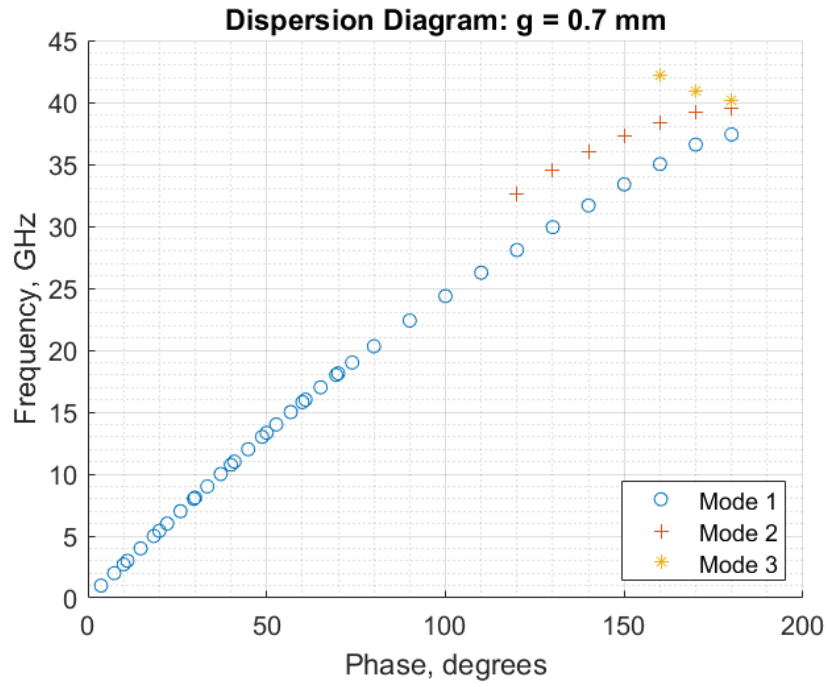


Figure 127: Square Duroid 5880: Dispersion Diagram, $g = 0.7$

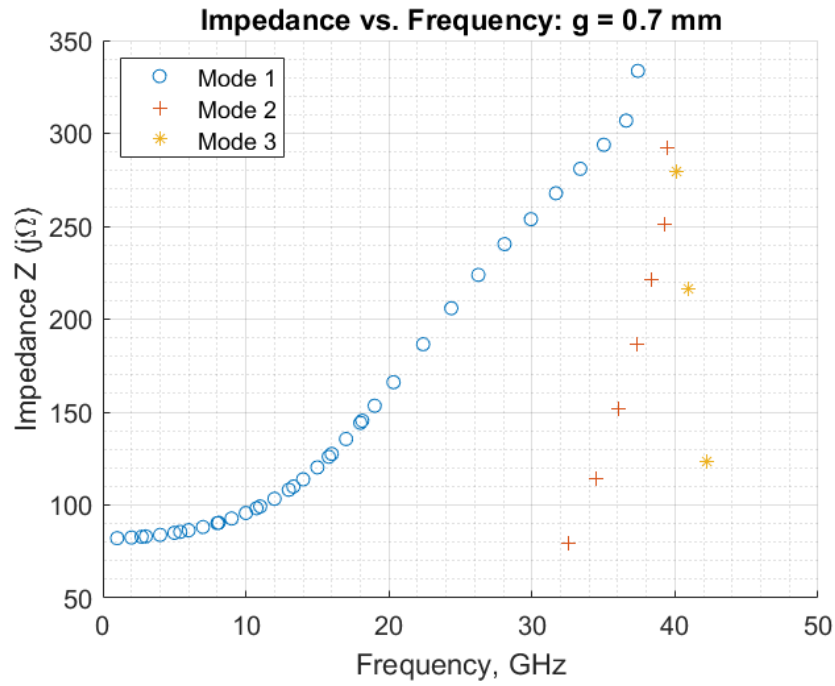


Figure 128: Square Duroid 5880: Impedance vs. Frequency, $g = 0.7$

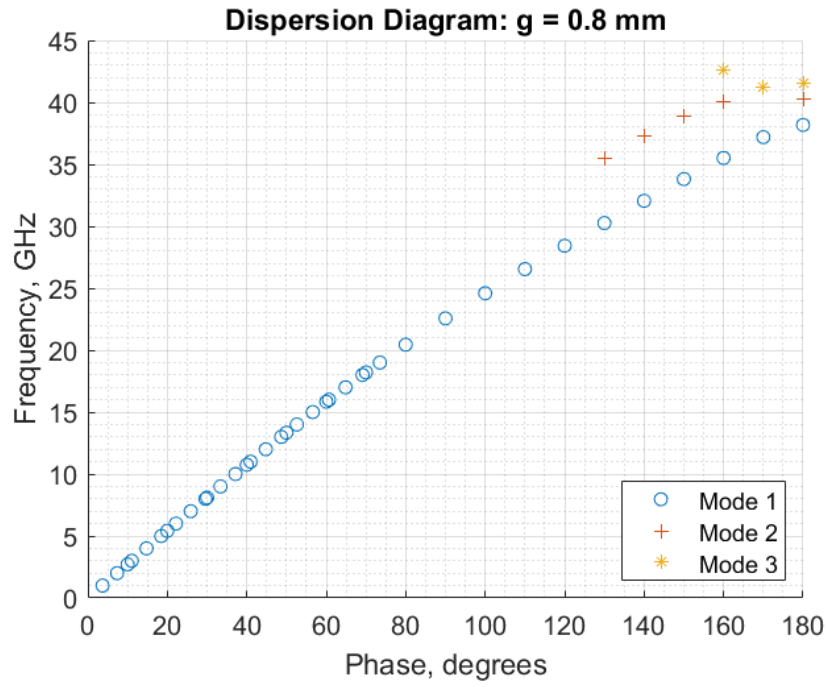


Figure 129: Square Duroid 5880: Dispersion Diagram, $g = 0.8$

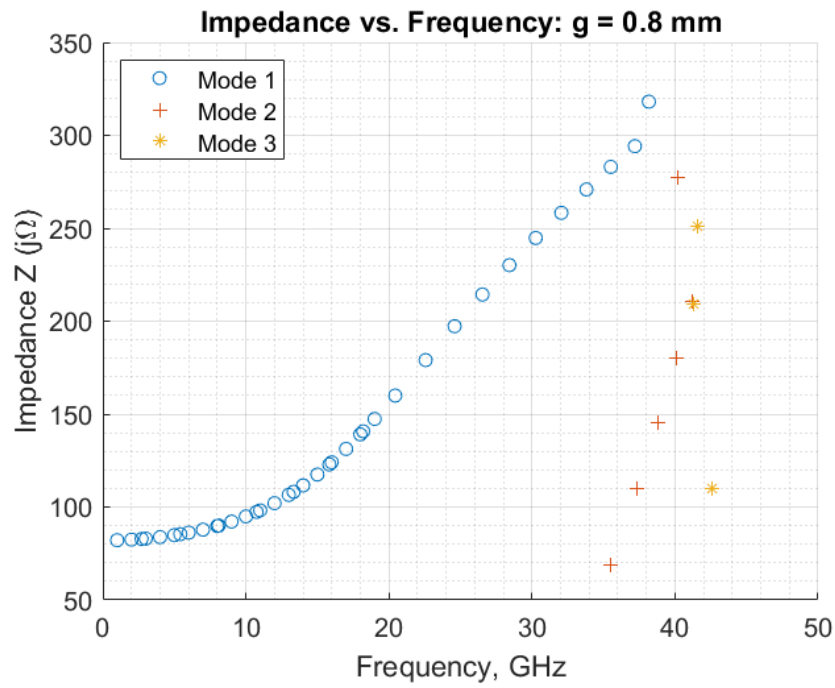


Figure 130: Square Duroid 5880: Impedance vs. Frequency, $g = 0.8$

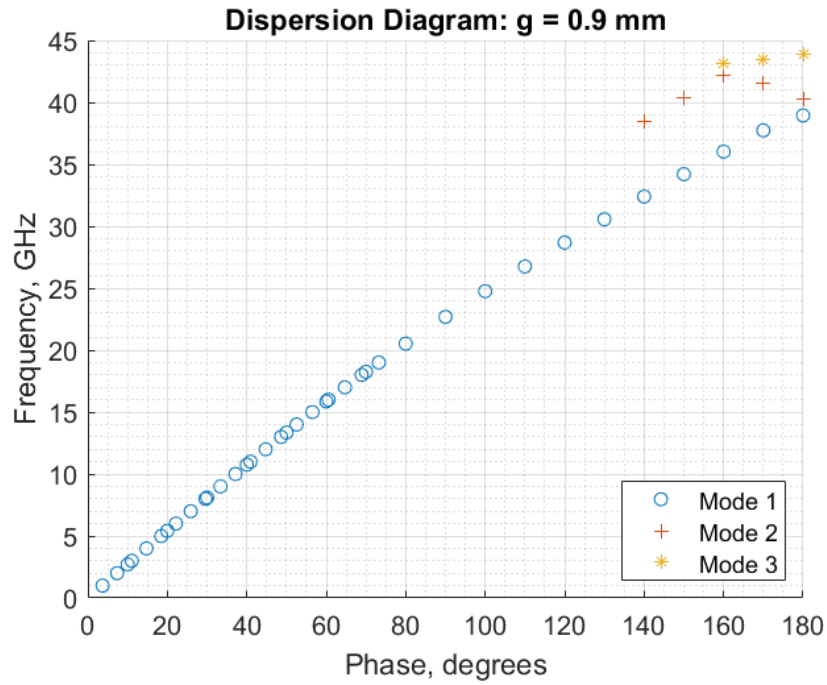


Figure 131: Square Duroid 5880: Dispersion Diagram, $g = 0.9$

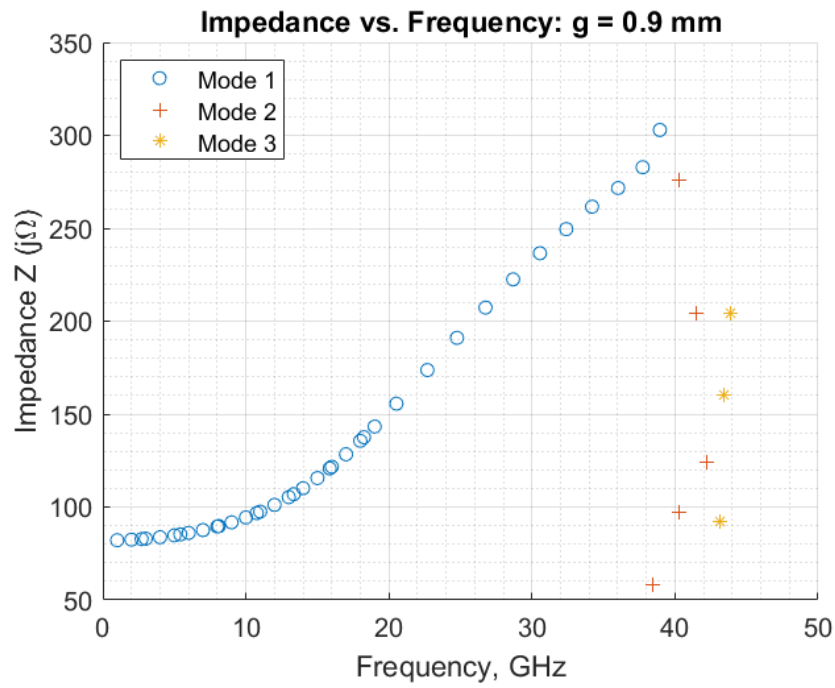


Figure 132: Square Duroid 5880: Impedance vs. Frequency, $g = 0.9$

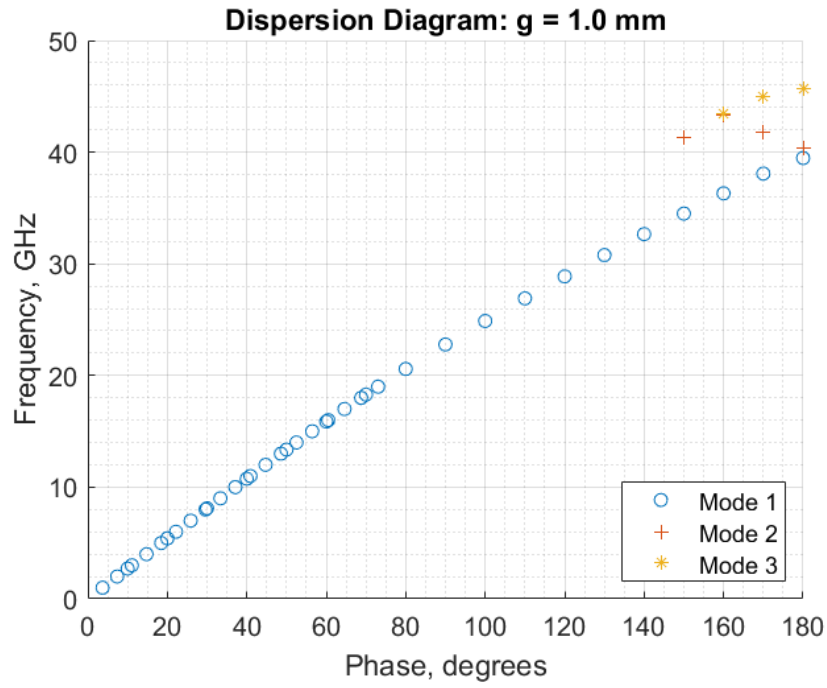


Figure 133: Square Duroid 5880: Dispersion Diagram, $g = 1.0$

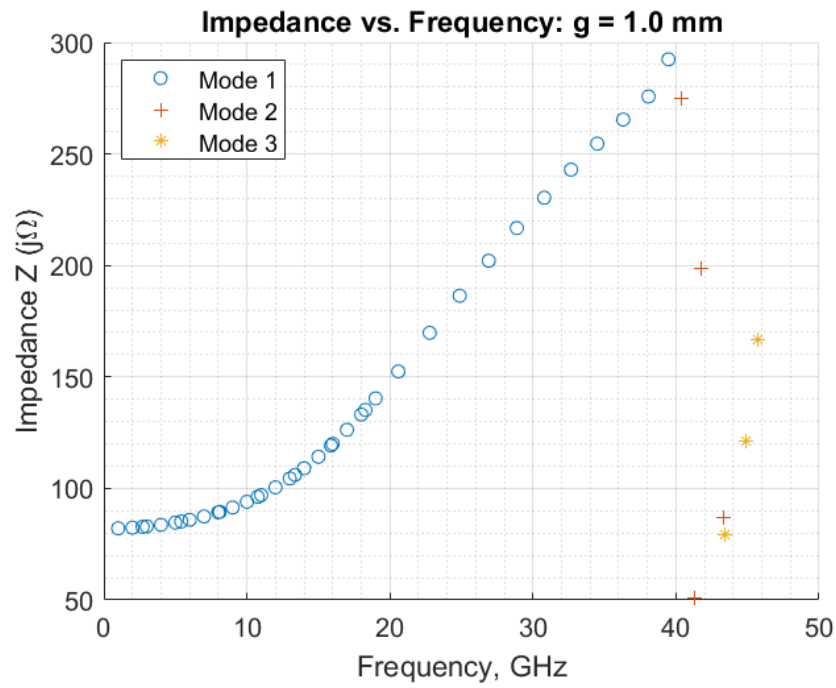


Figure 134: Square Duroid 5880: Impedance vs. Frequency, $g = 1.0$

Model: 1 GHz

Equation form: $y = c_0 + c_1x^1$

	<u>Coefficient</u>	<u>SE</u>	<u>tStat</u>	<u>pValue</u>
c_0 (intercept)	82.304	0.0086637	9499.9	3.7821×10^{-26}
c_1	-0.19302	0.013263	-14.553	1.7264×10^{-6}

Table 7: Square Duroid 5880: Model Coefficients, 1 GHz

Model Statistics

Error Degrees of Freedom: 7

Root Mean Squared Error (RMSE): 0.0103

R-squared: 0.968

Adjusted R-Squared: 0.963

F-statistic vs. constant model: 212

p-value = 1.73×10^{-6}

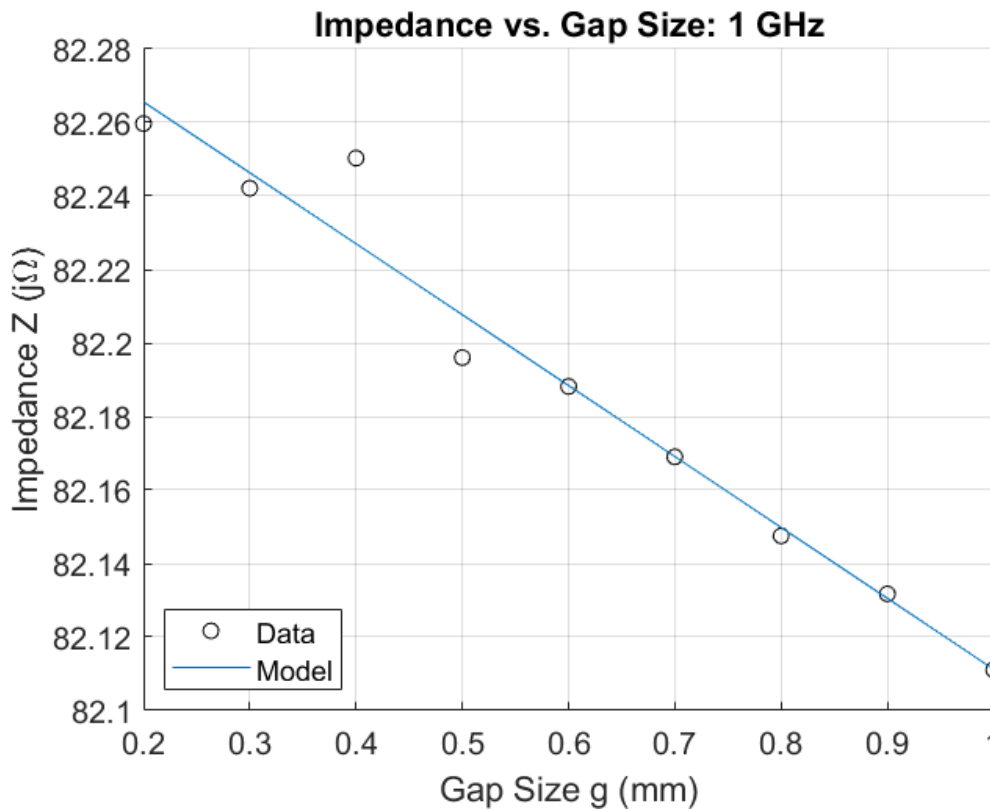


Figure 135: Square Duroid 5880: Impedance vs. Gap Size, 1 GHz

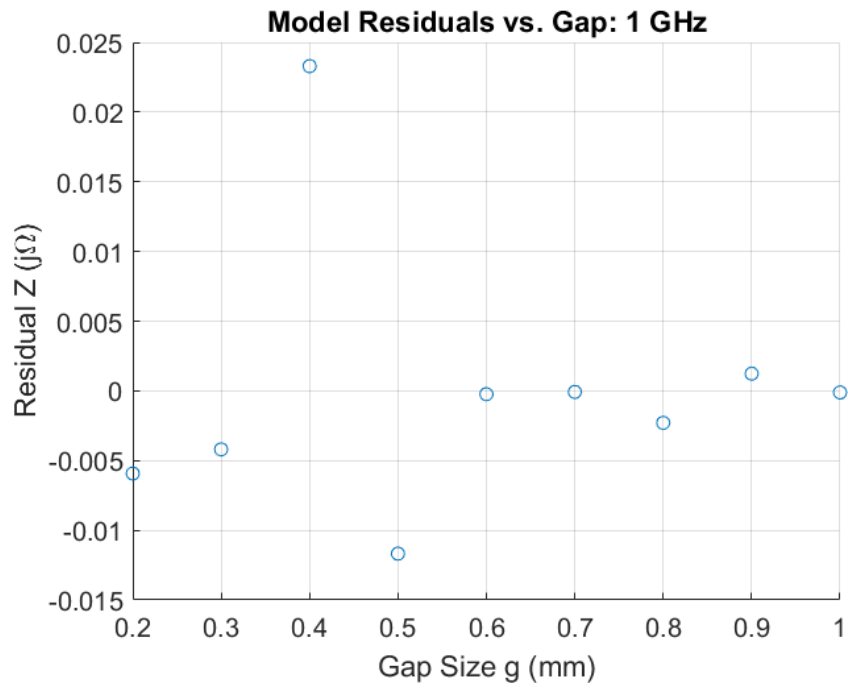


Figure 136: Square Duroid 5880: Residuals, 1 GHz

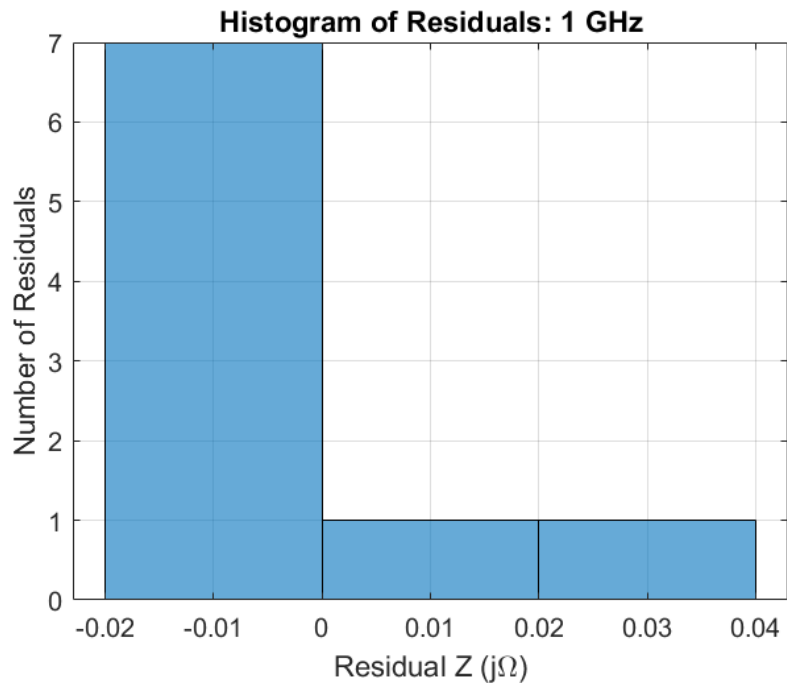


Figure 137: Square Duroid 5880: Histogram of Residuals, 1 GHz

Model: 2 GHz

Equation form: $y = c_0 + c_1x^1 + c_2x^2$

	<u>Coefficient</u>	<u>SE</u>	<u>tStat</u>	<u>pValue</u>
c_0 (intercept)	82.953	0.022376	3707.2	2.7106×10^{-17}
c_1	-0.88959	0.084953	-10.472	0.000137
c_2	0.36391	0.069084	5.2676	0.0032783

Table 8: Square Duroid 5880: Model Coefficients, 2 GHz

Model Statistics

Error Degrees of Freedom: 5
 Root Mean Squared Error (RMSE): 0.0114
 R-squared: 0.995
 Adjusted R-Squared: 0.993
 F-statistic vs. constant model: 472
 p-value = 2.01×10^{-6}

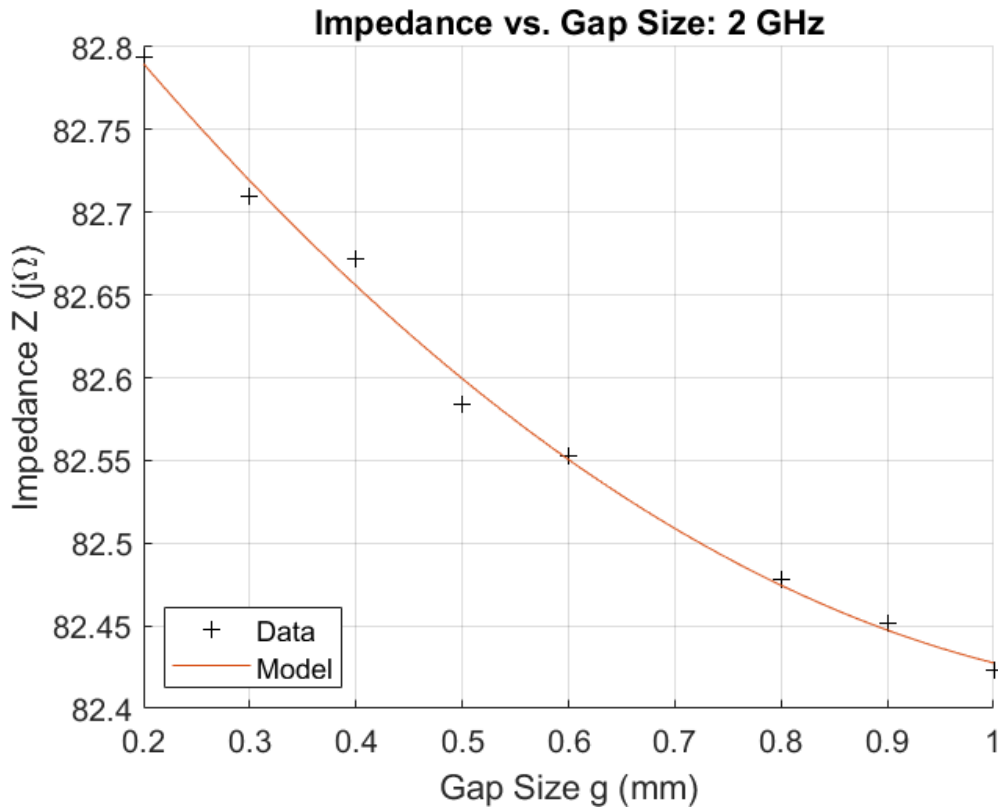


Figure 138: Square Duroid 5880: Impedance vs. Gap Size, 2 GHz

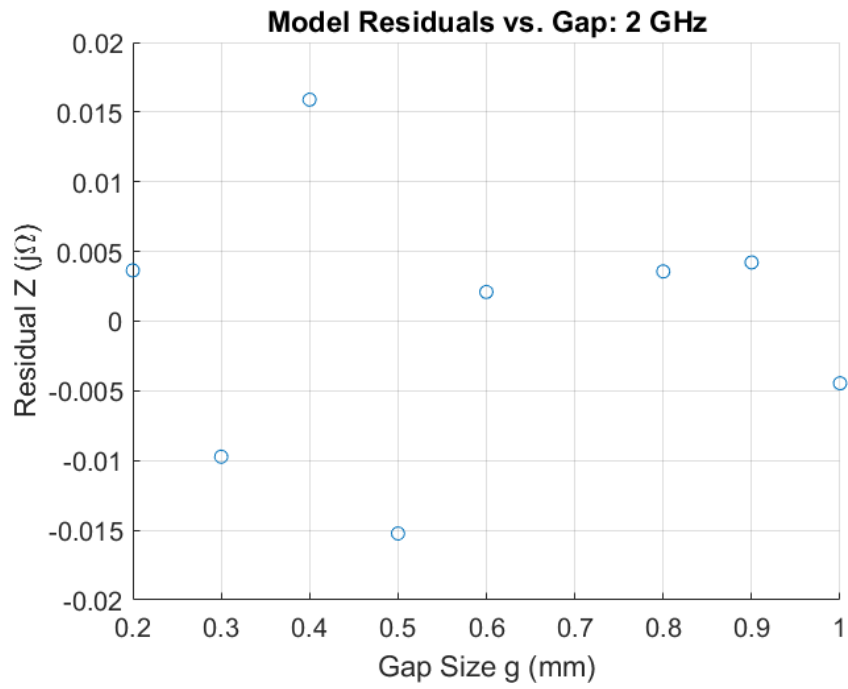


Figure 139: Square Duroid 5880: Residuals, 2 GHz

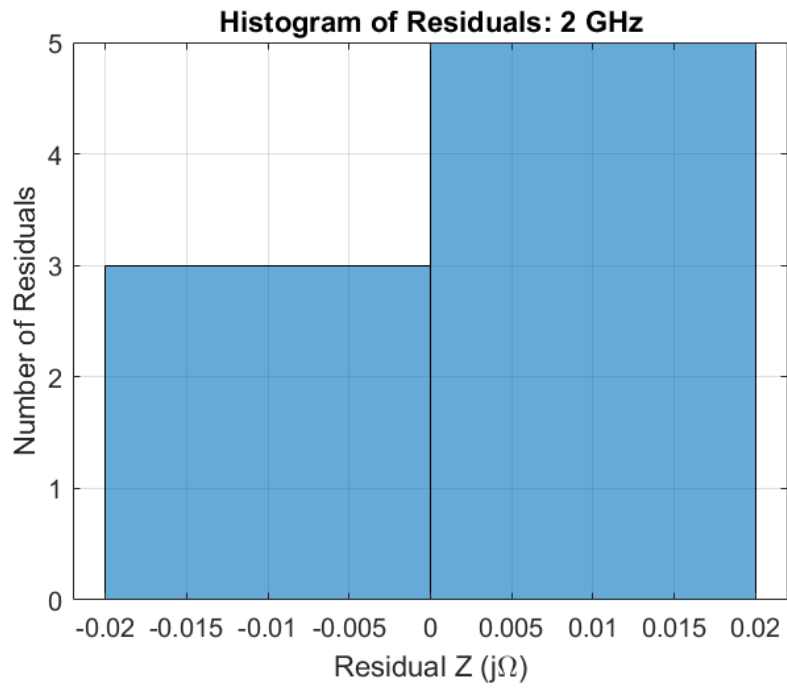


Figure 140: Square Duroid 5880: Histogram of Residuals, 2 GHz

Model: 3 GHz

Equation form: $y = c_0 + c_1 \frac{1}{x^1} + c_2 \frac{1}{x^2}$

	Coefficient	SE	tStat	pValue
c_0 (intercept)	82.599	0.022591	3656.3	2.825×10^{-20}
c_1	0.39393	0.019129	20.594	8.5286×10^{-07}
c_2	-0.034759	0.0032086	-10.833	3.6642×10^{-05}

Table 9: Square Duroid 5880: Model Coefficients: 3 GHz

Model Statistics

Error Degrees of Freedom: 6
 Root Mean Squared Error (RMSE): 0.0138
 R-squared: 0.998
 Adjusted R-Squared: 0.997
 F-statistic vs. constant model: 1350
 p-value = 1.08×10^{-8}

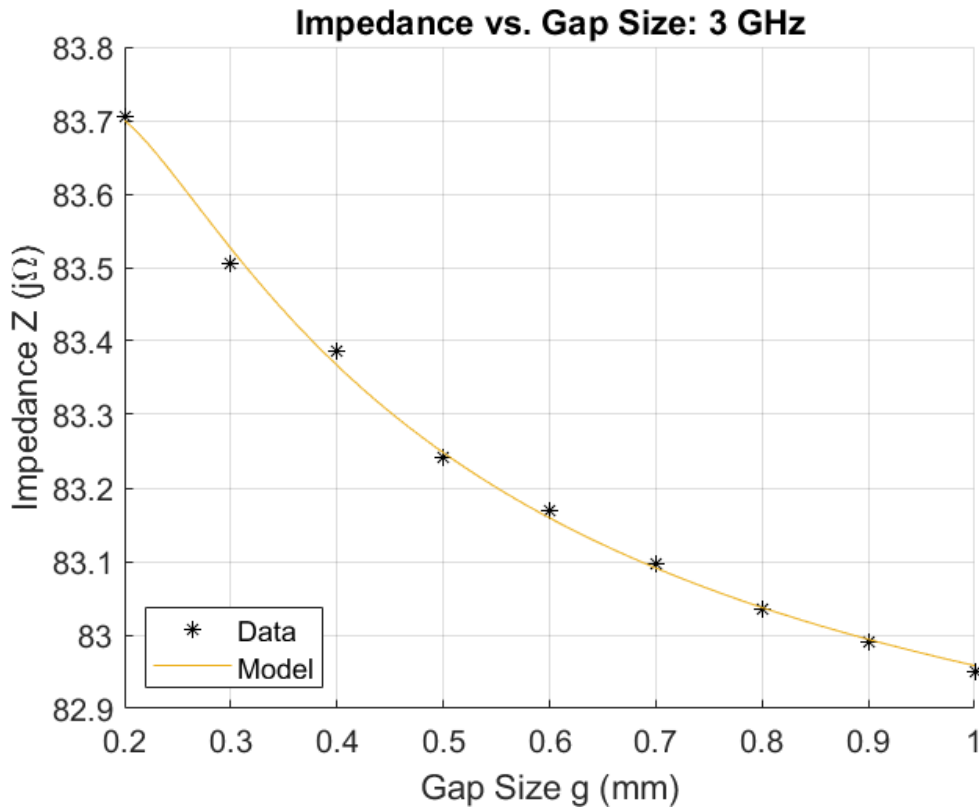


Figure 141: Square Duroid 5880: Impedance vs. Gap Size, 3 GHz

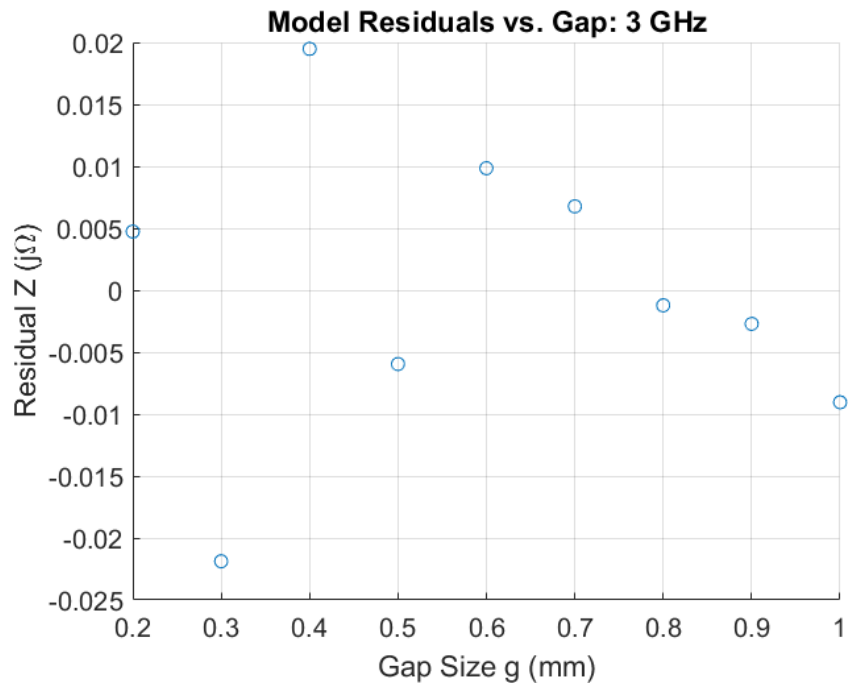


Figure 142: Square Duroid 5880: Residuals, 3 GHz

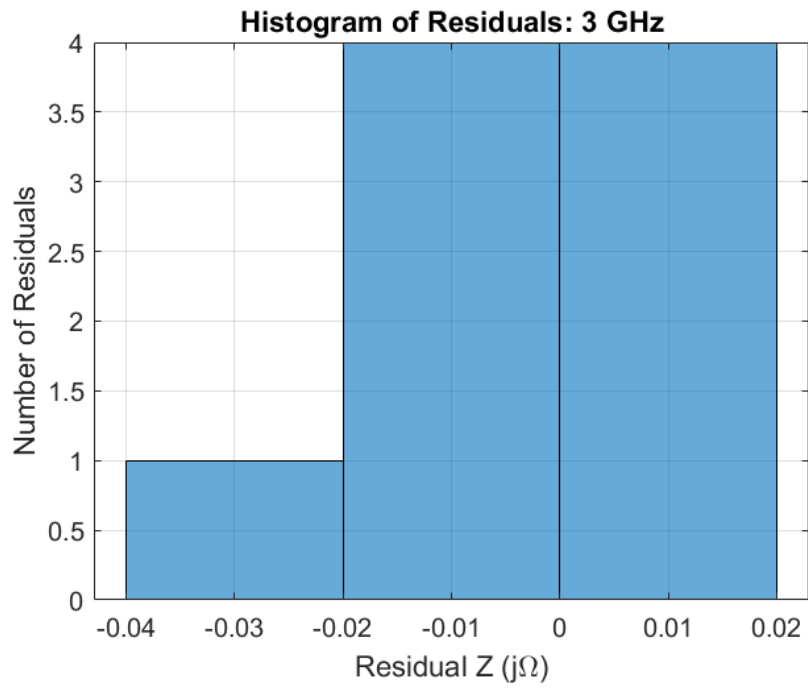


Figure 143: Square Duroid 5880: Histogram of Residuals, 3 GHz

Model: 4 GHz

Equation form: $y = c_0 + c_1 \frac{1}{x^1} + c_2 \frac{1}{x^2}$

	Coefficient	SE	tStat	pValue
c_0 (intercept)	83.118	0.023585	3524.2	3.5232×10^{-20}
c_1	0.64026	0.01997	20.594	6.1214×10^{-08}
c_2	-0.051864	0.0033498	-10.833	4.5923×10^{-06}

Table 10: Square Duroid 5880: Model Coefficients: 4 GHz

Model Statistics

Error Degrees of Freedom: 6
 Root Mean Squared Error (RMSE): 0.0144
 R-squared: 0.999
 Adjusted R-Squared: 0.999
 F-statistic vs. constant model: 3830
 p-value = 4.8×10^{-10}

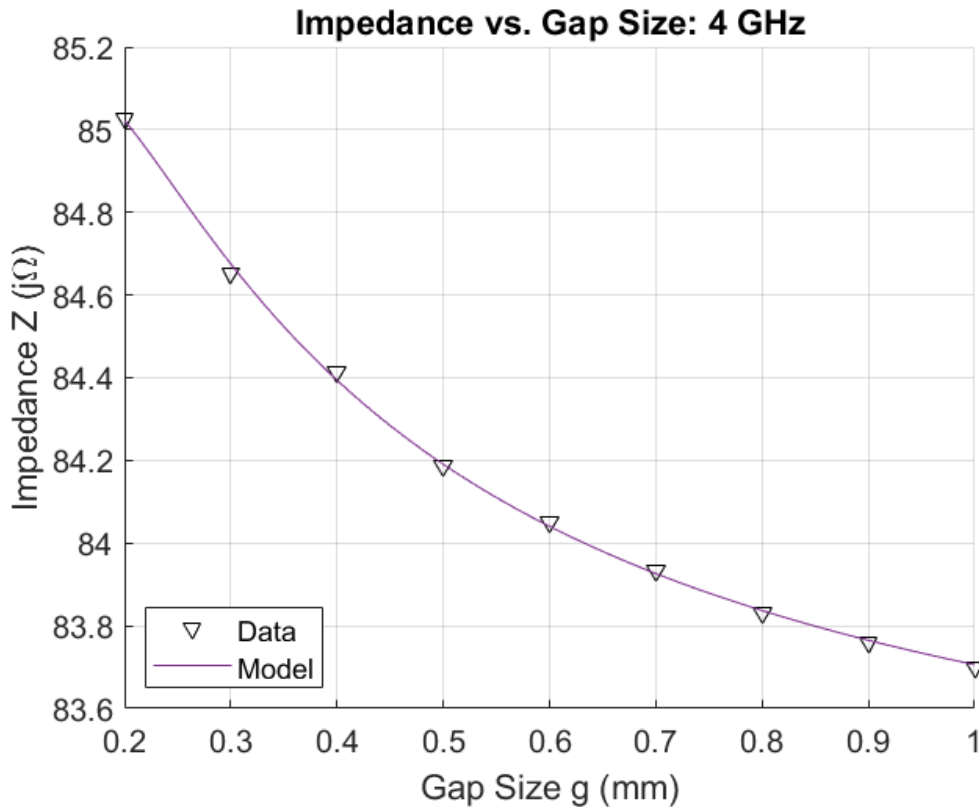


Figure 144: Square Duroid 5880: Impedance vs. Gap Size, 4 GHz

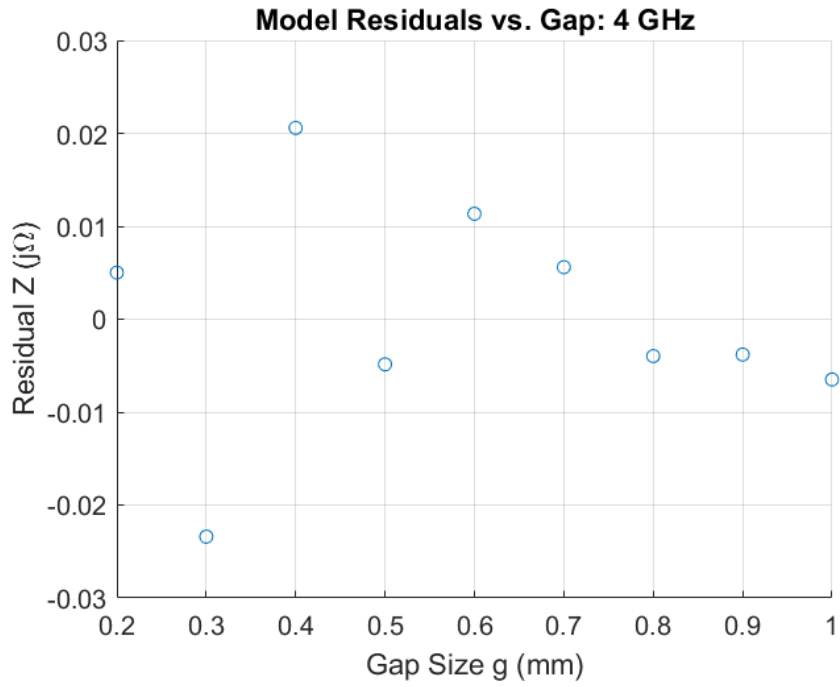


Figure 145: Square Duroid 5880: Residuals, 4 GHz

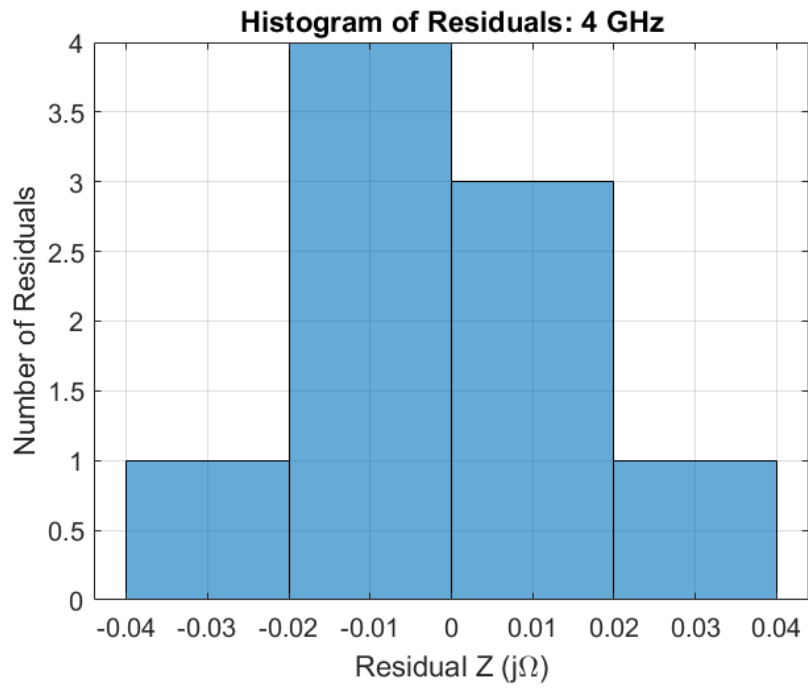


Figure 146: Square Duroid 5880: Histogram of Residuals, 4 GHz

Model: 5 GHz

Equation form: $y = c_0 + c_1 \frac{1}{x^1} + c_2 \frac{1}{x^2}$

	<u>Coefficient</u>	<u>SE</u>	<u>tStat</u>	<u>pValue</u>
c_0 (intercept)	83.787	0.025125	3334.8	4.9078×10^{-20}
c_1	0.97756	0.021275	45.95	7.1182×10^{-09}
c_2	-0.074666	0.0035686	-20.923	7.7632×10^{-07}

Table 11: Square Duroid 5880: Model Coefficients: 5 GHz

Model Statistics

Error Degrees of Freedom: 6

Root Mean Squared Error (RMSE): 0.0154

R-squared: 1

Adjusted R-Squared: 1

F-statistic vs. constant model: 8640

p-value = 4.18×10^{-11}

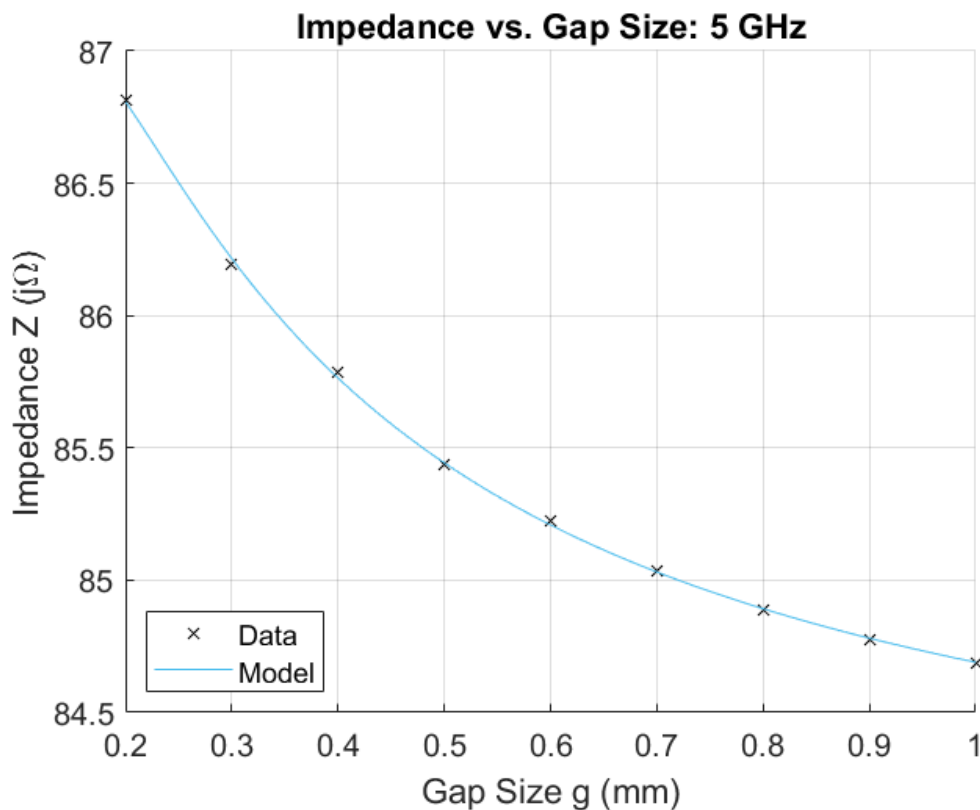


Figure 147: Square Duroid 5880: Impedance vs. Gap Size, 5 GHz

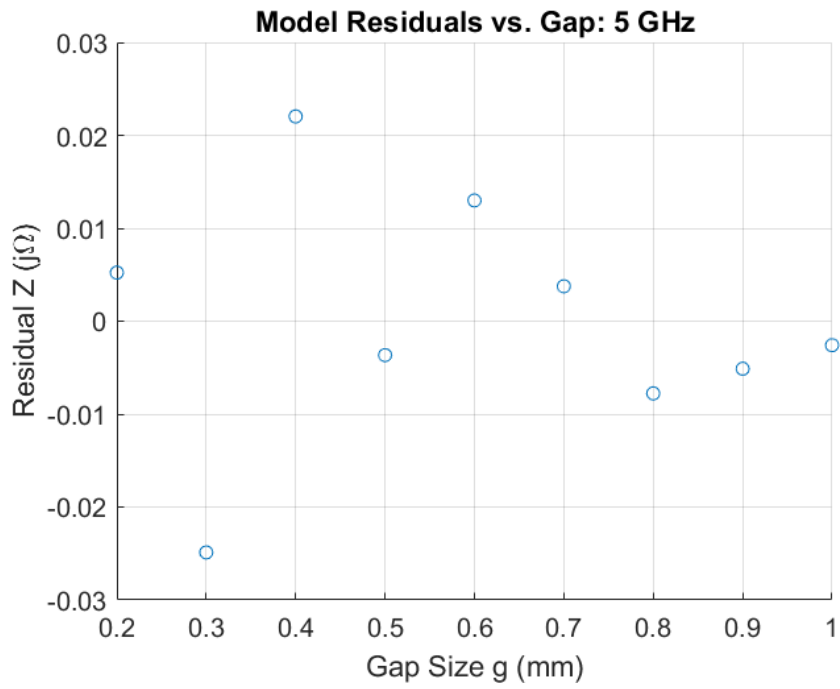


Figure 148: Square Duroid 5880: Residuals, 5 GHz

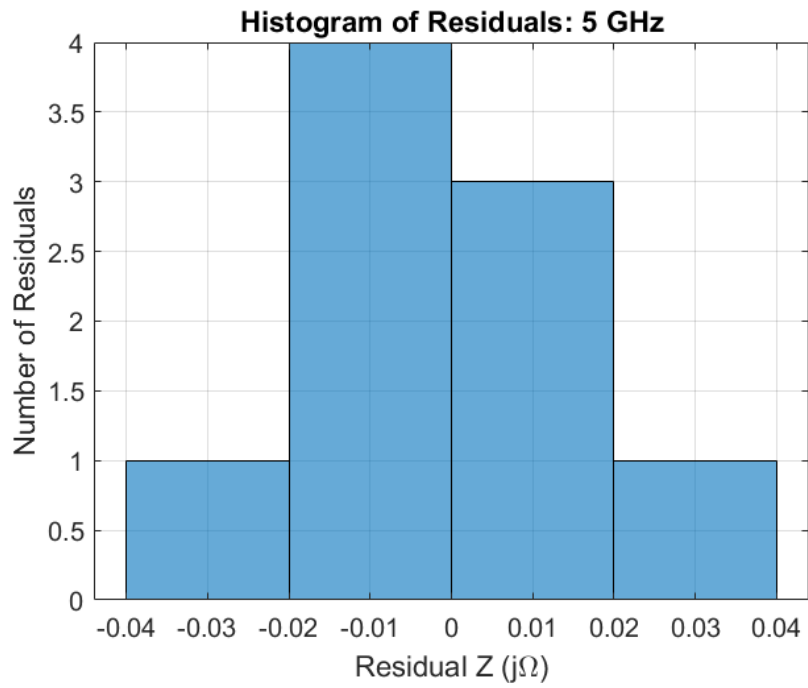


Figure 149: Square Duroid 5880: Histogram of Residuals, 5 GHz

Model: 6 GHz

Equation form: $y = c_0 + c_1 \frac{1}{x^1} + c_2 \frac{1}{x^2}$

	<u>Coefficient</u>	<u>SE</u>	<u>tStat</u>	<u>pValue</u>
c_0 (intercept)	84.608	0.027526	3073.7	8.0044×10^{-20}
c_1	1.4233	0.023308	61.065	1.2963×10^{-09}
c_2	-0.1037	0.0039097	-26.524	1.8956×10^{-07}

Table 12: Square Duroid 5880: Model Coefficients: 6 GHz

Model Statistics

Error Degrees of Freedom: 6

Root Mean Squared Error (RMSE): 0.0169

R-squared: 1

Adjusted R-Squared: 1

F-statistic vs. constant model: 16400

p-value = 6.17×10^{-12}

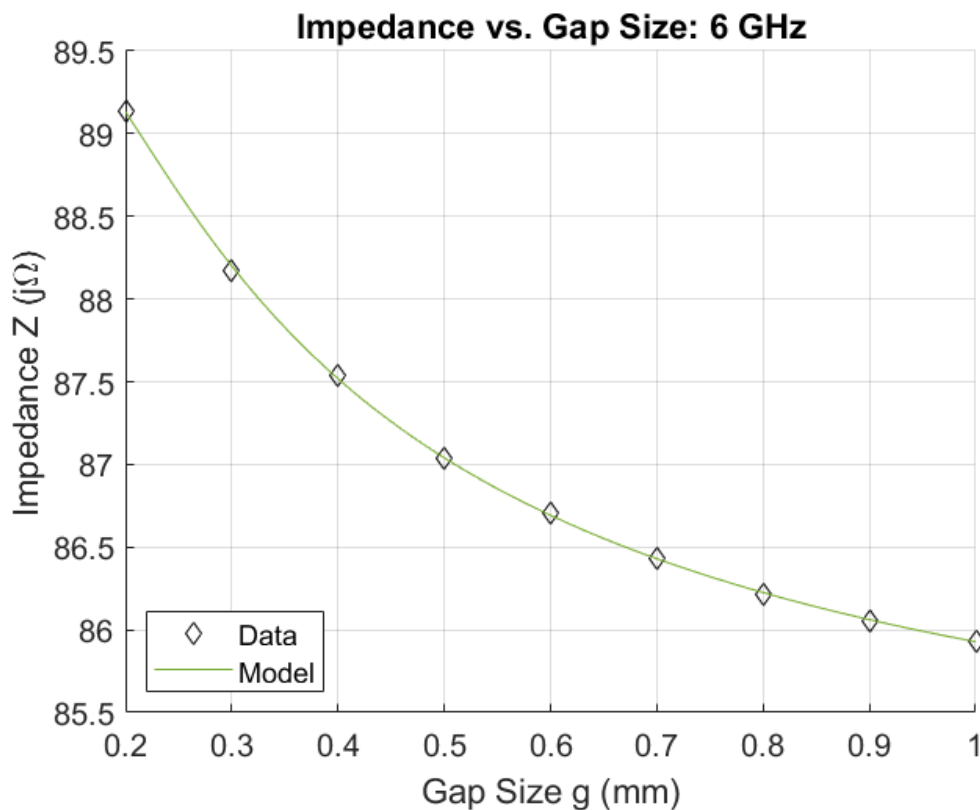


Figure 150: Square Duroid 5880: Impedance vs. Gap Size, 6 GHz

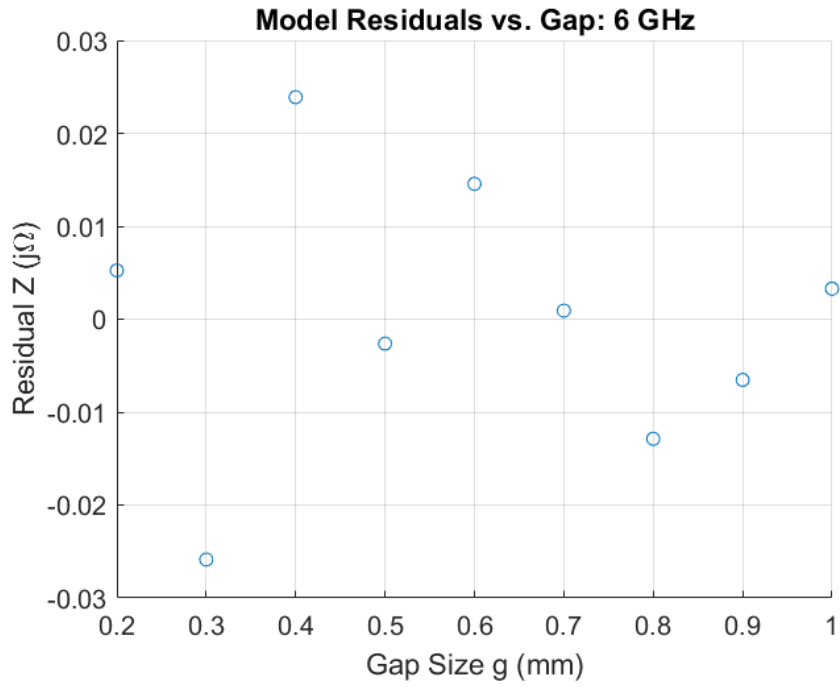


Figure 151: Square Duroid 5880: Residuals, 6 GHz

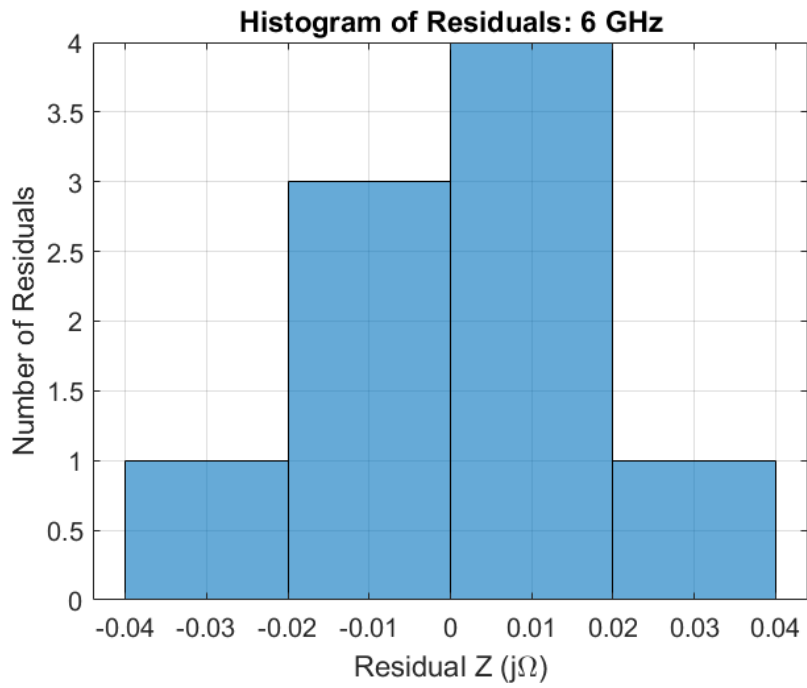


Figure 152: Square Duroid 5880: Histogram of Residuals, 6 GHz

Model: 7 GHz

Equation form: $y = c_0 + c_1 \frac{1}{x^1} + c_2 \frac{1}{x^2}$

	<u>Coefficient</u>	<u>SE</u>	<u>tStat</u>	<u>pValue</u>
c_0 (intercept)	85.582	0.031221	2741.2	1.5911×10^{-19}
c_1	2.0006	0.026436	75.676	3.584×10^{-10}
c_2	-0.13944	0.0044344	-31.445	6.872×10^{-08}

Table 13: Square Duroid 5880: Model Coefficients: 7 GHz

Model Statistics

Error Degrees of Freedom: 6
 Root Mean Squared Error (RMSE): 0.0191
 R-squared: 1
 Adjusted R-Squared: 1
 F-statistic vs. constant model: 26700
 p-value = 1.42×10^{-12}

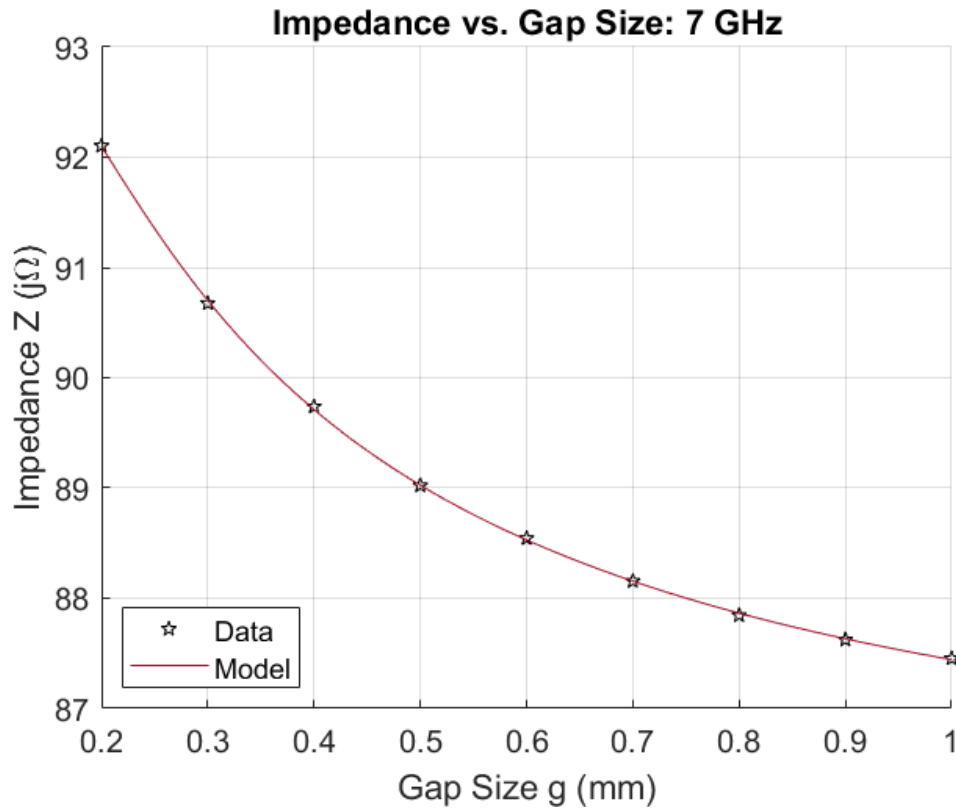


Figure 153: Square Duroid 5880: Impedance vs. Gap Size, 7 GHz

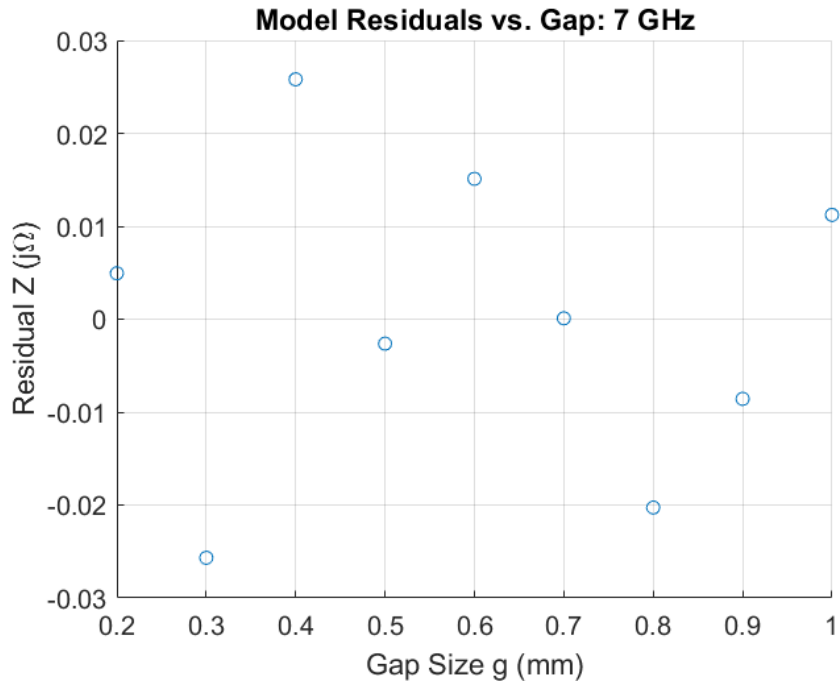


Figure 154: Square Duroid 5880: Residuals, 7 GHz

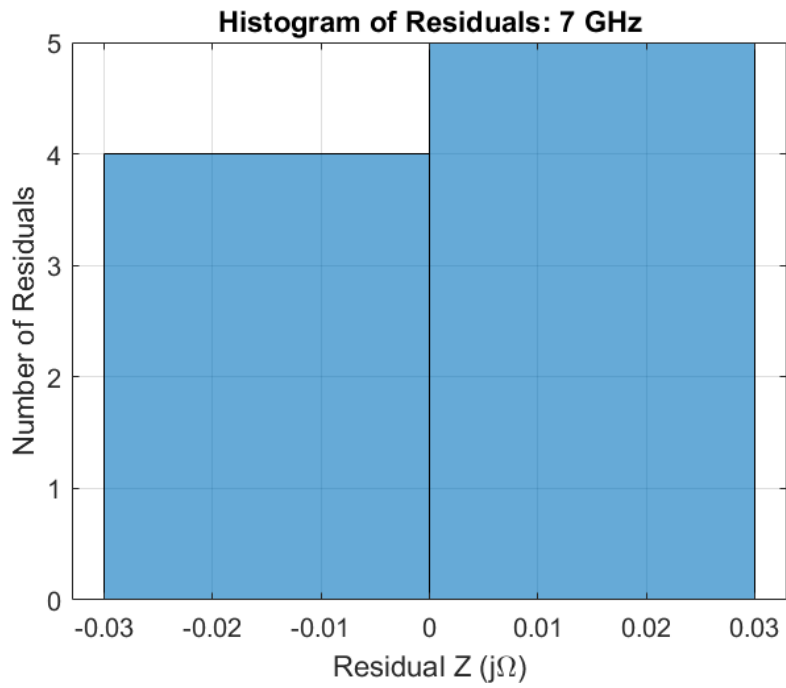


Figure 155: Square Duroid 5880: Histogram of Residuals, 7 GHz

Model: 8 GHz

Equation form: $y = c_0 + c_1 \frac{1}{x^1} + c_2 \frac{1}{x^2}$

	<u>Coefficient</u>	<u>SE</u>	<u>tStat</u>	<u>pValue</u>
c_0 (intercept)	86.705	0.035767	2424.1	3.3263×10^{-19}
c_1	2.7398	0.030286	90.463	1.2293×10^{-10}
c_2	-0.18205	0.0050802	-35.836	3.1484×10^{-08}

Table 14: Square Duroid 5880: Model Coefficients: 8 GHz

Model Statistics

Error Degrees of Freedom: 6

Root Mean Squared Error (RMSE): 0.0219

R-squared: 1

Adjusted R-Squared: 1

F-statistic vs. constant model: 40500

p-value = 4.07×10^{-13}

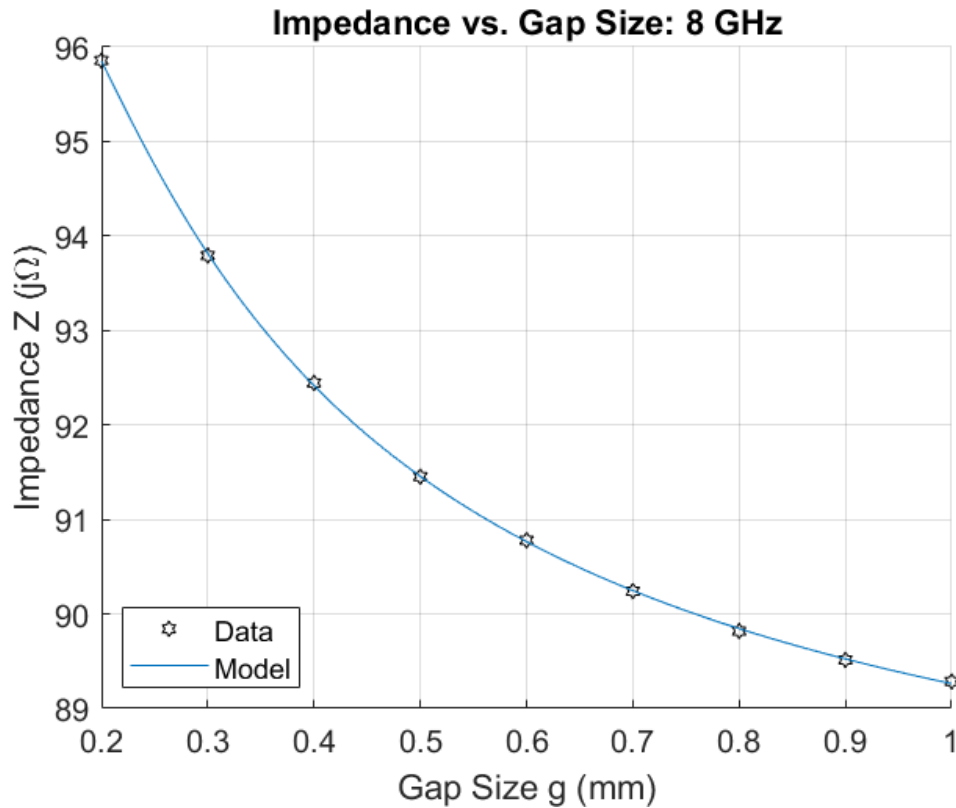


Figure 156: Square Duroid 5880: Impedance vs. Gap Size, 8 GHz

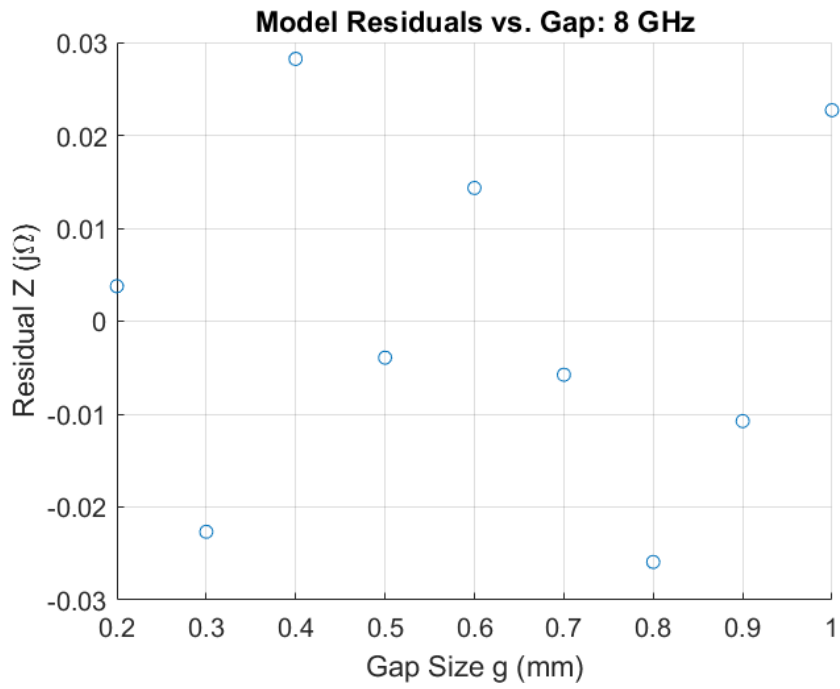


Figure 157: Square Duroid 5880: Residuals, 8 GHz

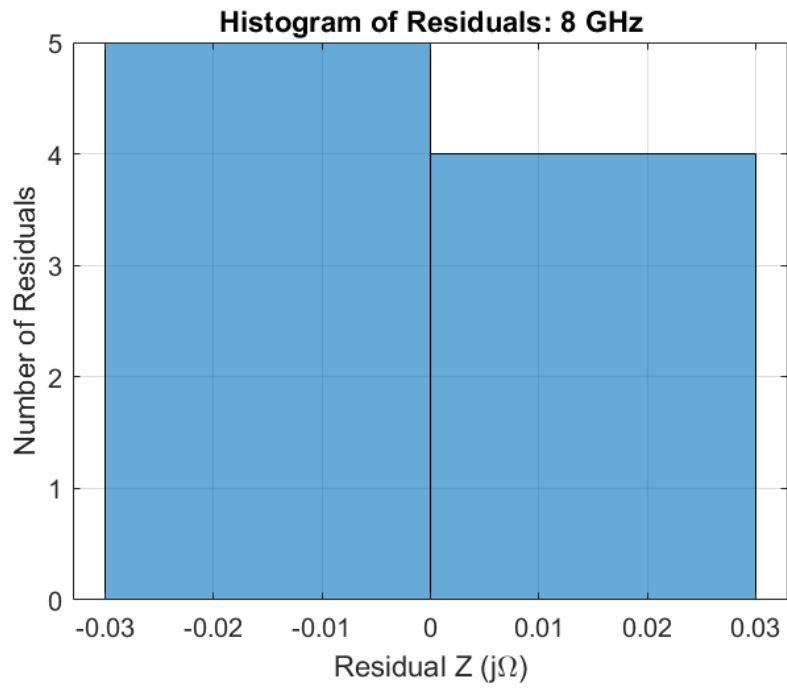


Figure 158: Square Duroid 5880: Histogram of Residuals, 8 GHz

Model: 9 GHz

Equation form: $y = c_0 + c_1 \frac{1}{x^1} + c_2 \frac{1}{x^2}$

	<u>Coefficient</u>	<u>SE</u>	<u>tStat</u>	<u>pValue</u>
c_0 (intercept)	87.971	0.045528	1932.3	1.2969×10^{-18}
c_1	3.6807	0.03855	95.478	8.8948×10^{-11}
c_2	-0.23131	0.0064664	-35.771	3.1825×10^{-08}

Table 15: Square Duroid 5880: Model Coefficients: 9 GHz

Model Statistics

Error Degrees of Freedom: 6

Root Mean Squared Error (RMSE): 0.0279

R-squared: 1

Adjusted R-Squared: 1

F-statistic vs. constant model: 48100

p-value = 2.42×10^{-13}

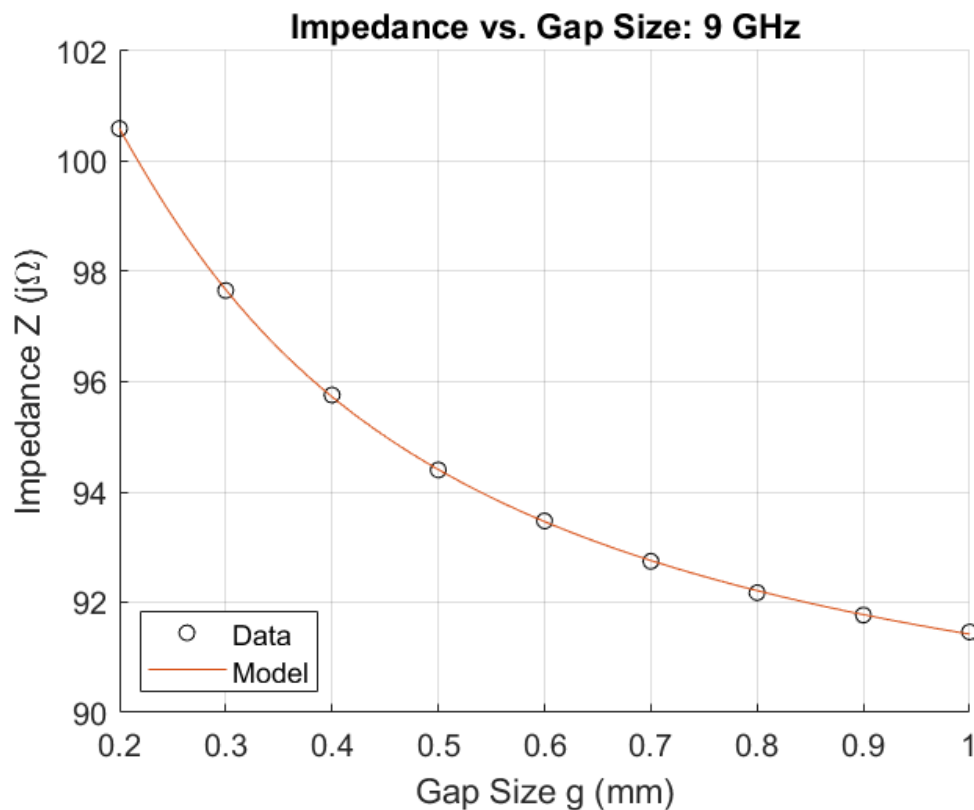


Figure 159: Square Duroid 5880: Impedance vs. Gap Size, 9 GHz

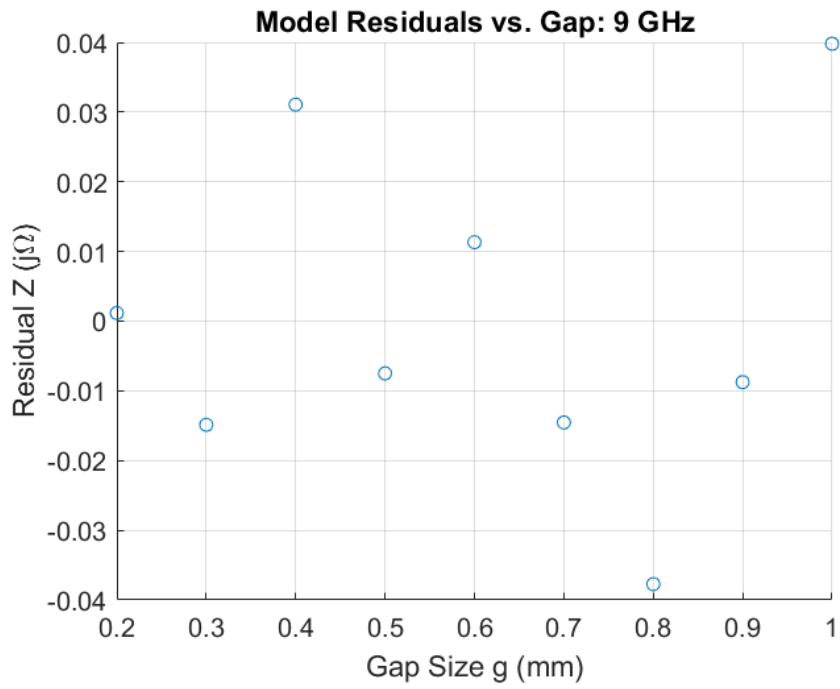


Figure 160: Square Duroid 5880: Residuals, 9 GHz

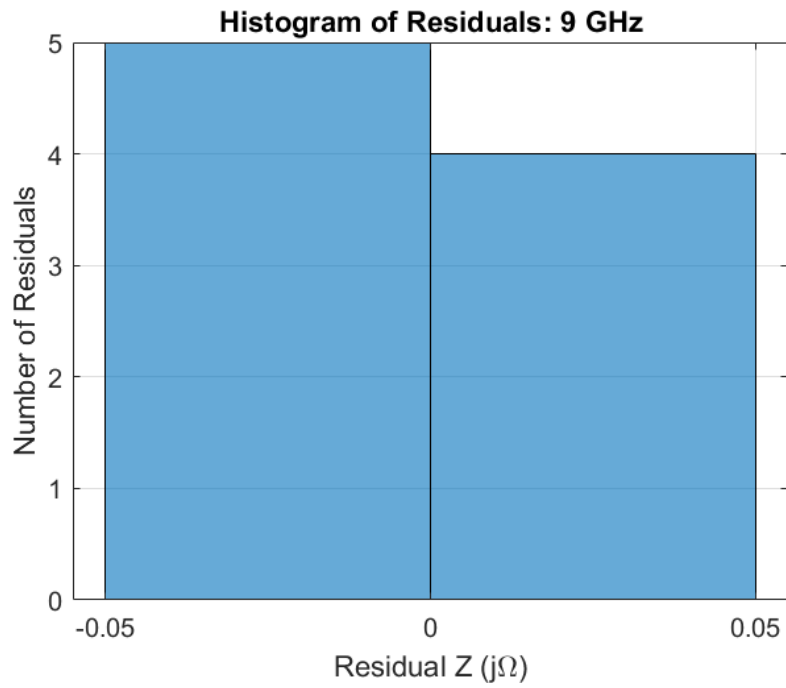


Figure 161: Square Duroid 5880: Histogram of Residuals, 9 GHz

Model: 10 GHz

Equation form: $y = c_0 + c_1 \frac{1}{x^1} + c_2 \frac{1}{x^2}$

	<u>Coefficient</u>	<u>SE</u>	<u>tStat</u>	<u>pValue</u>
c_0 (intercept)	89.364	0.064241	1391.1	9.3148×10^{-18}
c_1	4.8752	0.054396	89.625	1.2998×10^{-10}
c_2	-0.28634	0.0091243	-31.383	6.9542×10^{-08}

Table 16: Square Duroid 5880: Model Coefficients: 10 GHz

Model Statistics

Error Degrees of Freedom: 6
 Root Mean Squared Error (RMSE): 0.0394
 R-squared: 1
 Adjusted R-Squared: 1
 F-statistic vs. constant model: 45600
 p-value = 2.85×10^{-13}

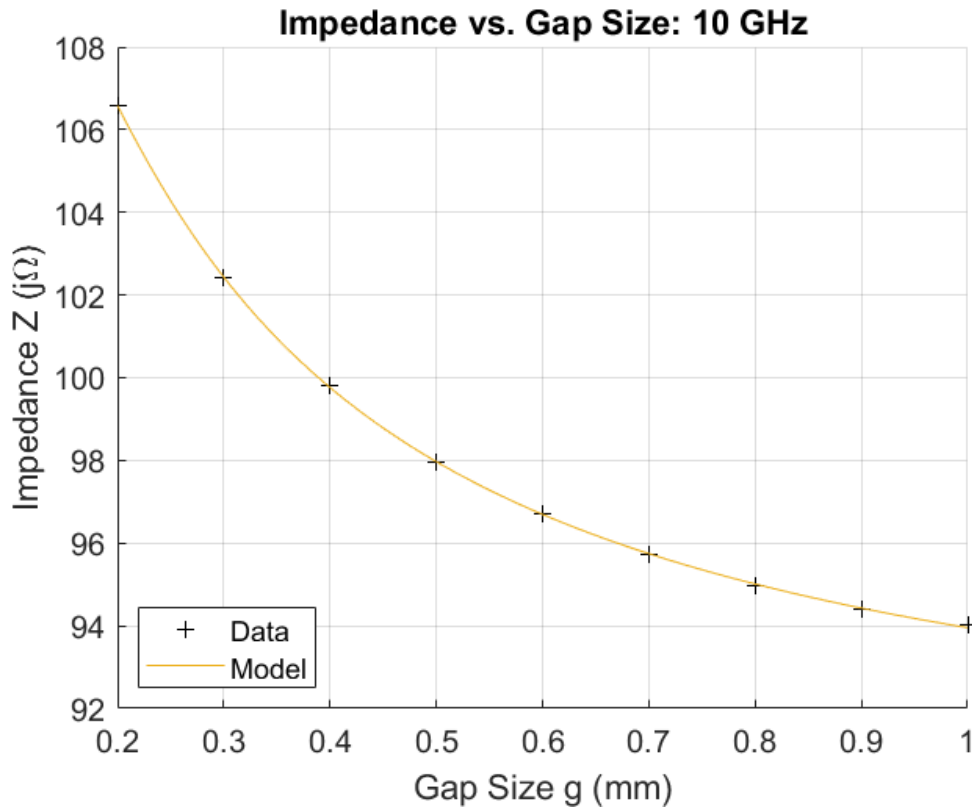


Figure 162: Square Duroid 5880: Impedance vs. Gap Size, 10 GHz

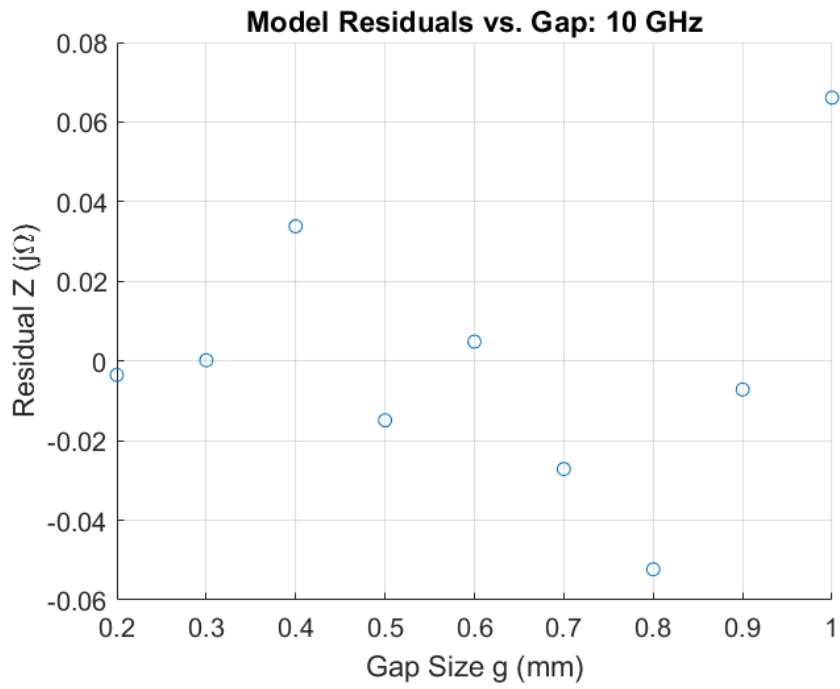


Figure 163: Square Duroid 5880: Residuals, 10 GHz

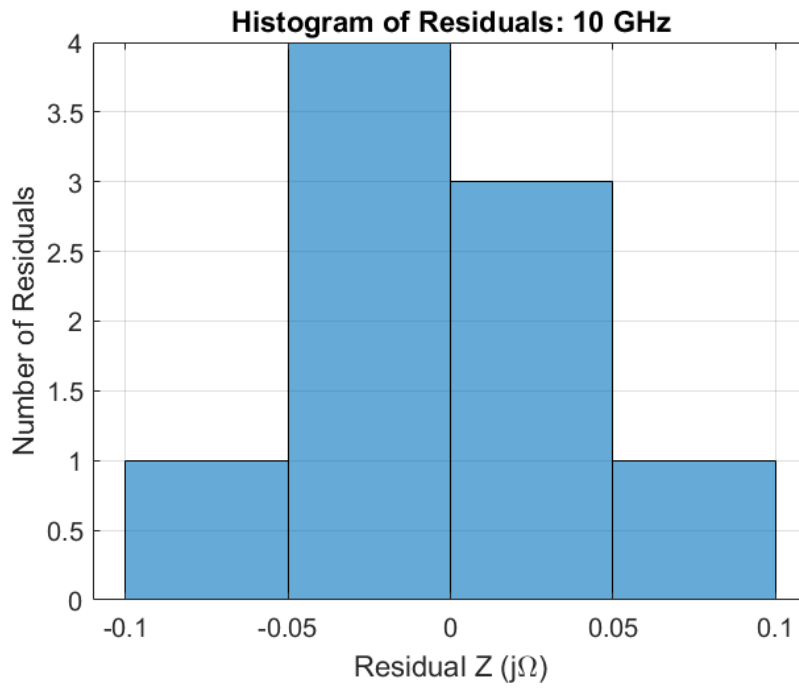


Figure 164: Square Duroid 5880: Histogram of Residuals, 10 GHz

Model: 11 GHz

Equation form: $y = c_0 + c_1 \frac{1}{x^1} + c_2 \frac{1}{x^2}$

	<u>Coefficient</u>	<u>SE</u>	<u>tStat</u>	<u>pValue</u>
c_0 (intercept)	90.864	0.096963	937.11	9.967×10^{-17}
c_1	6.3847	0.082103	77.764	3.0444×10^{-10}
c_2	-0.34499	0.013772	-25.05	2.6642×10^{-07}

Table 17: Square Duroid 5880: Model Coefficients: 11 GHz

Model Statistics

Error Degrees of Freedom: 6
 Root Mean Squared Error (RMSE): 0.0594
 R-squared: 1
 Adjusted R-Squared: 1
 F-statistic vs. constant model: 37200
 p-value = 5.26×10^{-13}

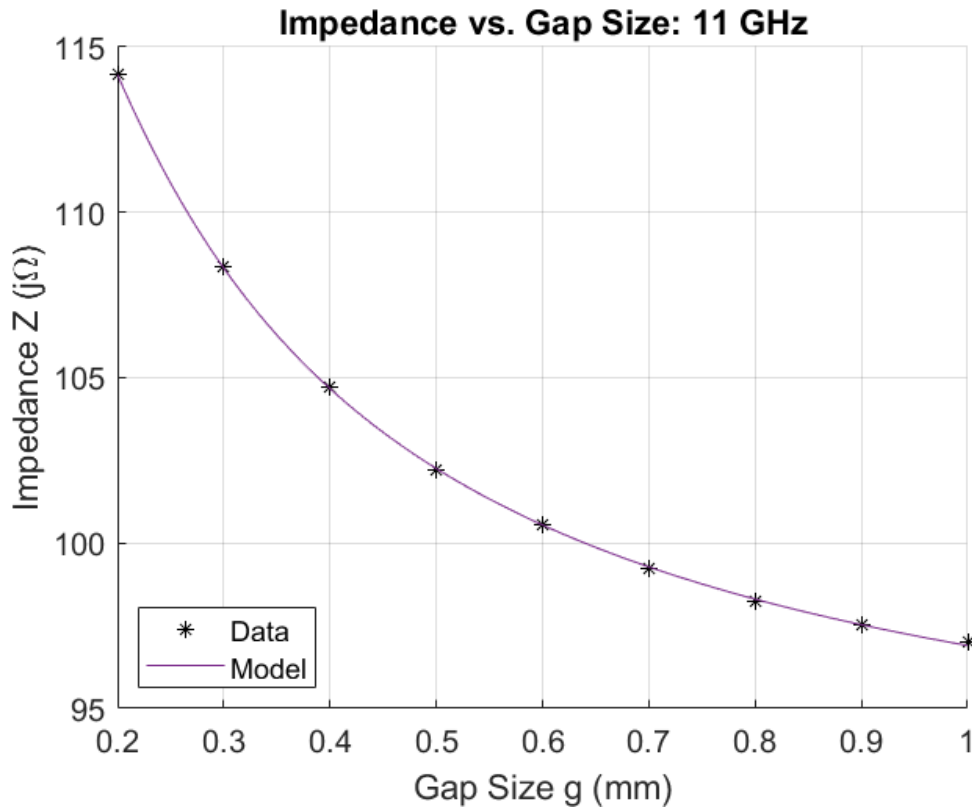


Figure 165: Square Duroid 5880: Impedance vs. Gap Size, 11 GHz

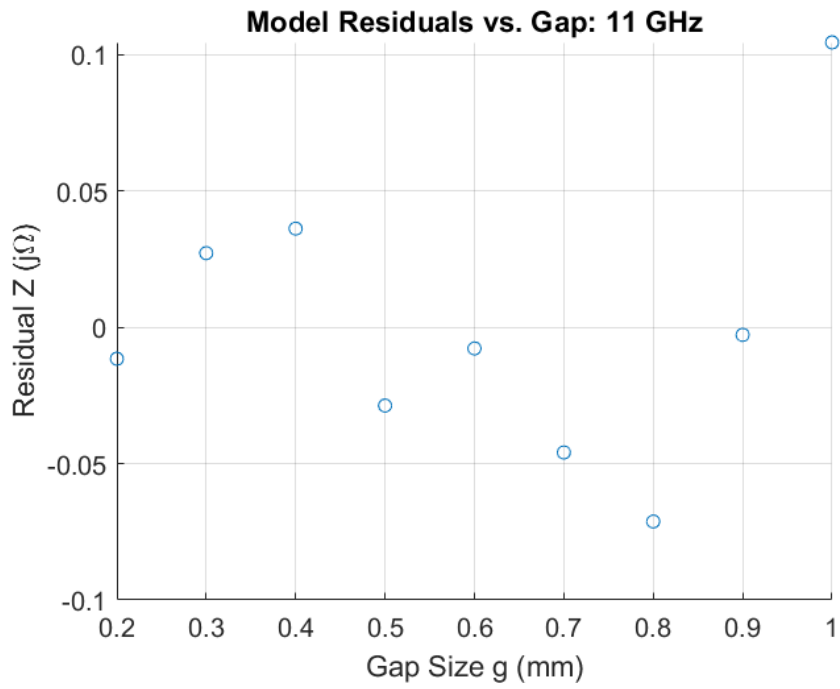


Figure 166: Square Duroid 5880: Residuals, 11 GHz

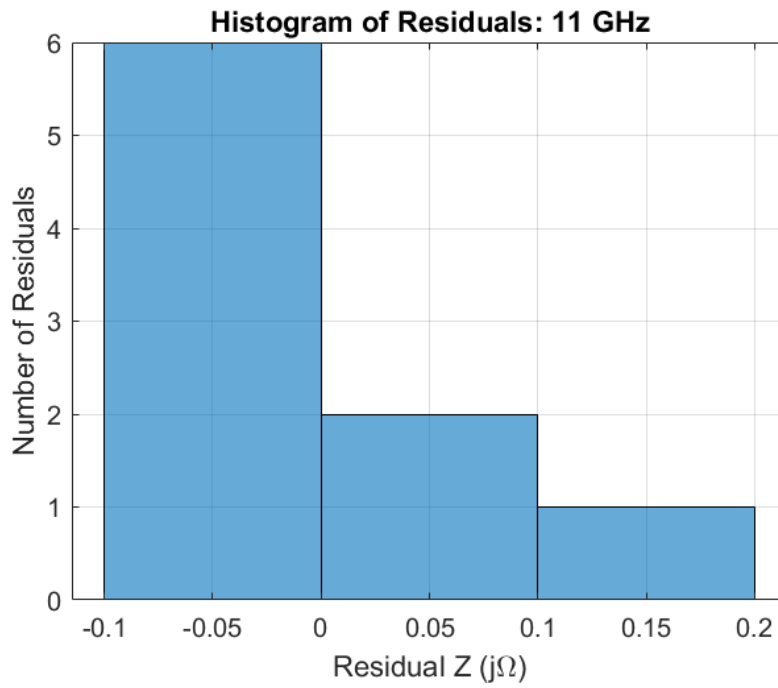


Figure 167: Square Duroid 5880: Histogram of Residuals, 11 GHz

Model: 12 GHz

Equation form: $y = c_0 + c_1 \frac{1}{x^1} + c_2 \frac{1}{x^2} + c_3 \frac{1}{x^3}$

	<u>Coefficient</u>	<u>SE</u>	<u>tStat</u>	<u>pValue</u>
c_0 (intercept)	93.145	0.32359	287.85	9.6031×10^{-12}
c_1	7.2958	0.4339	16.814	1.3601×10^{-5}
c_2	-0.012769	0.16819	-0.075921	0.94243
c_3	-0.044843	0.019081	-2.3501	0.065549

Table 18: Square Duroid 5880: Model Coefficients: 12 GHz

Model Statistics

Error Degrees of Freedom: 5
 Root Mean Squared Error (RMSE): 0.0698
 R-squared: 1
 Adjusted R-Squared: 1
 F-statistic vs. constant model: 32900
 p-value = 3.73×10^{-11}

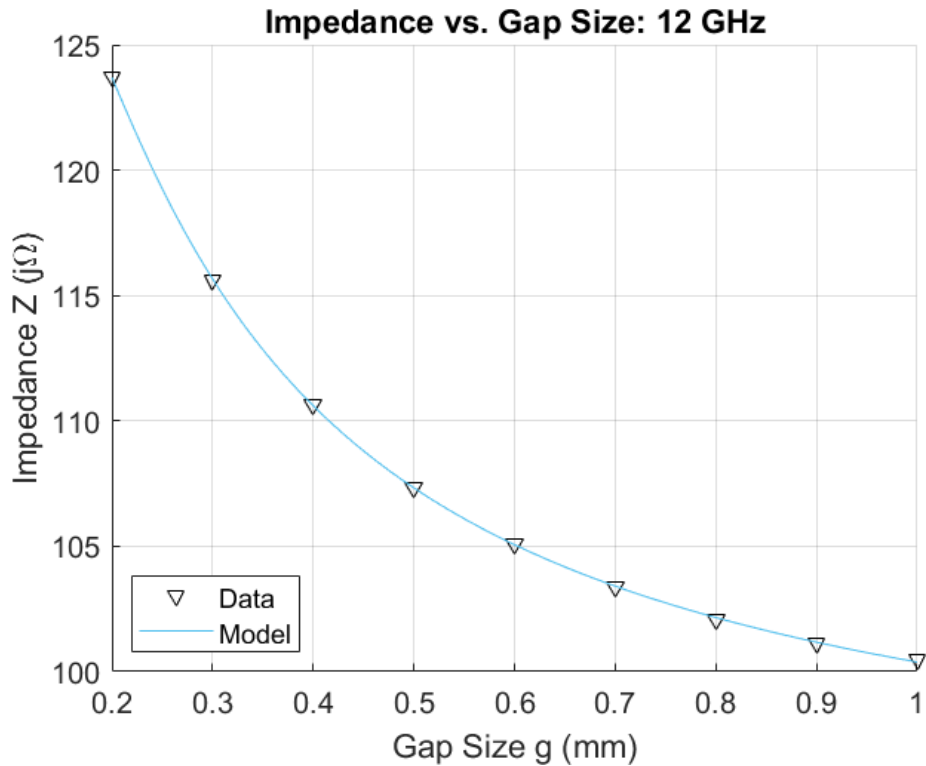


Figure 168: Square Duroid 5880: Impedance vs. Gap Size, 12 GHz

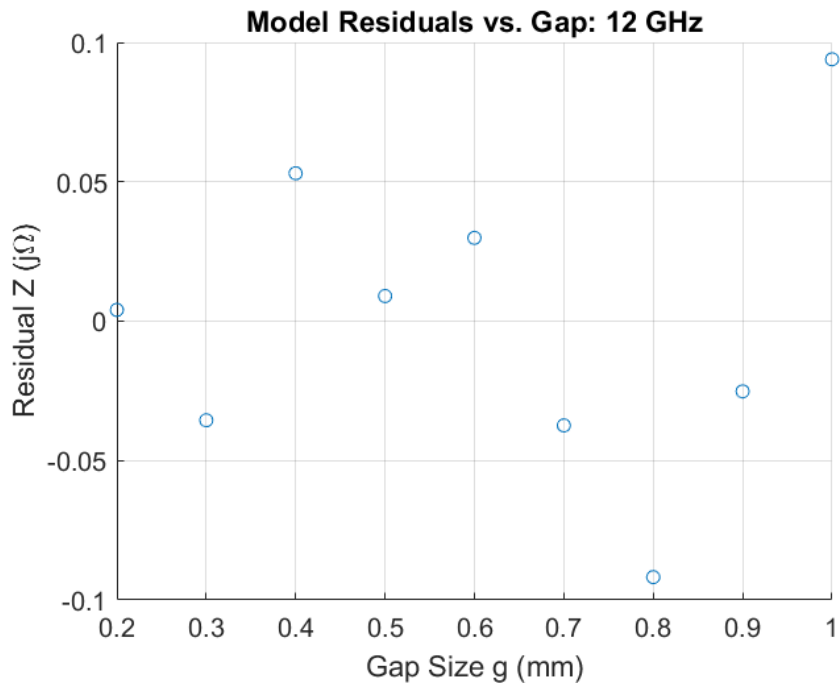


Figure 169: Square Duroid 5880: Residuals, 12 GHz

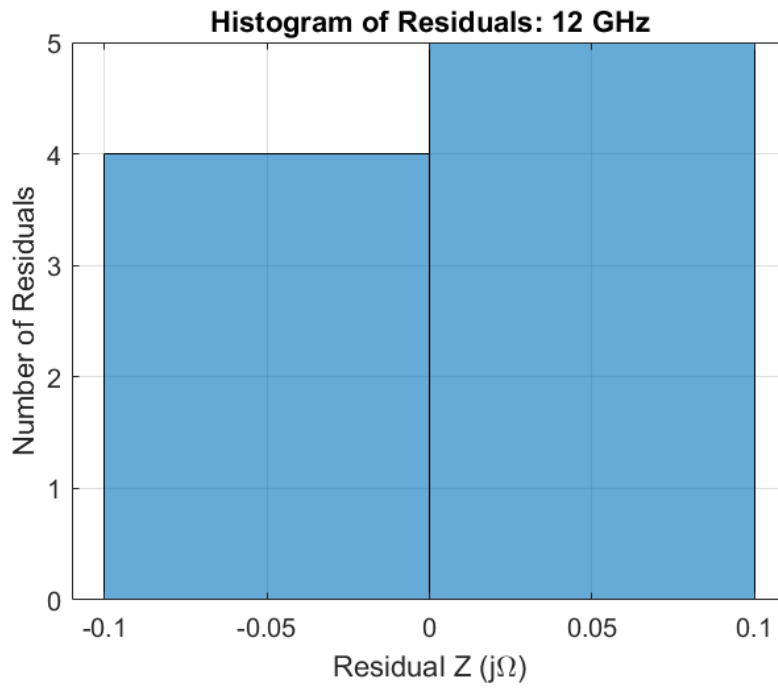


Figure 170: Square Duroid 5880: Histogram of Residuals, 12 GHz

Model: 13 GHz

Equation form: $y = c_0 + c_1 \frac{1}{x^1} + c_2 \frac{1}{x^2} + c_3 \frac{1}{x^3}$

	<u>Coefficient</u>	<u>SE</u>	<u>tStat</u>	<u>pValue</u>
c_0 (intercept)	95.267	0.42176	225.88	3.2271×10^{-11}
c_1	8.9427	0.56553	15.813	1.84×10^{-5}
c_2	0.22115	0.21921	1.0088	0.35935
c_3	-0.079475	0.02487	-3.1956	0.024113

Table 19: Square Duroid 5880: Model Coefficients: 13 GHz

Model Statistics

Error Degrees of Freedom: 5
 Root Mean Squared Error (RMSE): 0.091
 R-squared: 1
 Adjusted R-Squared: 1
 F-statistic vs. constant model: 34600
 p-value = 3.27×10^{-11}

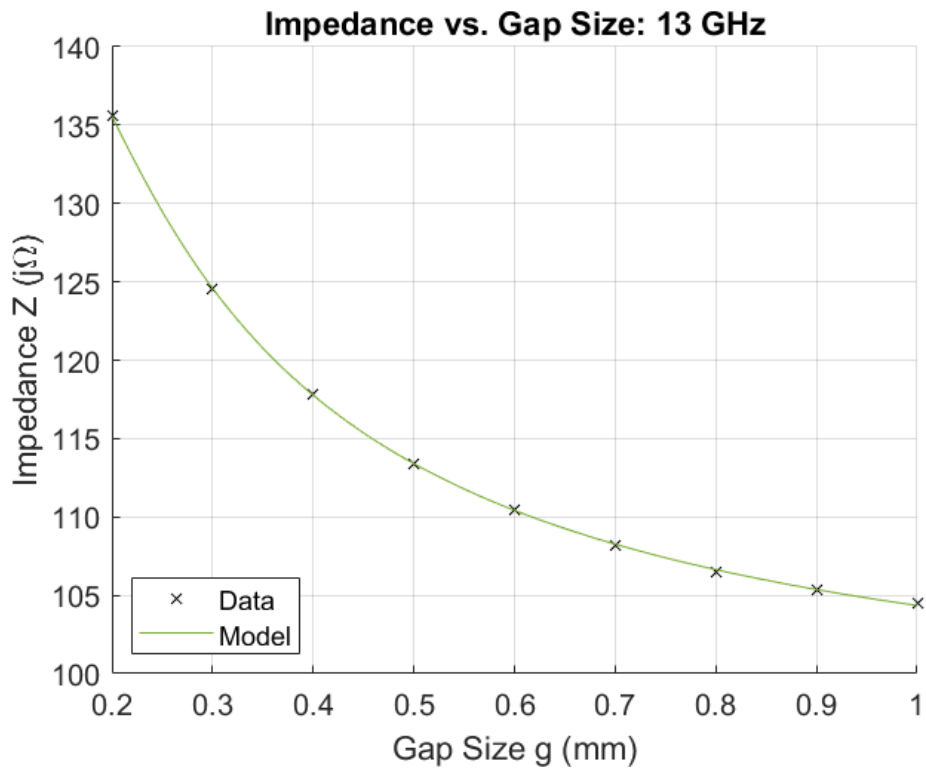


Figure 171: Square Duroid 5880: Impedance vs. Gap Size, 13 GHz

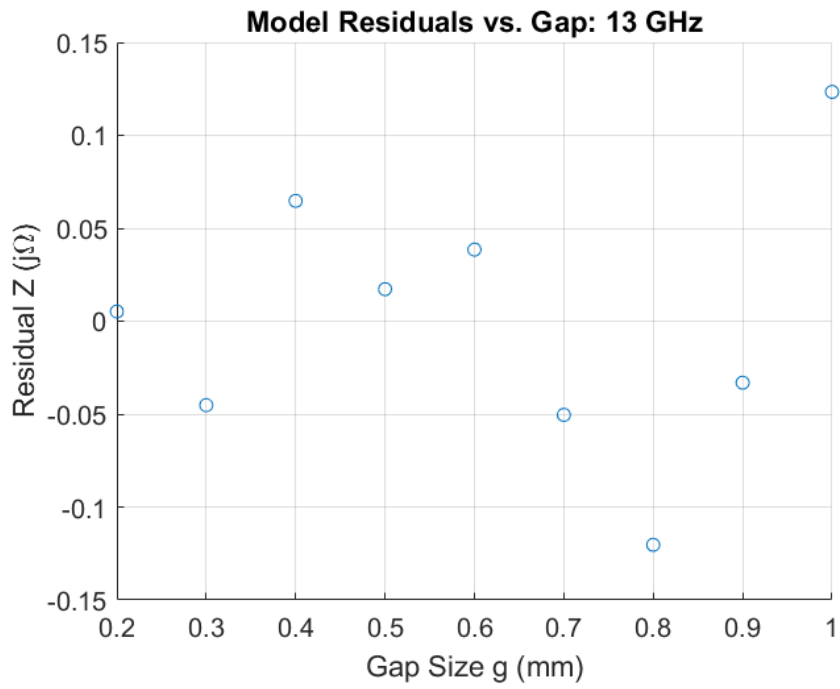


Figure 172: Square Duroid 5880: Residuals, 13 GHz

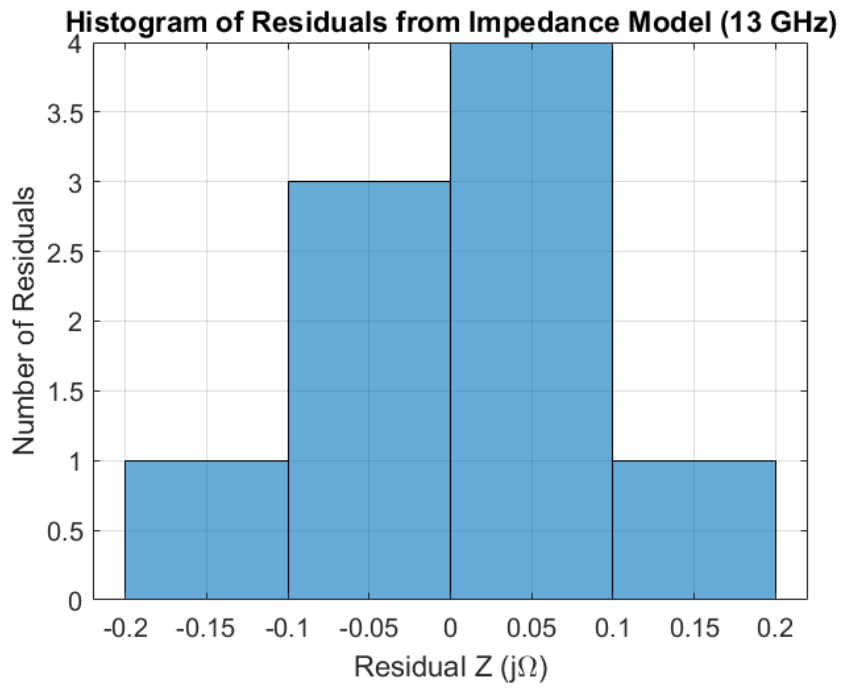


Figure 173: Square Duroid 5880: Histogram of Residuals, 13 GHz

Model: 14 GHz

Equation form: $y = c_0 + c_1 \frac{1}{x^1} + c_2 \frac{1}{x^2} + c_3 \frac{1}{x^3}$

	Coefficient	SE	tStat	pValue
c_0 (intercept)	97.573	0.54877	177.8	1.0677×10^{-10}
c_1	10.86	0.73584	14.758	2.5821×10^{-5}
c_2	0.58198	0.28523	2.0404	0.09682
c_3	-0.13239	0.032359	-4.0912	0.0094357

Table 20: Square Duroid 5880: Model Coefficients: 14 GHz

Model Statistics

Error Degrees of Freedom: 5
 Root Mean Squared Error (RMSE): 0.118
 R-squared: 1
 Adjusted R-Squared: 1
 F-statistic vs. constant model: 35300
 p-value = 3.12×10^{-11}

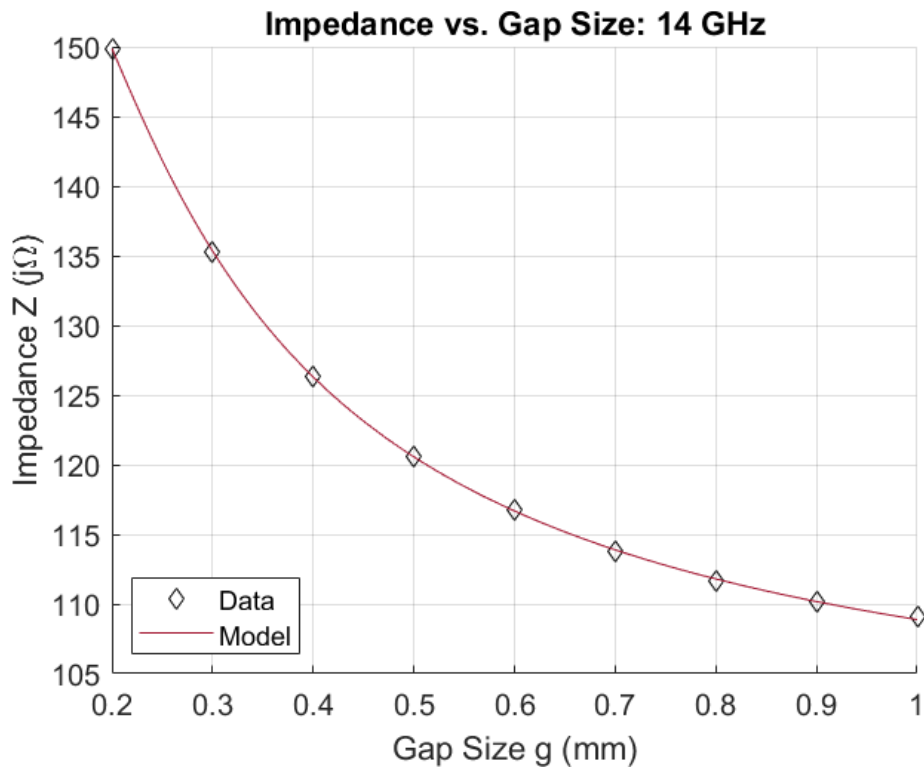


Figure 174: Square Duroid 5880: Impedance vs. Gap Size, 14 GHz

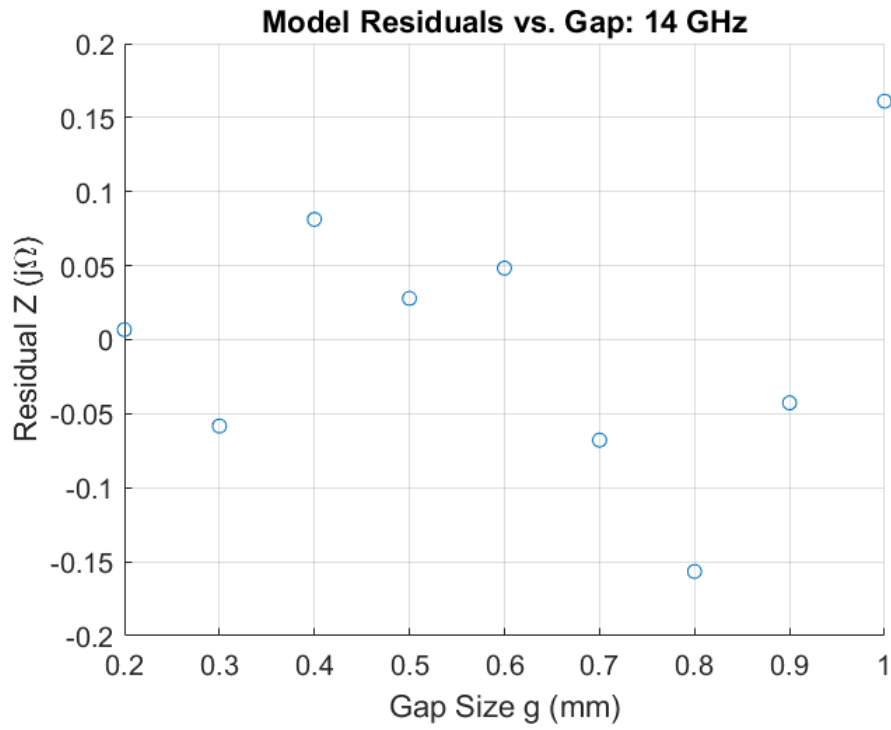


Figure 175: Square Duroid 5880: Residuals, 14 GHz

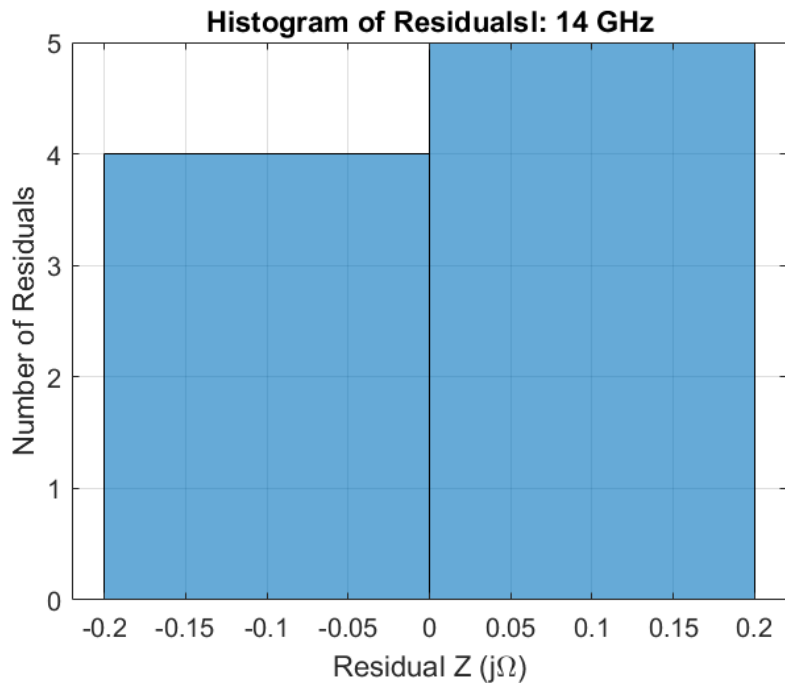


Figure 176: Square Duroid 5880: Histogram of Residuals, 14 GHz

Model: 15 GHz

Equation form: $y = c_0 + c_1 \frac{1}{x^1} + c_2 \frac{1}{x^2} + c_3 \frac{1}{x^3}$

	Coefficient	SE	tStat	pValue
c_0 (intercept)	99.98	0.71857	139.14	3.6379×10^{-10}
c_1	13.176	0.96353	13.674	3.7513×10^{-5}
c_2	1.0493	0.37349	2.8096	0.037566
c_3	-0.20691	0.042372	-4.8831	0.0045407

Table 21: Square Duroid 5880: Model Coefficients: 15 GHz

Model Statistics

Error Degrees of Freedom: 5
 Root Mean Squared Error (RMSE): 0.155
 R-squared: 1
 Adjusted R-Squared: 1
 F-statistic vs. constant model: 35300
 p-value = 3.54×10^{-11}

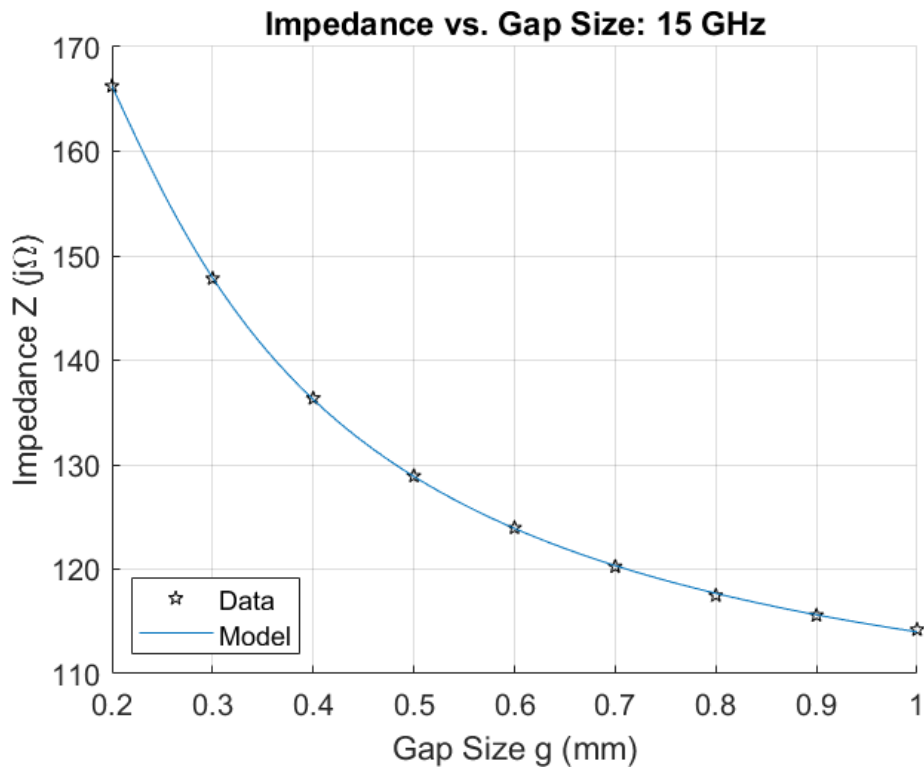


Figure 177: Square Duroid 5880: Impedance vs. Gap Size, 15 GHz

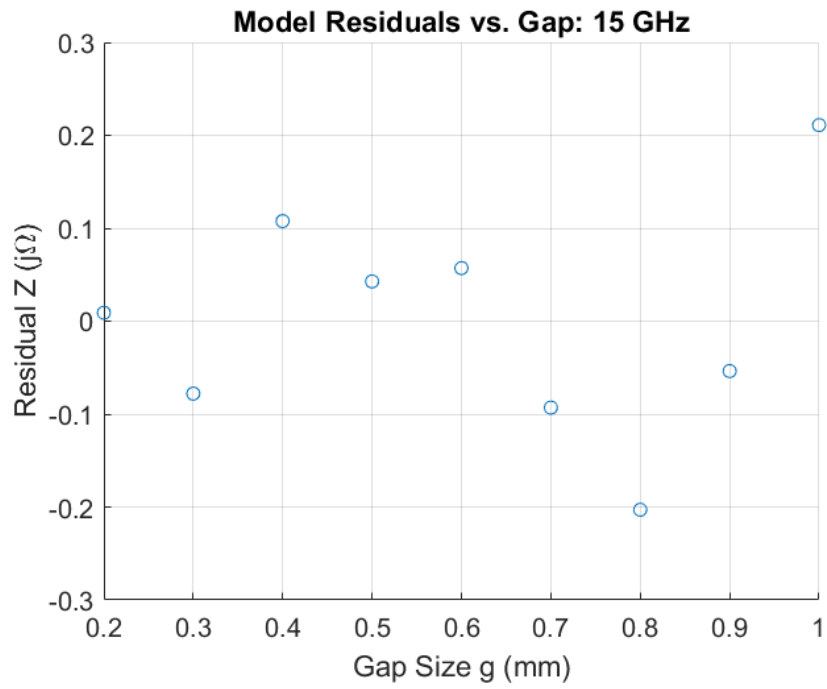


Figure 178: Square Duroid 5880: Residuals, 15 GHz

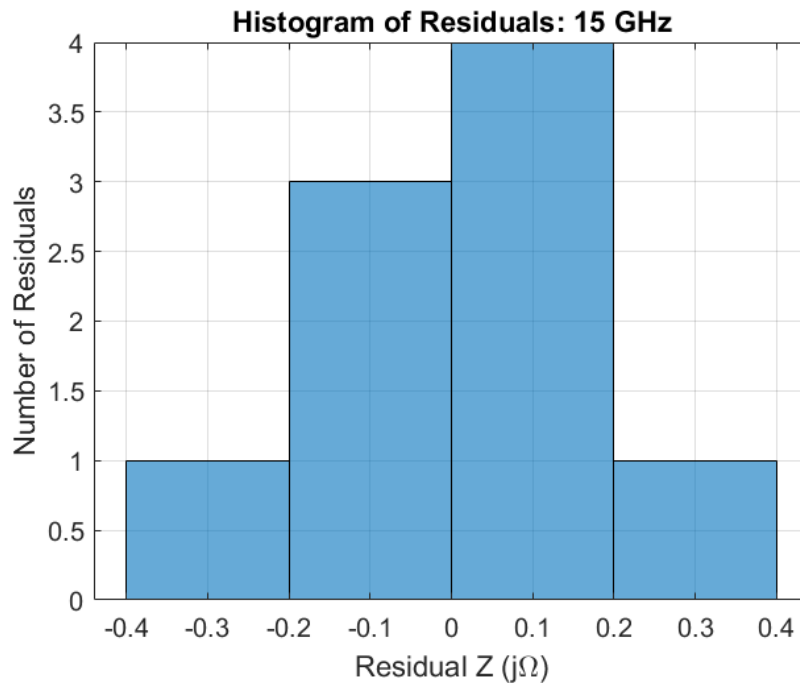


Figure 179: Square Duroid 5880: Histogram of Residuals, 15 GHz

Model: 16 GHz

Equation form: $y = c_0 + c_1 \frac{1}{x^1} + c_2 \frac{1}{x^2} + c_3 \frac{1}{x^3}$

	Coefficient	SE	tStat	pValue
c_0 (intercept)	102.3	0.95627	106.98	1.3533×10^{-9}
c_1	16.186	1.2823	12.623	5.5422×10^{-5}
c_2	1.5023	0.49703	3.0226	0.029329
c_3	-0.29567	0.056389	-5.2434	0.0033445

Table 22: Square Duroid 5880: Model Coefficients: 16 GHz

Model Statistics

Error Degrees of Freedom: 5
 Root Mean Squared Error (RMSE): 0.206
 R-squared: 1
 Adjusted R-Squared: 1
 F-statistic vs. constant model: 28800
 p-value = 5.2×10^{-11}

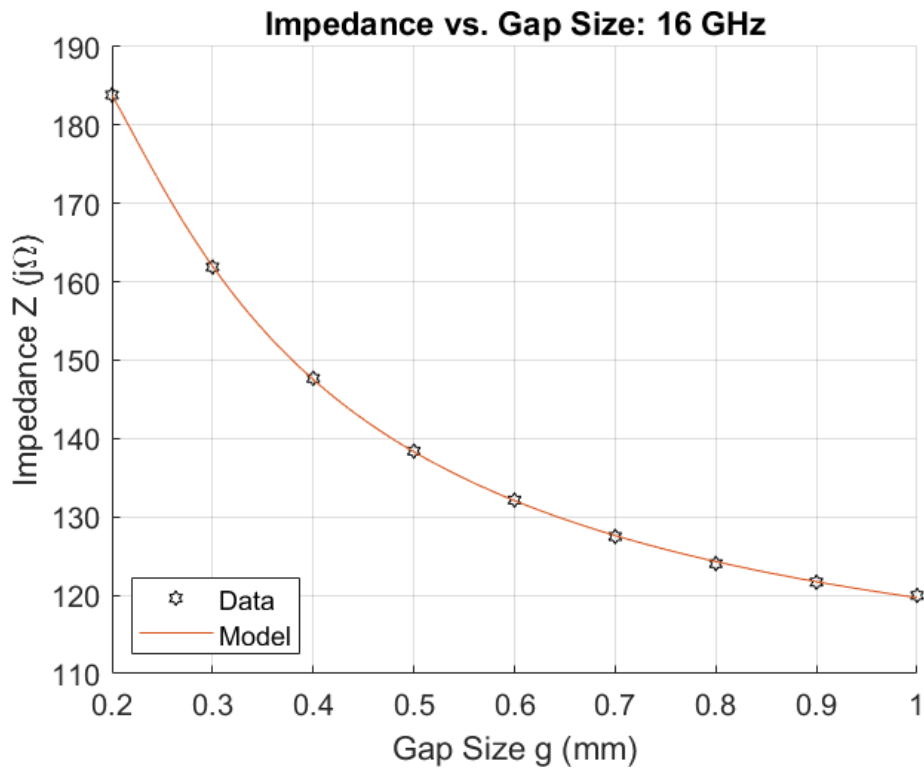


Figure 180: Square Duroid 5880: Impedance vs. Gap Size, 16 GHz

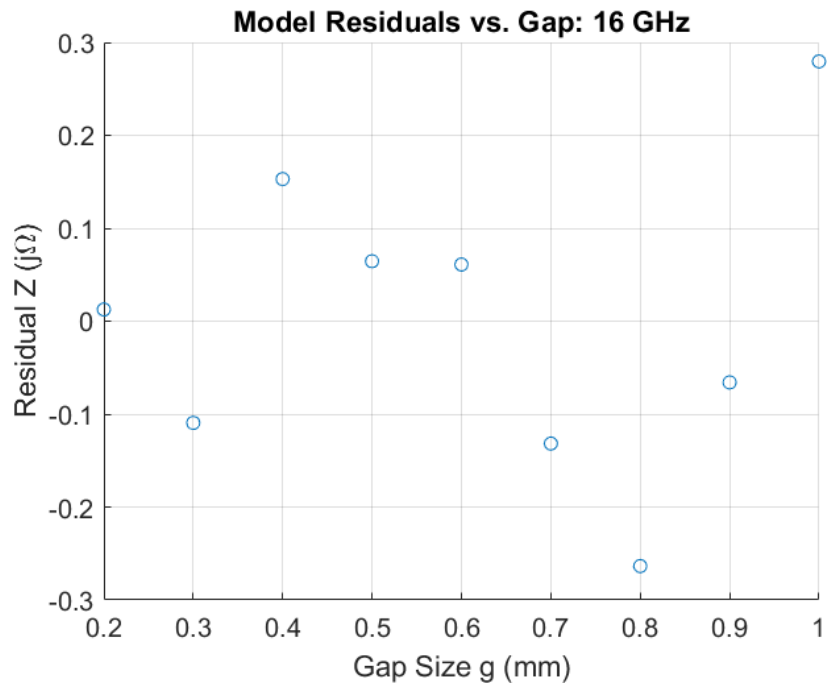


Figure 181: Square Duroid 5880: Residuals, 16 GHz

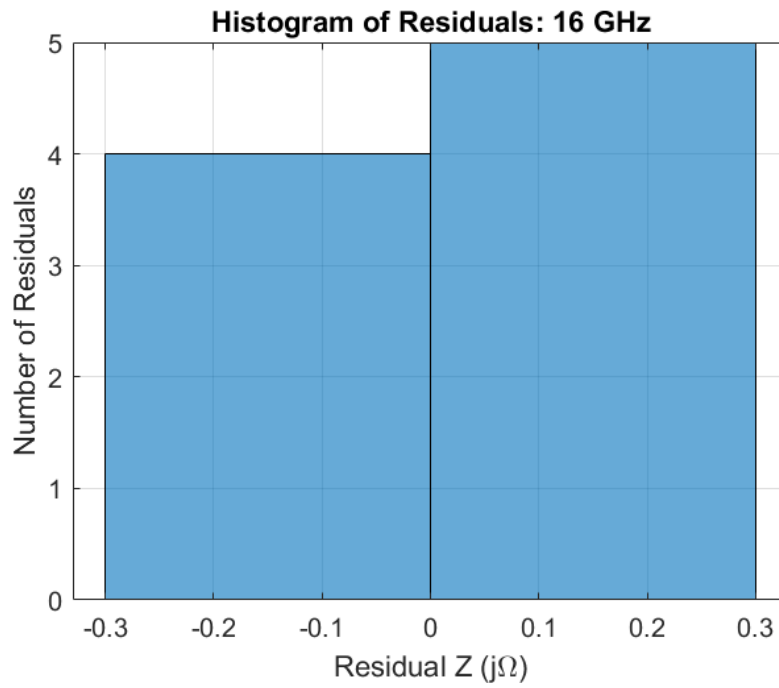


Figure 182: Square Duroid 5880: Histogram of Residuals, 16 GHz

Model: 17 GHz

Equation form: $y = c_0 + c_1 \frac{1}{x^1} + c_2 \frac{1}{x^2} + c_3 \frac{1}{x^3}$

	Coefficient	SE	tStat	pValue
c_0 (intercept)	104.33	1.2785	81.609	5.2349×10^{-9}
c_1	20.232	1.7143	11.802	7.6854×10^{-5}
c_2	1.7492	0.6645	2.6324	0.046398
c_3	-0.37996	0.075388	-5.0401	0.0039666

Table 23: Square Duroid 5880: Model Coefficients: 17 GHz

Model Statistics

Error Degrees of Freedom: 5
 Root Mean Squared Error (RMSE): 0.276
 R-squared: 1
 Adjusted R-Squared: 1
 F-statistic vs. constant model: 22700
 p-value = 9.42×10^{-11}

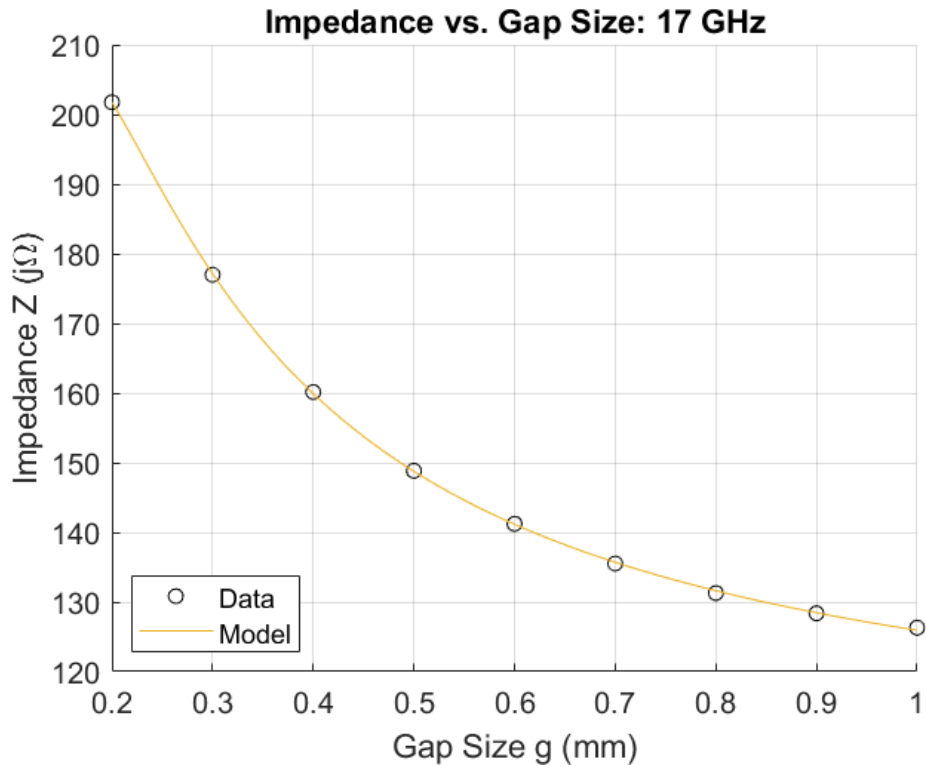


Figure 183: Square Duroid 5880: Impedance vs. Gap Size, 17 GHz

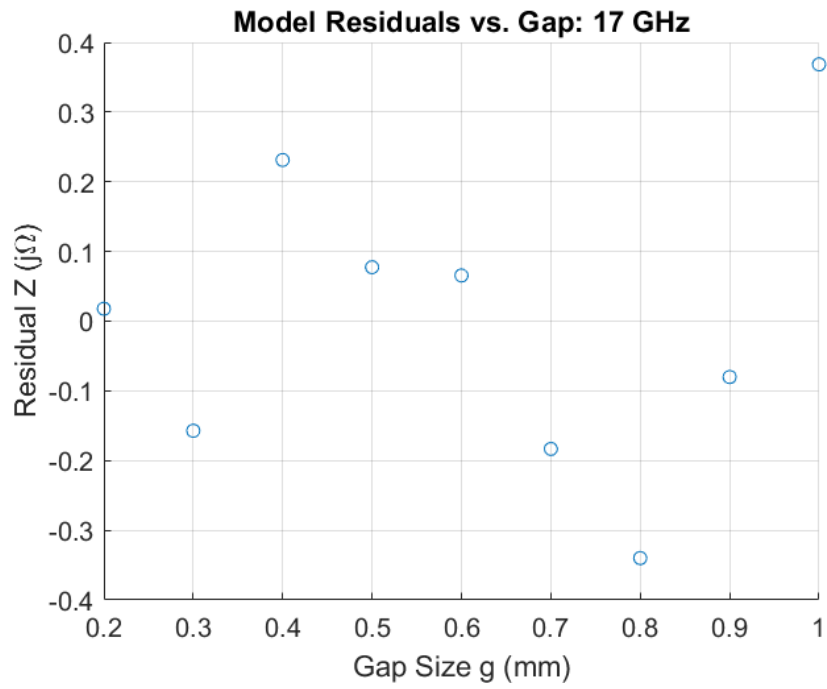


Figure 184: Square Duroid 5880: Residuals, 17 GHz

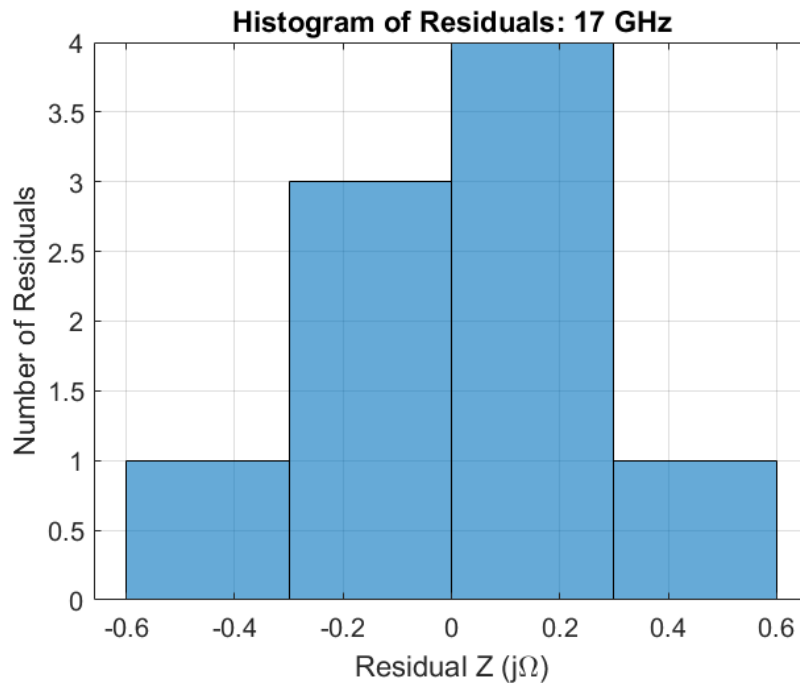


Figure 185: Square Duroid 5880: Histogram of Residuals, 17 GHz

Model: 18 GHz

Equation form: $y = c_0 + c_1 \frac{1}{x^1} + c_2 \frac{1}{x^2} + c_3 \frac{1}{x^3}$

	Coefficient	SE	tStat	pValue
c_0 (intercept)	105.77	1.7211	61.458	2.1586×10^{-8}
c_1	25.789	2.3078	11.175	0.00010011
c_2	1.5148	0.89454	1.6934	0.15116
c_3	-0.42754	0.10149	-4.2128	0.0083858

Table 24: Square Duroid 5880: Model Coefficients: 18 GHz

Model Statistics

Error Degrees of Freedom: 5
 Root Mean Squared Error (RMSE): 0.371
 R-squared: 1
 Adjusted R-Squared: 1
 F-statistic vs. constant model: 16500
 p-value = 2.1×10^{-10}

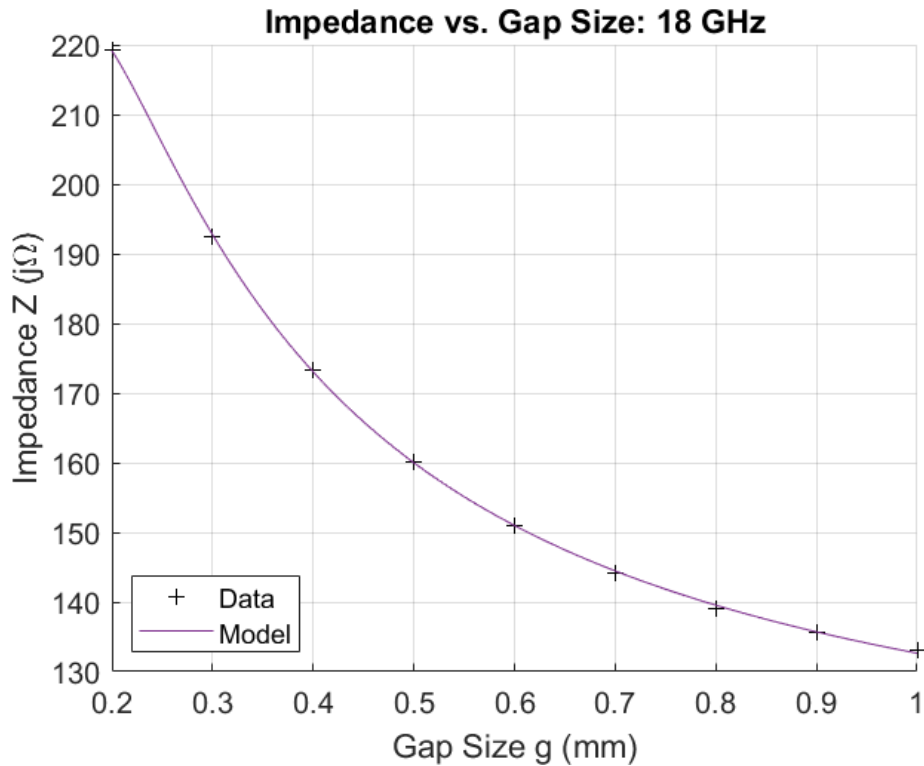


Figure 186: Square Duroid 5880: Impedance vs. Gap Size, 18 GHz

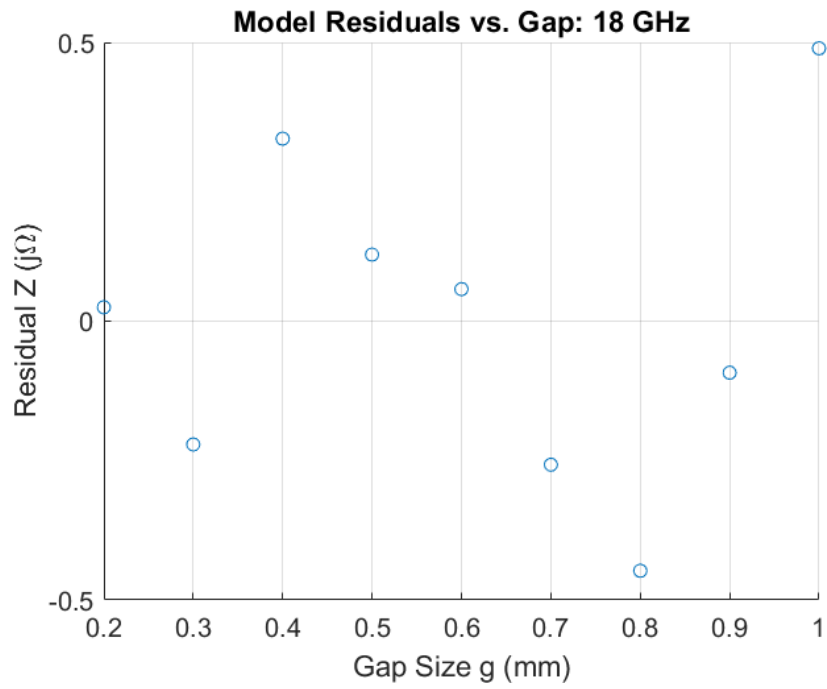


Figure 187: Square Duroid 5880: Residuals, 18 GHz

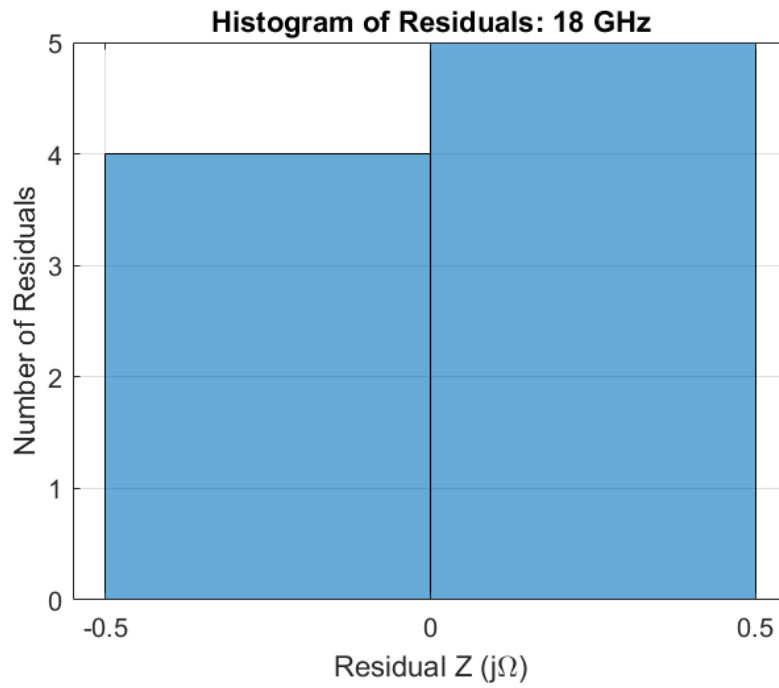


Figure 188: Square Duroid 5880: Histogram of Residuals, 18 GHz

Model: 19 GHz

Equation form: $y = c_0 + c_1 \frac{1}{x^1} + c_2 \frac{1}{x^2} + c_3 \frac{1}{x^3}$

	Coefficient	SE	tStat	pValue
c_0 (intercept)	106.6	2.2223	47.968	7.4394×10^{-8}
c_1	32.899	2.9799	11.04	0.00010617
c_2	0.67786	1.1551	0.58685	0.5828
c_3	-0.41965	0.13105	-3.2023	0.023933

Table 25: Square Duroid 5880: Model Coefficients: 19 GHz

Model Statistics

Error Degrees of Freedom: 5
 Root Mean Squared Error (RMSE): 0.479
 R-squared: 1
 Adjusted R-Squared: 1
 F-statistic vs. constant model: 12300
 p-value = 4.39×10^{-10}

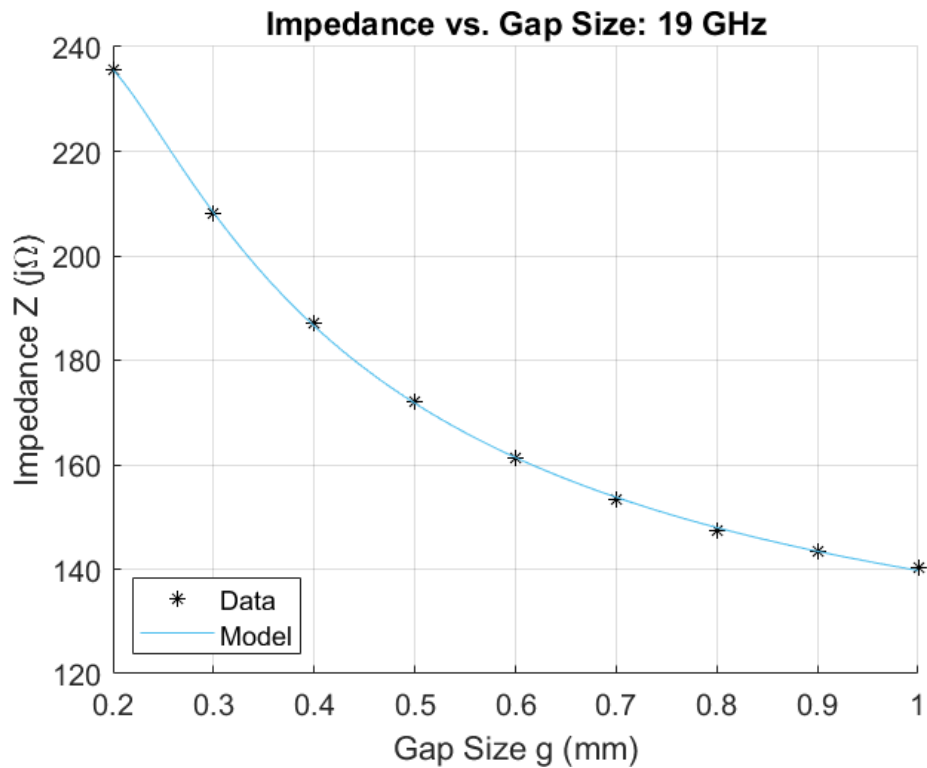


Figure 189: Square Duroid 5880: Impedance vs. Gap Size, 19 GHz

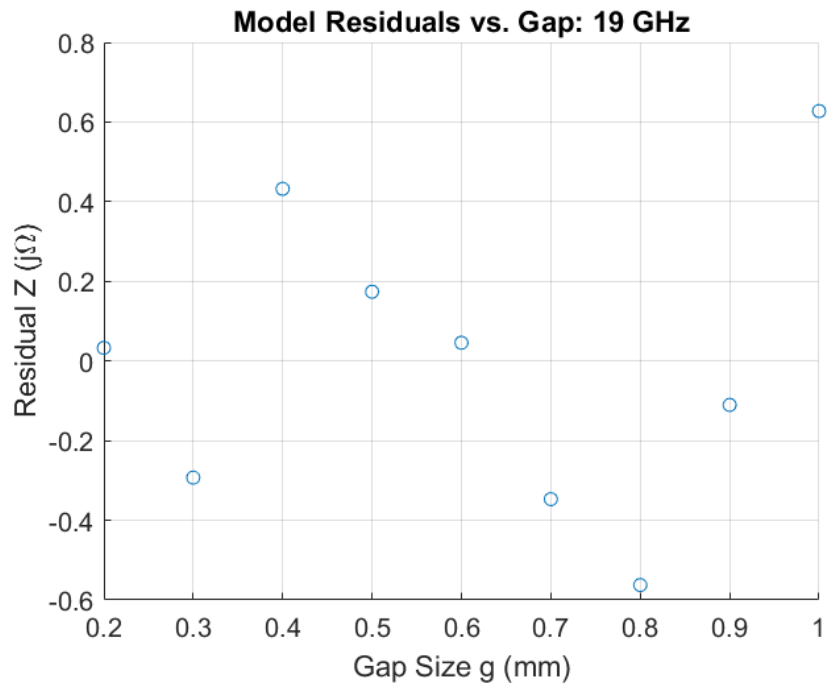


Figure 190: Square Duroid 5880: Residuals, 19 GHz

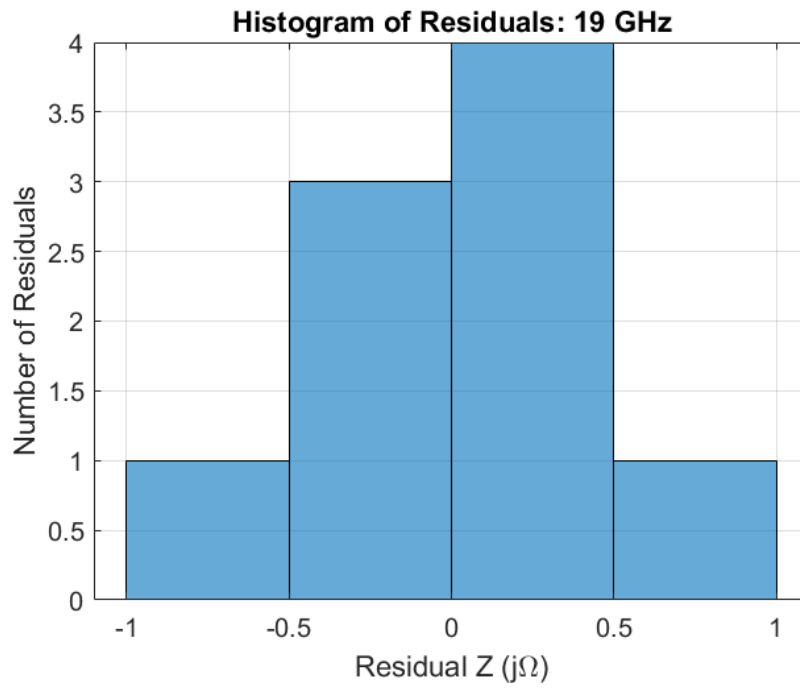


Figure 191: Square Duroid 5880: Histogram of Residuals, 19 GHz

Appendix B. Circular Duroid 5880 Unit Cell

Model Summary

Cell Parameters

Material: Duroid 5880

Dielectric Constant, ϵ_r : 2.2

Dissipation Constant, $\tan \delta$: 0.0009

Shape: circle

Dielectric Thickness: 1.575 mm

Copper Thickness: 0.035 mm

Cell Size, a : 3 mm

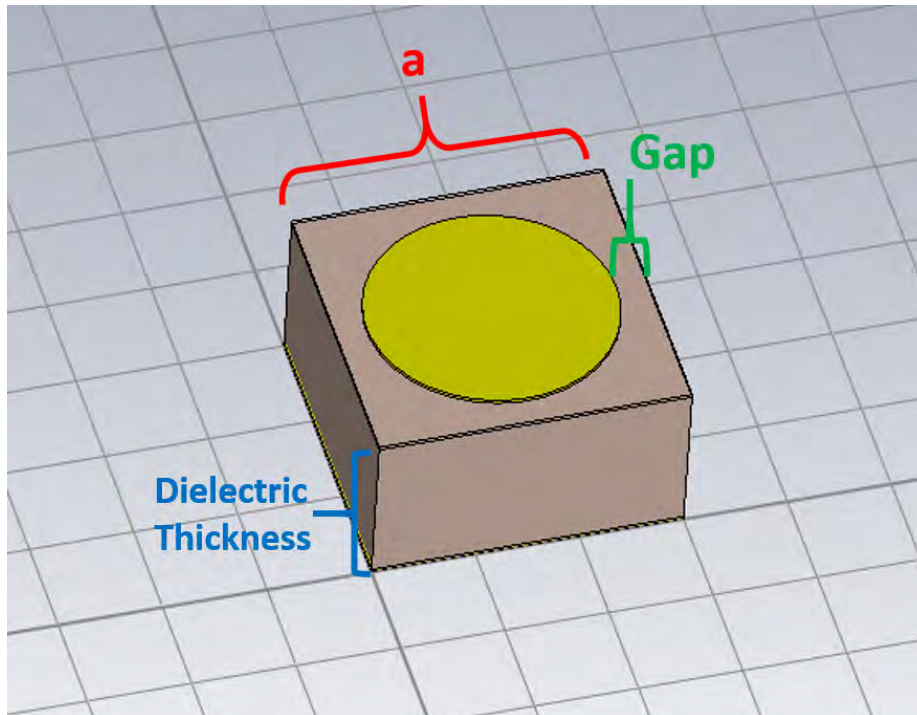


Figure 192: Circle Cell Geometry

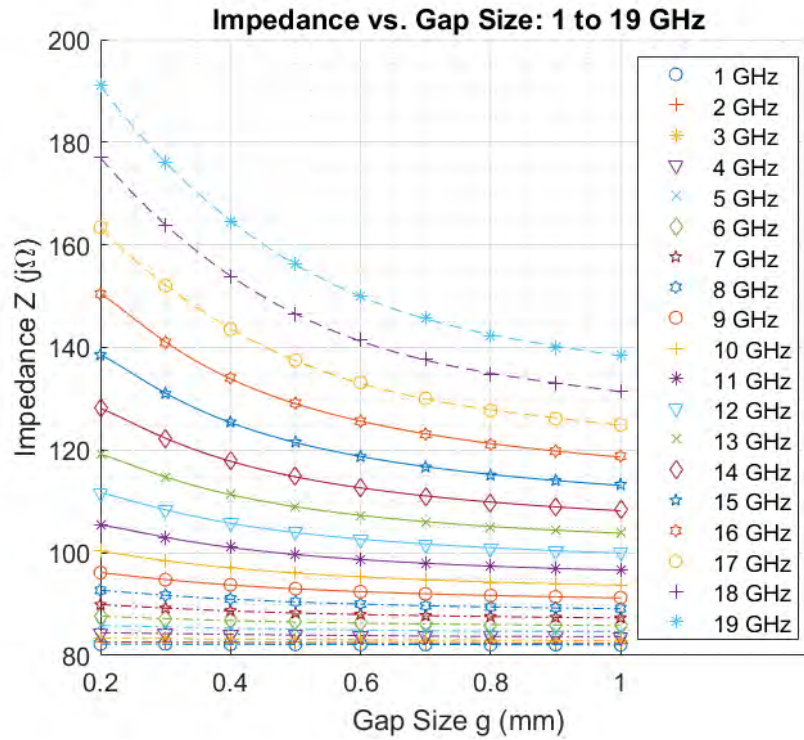


Figure 193: Circle Duroid 5880: Cell Impedance vs. Gap, 1-19 GHz

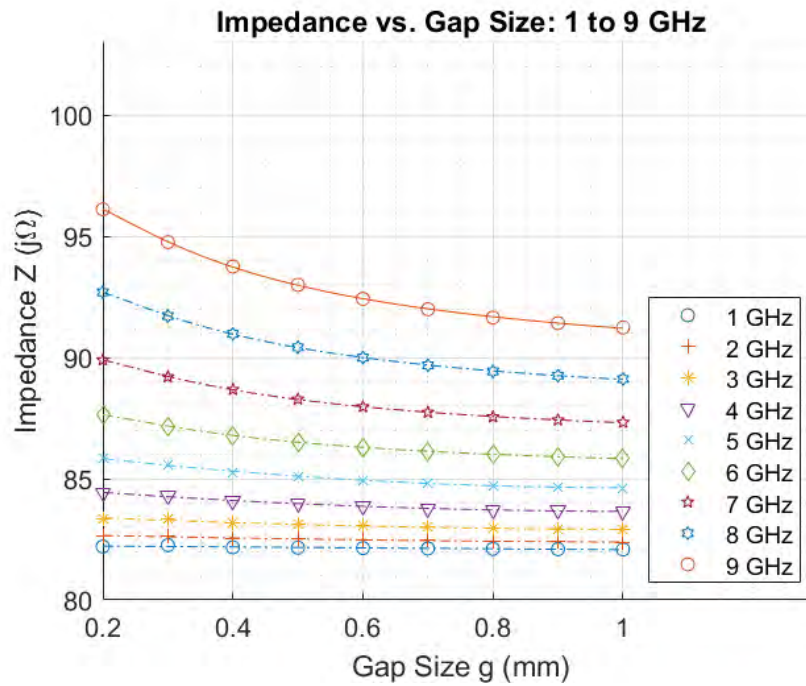


Figure 194: Circle Duroid 5880: Cell Impedance vs. Gap, 1-9 GHz

Unit Cell Impedance Model: Circle Duroid 5880

Frequency \rightarrow Parameter \downarrow	1 GHz	2 GHz	3 GHz	4 GHz	5 GHz	6 GHz	7 GHz	8 GHz	9 GHz	10 GHz
c_4	0	0	0	0	0	0	0	0	0	0
c_3	0	0	0	0	0	0	0	0	0	0
c_2	0	0.280465	0.622013	1.1291	1.835088	-0.07589	-0.10376	-0.1387	-0.18215	-0.23537
c_1	-0.19035	-0.67647	-1.34441	-2.33335	-3.70461	0.907279	1.268479	1.731144	2.320892	3.068749
c_0 (intercept)	82.26263	82.78515	83.63282	84.85761	86.50121	84.99389	86.14596	87.501	89.06668	90.85025
Z_{min}	82.08266	82.3893	82.90633	83.64291	84.61218	85.83167	87.32366	89.1156	82.08266	93.73631
Z_{max}	82.26028	82.65888	83.36755	84.42227	85.83052	87.63593	89.89725	92.69182	82.26028	100.3099
X	82.17147	82.52409	83.13694	84.03259	85.22135	86.7338	88.61045	90.90371	82.17147	97.02312
M	0.088814	0.13479	0.230609	0.389683	0.609174	0.90213	1.286794	1.788109	0.088814	3.286813
ϕ_{avg}	3.687144	7.37572	11.06723	14.76333	18.46591	22.1771	25.89986	29.63754	3.687144	37.17644
Inversion Factor	1	1	1	1	1	-1	-1	-1	-1	-1

Frequency \rightarrow Parameter \downarrow	11 GHz	12 GHz	13 GHz	14 GHz	15 GHz	16 GHz	17 GHz	18 GHz	19 GHz
c_4	0	0	0	0	0	0	0	0	0
c_3	-0.03036	-0.04176	-0.05792	-0.08062	-0.10883	-0.14187	-71.3965	-79.8501	-84.5961
c_2	-0.04574	-0.02523	0.020828	0.102113	0.20597	0.315224	197.504	224.538	243.8315
c_1	3.421354	4.367988	5.508289	6.865196	8.496999	10.45299	-196.612	-227.425	-253.397
c_0 (intercept)	93.25119	95.6468	98.32793	101.3013	104.5426	108.0184	195.3077	214.1067	232.506
Z_{min}	96.64634	100.0163	103.8913	108.3097	113.2954	118.8488	124.9402	131.509	138.4708
Z_{max}	105.4215	111.6385	119.1546	128.1093	138.5813	150.4412	163.4431	177.0861	190.9976
X	101.0339	105.8274	111.523	118.2095	125.9384	134.645	144.1916	154.2975	164.7342
M	4.387556	5.811111	7.631677	9.899806	12.64292	15.7962	19.25145	22.78857	26.26337
ϕ_{avg}	40.99098	44.84693	48.7564	52.73356	56.79438	60.95456	65.22776	69.62241	74.14292
Inversion Factor	-1	-1	-1	-1	-1	-1	1	1	1

Table 26: Unit Cell Impedance Model: Circle Duroid 5880

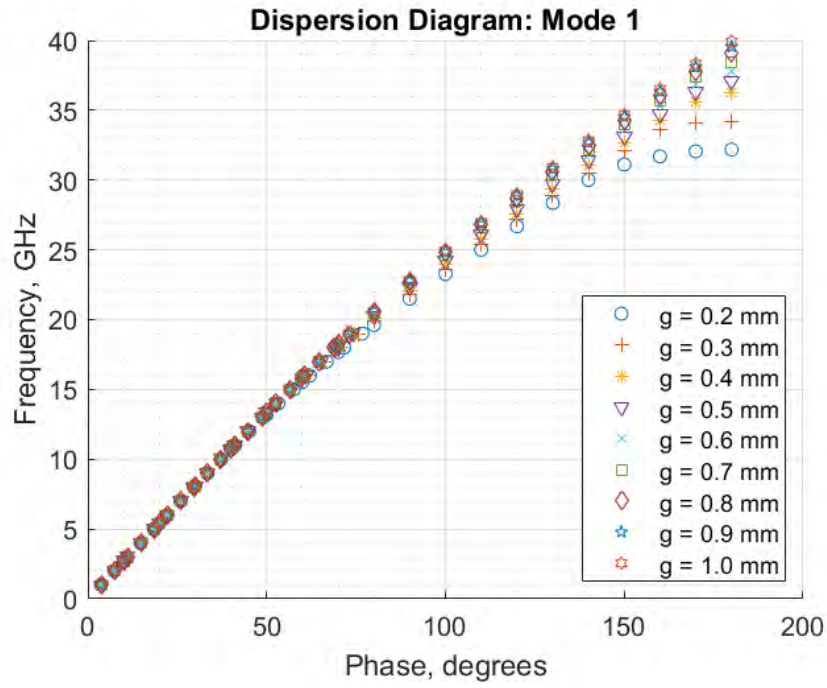


Figure 195: Circle Duroid 5880: Dispersion Diagram, Mode 1

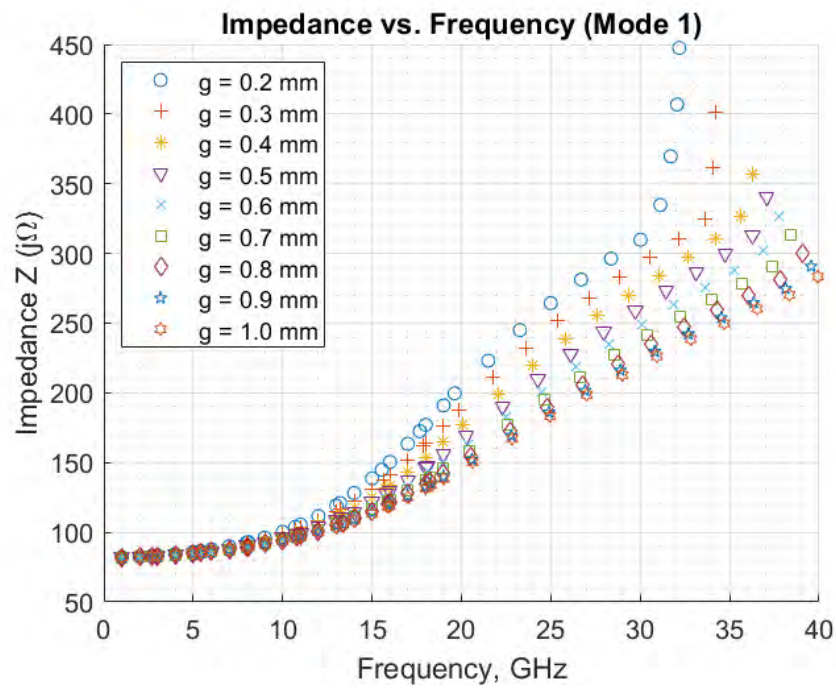


Figure 196: Circle Duroid 5880: Impedance vs. Frequency, Mode 1

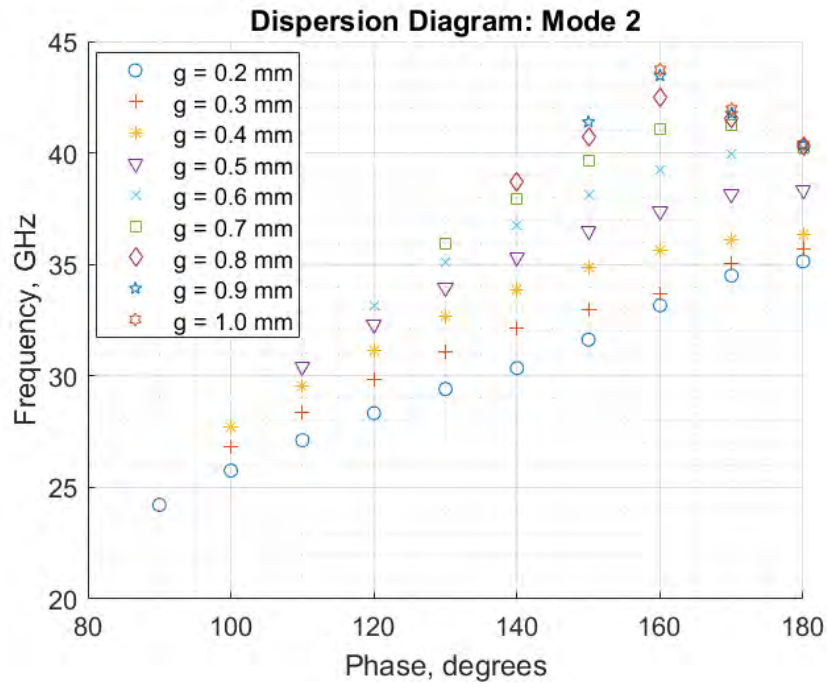


Figure 197: Circle Duroid 5880: Dispersion Diagram, Mode 2

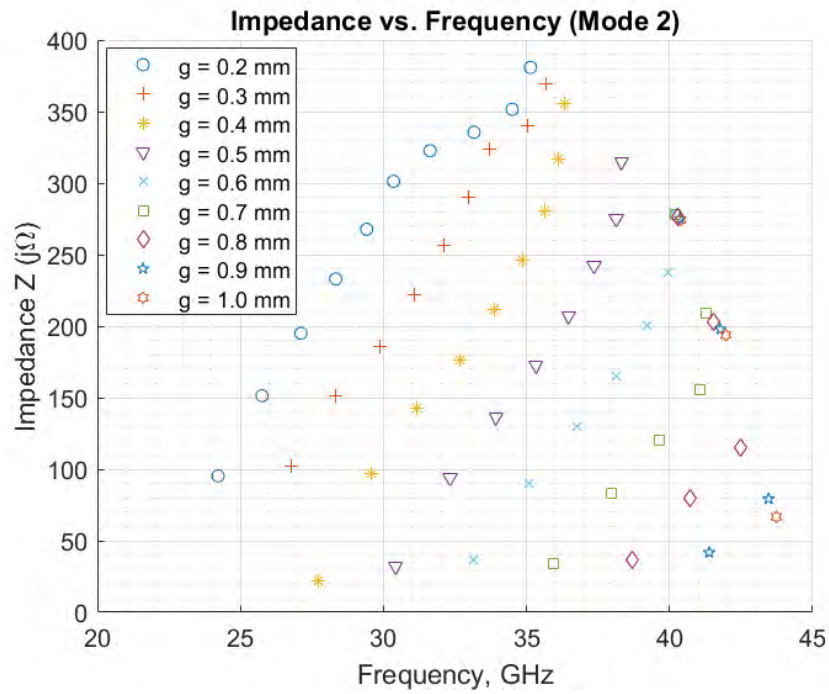


Figure 198: Circle Duroid 5880: Impedance vs. Frequency, Mode 2

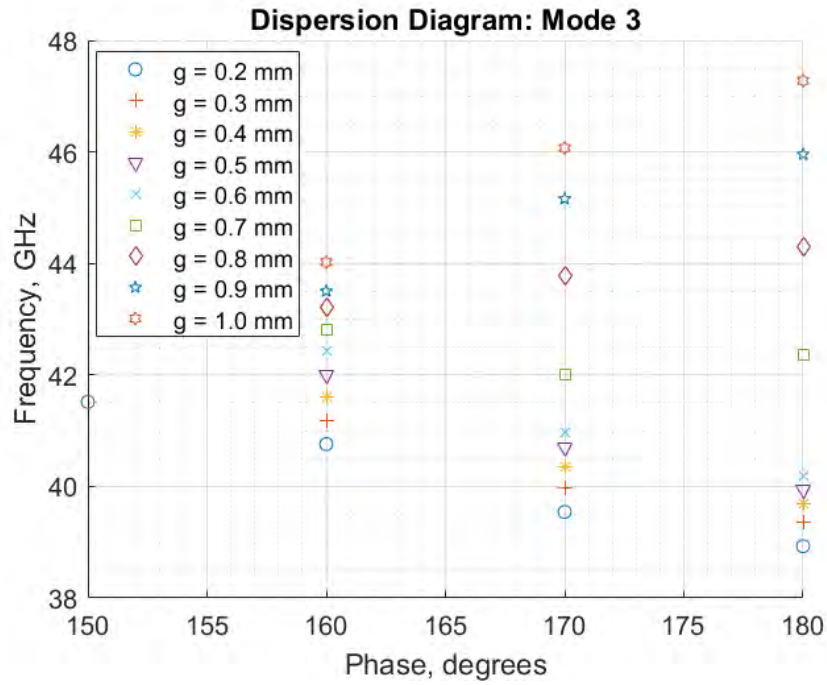


Figure 199: Circle Duroid 5880: Dispersion Diagram, Mode 3

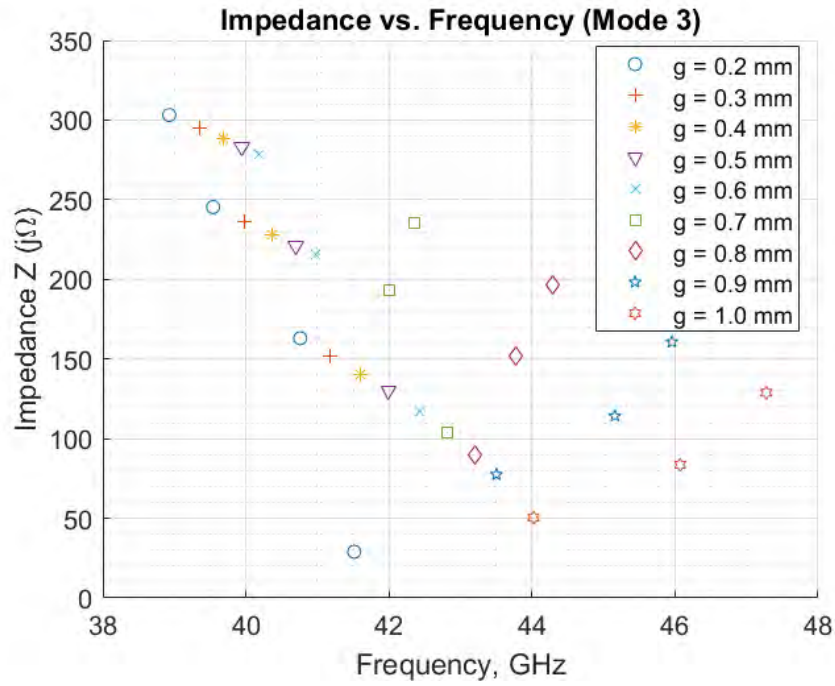


Figure 200: Circle Duroid 5880: Impedance vs. Frequency, Mode 3

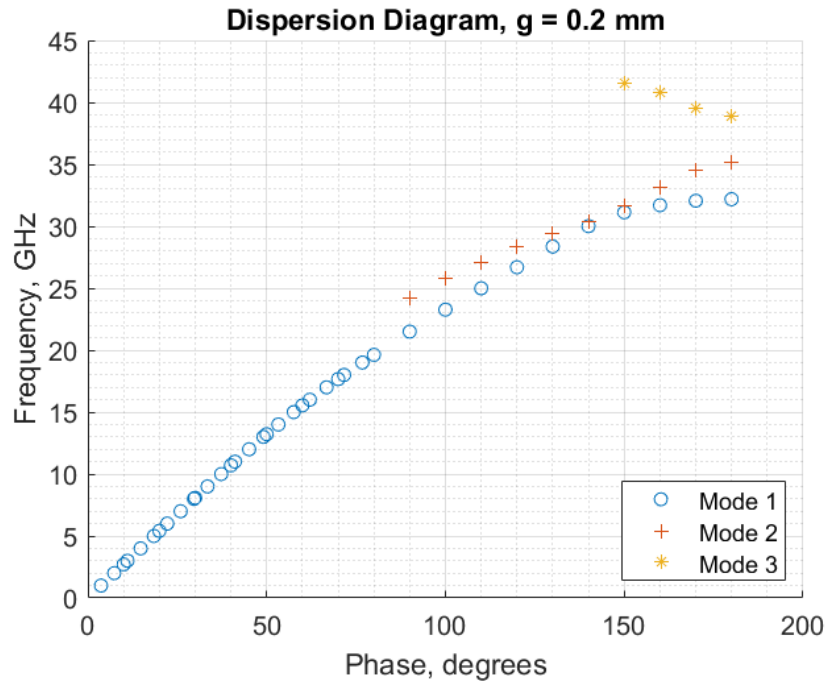


Figure 201: Circle Duroid 5880: Dispersion Diagram, $g = 0.2$

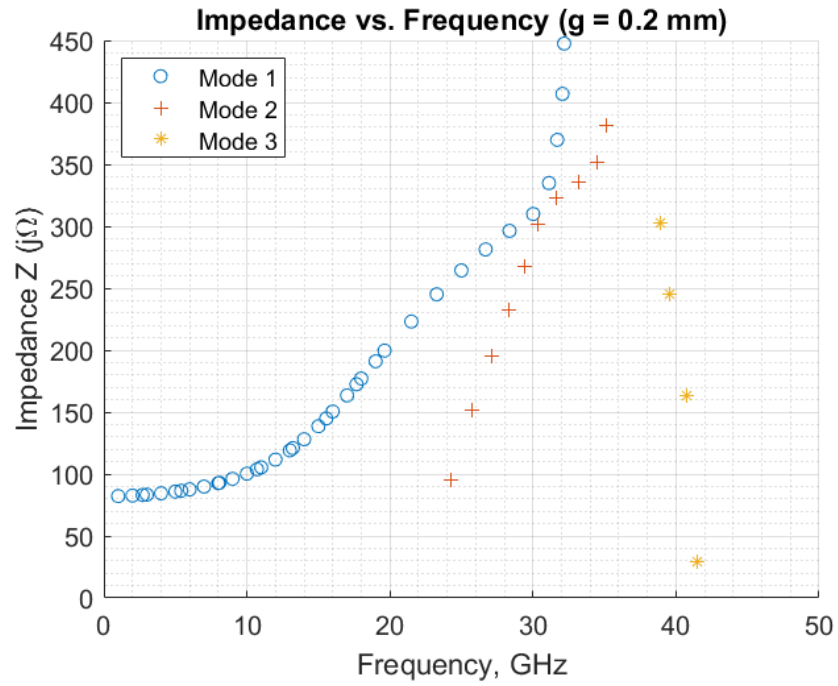


Figure 202: Circle Duroid 5880: Impedance vs. Frequency, $g = 0.2$

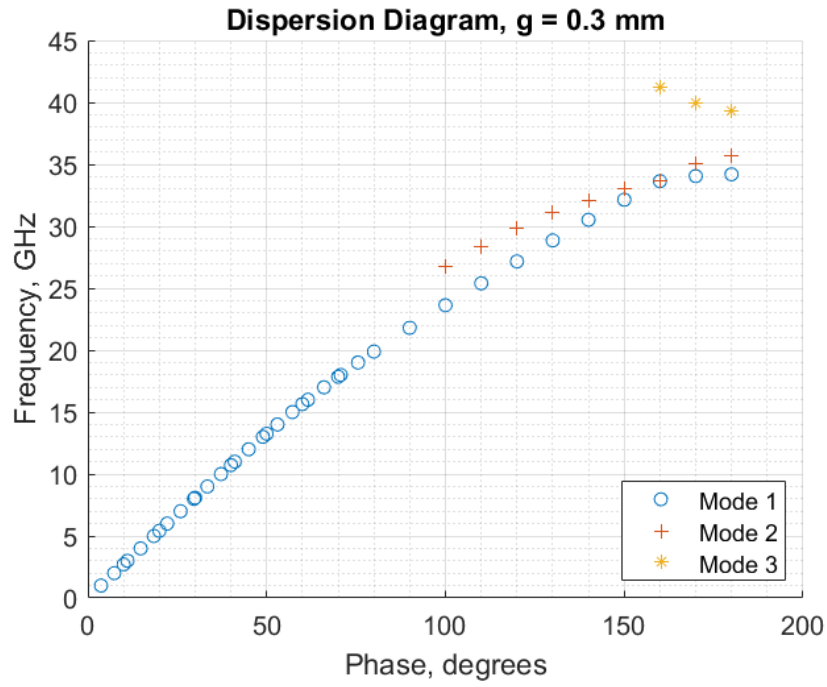


Figure 203: Circle Duroid 5880: Dispersion Diagram, $g = 0.3$

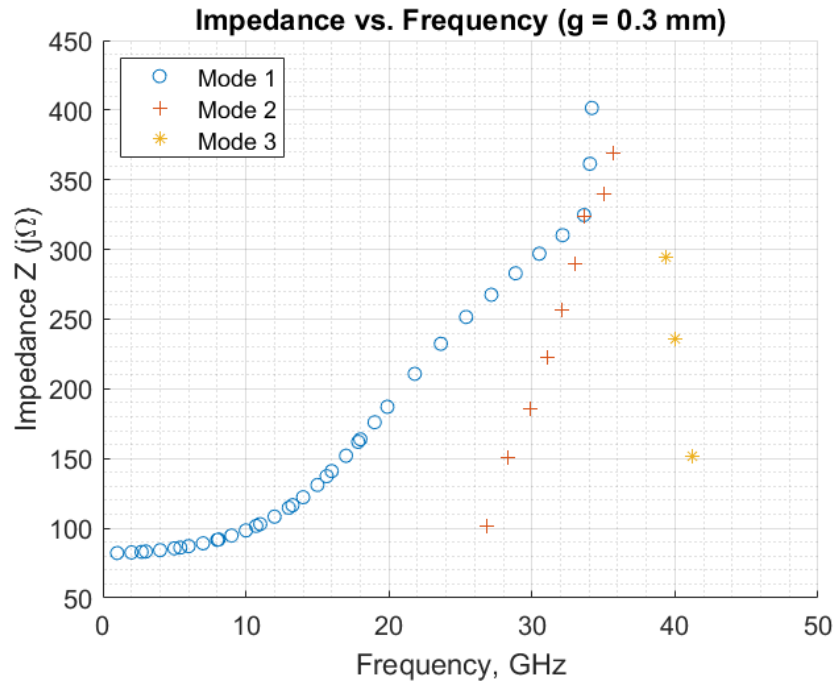


Figure 204: Circle Duroid 5880: Impedance vs. Frequency, $g = 0.3$

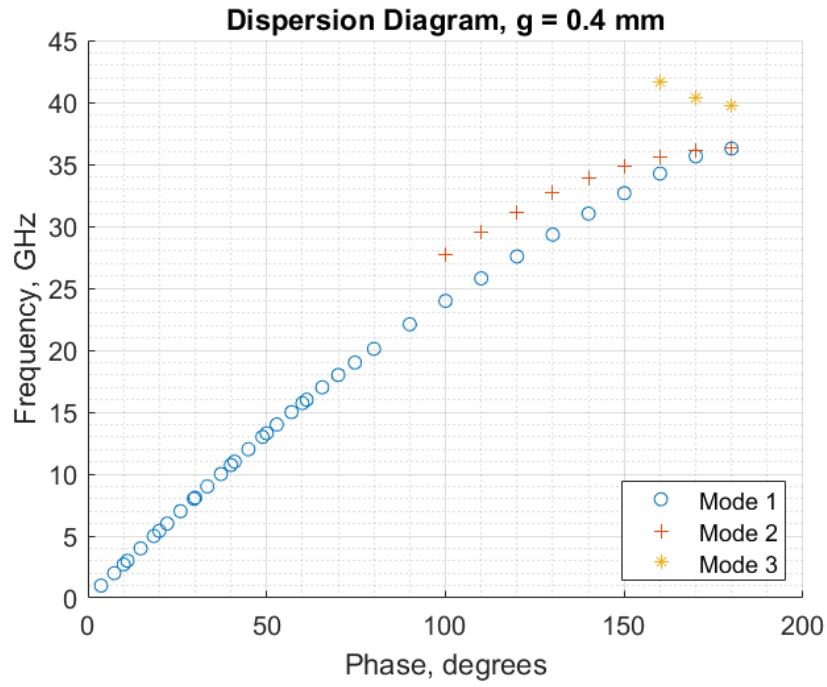


Figure 205: Circle Duroid 5880: Dispersion Diagram, $g = 0.4$

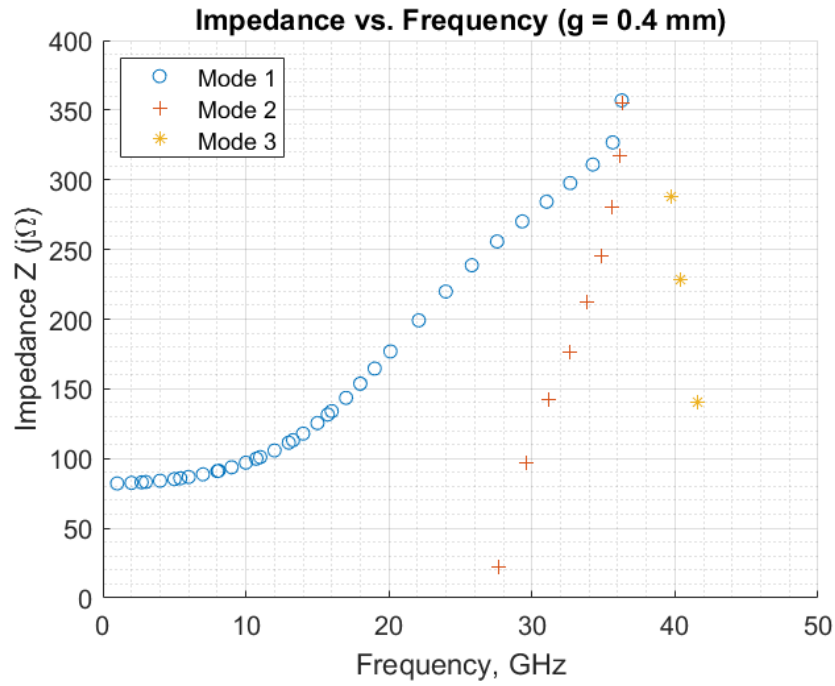


Figure 206: Circle Duroid 5880: Impedance vs. Frequency, $g = 0.4$

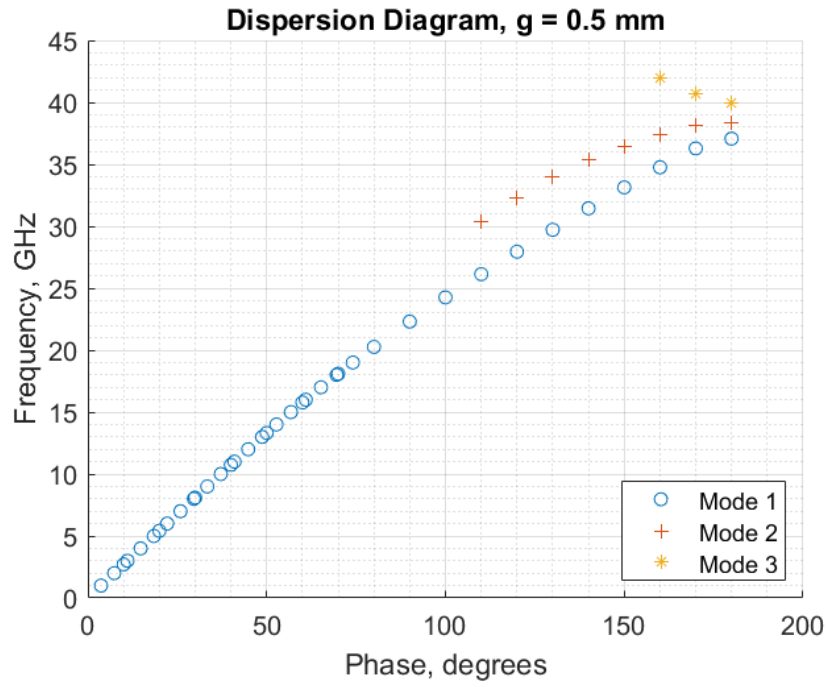


Figure 207: Circle Duroid 5880: Dispersion Diagram, $g = 0.5$

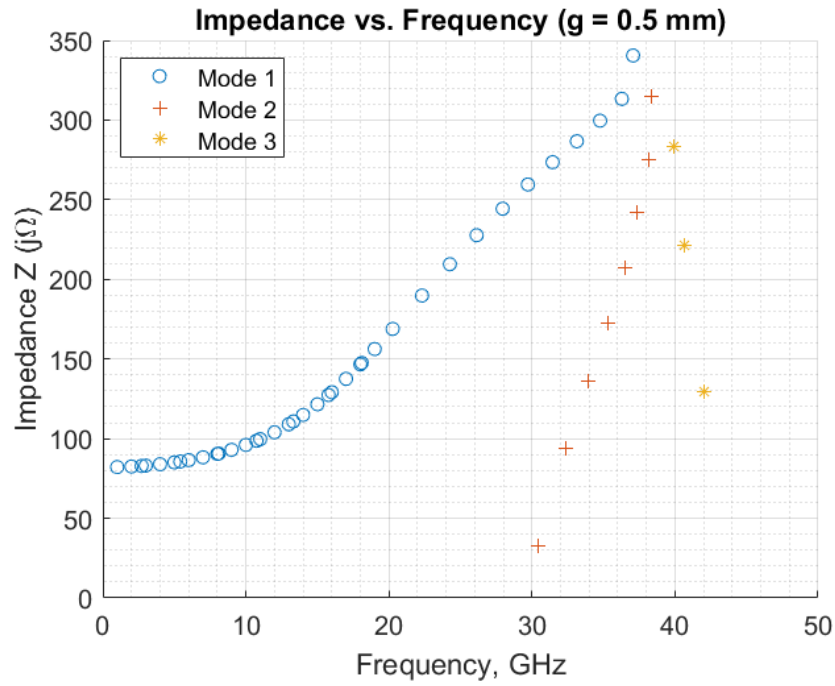


Figure 208: Circle Duroid 5880: Impedance vs. Frequency, $g = 0.5$

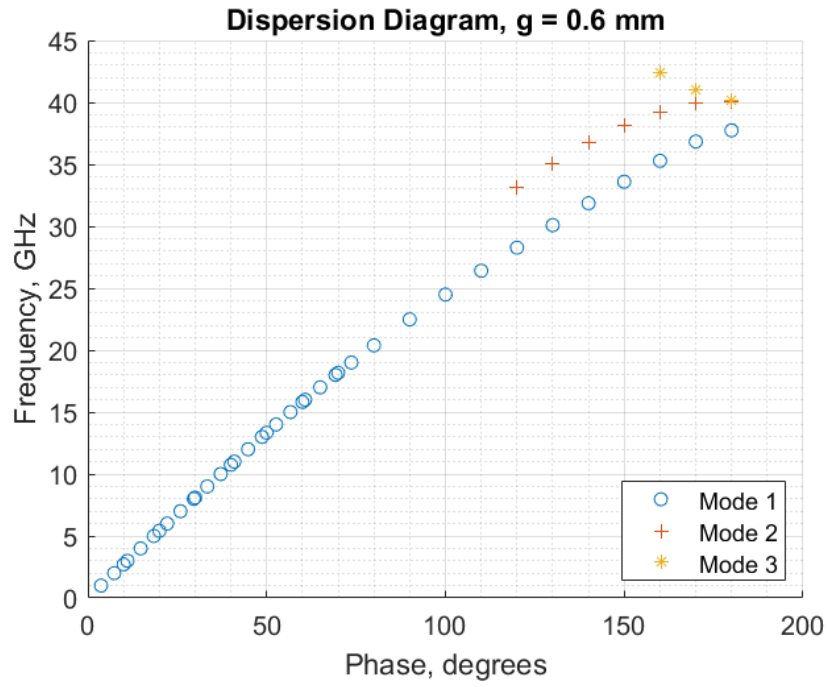


Figure 209: Circle Duroid 5880: Dispersion Diagram, g = 0.6

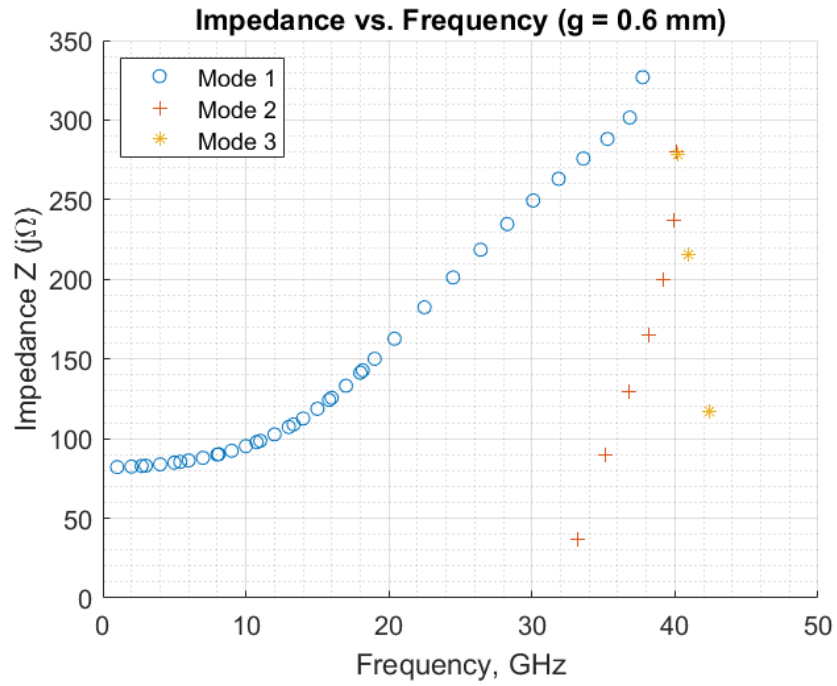


Figure 210: Circle Duroid 5880: Impedance vs. Frequency, g = 0.6

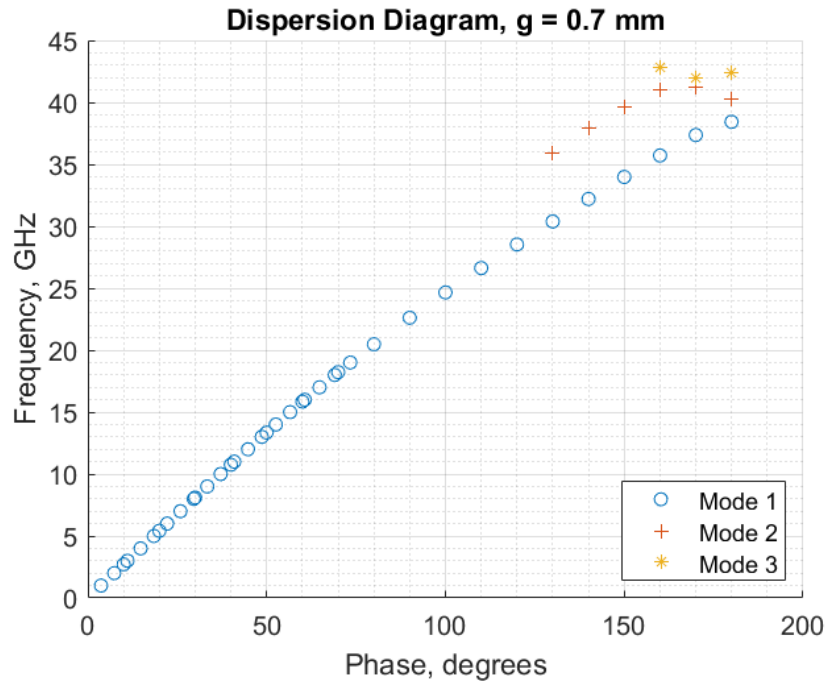


Figure 211: Circle Duroid 5880: Dispersion Diagram, $g = 0.7$

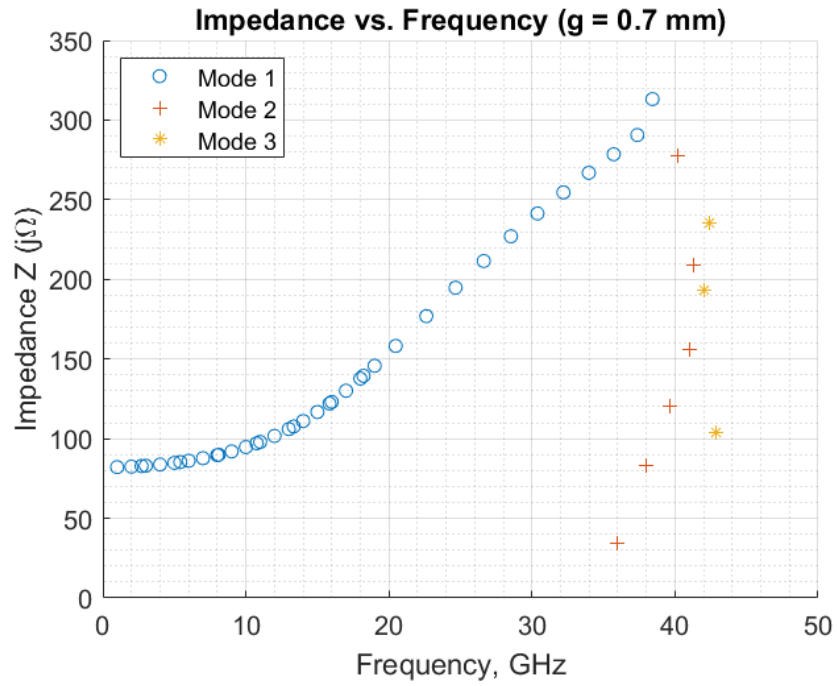


Figure 212: Circle Duroid 5880: Impedance vs. Frequency, $g = 0.7$

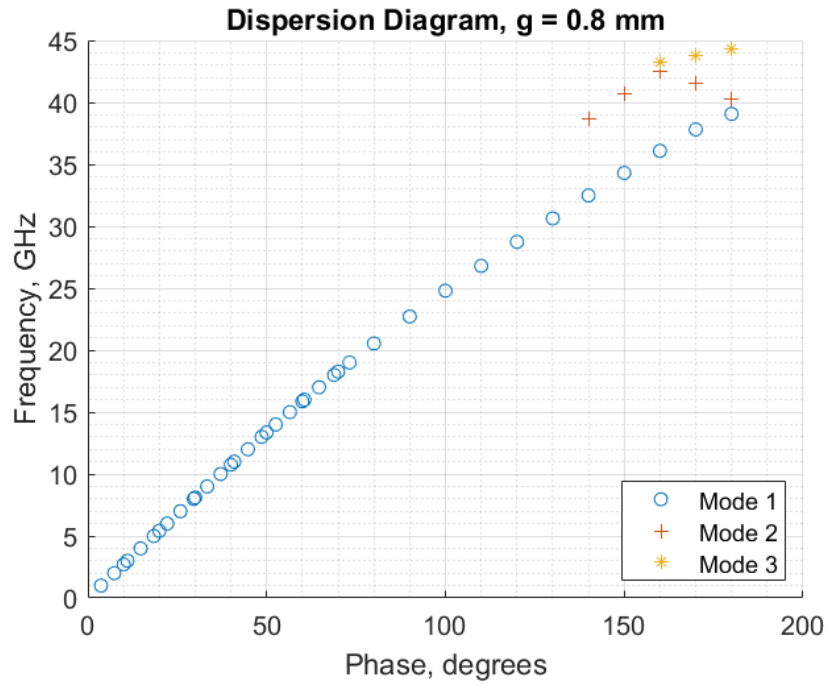


Figure 213: Circle Duroid 5880: Dispersion Diagram, $g = 0.8$

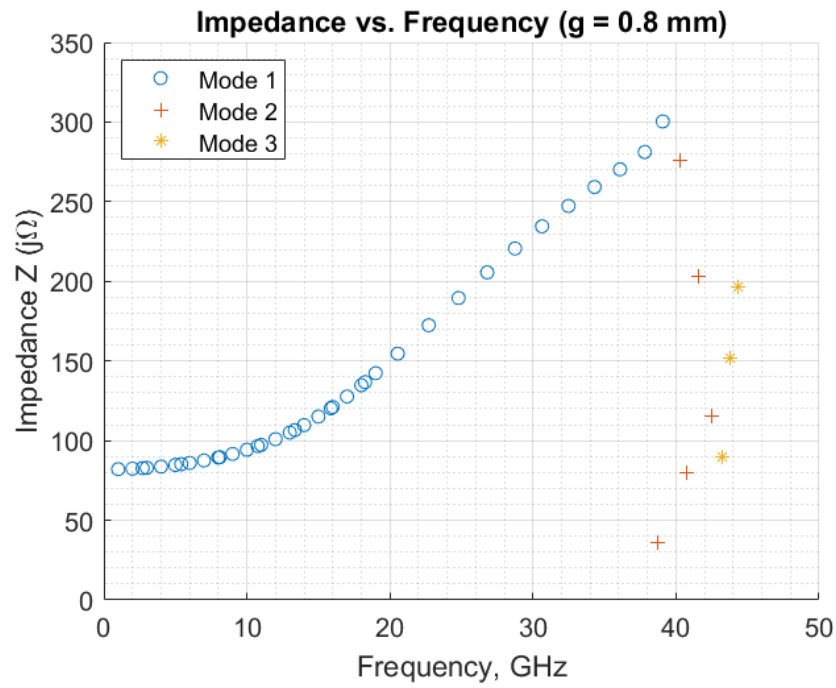


Figure 214: Circle Duroid 5880: Impedance vs. Frequency, $g = 0.8$

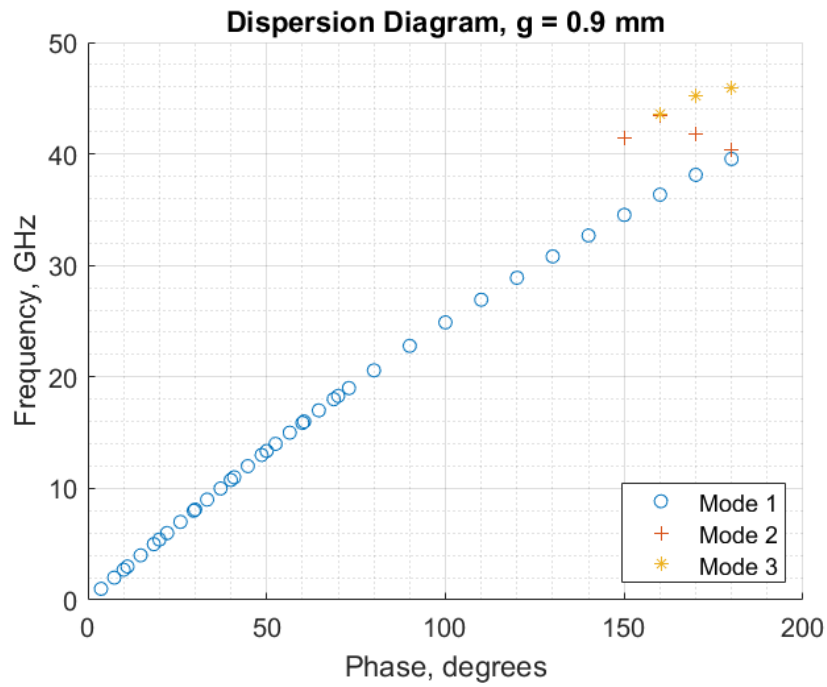


Figure 215: Circle Duroid 5880: Dispersion Diagram, $g = 0.9$

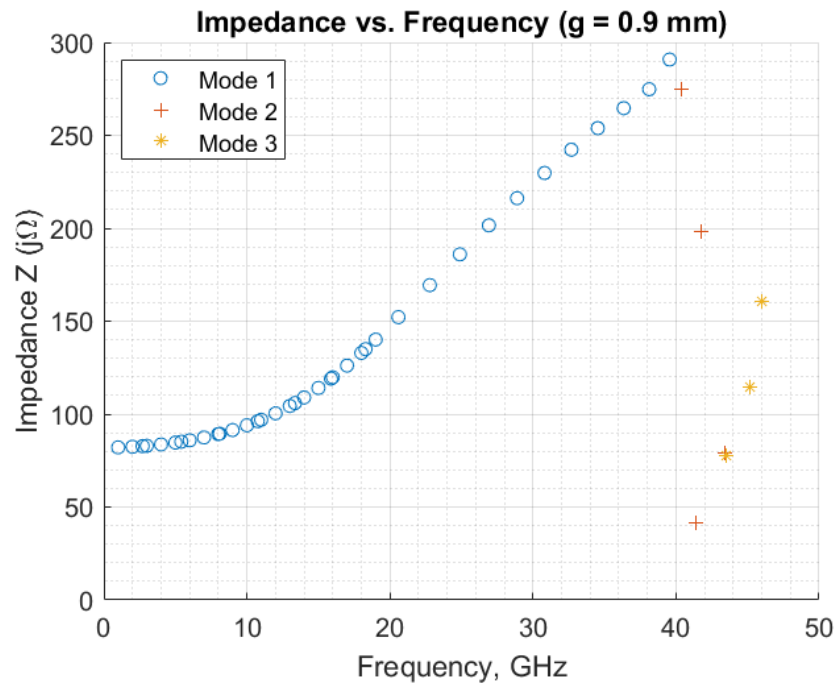


Figure 216: Circle Duroid 5880: Impedance vs. Frequency, $g = 0.9$

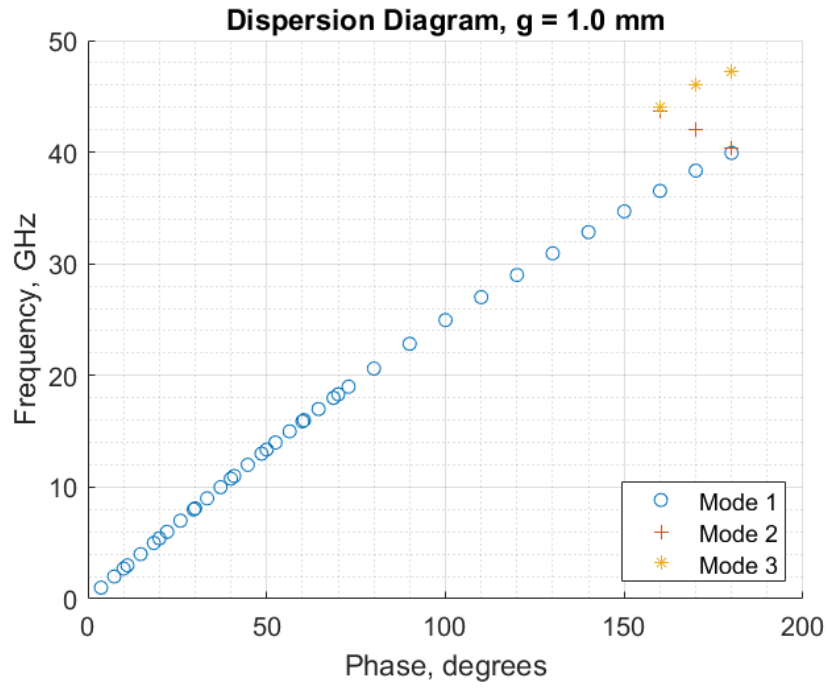


Figure 217: Circle Duroid 5880: Dispersion Diagram, $g = 1.0$

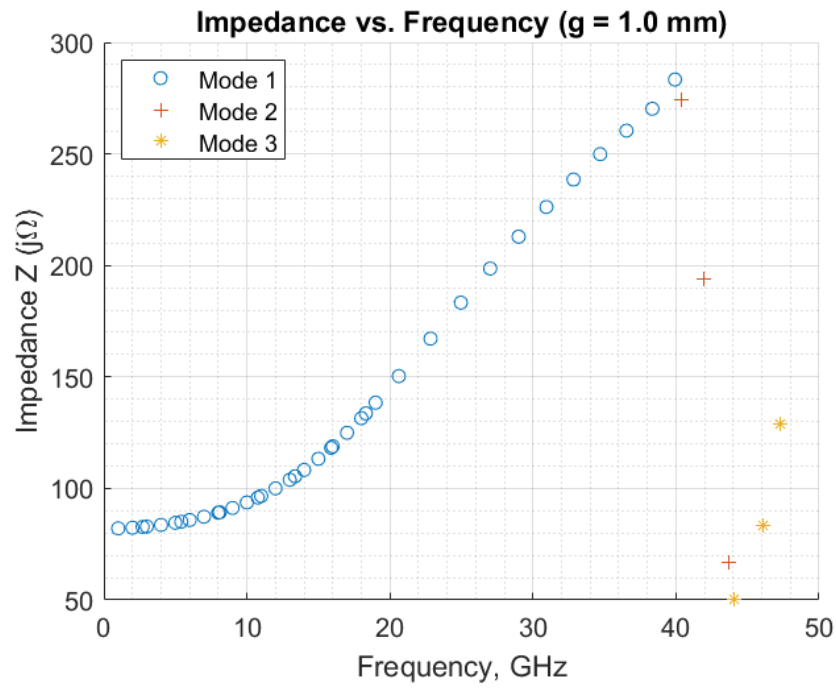


Figure 218: Circle Duroid 5880: Impedance vs. Frequency, $g = 1.0$

Model: 1 GHz

Equation form: $y = c_0 + c_1x^1$

	<u>Coefficient</u>	<u>SE</u>	<u>tStat</u>	<u>pValue</u>
c_0 (intercept)	82.263	0.020404	4031.7	1.5253×10^{-23}
c_1	-0.19035	0.031237	-6.0937	0.00049415

Table 27: Model Coefficients: 1 GHz

Model Statistics

Error Degrees of Freedom: 7
 Root Mean Squared Error (RMSE): 0.0242
 R-squared: 0.841
 Adjusted R-Squared: 0.819
 F-statistic vs. constant model: 37.1
 p-value = 0.000494

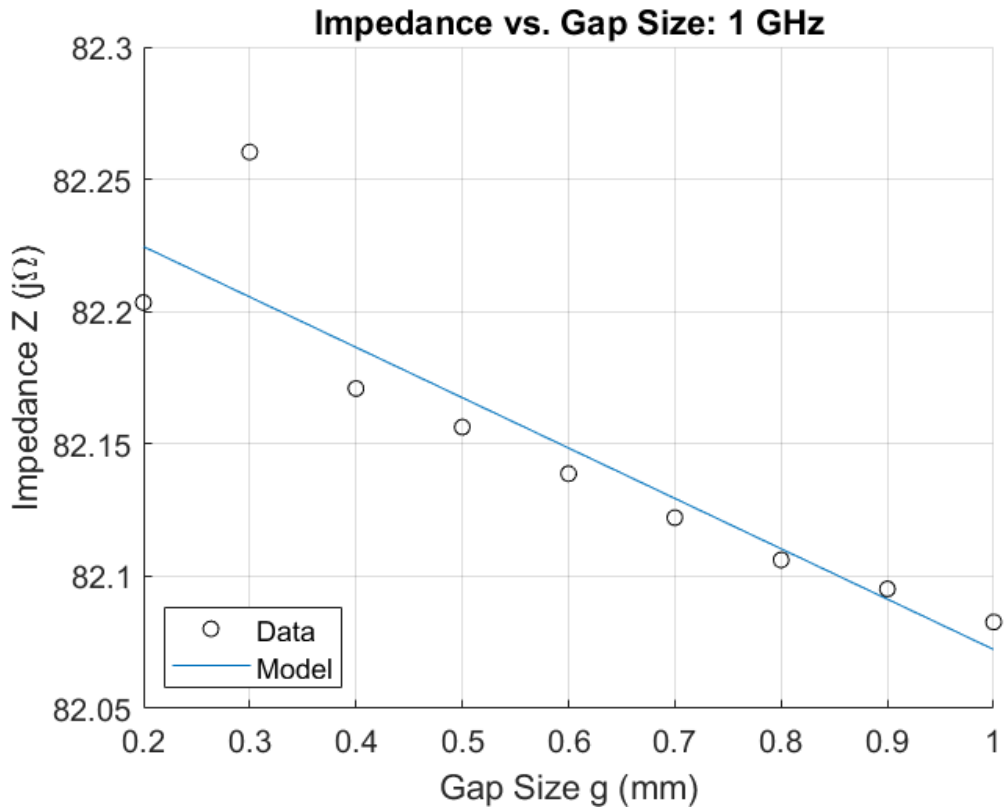


Figure 219: Circle Duroid 5880: Impedance vs. Gap Size, 1 GHz

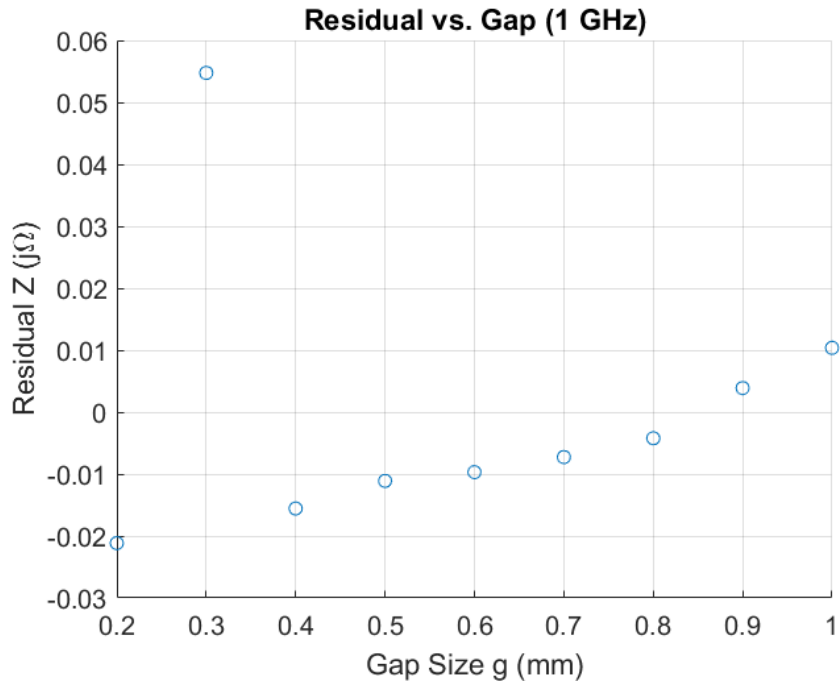


Figure 220: Circle Duroid 5880: Residuals, 1 GHz

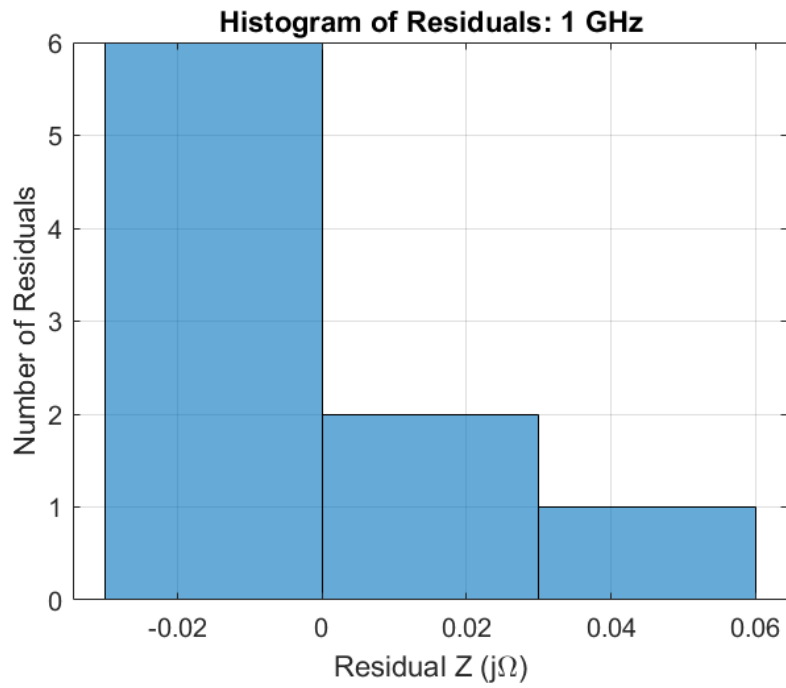


Figure 221: Circle Duroid 5880: Histogram of Residuals, 1 GHz

Model: 2 GHz

Equation form: $y = c_0 + c_1x^1 + c_2x^2$

	<u>Coefficient</u>	<u>SE</u>	<u>tStat</u>	<u>pValue</u>
c_0 (intercept)	82.785	0.046358	1785.8	2.0812×10^{-8}
c_1	-0.67647	0.17231	-3.9259	0.0077488
c_2	0.28046	0.1411	1.9878	0.094009

Table 28: Model Coefficients: 2 GHz

Model Statistics

Error Degrees of Freedom: 6
 Root Mean Squared Error (RMSE): 0.0248
 R-squared: 0.951
 Adjusted R-Squared: 0.935
 F-statistic vs. constant model: 58.5
 p-value = 0.000116

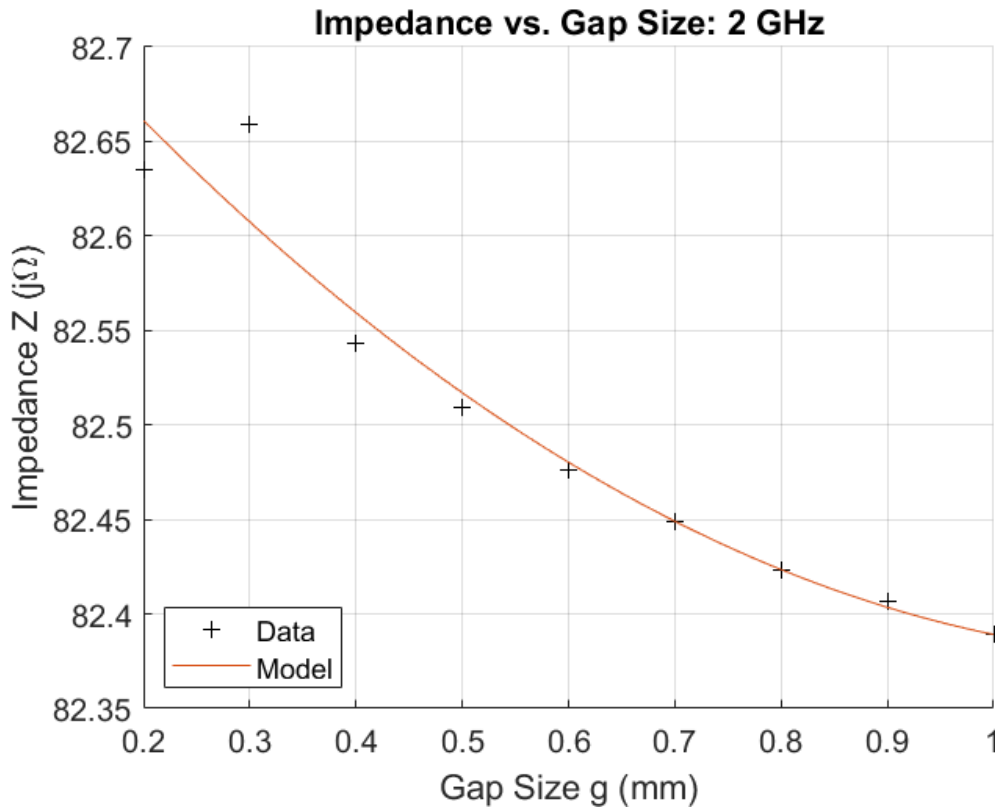


Figure 222: Circle Duroid 5880: Impedance vs. Gap Size, 2 GHz

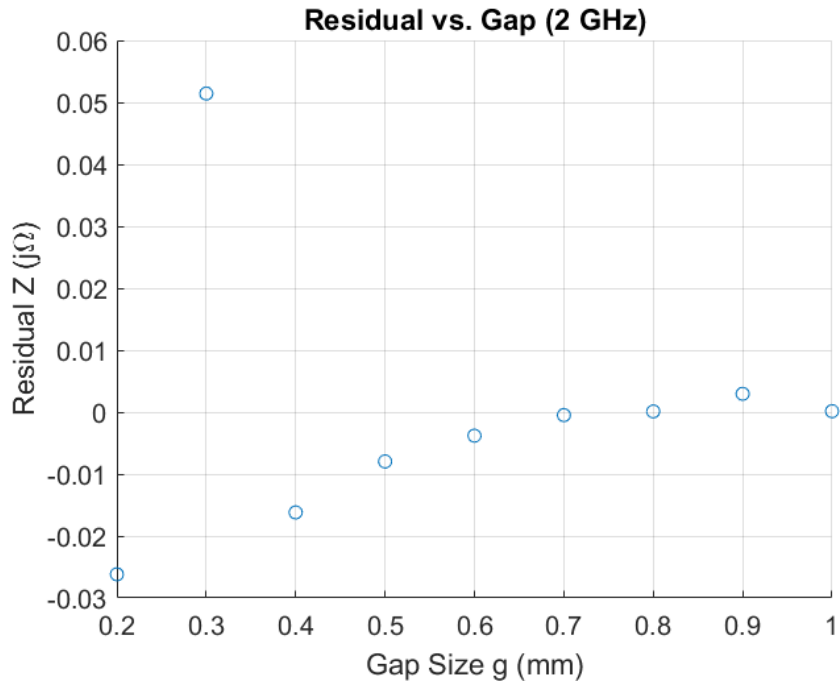


Figure 223: Circle Duroid 5880: Residuals, 2 GHz

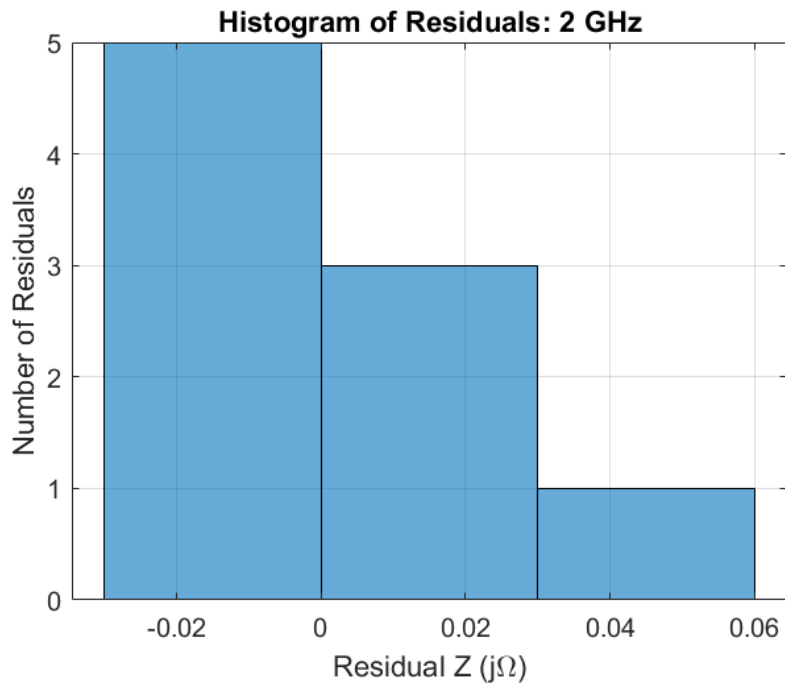


Figure 224: Circle Duroid 5880: Histogram of Residuals, 2 GHz

Model: 3 GHz

Equation form: $y = c_0 + c_1x^1 + c_2x^2$

	<u>Coefficient</u>	<u>SE</u>	<u>tStat</u>	<u>pValue</u>
c_0 (intercept)	83.633	0.045129	1853.2	1.6664×10^{-18}
c_1	-1.3444	0.16774	-8.0148	0.00020139
c_2	0.62201	0.13736	4.5284	0.0039819

Table 29: Model Coefficients: 3 GHz

Model Statistics

Error Degrees of Freedom: 6
 Root Mean Squared Error (RMSE): 0.0241
 R-squared: 0.985
 Adjusted R-Squared: 0.98
 F-statistic vs. constant model: 195
 p-value = 3.49×10^{-6}

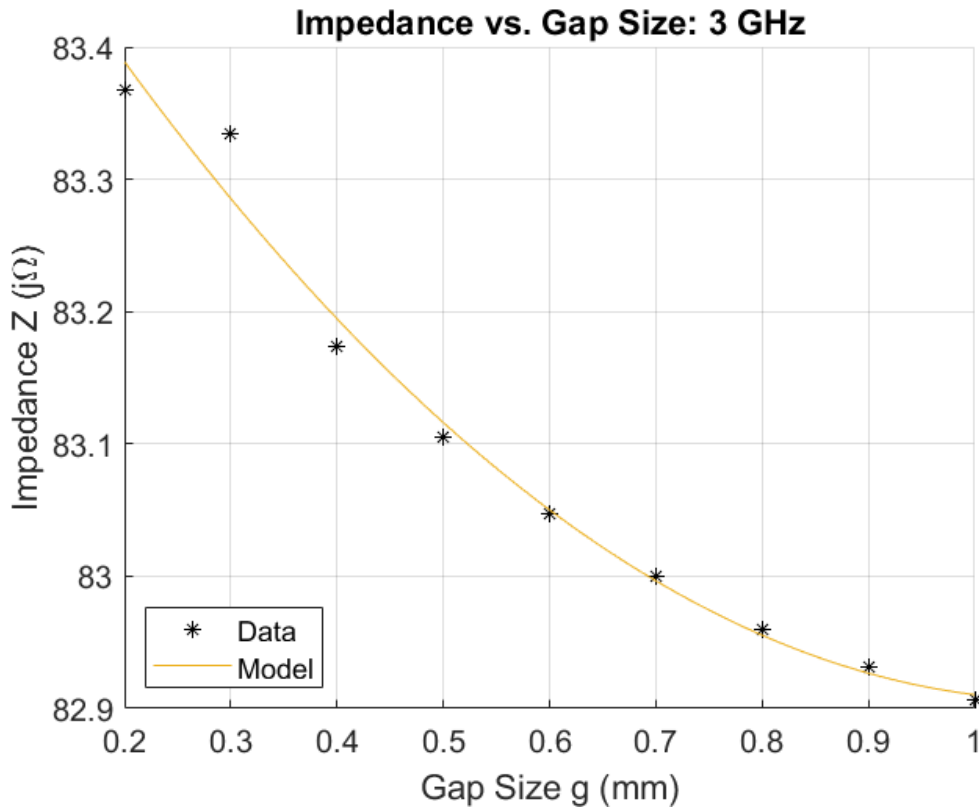


Figure 225: Circle Duroid 5880: Impedance vs. Gap Size, 3 GHz

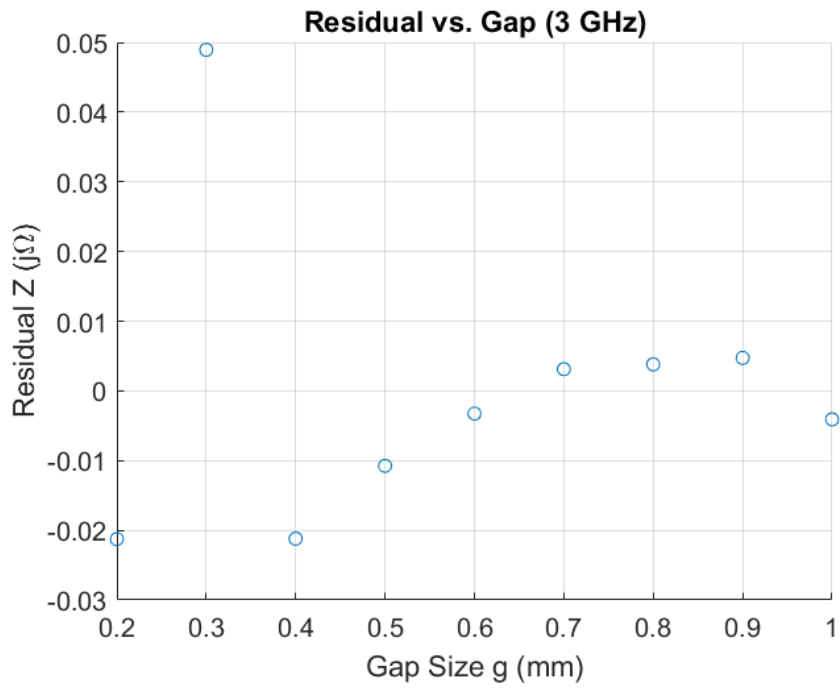


Figure 226: Circle Duroid 5880: Residuals, 3 GHz

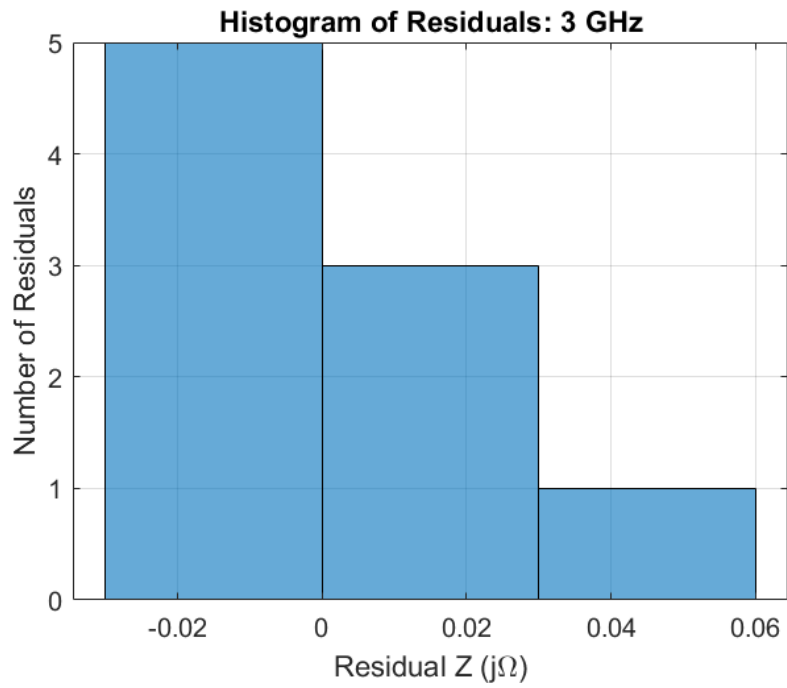


Figure 227: Circle Duroid 5880: Histogram of Residuals, 3 GHz

Model: 4 GHz

Equation form: $y = c_0 + c_1x^1 + c_2x^2$

	<u>Coefficient</u>	<u>SE</u>	<u>tStat</u>	<u>pValue</u>
c_0 (intercept)	84.858	0.045925	1847.8	1.696×10^{-18}
c_1	-2.3333	0.1707	-13.669	9.5226×10^{-6}
c_2	1.1291	0.13978	8.0778	0.00019282

Table 30: Model Coefficients: 4 GHz

Model Statistics

Error Degrees of Freedom: 6
 Root Mean Squared Error (RMSE): 0.0245
 R-squared: 0.994
 Adjusted R-Squared: 0.992
 F-statistic vs. constant model: 510
 p-value = 2×10^{-7}

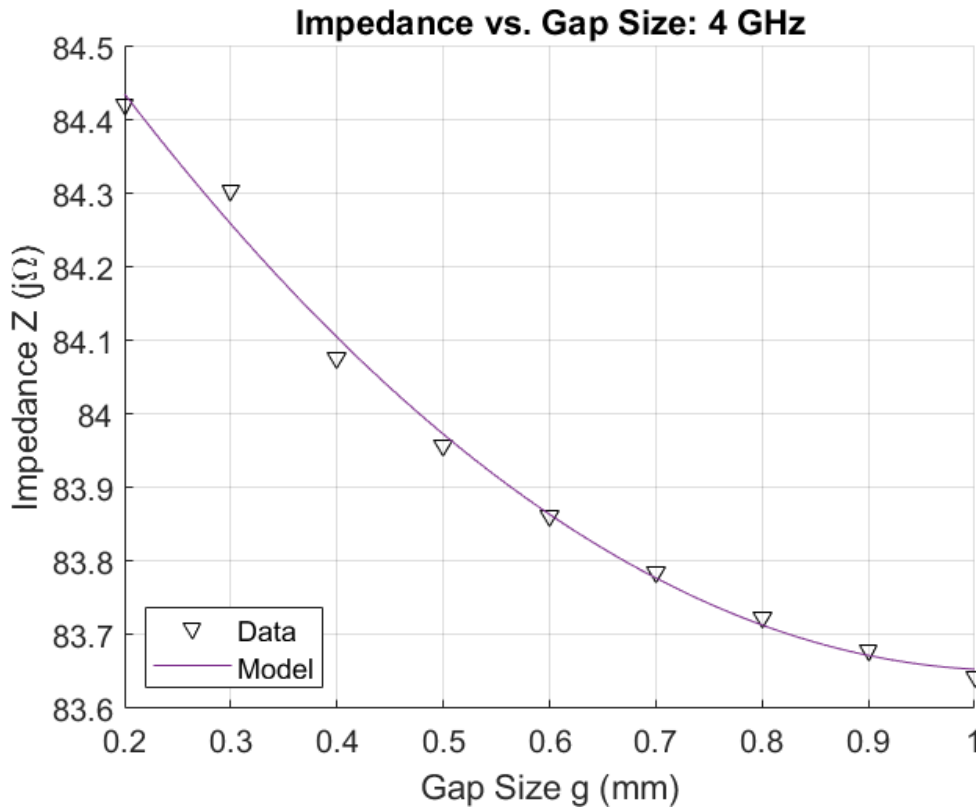


Figure 228: Circle Duroid 5880: Impedance vs. Gap Size, 4 GHz

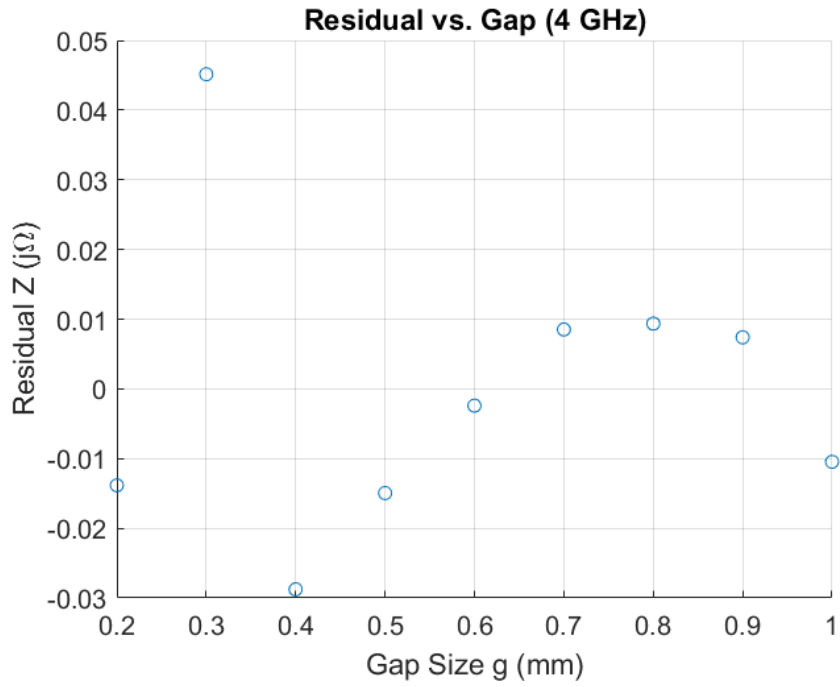


Figure 229: Circle Duroid 5880: Residuals, 4 GHz

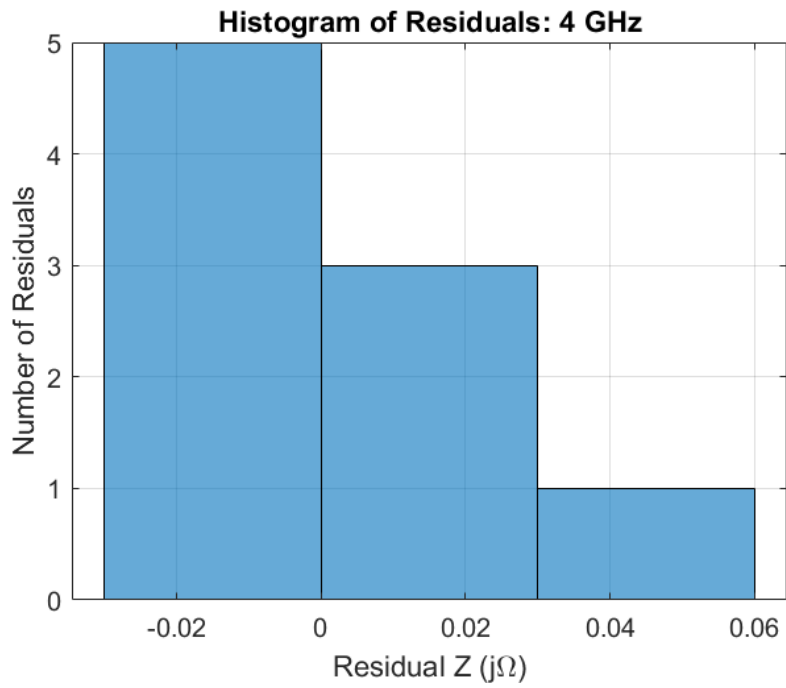


Figure 230: Circle Duroid 5880: Histogram of Residuals, 4 GHz

Model: 5 GHz

Equation form: $y = c_0 + c_1x^1 + c_2x^2$

	<u>Coefficient</u>	<u>SE</u>	<u>tStat</u>	<u>pValue</u>
c_0 (intercept)	86.501	0.052054	1661.8	3.2056×10^{-18}
c_1	-3.7046	0.19348	-19.147	1.3127×10^{-6}
c_2	1.8351	0.15844	11.583	2.4921×10^{-5}

Table 31: Model Coefficients: 5 GHz

Model Statistics

Error Degrees of Freedom: 6
 Root Mean Squared Error (RMSE): 0.0278
 R-squared: 0.997
 Adjusted R-Squared: 0.996
 F-statistic vs. constant model: 943
 p-value = 3.19×10^{-8}

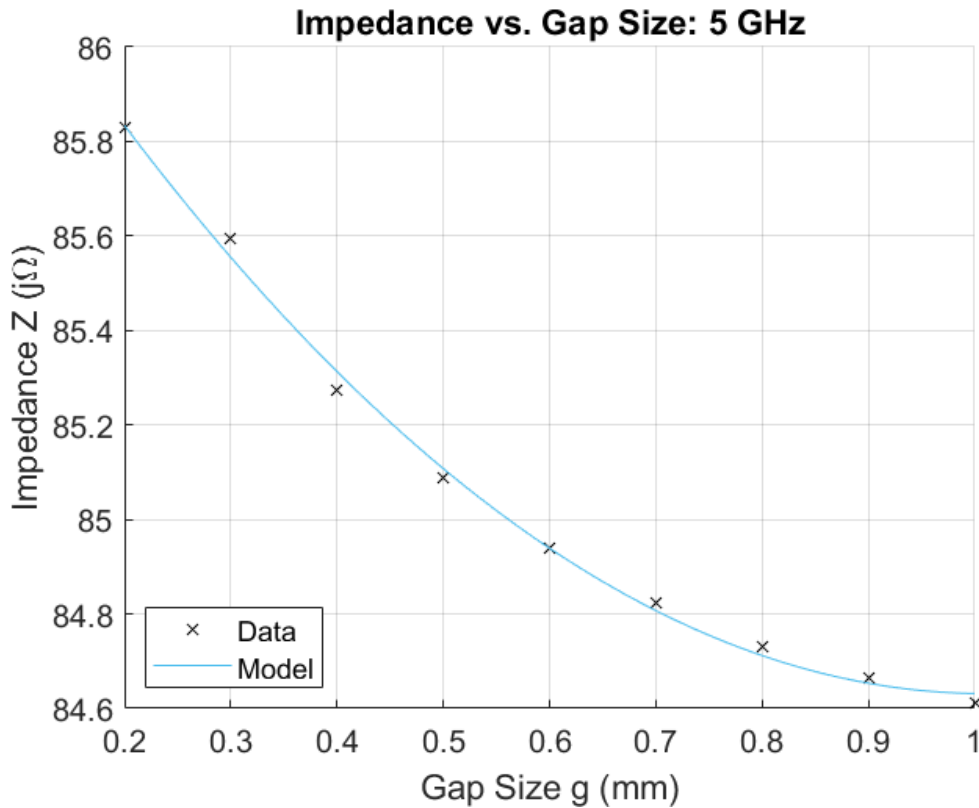


Figure 231: Circle Duroid 5880: Impedance vs. Gap Size, 5 GHz

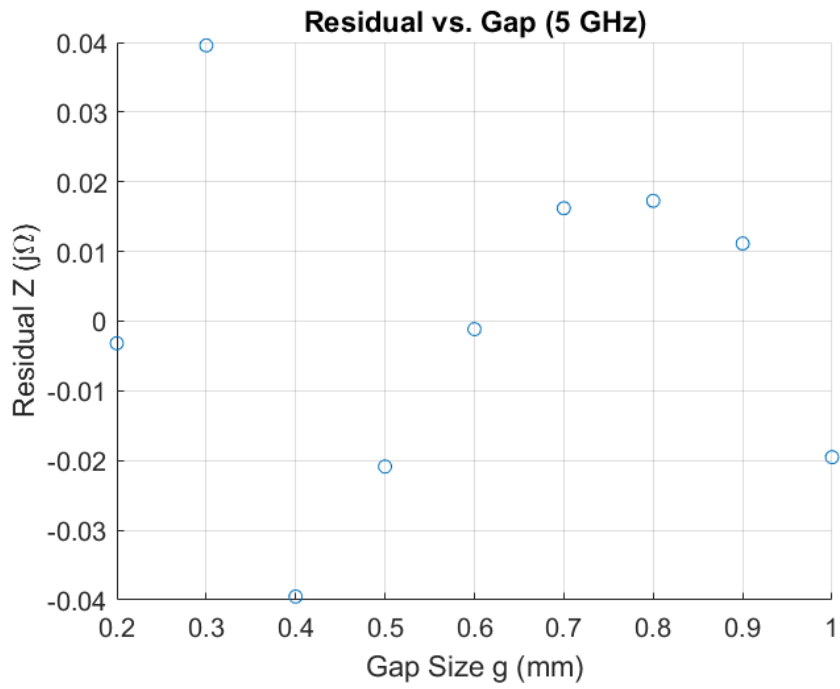


Figure 232: Circle Duroid 5880: Residuals, 5 GHz

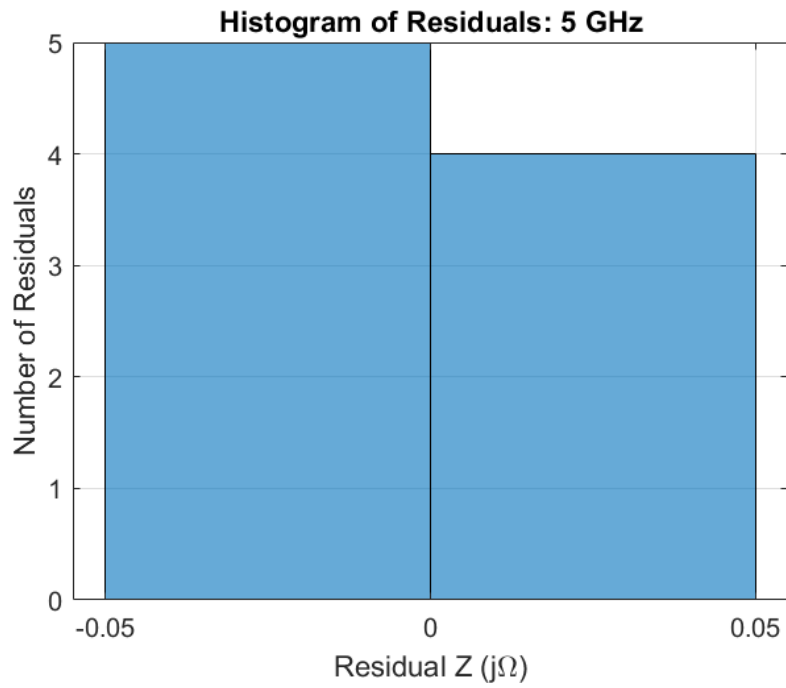


Figure 233: Circle Duroid 5880: Histogram of Residuals, 5 GHz

Model: 6 GHz

Equation form: $y = c_0 + c_1 \frac{1}{x^1} + c_2 \frac{1}{x^2}$

	<u>Coefficient</u>	<u>SE</u>	<u>tStat</u>	<u>pValue</u>
c_0 (intercept)	84.994	0.016438	5170.7	3.5318×10^{-21}
c_1	0.90728	0.013918	65.185	8.766×10^{-10}
c_2	-0.075891	0.0023347	-32.506	5.6371×10^{-8}

Table 32: Model Coefficients: 6 GHz

Model Statistics

Error Degrees of Freedom: 6
 Root Mean Squared Error (RMSE): 0.0101
 R-squared: 1
 Adjusted R-Squared: 1
 F-statistic vs. constant model: 1.5×10^4
 p-value = 8.04×10^{-12}

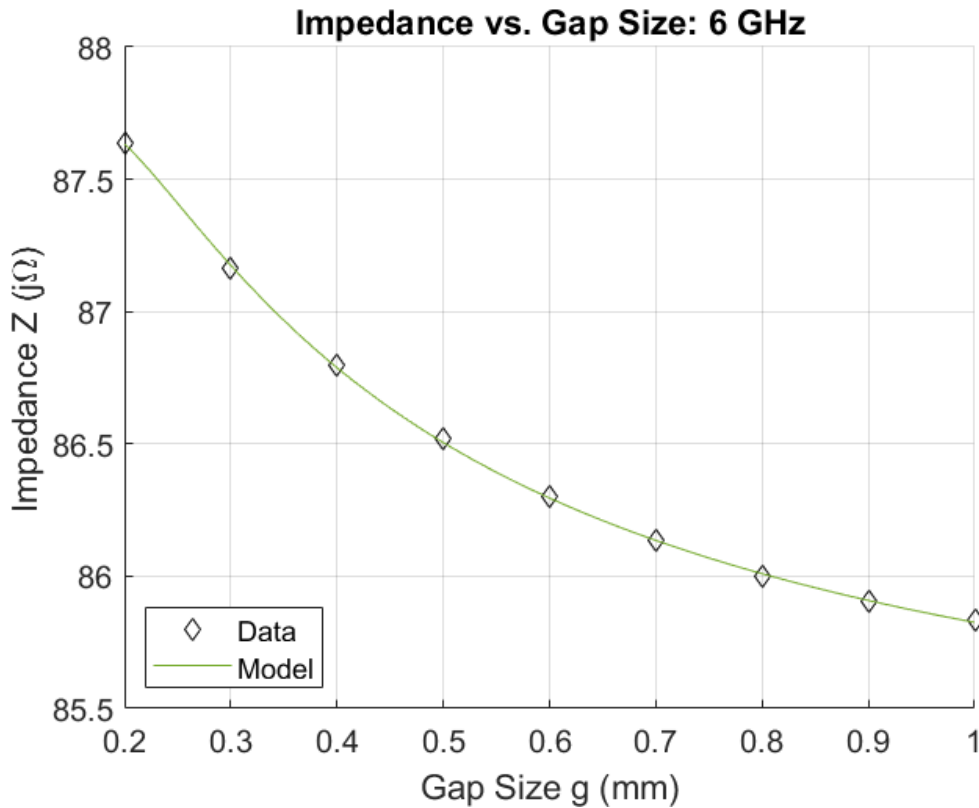


Figure 234: Circle Duroid 5880: Impedance vs. Gap Size, 6 GHz

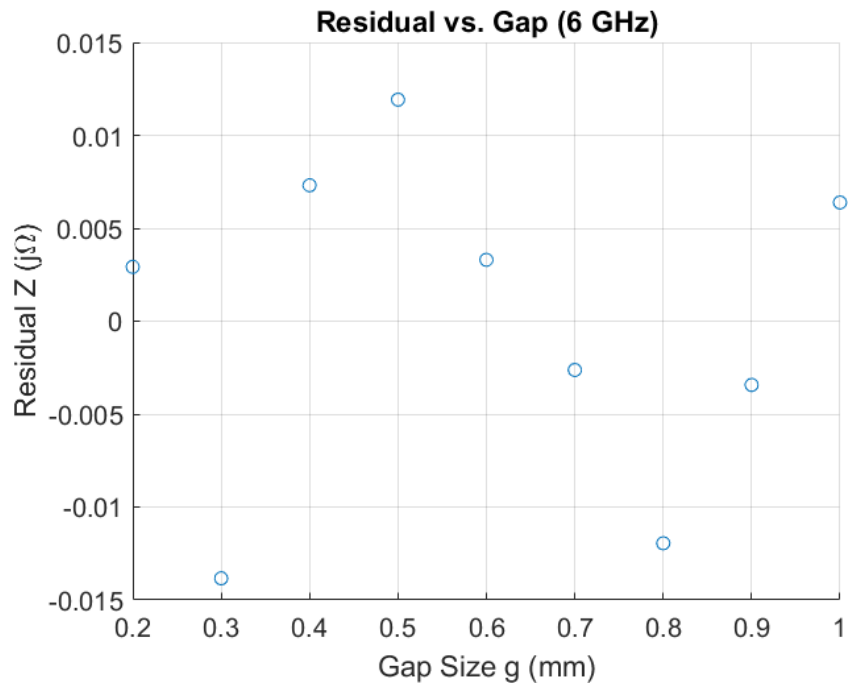


Figure 235: Circle Duroid 5880: Residuals, 6 GHz

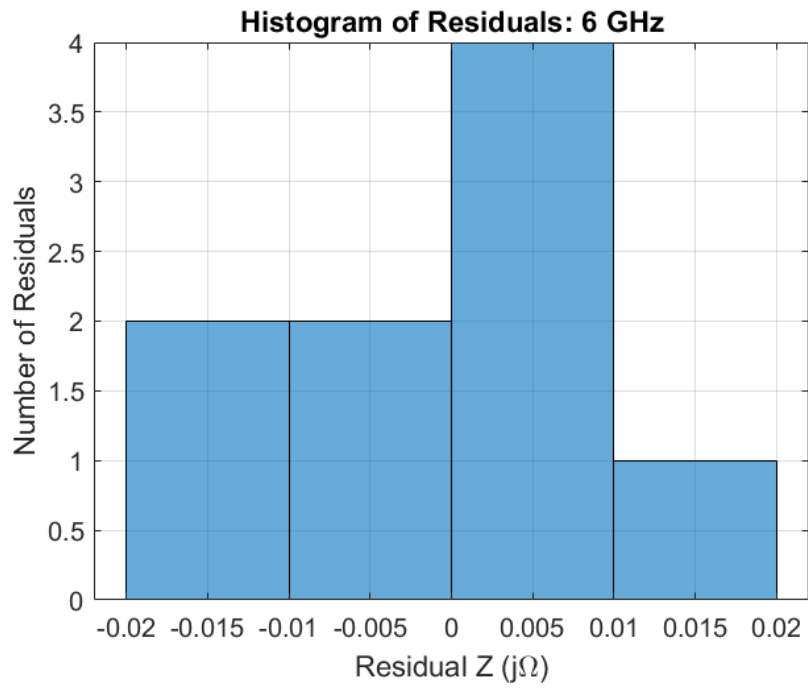


Figure 236: Circle Duroid 5880: Histogram of Residuals, 6 GHz

Model: 7 GHz

Equation form: $y = c_0 + c_1 \frac{1}{x^1} + c_2 \frac{1}{x^2}$

	<u>Coefficient</u>	<u>SE</u>	<u>tStat</u>	<u>pValue</u>
c_0 (intercept)	86.146	0.022033	3909.8	1.8895×10^{-20}
c_1	1.2685	0.018657	67.991	6.8096×10^{-10}
c_2	-0.10376	0.0031294	-33.156	5.0083×10^{-8}

Table 33: Model Coefficients: 7 GHz

Model Statistics

Error Degrees of Freedom: 6
 Root Mean Squared Error (RMSE): 0.0135
 R-squared: 1
 Adjusted R-Squared: 1
 F-statistic vs. constant model: 1.69×10^4
 p-value = 5.55×10^{-12}

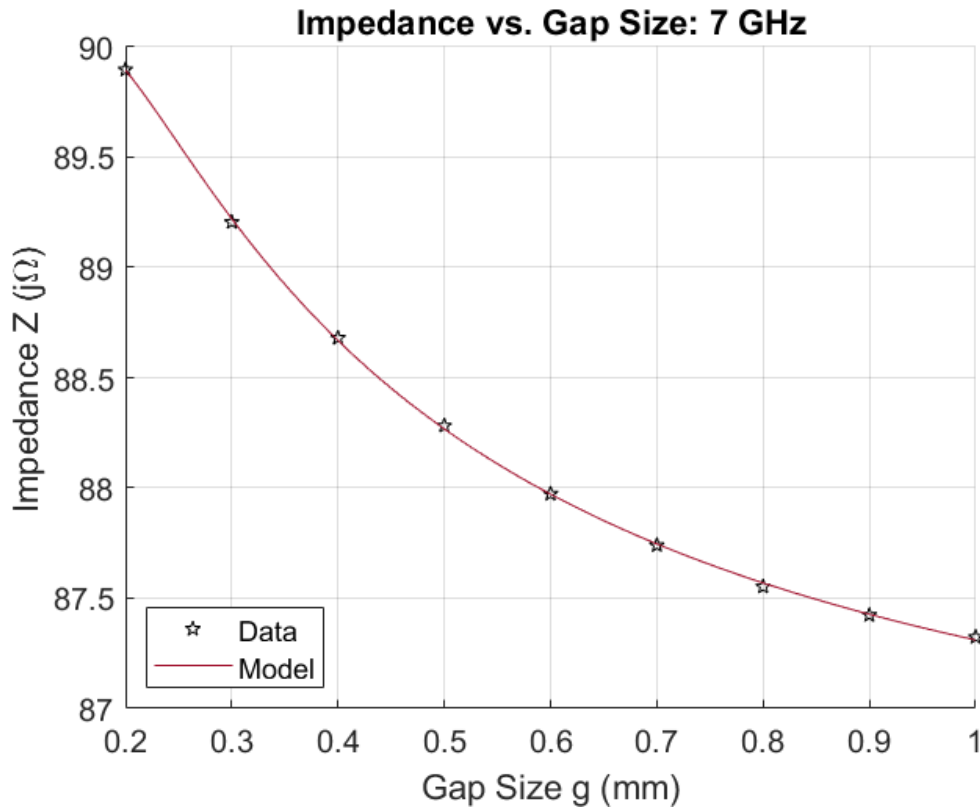


Figure 237: Circle Duroid 5880: Impedance vs. Gap Size, 7 GHz

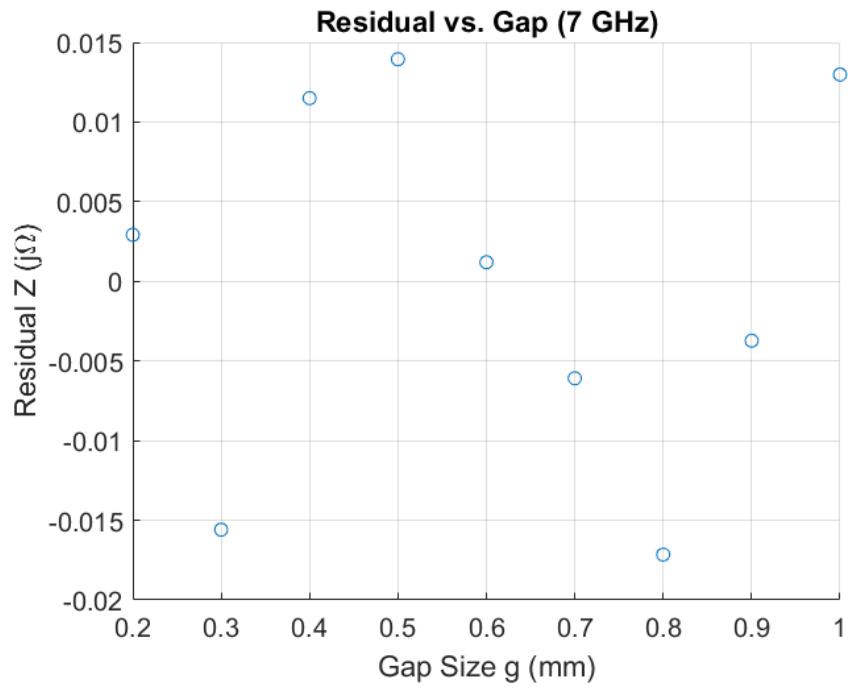


Figure 238: Circle Duroid 5880: Residuals, 7 GHz

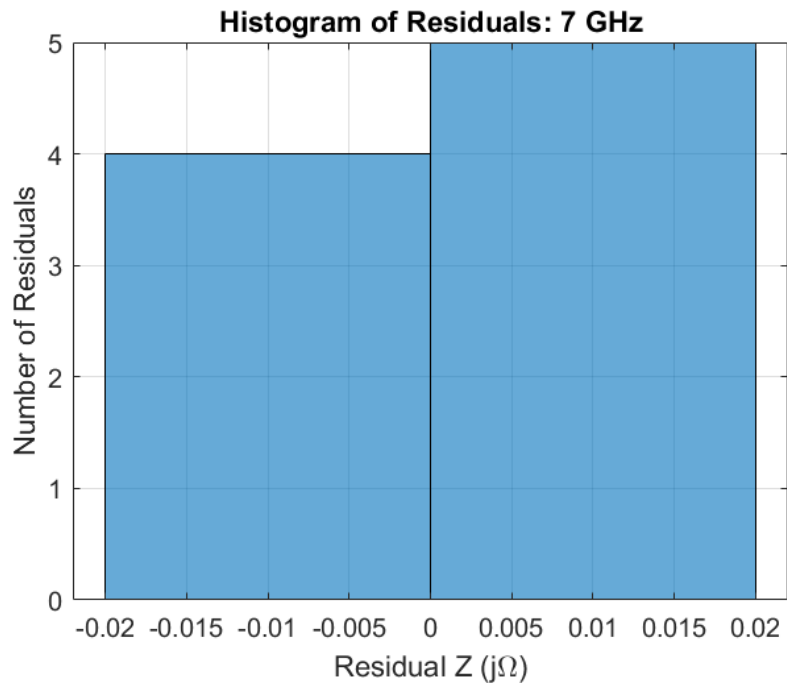


Figure 239: Circle Duroid 5880: Histogram of Residuals, 7 GHz

Model: 8 GHz

Equation form: $y = c_0 + c_1 \frac{1}{x^1} + c_2 \frac{1}{x^2}$

	Coefficient	SE	tStat	pValue
c_0 (intercept)	87.501	0.030007	2916	1.098×10^{-19}
c_1	1.7311	0.025409	68.132	6.7256×10^{-10}
c_2	-0.1387	0.004262	-32.543	5.5987×10^{-8}

Table 34: Model Coefficients: 8 GHz

Model Statistics

Error Degrees of Freedom: 6
 Root Mean Squared Error (RMSE): 0.0184
 R-squared: 1
 Adjusted R-Squared: 1
 F-statistic vs. constant model: 1.76×10^4
 p-value = 4.94×10^{-12}

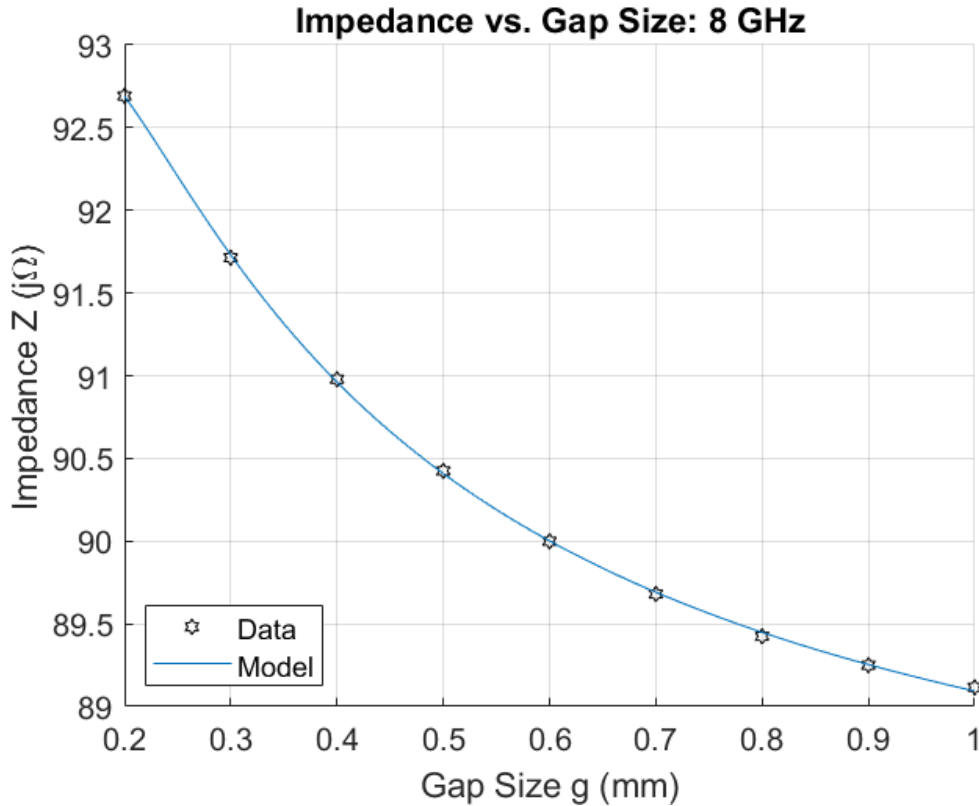


Figure 240: Circle Duroid 5880: Impedance vs. Gap Size, 8 GHz

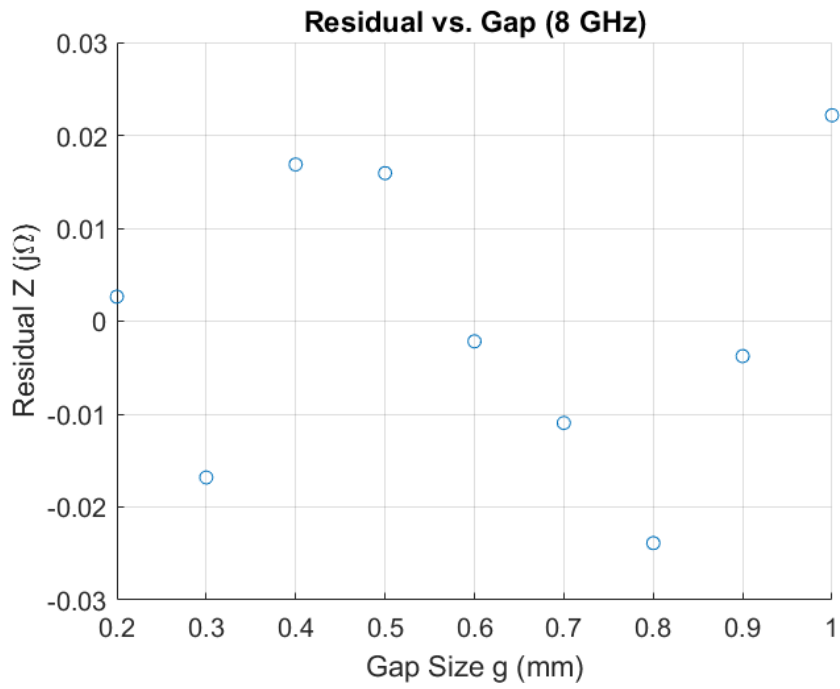


Figure 241: Circle Duroid 5880: Residuals, 8 GHz

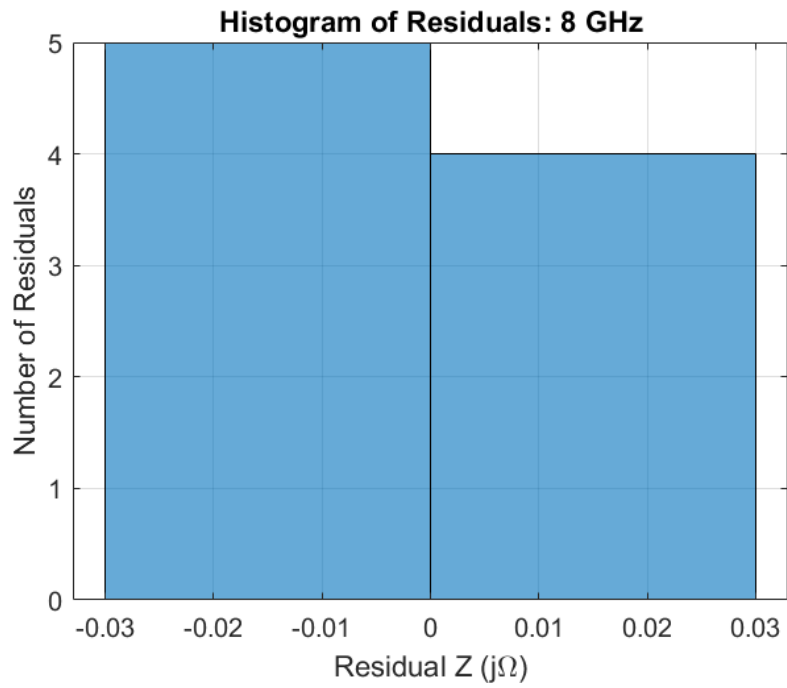


Figure 242: Circle Duroid 5880: Histogram of Residuals, 8 GHz

Model: 9 GHz

Equation form: $y = c_0 + c_1 \frac{1}{x^1} + c_2 \frac{1}{x^2}$

	<u>Coefficient</u>	<u>SE</u>	<u>tStat</u>	<u>pValue</u>
c_0 (intercept)	89.067	0.041146	2164.6	6.5613×10^{-19}
c_1	2.3209	0.034841	66.615	7.6975×10^{-10}
c_2	-0.18215	0.0058441	-31.168	7.2455×10^{-8}

Table 35: Model Coefficients: 9 GHz

Model Statistics

Error Degrees of Freedom: 6
 Root Mean Squared Error (RMSE): 0.0252
 R-squared: 1
 Adjusted R-Squared: 1
 F-statistic vs. constant model: 1.74×10^4
 p-value = 5.12×10^{-12}

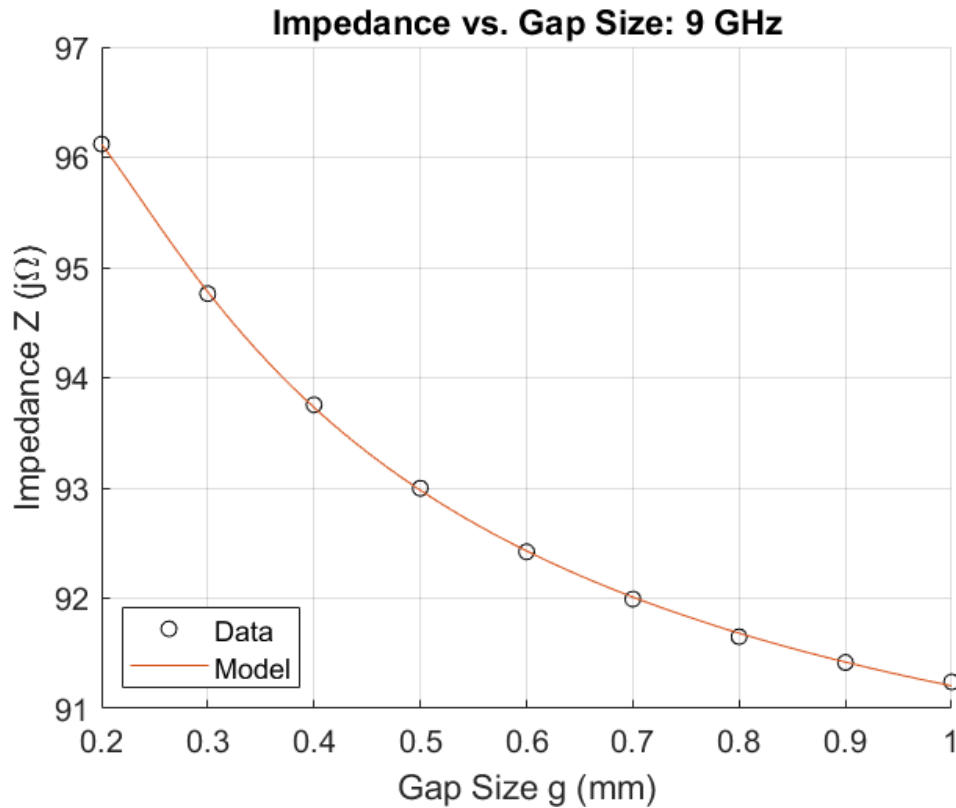


Figure 243: Circle Duroid 5880: Impedance vs. Gap Size, 9 GHz

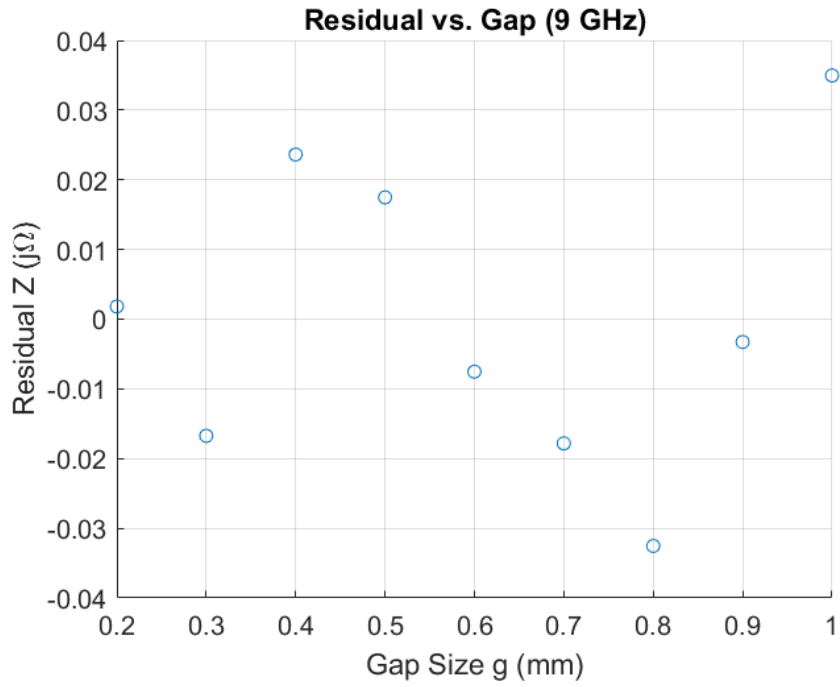


Figure 244: Circle Duroid 5880: Residuals, 9 GHz

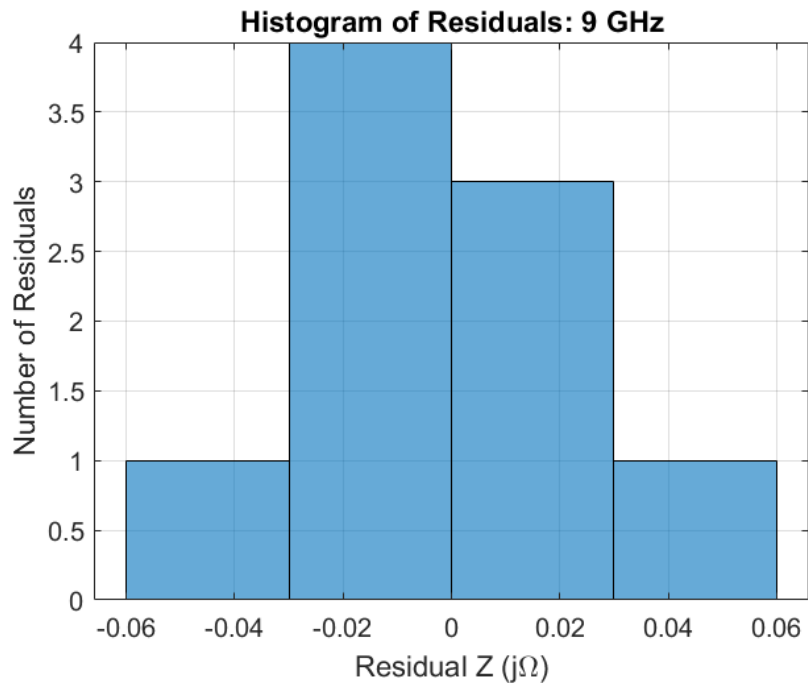


Figure 245: Circle Duroid 5880: Histogram of Residuals, 9 GHz

Model: 10 GHz

Equation form: $y = c_0 + c_1 \frac{1}{x^1} + c_2 \frac{1}{x^2}$

	<u>Coefficient</u>	<u>SE</u>	<u>tStat</u>	<u>pValue</u>
c_0 (intercept)	90.85	0.056798	1599.5	4.0302×10^{-18}
c_1	3.0687	0.048094	63.808	9.9627×10^{-10}
c_2	-0.23537	0.0080672	-29.176	1.0743×10^{-7}

Table 36: Model Coefficients: 10 GHz

Model Statistics

Error Degrees of Freedom: 6
 Root Mean Squared Error (RMSE): 0.0348
 R-squared: 1
 Adjusted R-Squared: 1
 F-statistic vs. constant model: 1.66×10^4
 p-value = 5.95×10^{-12}

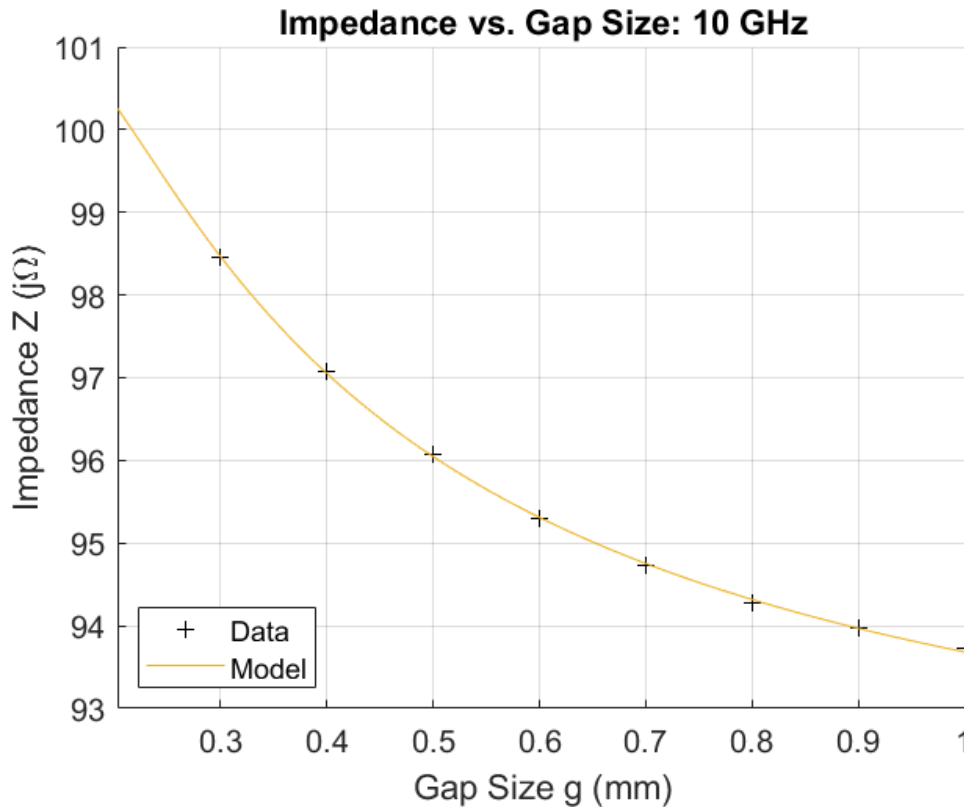


Figure 246: Circle Duroid 5880: Impedance vs. Gap Size, 10 GHz

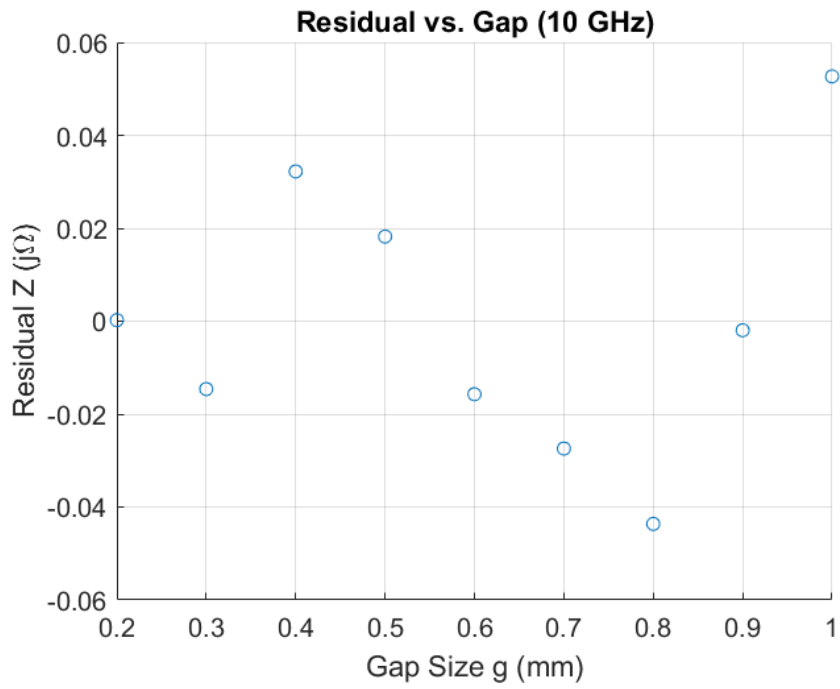


Figure 247: Circle Duroid 5880: Residuals, 10 GHz

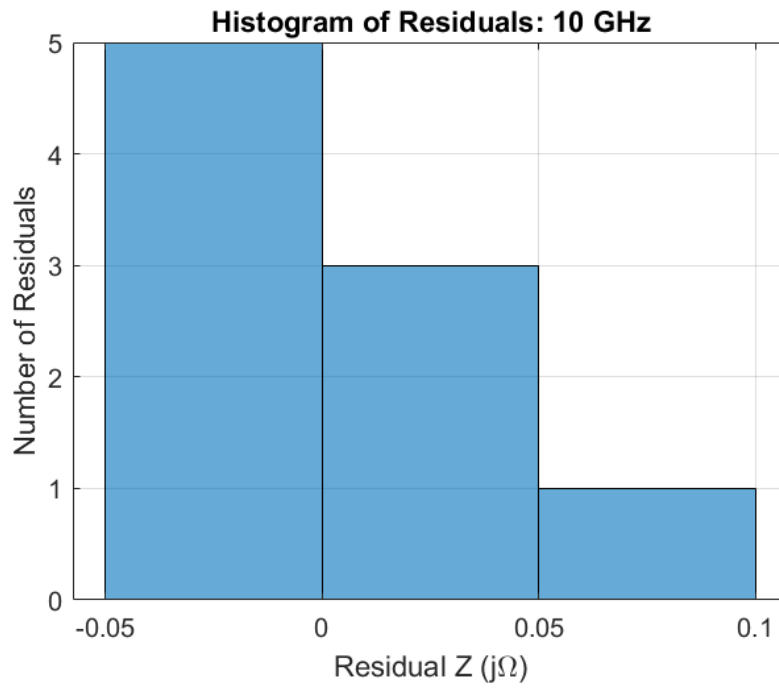


Figure 248: Circle Duroid 5880: Histogram of Residuals, 10 GHz

Model: 11 GHz

Equation form: $y = c_0 + c_1 \frac{1}{x^1} + c_2 \frac{1}{x^2} + c_3 \frac{1}{x^3}$

	<u>Coefficient</u>	<u>SE</u>	<u>tStat</u>	<u>pValue</u>
c_0 (intercept)	93.251	0.17509	532.59	4.4292×10^{-13}
c_2	3.4214	0.23478	14.573	2.7475×10^{-5}
c_2	-0.045742	0.091005	-0.50263	0.63657
c_3	-0.03036	0.010325	-2.9406	0.032236

Table 37: Model Coefficients: 11 GHz

Model Statistics

Error Degrees of Freedom: 5
 Root Mean Squared Error (RMSE): 0.0378
 R-squared: 1
 Adjusted R-Squared: 1
 F-statistic vs. constant model: 1.68×10^4
 p-value = 1.98×10^{-10}

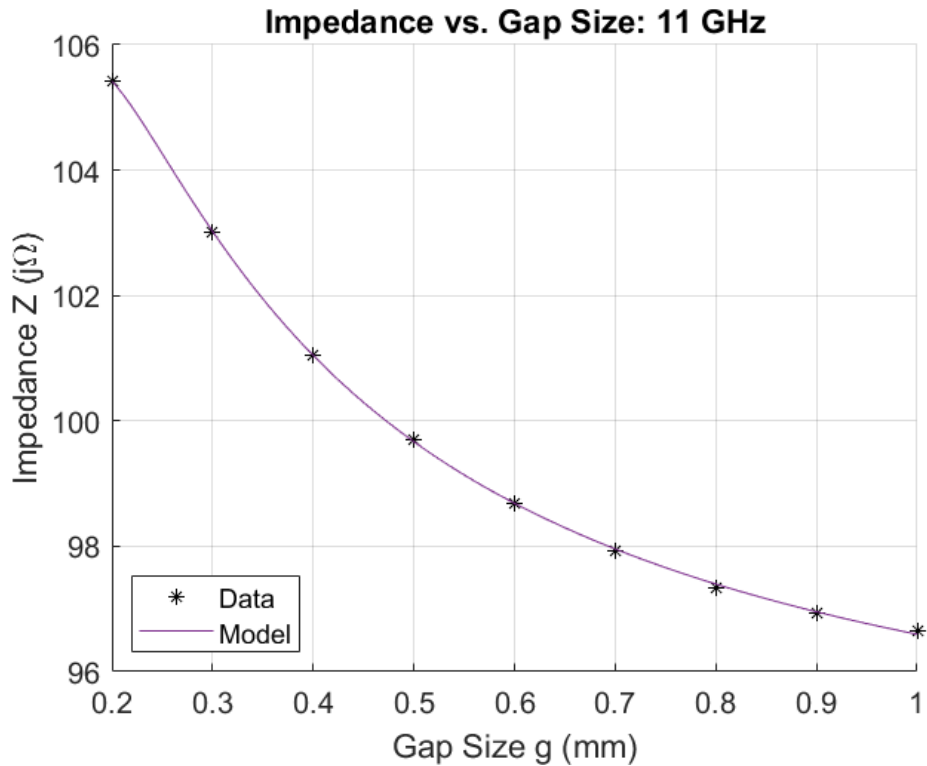


Figure 249: Circle Duroid 5880: Impedance vs. Gap Size, 11 GHz

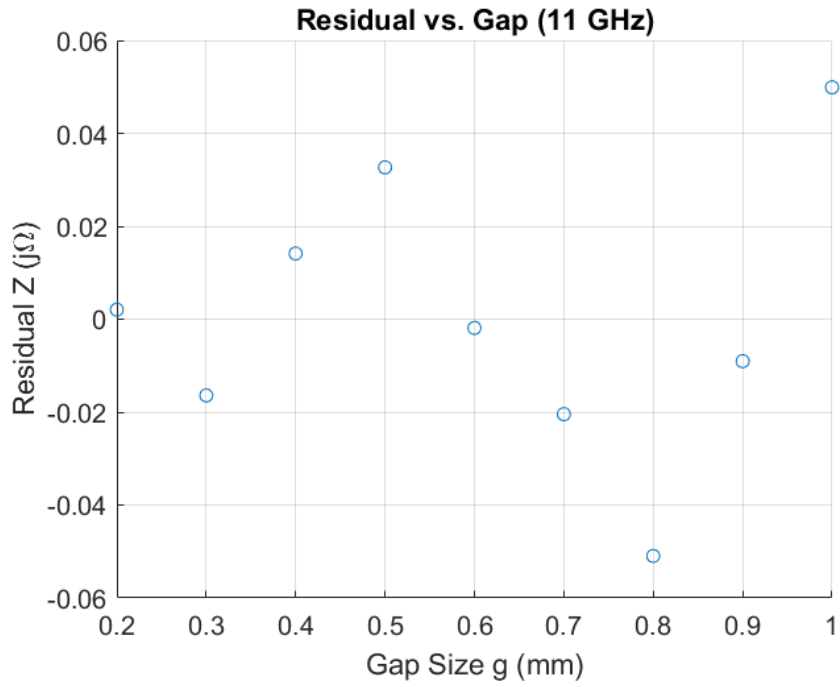


Figure 250: Circle Duroid 5880: Residuals, 11 GHz

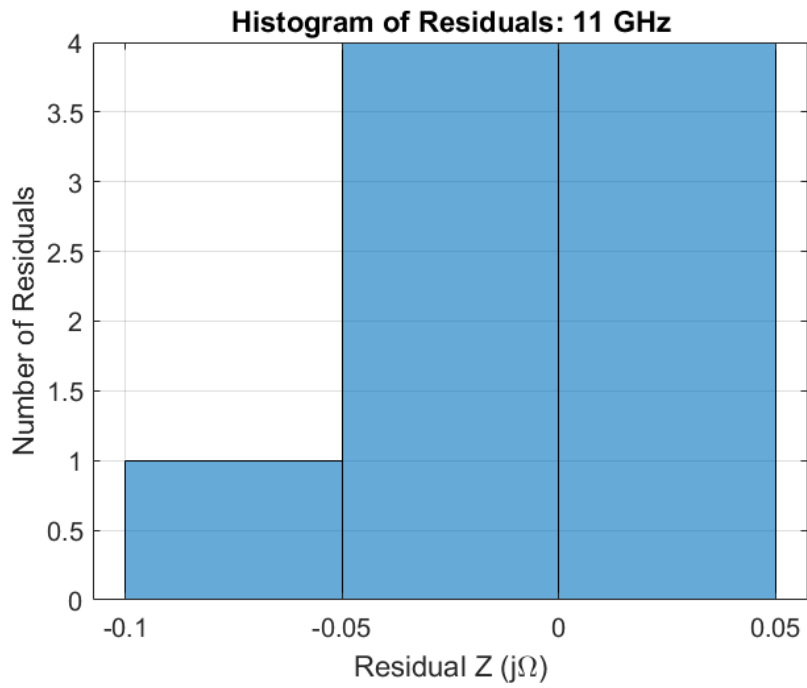


Figure 251: Circle Duroid 5880: Histogram of Residuals, 11 GHz

Model: 12 GHz

Equation form: $y = c_0 + c_1 \frac{1}{x^1} + c_2 \frac{1}{x^2} + c_3 \frac{1}{x^3}$

	<u>Coefficient</u>	<u>SE</u>	<u>tStat</u>	<u>pValue</u>
c_0 (intercept)	95.647	0.24141	396.2	1.944×10^{-12}
c_2	4.368	0.3237	13.494	4.0033×10^{-5}
c_2	-0.025229	0.12548	-0.20106	0.84857
c_3	-0.041765	0.014235	-2.9339	0.032485

Table 38: Model Coefficients: 12 GHz

Model Statistics

Error Degrees of Freedom: 5
 Root Mean Squared Error (RMSE): 0.0521
 R-squared: 1
 Adjusted R-Squared: 1
 F-statistic vs. constant model: 1.55×10^4
 p-value = 2.45×10^{-10}

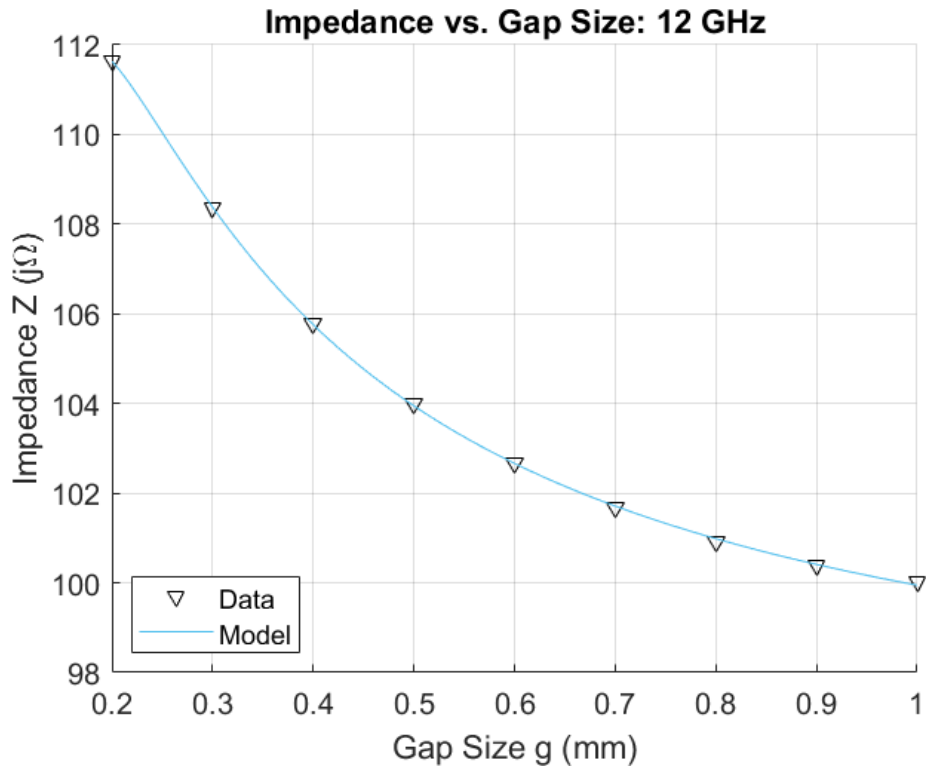


Figure 252: Circle Duroid 5880: Impedance vs. Gap Size, 12 GHz

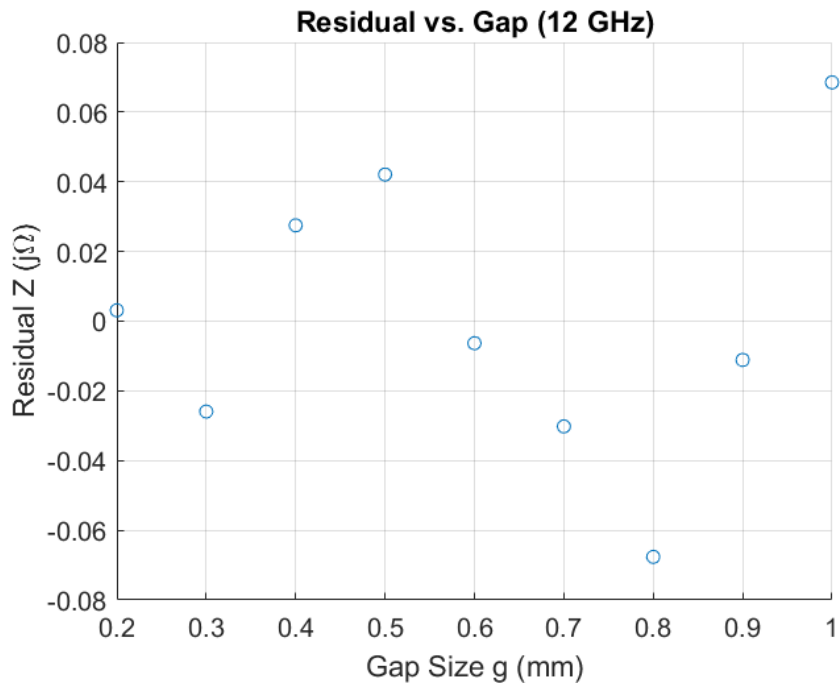


Figure 253: Circle Duroid 5880: Residuals, 12 GHz

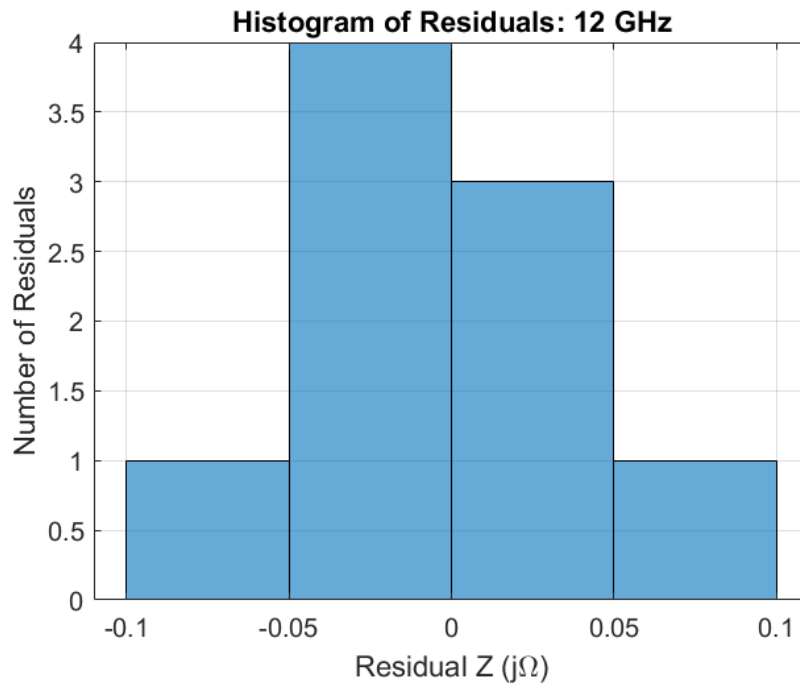


Figure 254: Circle Duroid 5880: Histogram of Residuals, 12 GHz

Model: 13 GHz

Equation form: $y = c_0 + c_1 \frac{1}{x^1} + c_2 \frac{1}{x^2} + c_3 \frac{1}{x^3}$

	Coefficient	SE	tStat	pValue
c_0 (intercept)	98.328	0.32762	300.13	7.7931×10^{-12}
c_2	5.5083	0.4393	12.539	5.7265×10^{-5}
c_2	0.020828	0.17028	0.12231	0.90742
c_3	-0.05792	0.019319	-2.9981	0.030165

Table 39: Model Coefficients: 13 GHz

Model Statistics

Error Degrees of Freedom: 5
 Root Mean Squared Error (RMSE): 0.0707
 R-squared: 1
 Adjusted R-Squared: 1
 F-statistic vs. constant model: 1.45×10^4
 p-value = 2.91×10^{-10}

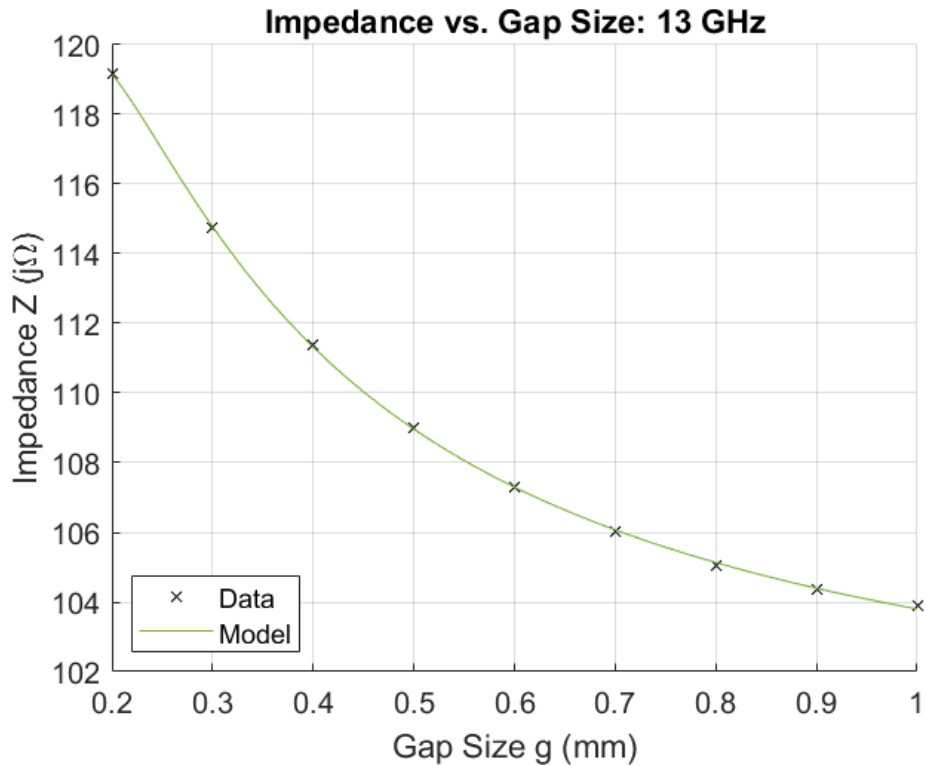


Figure 255: Circle Duroid 5880: Impedance vs. Gap Size, 13 GHz

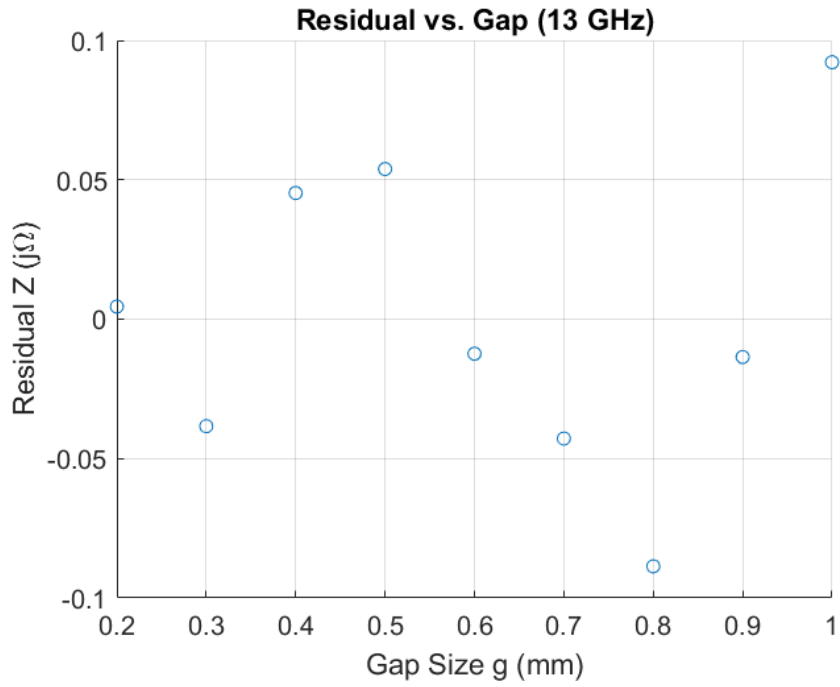


Figure 256: Circle Duroid 5880: Residuals, 13 GHz

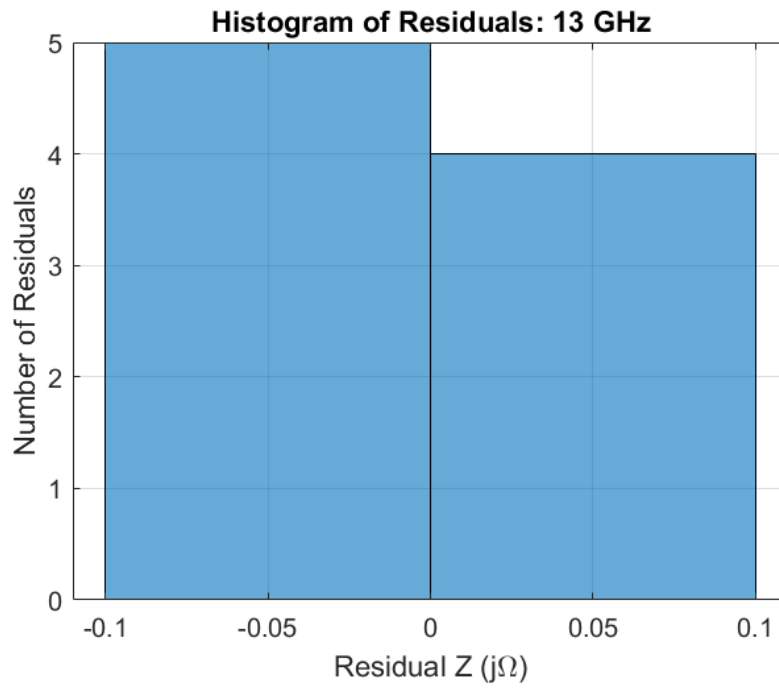


Figure 257: Circle Duroid 5880: Histogram of Residuals, 13 GHz

Model: 14 GHz

Equation form: $y = c_0 + c_1 \frac{1}{x^1} + c_2 \frac{1}{x^2} + c_3 \frac{1}{x^3}$

	<u>Coefficient</u>	<u>SE</u>	<u>tStat</u>	<u>pValue</u>
c_0 (intercept)	101.3	0.43706	231.78	2.8368×10^{-11}
c_2	6.8652	0.58605	11.714	7.9685×10^{-5}
c_2	0.10211	0.22717	0.44951	0.67188
c_3	-0.080617	0.025772	-3.1281	0.026014

Table 40: Model Coefficients: 14 GHz

Model Statistics

Error Degrees of Freedom: 5
 Root Mean Squared Error (RMSE): 0.0943
 R-squared: 1
 Adjusted R-Squared: 1
 F-statistic vs. constant model: 1.36×10^4
 p-value = 3.36×10^{-10}

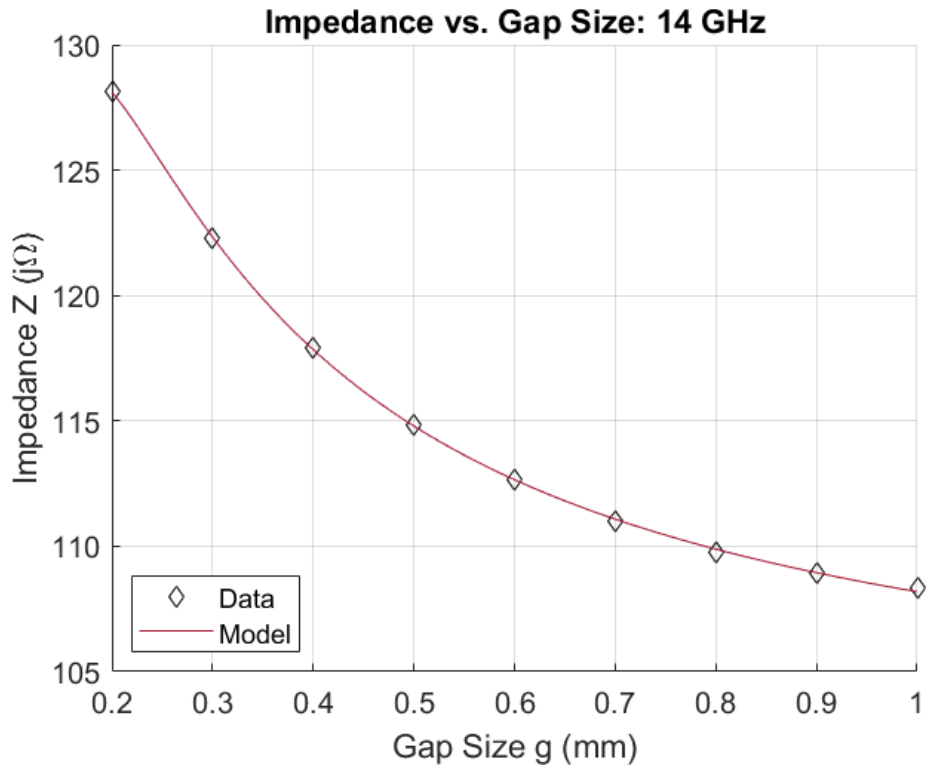


Figure 258: Circle Duroid 5880: Impedance vs. Gap Size, 14 GHz

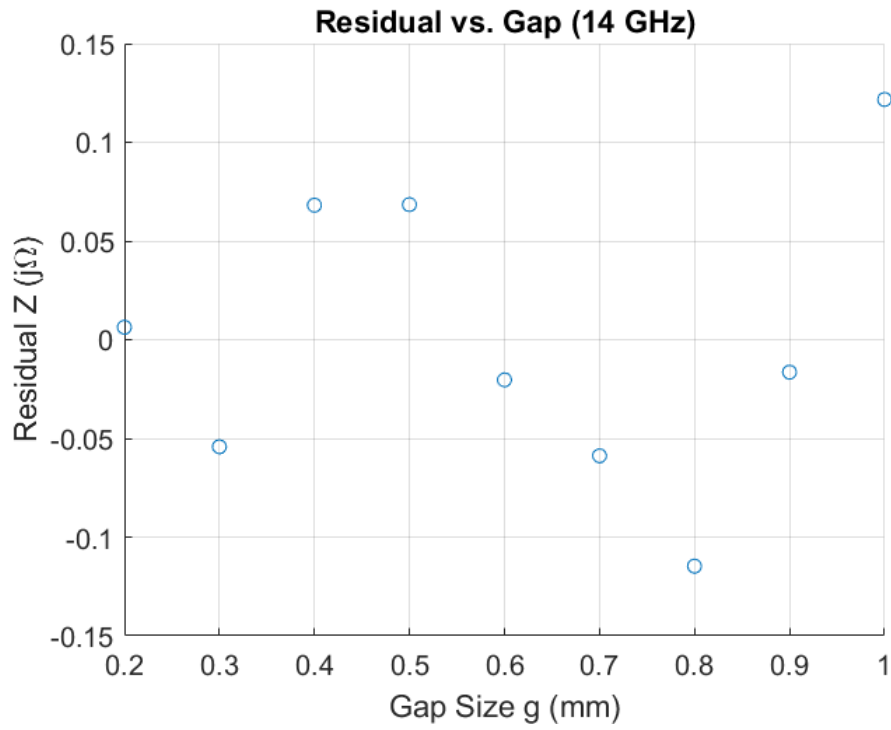


Figure 259: Circle Duroid 5880: Residuals, 14 GHz

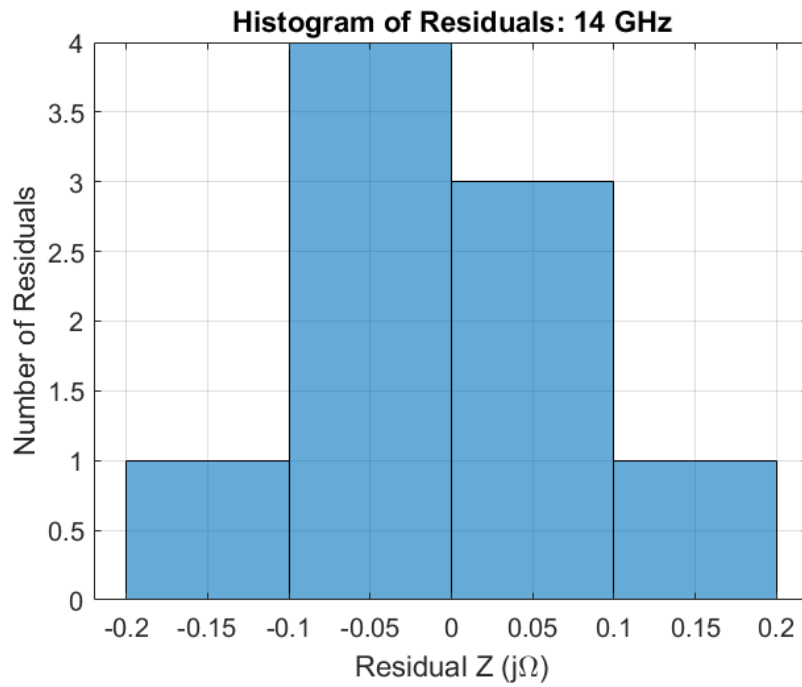


Figure 260: Circle Duroid 5880: Histogram of Residuals, 14 GHz

Model: 15 GHz

Equation form: $y = c_0 + c_1 \frac{1}{x^1} + c_2 \frac{1}{x^2} + c_3 \frac{1}{x^3}$

	<u>Coefficient</u>	<u>SE</u>	<u>tStat</u>	<u>pValue</u>
c_0 (intercept)	104.54	0.57615	181.45	9.6469×10^{-11}
c_2	8.497	0.77256	10.998	0.00010813
c_2	0.20597	0.29946	0.6878	0.52218
c_3	-0.10883	0.033974	-3.2034	0.023904

Table 41: Model Coefficients: 15 GHz

Model Statistics

Error Degrees of Freedom: 5
 Root Mean Squared Error (RMSE): 0.124
 R-squared: 1
 Adjusted R-Squared: 1
 F-statistic vs. constant model: 1.28×10^4
 p-value = 3.95×10^{-10}

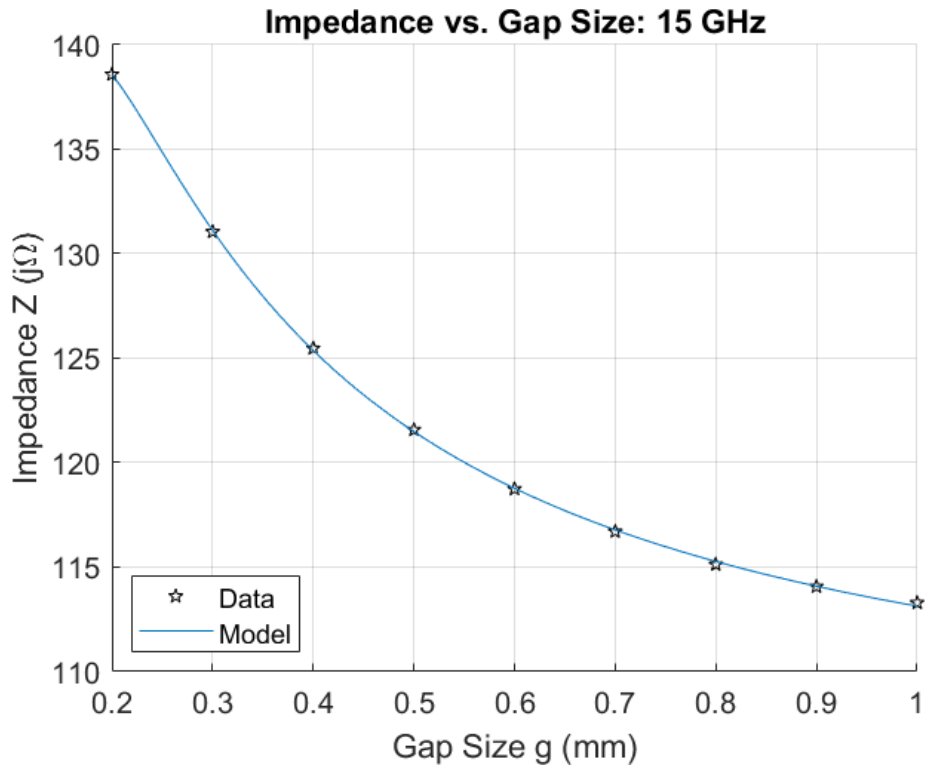


Figure 261: Circle Duroid 5880: Impedance vs. Gap Size, 15 GHz

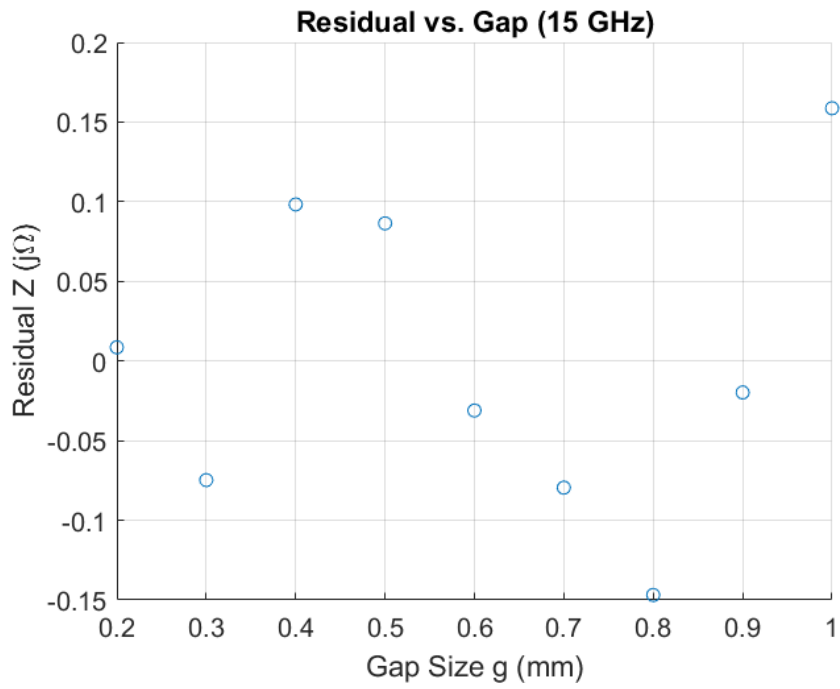


Figure 262: Circle Duroid 5880: Residuals, 15 GHz

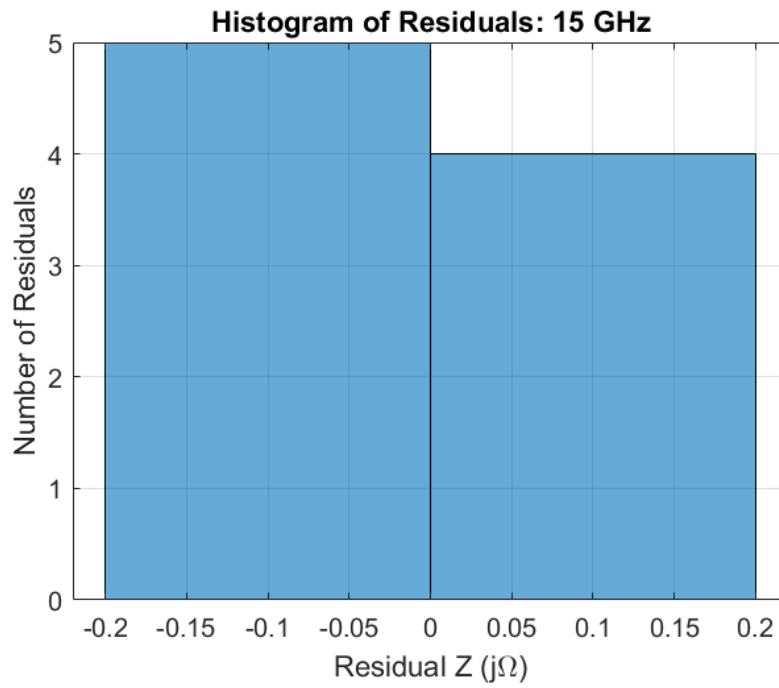


Figure 263: Circle Duroid 5880: Histogram of Residuals, 15 GHz

Model: 16 GHz

Equation form: $y = c_0 + c_1 \frac{1}{x^1} + c_2 \frac{1}{x^2} + c_3 \frac{1}{x^3}$

	<u>Coefficient</u>	<u>SE</u>	<u>tStat</u>	<u>pValue</u>
c_0 (intercept)	108.02	0.74889	144.24	3.0386×10^{-10}
c_2	10.453	1.0042	10.409	0.00014098
c_2	0.31522	0.38924	0.80984	0.45483
c_3	-0.14187	0.04416	-3.2127	0.023657

Table 42: Model Coefficients: 16 GHz

Model Statistics

Error Degrees of Freedom: 5
 Root Mean Squared Error (RMSE): 0.162
 R-squared: 1
 Adjusted R-Squared: 1
 F-statistic vs. constant model: 1.18×10^4
 p-value = 4.81×10^{-10}

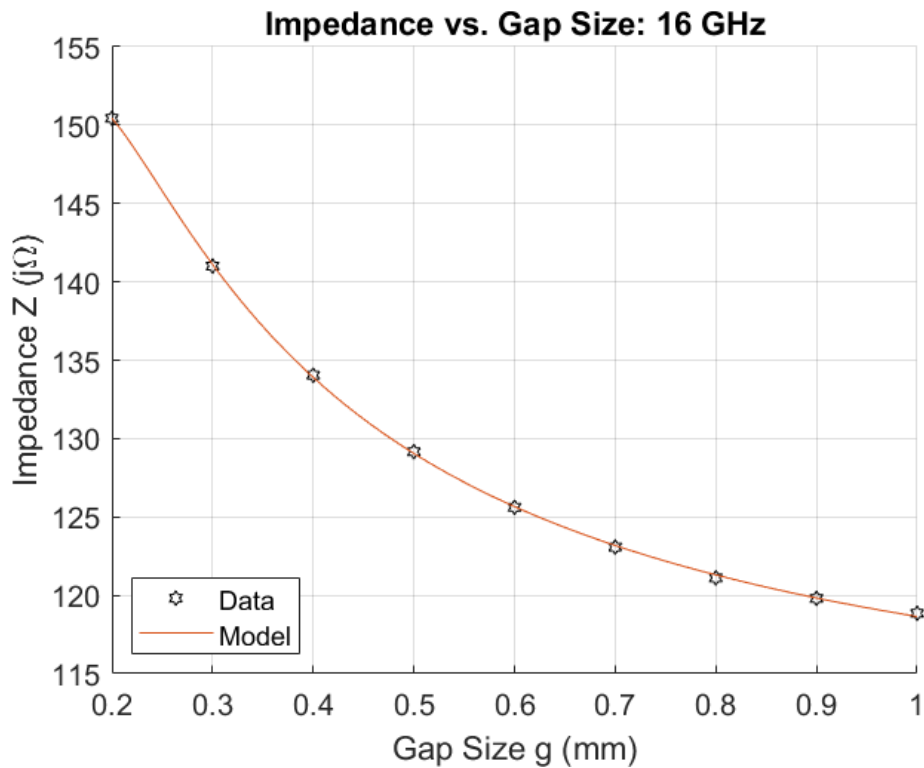


Figure 264: Circle Duroid 5880: Impedance vs. Gap Size, 16 GHz

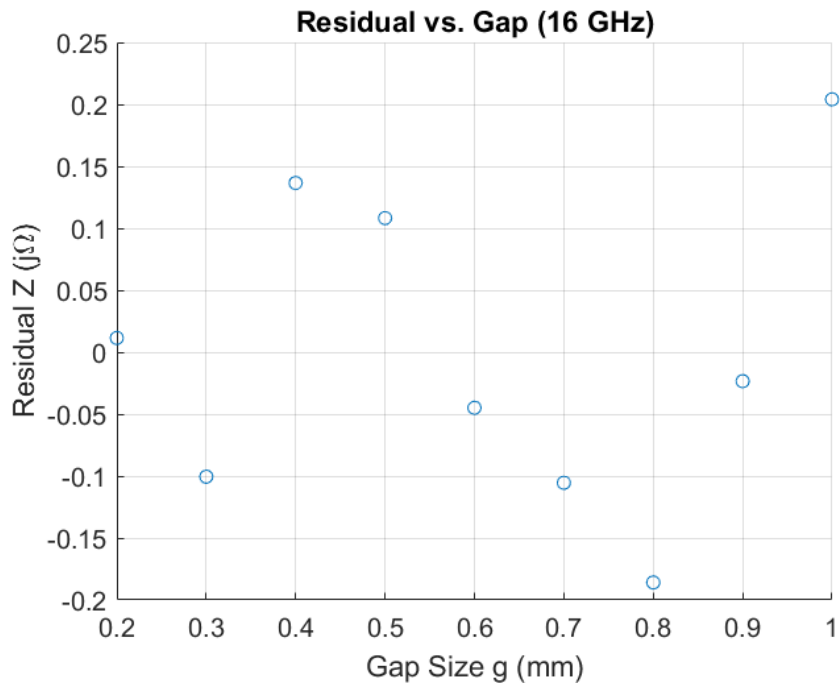


Figure 265: Circle Duroid 5880: Residuals, 16 GHz

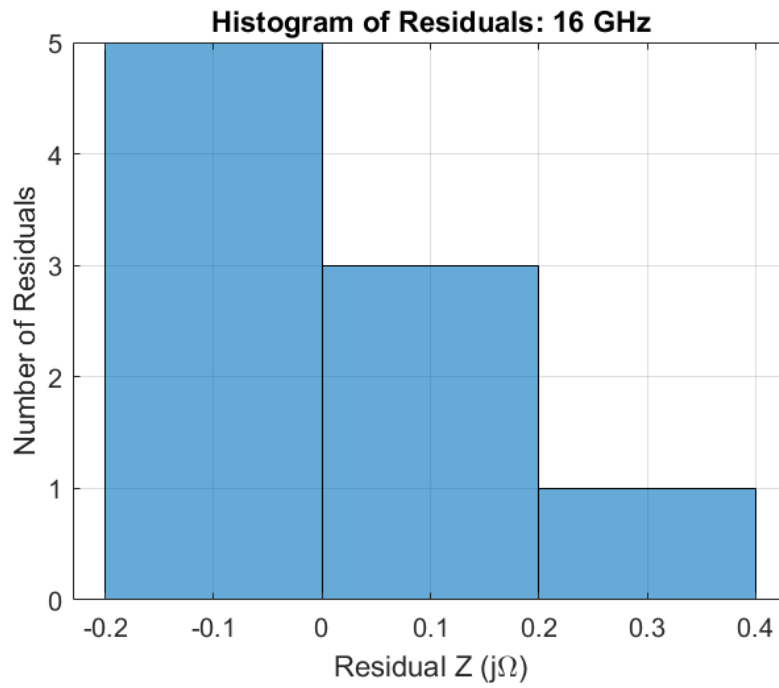


Figure 266: Circle Duroid 5880: Histogram of Residuals, 16 GHz

Model: 17 GHz

Equation form: $y = c_0 + c_1x^1 + c_2x^2 + c_3x^3$

	<u>Coefficient</u>	<u>SE</u>	<u>tStat</u>	<u>pValue</u>
c_0 (intercept)	195.31	0.87933	222.11	3.5105×10^{-11}
c_2	-196.61	5.43	-36.209	3.0249×10^{-7}
c_2	197.5	9.8708	20.009	5.7629×10^{-6}
c_3	-71.397	5.445	-13.112	4.60451×10^{-5}

Table 43: Model Coefficients: 17 GHz

Model Statistics

Error Degrees of Freedom: 5
 Root Mean Squared Error (RMSE): 0.206
 R-squared: 1
 Adjusted R-Squared: 1
 F-statistic vs. constant model: 1.09×10^4
 p-value = 5.95×10^{-10}

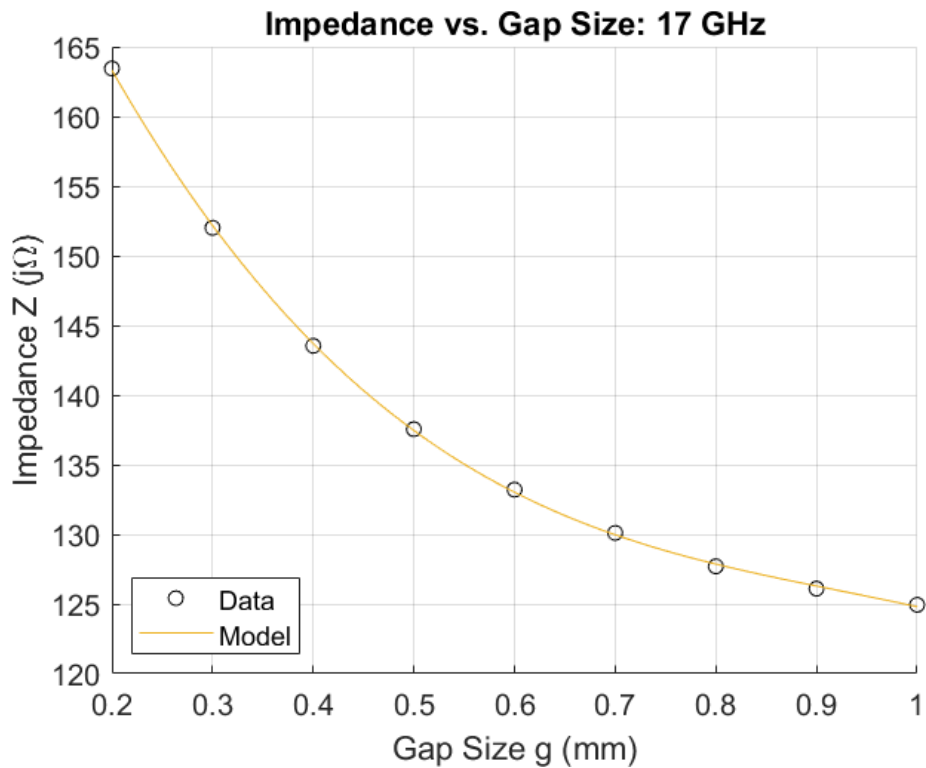


Figure 267: Circle Duroid 5880: Impedance vs. Gap Size, 17 GHz

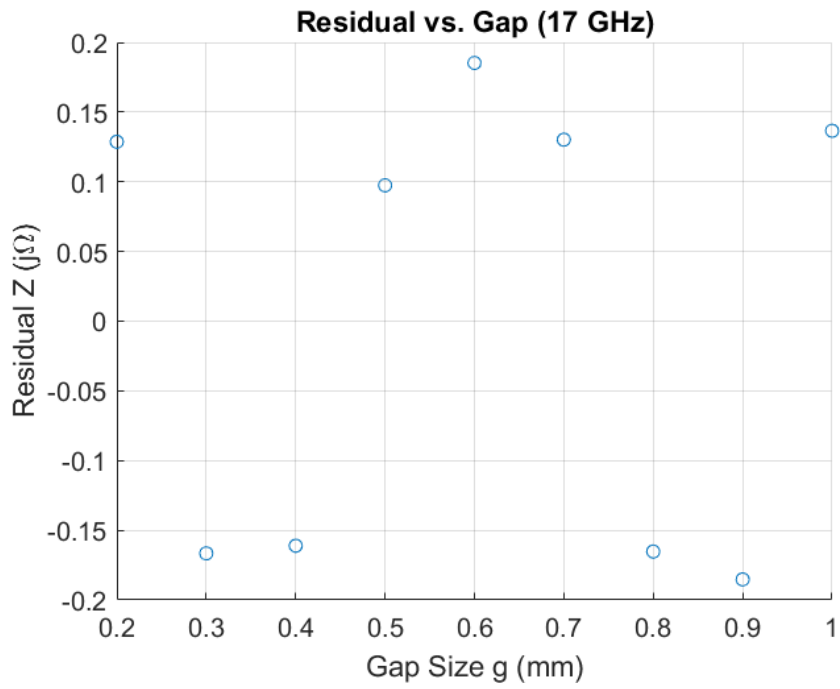


Figure 268: Circle Duroid 5880: Residuals, 17 GHz

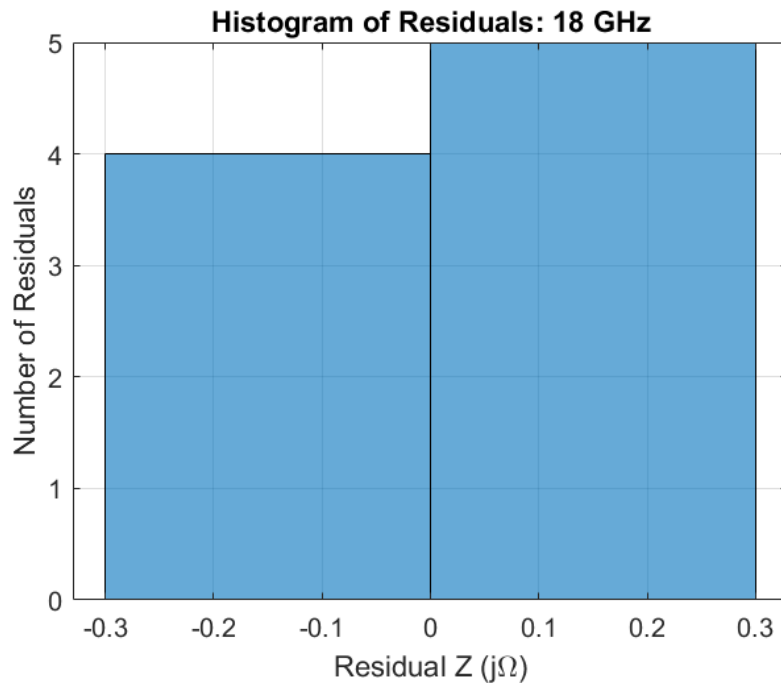


Figure 269: Circle Duroid 5880: Histogram of Residuals, 17 GHz

Model: 18 GHz

Equation form: $y = c_0 + c_1x^1 + c_2x^2 + c_3x^3$

	<u>Coefficient</u>	<u>SE</u>	<u>tStat</u>	<u>pValue</u>
c_0 (intercept)	214.11	0.88581	241.71	2.3003×10^{-11}
c_2	-227.42	5.47	-41.577	1.5183×10^{-7}
c_2	224.54	9.9436	22.581	3.1659×10^{-6}
c_3	-79.85	5.4852	-14.557	2.7617×10^{-5}

Table 44: Model Coefficients: 18 GHz

Model Statistics

Error Degrees of Freedom: 5
 Root Mean Squared Error (RMSE): 0.207
 R-squared: 1
 Adjusted R-Squared: 1
 F-statistic vs. constant model: 1.5×10^4
 p-value = 2.63×10^{-10}

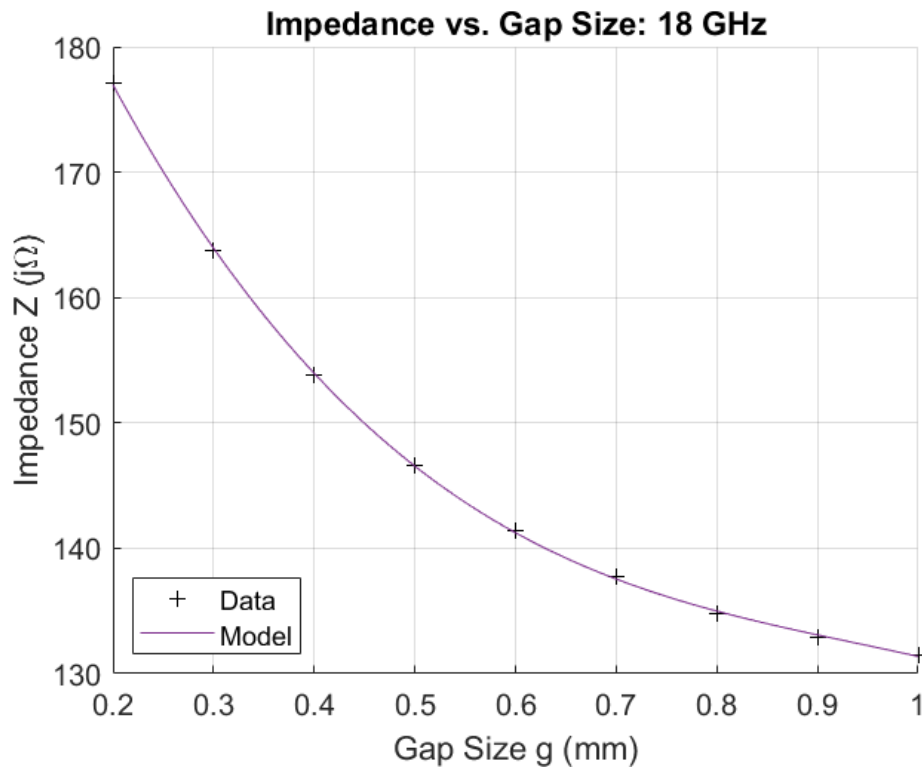


Figure 270: Circle Duroid 5880: Impedance vs. Gap Size, 18 GHz

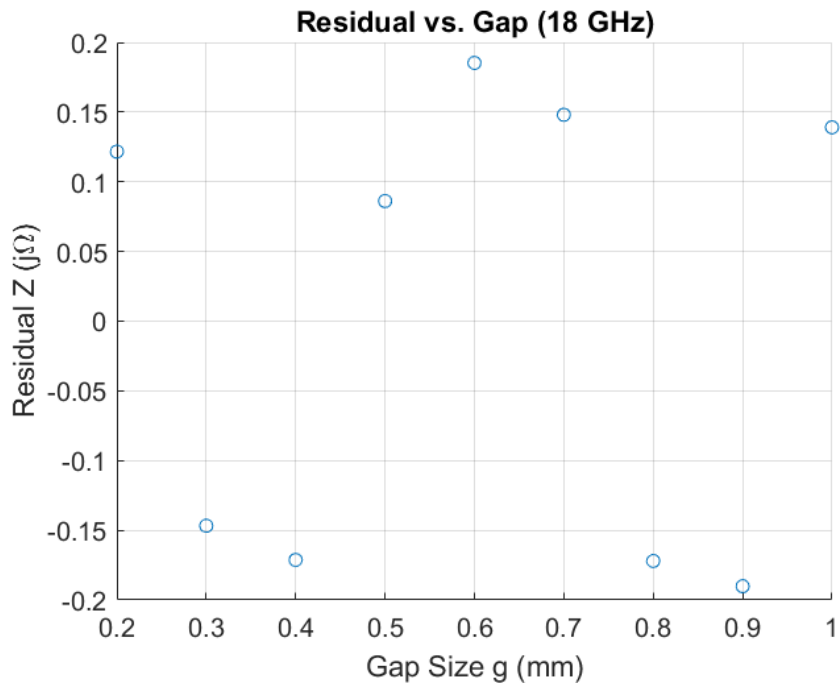


Figure 271: Circle Duroid 5880: Residuals, 18 GHz

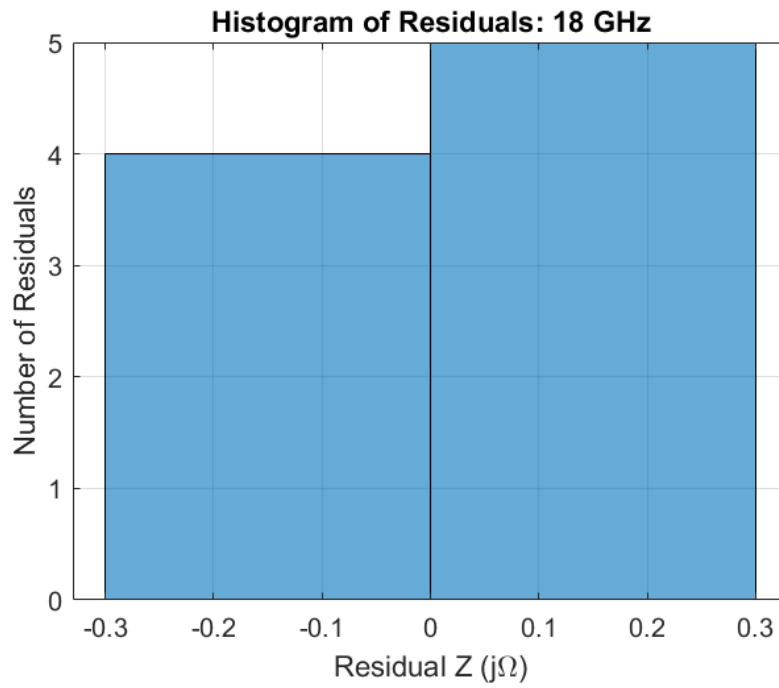


Figure 272: Circle Duroid 5880: Histogram of Residuals, 18 GHz

Model: 19 GHz

Equation form: $y = c_0 + c_1x^1 + c_2x^2 + c_3x^3$

	<u>Coefficient</u>	<u>SE</u>	<u>tStat</u>	<u>pValue</u>
c_0 (intercept)	232.51	0.80474	288.92	9.4266×10^{-12}
c_2	-253.4	4.9694	-50.992	5.483×10^{-8}
c_2	243.83	9.0336	26.992	1.3055×10^{-6}
c_3	-84.596	4.9832	-16.976	1.2974×10^{-5}

Table 45: Model Coefficients: 19 GHz

Model Statistics

Error Degrees of Freedom: 5
 Root Mean Squared Error (RMSE): 0.188
 R-squared: 1
 Adjusted R-Squared: 1
 F-statistic vs. constant model: 2.43×10^4
 p-value = 7.9×10^{-11}

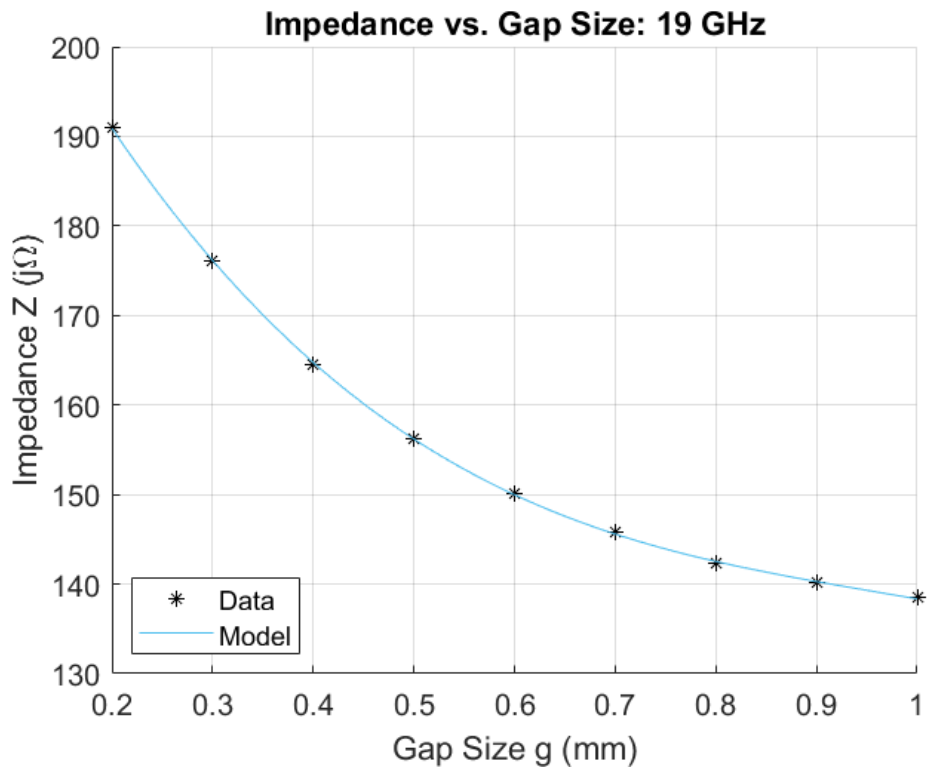


Figure 273: Circle Duroid 5880: Impedance vs. Gap Size, 19 GHz

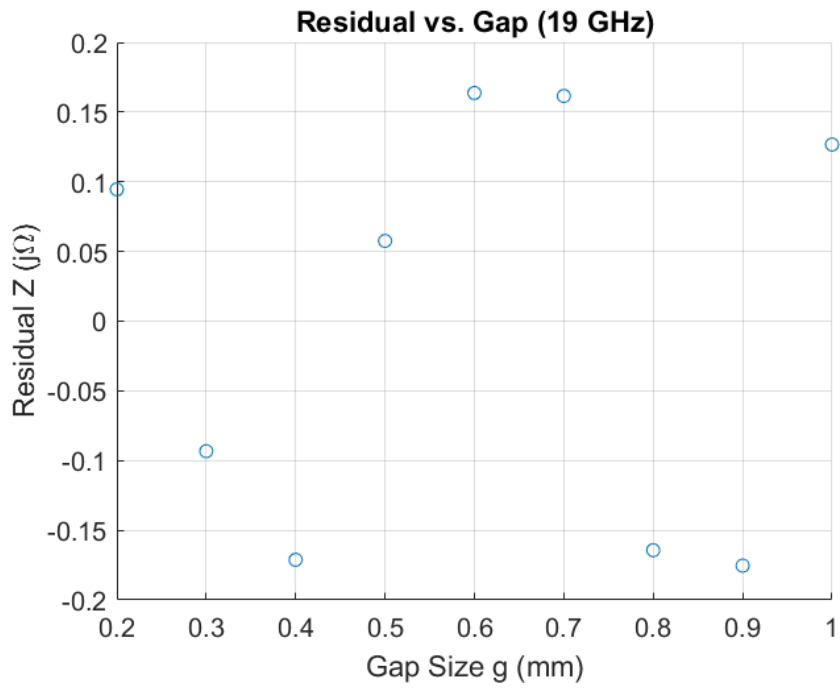


Figure 274: Circle Duroid 5880: Residuals, 19 GHz

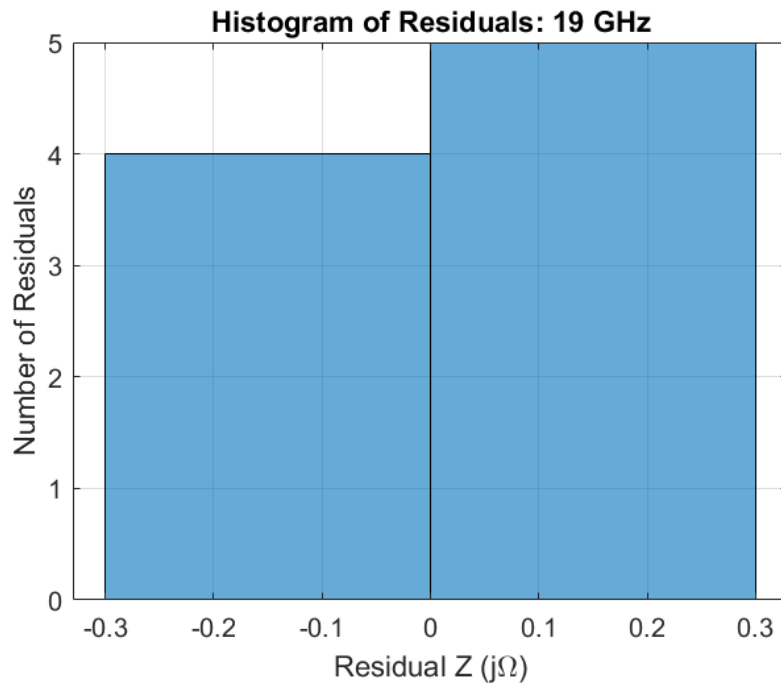


Figure 275: Circle Duroid 5880: Histogram of Residuals, 19 GHz

Appendix C. Fractal Duroid 5880 Unit Cell

Model Summary

Cell Parameters

Material: Duroid 5880

Dielectric Constant, ϵ_r : 2.2

Dissipation Constant, $\tan \delta$: 0.0009

Shape: circle

Dielectric Thickness: 1.575 mm

Copper Thickness: 0.035 mm

Cell Size, a : 4 mm

Subcell Size, $b = \frac{a-2g}{3}$

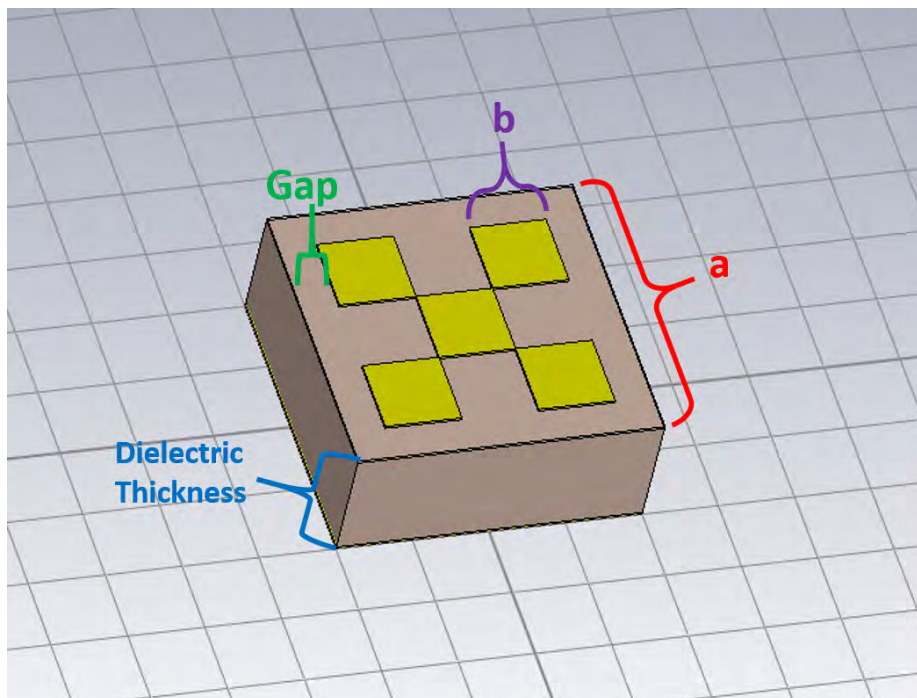


Figure 276: Circle Cell Geometry

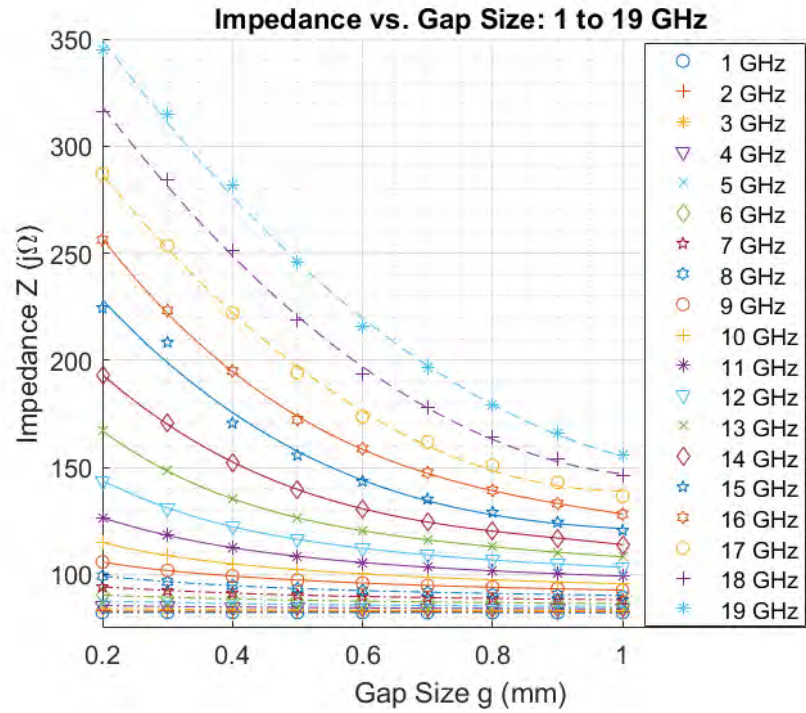


Figure 277: Fractal Duroid 5880: Cell Impedance vs. Gap, 1-19 GHz

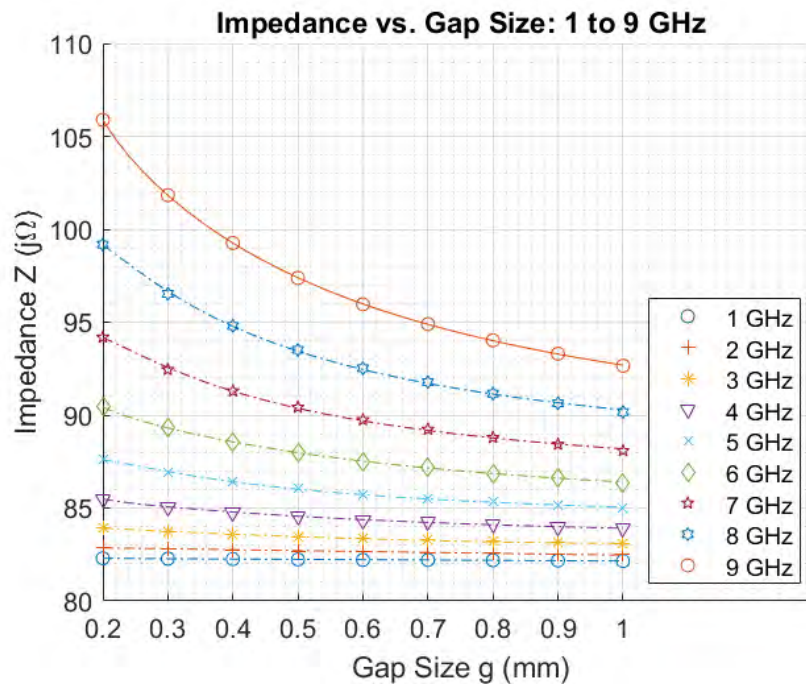


Figure 278: Fractal Duroid 5880: Cell Impedance vs. Gap, 1-9 GHz

Unit Cell Impedance Model: Fractal Duroid 5880

Frequency \rightarrow Parameter \downarrow	1 GHz	2 GHz	3 GHz	4 GHz	5 GHz	6 GHz	7 GHz	8 GHz	9 GHz	10 GHz
c_4	0	0	0	0	0	0	0	0	0	0
c_3	0	0	0	0.017972	0	0.036384	0	0	0.073354	0.081324
c_2	0	0	1.002568	-0.22893	-0.11092	-0.48242	-0.23014	-0.31337	-1.05622	-1.2367
c_1	-0.17707	-0.48866	-2.24027	1.210418	1.300837	2.776585	2.874584	4.093275	7.361915	9.756483
c_0 (intercept)	82.32672	82.95448	84.32895	82.91051	83.85627	84.06691	85.53879	86.5022	86.30852	87.05939
Z_{min}	82.14573	82.488	83.06657	83.89395	84.98842	86.37482	88.08554	90.16176	92.6548	95.62733
Z_{max}	82.2966	82.90321	83.94778	85.48539	87.6037	90.43675	94.18848	99.17278	105.8812	115.09
X	82.22116	82.6956	83.50718	84.68967	86.29606	88.40578	91.13701	94.66727	99.26801	105.3587
M	0.075438	0.207601	0.440606	0.795721	1.307639	2.030965	3.051471	4.505512	6.613205	9.73132
ϕ_{avg}	4.916388	9.83518	14.75896	19.69069	24.63402	29.59364	34.57593	39.58996	44.64927	49.77495
Inversion Factor	1	1	1	-1	-1	-1	-1	-1	-1	-1

Frequency \rightarrow Parameter \downarrow	11 GHz	12 GHz	13 GHz	14 GHz	15 GHz	16 GHz	17 GHz	18 GHz	19 GHz
c_4	0	0	121.6705	0	0	0	0	0	0
c_3	0	-0.07739	-437.878	-153.85	-117.9	-181.588	0	0	0
c_2	-0.82887	-0.36327	613.3157	420.0307	404.7	540.1235	228.9707	222.7191	204.169
c_1	11.75645	14.63689	-418.331	-412.517	-473	-583.834	-459.375	-481.595	-487.883
c_0 (intercept)	88.27557	89.17619	229.4454	260.2047	307.6	353.4645	369.389	405.7554	438.9874
Z_{min}	99.15392	103.32	108.2175	113.9362	120.5487	128.0922	136.5543	145.872	155.9494
Z_{max}	126.3337	143.6057	166.9954	193.0362	224.4749	256.264	286.8755	316.206	345.1874
X	112.7438	123.4628	137.6064	153.4862	172.5118	192.1781	211.7149	231.039	250.5684
M	13.58989	20.14285	29.38893	39.55	51.96306	64.0859	75.16059	85.16697	94.61903
ϕ_{avg}	54.99284	60.36722	65.97269	71.87686	78.28756	84.87478	92.07889	99.82021	108.137
Inversion Factor	-1	-1	1	1	1	1	1	1	1

Table 46: Unit Cell Impedance Model: Fractal Duroid 5880

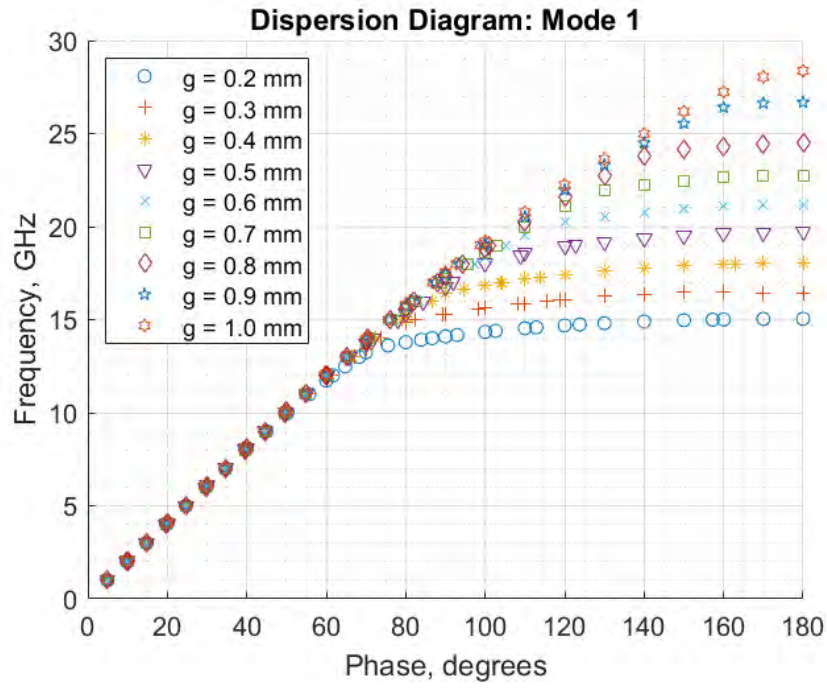


Figure 279: Fractal Duroid 5880: Dispersion Diagram, Mode 1

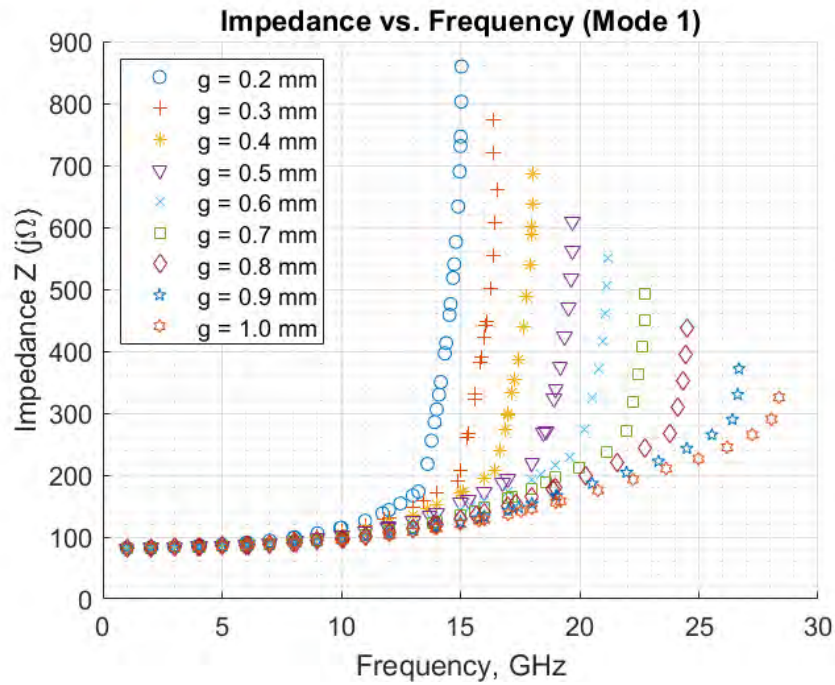


Figure 280: Fractal Duroid 5880: Impedance vs. Frequency, Mode 1

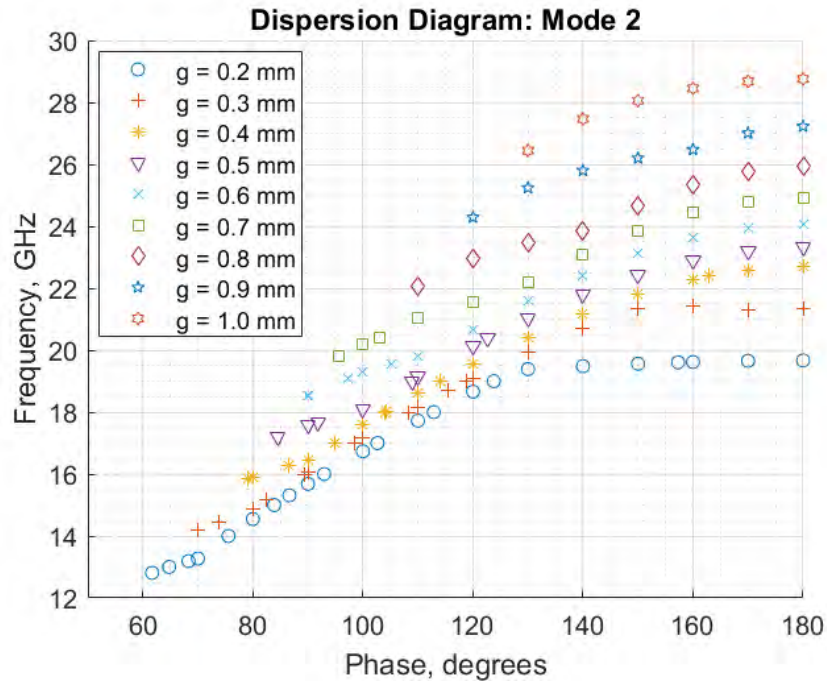


Figure 281: Fractal Duroid 5880: Dispersion Diagram, Mode 2

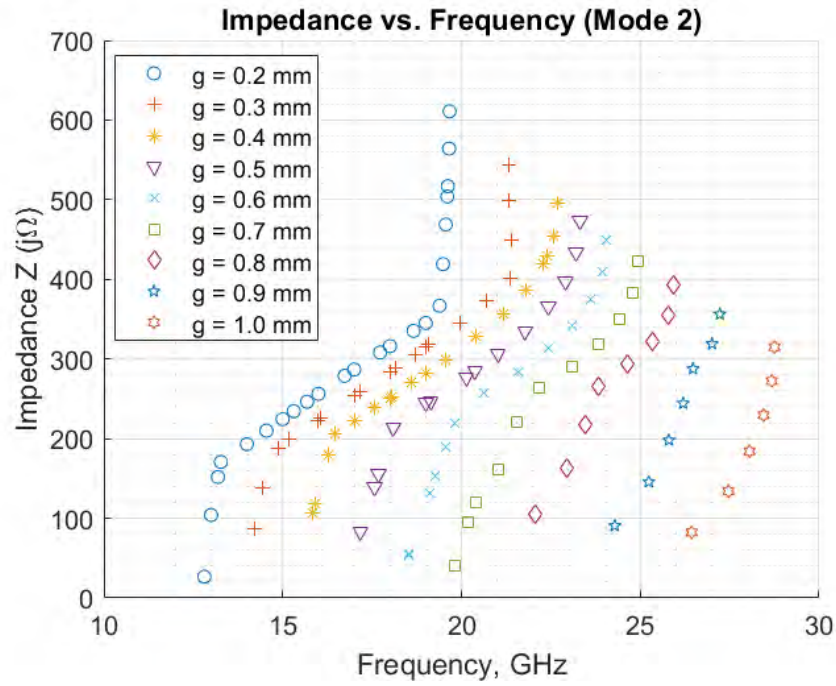


Figure 282: Fractal Duroid 5880: Impedance vs. Frequency, Mode 2

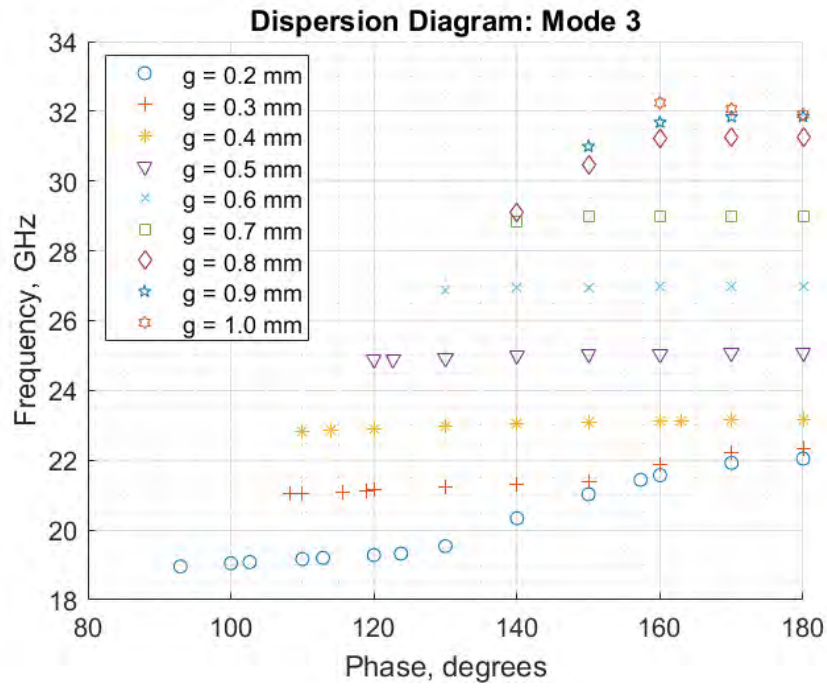


Figure 283: Fractal Duroid 5880: Dispersion Diagram, Mode 3

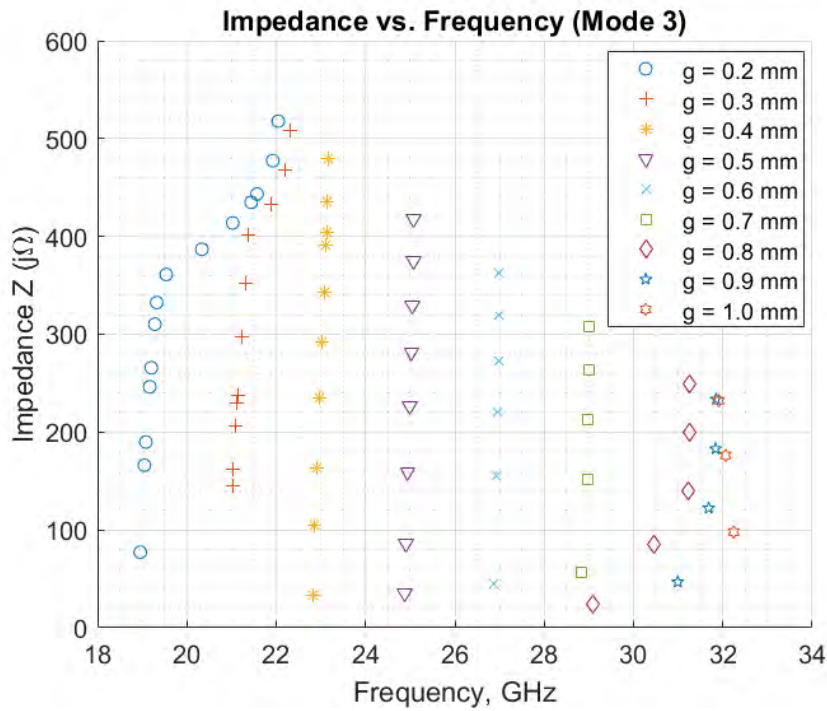


Figure 284: Fractal Duroid 5880: Impedance vs. Frequency, Mode 3

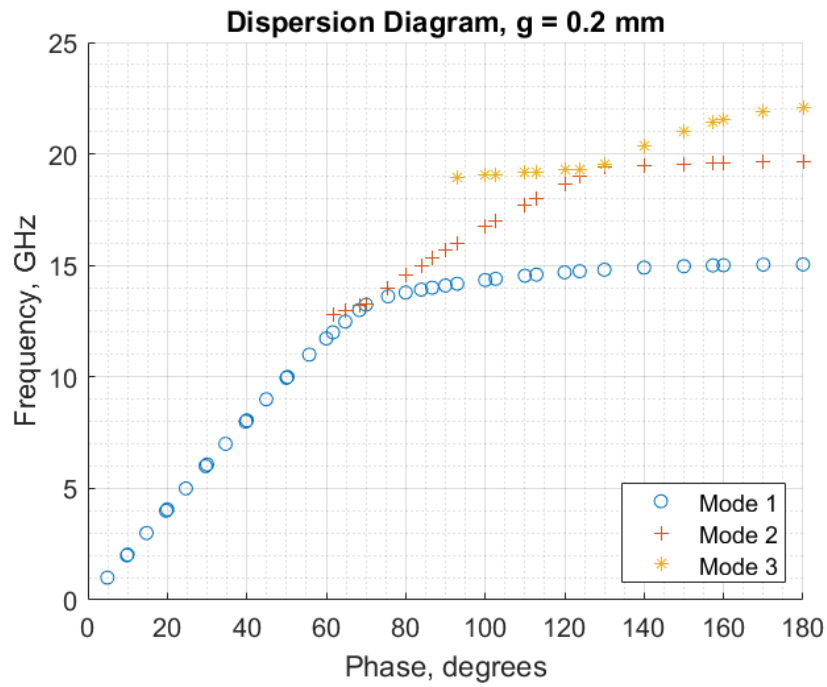


Figure 285: Fractal Duroid 5880: Dispersion Diagram, g = 0.2

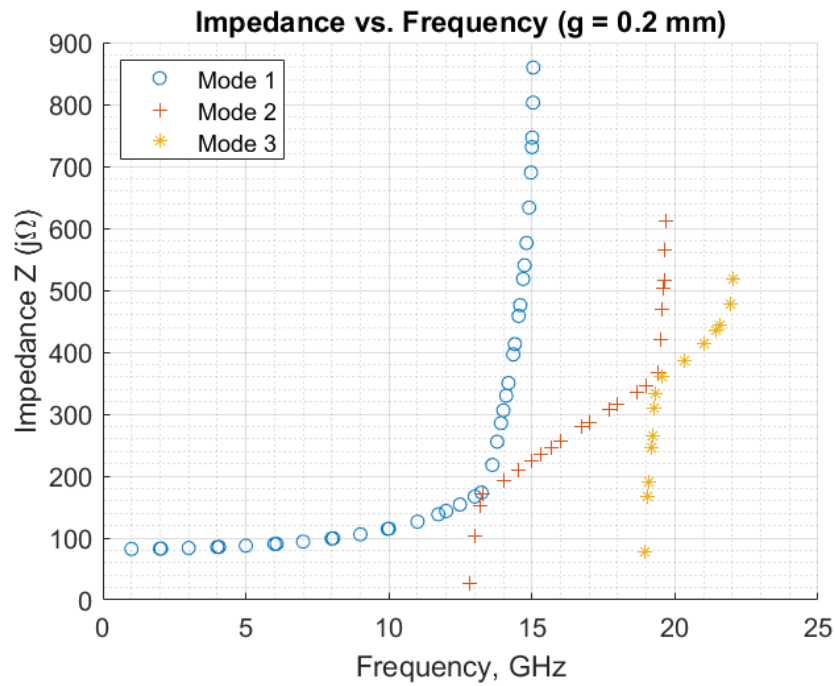


Figure 286: Fractal Duroid 5880: Impedance vs. Frequency, g = 0.2

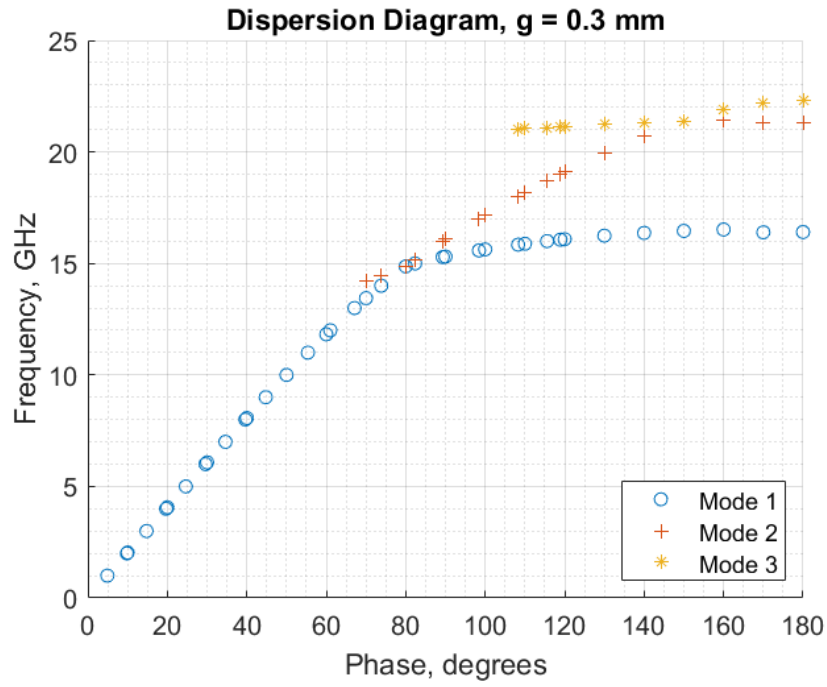


Figure 287: Fractal Duroid 5880: Dispersion Diagram, $g = 0.3$

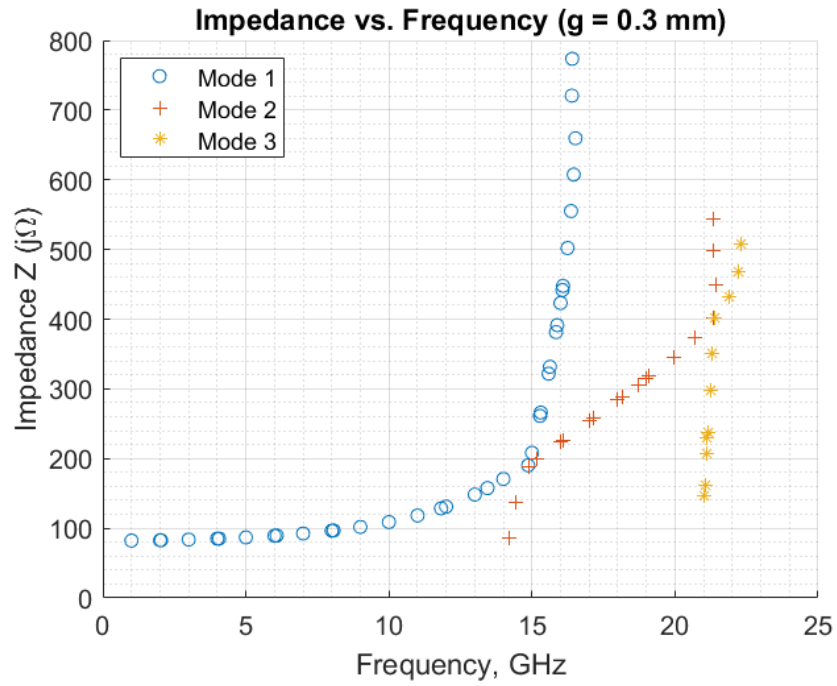


Figure 288: Fractal Duroid 5880: Impedance vs. Frequency, $g = 0.3$

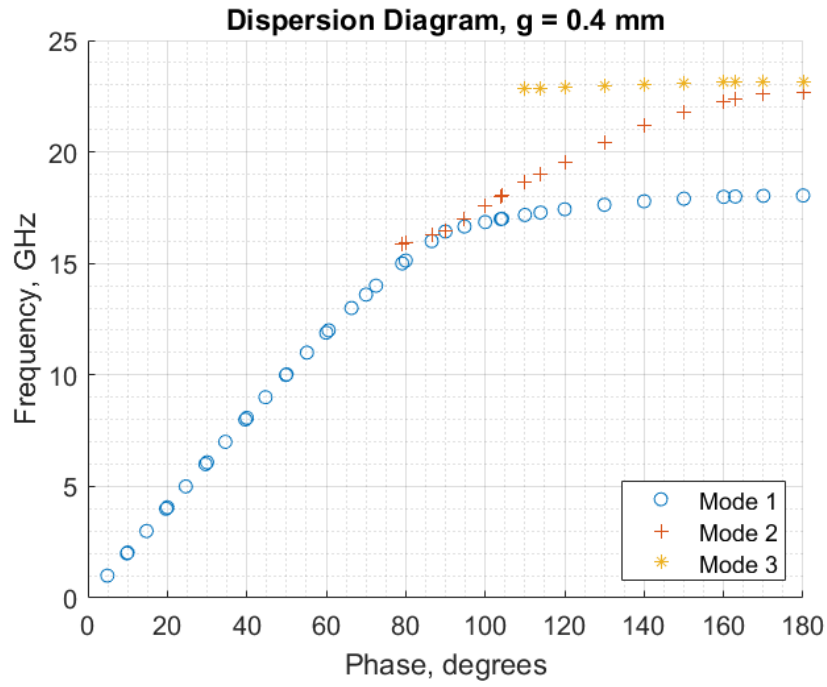


Figure 289: Fractal Duroid 5880: Dispersion Diagram, g = 0.4

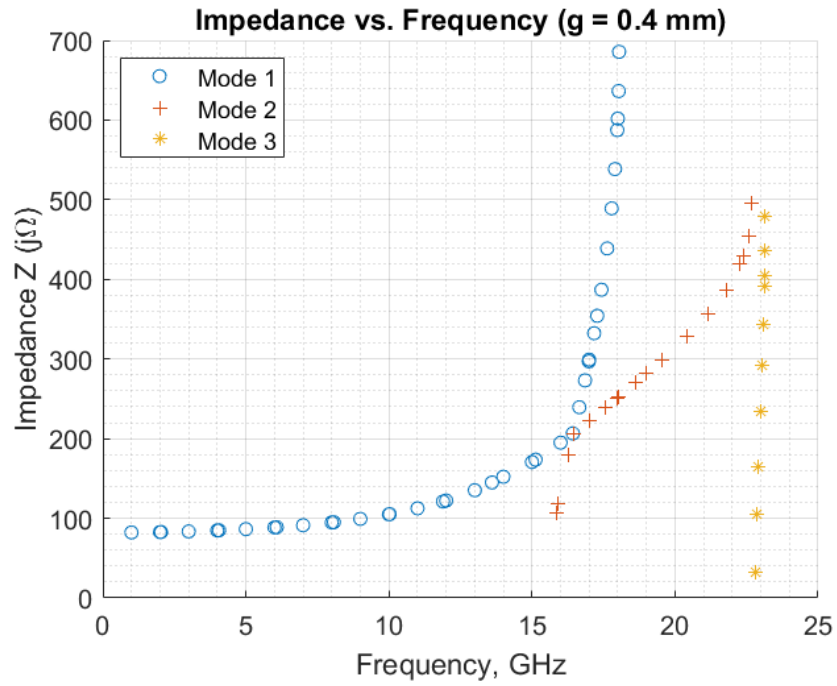


Figure 290: Fractal Duroid 5880: Impedance vs. Frequency, g = 0.4

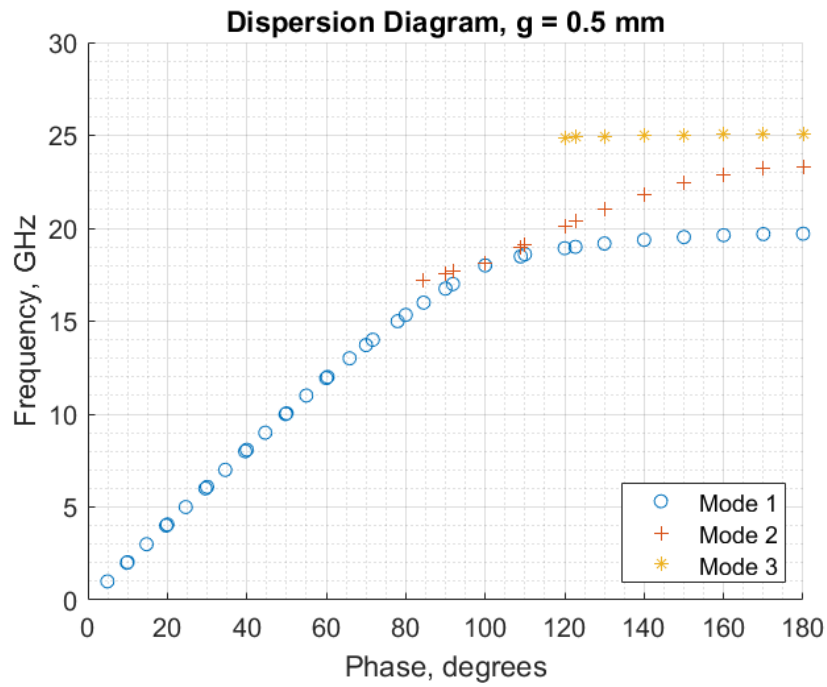


Figure 291: Fractal Duroid 5880: Dispersion Diagram, $g = 0.5$

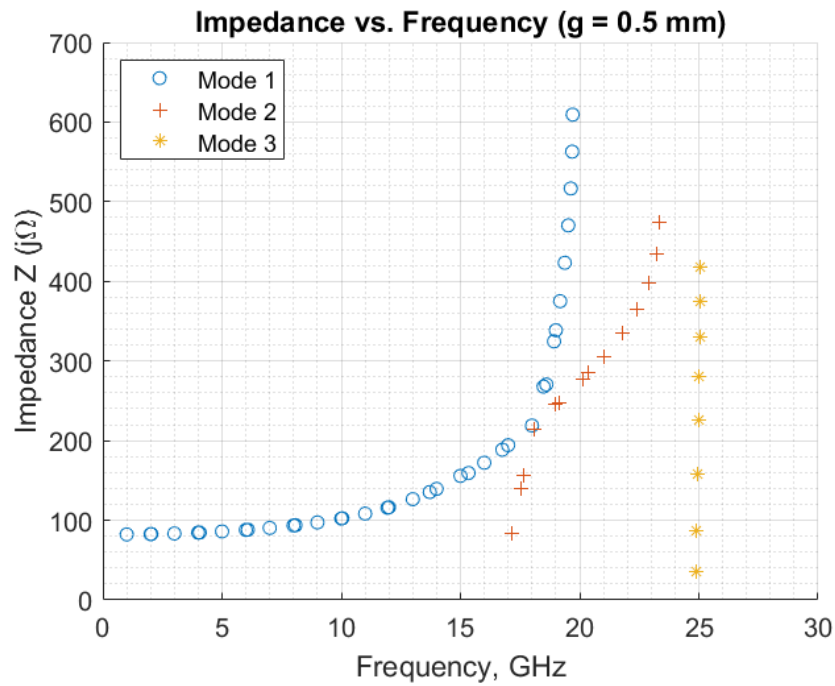


Figure 292: Fractal Duroid 5880: Impedance vs. Frequency, $g = 0.5$

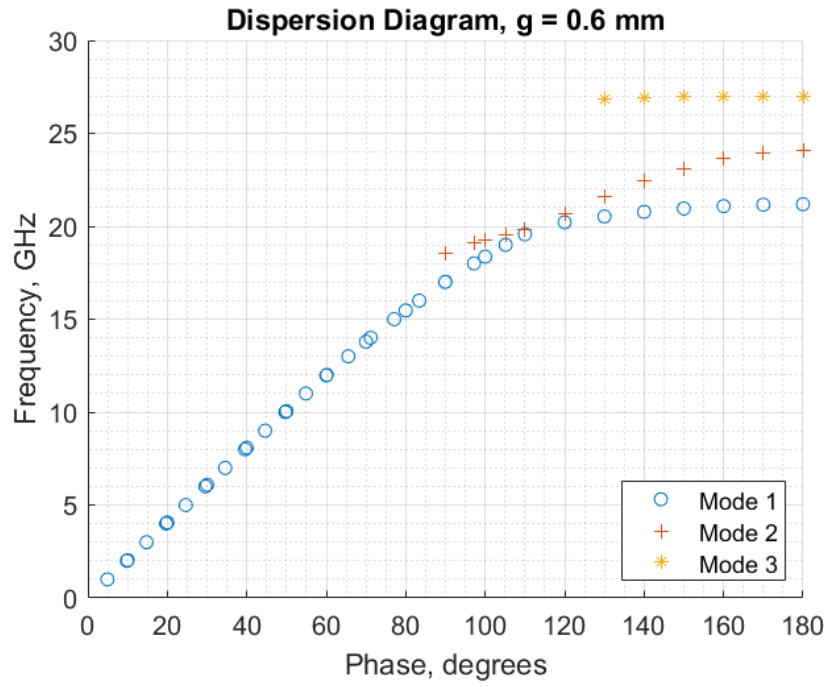


Figure 293: Fractal Duroid 5880: Dispersion Diagram, g = 0.6

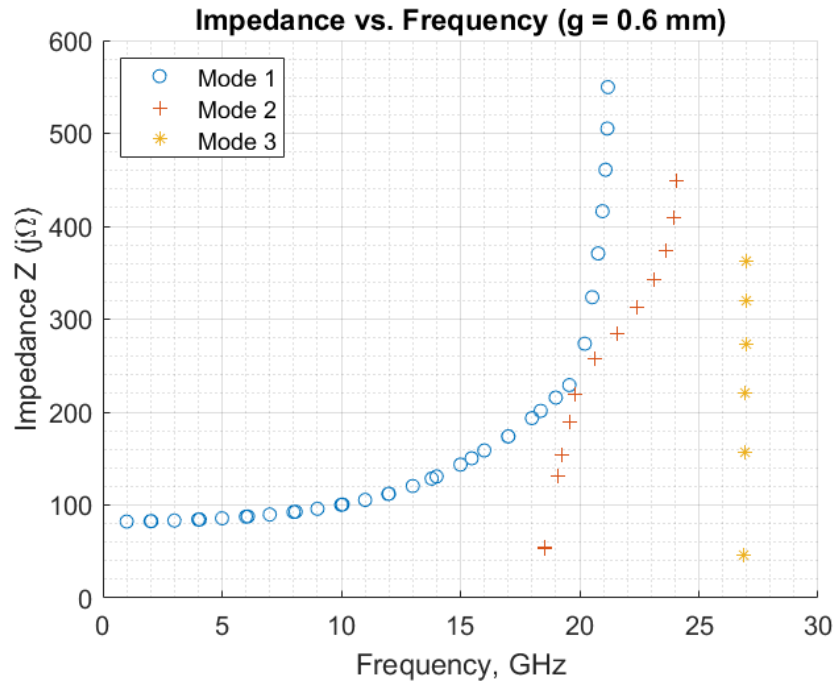


Figure 294: Fractal Duroid 5880: Impedance vs. Frequency, g = 0.6

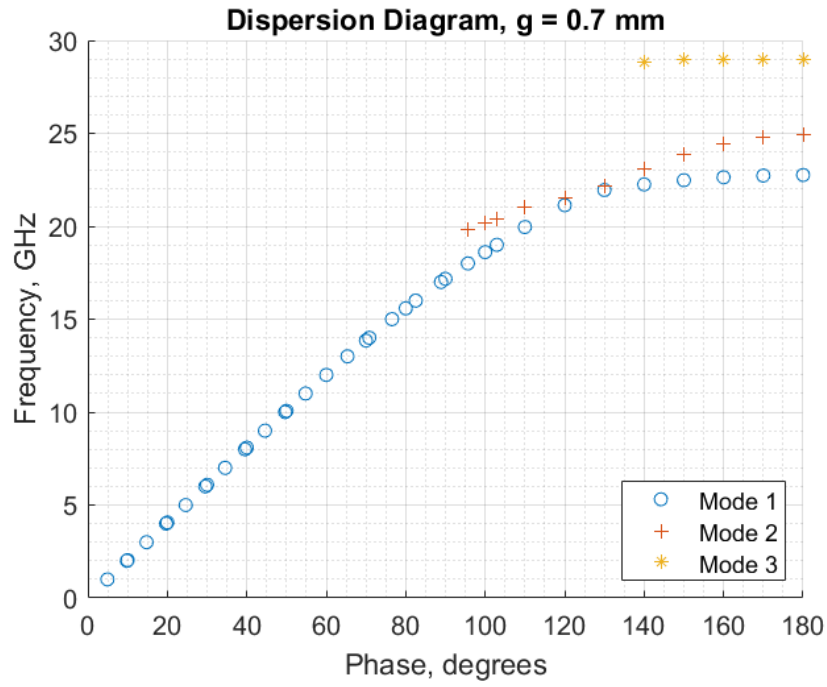


Figure 295: Fractal Duroid 5880: Dispersion Diagram, g = 0.7

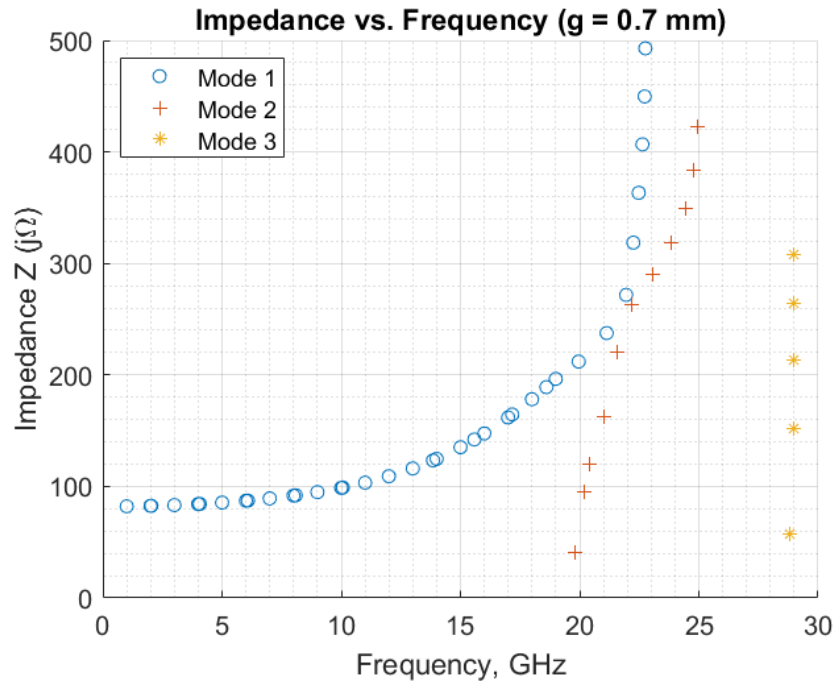


Figure 296: Fractal Duroid 5880: Impedance vs. Frequency, g = 0.7

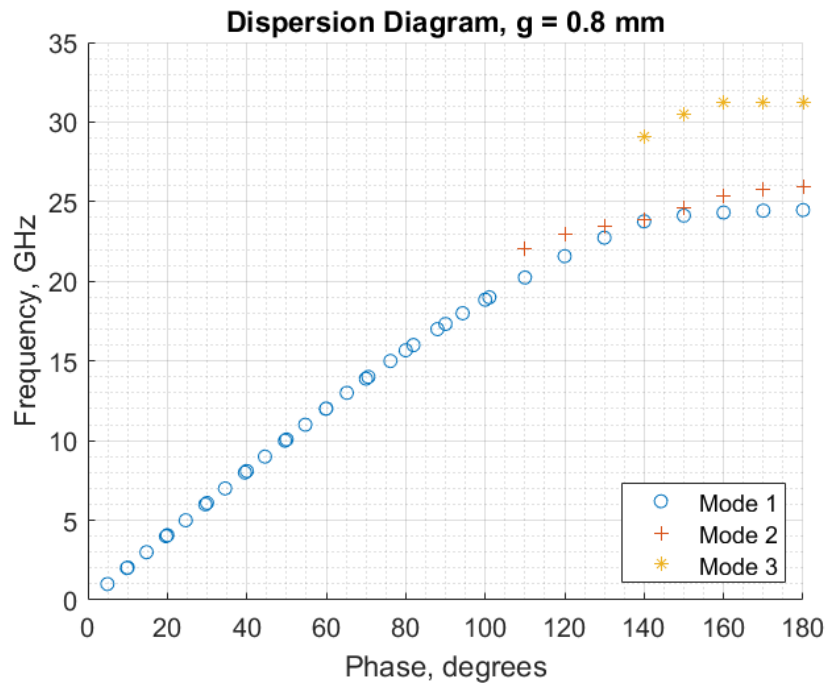


Figure 297: Fractal Duroid 5880: Dispersion Diagram, g = 0.8

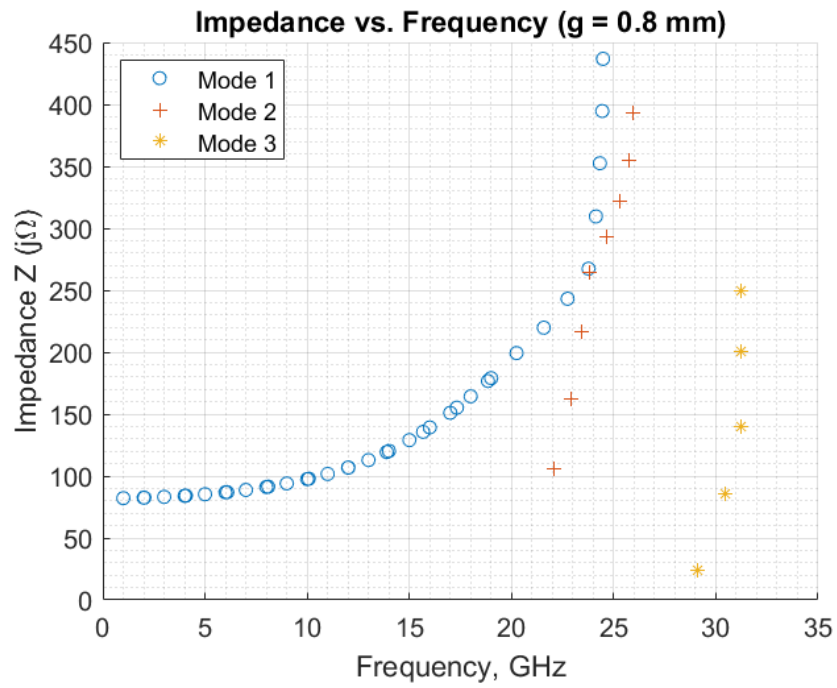


Figure 298: Fractal Duroid 5880: Impedance vs. Frequency, g = 0.8

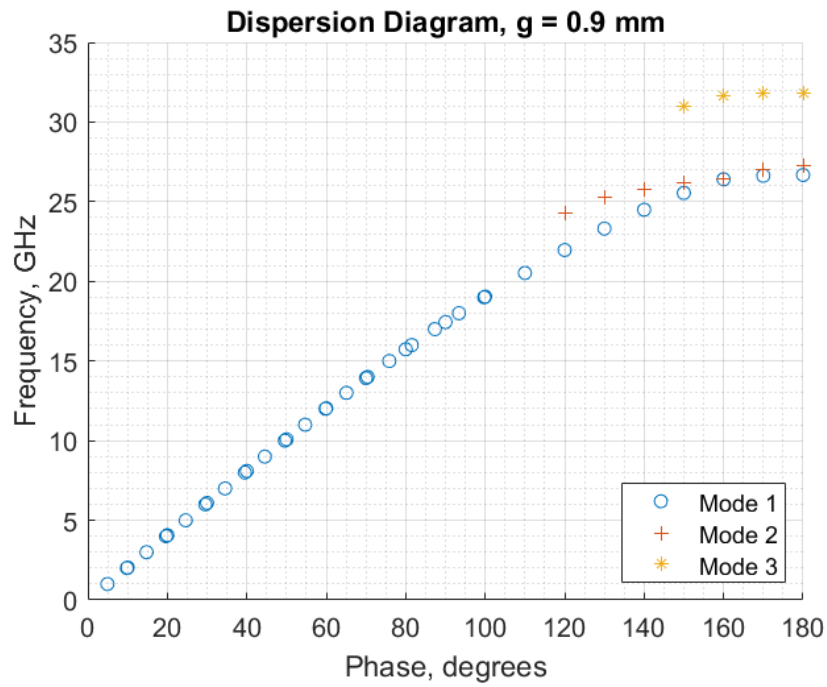


Figure 299: Fractal Duroid 5880: Dispersion Diagram, $g = 0.9$

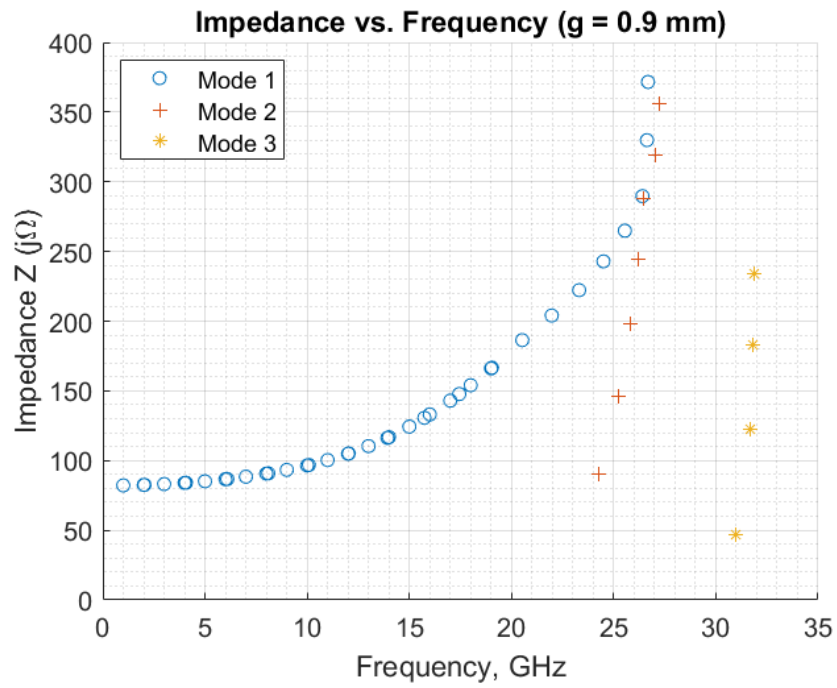


Figure 300: Fractal Duroid 5880: Impedance vs. Frequency, $g = 0.9$

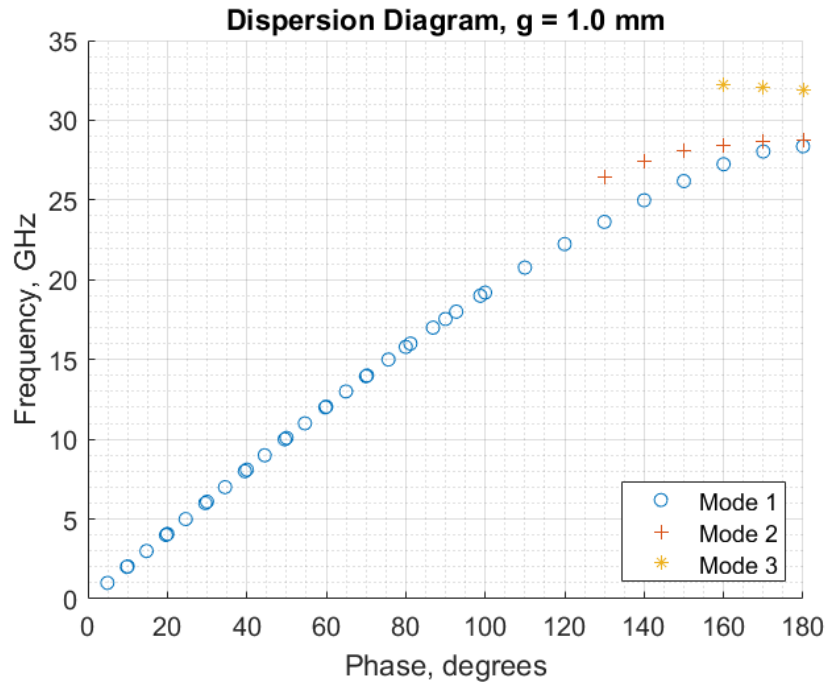


Figure 301: Fractal Duroid 5880: Dispersion Diagram, $g = 1.0$

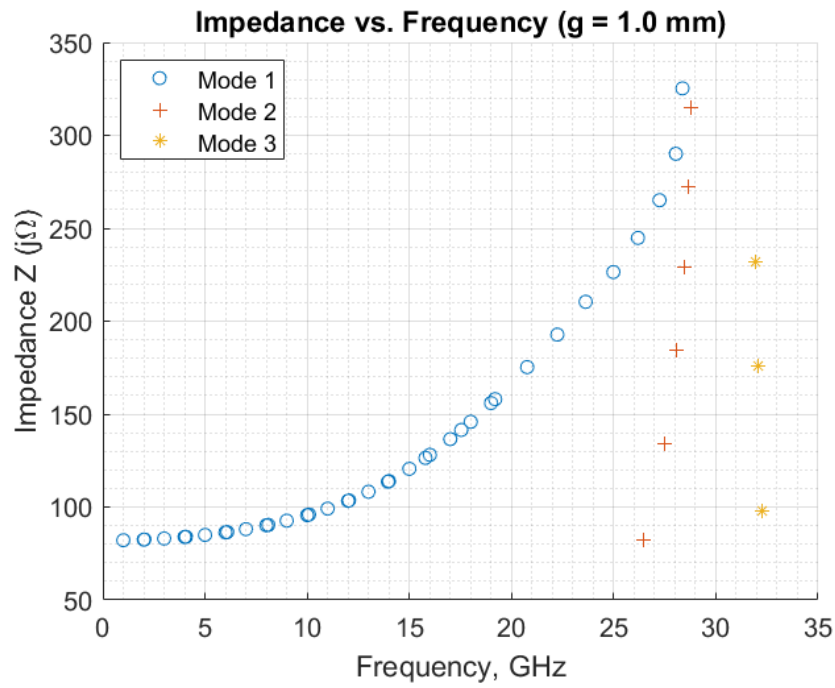


Figure 302: Fractal Duroid 5880: Impedance vs. Frequency, $g = 1.0$

Model: 1 GHz

Equation form: $y = c_0 + c_1x^1$

	Coefficient	SE	tStat	pValue
c_0 (intercept)	82.327	0.0051225	16072	9.5355×10^{-28}
c_1	-0.17707	0.0078421	-22.579	8.461×10^{-8}

Table 47: Model Coefficients: 1 GHz

Model Statistics

Error Degrees of Freedom: 7
 Root Mean Squared Error (RMSE): 0.00607
 R-squared: 0.986
 Adjusted R-Squared: 0.985
 F-statistic vs. constant model: 510
 p-value = 8.46×10^{-8}

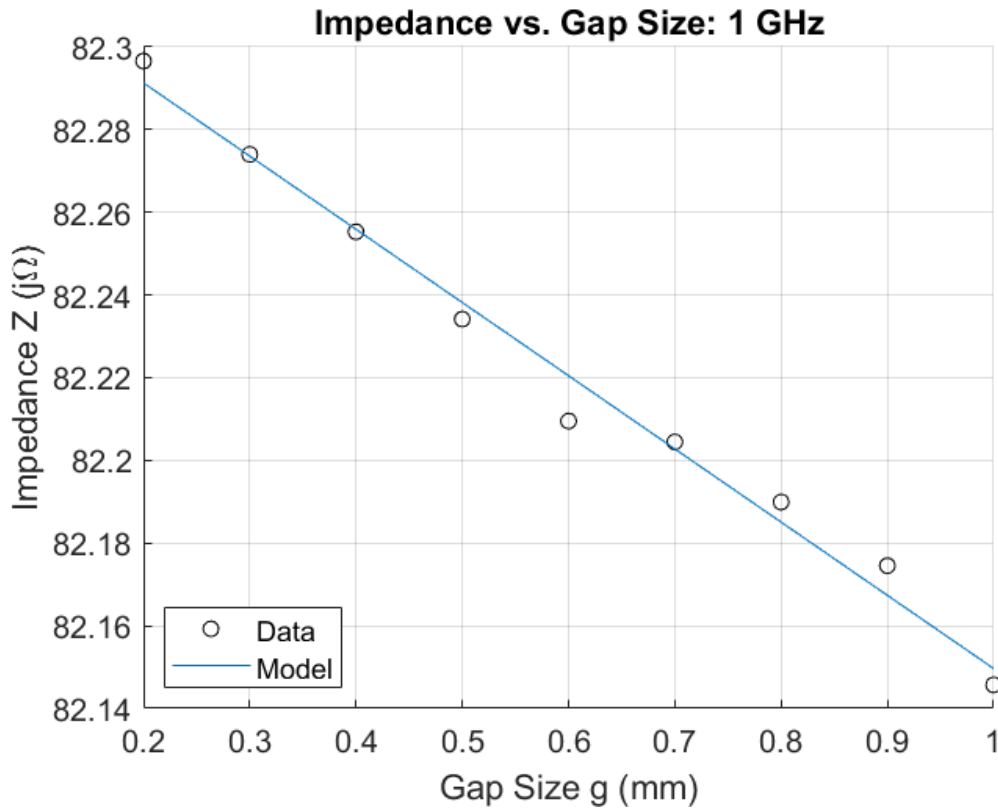


Figure 303: Fractal Duroid 5880: Impedance vs. Gap Size, 1 GHz

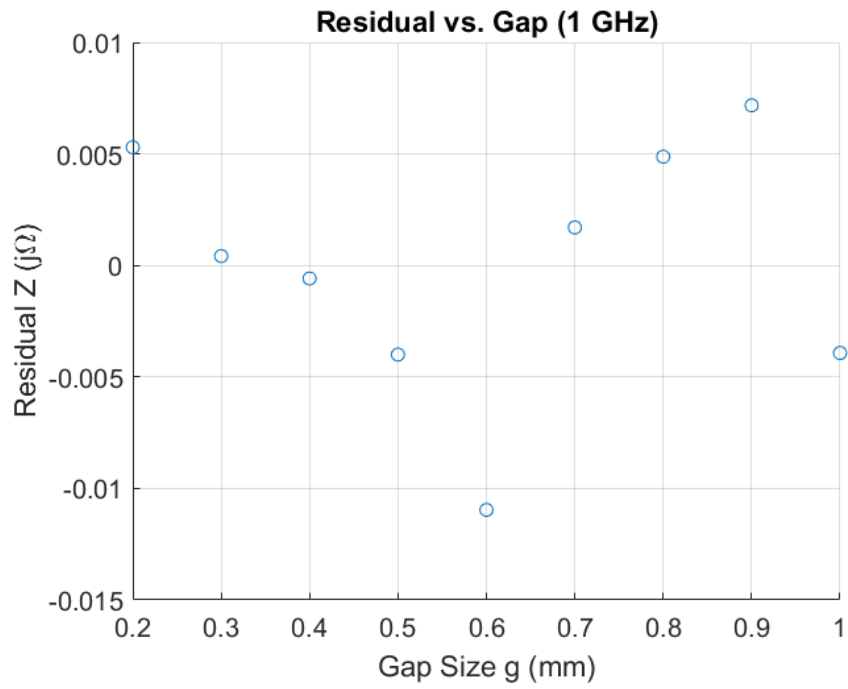


Figure 304: Fractal Duroid 5880: Residuals, 1 GHz

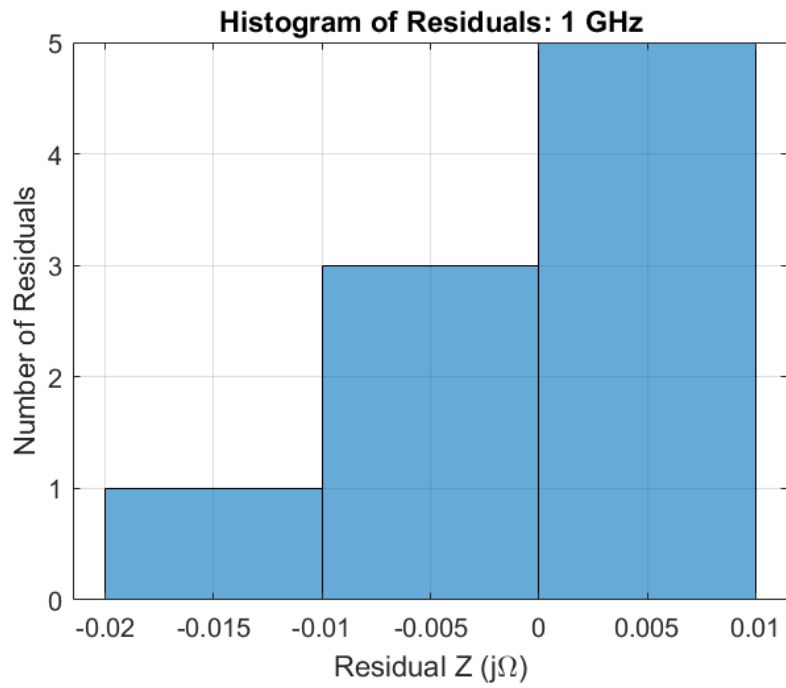


Figure 305: Fractal Duroid 5880: Histogram of Residuals, 1 GHz

Model: 2 GHz

Equation form: $y = c_0 + c_1x^1$

	<u>Coefficient</u>	<u>SE</u>	<u>tStat</u>	<u>pValue</u>
c_0 (intercept)	82.954	0.023052	3598.6	3.3795×10^{-23}
c_1	-0.48866	0.035291	-13.847	2.4204×10^{-6}

Table 48: Model Coefficients: 2 GHz

Model Statistics

Error Degrees of Freedom: 7

Root Mean Squared Error (RMSE): 0.0273

R-squared: 0.965

Adjusted R-Squared: 0.96

F-statistic vs. constant model: 192

p-value = 2.42×10^{-6}

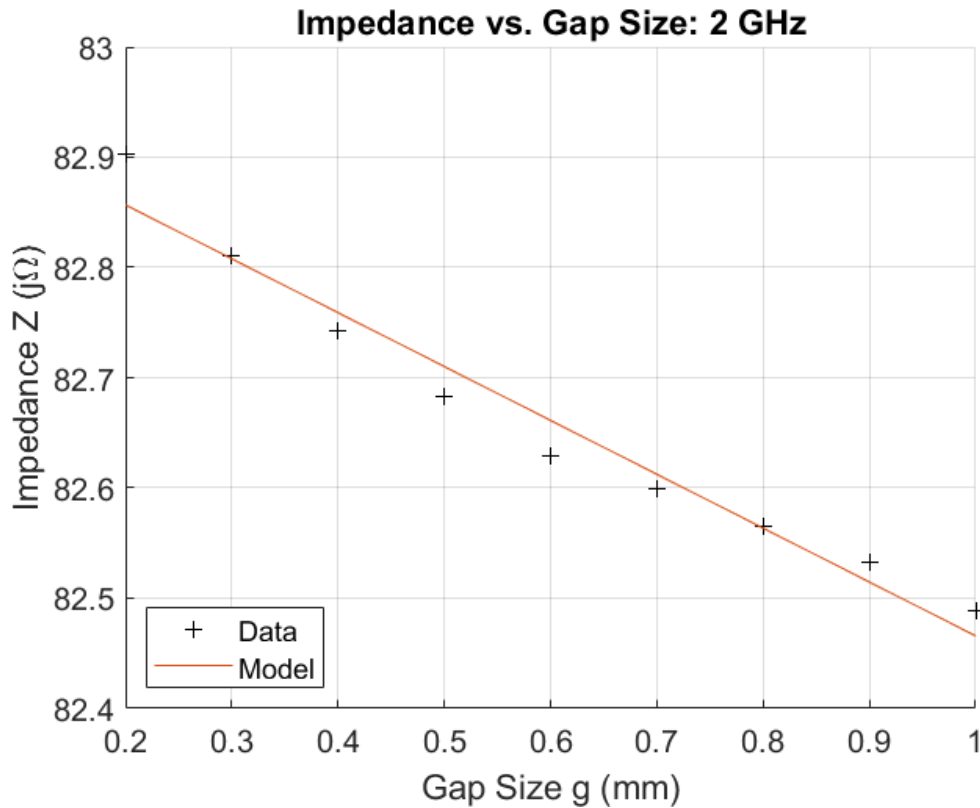


Figure 306: Fractal Duroid 5880: Impedance vs. Gap Size, 2 GHz

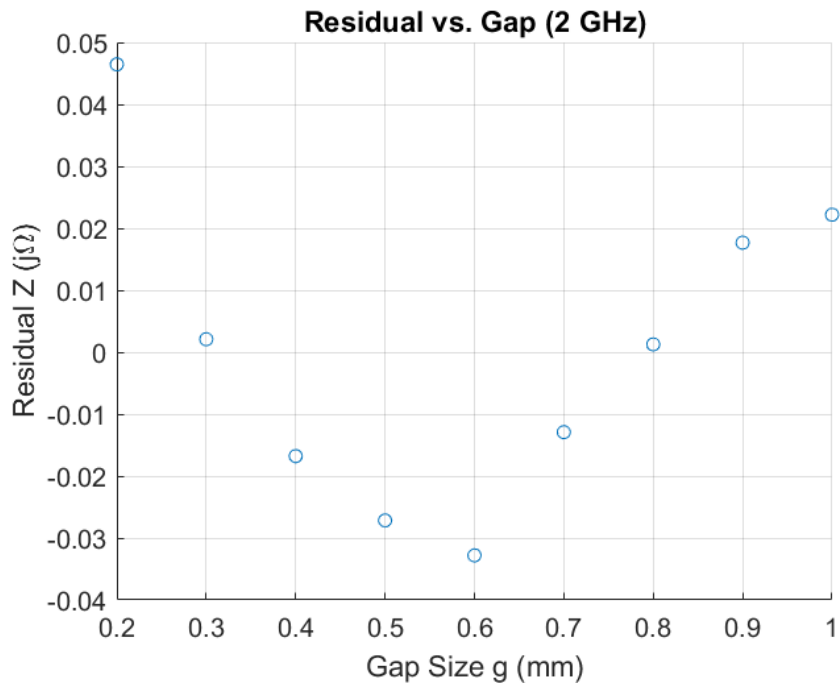


Figure 307: Fractal Duroid 5880: Residuals, 2 GHz

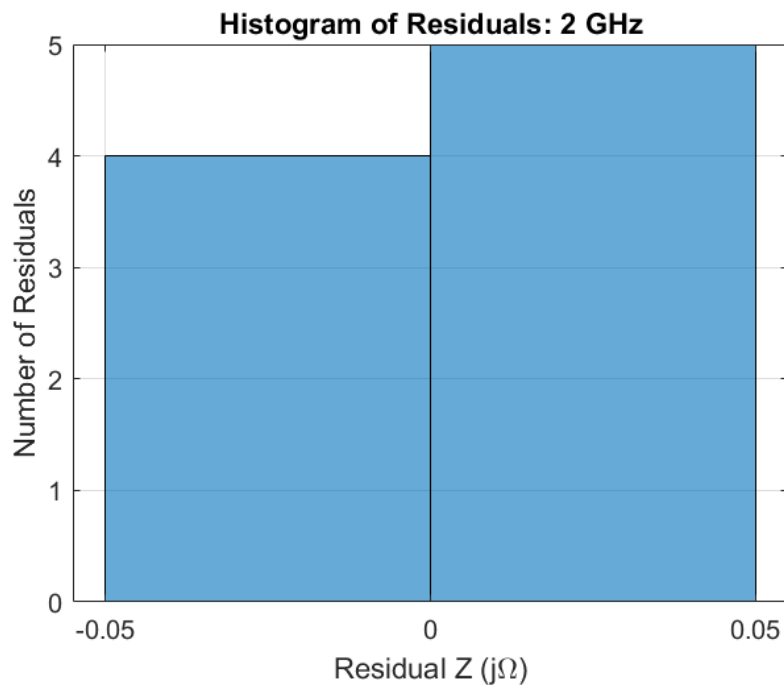


Figure 308: Fractal Duroid 5880: Histogram of Residuals, 2 GHz

Model: 3 GHz

Equation form: $y = c_0 + c_1 \frac{1}{x^1} + c_2 \frac{1}{x^2}$

	Coefficient	SE	tStat	pValue
c_0 (intercept)	84.329	0.042944	1963.7	1.1772×10^{-18}
c_1	-2.2403	0.15962	-14.035	8.1616×10^{-6}
c_2	1.0026	0.13071	7.6704	0.00025677

Table 49: Model Coefficients: 3 GHz

Model Statistics

Error Degrees of Freedom: 6
 Root Mean Squared Error (RMSE): 0.0229
 R-squared: 0.995
 Adjusted R-Squared: 0.994
 F-statistic vs. constant model: 643
 p-value = 1×10^{-7}

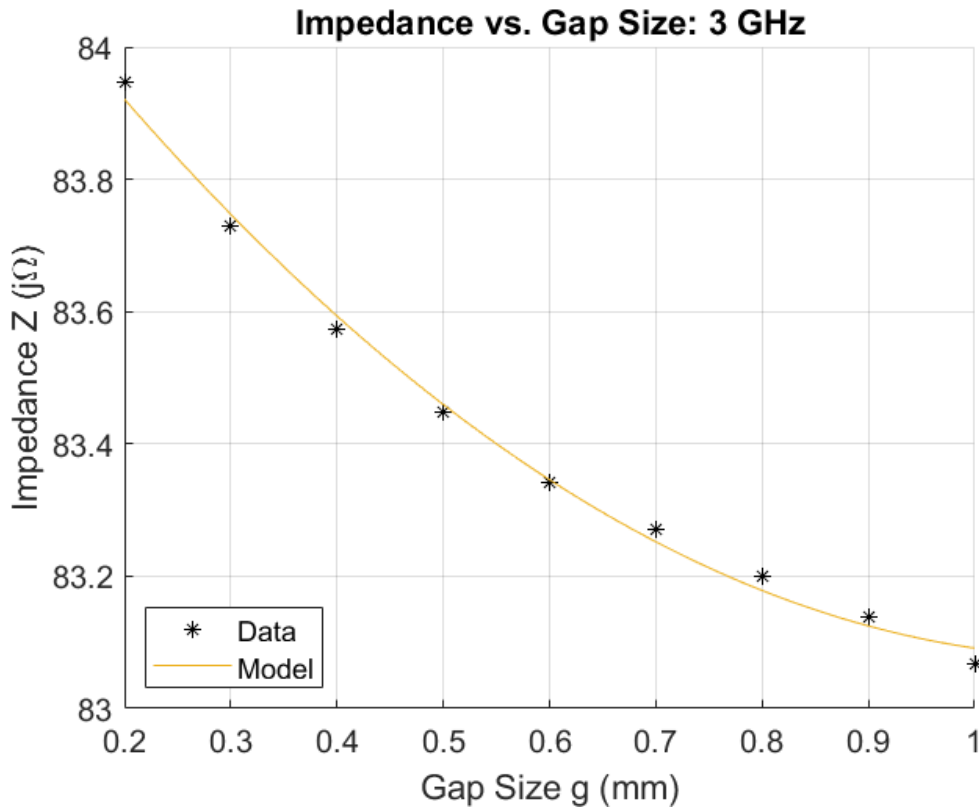


Figure 309: Fractal Duroid 5880: Impedance vs. Gap Size, 3 GHz

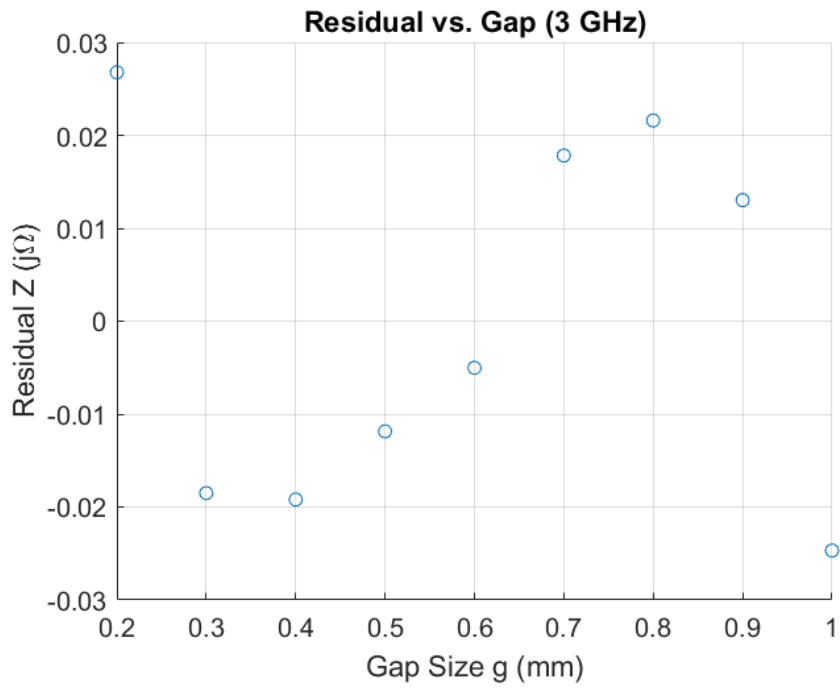


Figure 310: Fractal Duroid 5880: Residuals, 3 GHz

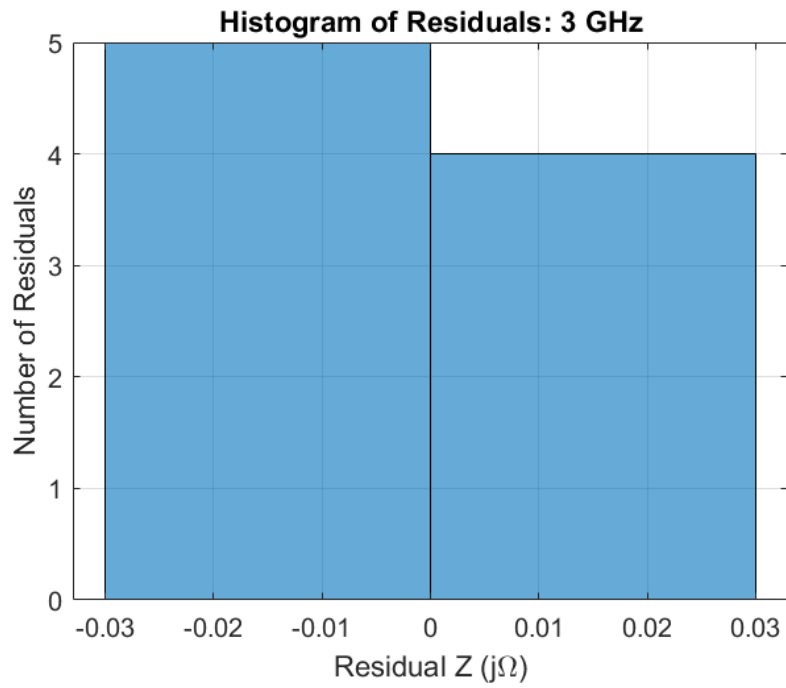


Figure 311: Fractal Duroid 5880: Histogram of Residuals, 3 GHz

Model: 4 GHz

Equation form: $y = c_0 + c_1 \frac{1}{x^1} + c_2 \frac{1}{x^2} + c_3 \frac{1}{x^3}$

	<u>Coefficient</u>	<u>SE</u>	<u>tStat</u>	<u>pValue</u>
c_0 (intercept)	82.911	0.051621	1606.1	1.17758×10^{-15}
c_1	1.2104	0.069219	17.487	1.1211×10^{-5}
c_2	-0.22893	0.026831	-8.5324	0.00036397
c_3	0.017972	0.003044	5.9043	0.0019837

Table 50: Model Coefficients: 4 GHz

Model Statistics

Error Degrees of Freedom: 5
 Root Mean Squared Error (RMSE): 0.0111
 R-squared: 1
 Adjusted R-Squared: 1
 F-statistic vs. constant model: 6×10^3
 p-value = 2.62×10^{-9}

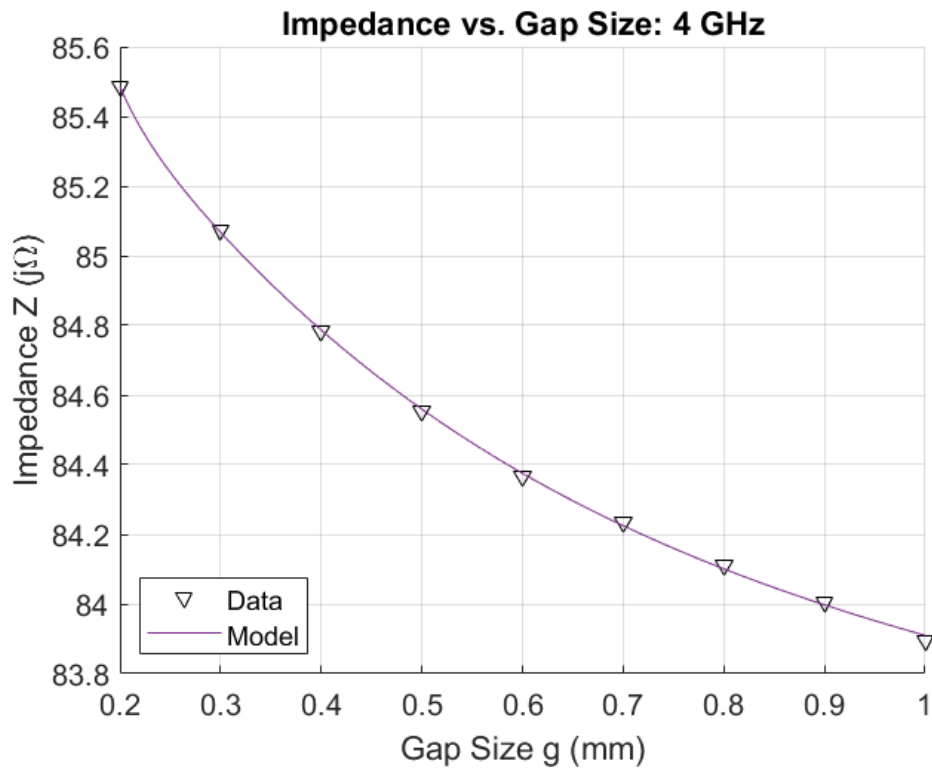


Figure 312: Fractal Duroid 5880: Impedance vs. Gap Size, 4 GHz

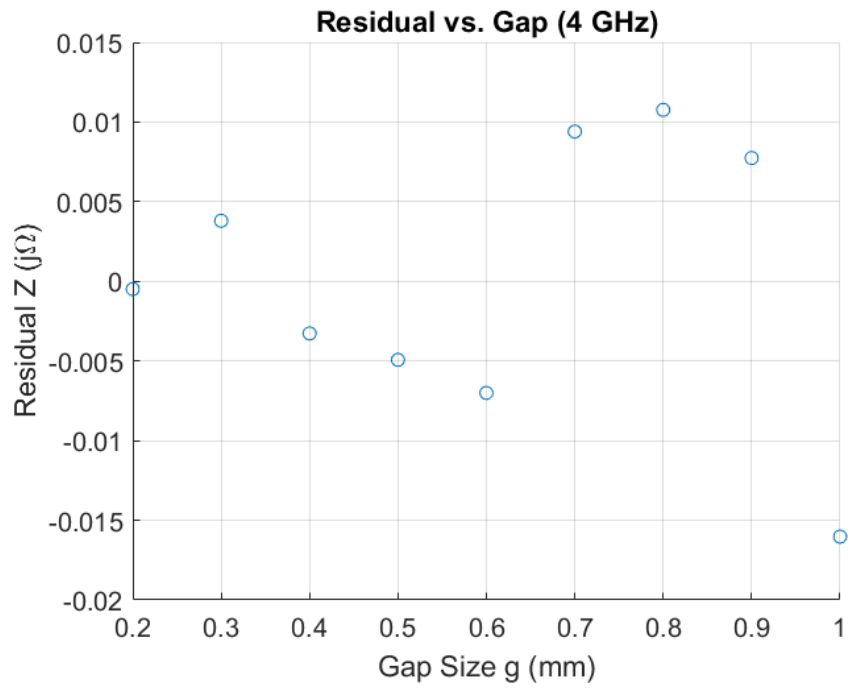


Figure 313: Fractal Duroid 5880: Residuals, 4 GHz

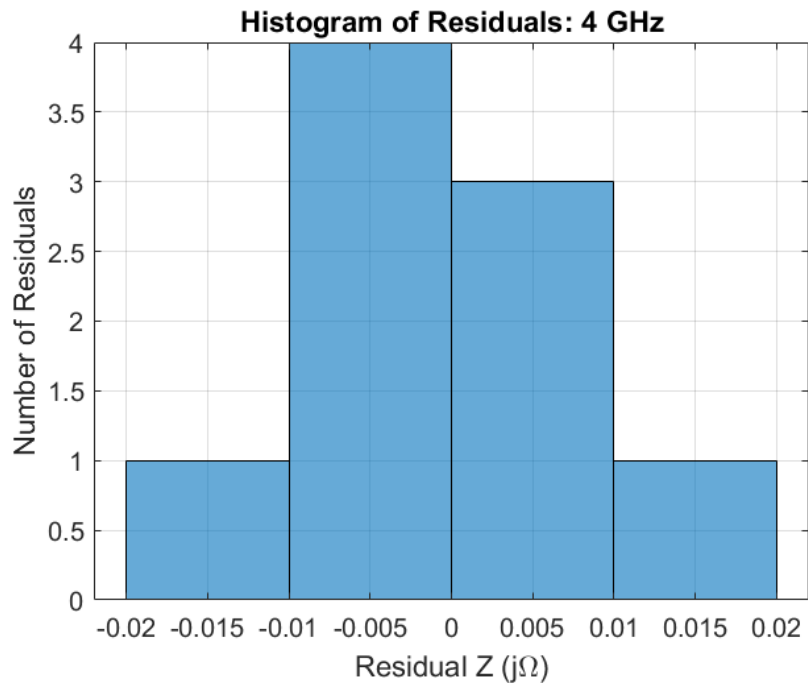


Figure 314: Fractal Duroid 5880: Histogram of Residuals, 4 GHz

Model: 5 GHz

Equation form: $y = c_0 + c_1 \frac{1}{x^1} + c_2 \frac{1}{x^2}$

	<u>Coefficient</u>	<u>SE</u>	<u>tStat</u>	<u>pValue</u>
c_0 (intercept)	83.856	0.066841	1254.6	1.7313×10^{-17}
c_1	1.3008	0.056598	22.984	4.4453×10^{-7}
c_2	-0.11092	0.0094937	-11.683	2.3704×10^{-5}

Table 51: Model Coefficients: 5 GHz

Model Statistics

Error Degrees of Freedom: 6
 Root Mean Squared Error (RMSE): 0.041
 R-squared: 0.998
 Adjusted R-Squared: 0.998
 F-statistic vs. constant model: 1.8×10^3
 p-value = 4.62×10^{-9}

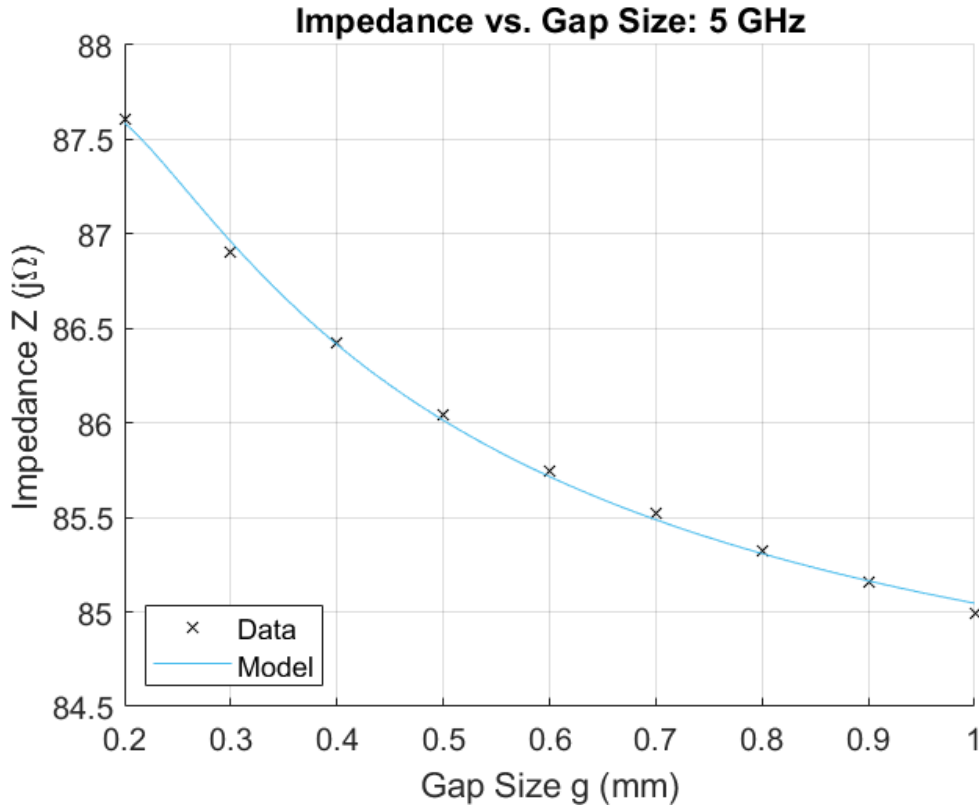


Figure 315: Fractal Duroid 5880: Impedance vs. Gap Size, 5 GHz

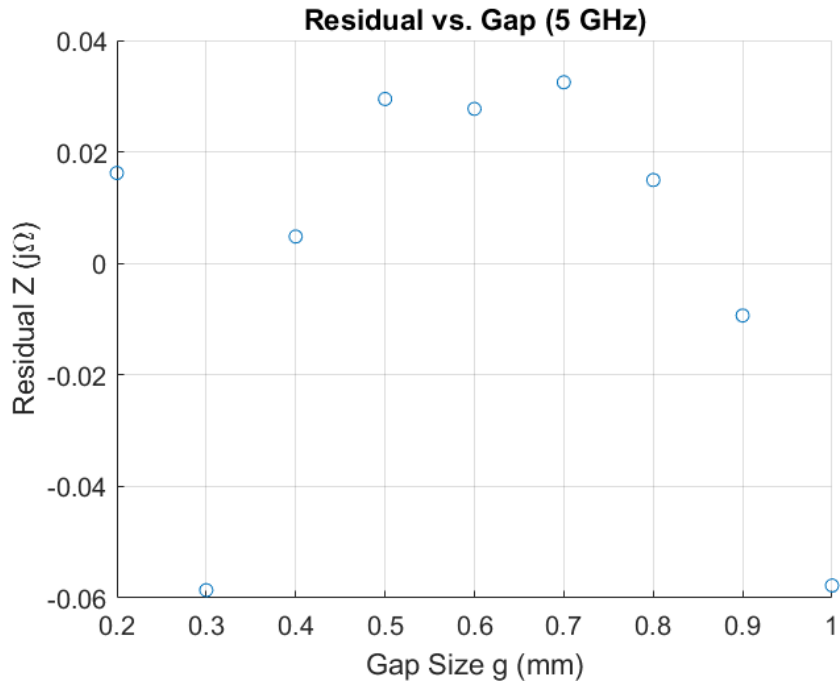


Figure 316: Fractal Duroid 5880: Residuals, 5 GHz

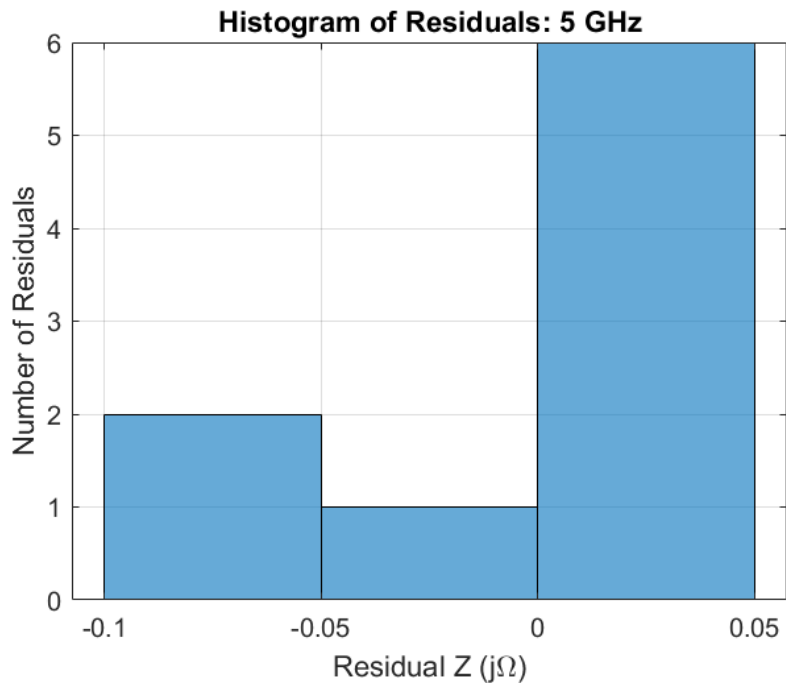


Figure 317: Fractal Duroid 5880: Histogram of Residuals, 5 GHz

Model: 6 GHz

Equation form: $y = c_0 + c_1 \frac{1}{x^1} + c_2 \frac{1}{x^2} + c_3 \frac{1}{x^3}$

	<u>Coefficient</u>	<u>SE</u>	<u>tStat</u>	<u>pValue</u>
c_0 (intercept)	84.067	0.072415	1160.9	9.0018×10^{-15}
c_1	2.7766	0.097102	28.595	9.7996×10^{-7}
c_2	-0.48242	0.037639	-12.817	5.1458×10^{-5}
c_3	0.036384	0.0042701	8.5206	0.00036635

Table 52: Model Coefficients: 6 GHz

Model Statistics

Error Degrees of Freedom: 5
 Root Mean Squared Error (RMSE): 0.0156
 R-squared: 1
 Adjusted R-Squared: 1
 F-statistic vs. constant model: 1.99×10^4
 p-value = 1.3×10^{-10}

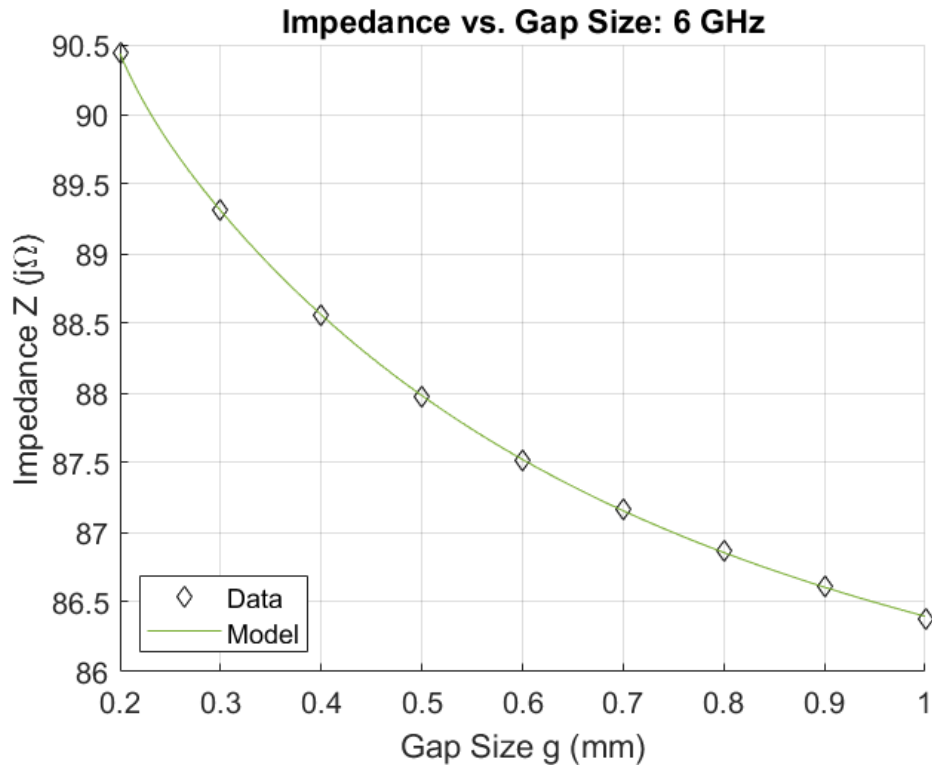


Figure 318: Fractal Duroid 5880: Impedance vs. Gap Size, 6 GHz

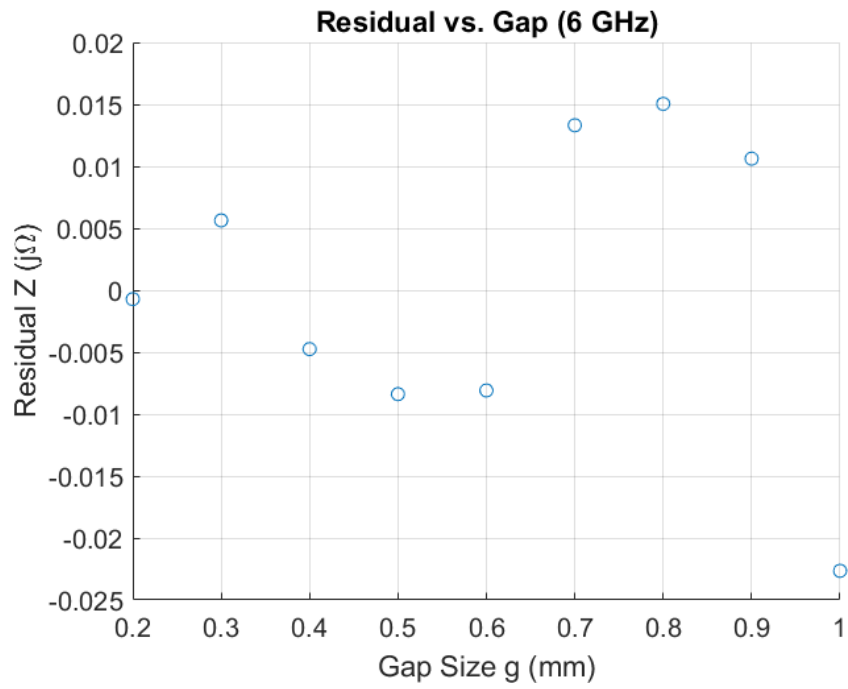


Figure 319: Fractal Duroid 5880: Residuals, 6 GHz

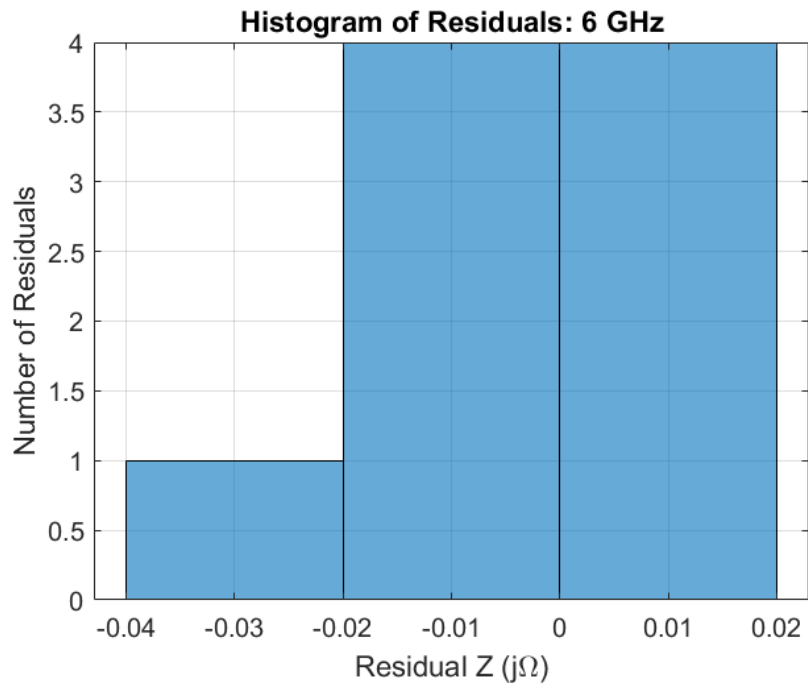


Figure 320: Fractal Duroid 5880: Histogram of Residuals, 6 GHz

Model: 7 GHz

Equation form: $y = c_0 + c_1 \frac{1}{x^1} + c_2 \frac{1}{x^2}$

	Coefficient	SE	tStat	pValue
c_0 (intercept)	85.539	0.12073	708.5	5.3362×10^{-16}
c_1	2.8746	0.10223	28.119	1.3387×10^{-7}
c_2	-0.23014	0.017148	-13.421	1.0599×10^{-5}

Table 53: Model Coefficients: 7 GHz

Model Statistics

Error Degrees of Freedom: 6
 Root Mean Squared Error (RMSE): 0.074
 R-squared: 0.999
 Adjusted R-Squared: 0.999
 F-statistic vs. constant model: 3×10^3
 p-value = 9.94×10^{-10}

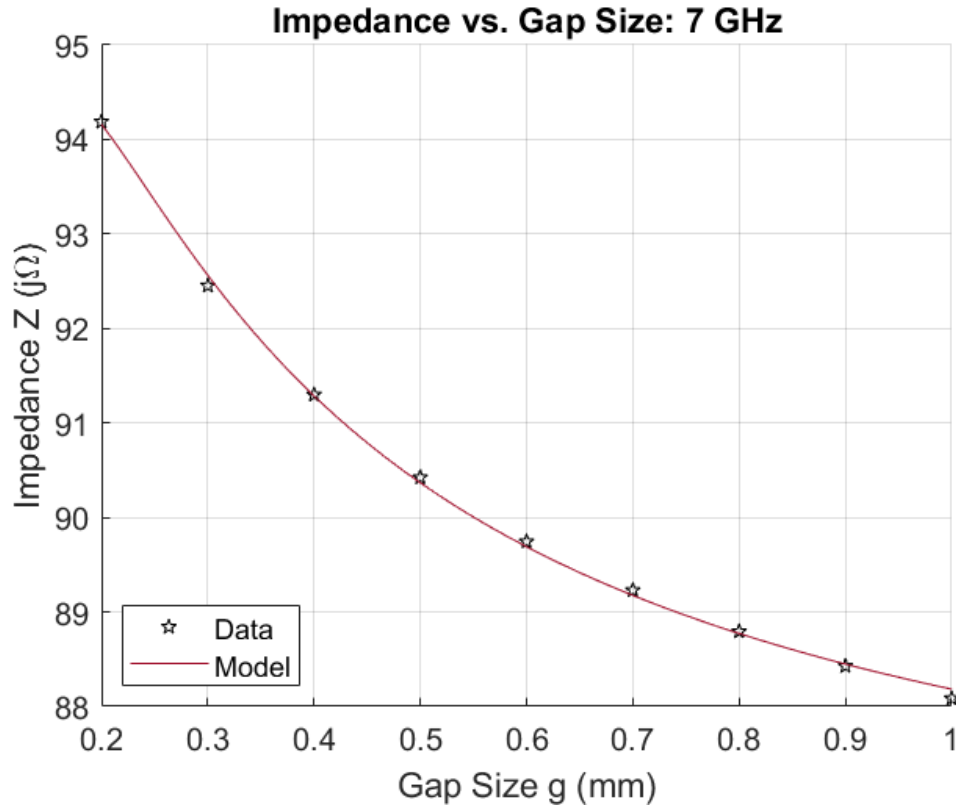


Figure 321: Fractal Duroid 5880: Impedance vs. Gap Size, 7 GHz

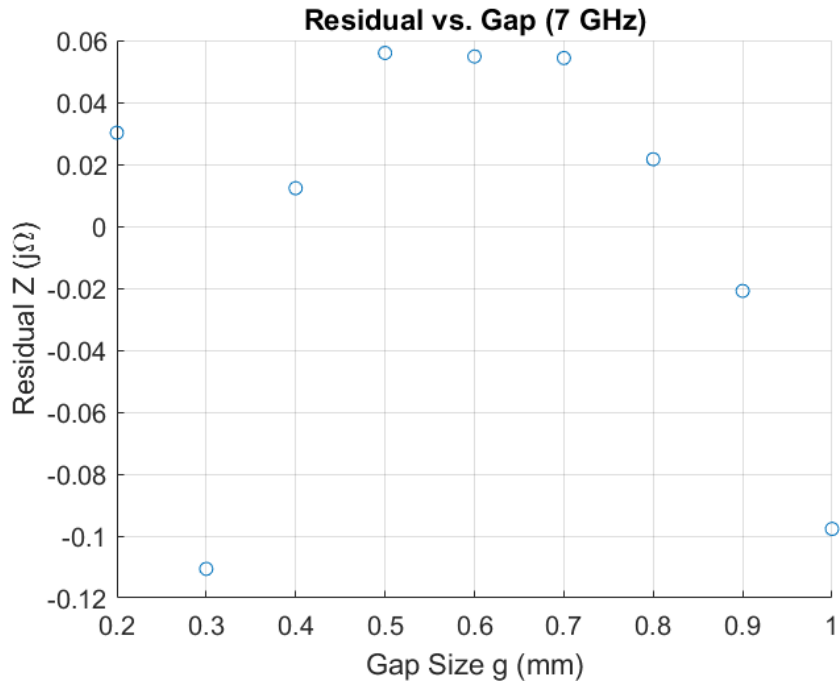


Figure 322: Fractal Duroid 5880: Residuals, 7 GHz

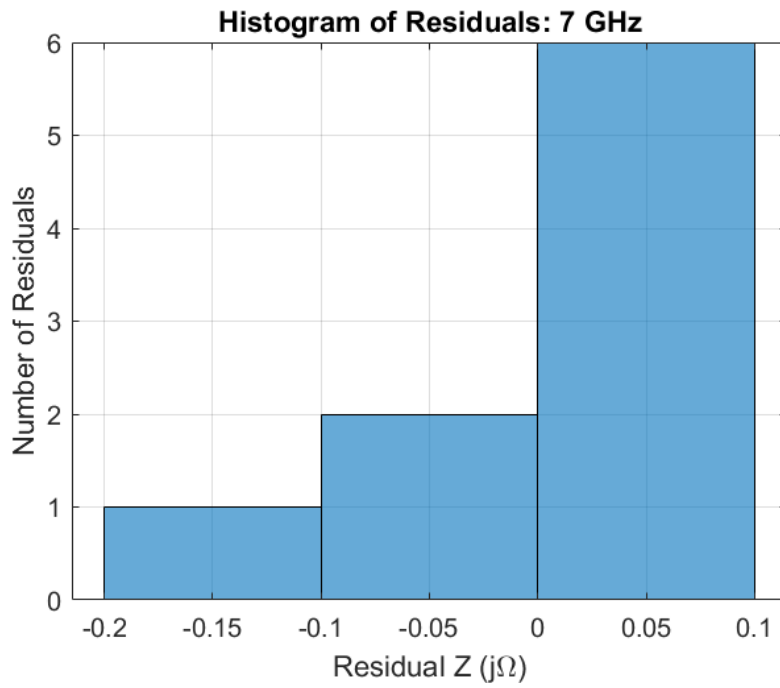


Figure 323: Fractal Duroid 5880: Histogram of Residuals, 7 GHz

Model: 8 GHz

Equation form: $y = c_0 + c_1 \frac{1}{x^1} + c_2 \frac{1}{x^2}$

	<u>Coefficient</u>	<u>SE</u>	<u>tStat</u>	<u>pValue</u>
c_0 (intercept)	86.502	0.15223	568.24	2.005×10^{-15}
c_1	4.0933	0.1289	31.755	6.4809×10^{-8}
c_2	-0.31337	0.021622	-14.493	6.7634×10^{-6}

Table 54: Model Coefficients: 8 GHz

Model Statistics

Error Degrees of Freedom: 6
 Root Mean Squared Error (RMSE): 0.0933
 R-squared: 0.999
 Adjusted R-Squared: 0.999
 F-statistic vs. constant model: 4.11×10^3
 p-value = 3.87×10^{-10}

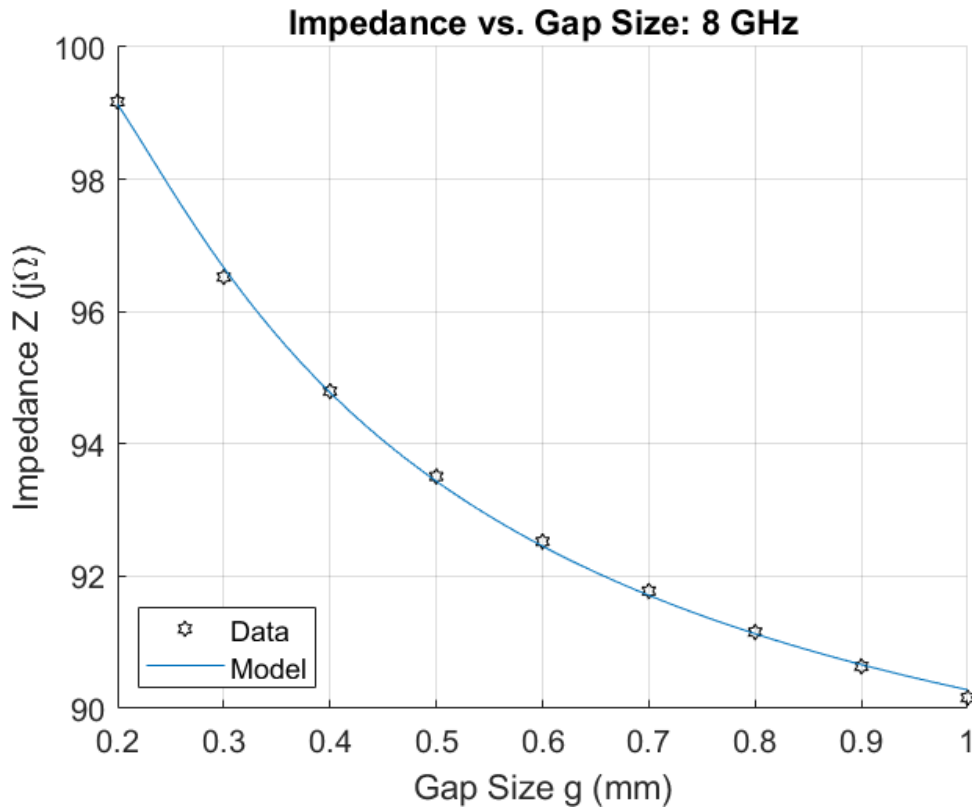


Figure 324: Fractal Duroid 5880: Impedance vs. Gap Size, 8 GHz

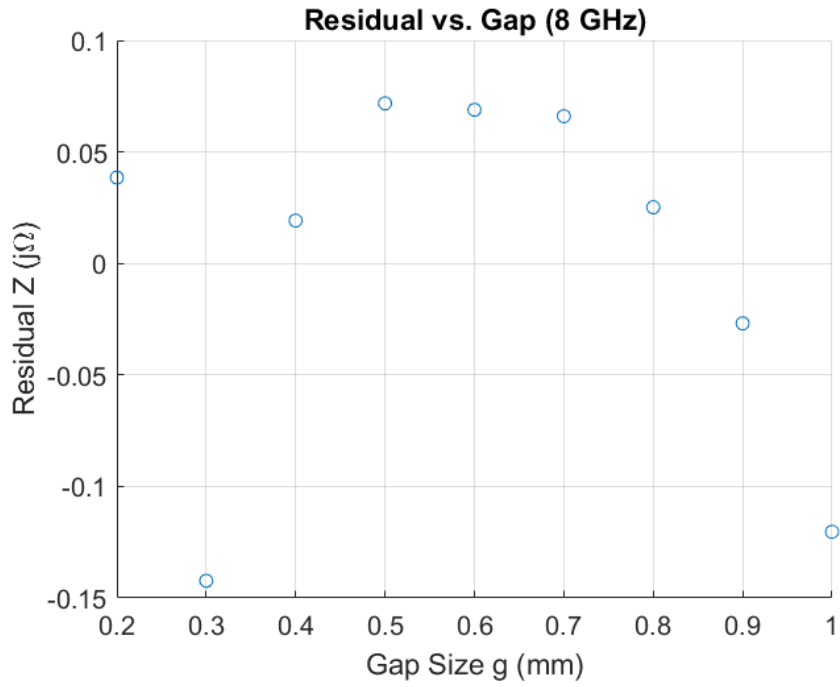


Figure 325: Fractal Duroid 5880: Residuals, 8 GHz

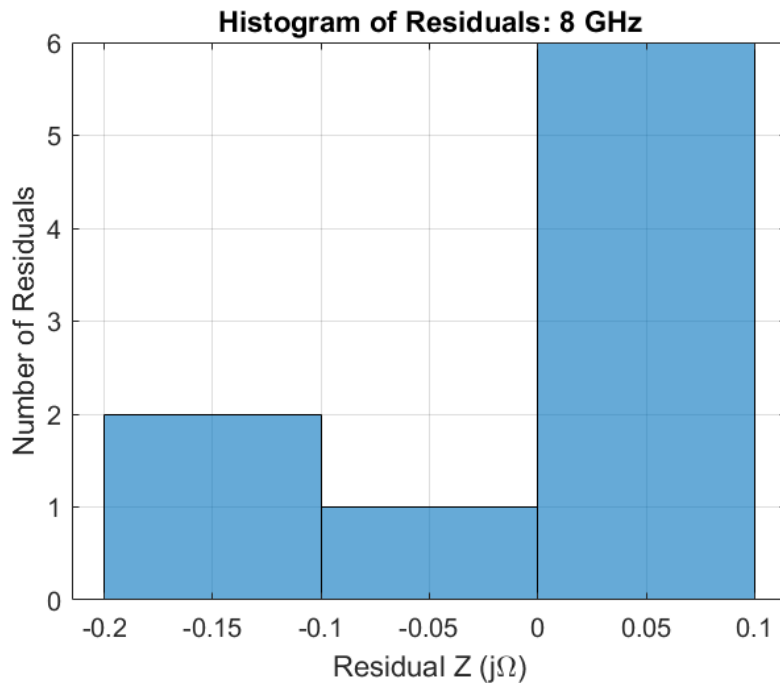


Figure 326: Fractal Duroid 5880: Histogram of Residuals, 8 GHz

Model: 9 GHz

Equation form: $y = c_0 + c_1 \frac{1}{x^1} + c_2 \frac{1}{x^2} + c_3 \frac{1}{x^3}$

	<u>Coefficient</u>	<u>SE</u>	<u>tStat</u>	<u>pValue</u>
c_0 (intercept)	86.309	0.10936	789.2	6.1955×10^{-14}
c_1	7.3619	0.14664	50.203	5.9266×10^{-8}
c_2	-1.0562	0.056842	-18.582	8.3079×10^{-6}
c_3	0.073354	0.0064488	11.375	9.1888×10^{-5}

Table 55: Model Coefficients: 9 GHz

Model Statistics

Error Degrees of Freedom: 5
 Root Mean Squared Error (RMSE): 0.0236
 R-squared: 1
 Adjusted R-Squared: 1
 F-statistic vs. constant model: 9.21×10^4
 p-value = 2.83×10^{-12}

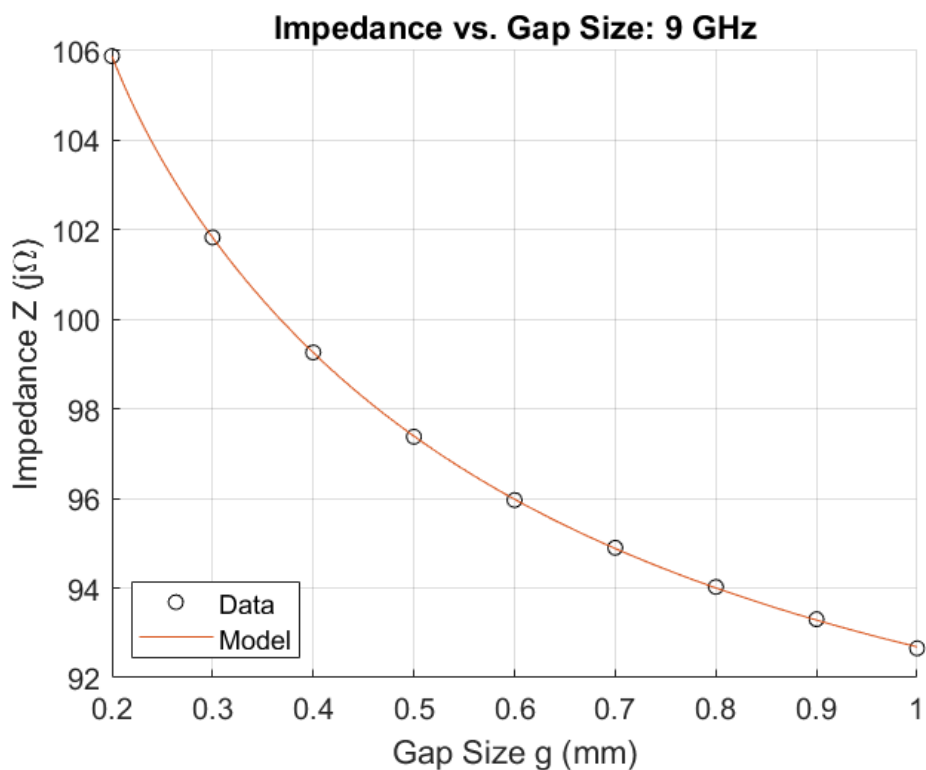


Figure 327: Fractal Duroid 5880: Impedance vs. Gap Size, 9 GHz

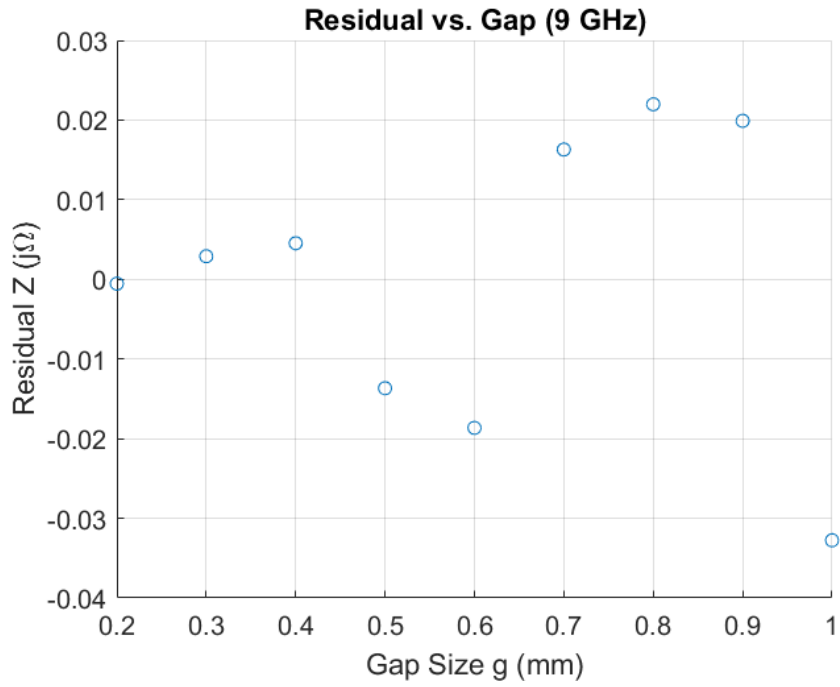


Figure 328: Fractal Duroid 5880: Residuals, 9 GHz

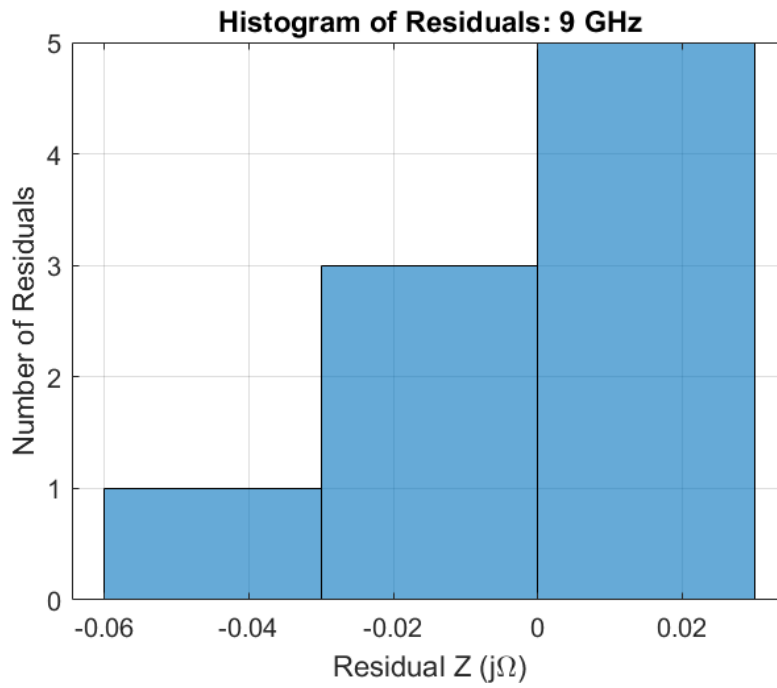


Figure 329: Fractal Duroid 5880: Histogram of Residuals, 9 GHz

Model: 10 GHz

Equation form: $y = c_0 + c_1 \frac{1}{x^1} + c_2 \frac{1}{x^2} + c_3 \frac{1}{x^3}$

	<u>Coefficient</u>	<u>SE</u>	<u>tStat</u>	<u>pValue</u>
c_0 (intercept)	87.059	0.12799	680.21	1.3034×10^{-13}
c_1	9.7565	0.17162	56.849	3.1859×10^{-8}
c_2	-1.2367	0.066524	-18.59	8.2889×10^{-6}
c_3	0.081324	0.0075471	10.775	0.00011936

Table 56: Model Coefficients: 10 GHz

Model Statistics

Error Degrees of Freedom: 5
 Root Mean Squared Error (RMSE): 0.0276
 R-squared: 1
 Adjusted R-Squared: 1
 F-statistic vs. constant model: 1.45×10^5
 p-value = 9.1×10^{-13}

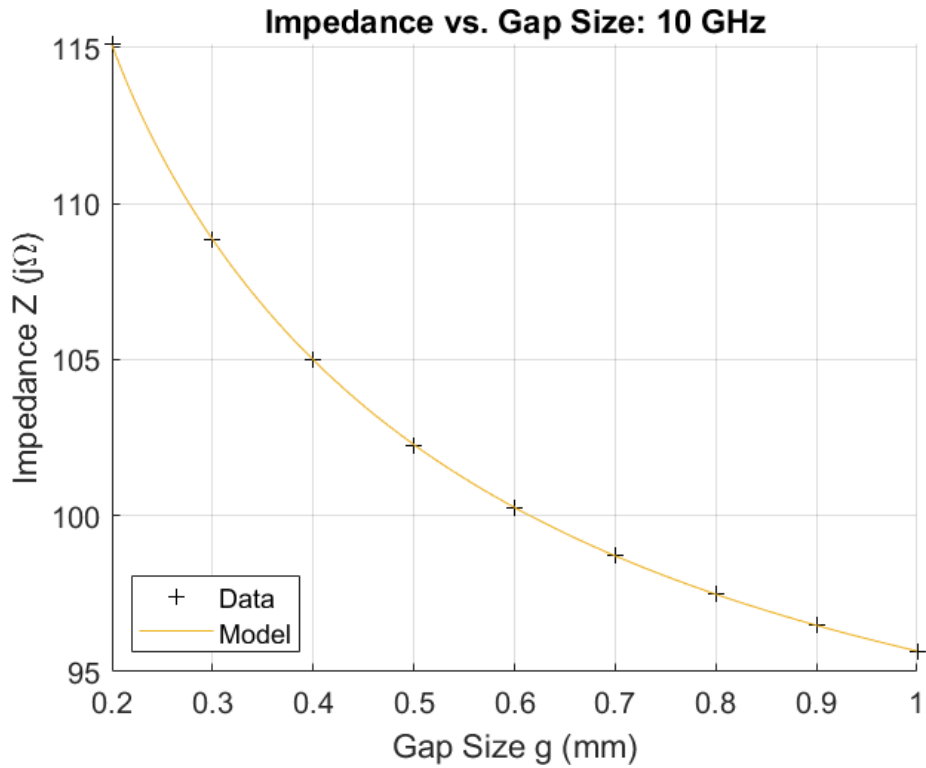


Figure 330: Fractal Duroid 5880: Impedance vs. Gap Size, 10 GHz

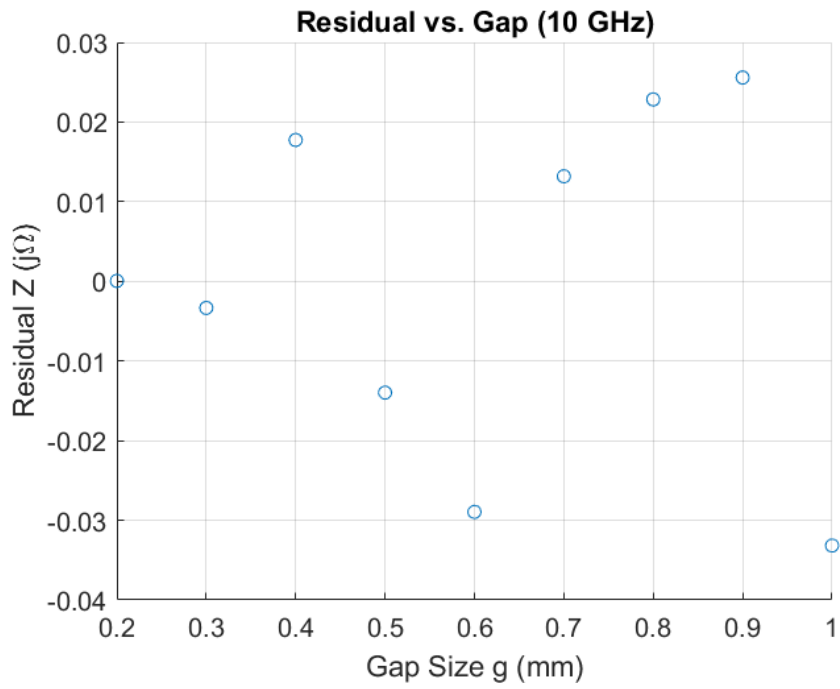


Figure 331: Fractal Duroid 5880: Residuals, 10 GHz

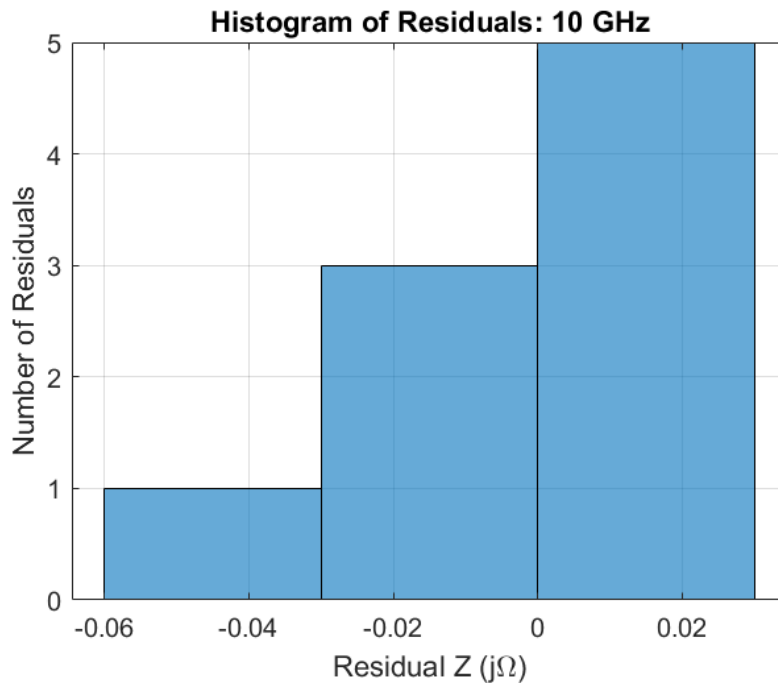


Figure 332: Fractal Duroid 5880: Histogram of Residuals, 10 GHz

Model: 11 GHz

Equation form: $y = c_0 + c_1 \frac{1}{x^1} + c_2 \frac{1}{x^2}$

	<u>Coefficient</u>	<u>SE</u>	<u>tStat</u>	<u>pValue</u>
c_0 (intercept)	88.276	0.054561	1617.9	3.763×10^{-18}
c_1	11.756	0.046199	254.47	2.4852×10^{-13}
c_2	-0.82887	0.0077494	-106.96	4.5021×10^{-11}

Table 57: Model Coefficients: ‘11 GHz

Model Statistics

Error Degrees of Freedom: 6
 Root Mean Squared Error (RMSE): 0.0334
 R-squared: 1
 Adjusted R-Squared: 1
 F-statistic vs. constant model: 2.97×10^5
 p-value = 1.03×10^{-15}

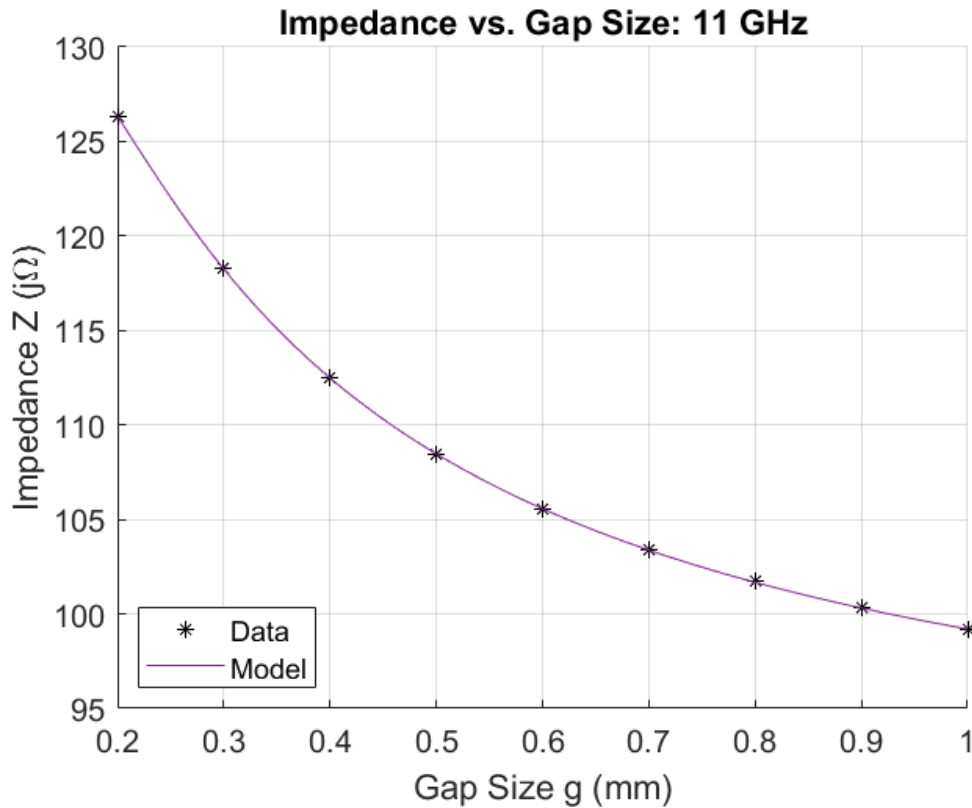


Figure 333: Fractal Duroid 5880: Impedance vs. Gap Size, 11 GHz

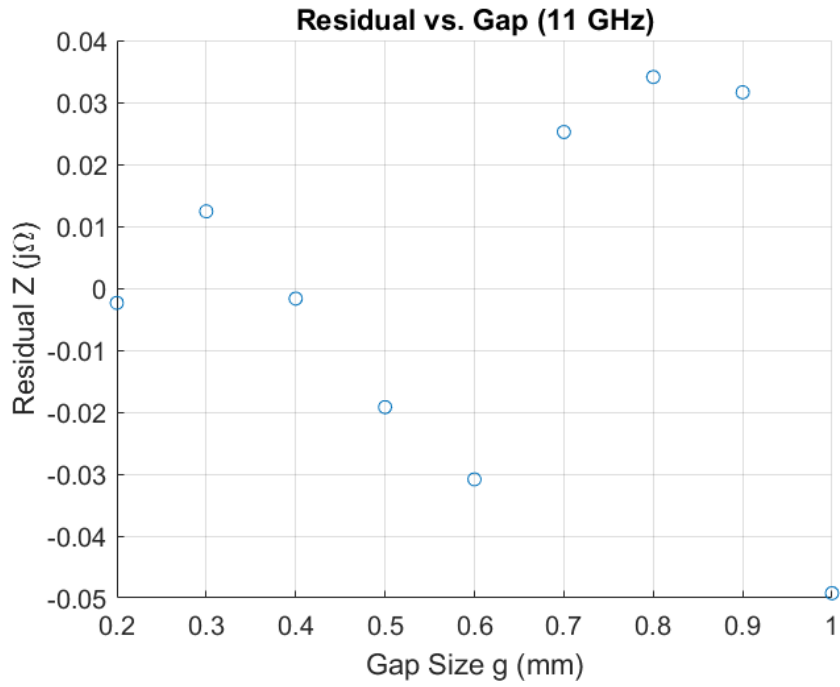


Figure 334: Fractal Duroid 5880: Residuals, 11 GHz

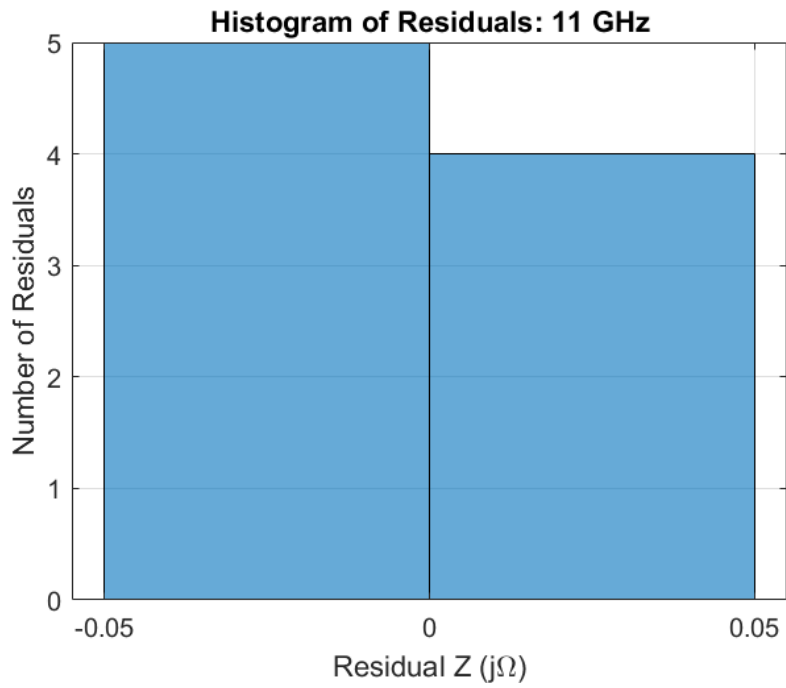


Figure 335: Fractal Duroid 5880: Histogram of Residuals, 11 GHz

Model: 12 GHz

Equation form: $y = c_0 + c_1 \frac{1}{x^1} + c_2 \frac{1}{x^2} + c_3 \frac{1}{x^3}$

	Coefficient	SE	tStat	pValue
c_0 (intercept)	89.176	0.19961	446.75	1.0665×10^{-12}
c_1	14.637	0.26766	54.685	3.8674×10^{-8}
c_2	-0.36327	0.10375	-3.5014	0.017259
c_3	-0.077385	0.011771	-6.5745	0.0012217

Table 58: Model Coefficients: '12 GHz

Model Statistics

Error Degrees of Freedom: 5
 Root Mean Squared Error (RMSE): 0.0431
 R-squared: 1
 Adjusted R-Squared: 1
 F-statistic vs. constant model: 2.62×10^5
 p-value = 2.08×10^{-13}

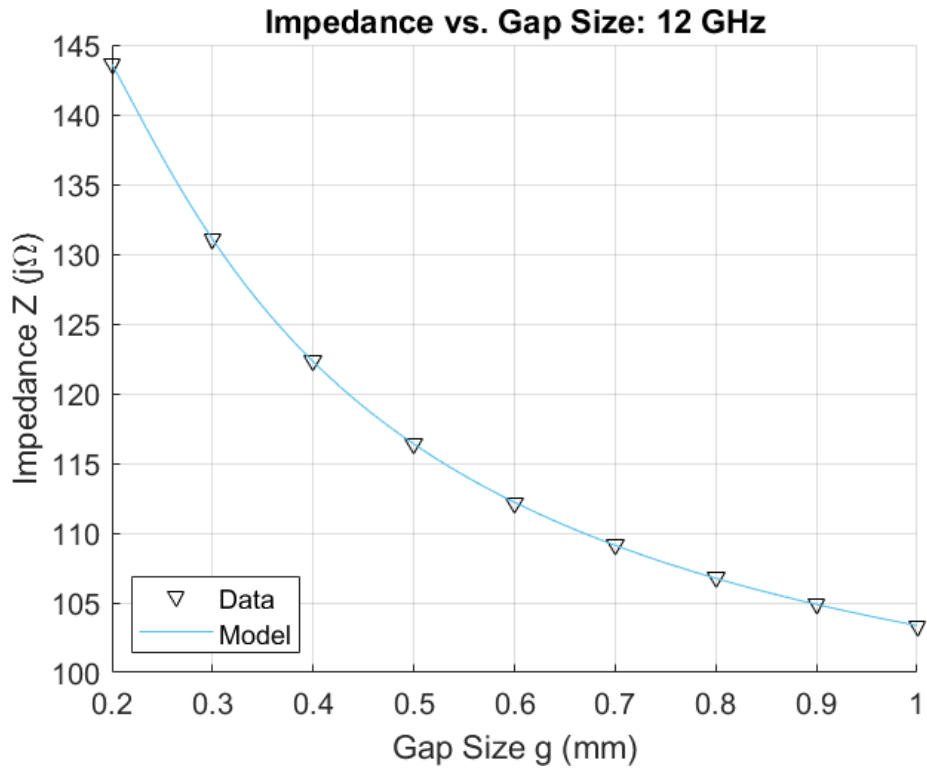


Figure 336: Fractal Duroid 5880: Impedance vs. Gap Size, 12 GHz

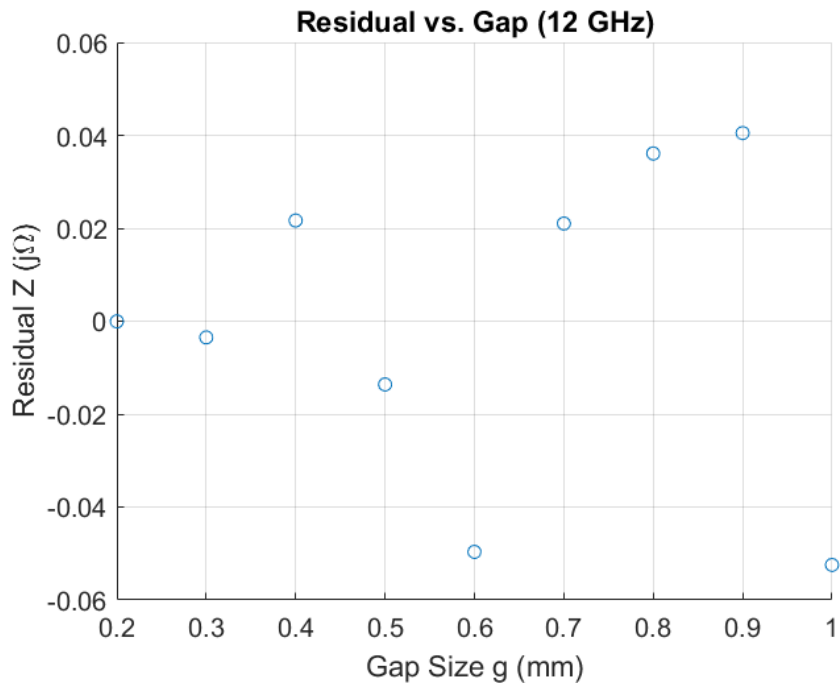


Figure 337: Fractal Duroid 5880: Residuals, 12 GHz

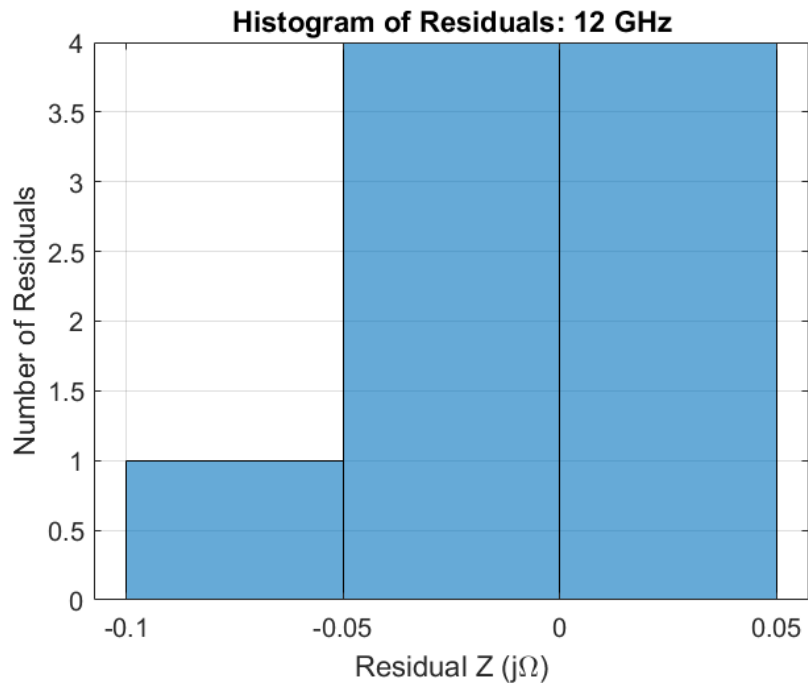


Figure 338: Fractal Duroid 5880: Histogram of Residuals, 12 GHz

Model: 13 GHz

Equation form: $y = c_0 + c_1x^1 + c_2x^2 + c_3x^3 + c_4x^4$

	<u>Coefficient</u>	<u>SE</u>	<u>tStat</u>	<u>pValue</u>
c_0 (intercept)	229.45	0.46817	490.09	1.04×10^{-10}
c_1	-418.33	4.0518	-103.24	5.2773×10^{-8}
c_2	613.32	11.798	51.983	8.1965×10^{-7}
c_3	-437.88	14.003	-31.271	6.2321×10^{-6}
c_4	121.67	5.8137	20.928	3.0806×10^{-5}

Table 59: Model Coefficients: '13 GHz

Model Statistics

Error Degrees of Freedom: 4
 Root Mean Squared Error (RMSE): 0.0446
 R-squared: 1
 Adjusted R-Squared: 1
 F-statistic vs. constant model: 3.91×10^5
 p-value = 1.96×10^{-11}

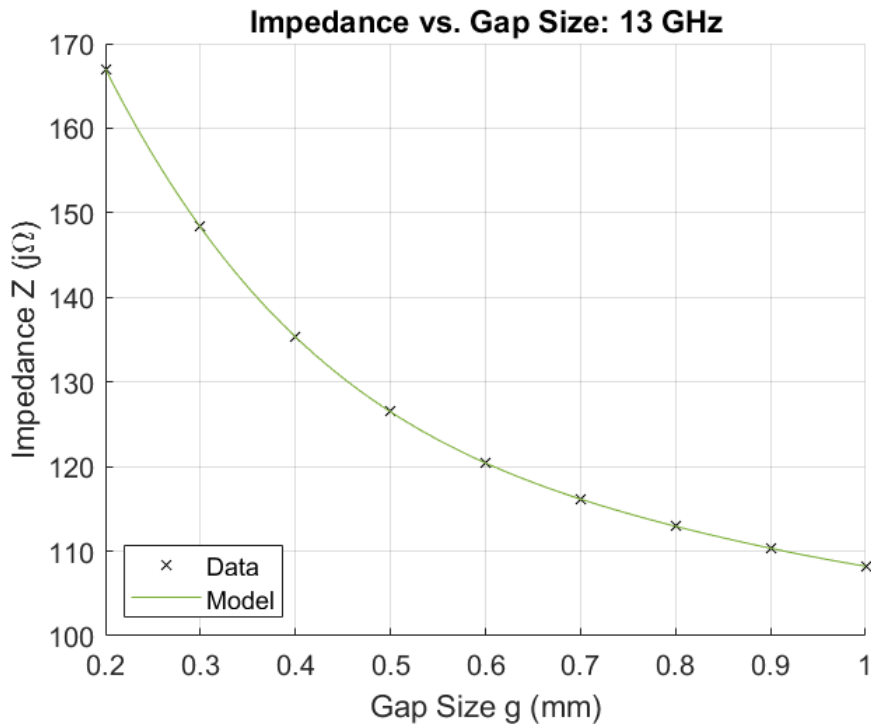


Figure 339: Fractal Duroid 5880: Impedance vs. Gap Size, 13 GHz

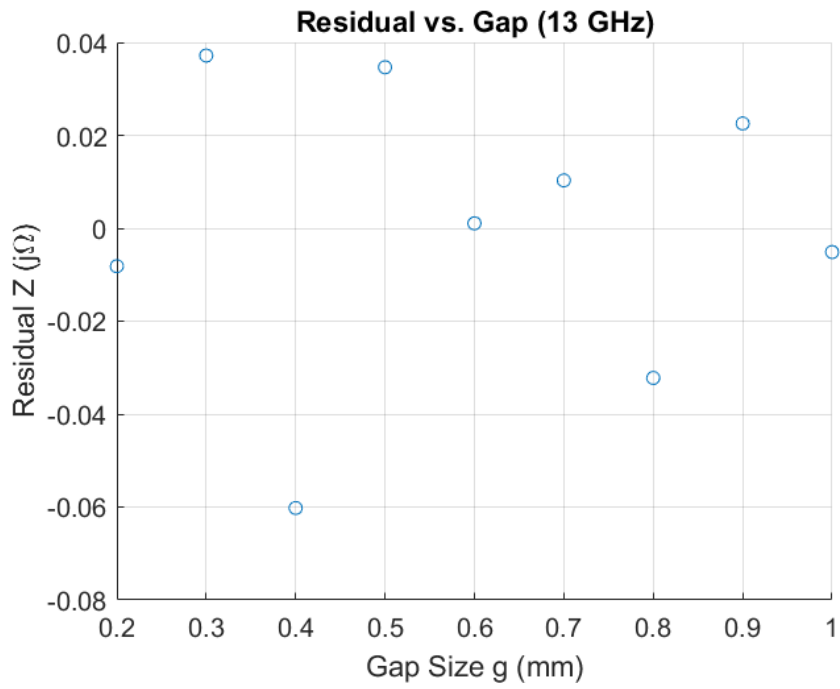


Figure 340: Fractal Duroid 5880: Residuals, 13 GHz

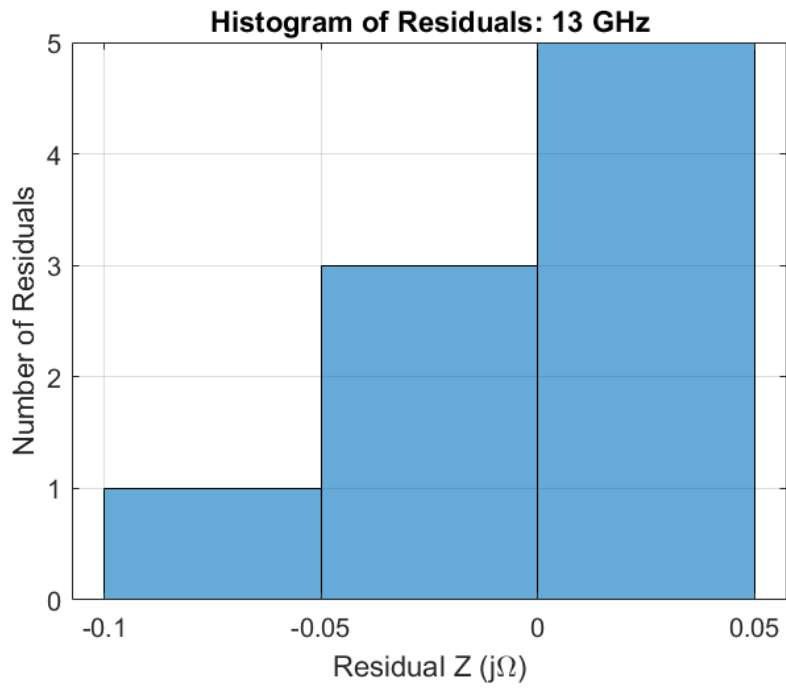


Figure 341: Fractal Duroid 5880: Histogram of Residuals, 13 GHz

Model: 14 GHz

Equation form: $y = c_0 + c_1x^1 + c_2x^2 + c_3x^3$

	<u>Coefficient</u>	<u>SE</u>	<u>tStat</u>	<u>pValue</u>
c_0 (intercept)	260.2	1.7688	147.11	2.7534×10^{-10}
c_1	-412.52	10.922	-37.768	2.4515×10^{-7}
c_2	420.03	19.855	21.155	4.3746×10^{-6}
c_3	-153.85	10.953	-14.047	3.2895×10^{-5}

Table 60: Model Coefficients: '14 GHz

Model Statistics

Error Degrees of Freedom: 5
 Root Mean Squared Error (RMSE): 0.414
 R-squared: 1
 Adjusted R-Squared: 1
 F-statistic vs. constant model: 1.14×10^4
 p-value = 5.3×10^{-10}

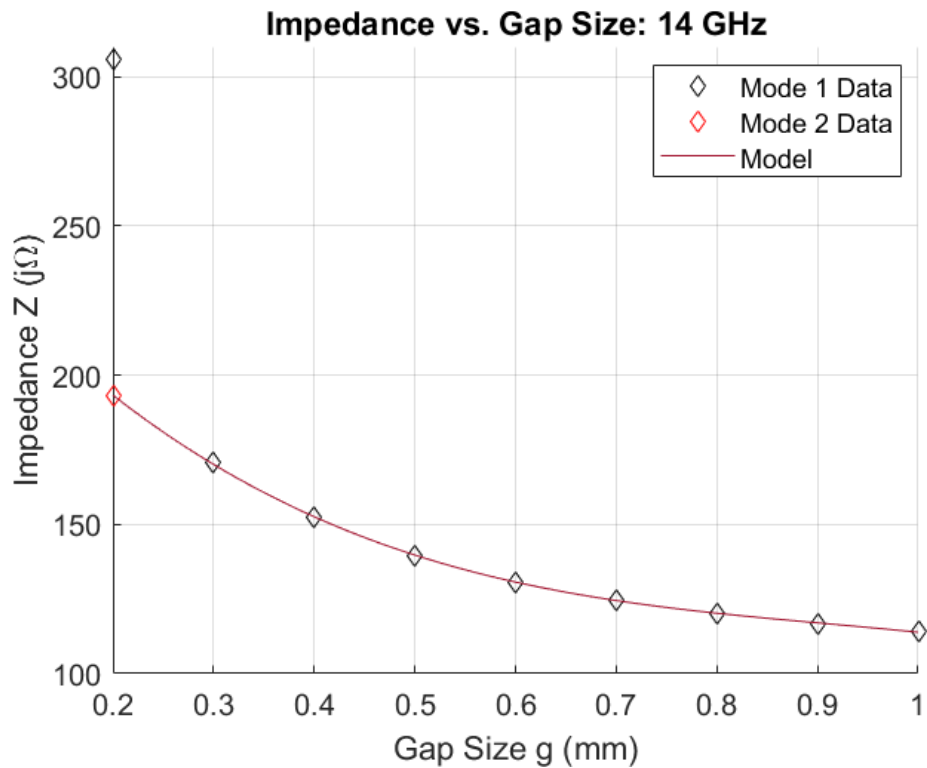


Figure 342: Fractal Duroid 5880: Impedance vs. Gap Size, 14 GHz

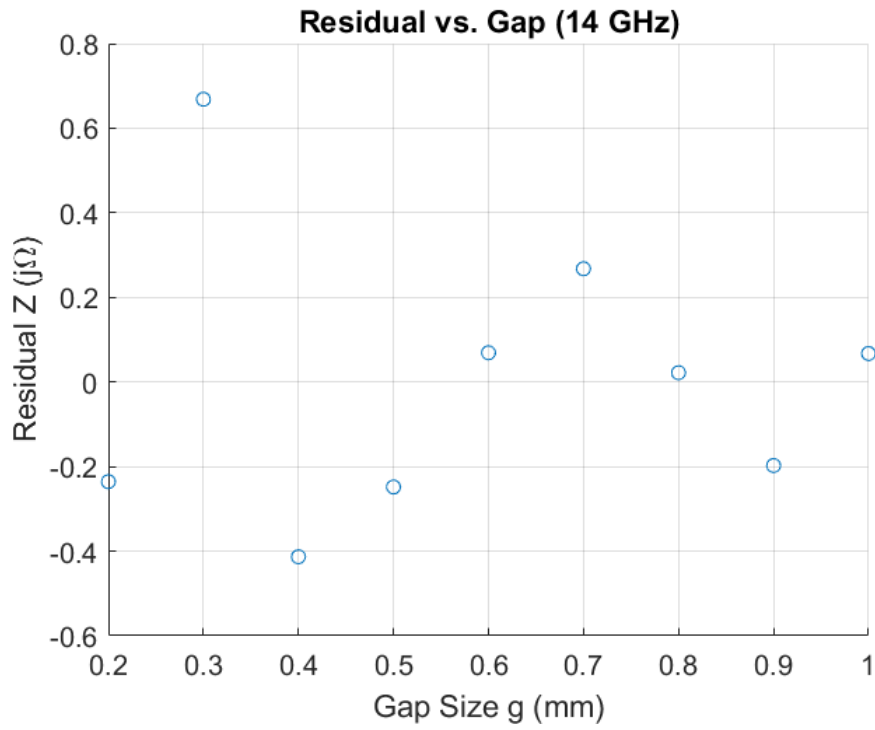


Figure 343: Fractal Duroid 5880: Residuals, 14 GHz

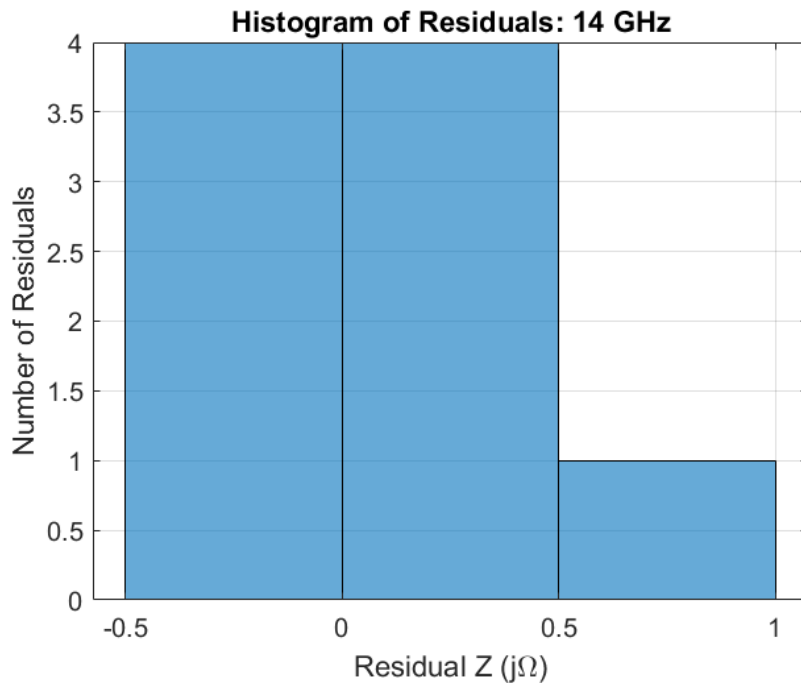


Figure 344: Fractal Duroid 5880: Histogram of Residuals, 14 GHz

Model: 15 GHz

Equation form: $y = c_0 + c_1x^1 + c_2x^2 + c_3x^3$

	<u>Coefficient</u>
c_0 (intercept)	307.6
c_1	-473
c_2	404.7
c_3	-117.9

Table 61: Model Coefficients: '15 GHz

Model Statistics

Error Degrees of Freedom: 5
Sum Squared Error (SSE): 134.2
Root Mean Squared Error (RMSE): 5.18
R-squared: 0.988
Adjusted R-Squared: 0.9809

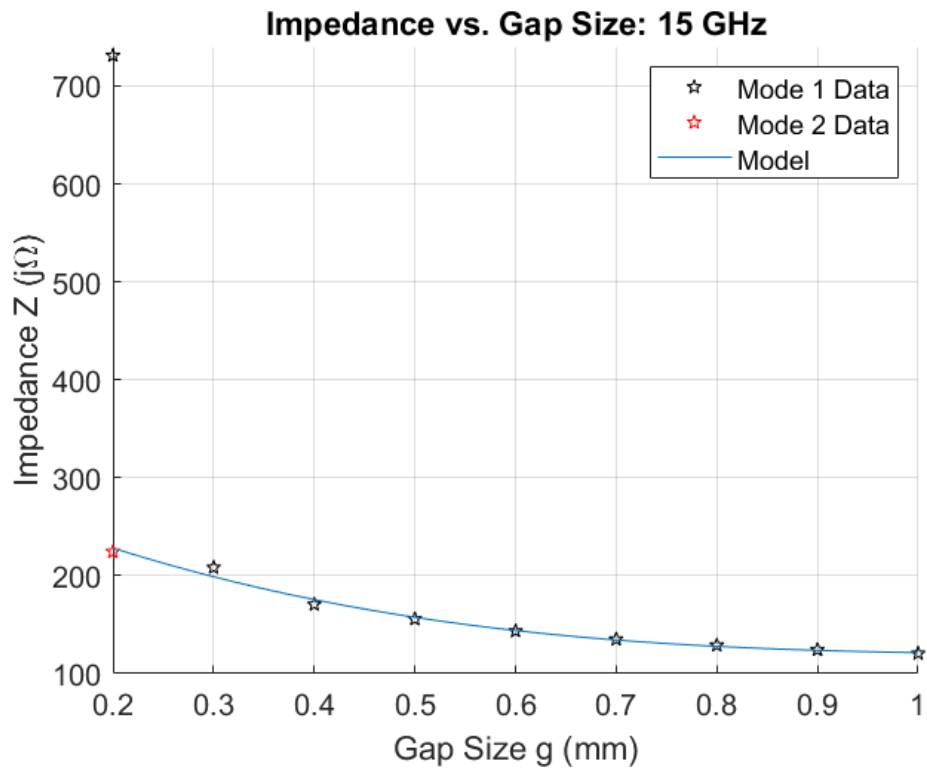


Figure 345: Fractal Duroid 5880: Impedance vs. Gap Size, 15 GHz

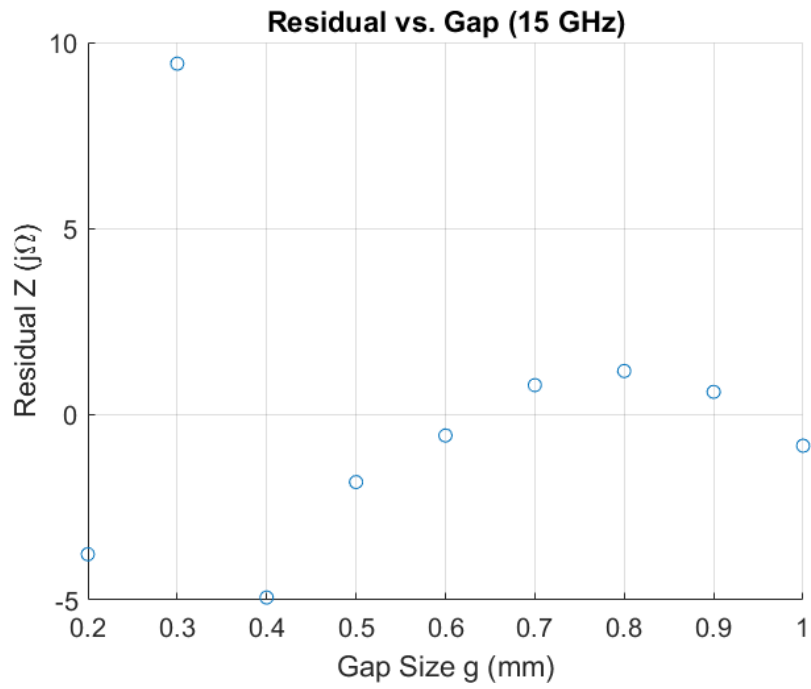


Figure 346: Fractal Duroid 5880: Residuals, 15 GHz

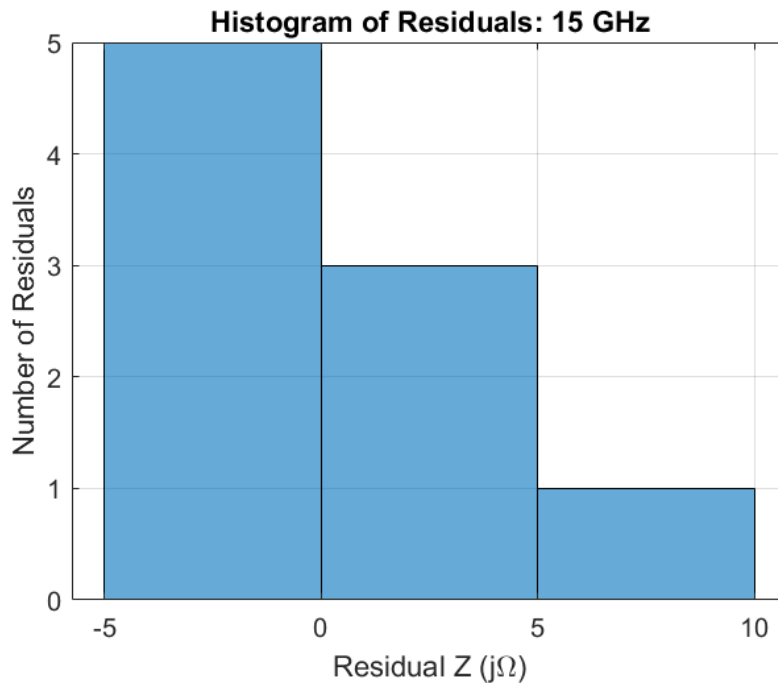


Figure 347: Fractal Duroid 5880: Histogram of Residuals, 15 GHz

Model: 16 GHz

Equation form: $y = c_0 + c_1x^1 + c_2x^2 + c_3x^3$

	Coefficient	SE	tStat	pValue
c_0 (intercept)	353.46	4.1369	85.441	4.1622×10^{-9}
c_1	-583.83	25.546	-22.854	2.9827×10^{-6}
c_2	540.12	46.439	11.631	8.2498×10^{-5}
c_3	-181.59	25.617	-7.0886	0.00086516

Table 62: Model Coefficients: '16 GHz

Model Statistics

Error Degrees of Freedom: 5
 Root Mean Squared Error (RMSE): 0.967
 R-squared: 1
 Adjusted R-Squared: 1
 F-statistic vs. constant model: 5.54×10^3
 p-value = 3.2×10^{-9}

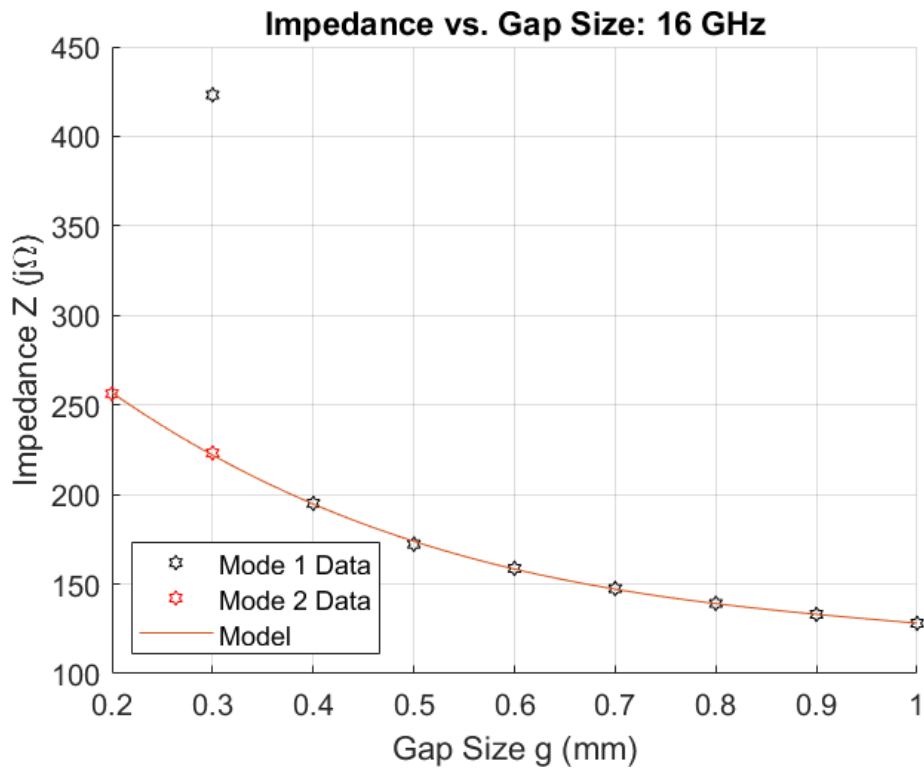


Figure 348: Fractal Duroid 5880: Impedance vs. Gap Size, 16 GHz

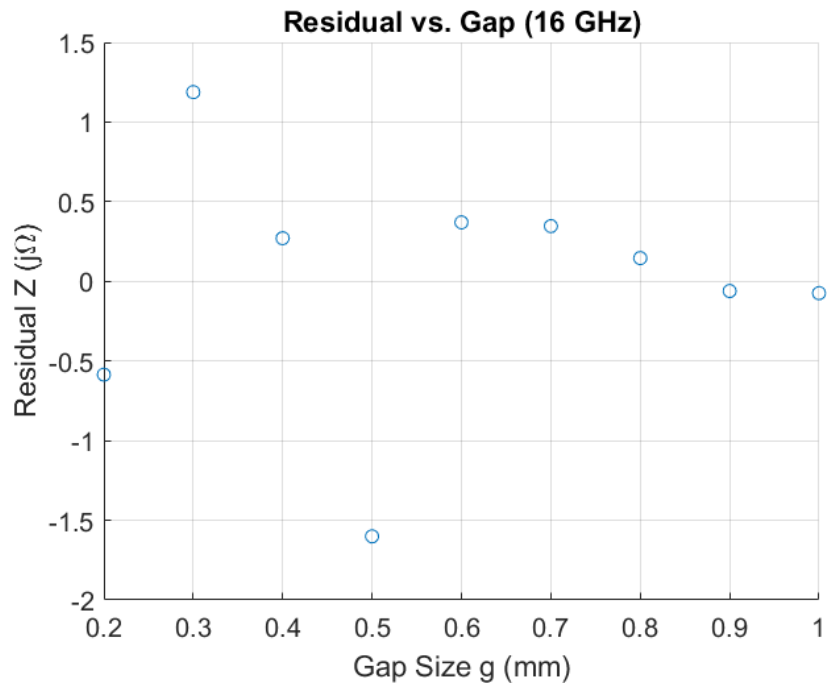


Figure 349: Fractal Duroid 5880: Residuals, 16 GHz

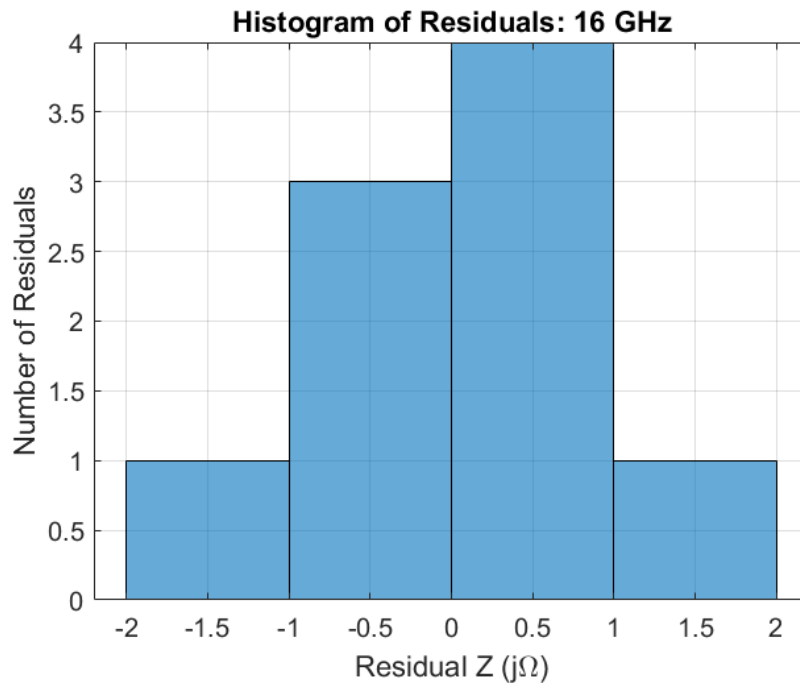


Figure 350: Fractal Duroid 5880: Histogram of Residuals, 16 GHz

Model: 17 GHz

Equation form: $y = c_0 + c_1x^1 + c_2x^2$

	<u>Coefficient</u>	<u>SE</u>	<u>tStat</u>	<u>pValue</u>
c_0 (intercept)	369.39	4.4177	83.616	1.9705×10^{-10}
c_1	-459.38	16.42	-27.976	1.3799×10^{-7}
c_2	228.97	13.446	17.029	2.623×10^{-6}

Table 63: Model Coefficients: '17 GHz

Model Statistics

Error Degrees of Freedom: 6
 Root Mean Squared Error (RMSE): 2.36
 R-squared: 0.998
 Adjusted R-Squared: 0.998
 F-statistic vs. constant model: 1.98×10^3
 p-value = 3.46×10^{-9}

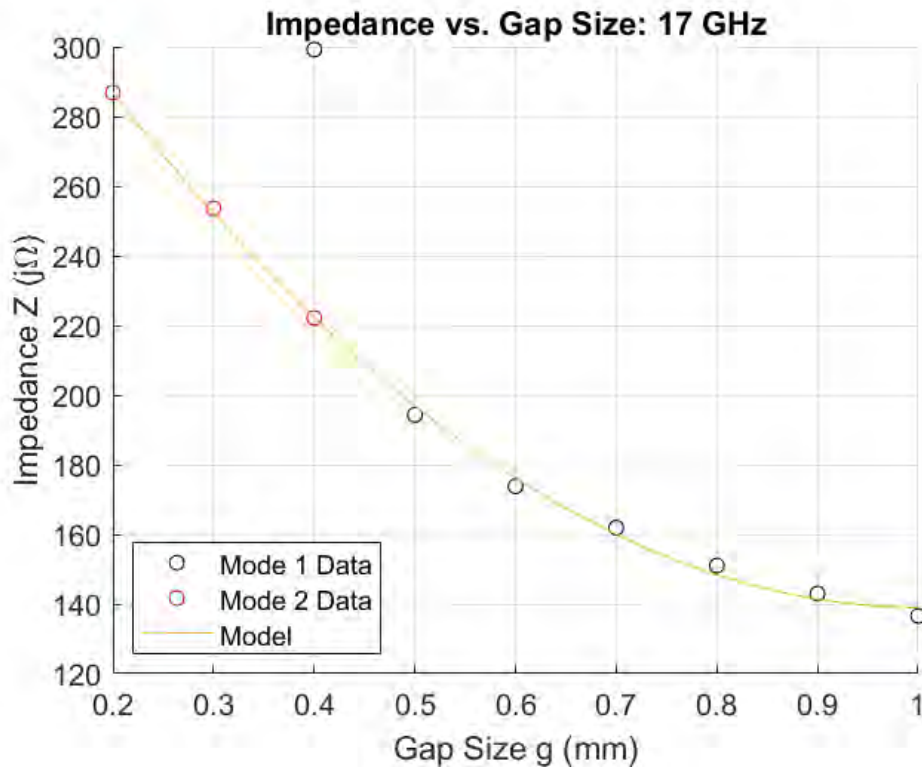


Figure 351: Fractal Duroid 5880: Impedance vs. Gap Size, 17 GHz

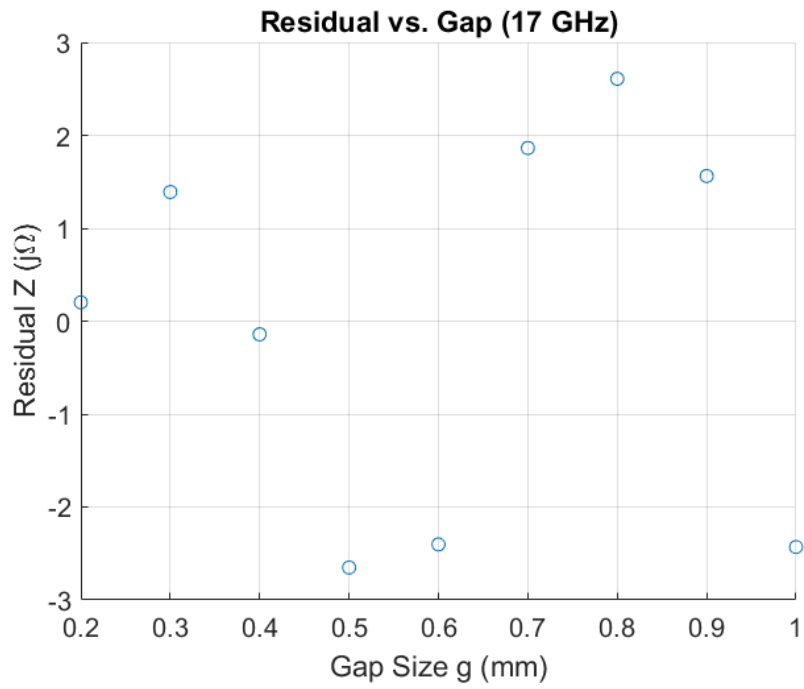


Figure 352: Fractal Duroid 5880: Residuals, 17 GHz

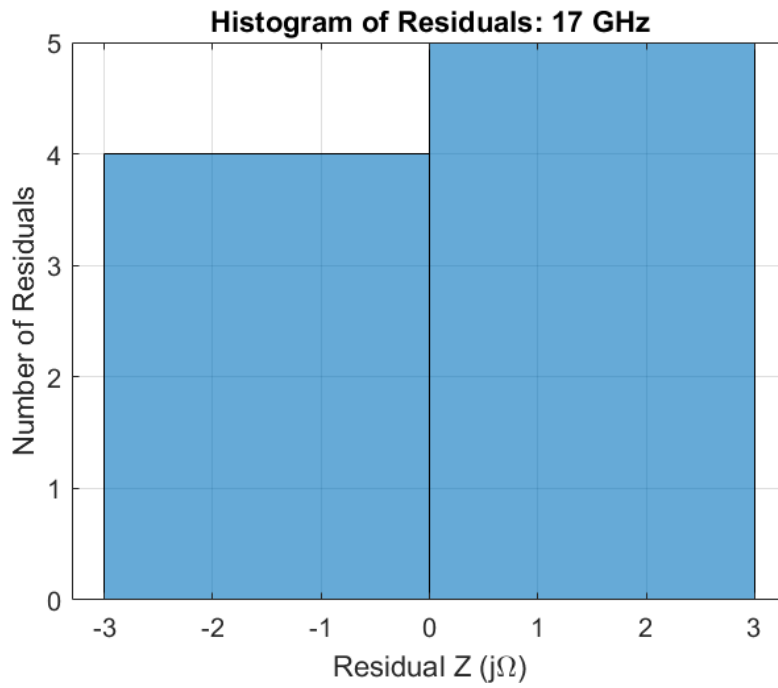


Figure 353: Fractal Duroid 5880: Histogram of Residuals, 17 GHz

Model: 18 GHz

Equation form: $y = c_0 + c_1x^1 + c_2x^2$

	Coefficient	SE	tStat	pValue
c_0 (intercept)	405.76	4.6715	86.858	1.568×10^{-10}
c_1	-481.59	17.363	-27.736	1.4527×10^{-7}
c_2	222.72	14.218	15.664	4.2884×10^{-6}

Table 64: Model Coefficients: '18 GHz

Model Statistics

Error Degrees of Freedom: 6
 Root Mean Squared Error (RMSE): 2.5
 R-squared: 0.999
 Adjusted R-Squared: 0.998
 F-statistic vs. constant model: 2.34×10^3
 p-value = 2.11×10^{-9}

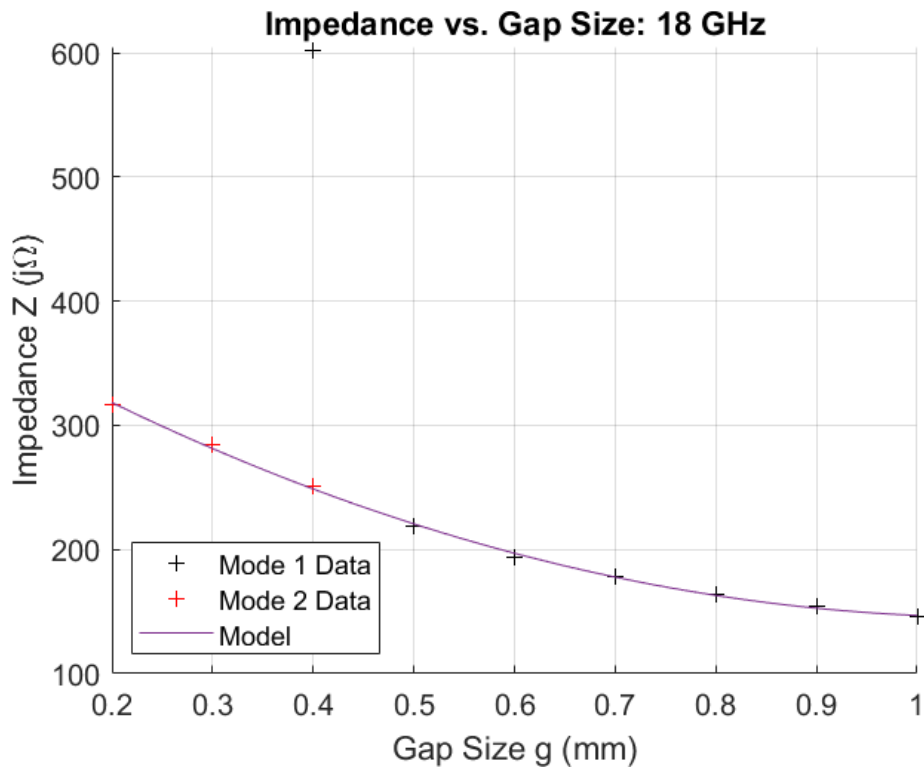


Figure 354: Fractal Duroid 5880: Impedance vs. Gap Size, 18 GHz

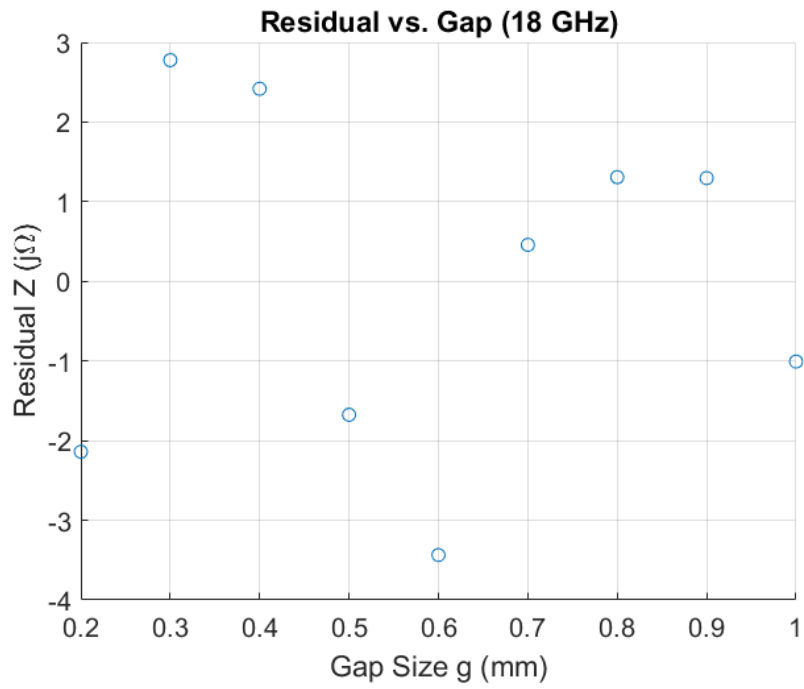


Figure 355: Fractal Duroid 5880: Residuals, 18 GHz

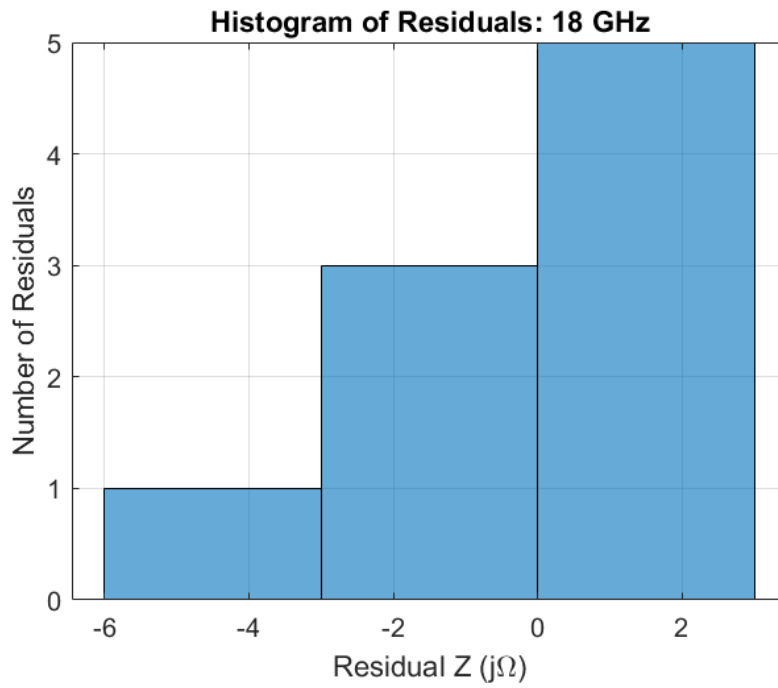


Figure 356: Fractal Duroid 5880: Histogram of Residuals, 18 GHz

Model: 19 GHz

Equation form: $y = c_0 + c_1x^1 + c_2x^2$

	Coefficient	SE	tStat	pValue
c_0 (intercept)	438.99	6.8132	64.432	9.398×10^{-10}
c_1	-487.88	25.324	-19.266	1.2656×10^{-6}
c_2	204.17	20.737	9.8457	6.3287×10^{-5}

Table 65: Model Coefficients: '19 GHz

Model Statistics

Error Degrees of Freedom: 6
 Root Mean Squared Error (RMSE): 3.64
 R-squared: 0.998
 Adjusted R-Squared: 0.997
 F-statistic vs. constant model: 1.38×10^3
 p-value = 1.01×10^8

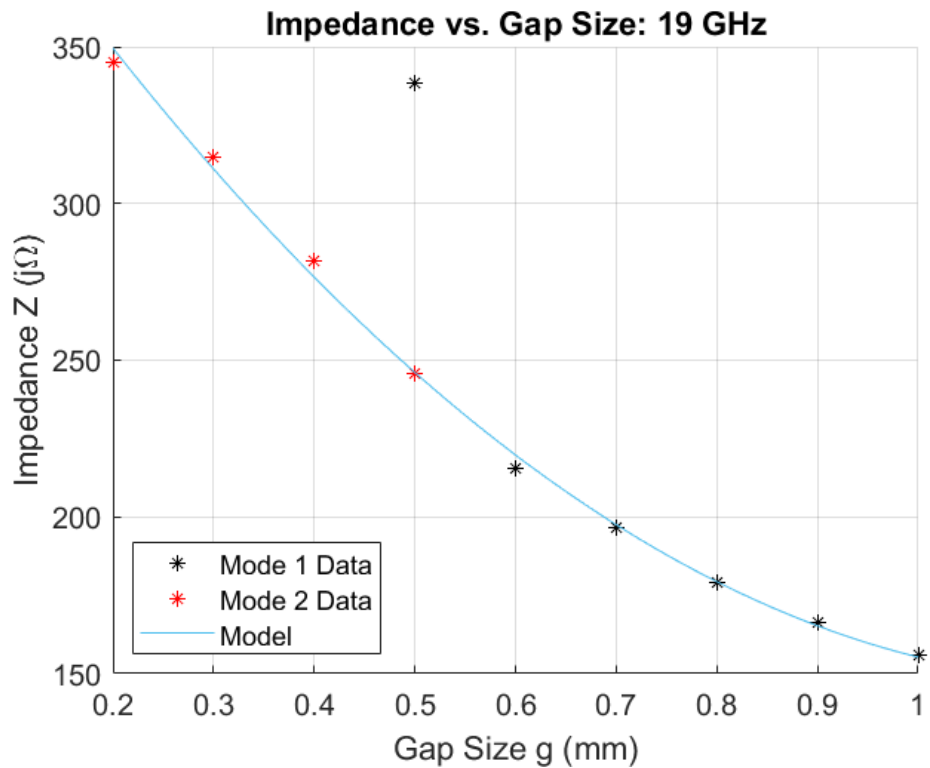


Figure 357: Fractal Duroid 5880: Impedance vs. Gap Size, 19 GHz

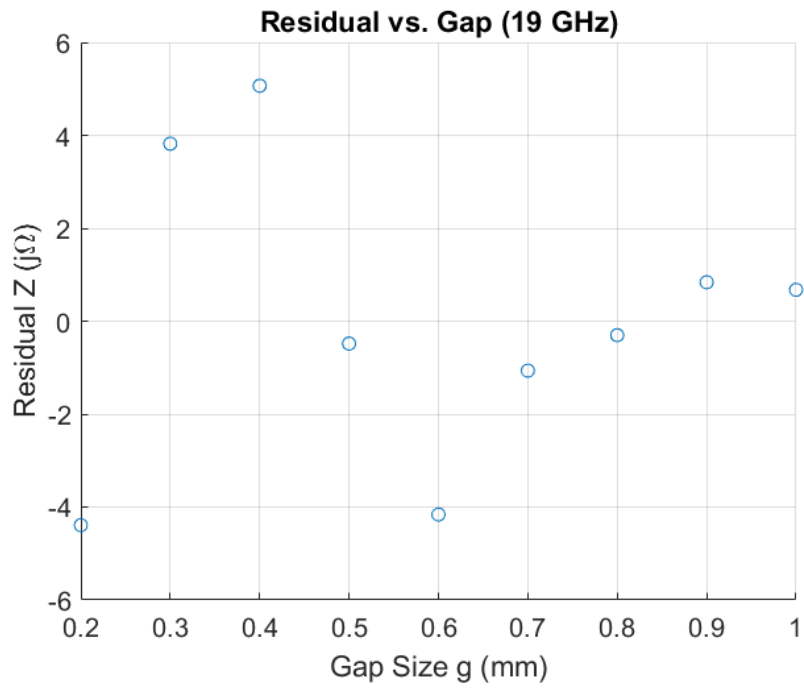


Figure 358: Fractal Duroid 5880: Residuals, 19 GHz

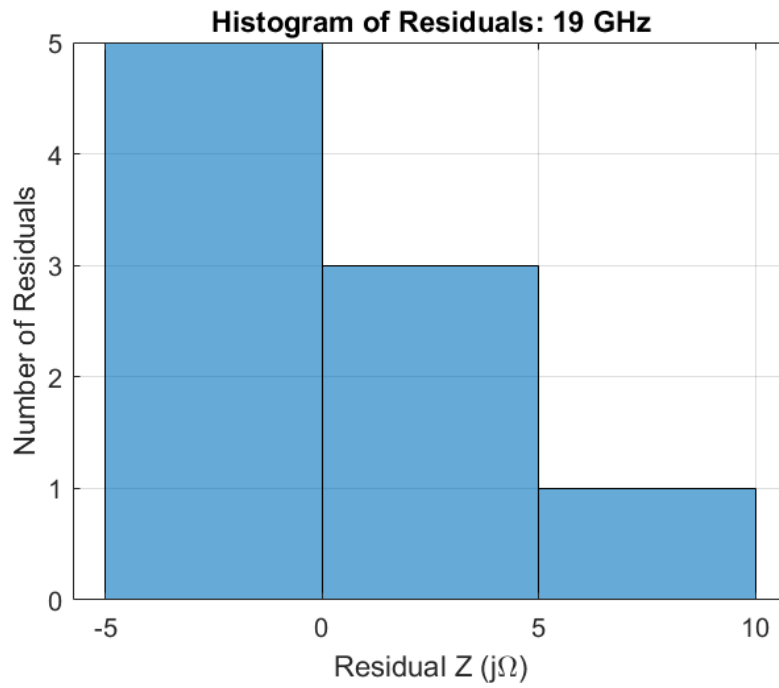


Figure 359: Fractal Duroid 5880: Histogram of Residuals, 19 GHz

Appendix D. Square FR4 Unit Cell

Model Summary

Cell Parameters

Material: FR4

Dielectric Constant, ϵ_r : 4.3

Dissipation Constant, $\tan \delta$: 0.025

Shape: square

Dielectric Thickness: 0.7874 mm

Copper Thickness: 0.035 mm

Cell Size, a : 3 mm

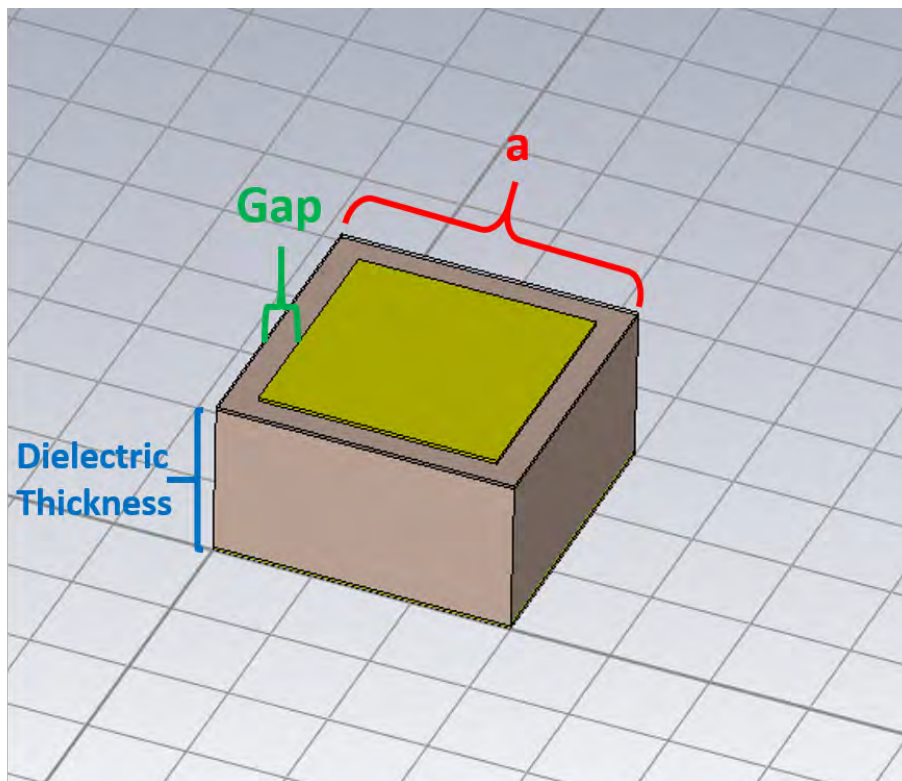


Figure 360: Square Cell Geometry

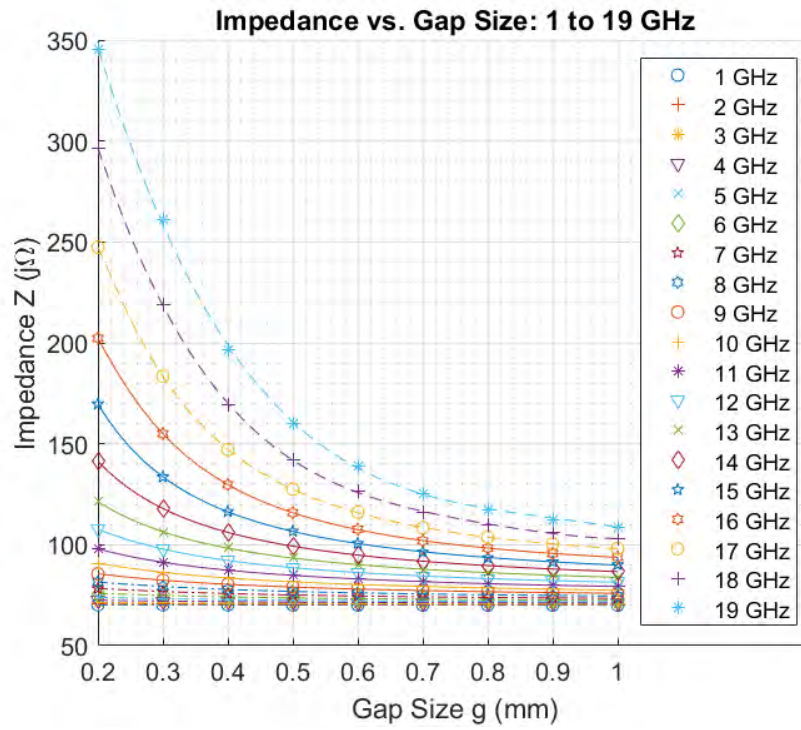


Figure 361: Square FR4: Cell Impedance vs. Gap, 1-19 GHz

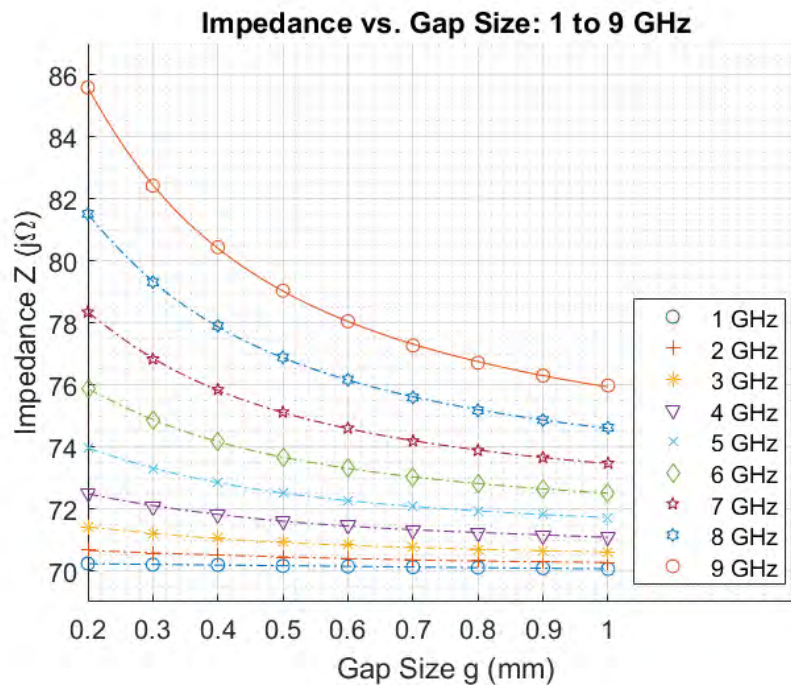


Figure 362: Square FR4: Cell Impedance vs. Gap, 1-9 GHz

Unit Cell Impedance Model: Square FR4										
Frequency \rightarrow Parameter \downarrow	1 GHz	2 GHz	3 GHz	4 GHz	5 GHz	6 GHz	7 GHz	8 GHz	9 GHz	10 GHz
c_4	0	0	0	0	0	0	0	0	0	0
c_3	0	0	0	-2.48777	0	0	0	0	0	0
c_2	0	0.417304	-0.03414	6.580462	-0.07641	-0.10638	-0.14226	-0.18317	-0.22654	-0.26604
c_1	-0.20901	-0.9825	0.40262	-6.56753	1.015885	1.478806	2.07285	2.825728	3.771856	4.951123
c_0 (intercept)	70.2695	70.83604	70.2455	73.55117	70.78012	71.13143	71.52616	71.94975	72.38204	72.79677
Z_{min}	70.05957	70.2609	70.59973	71.08112	71.71235	72.50325	73.46614	74.61675	70.05957	77.56206
Z_{max}	70.23304	70.66747	71.41003	72.49053	73.95513	75.87187	78.33975	81.50362	70.23304	90.89737
X	70.14631	70.46418	71.00488	71.78583	72.83374	74.18756	75.90295	78.06018	70.14631	84.22971
M	0.086736	0.203286	0.405149	0.704703	1.121393	1.684314	2.436804	3.443434	0.086736	6.667656
ϕ_{avg}	3.664405	7.329794	10.99721	14.6678	18.34292	22.02423	25.71382	29.41449	3.664405	36.8661
Inversion Factor	1	1	-1	1	-1	-1	-1	-1	-1	-1

Frequency \rightarrow Parameter \downarrow	11 GHz	12 GHz	13 GHz	14 GHz	15 GHz	16 GHz	17 GHz	18 GHz	19 GHz
c_4	0	0	0	0	0	0	0	867.9965	398.3
c_3	0	-0.05676	-0.09609	-0.15737	-0.27519	-0.86165	-1.63348	-2853.92	-1741
c_2	-0.28727	0.238341	0.72012	1.606061	3.287676	8.564719	15.69921	3585.567	2769
c_1	6.402039	6.888048	8.030685	8.867795	8.75579	2.459537	-6.23295	-2089.18	-1958
c_0 (intercept)	73.16456	74.36185	75.20913	76.35784	78.13789	83.56315	90.22791	592.5628	640.4
Z_{min}	79.40806	81.54546	84.01295	86.85488	90.12041	93.86184	98.13132	102.9759	108.4319
Z_{max}	97.97932	107.6725	121.3635	141.1882	169.7225	202.2746	247.3527	296.5458	345.4687
X	88.69369	94.60897	102.6882	114.0215	129.9215	148.0682	172.742	199.7609	226.9503
M	9.285627	13.06352	18.67526	27.16664	39.80107	54.2064	74.61071	96.78492	118.5184
ϕ_{avg}	40.63097	44.43804	48.30986	52.28563	56.431	60.79034	65.53151	70.70345	76.34897
Inversion Factor	-1	-1	-1	-1	-1	-1	-1	1	1

Table 66: Unit Cell Impedance Model: Square FR4

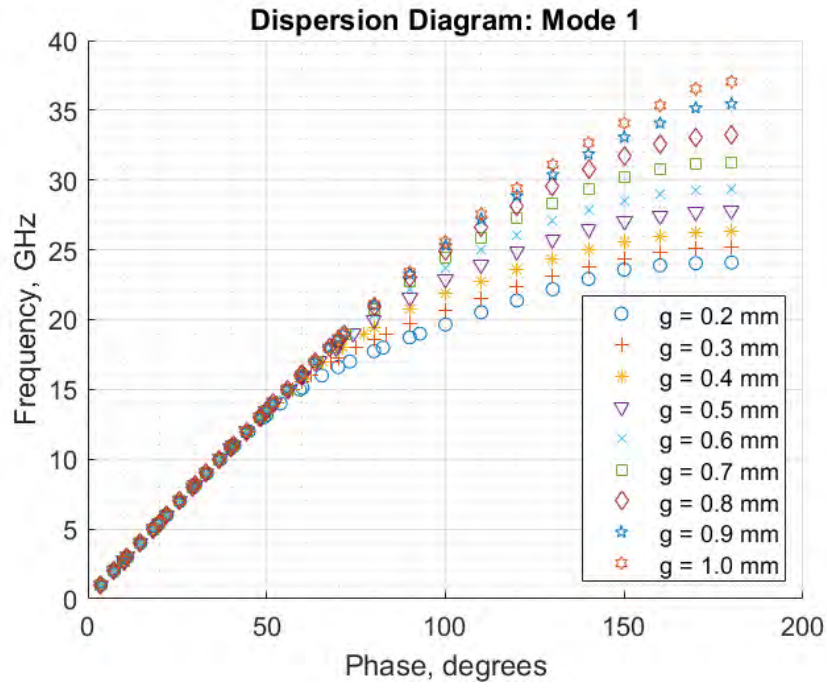


Figure 363: Square FR4: Dispersion Diagram, Mode 1

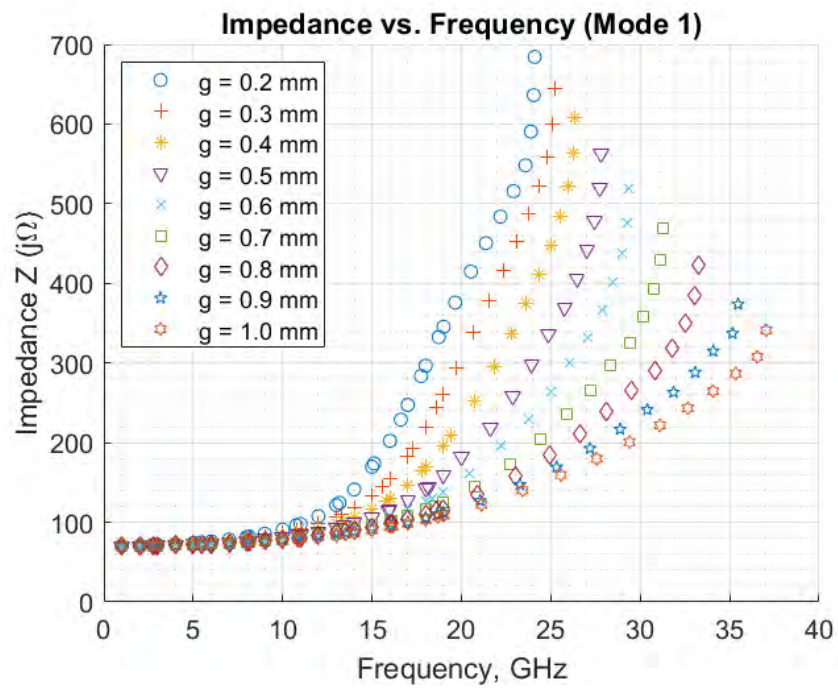


Figure 364: Square FR4: Impedance vs. Frequency, Mode 1

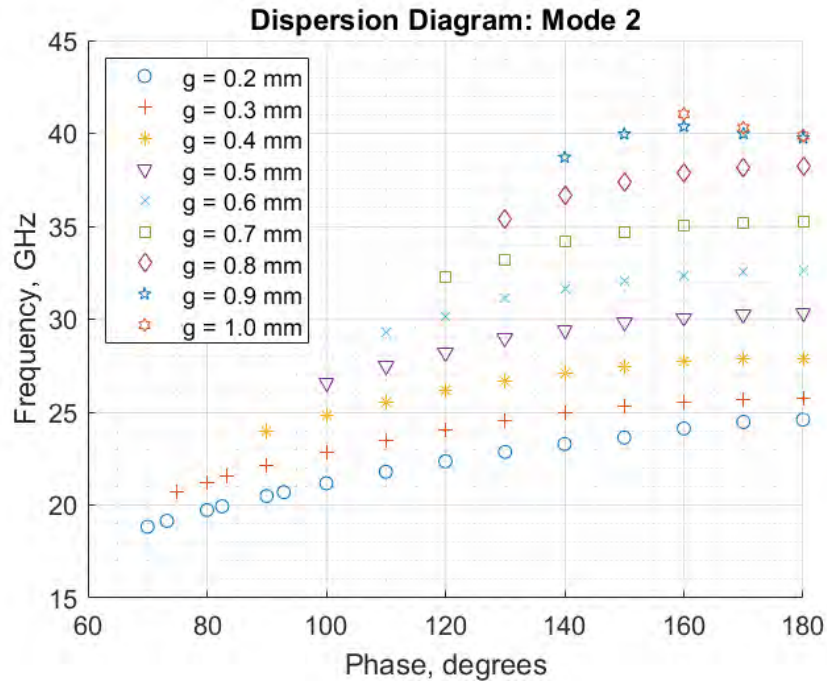


Figure 365: Square FR4: Dispersion Diagram, Mode 2

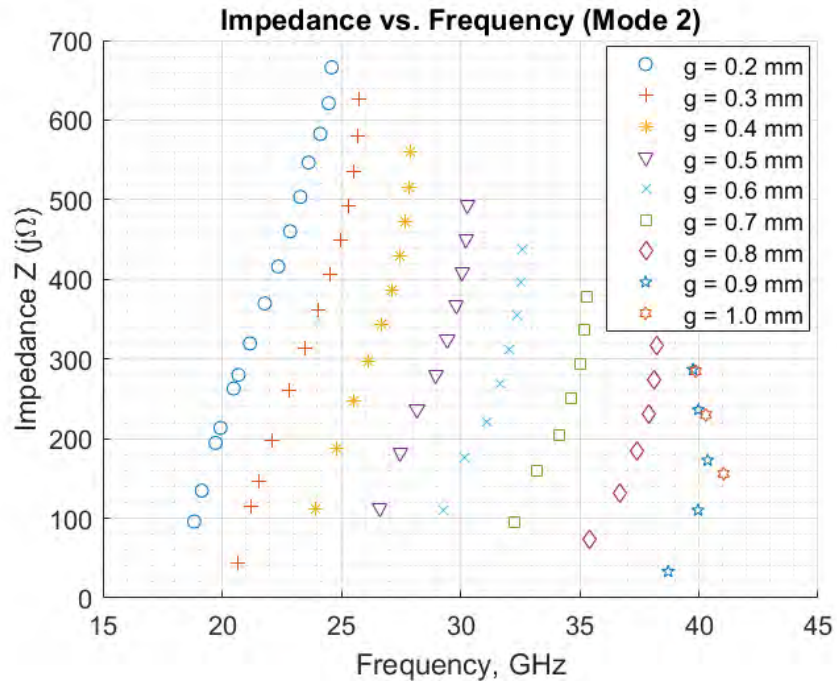


Figure 366: Square FR4: Impedance vs. Frequency, Mode 2

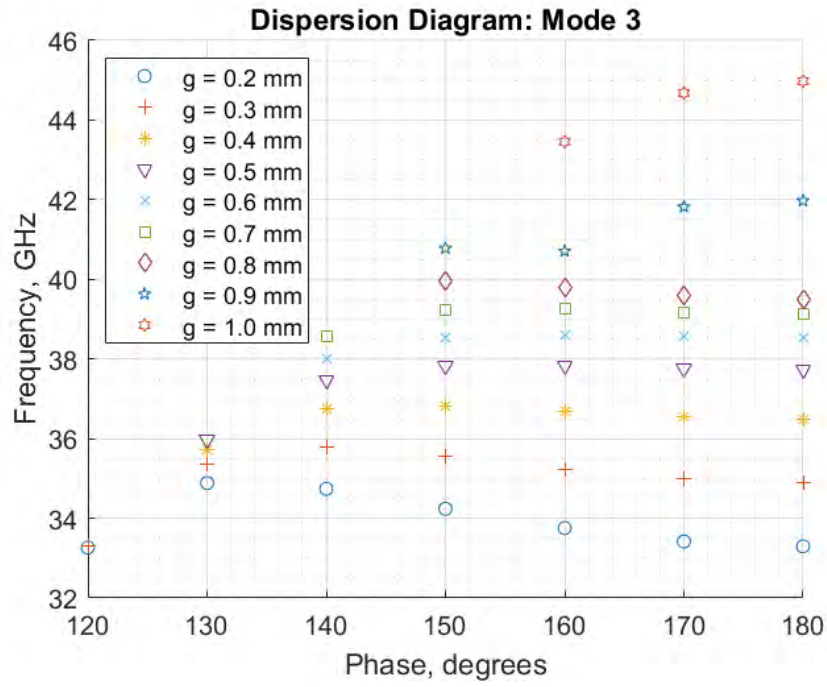


Figure 367: Square FR4: Dispersion Diagram, Mode 3

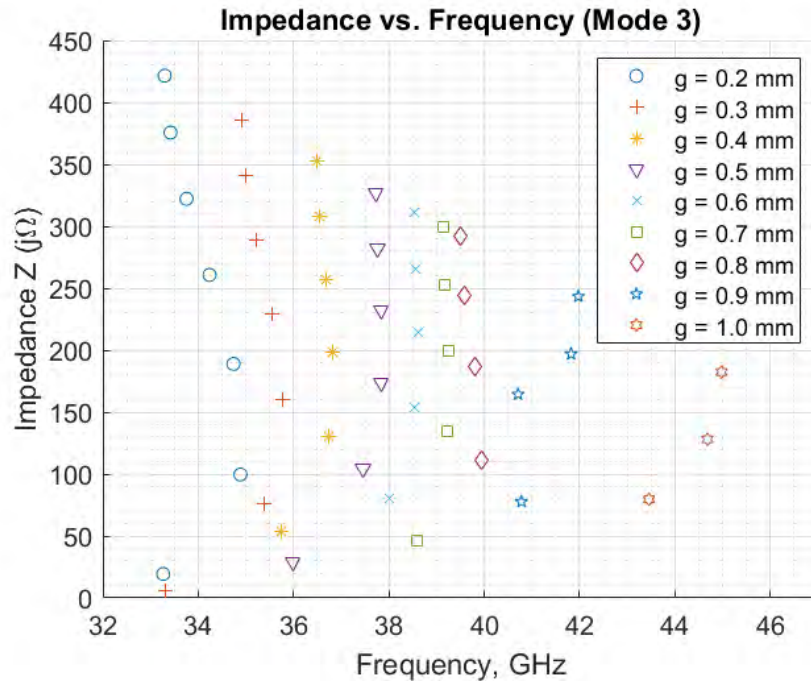


Figure 368: Square FR4: Impedance vs. Frequency, Mode 3

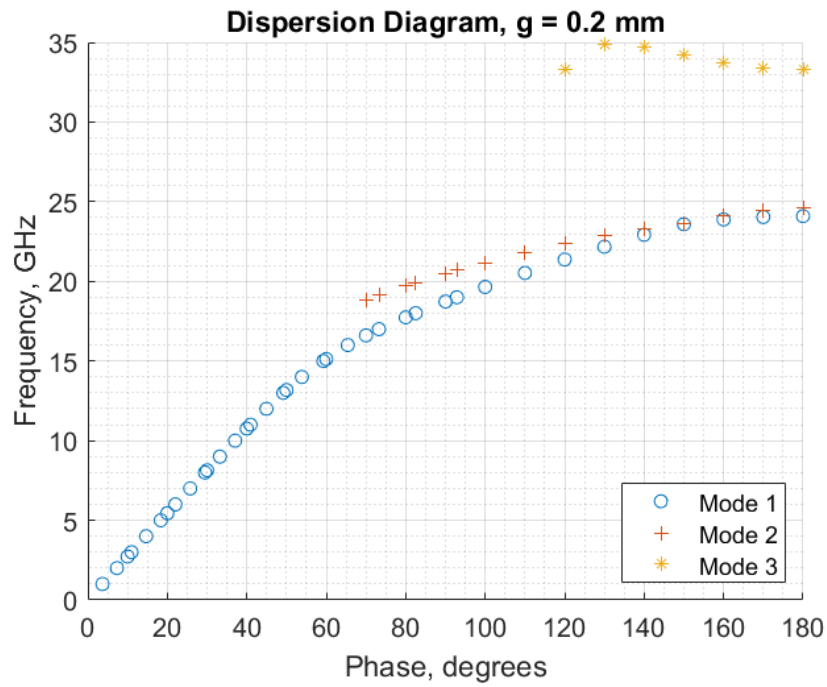


Figure 369: Square FR4: Dispersion Diagram, $g = 0.2$

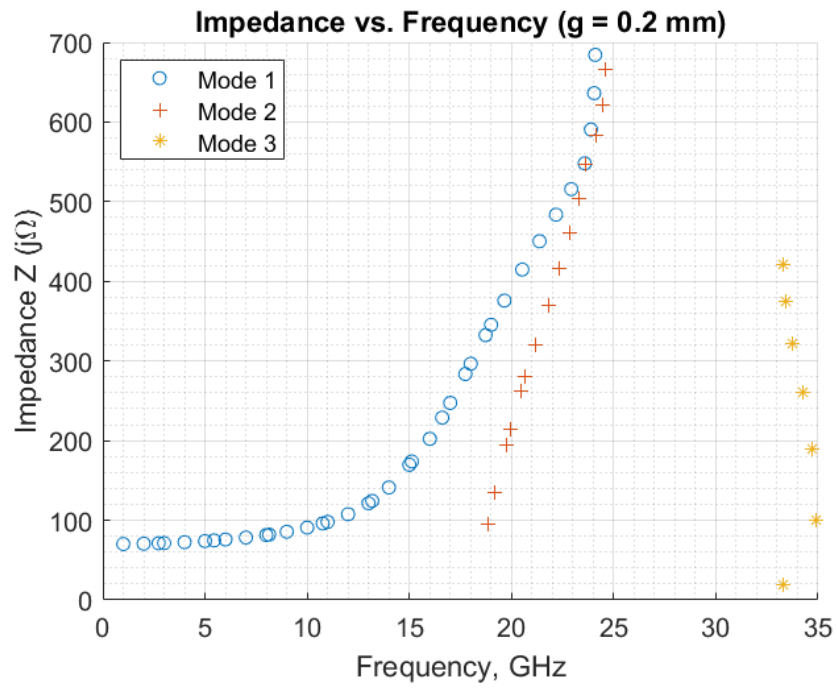


Figure 370: Square FR4: Impedance vs. Frequency, $g = 0.2$

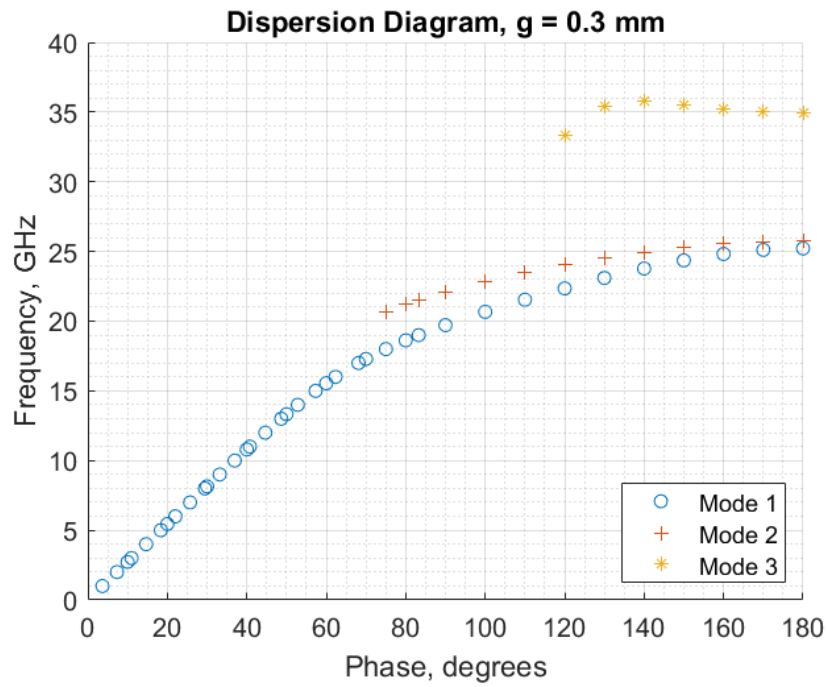


Figure 371: Square FR4: Dispersion Diagram, $g = 0.3$

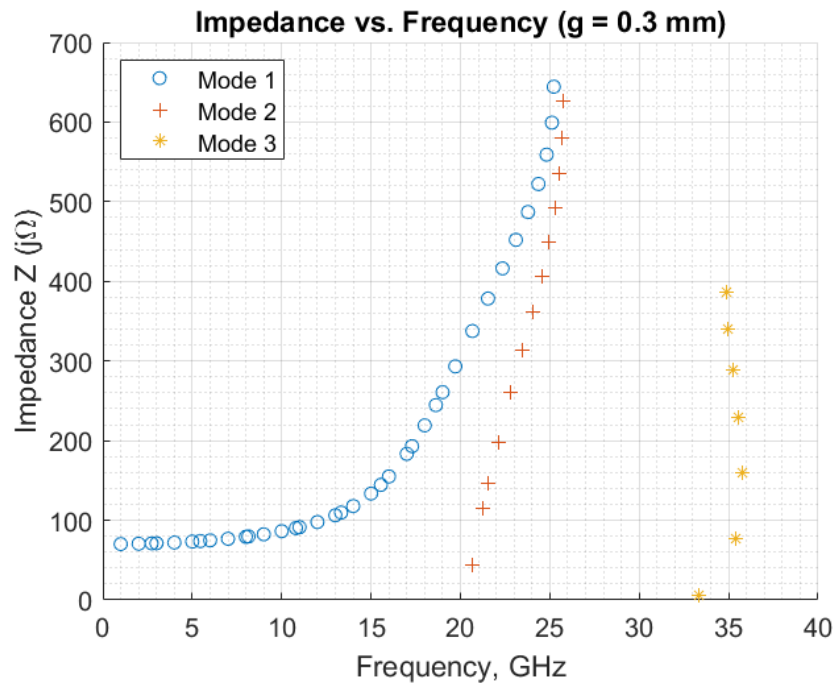


Figure 372: Square FR4: Impedance vs. Frequency, $g = 0.3$

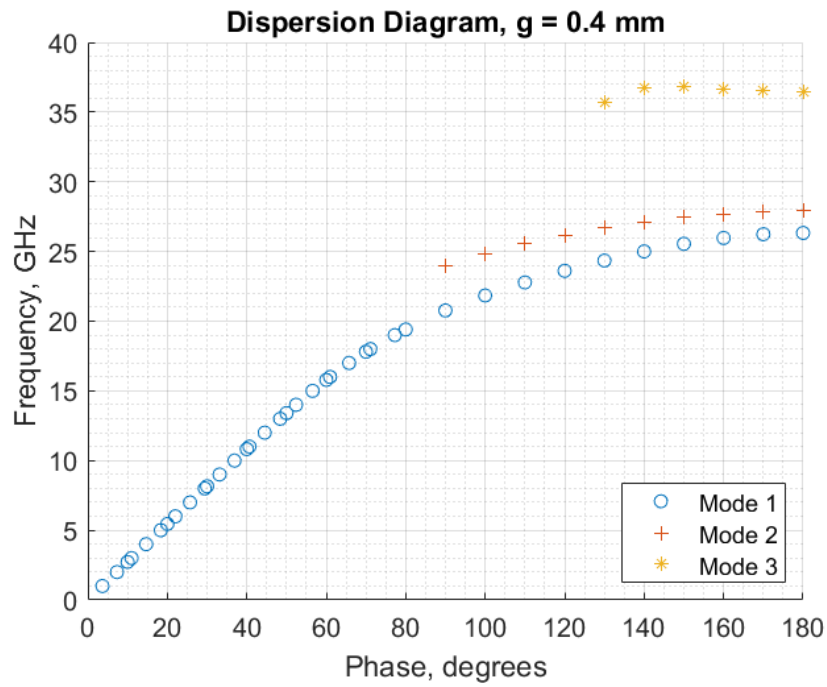


Figure 373: Square FR4: Dispersion Diagram, g = 0.4

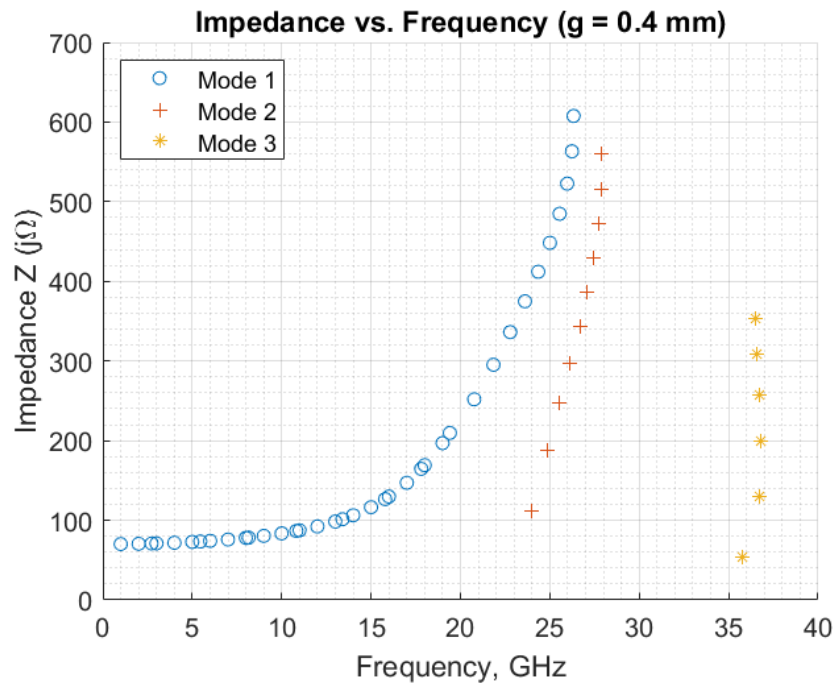


Figure 374: Square FR4: Impedance vs. Frequency, g = 0.4

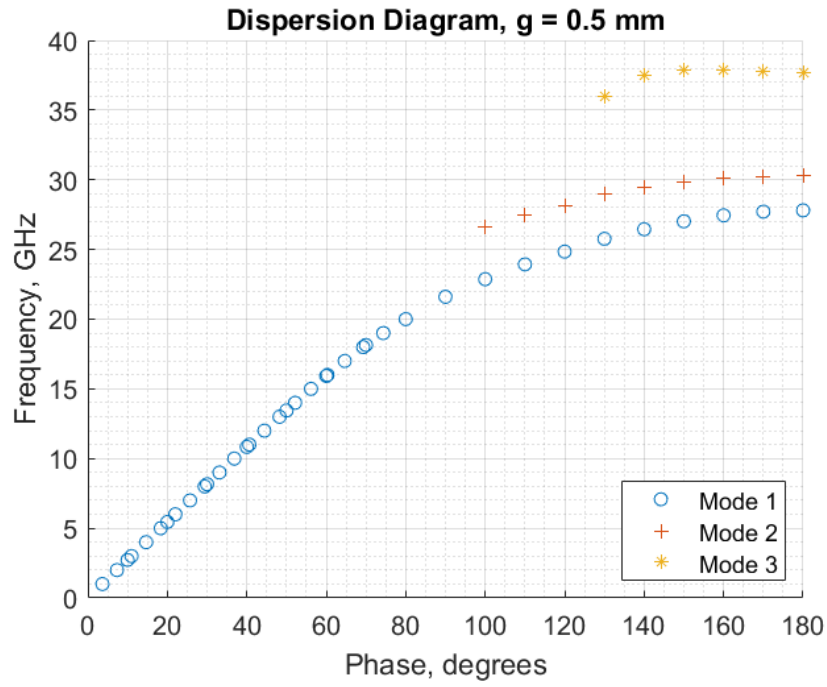


Figure 375: Square FR4: Dispersion Diagram, g = 0.5

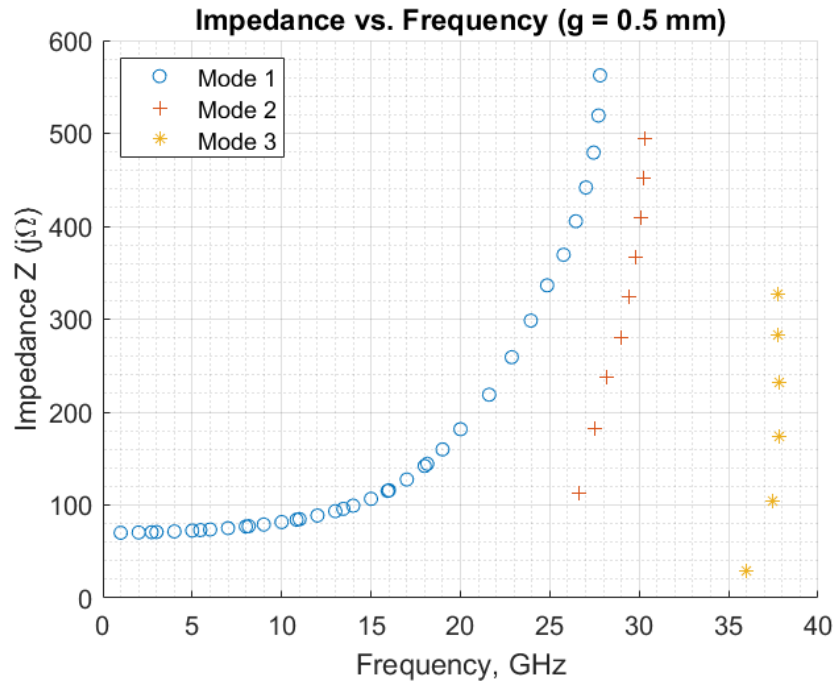


Figure 376: Square FR4: Impedance vs. Frequency, g = 0.5

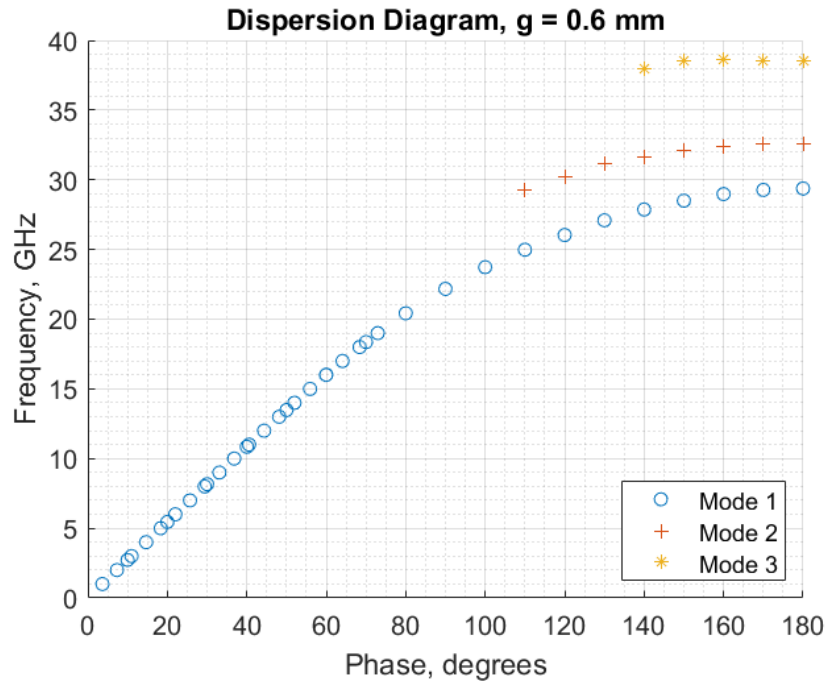


Figure 377: Square FR4: Dispersion Diagram, $g = 0.6$

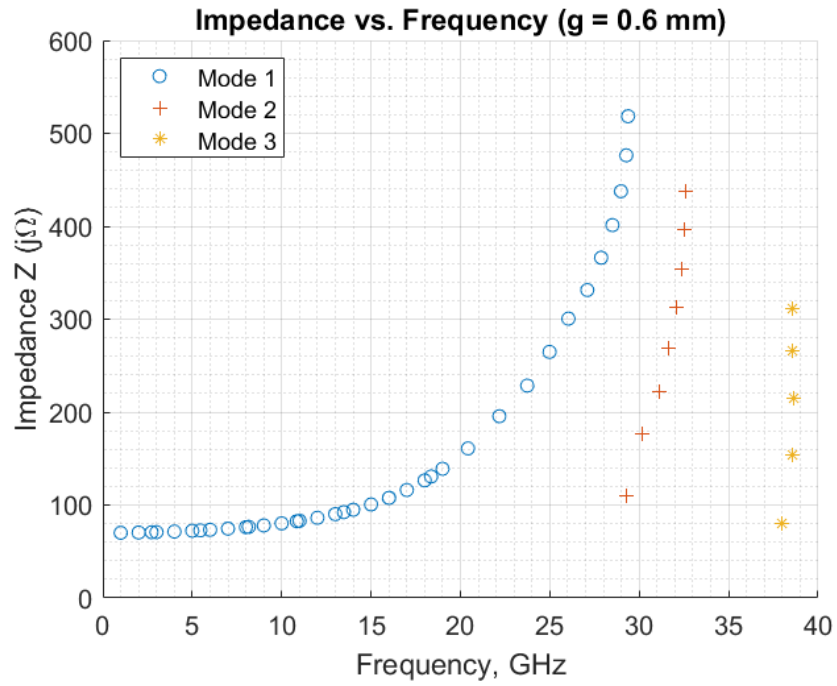


Figure 378: Square FR4: Impedance vs. Frequency, $g = 0.6$

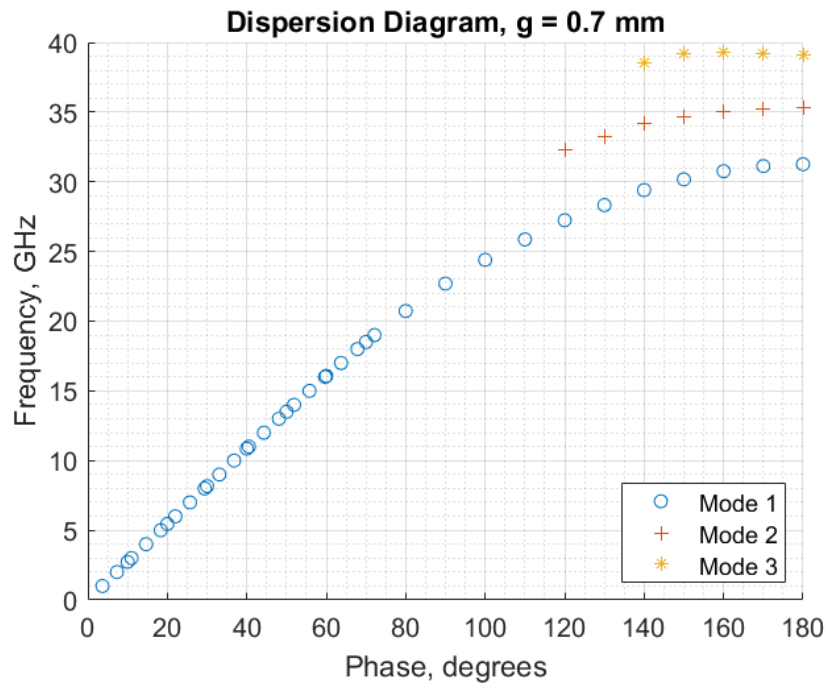


Figure 379: Square FR4: Dispersion Diagram, $g = 0.7$

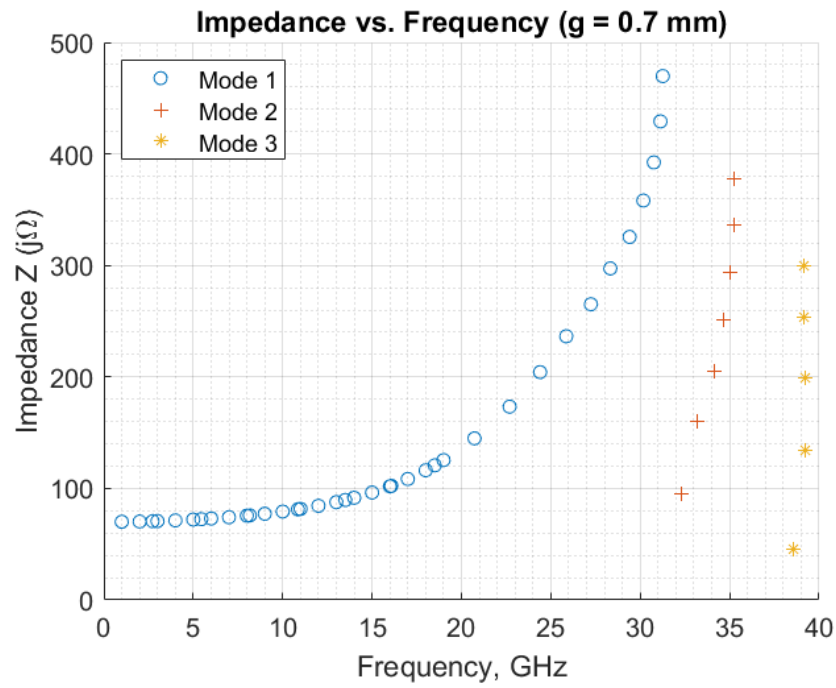


Figure 380: Square FR4: Impedance vs. Frequency, $g = 0.7$

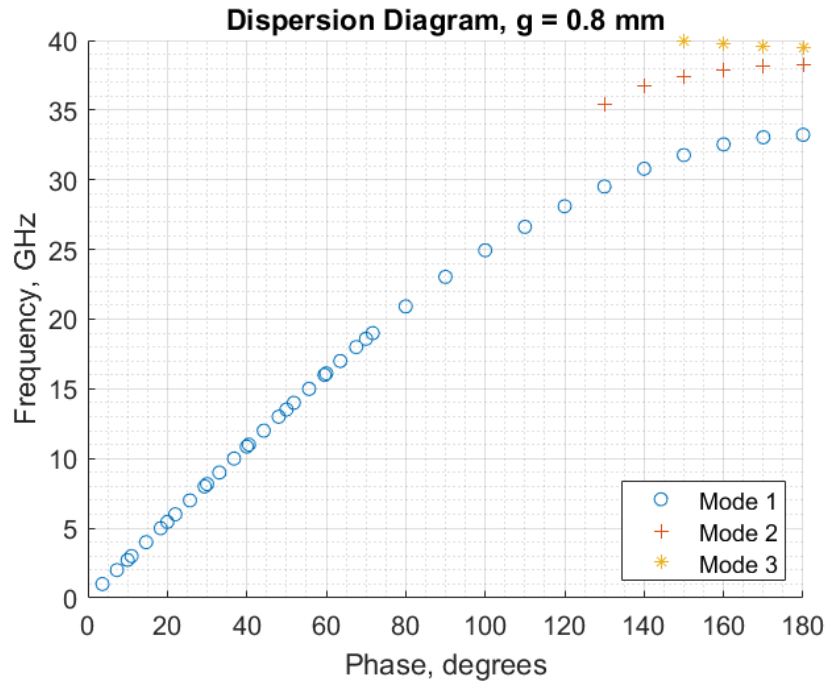


Figure 381: Square FR4: Dispersion Diagram, $g = 0.8$

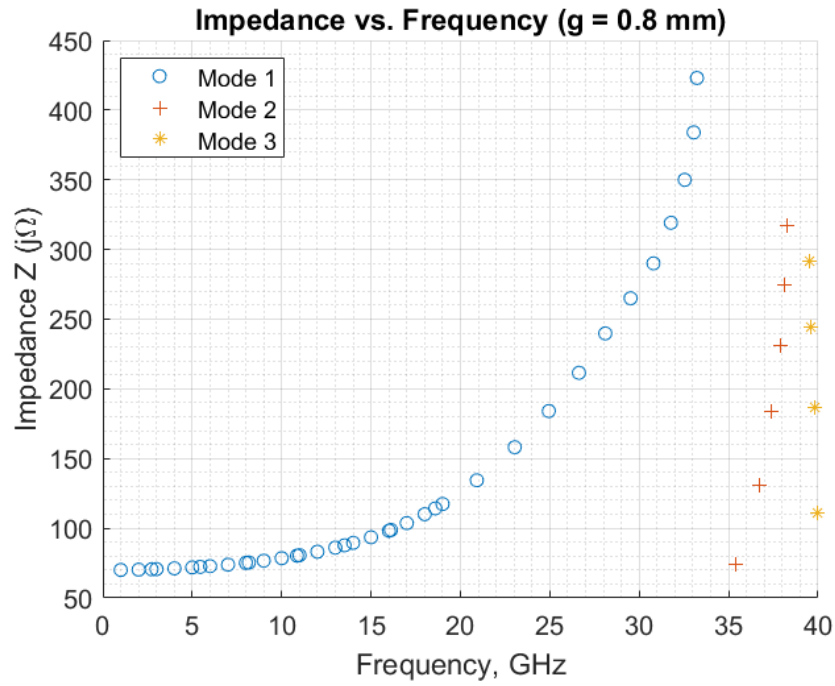


Figure 382: Square FR4: Impedance vs. Frequency, $g = 0.8$

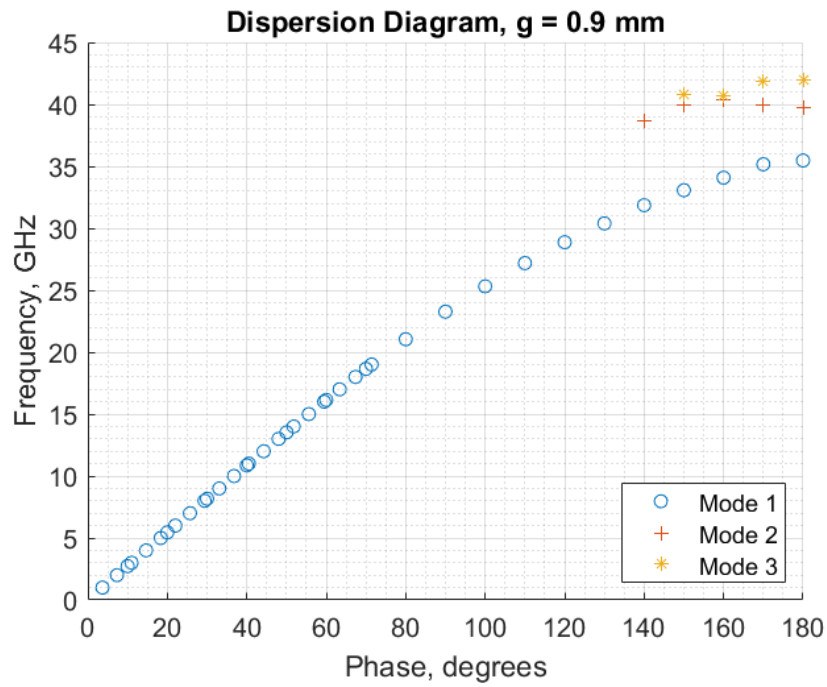


Figure 383: Square FR4: Dispersion Diagram, $g = 0.9$

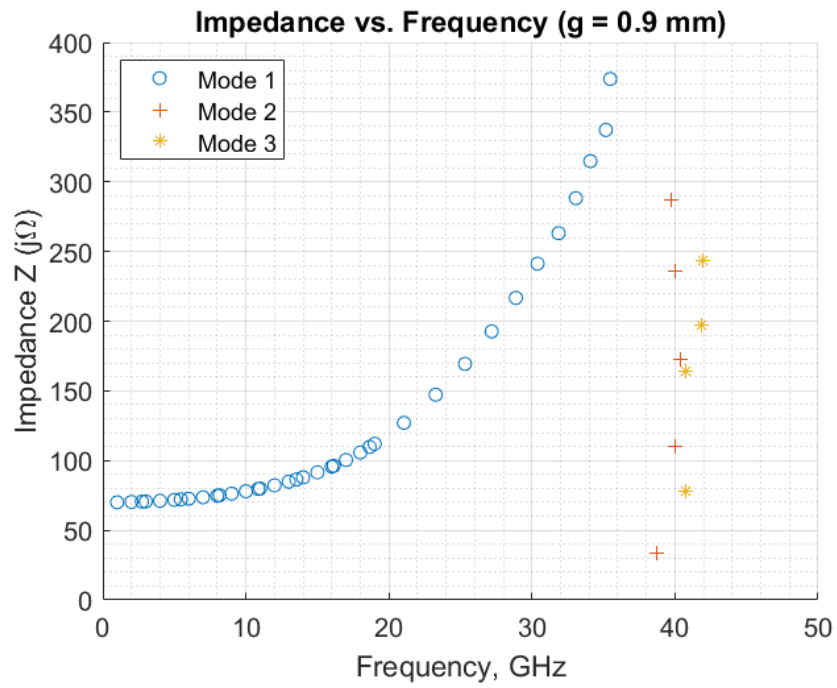


Figure 384: Square FR4: Impedance vs. Frequency, $g = 0.9$

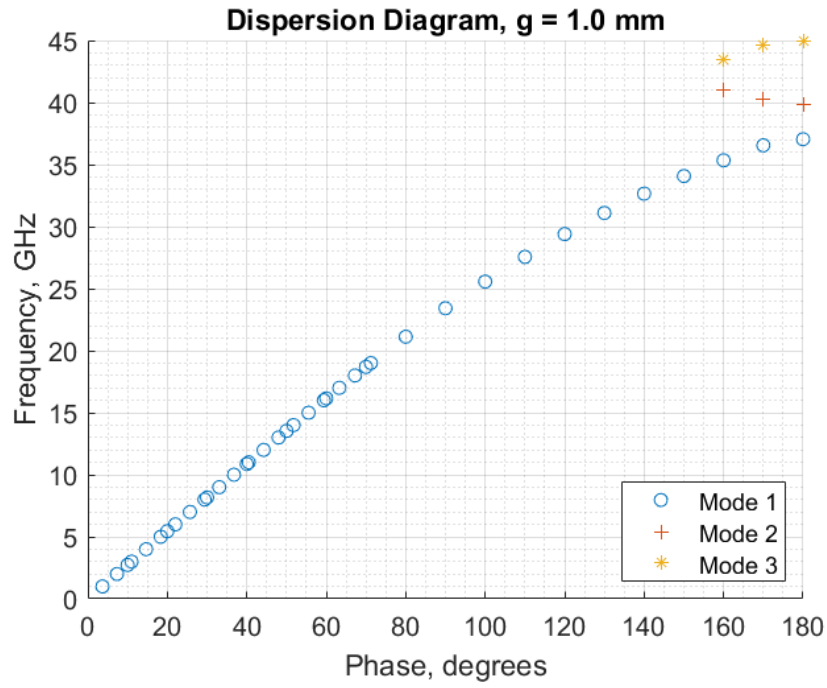


Figure 385: Square FR4: Dispersion Diagram, g = 1.0

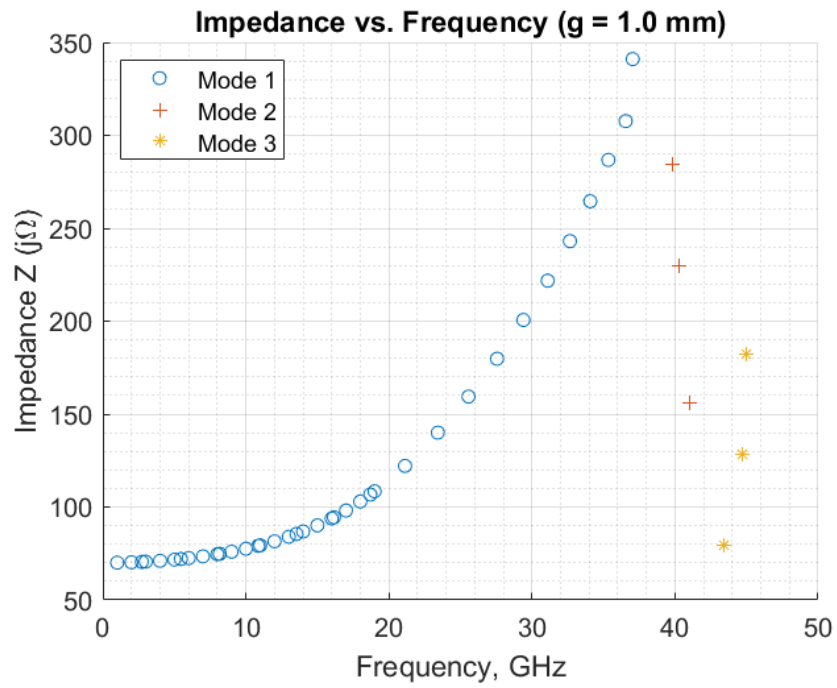


Figure 386: Square FR4: Impedance vs. Frequency, g = 1.0

Model: 1 GHz

Equation form: $y = c_0 + c_1x^1$

	Coefficient	SE	tStat	pValue
c_0 (intercept)	70.27	0.0042223	16642	7.4692×10^{-28}
c_1	-0.20901	0.0064641	-32.333	7.0017×10^{-9}

Table 67: Model Coefficients: 1 GHz

Model Statistics

Error Degrees of Freedom: 7
 Root Mean Squared Error (RMSE): 0.00501
 R-squared: 0.993
 Adjusted R-Squared: 0.992
 F-statistic vs. constant model: 1.05×10^3
 p-value = 7×10^{-9}

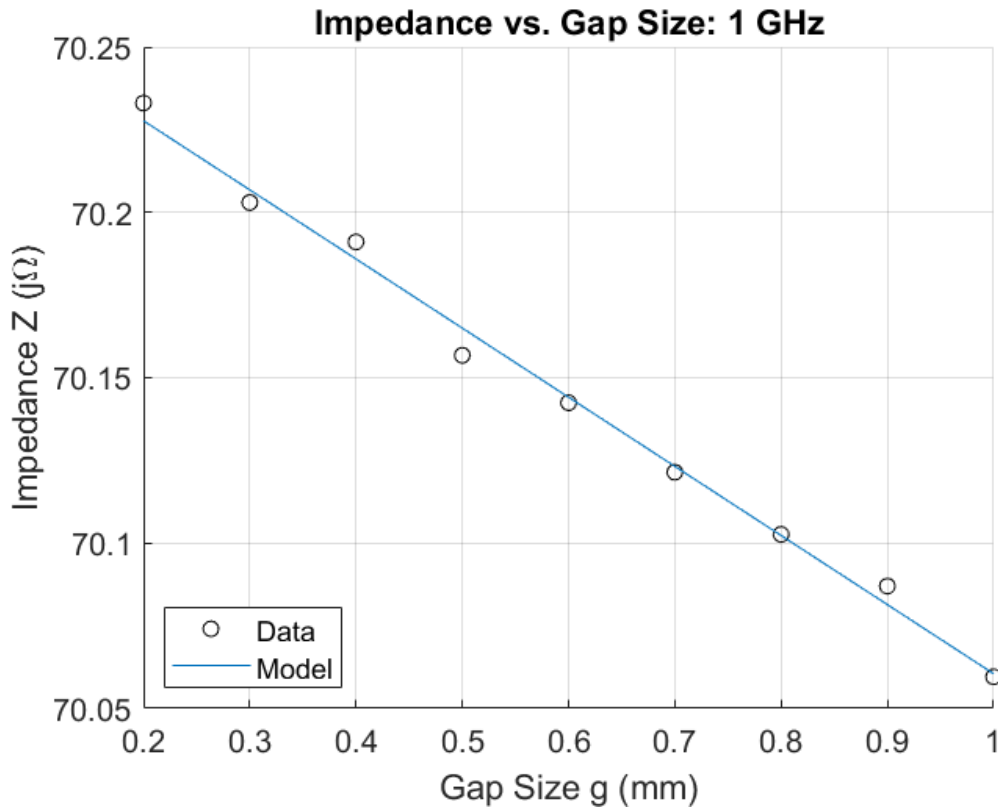


Figure 387: Square FR4: Impedance vs. Gap Size, 1 GHz

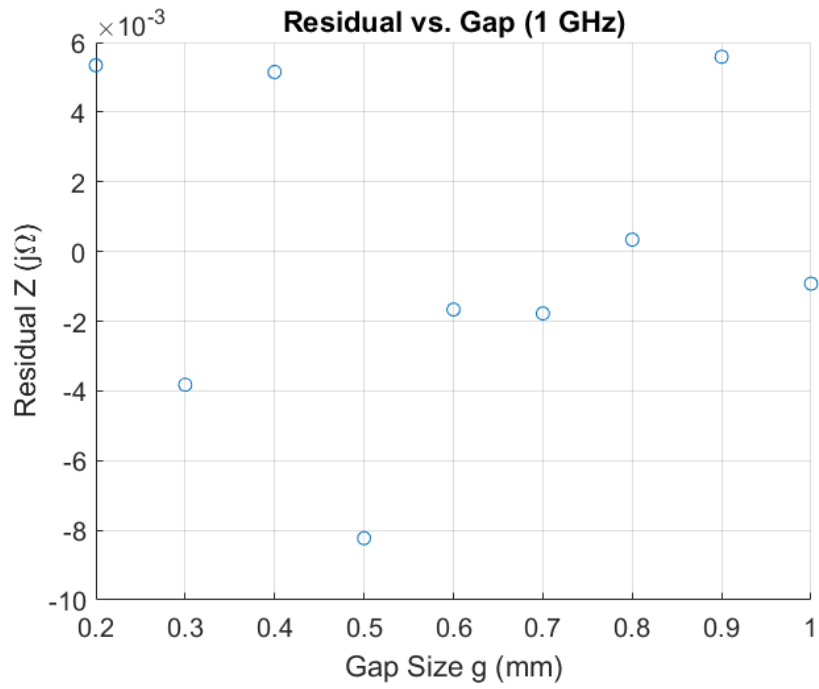


Figure 388: Square FR4: Residuals, 1 GHz

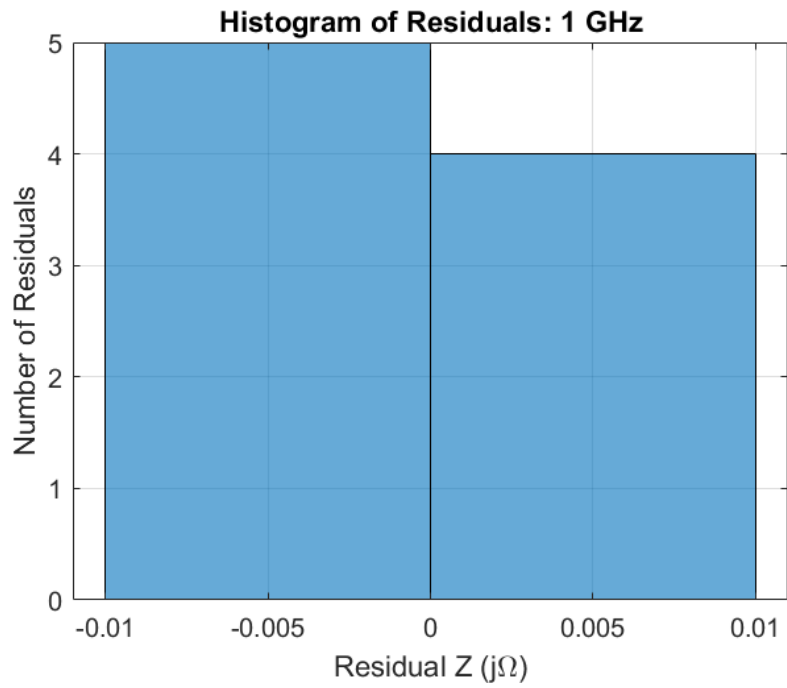


Figure 389: Square FR4: Histogram of Residuals, 1 GHz

Model: 2 GHz

Equation form: $y = c_0 + c_1x^1 + c_2x^2$

	<u>Coefficient</u>	<u>SE</u>	<u>tStat</u>	<u>pValue</u>
c_0 (intercept)	70.836	0.018206	3890.8	1.9458×10^{-20}
c_1	-0.9825	0.067671	-14.519	6.6944×10^{-6}
c_2	0.4173	0.055413	7.5307	0.00028411

Table 68: Model Coefficients: 2 GHz

Model Statistics

Error Degrees of Freedom: 6
 Root Mean Squared Error (RMSE): 0.00972
 R-squared: 0.996
 Adjusted R-Squared: 0.995
 F-statistic vs. constant model: 764
 p-value = 5.97×10^{-8}

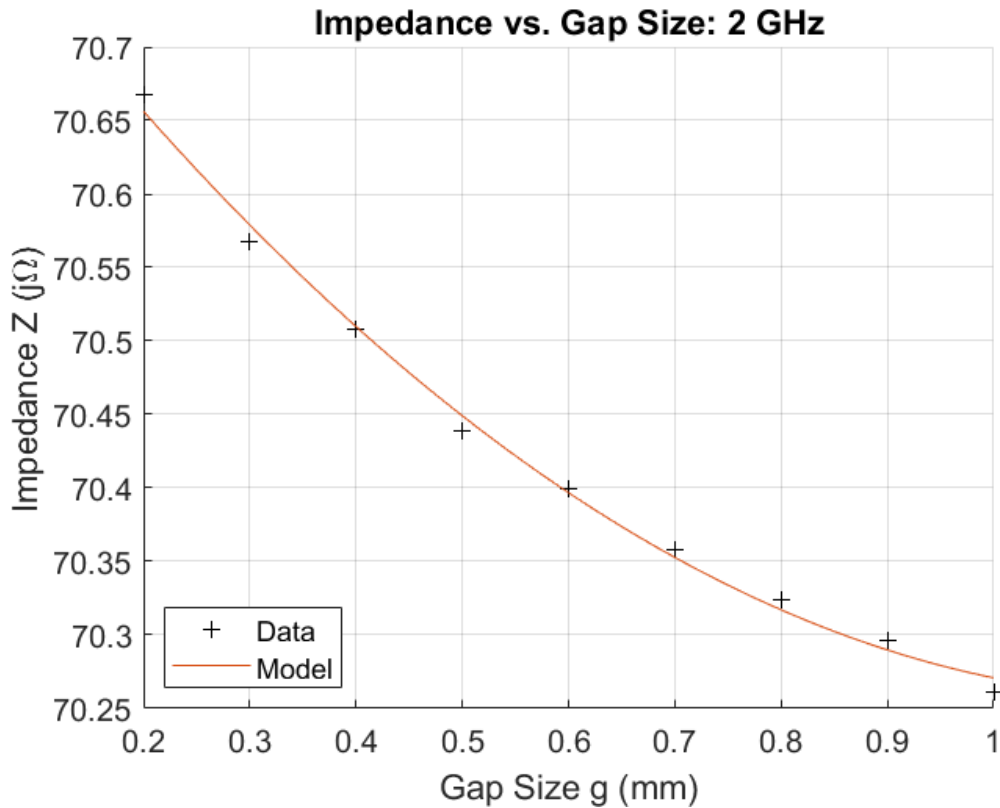


Figure 390: Square FR4: Impedance vs. Gap Size, 2 GHz

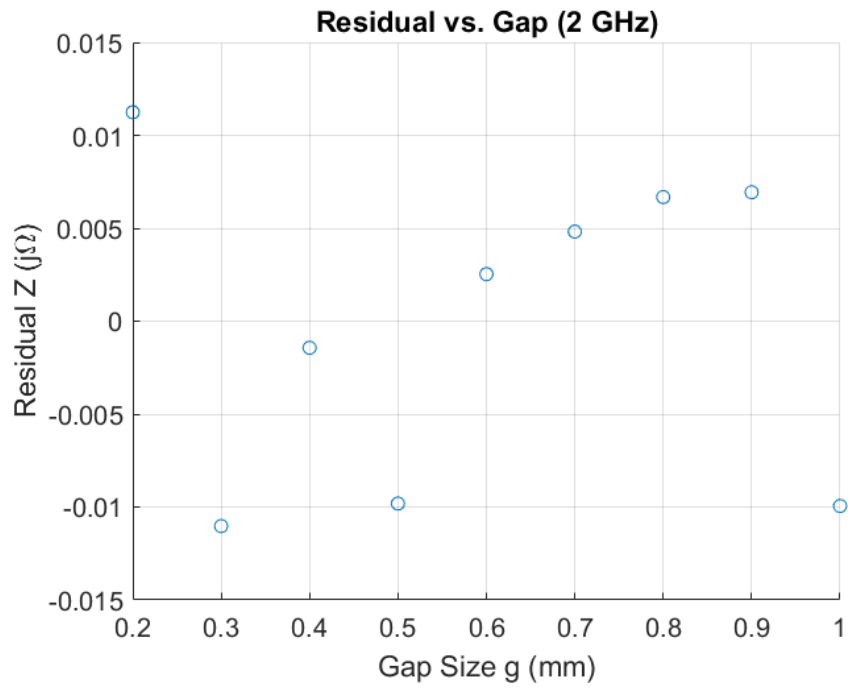


Figure 391: Square FR4: Residuals, 2 GHz

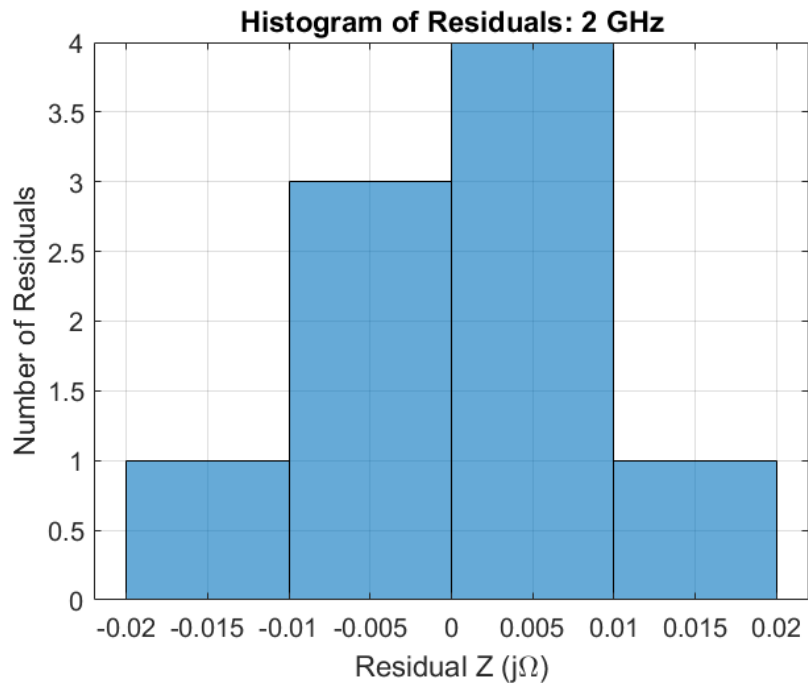


Figure 392: Square FR4: Histogram of Residuals, 2 GHz

Model: 3 GHz

Equation form: $y = c_0 + c_1 \frac{1}{x^1} + c_2 \frac{1}{x^2}$

	<u>Coefficient</u>	<u>SE</u>	<u>tStat</u>	<u>pValue</u>
c_0 (intercept)	70.246	0.019403	3620.4	2.9975×10^{-20}
c_1	0.40262	0.016429	24.506	3.036×10^{-7}
c_2	-0.034137	0.0027558	-12.387	1.6893×10^{-5}

Table 69: Model Coefficients: 3 GHz

Model Statistics

Error Degrees of Freedom: 6
 Root Mean Squared Error (RMSE): 0.0119
 R-squared: 0.999
 Adjusted R-Squared: 0.998
 F-statistic vs. constant model: 2.07×10^3
 p-value = 3.05×10^{-9}

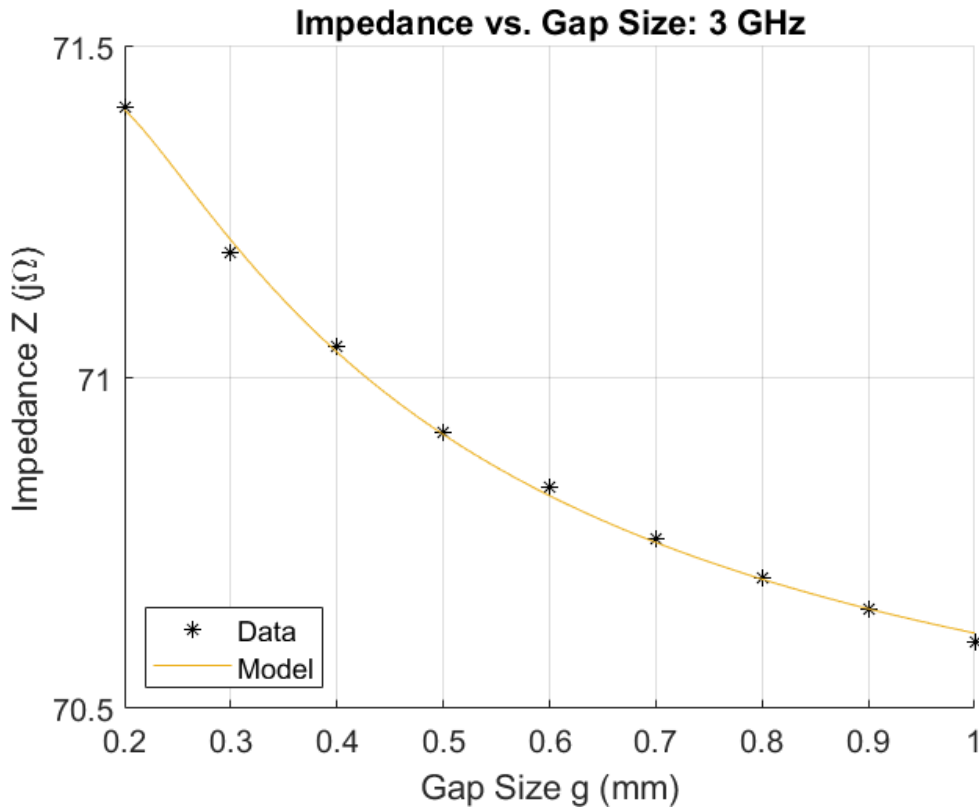


Figure 393: Square FR4: Impedance vs. Gap Size, 3 GHz

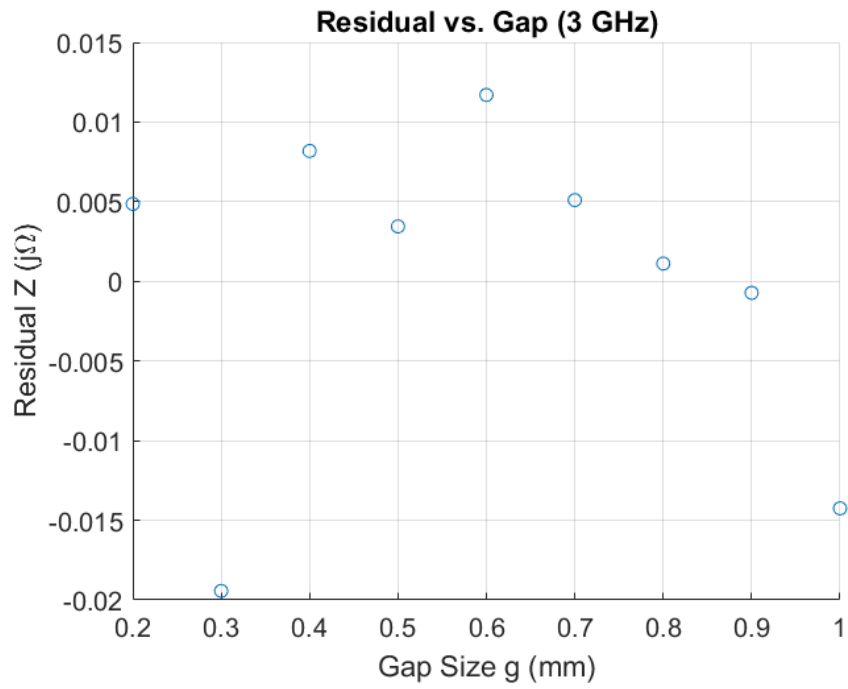


Figure 394: Square FR4: Residuals, 3 GHz

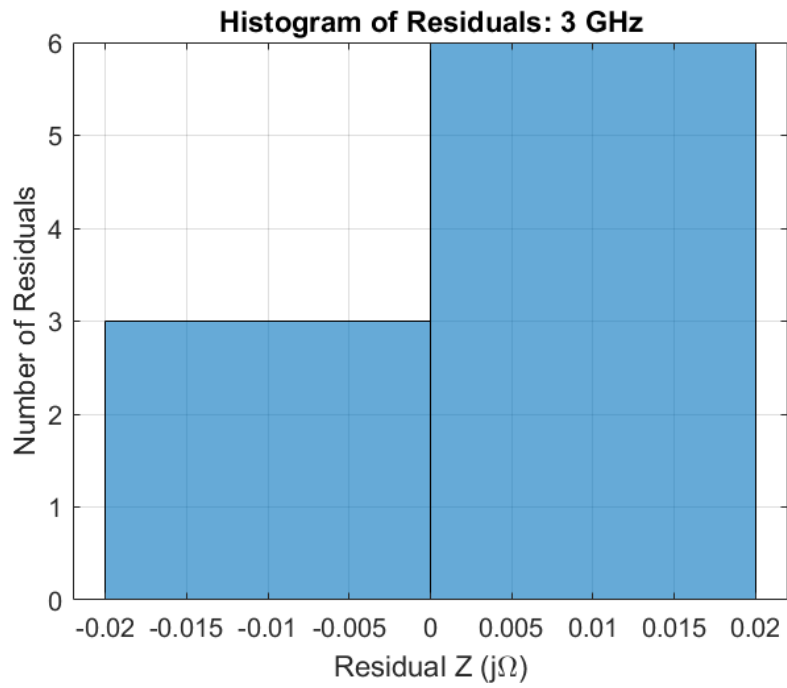


Figure 395: Square FR4: Histogram of Residuals, 3 GHz

Model: 4 GHz

Equation form: $y = c_0 + c_1x^1 + c_2x^2 + c_3x^3$

	<u>Coefficient</u>	<u>SE</u>	<u>tStat</u>	<u>pValue</u>
c_0 (intercept)	73.551	0.051618	1424.9	3.2312×10^{-15}
c_1	-6.5675	0.31875	-20.604	4.9847×10^{-6}
c_2	6.5805	0.57944	11.357	9.2605×10^{-5}
c_3	-2.4878	0.31963	-7.7832	0.00056056

Table 70: Model Coefficients: 4 GHz

Model Statistics

Error Degrees of Freedom: 5
 Root Mean Squared Error (RMSE): 0.0121
 R-squared: 1
 Adjusted R-Squared: 0.999
 F-statistic vs. constant model: 4.08×10^3
 p-value = 6.88×10^{-9}

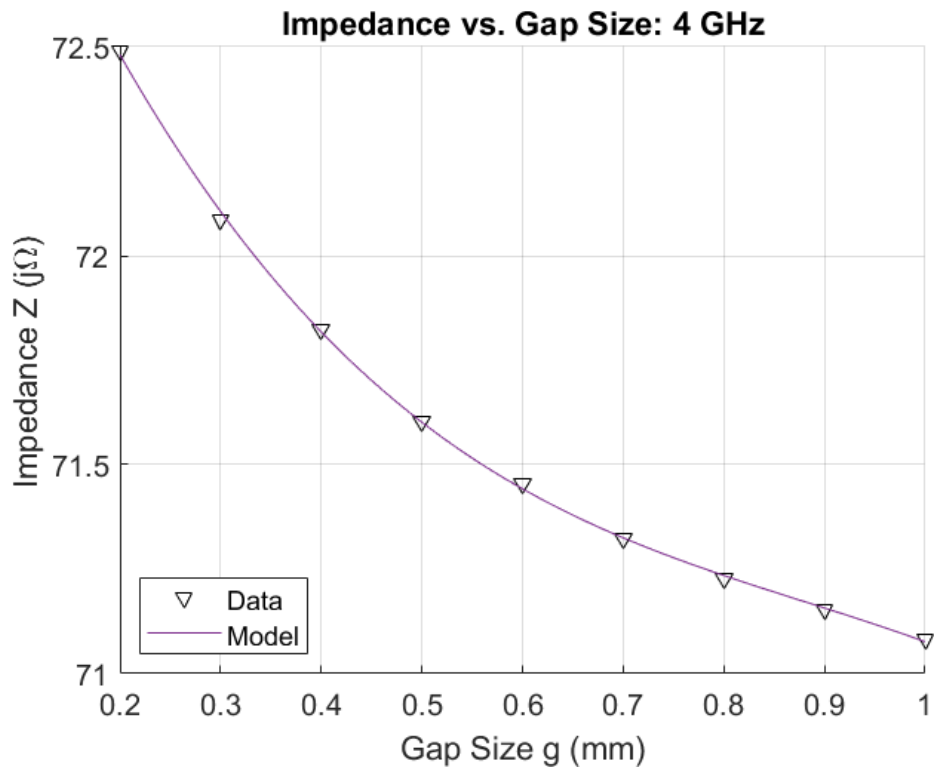


Figure 396: Square FR4: Impedance vs. Gap Size, 4 GHz

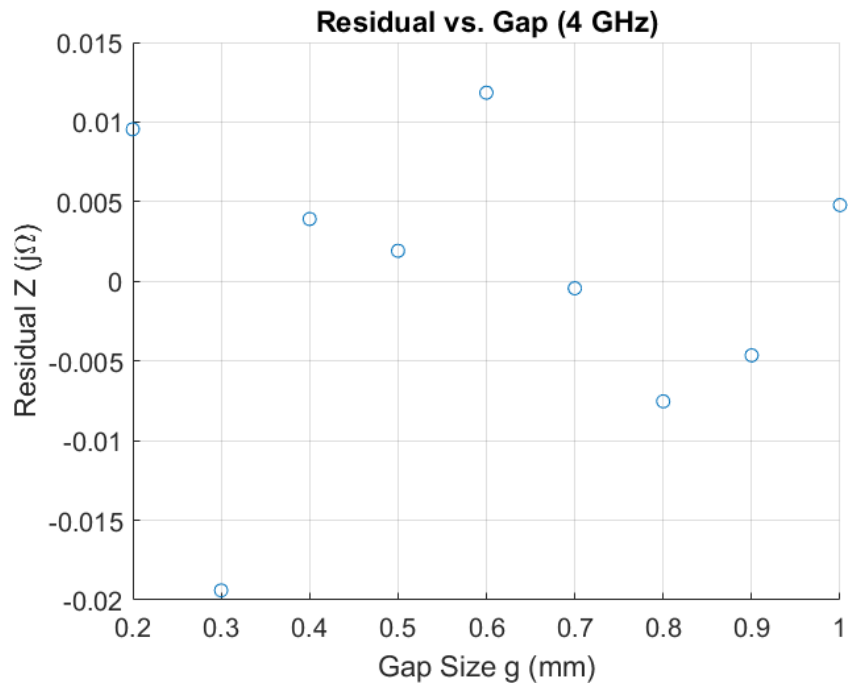


Figure 397: Square FR4: Residuals, 4 GHz

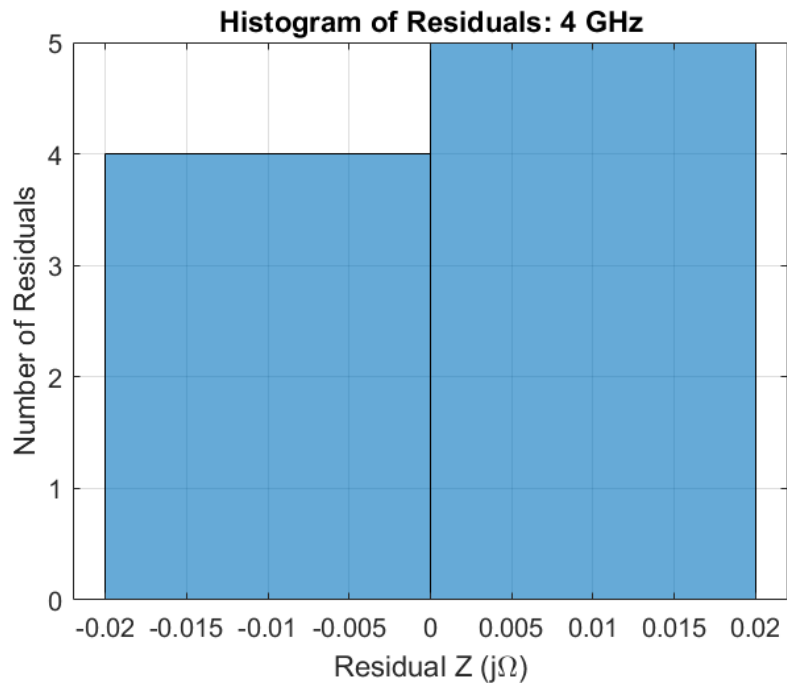


Figure 398: Square FR4: Histogram of Residuals, 4 GHz

Model: 5 GHz

Equation form: $y = c_0 + c_1 \frac{1}{x^1} + c_2 \frac{1}{x^2}$

	<u>Coefficient</u>	<u>SE</u>	<u>tStat</u>	<u>pValue</u>
c_0 (intercept)	70.78	0.022981	3079.9	7.9081×10^{-20}
c_1	1.0159	0.019459	52.205	3.3151×10^{-9}
c_2	-0.076408	0.0032641	-23.409	3.9868×10^{-7}

Table 71: Model Coefficients: 5 GHz

Model Statistics

Error Degrees of Freedom: 6
 Root Mean Squared Error (RMSE): 0.0141
 R-squared: 1
 Adjusted R-Squared: 1
 F-statistic vs. constant model: 1.14×10^4
 p-value = 1.81×10^{-11}

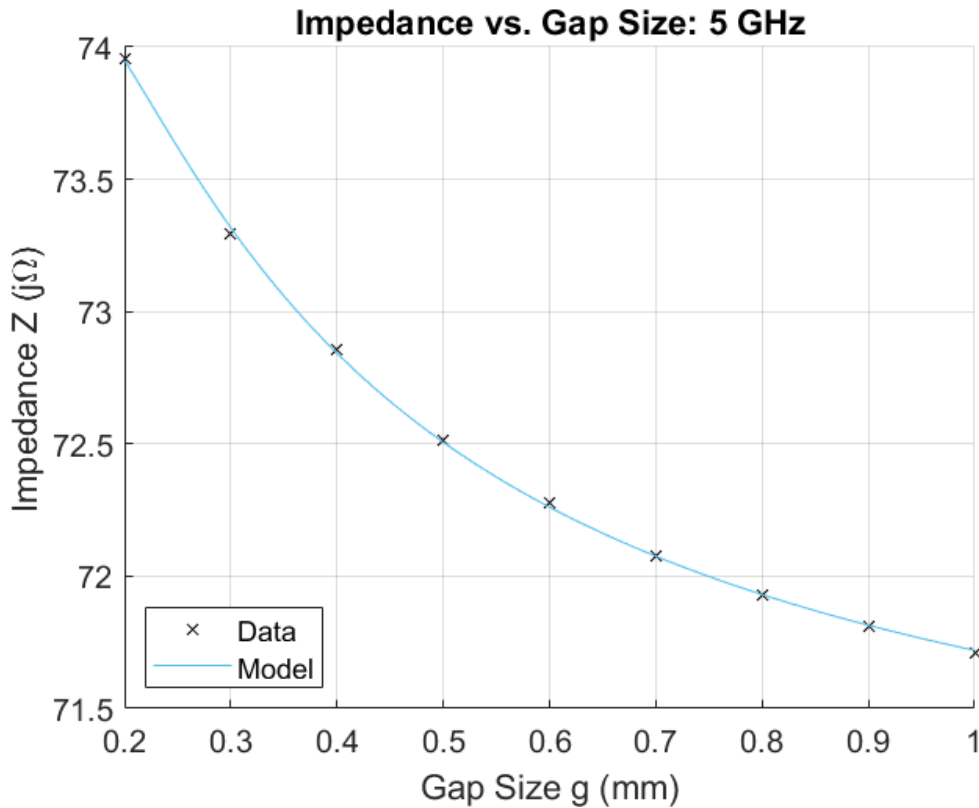


Figure 399: Square FR4: Impedance vs. Gap Size, 5 GHz

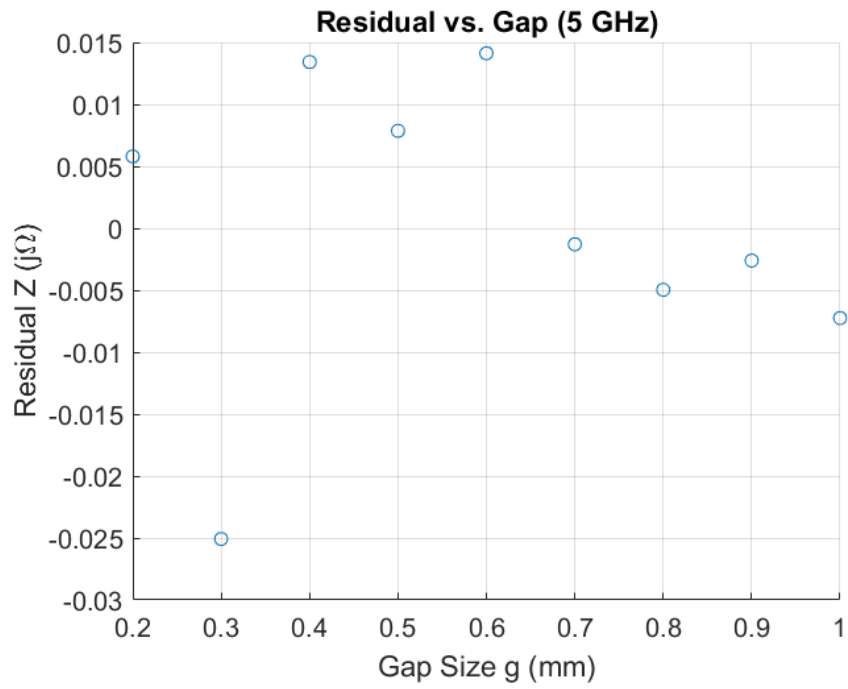


Figure 400: Square FR4: Residuals, 5 GHz

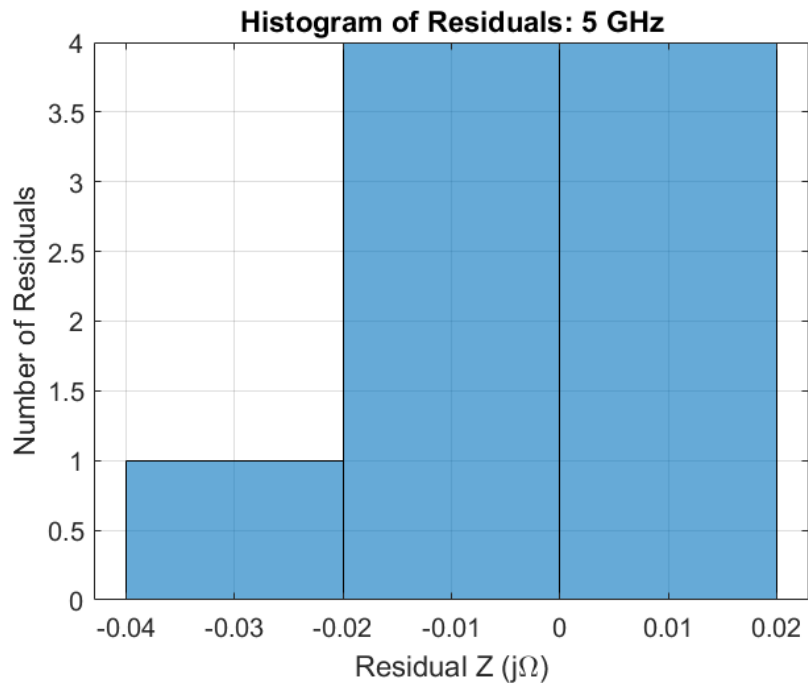


Figure 401: Square FR4: Histogram of Residuals, 5 GHz

Model: 6 GHz

Equation form: $y = c_0 + c_1 \frac{1}{x^1} + c_2 \frac{1}{x^2}$

	<u>Coefficient</u>	<u>SE</u>	<u>tStat</u>	<u>pValue</u>
c_0 (intercept)	71.131	0.026519	2682.3	1.8126×10^{-19}
c_1	1.4788	0.022455	65.856	8.2444×10^{-10}
c_2	-0.10638	0.0037666	-28.244	1.3037×10^{-7}

Table 72: Model Coefficients: 6 GHz

Model Statistics

Error Degrees of Freedom: 6
 Root Mean Squared Error (RMSE): 0.0162
 R-squared: 1
 Adjusted R-Squared: 1
 F-statistic vs. constant model: 1.94×10^4
 p-value = 3.72×10^{-12}

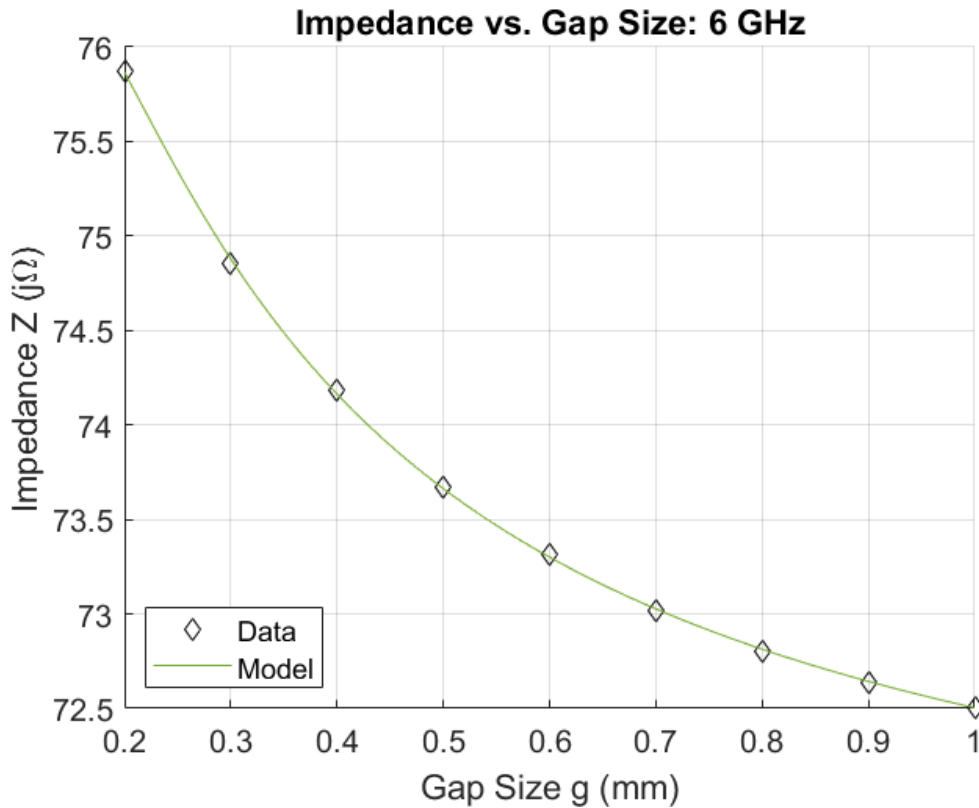


Figure 402: Square FR4: Impedance vs. Gap Size, 6 GHz

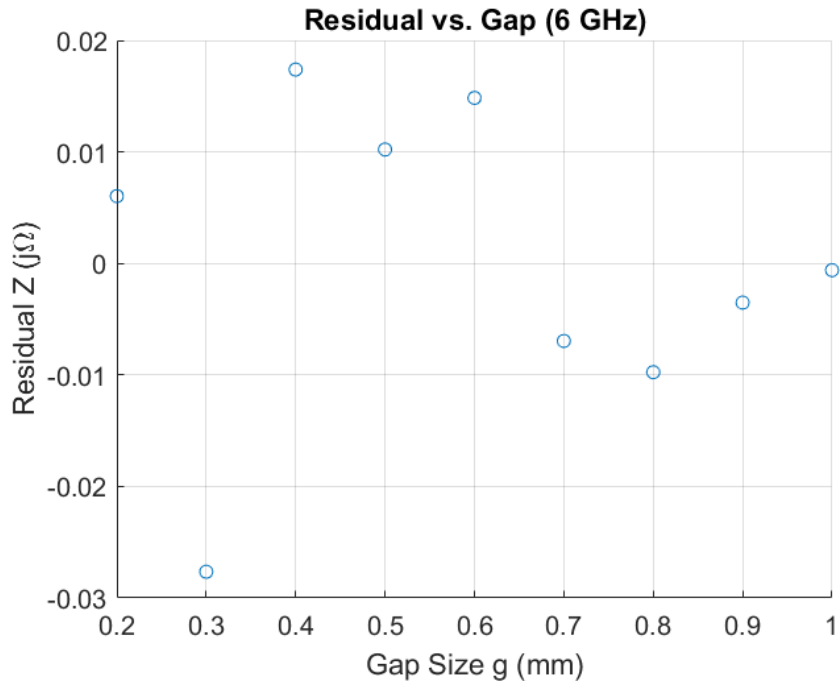


Figure 403: Square FR4: Residuals, 6 GHz

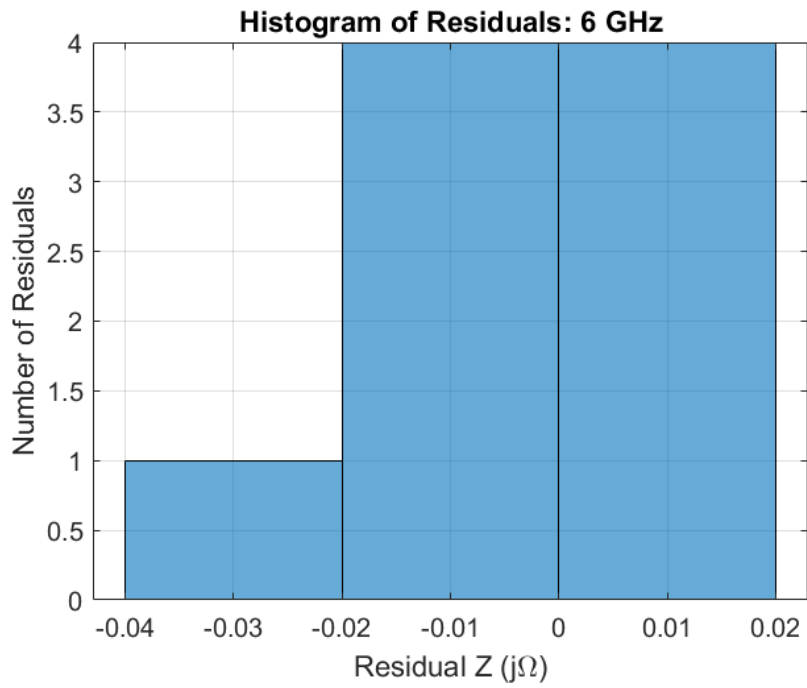


Figure 404: Square FR4: Histogram of Residuals, 6 GHz

Model: 7 GHz

Equation form: $y = c_0 + c_1 \frac{1}{x^1} + c_2 \frac{1}{x^2}$

	Coefficient	SE	tStat	pValue
c_0 (intercept)	71.526	0.032089	2229	5.5038×10^{-19}
c_1	2.0728	0.027172	76.288	3.4151×10^{-10}
c_2	-0.14226	0.0045577	-31.212	7.1839×10^{-8}

Table 73: Model Coefficients: 7 GHz

Model Statistics

Error Degrees of Freedom: 6
 Root Mean Squared Error (RMSE): 0.0197
 R-squared: 1
 Adjusted R-Squared: 1
 F-statistic vs. constant model: 2.77×10^4
 p-value = 1.28×10^{-12}

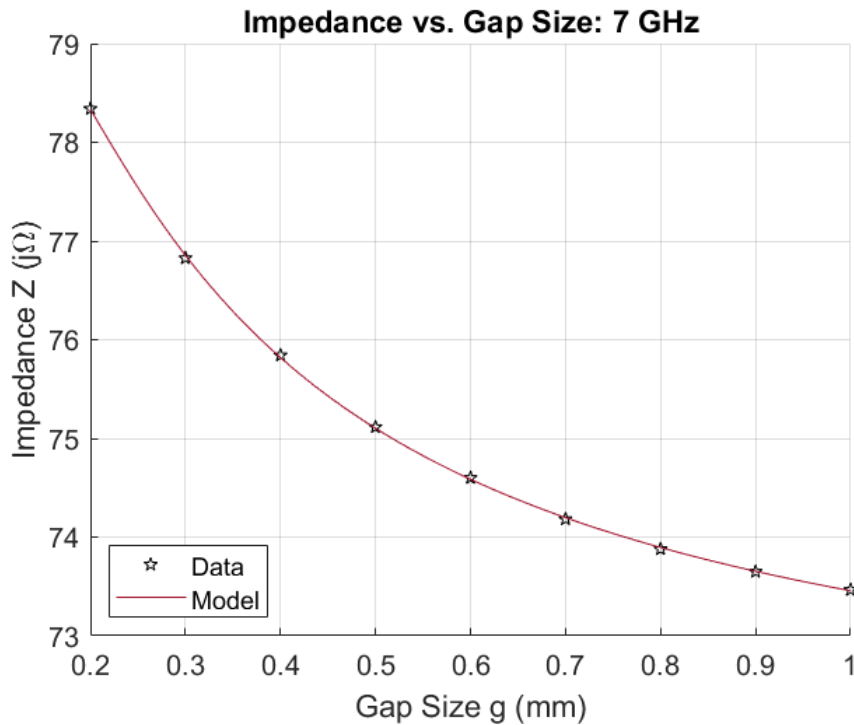


Figure 405: Square FR4: Impedance vs. Gap Size, 7 GHz

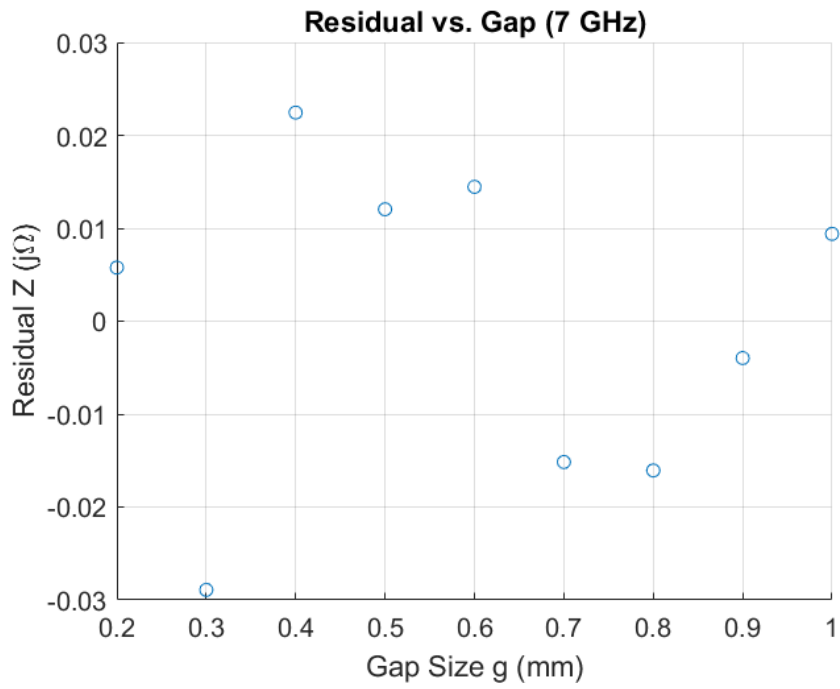


Figure 406: Square FR4: Residuals, 7 GHz

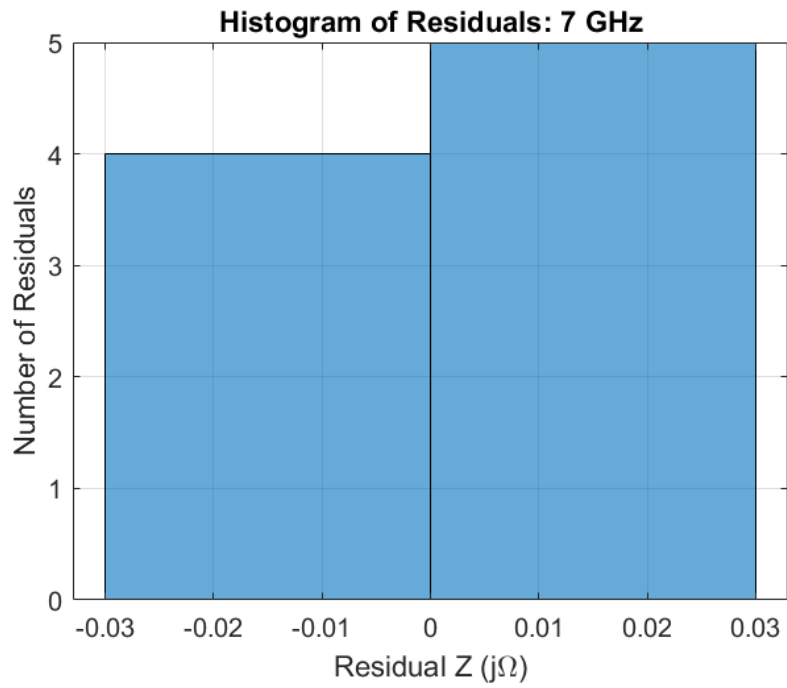


Figure 407: Square FR4: Histogram of Residuals, 7 GHz

Model: 8 GHz

Equation form: $y = c_0 + c_1 \frac{1}{x^1} + c_2 \frac{1}{x^2}$

	<u>Coefficient</u>	<u>SE</u>	<u>tStat</u>	<u>pValue</u>
c_0 (intercept)	71.95	0.041226	1745.2	2.3887×10^{-18}
c_1	2.8257	0.034908	80.947	2.3936×10^{-10}
c_2	-0.18317	0.0058555	-31.282	7.0884×10^{-8}

Table 74: Model Coefficients: 8 GHz

Model Statistics

Error Degrees of Freedom: 6
 Root Mean Squared Error (RMSE): 0.0253
 R-squared: 1
 Adjusted R-Squared: 1
 F-statistic vs. constant model: 3.34×10^4
 p-value = 7.25×10^{-13}

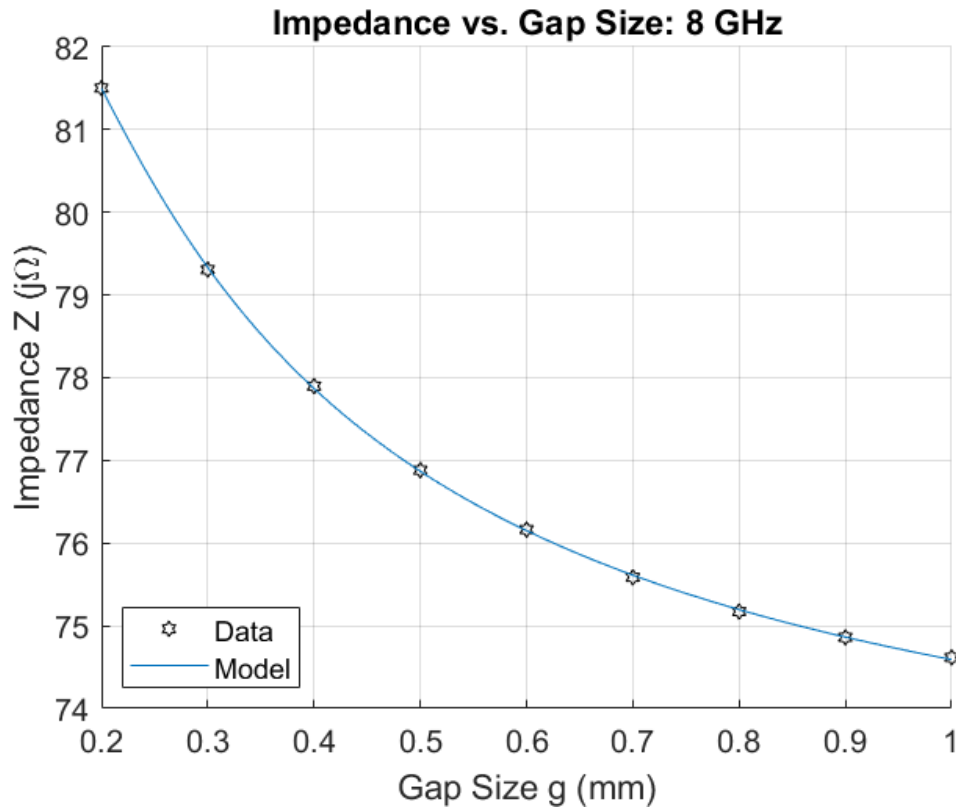


Figure 408: Square FR4: Impedance vs. Gap Size, 8 GHz

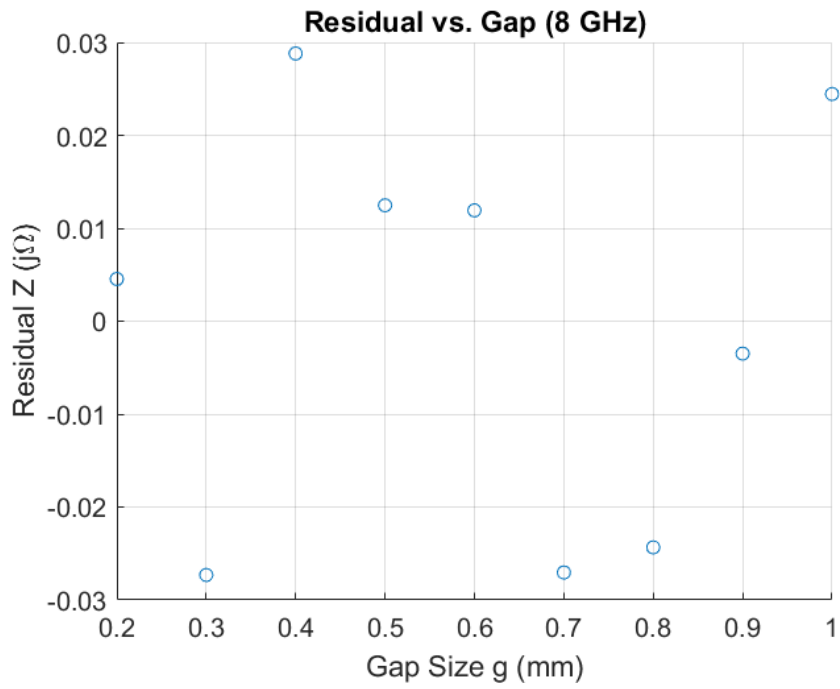


Figure 409: Square FR4: Residuals, 8 GHz

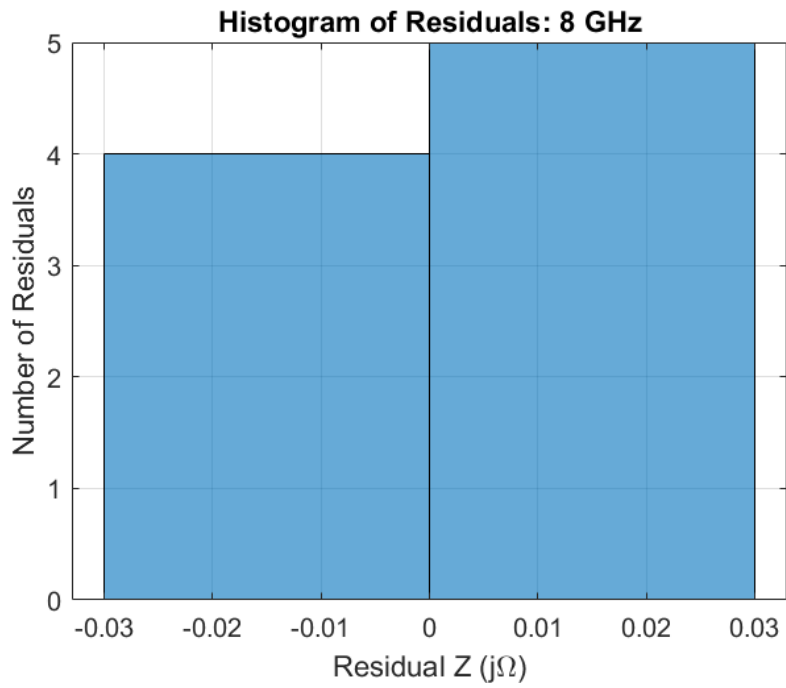


Figure 410: Square FR4: Histogram of Residuals, 8 GHz

Model: 9 GHz

Equation form: $y = c_0 + c_1 \frac{1}{x^1} + c_2 \frac{1}{x^2}$

	<u>Coefficient</u>	<u>SE</u>	<u>tStat</u>	<u>pValue</u>
c_0 (intercept)	72.382	0.056898	1272.1	1.5926×10^{-17}
c_1	3.7719	0.048179	78.289	2.9241×10^{-10}
c_2	-0.22654	0.0080815	-28.032	1.3635×10^{-7}

Table 75: Model Coefficients: 9 GHz

Model Statistics

Error Degrees of Freedom: 6
 Root Mean Squared Error (RMSE): 0.0349
 R-squared: 1
 Adjusted R-Squared: 1
 F-statistic vs. constant model: 3.4×10^4
 p-value = 6.87×10^{-13}

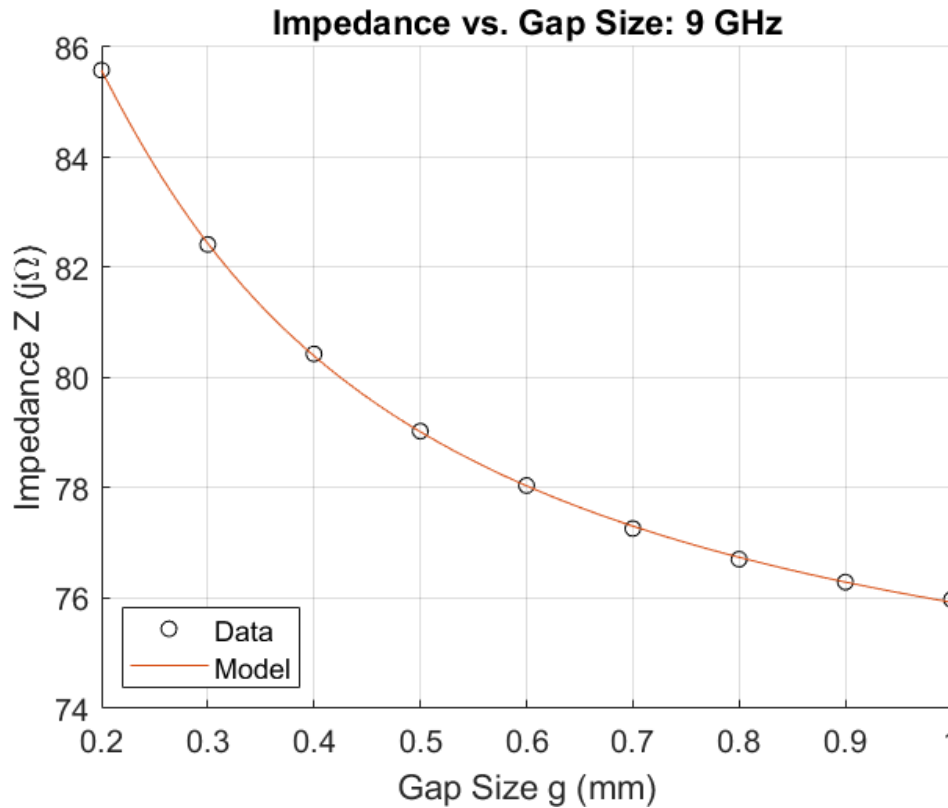


Figure 411: Square FR4: Impedance vs. Gap Size, 9 GHz

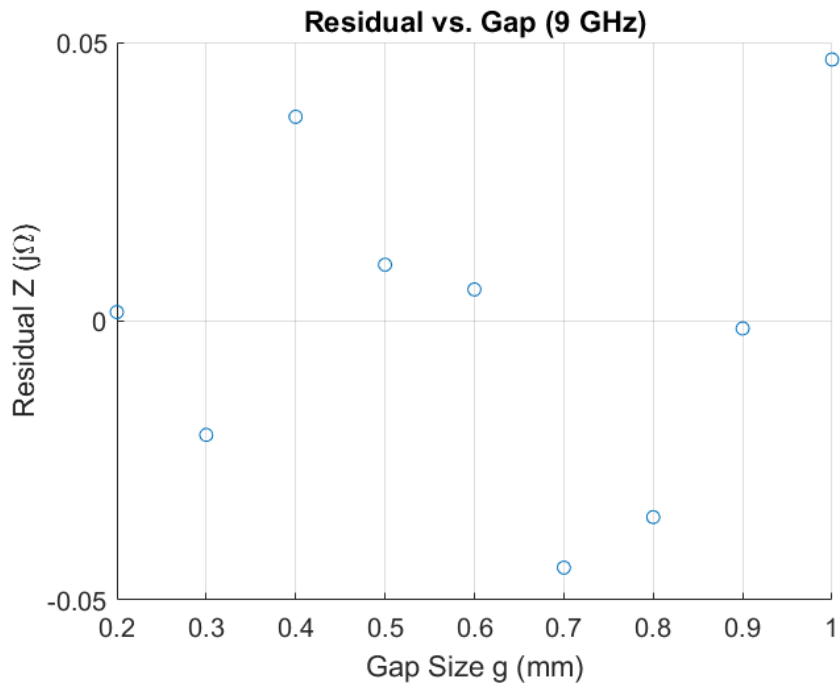


Figure 412: Square FR4: Residuals, 9 GHz

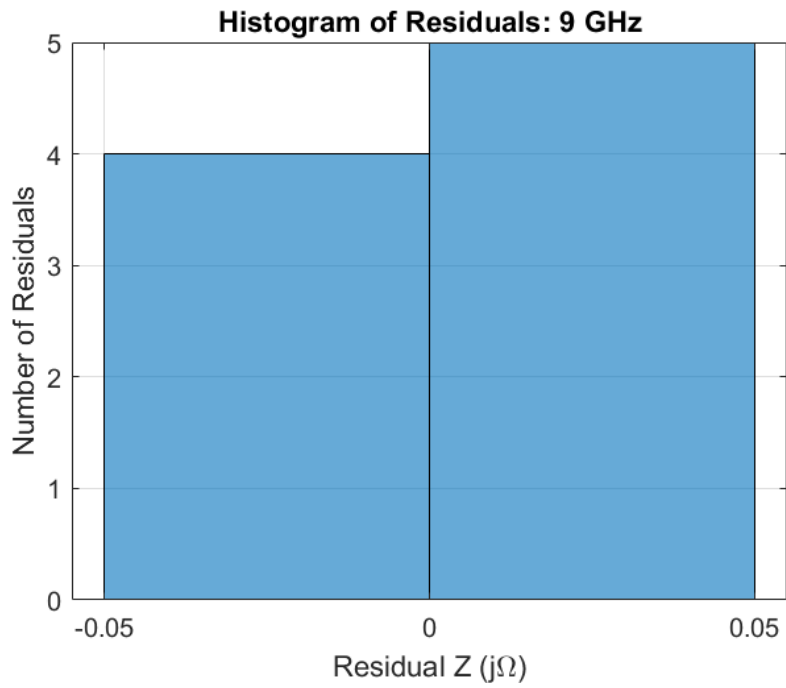


Figure 413: Square FR4: Histogram of Residuals, 9 GHz

Model: 10 GHz

Equation form: $y = c_0 + c_1 \frac{1}{x^1} + c_2 \frac{1}{x^2}$

	<u>Coefficient</u>	<u>SE</u>	<u>tStat</u>	<u>pValue</u>
c_0 (intercept)	72.797	0.083845	868.23	1.5757×10^{-16}
c_1	4.9511	0.070996	69.739	5.8487×10^{-10}
c_2	-0.26604	0.011909	-22.34	5.2623×10^{-7}

Table 76: Model Coefficients: 10 GHz

Model Statistics

Error Degrees of Freedom: 6
 Root Mean Squared Error (RMSE): 0.0514
 R-squared: 1
 Adjusted R-Squared: 1
 F-statistic vs. constant model: 3×10^4
 p-value = 9.96×10^{-13}

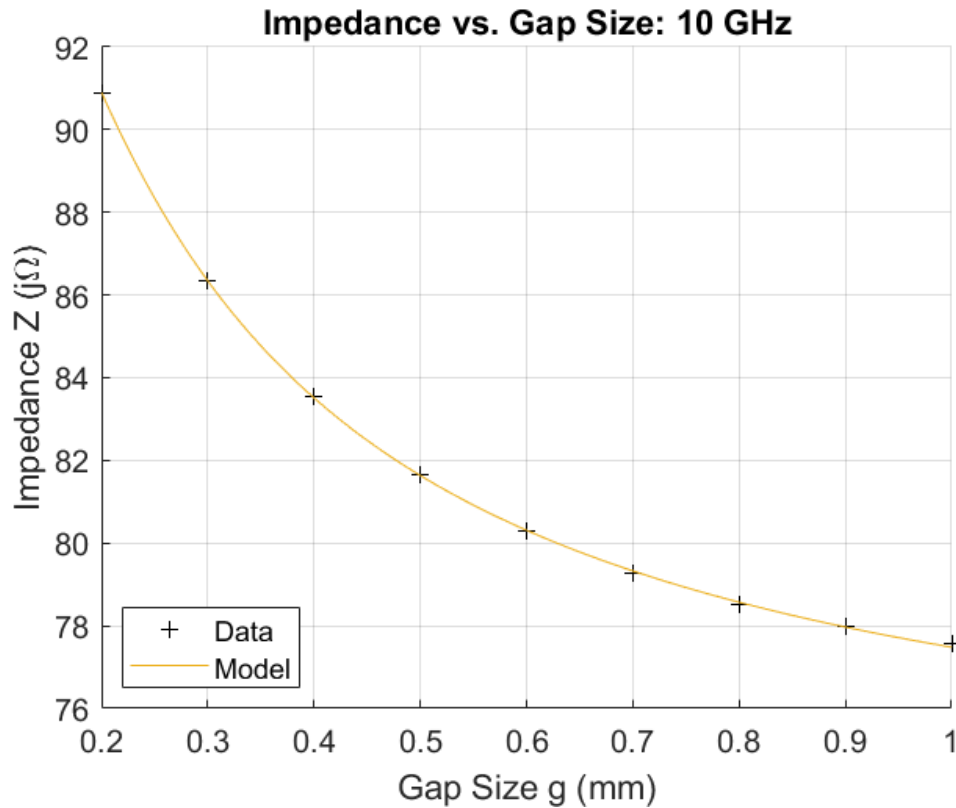


Figure 414: Square FR4: Impedance vs. Gap Size, 10 GHz

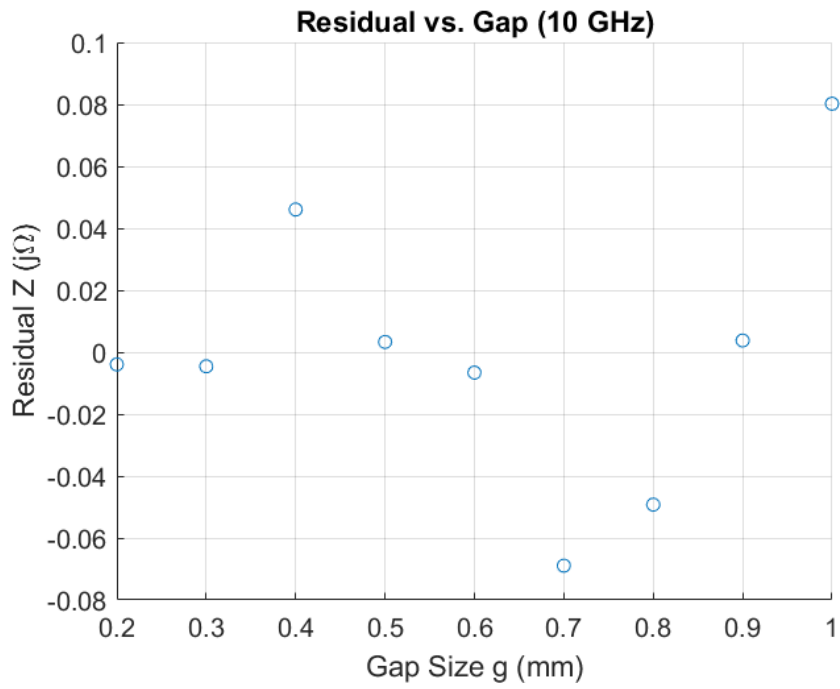


Figure 415: Square FR4: Residuals, 10 GHz

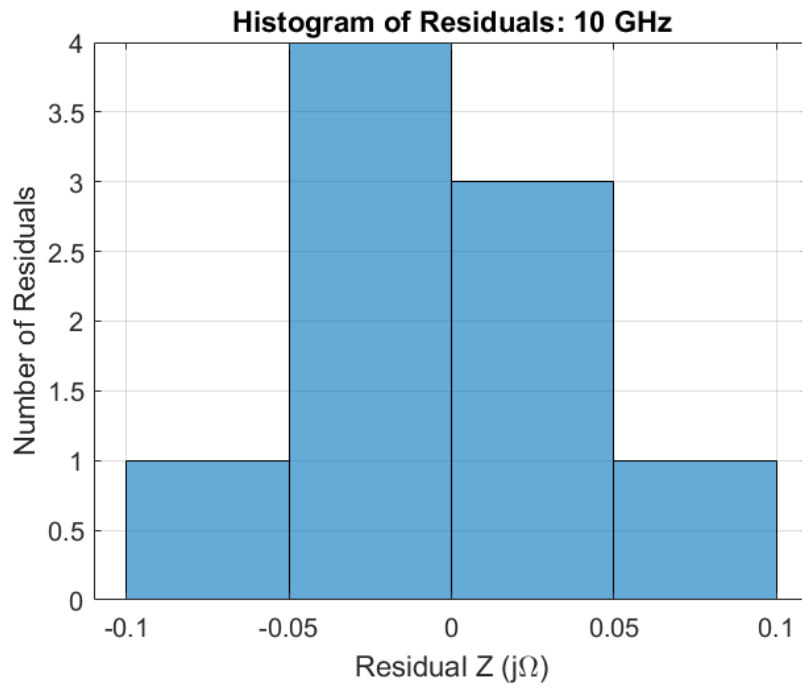


Figure 416: Square FR4: Histogram of Residuals, 10 GHz

Model: 11 GHz

Equation form: $y = c_0 + c_1 \frac{1}{x^1} + c_2 \frac{1}{x^2}$

	<u>Coefficient</u>	<u>SE</u>	<u>tStat</u>	<u>pValue</u>
c_0 (intercept)	73.165	0.12842	569.71	1.974×10^{-15}
c_1	6.402	0.10874	58.873	1.6137×10^{-9}
c_2	-0.28727	0.01824	-15.749	4.1548×10^{-6}

Table 77: Model Coefficients: 11 GHz

Model Statistics

Error Degrees of Freedom: 6

Root Mean Squared Error (RMSE): 0.0787

R-squared: 1

Adjusted R-Squared: 1

F-statistic vs. constant model: 2.47×10^4

p-value = 1.8×10^{-12}

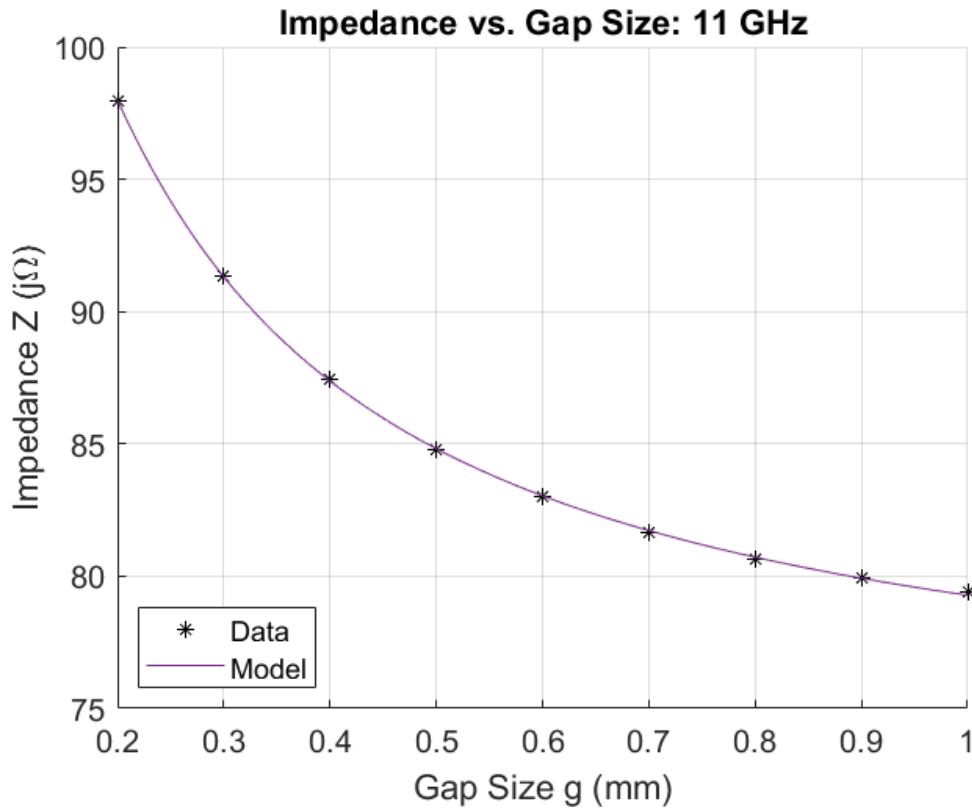


Figure 417: Square FR4: Impedance vs. Gap Size, 11 GHz

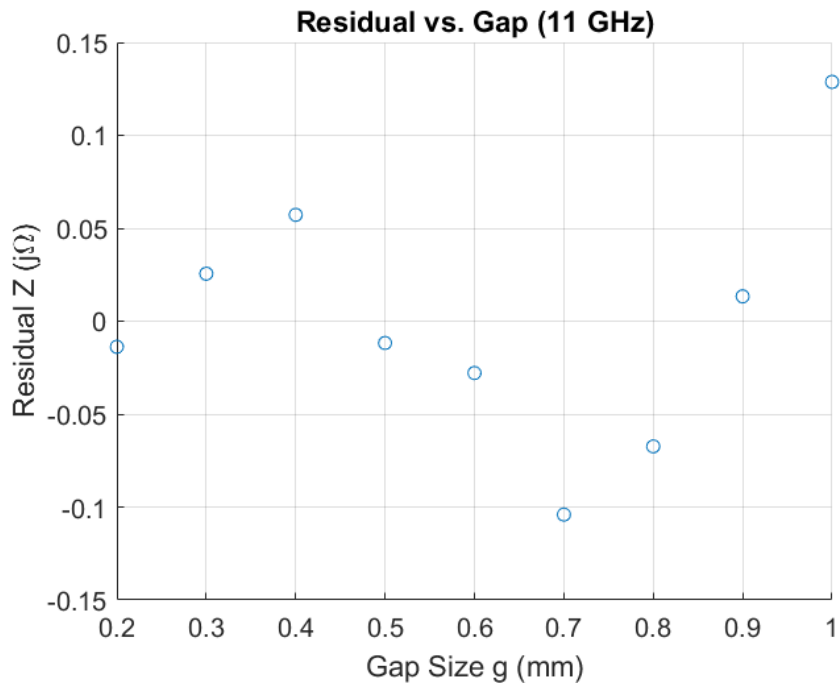


Figure 418: Square FR4: Residuals, 11 GHz

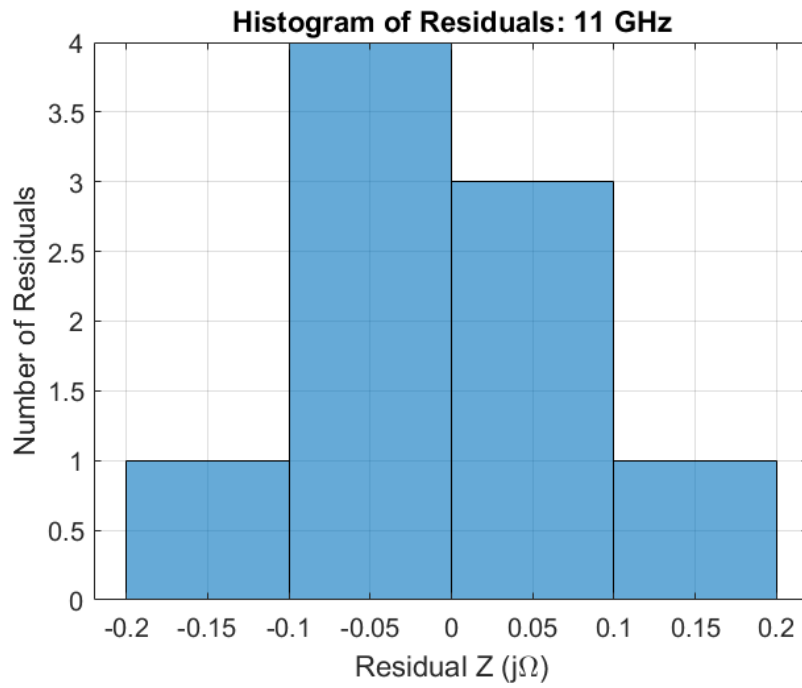


Figure 419: Square FR4: Histogram of Residuals, 11 GHz

Model: 12 GHz

Equation form: $y = c_0 + c_1 \frac{1}{x^1} + c_2 \frac{1}{x^2} + c_3 \frac{1}{x^3}$

	Coefficient	SE	tStat	pValue
c_0 (intercept)	74.362	0.44184	168.3	1.4051×10^{-10}
c_1	6.888	0.59246	11.626	8.266×10^{-5}
c_2	0.23834	0.22965	1.0378	0.34691
c_3	-0.056759	0.026054	-2.1785	0.081264

Table 78: Model Coefficients: 12 GHz

Model Statistics

Error Degrees of Freedom: 5
 Root Mean Squared Error (RMSE): 0.0953
 R-squared: 1
 Adjusted R-Squared: 1
 F-statistic vs. constant model: 2.2×10^4
 p-value = 1.01×10^{-10}

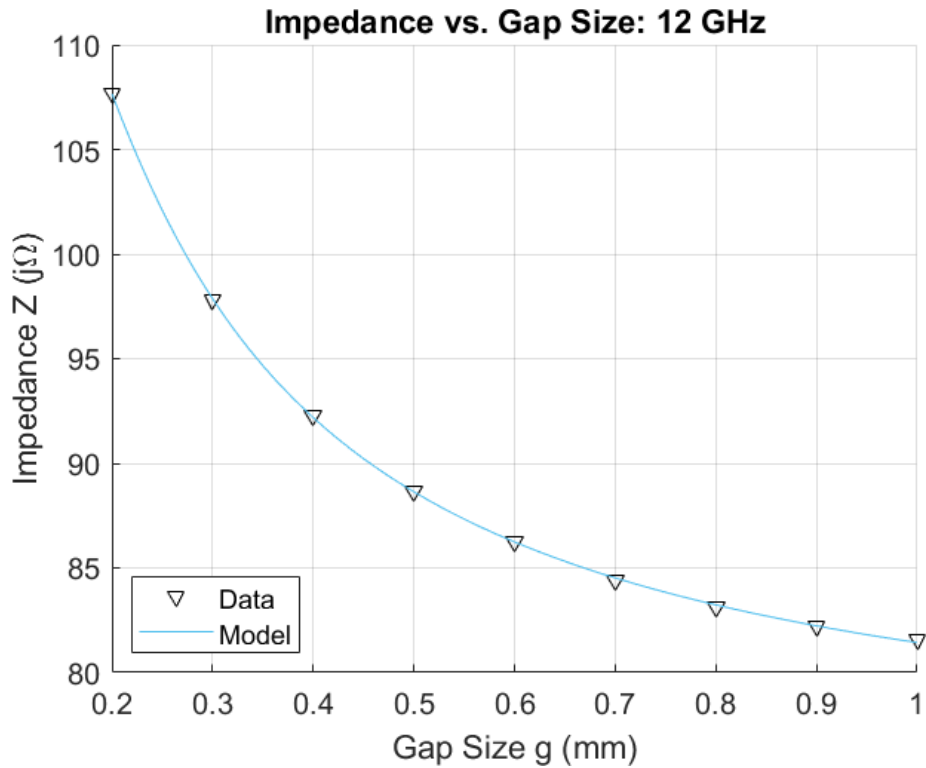


Figure 420: Square FR4: Impedance vs. Gap Size, 12 GHz

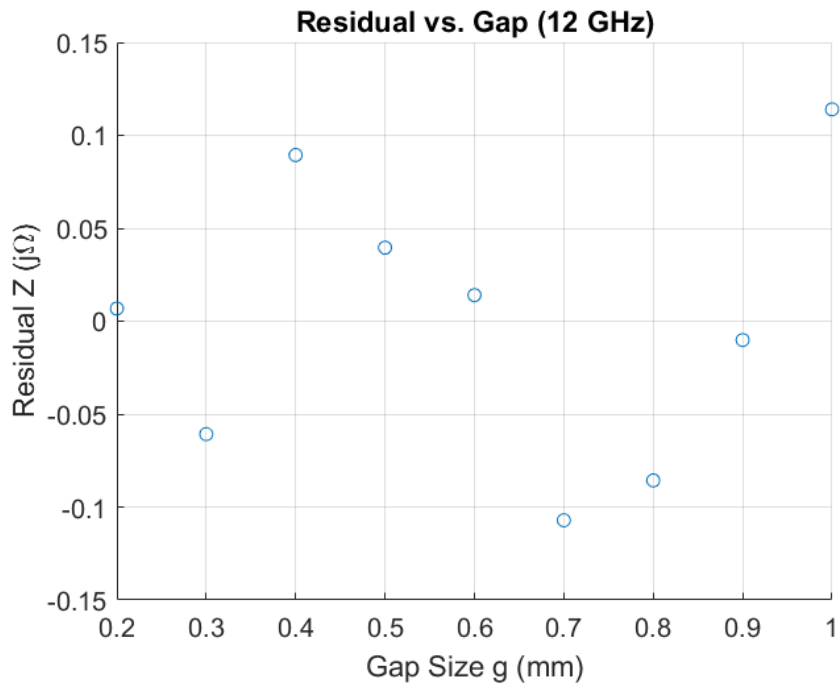


Figure 421: Square FR4: Residuals, 12 GHz

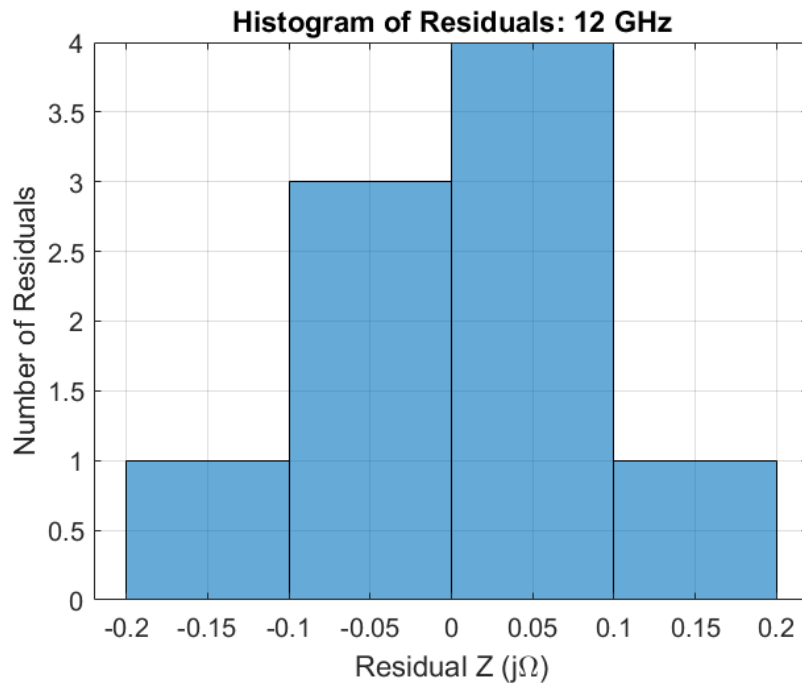


Figure 422: Square FR4: Histogram of Residuals, 12 GHz

Model: 13 GHz

Equation form: $y = c_0 + c_1 \frac{1}{x^1} + c_2 \frac{1}{x^2} + c_3 \frac{1}{x^3}$

	Coefficient	SE	tStat	pValue
c_0 (intercept)	75.209	0.5748	130.84	4.9461×10^{-10}
c_1	8.0307	0.77075	10.419	0.00014034
c_2	0.72012	0.29876	2.4104	0.060836
c_3	-0.096087	0.033894	-2.8349	0.036465

Table 79: Model Coefficients: 13 GHz

Model Statistics

Error Degrees of Freedom: 5
 Root Mean Squared Error (RMSE): 0.124
 R-squared: 1
 Adjusted R-Squared: 1
 F-statistic vs. constant model: 2.64×10^4
 p-value = 6.47×10^{-11}

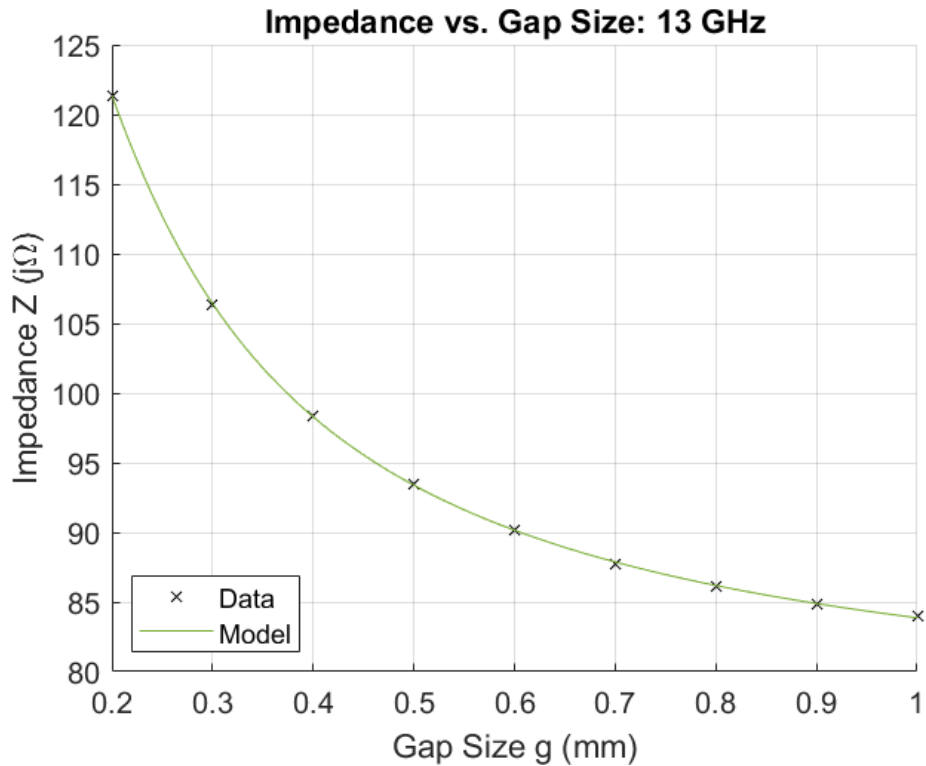


Figure 423: Square FR4: Impedance vs. Gap Size, 13 GHz

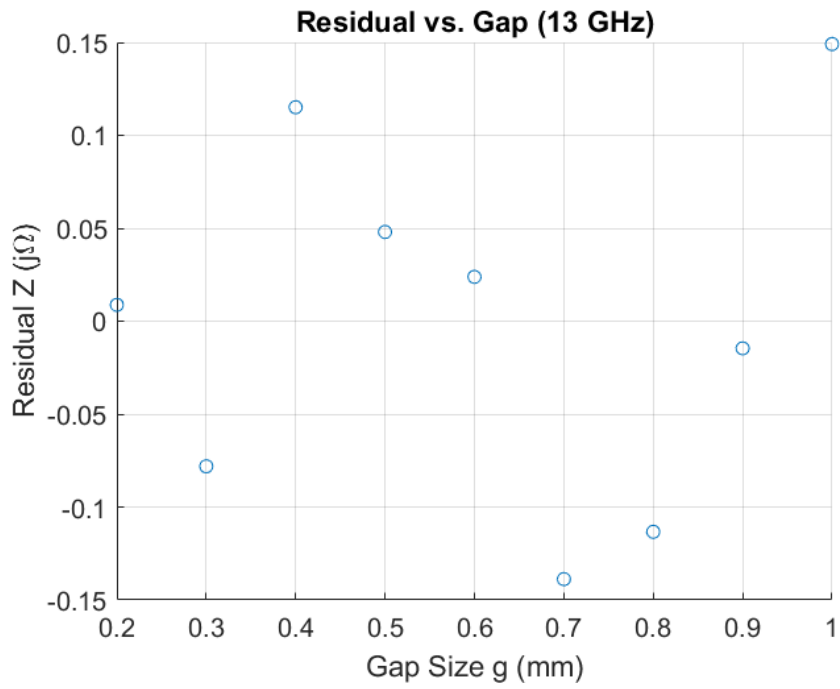


Figure 424: Square FR4: Residuals, 13 GHz

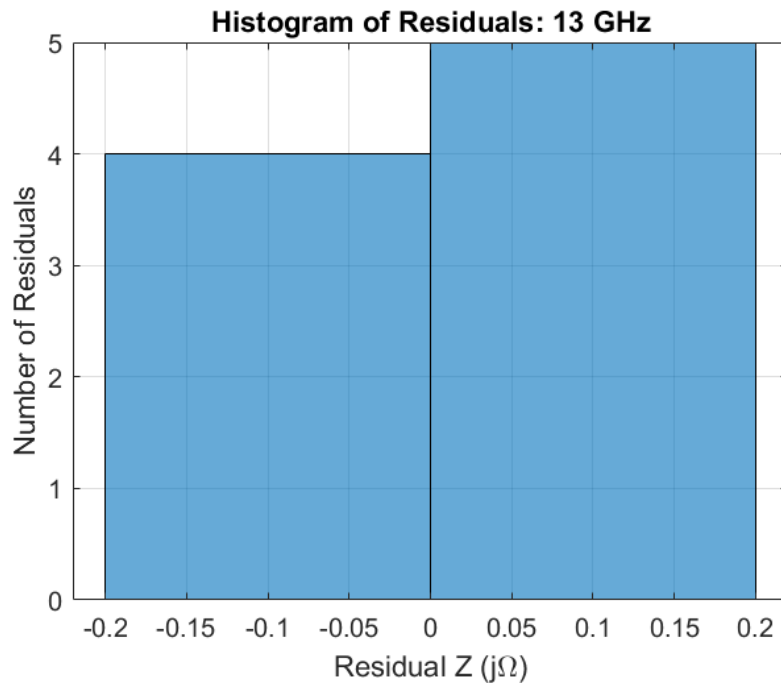


Figure 425: Square FR4: Histogram of Residuals, 13 GHz

Model: 14 GHz

Equation form: $y = c_0 + c_1 \frac{1}{x^1} + c_2 \frac{1}{x^2} + c_3 \frac{1}{x^3}$

	<u>Coefficient</u>	<u>SE</u>	<u>tStat</u>	<u>pValue</u>
c_0 (intercept)	76.358	0.70728	107.96	1.293×10^{-9}
c_1	8.8678	0.94839	9.3504	0.0002357
c_2	1.6061	0.36762	4.3689	0.0072298
c_3	-0.15737	0.041706	-3.7733	0.012979

Table 80: Model Coefficients: 14 GHz

Model Statistics

Error Degrees of Freedom: 5
 Root Mean Squared Error (RMSE): 0.153
 R-squared: 1
 Adjusted R-Squared: 1
 F-statistic vs. constant model: 3.65×10^4
 p-value = 2.86×10^{-11}

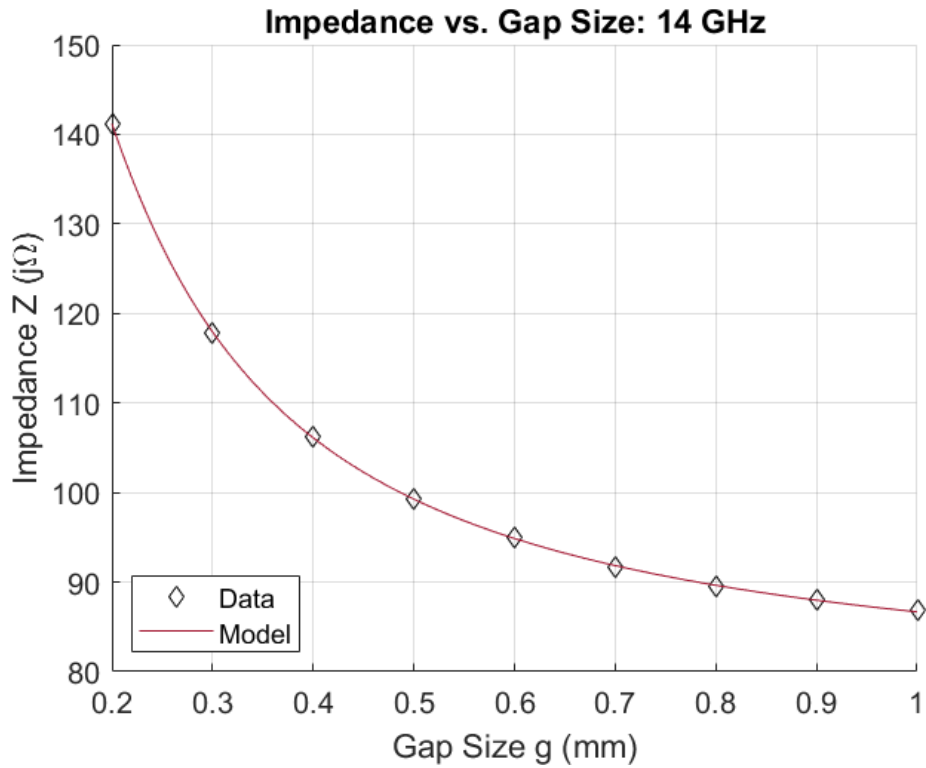


Figure 426: Square FR4: Impedance vs. Gap Size, 14 GHz

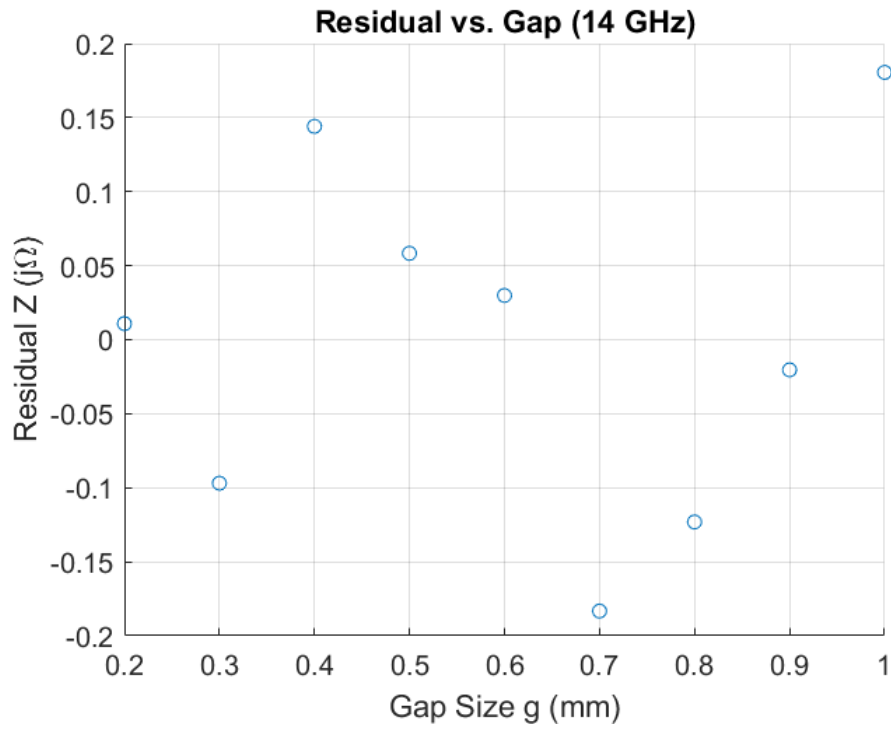


Figure 427: Square FR4: Residuals, 14 GHz

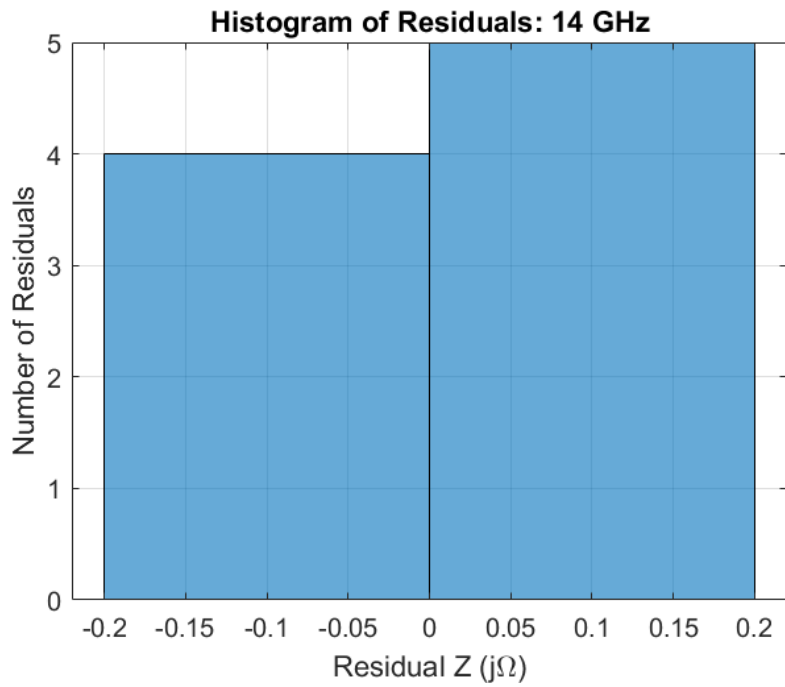


Figure 428: Square FR4: Histogram of Residuals, 14 GHz

Model: 15 GHz

Equation form: $y = c_0 + c_1 \frac{1}{x^1} + c_2 \frac{1}{x^2} + c_3 \frac{1}{x^3}$

	<u>Coefficient</u>	<u>SE</u>	<u>tStat</u>	<u>pValue</u>
c_0 (intercept)	78.138	0.83627	93.436	2.6619×10^{-9}
c_1	8.7558	1.1213	7.8083	0.00055219
c_2	3.2877	0.43466	7.5638	0.00064052
c_3	-0.27519	0.049312	-5.5805	0.002547

Table 81: Model Coefficients: 15 GHz

Model Statistics

Error Degrees of Freedom: 5
 Root Mean Squared Error (RMSE): 0.18
 R-squared: 1
 Adjusted R-Squared: 1
 F-statistic vs. constant model: 5.58×10^4
 p-value = 9.92×10^{-12}

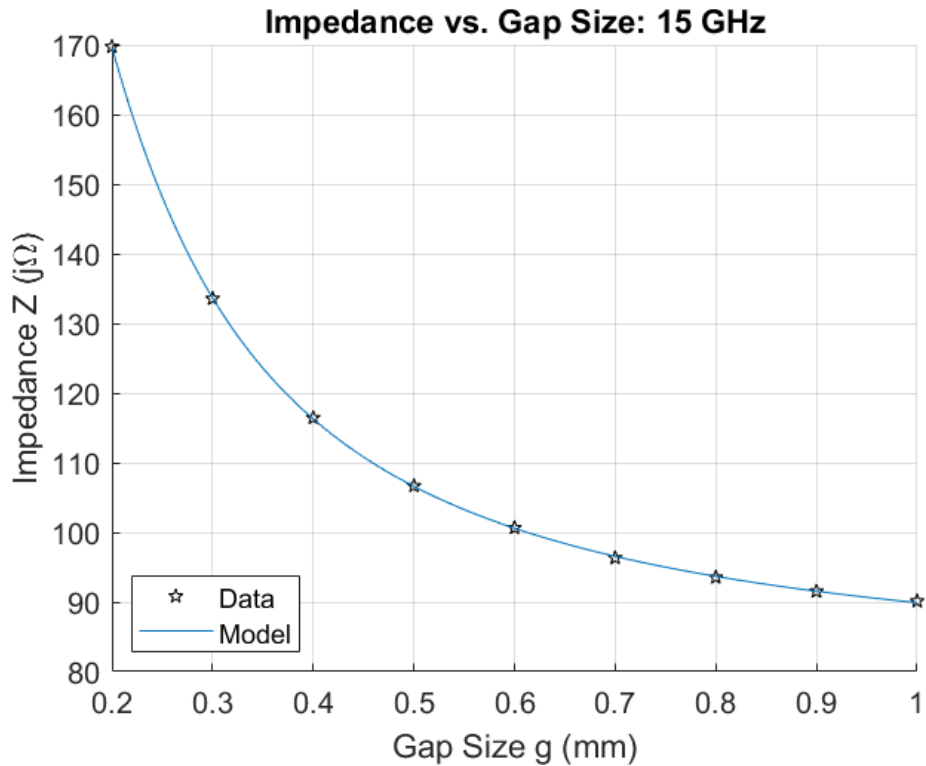


Figure 429: Square FR4: Impedance vs. Gap Size, 15 GHz

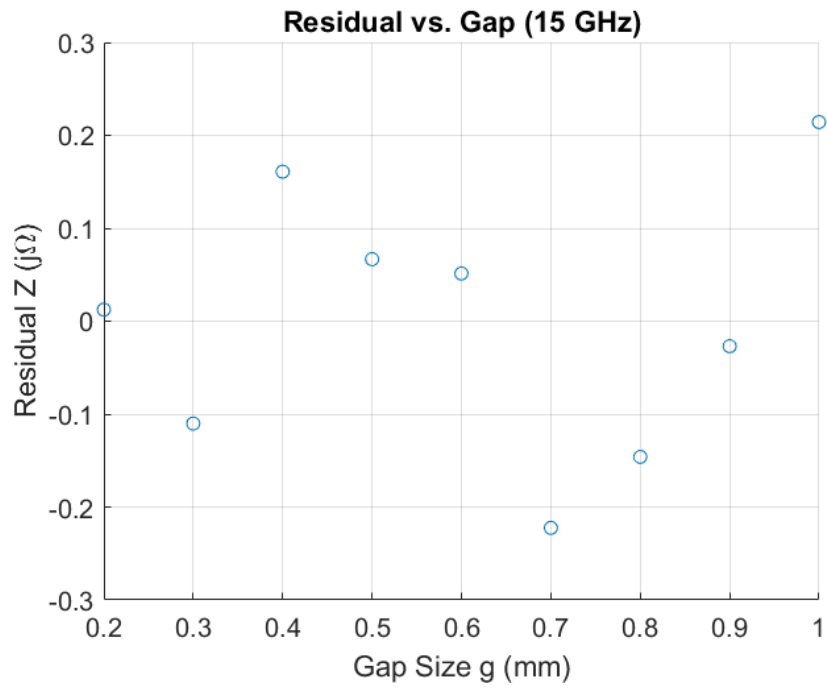


Figure 430: Square FR4: Residuals, 15 GHz

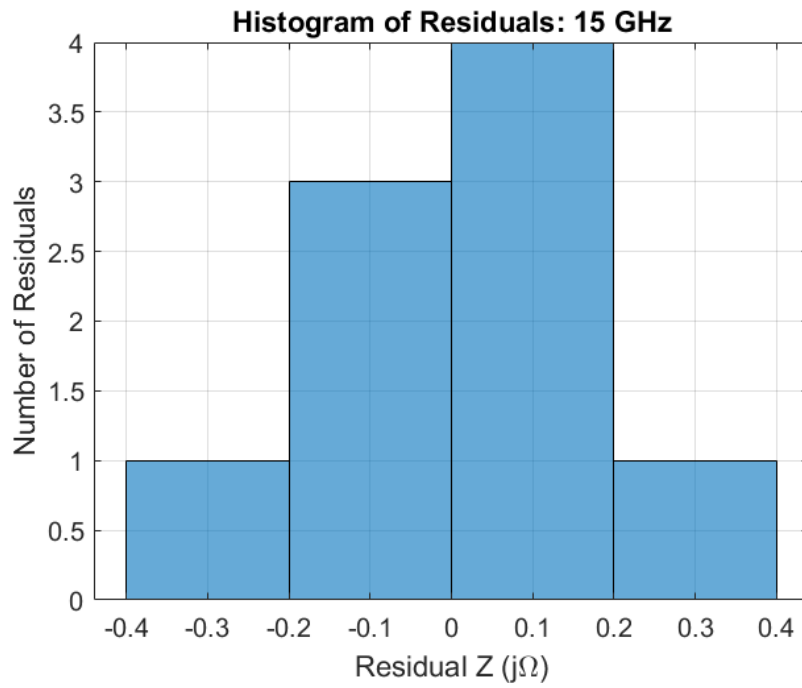


Figure 431: Square FR4: Histogram of Residuals, 15 GHz

Model: 16 GHz

Equation form: $y = c_0 + c_1 \frac{1}{x^1} + c_2 \frac{1}{x^2} + c_3 \frac{1}{x^3}$

	Coefficient	SE	tStat	pValue
c_0 (intercept)	83.563	0.62042	134.69	4.2796×10^{-10}
c_1	2.4595	0.83192	2.9565	0.031648
c_2	8.5647	0.32247	26.56	1.4145×10^{-6}
c_3	-0.86165	0.036584	-23.552	2.5691×10^{-6}

Table 82: Model Coefficients: 16 GHz

Model Statistics

Error Degrees of Freedom: 5
 Root Mean Squared Error (RMSE): 0.134
 R-squared: 1
 Adjusted R-Squared: 1
 F-statistic vs. constant model: 1.92×10^5
 p-value = 4.55×10^{-13}

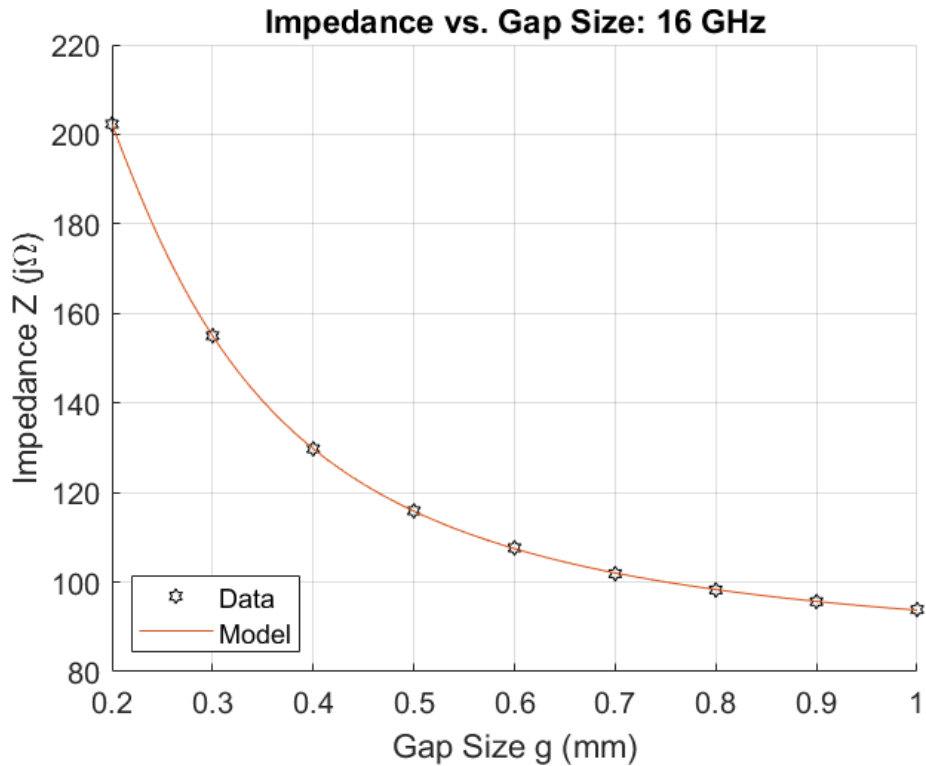


Figure 432: Square FR4: Impedance vs. Gap Size, 16 GHz

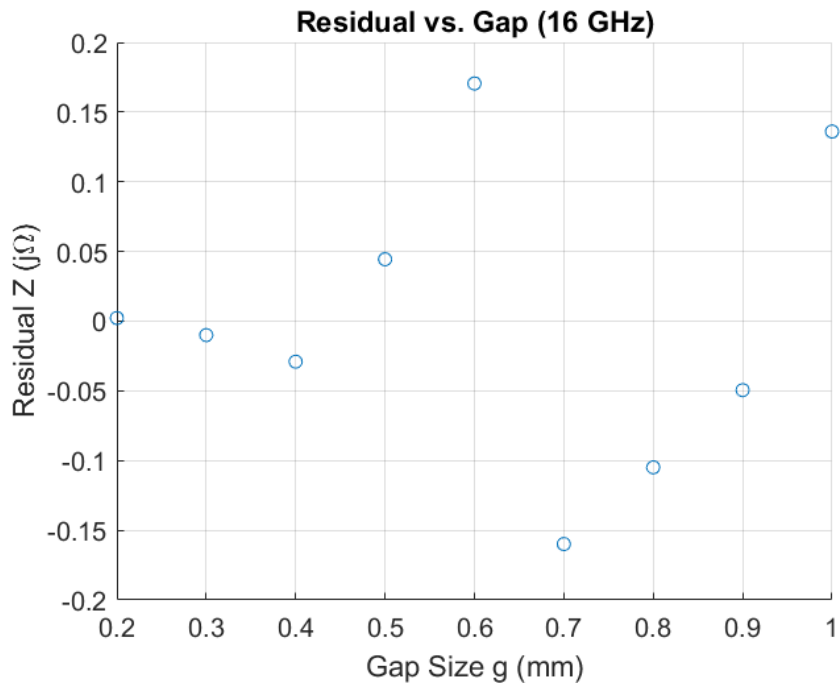


Figure 433: Square FR4: Residuals, 16 GHz

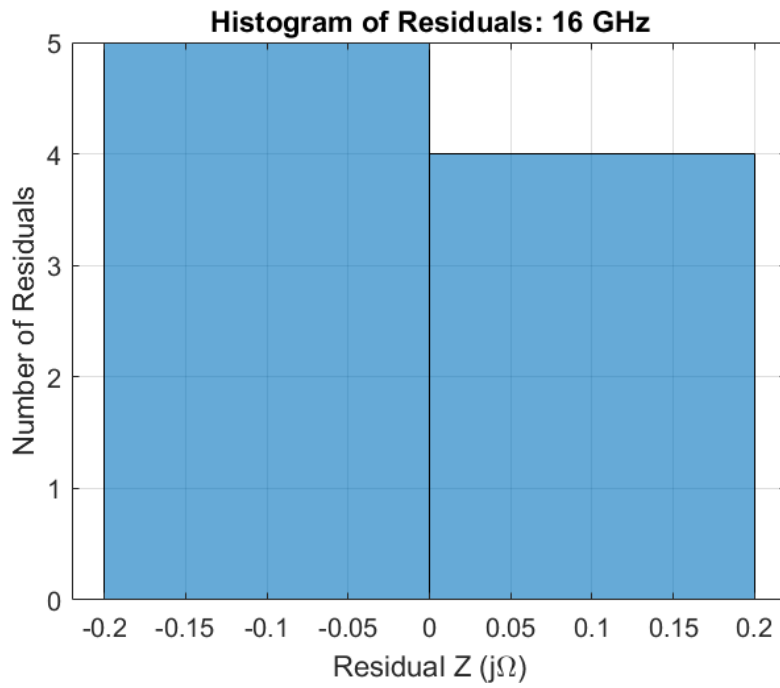


Figure 434: Square FR4: Histogram of Residuals, 16 GHz

Model: 17 GHz

Equation form: $y = c_0 + c_1 \frac{1}{x^1} + c_2 \frac{1}{x^2} + c_3 \frac{1}{x^3}$

	<u>Coefficient</u>	<u>SE</u>	<u>tStat</u>	<u>pValue</u>
c_0 (intercept)	90.228	0.7494	120.4	7.4965×10^{-10}
c_1	-6.2329	1.0049	-6.2027	0.0015902
c_2	15.699	0.38951	40.305	1.7728×10^{-7}
c_3	-1.6335	0.04419	-36.965	2.7288×10^{-7}

Table 83: Model Coefficients: 17 GHz

Model Statistics

Error Degrees of Freedom: 5
 Root Mean Squared Error (RMSE): 0.162
 R-squared: 1
 Adjusted R-Squared: 1
 F-statistic vs. constant model: 2.52×10^5
 p-value = 2.3×10^{-13}

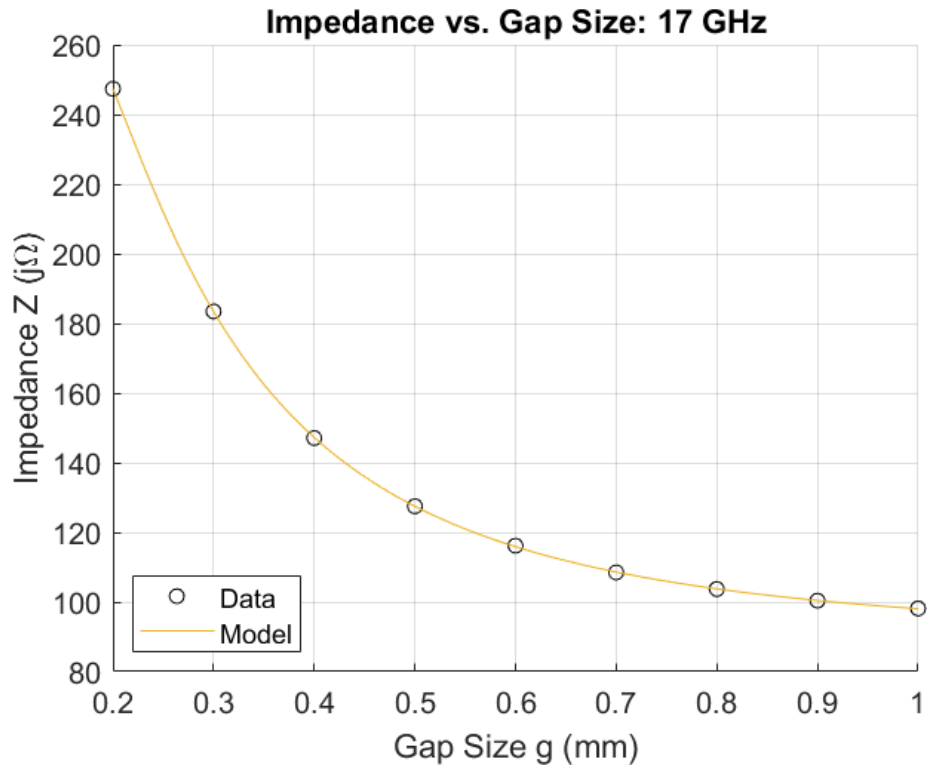


Figure 435: Square FR4: Impedance vs. Gap Size, 17 GHz

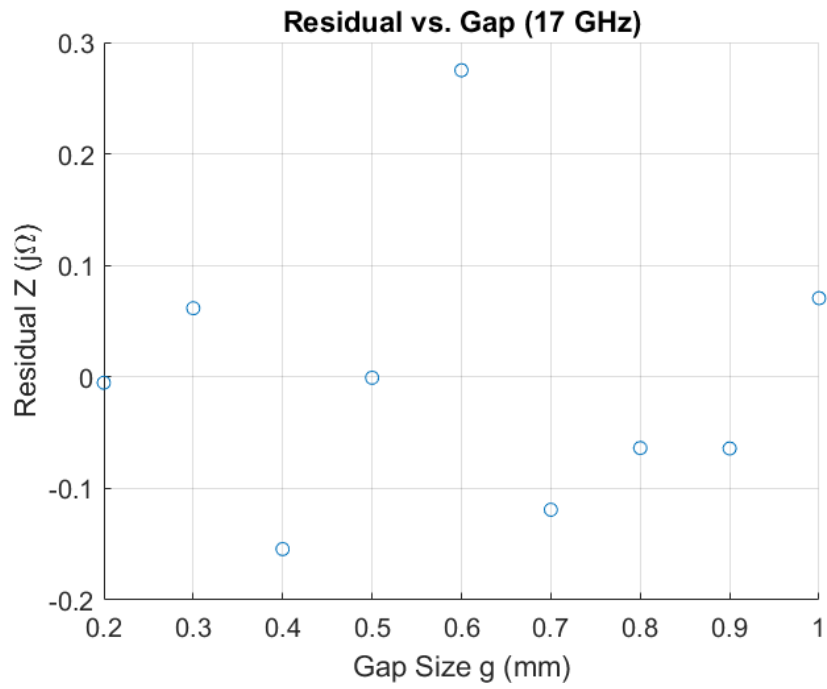


Figure 436: Square FR4: Residuals, 17 GHz

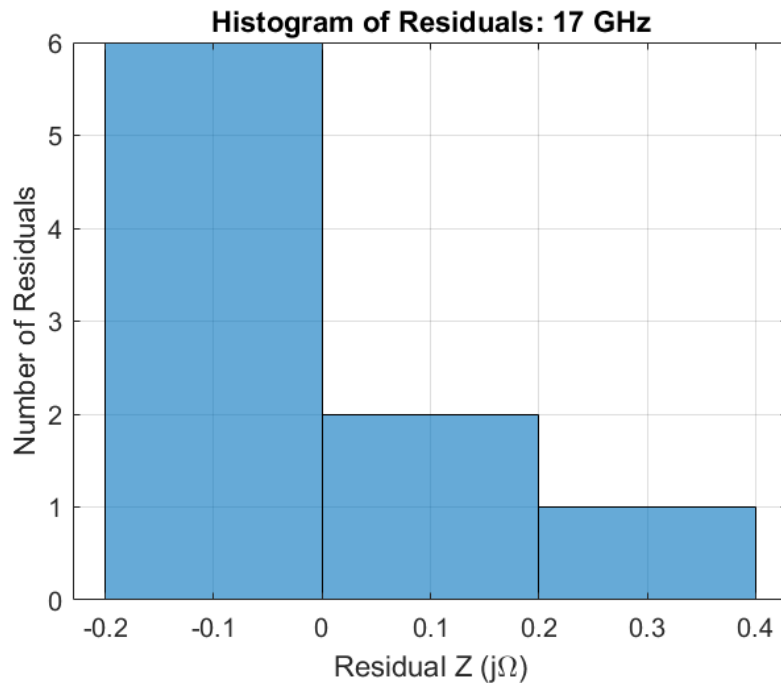


Figure 437: Square FR4: Histogram of Residuals, 17 GHz

Model: 18 GHz

Equation form: $y = c_0 + c_1x^1 + c_2x^2 + c_3x^3 + c_4x^4$

	Coefficient	SE	tStat	pValue
c_0 (intercept)	592.56	7.0348	84.233	1.1907×10^{-7}
c_1	-2089.2	60.884	-34.314	4.3033×10^{-6}
c_2	3585.6	177.28	20.225	3.5282×10^{-5}
c_3	-2853.9	210.41	-13.564	0.00017102
c_4	868	87.358	9.9361	0.00057612

Table 84: Model Coefficients: 18 GHz

Model Statistics

Error Degrees of Freedom: 4
 Root Mean Squared Error (RMSE): 0.67
 R-squared: 1
 Adjusted R-Squared: 1
 F-statistic vs. constant model: 1.89×10^4
 p-value = 8.38×10^{-9}

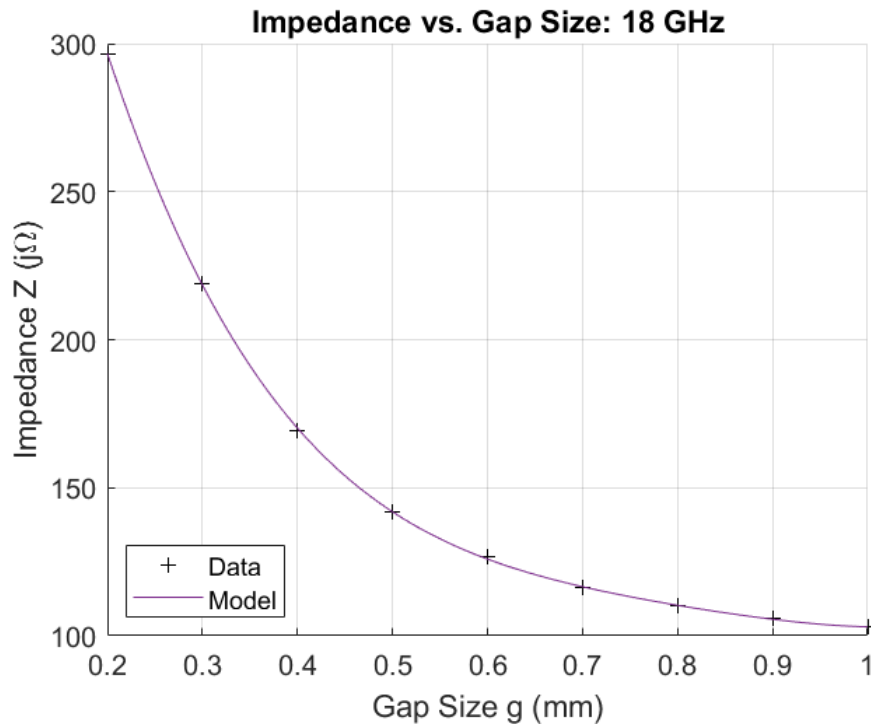


Figure 438: Square FR4: Impedance vs. Gap Size, 18 GHz

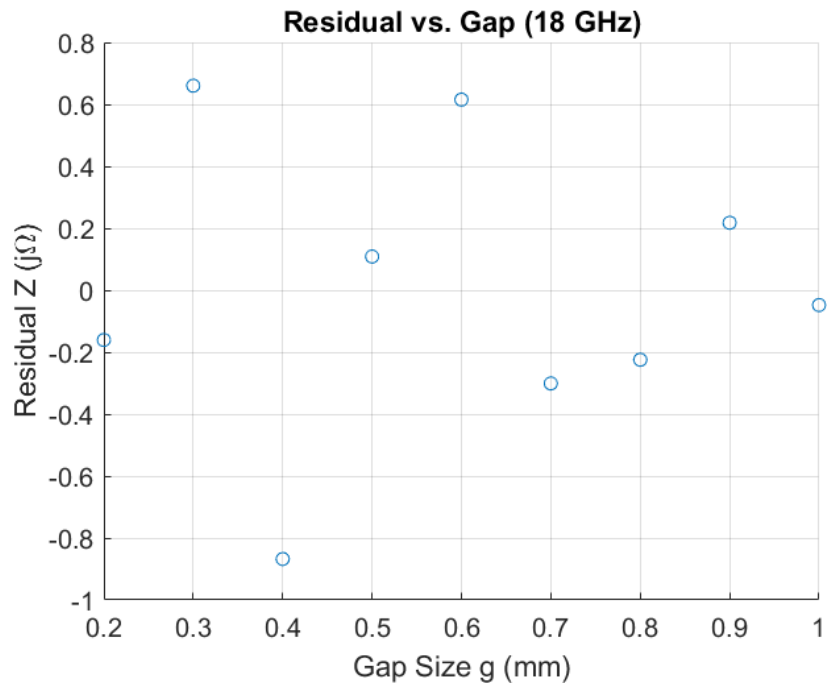


Figure 439: Square FR4: Residuals, 18 GHz

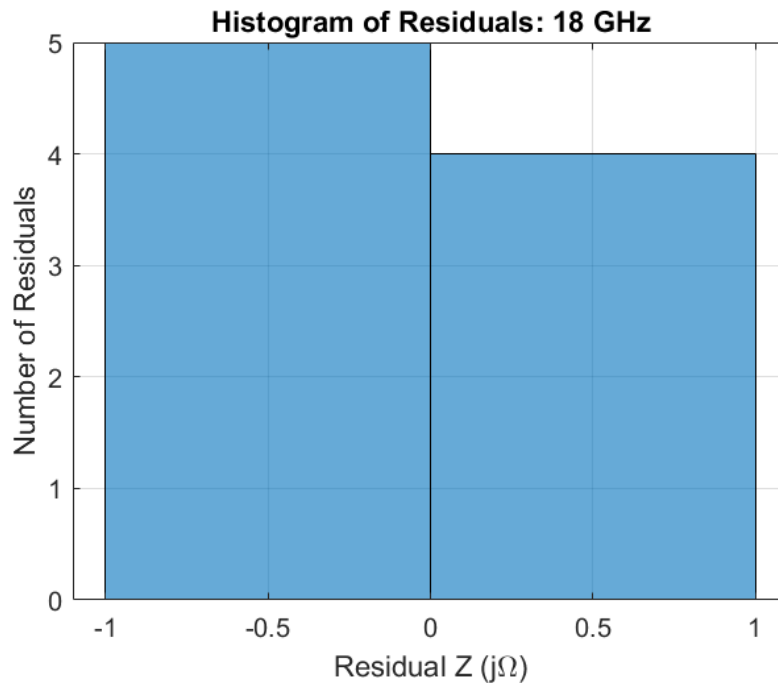


Figure 440: Square FR4: Histogram of Residuals, 18 GHz

Model: 19 GHz

Equation form: $y = c_0 + c_1x^1 + c_2x^2 + c_3x^3 + c_4x^4$

	<u>Coefficient</u>
c_0 (intercept)	640.4
c_1	-1958
c_2	2769
c_3	-1741
c_4	398.3

Table 85: Model Coefficients: 19 GHz

Model Statistics

Error Degrees of Freedom: 4

Root Mean Squared Error (RMSE): 1.91

Sum Squared Error (SSE): 14.59

R-squared: 0.9997

Adjusted R-Squared: 0.9994

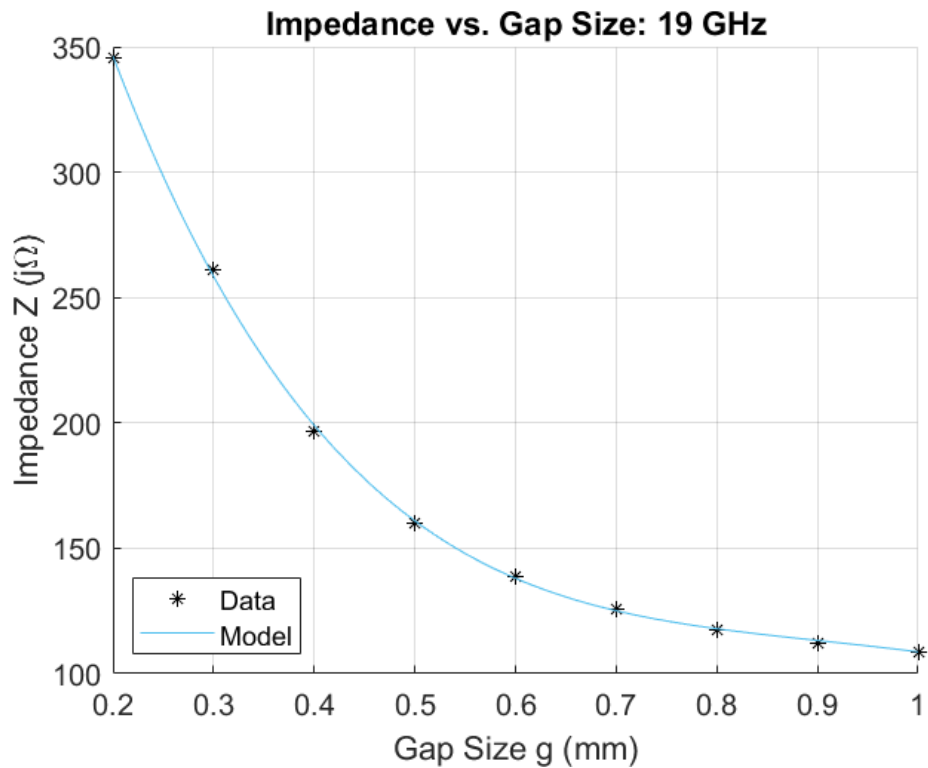


Figure 441: Square FR4: Impedance vs. Gap Size, 19 GHz

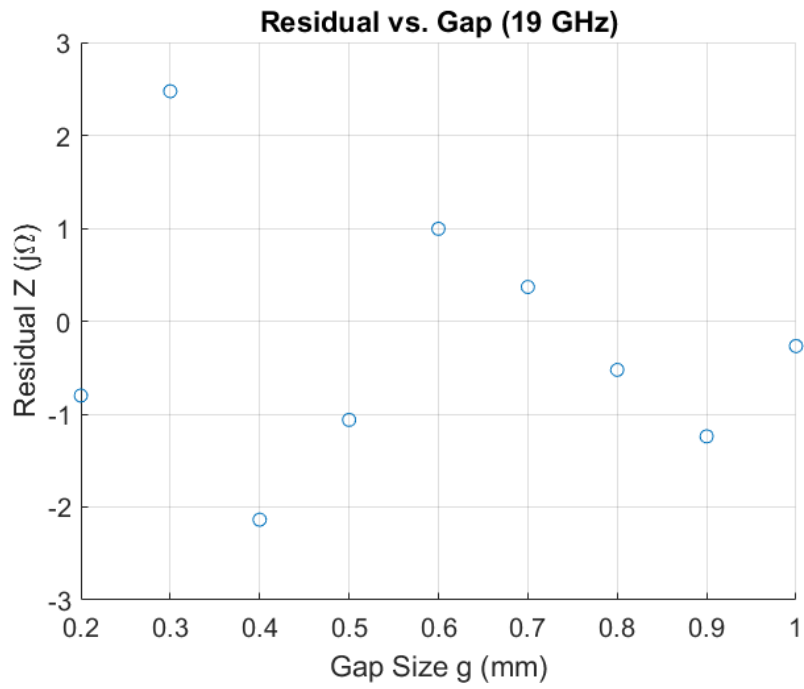


Figure 442: Square FR4: Residuals, 19 GHz

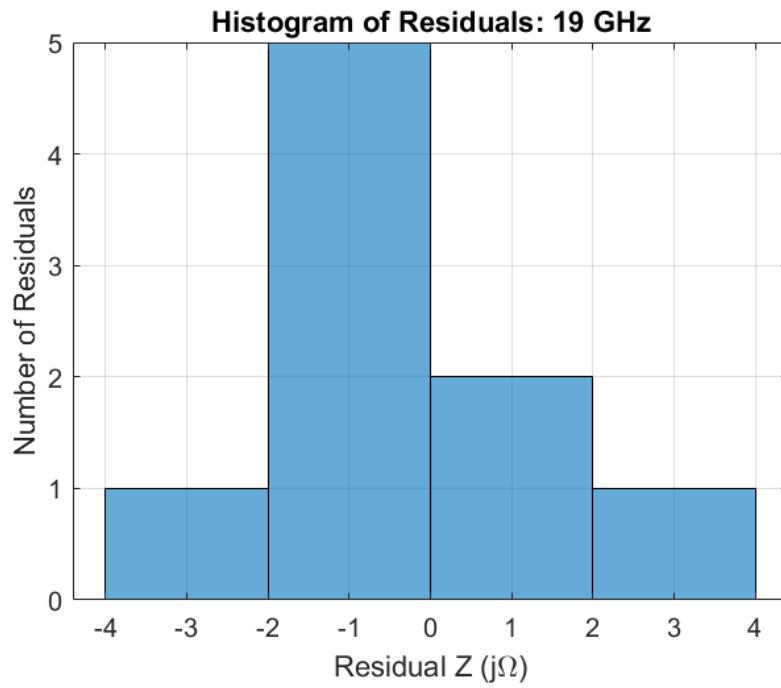


Figure 443: Square FR4: Histogram of Residuals, 19 GHz

Appendix E. Circular Rogers 3010 Unit Cell

Model Summary

Cell Parameters

Material: Rogers 3010

Dielectric Constant, ϵ_r : 11.2

Dissipation Constant, $\tan \delta$: 0.0022

Shape: circle

Dielectric Thickness: 1.27 mm

Copper Thickness: 0.035 mm

Cell Size, a : 3 mm

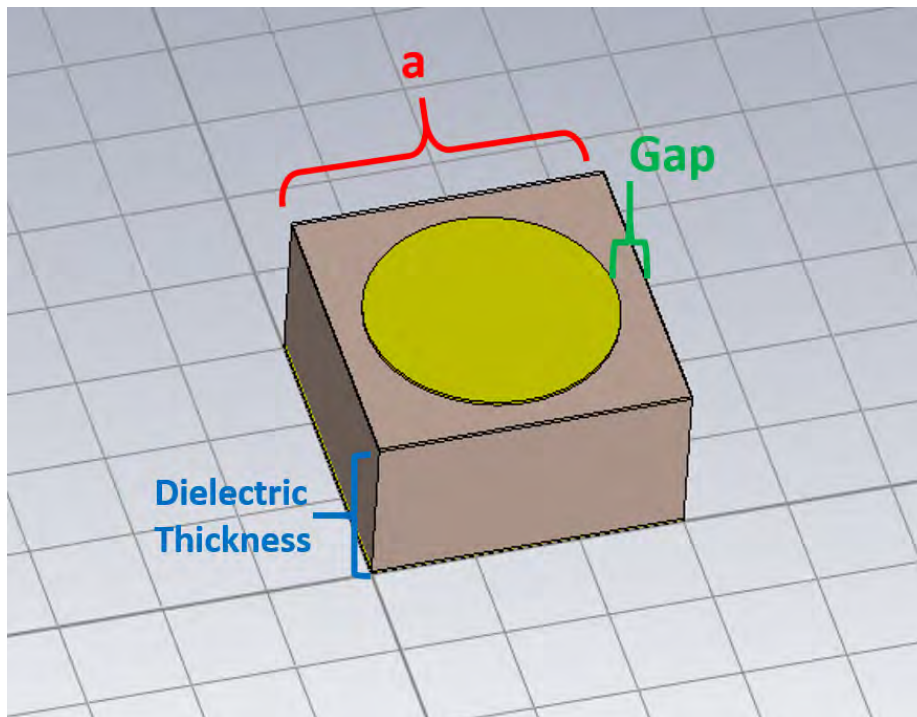


Figure 444: Circle Cell Geometry

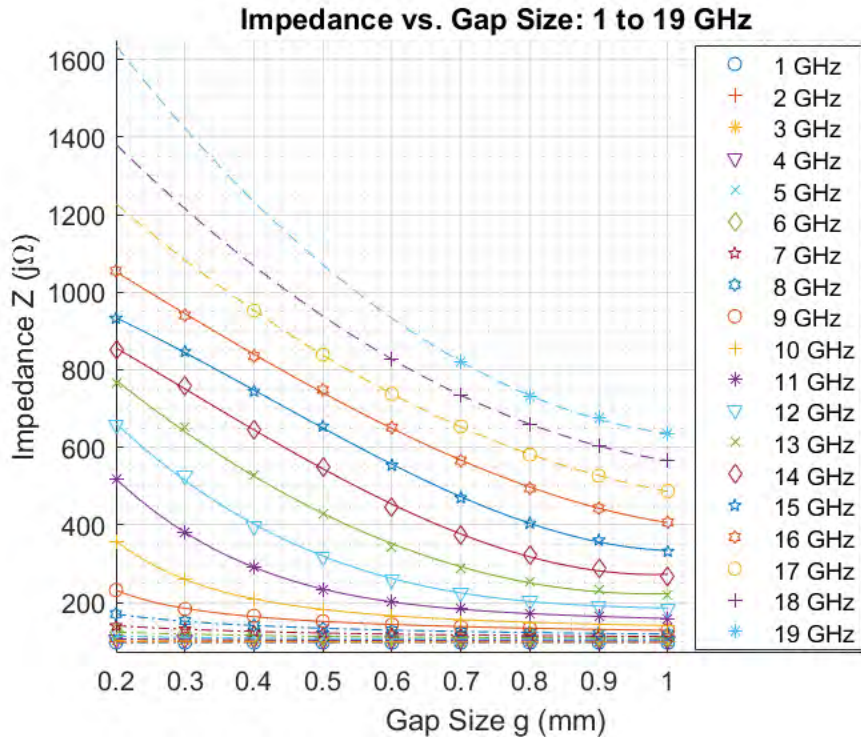


Figure 445: Circle Rogers 3010: Cell Impedance vs. Gap, 1-19 GHz

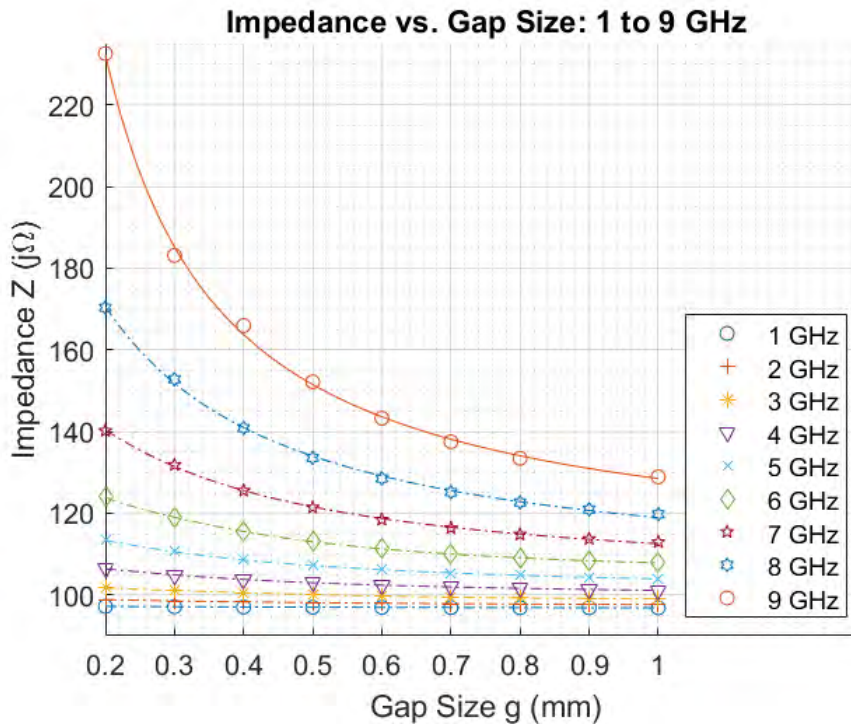


Figure 446: Circle Rogers 3010: Cell Impedance vs. Gap, 1-9 GHz

Unit Cell Impedance Model: Circle Rogers 3010

Frequency → Parameter ↓	1 GHz	2 GHz	3 GHz	4 GHz	5 GHz	6 GHz	7 GHz	8 GHz	9 GHz	10 GHz
c_4	0	0	0	0	0	0.063212	0	0	0	0
c_3	-0.25448	0	0	0	0	-0.76108	0	0	0	-1.69957
c_2	0.864475	-0.0514	4.2457	-0.18867	-0.30141	2.72754	-0.69131	-0.71299	0.975632	17.82036
c_1	-1.16778	0.602613	-8.31314	2.446404	4.157723	1.408637	11.09149	17.19171	20.06911	-0.0238
c_0 (intercept)	97.39951	97.10945	103.1982	98.85864	100.0842	104.3983	102.1603	102.4628	107.4676	124.7697
Z_{min}	96.84171	97.66159	99.07436	101.1559	104.027	107.8723	112.9719	119.757	128.9015	141.4743
Z_{max}	97.19838	98.8397	101.7745	106.3725	113.3281	124.0015	140.2208	170.3308	232.5729	357.7722
X	97.02005	98.25065	100.4244	103.7642	108.6775	115.9369	126.5964	145.0439	180.7372	249.6232
M	0.178333	0.589053	1.350052	2.608284	4.650518	8.064629	13.62445	25.28691	51.8357	108.1489
ϕ_{avg}	3.719948	7.445195	11.18193	14.93846	18.72741	22.57037	26.50661	30.63485	35.30223	40.98366
Inversion Factor	1	-1	1	-1	-1	-1	-1	-1	-1	-1

Frequency → Parameter ↓	11 GHz	12 GHz	13 GHz	14 GHz	15 GHz	16 GHz	17 GHz	18 GHz	19 GHz
c_4	977.1859	0	0	0	0	0	0	0	0
c_3	-3604.35	-797.355	0	739.4	903.942	399.9457	0	0	0
c_2	5076.849	2443.464	913.5814	-638.5	-1142.65	-219.574	744.0208	912.2231	1265.586
c_1	-3291.72	-2538.18	-1784.13	-879.9	-499.42	-1040.15	-1818.79	-2113.92	-2768.27
c_0 (intercept)	1001.056	1077.858	1093.552	1052	1072.313	1265.679	1561.561	1767.303	2138.607
Z_{min}	159.1489	184.3592	220.0549	268.8579	331.9371	407.0824	487.4198	564.9509	635.0481
Z_{max}	518.2766	656.7574	764.9913	852.7016	932.655	1055.014	952.2567	827.8944	821.8337
X	338.7128	420.5583	492.5231	560.7798	632.2961	731.0481	719.8383	696.4226	728.4409
M	179.5638	236.1991	272.4682	291.9219	300.359	323.9657	232.4184	131.4718	93.39284
ϕ_{avg}	48.81687	58.82049	71.06865	85.35199	101.5397	120.3136	127.3524	133.7662	147.0792
Inversion Factor	1	1	1	1	1	1	1	1	1

Table 86: Unit Cell Impedance Model: Circle Rogers 3010

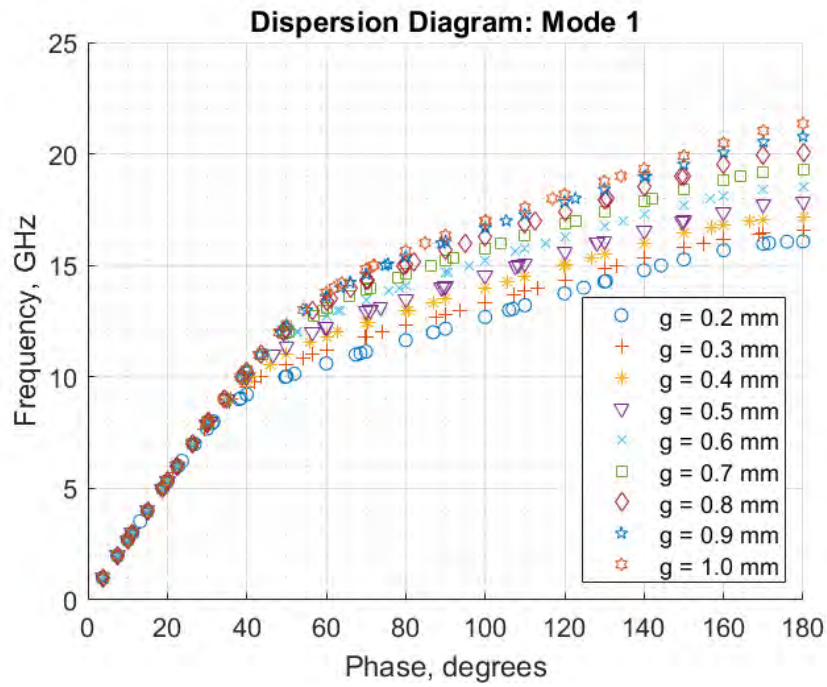


Figure 447: Circle Rogers 3010: Dispersion Diagram, Mode 1

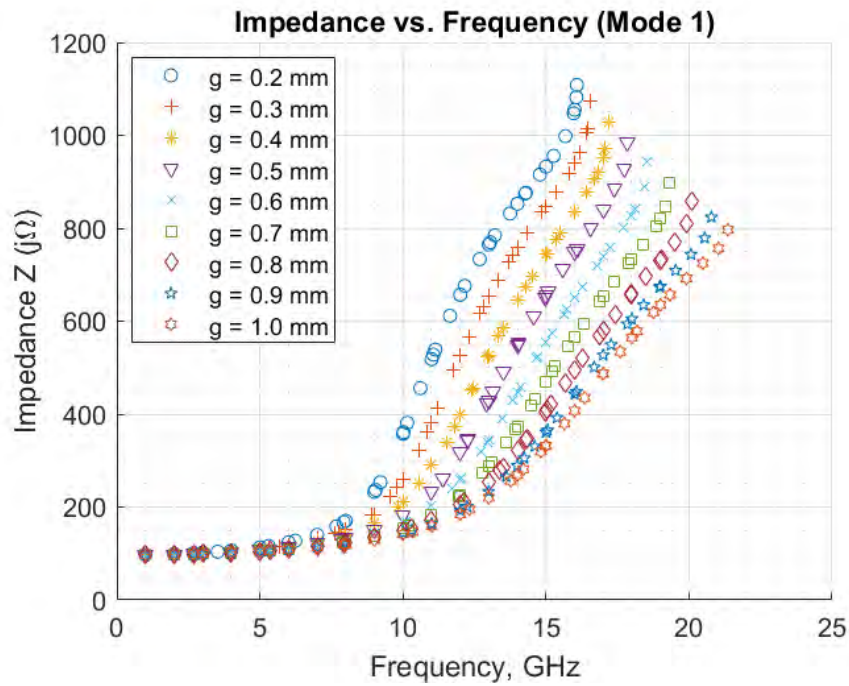


Figure 448: Circle Rogers 3010: Impedance vs. Frequency, Mode 1

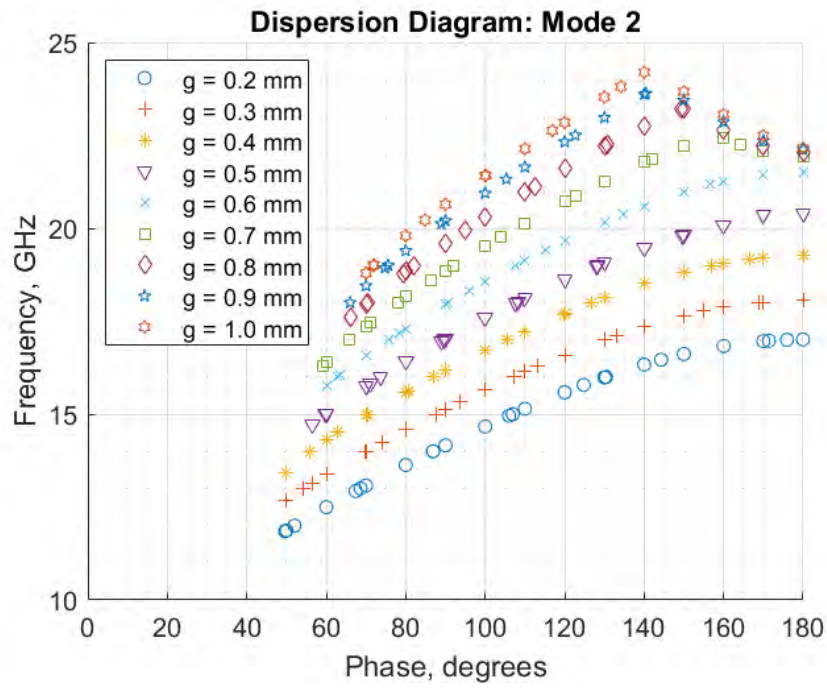


Figure 449: Circle Rogers 3010: Dispersion Diagram, Mode 2

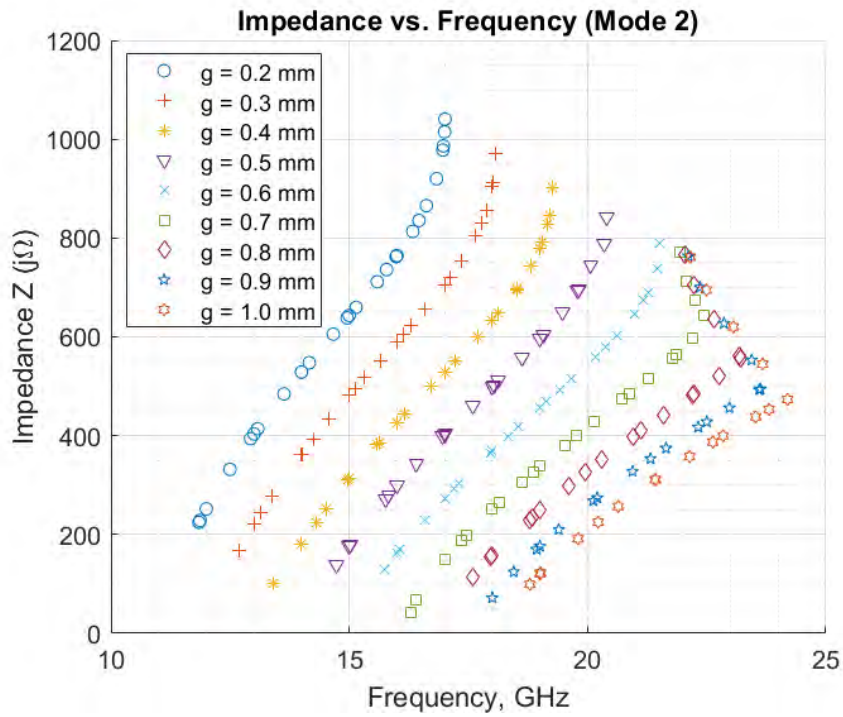


Figure 450: Circle Rogers 3010: Impedance vs. Frequency, Mode 2

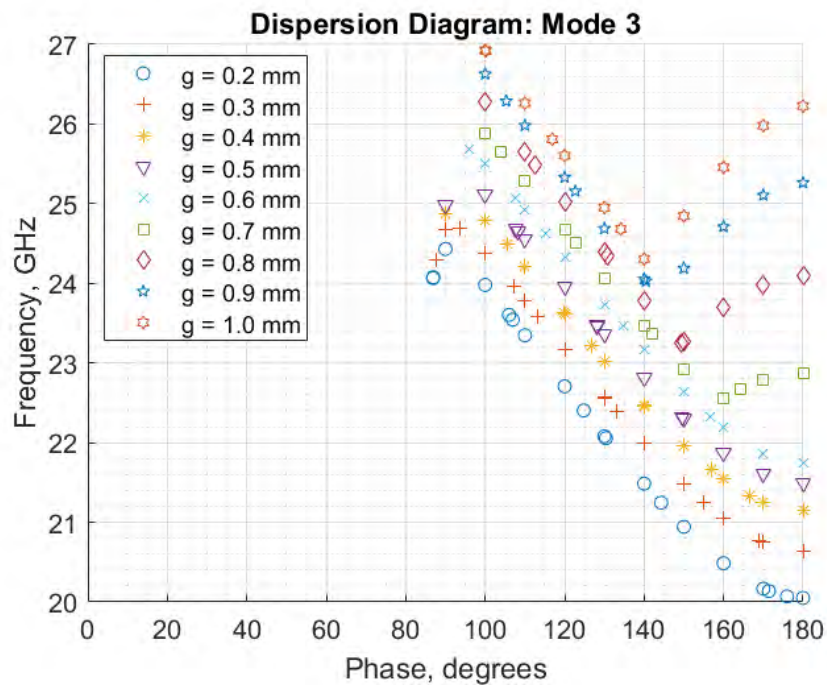


Figure 451: Circle Rogers 3010: Dispersion Diagram, Mode 3

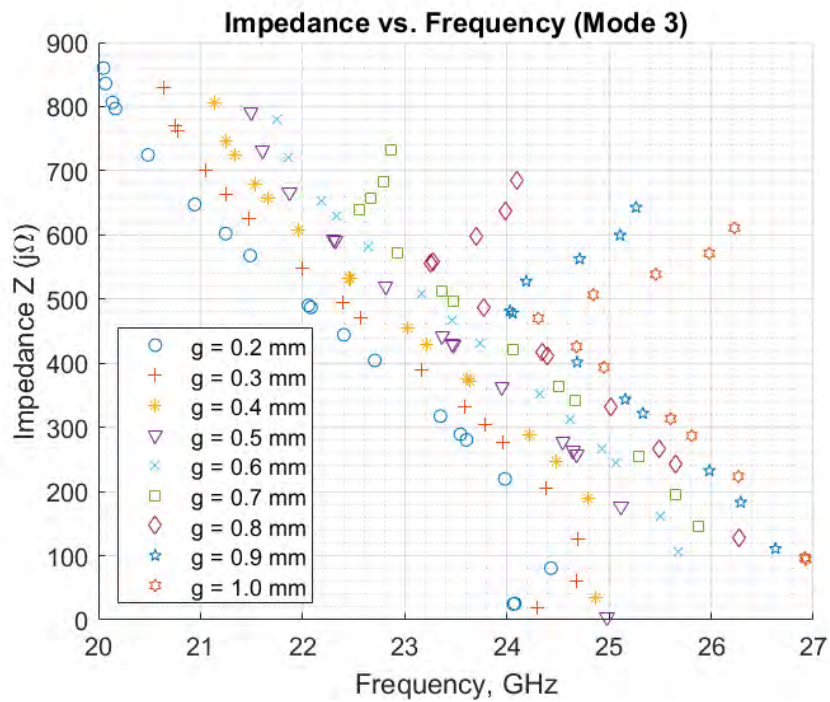


Figure 452: Circle Rogers 3010: Impedance vs. Frequency, Mode 3

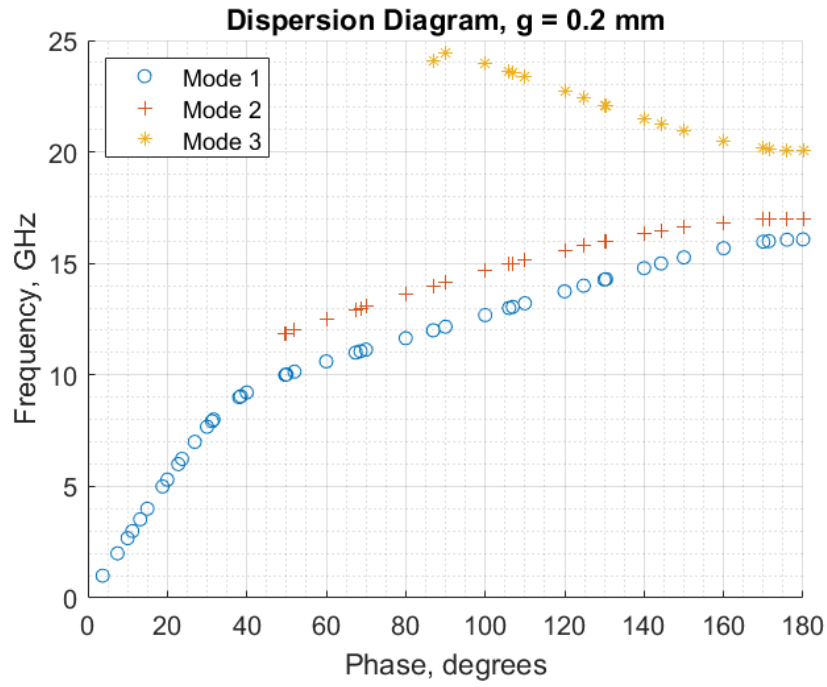


Figure 453: Circle Rogers 3010: Dispersion Diagram, $g = 0.2$

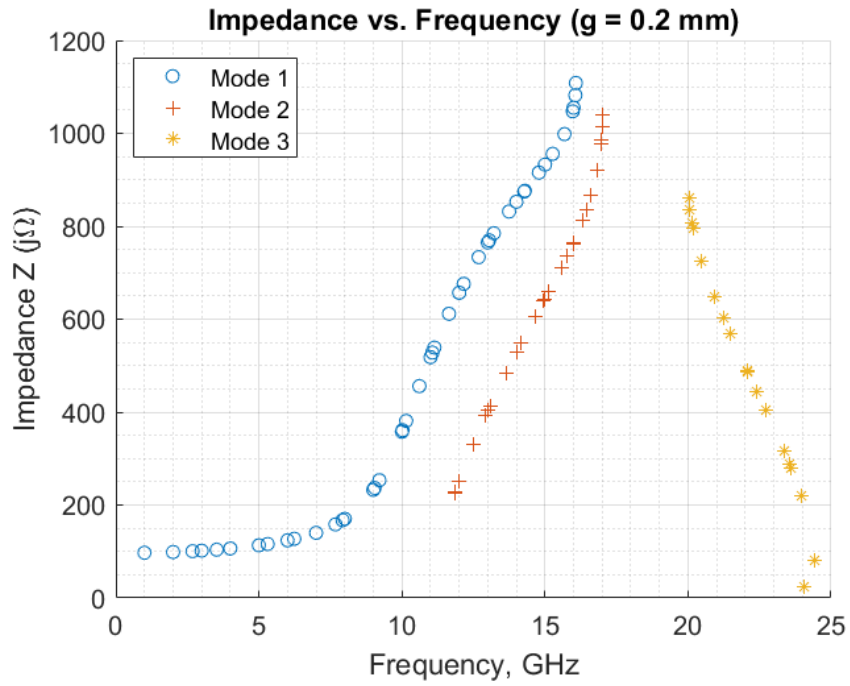


Figure 454: Circle Rogers 3010: Impedance vs. Frequency, $g = 0.2$

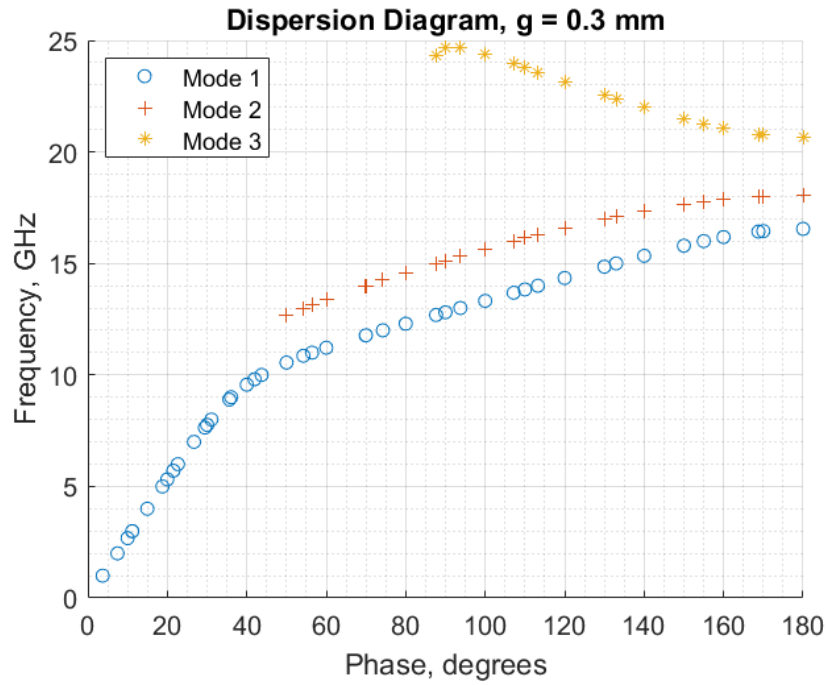


Figure 455: Circle Rogers 3010: Dispersion Diagram, $g = 0.3$

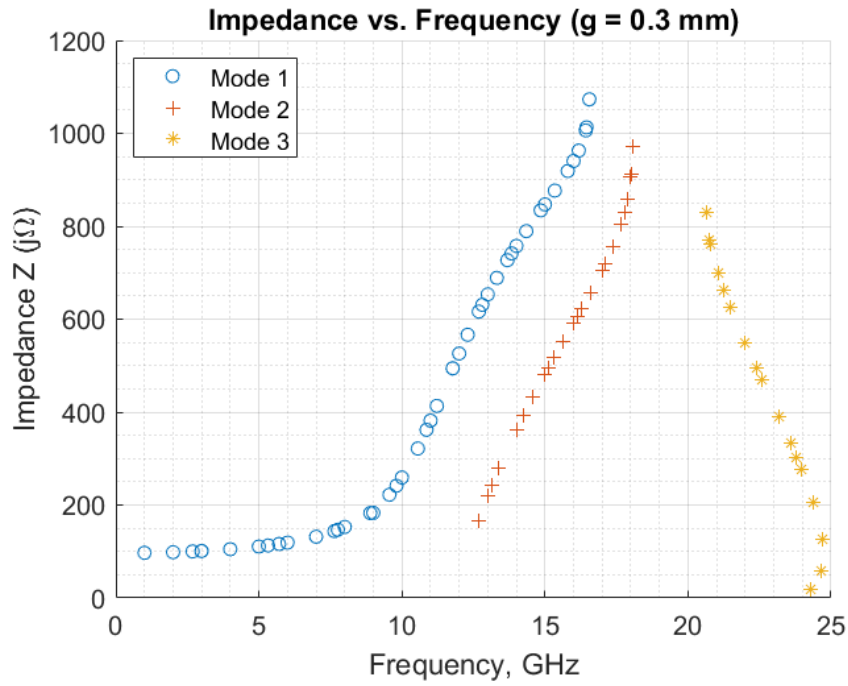


Figure 456: Circle Rogers 3010: Impedance vs. Frequency, $g = 0.3$

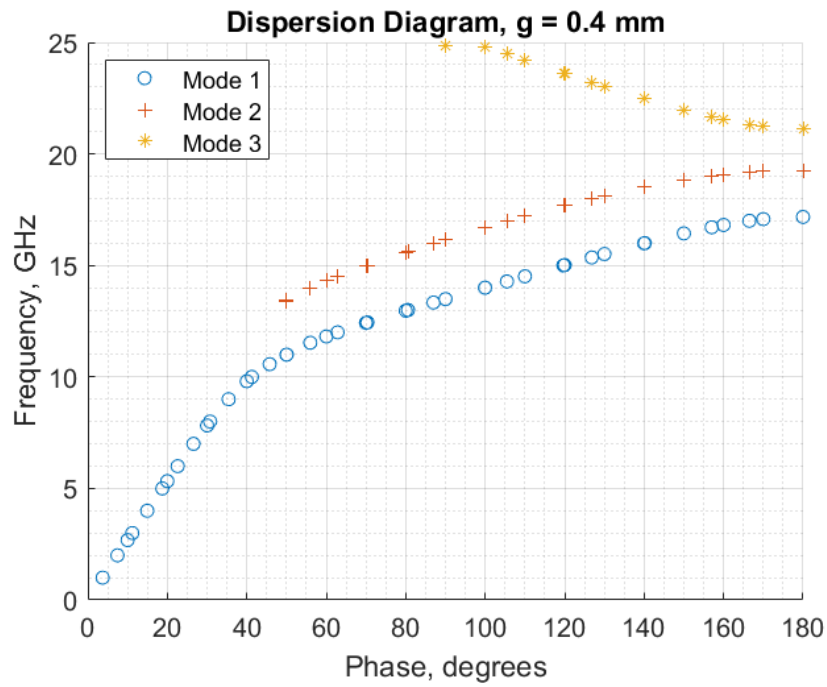


Figure 457: Circle Rogers 3010: Dispersion Diagram, g = 0.4

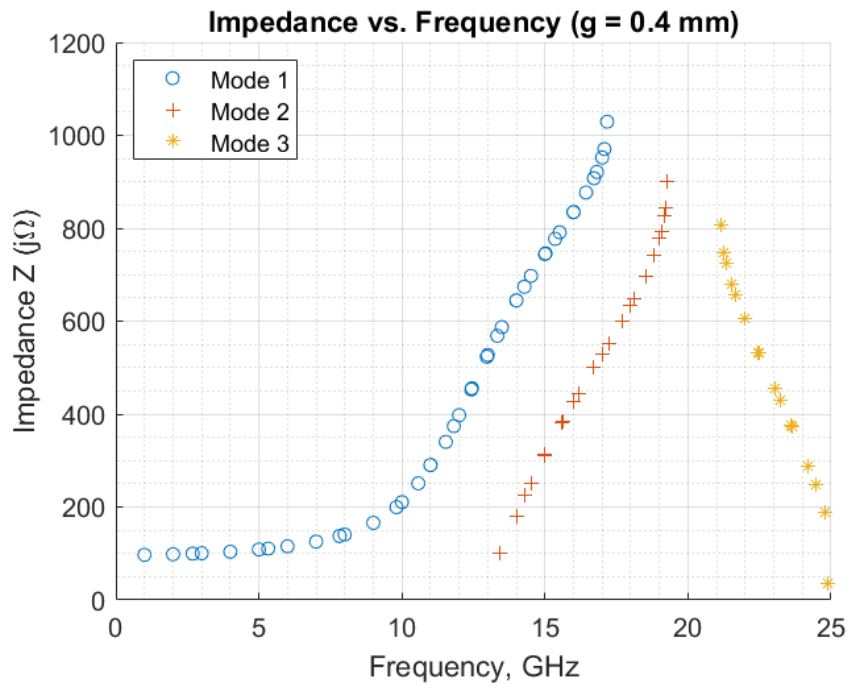


Figure 458: Circle Rogers 3010: Impedance vs. Frequency, g = 0.4

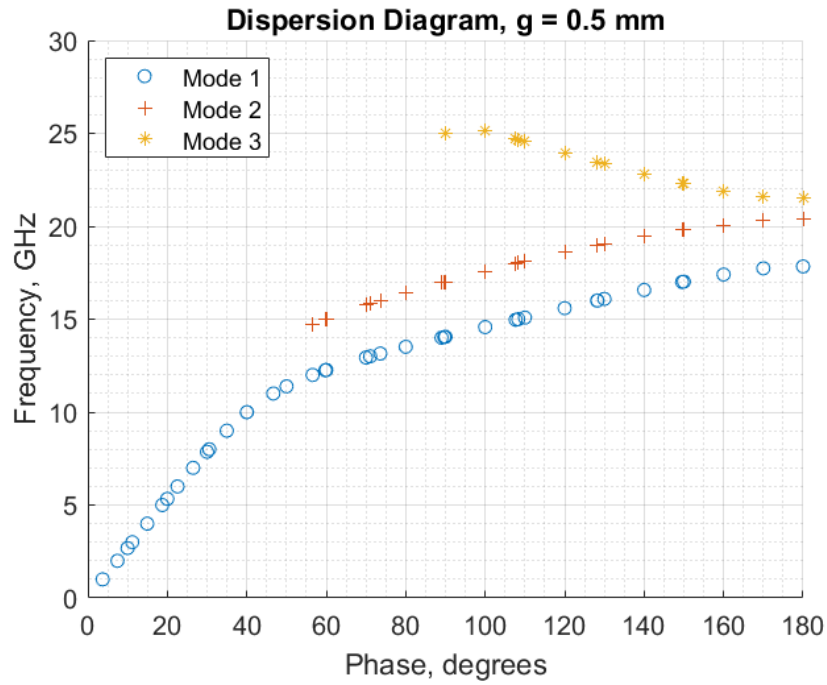


Figure 459: Circle Rogers 3010: Dispersion Diagram, g = 0.5

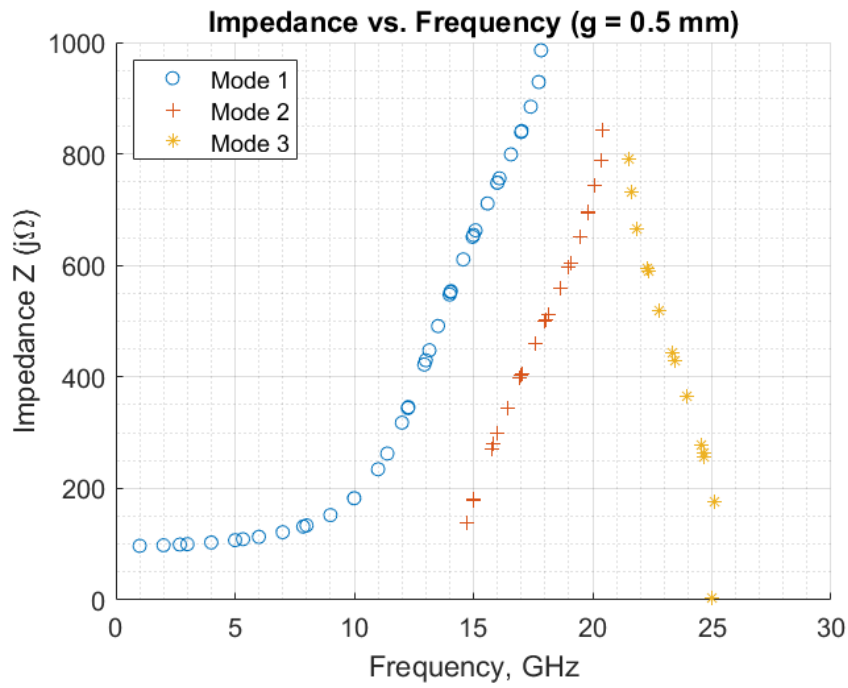


Figure 460: Circle Rogers 3010: Impedance vs. Frequency, g = 0.5

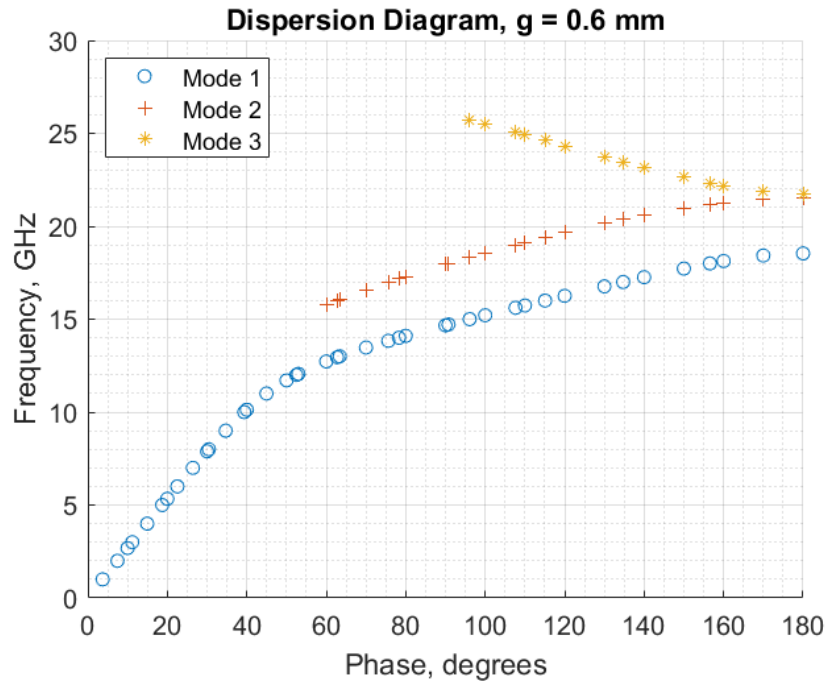


Figure 461: Circle Rogers 3010: Dispersion Diagram, $g = 0.6$

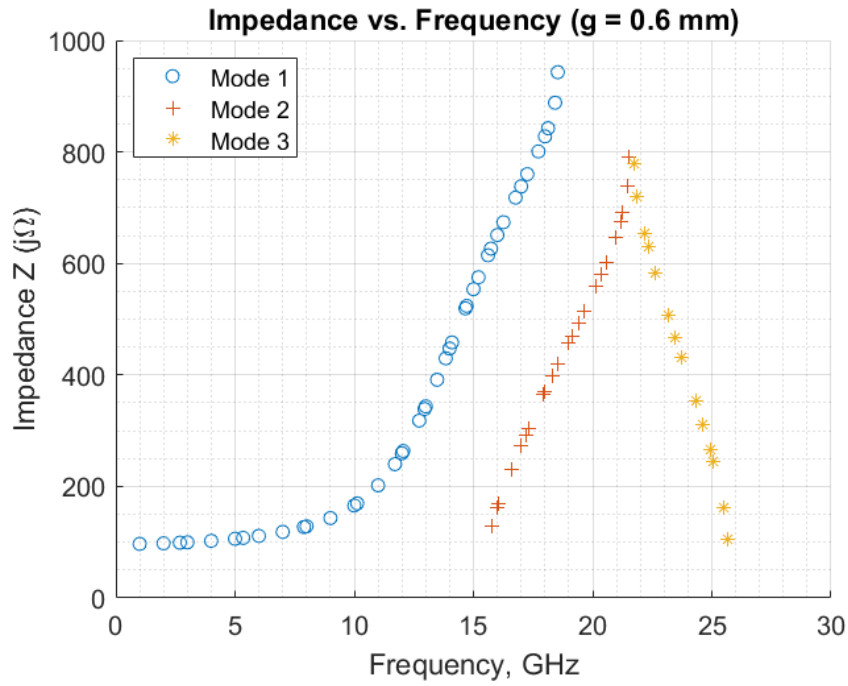


Figure 462: Circle Rogers 3010: Impedance vs. Frequency, $g = 0.6$

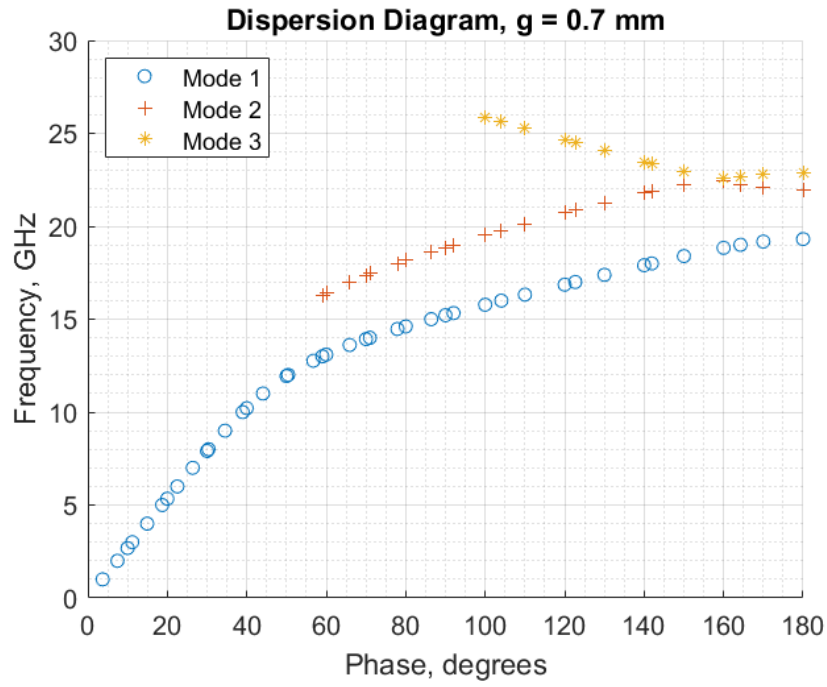


Figure 463: Circle Rogers 3010: Dispersion Diagram, g = 0.7

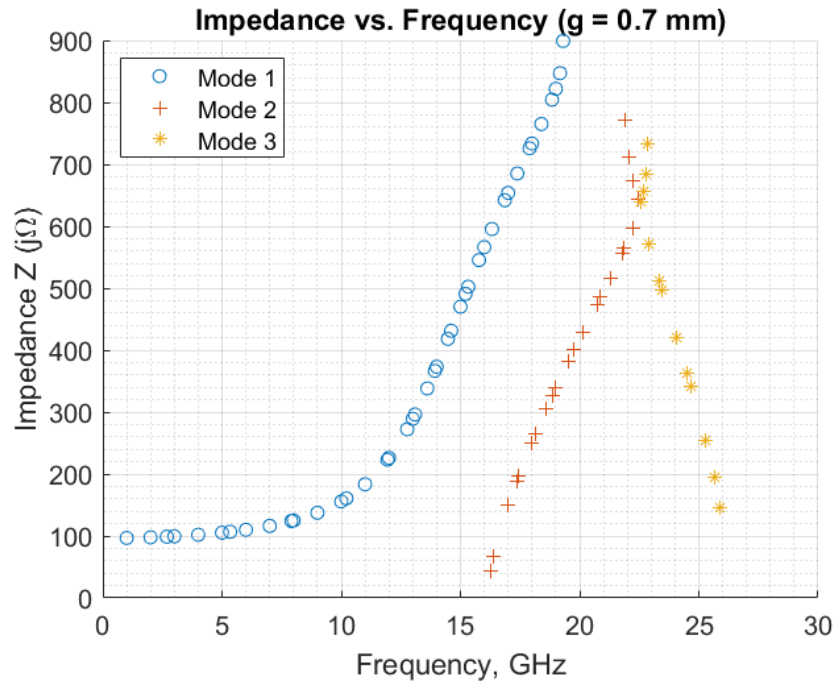


Figure 464: Circle Rogers 3010: Impedance vs. Frequency, g = 0.7

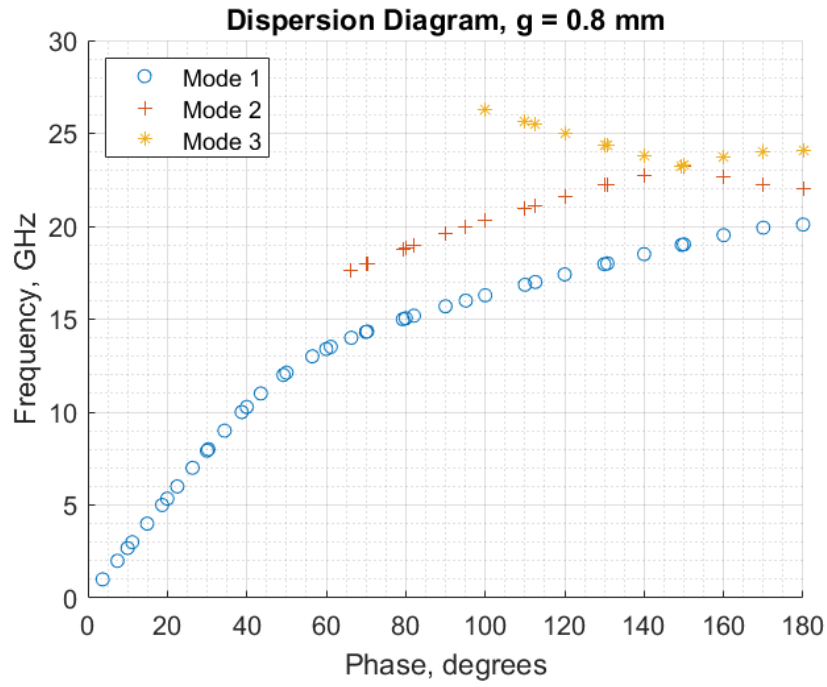


Figure 465: Circle Rogers 3010: Dispersion Diagram, $g = 0.8$

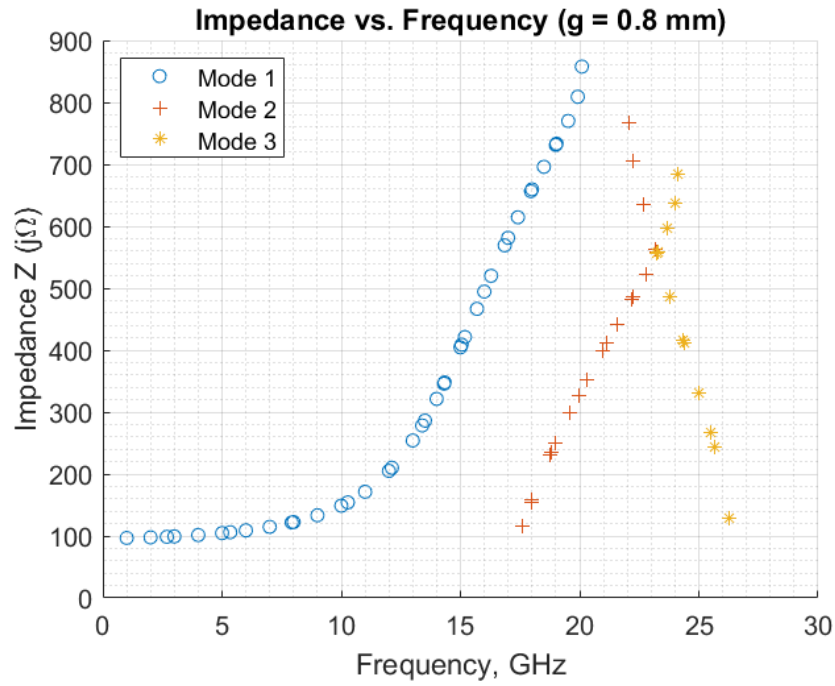


Figure 466: Circle Rogers 3010: Impedance vs. Frequency, $g = 0.8$

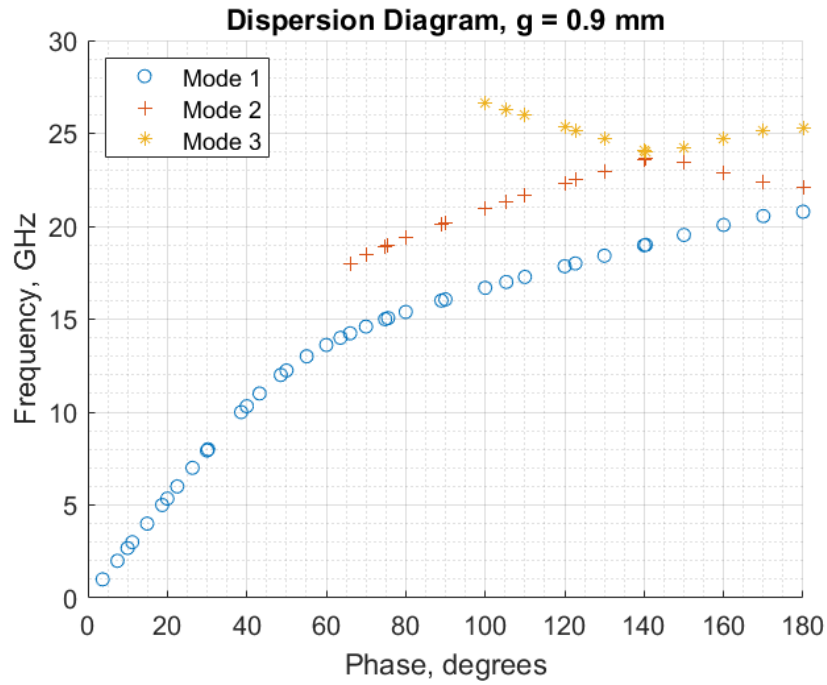


Figure 467: Circle Rogers 3010: Dispersion Diagram, g = 0.9

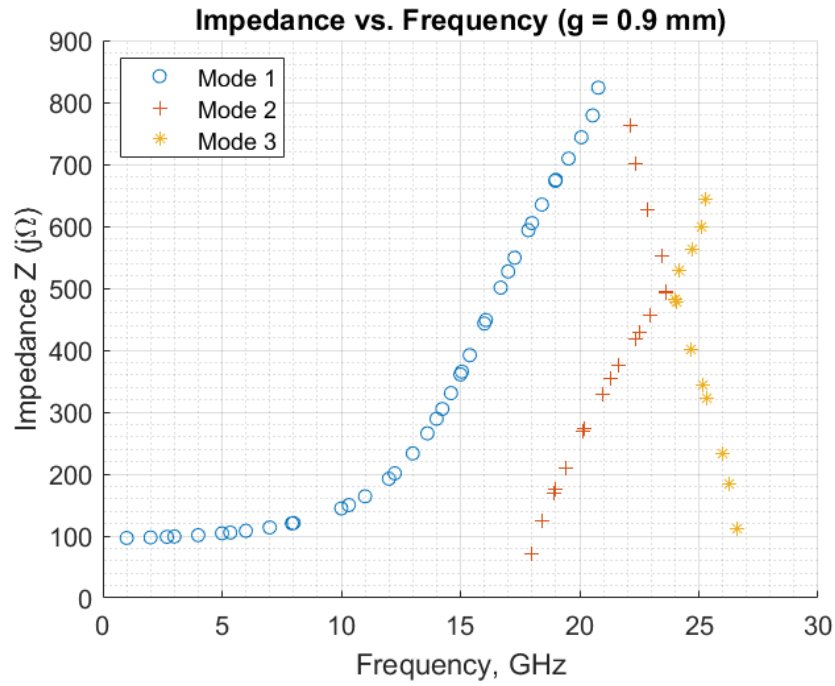


Figure 468: Circle Rogers 3010: Impedance vs. Frequency, g = 0.9

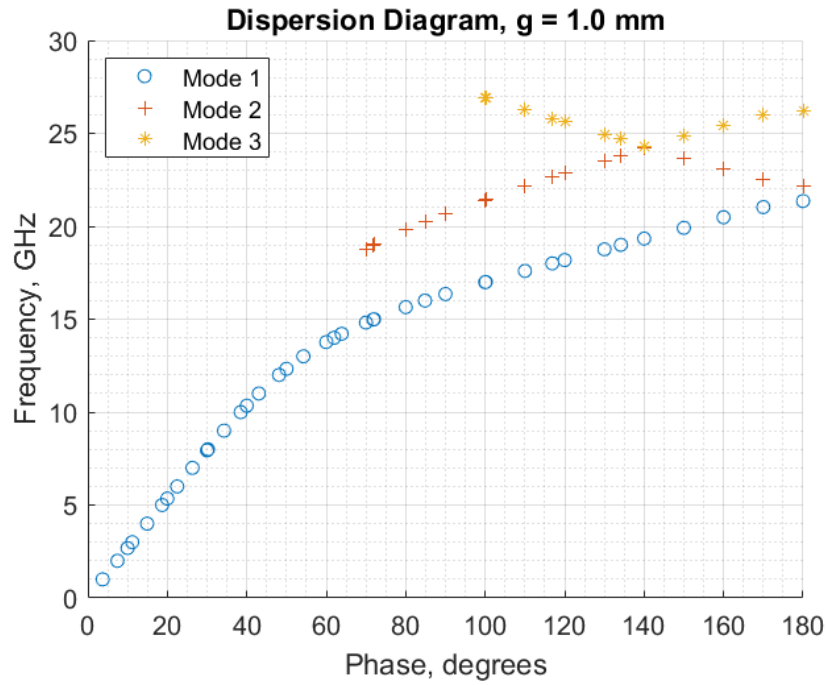


Figure 469: Circle Rogers 3010: Dispersion Diagram, g = 1.0

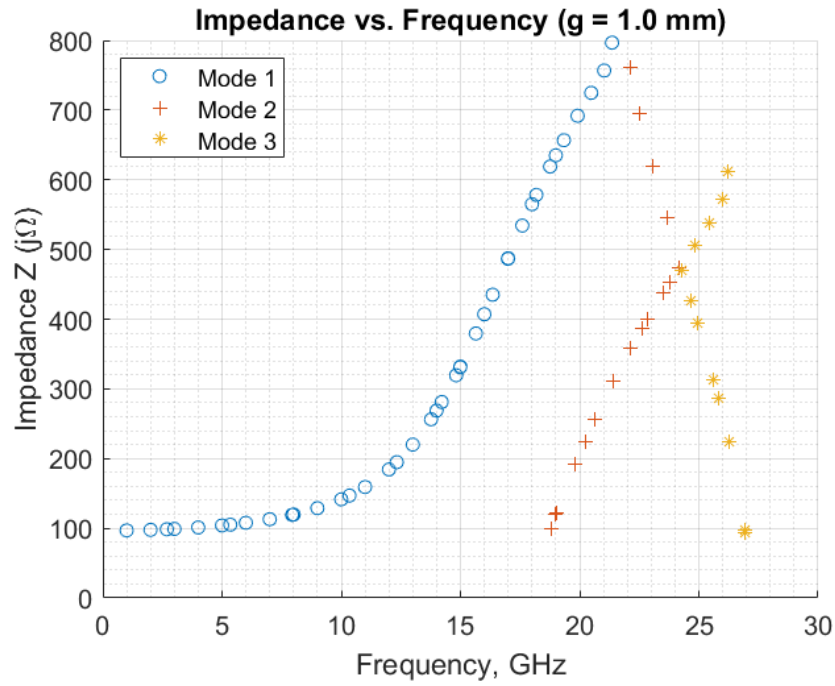


Figure 470: Circle Rogers 3010: Impedance vs. Frequency, g = 1.0

Model: 1 GHz

Equation form: $y = c_0 + c_1x^1 + c_2x^2 + c_3x^3$

	Coefficient	SE	tStat	pValue
c_0 (intercept)	97.4	0.0051544	18896	7.8781×10^{-21}
c_1	-1.1678	0.031829	-36.689	2.8326×10^{-7}
c_2	0.86447	0.057861	14.941	2.4313×10^{-5}
c_3	-0.25448	0.031918	-7.9729	0.00050081

Table 87: Model Coefficients: 1 GHz

Model Statistics

Error Degrees of Freedom: 5
 Root Mean Squared Error (RMSE): 0.00121
 R-squared: 1
 Adjusted R-Squared: 1
 F-statistic vs. constant model: 2.73×10^4
 p-value = 5.94×10^{-11}

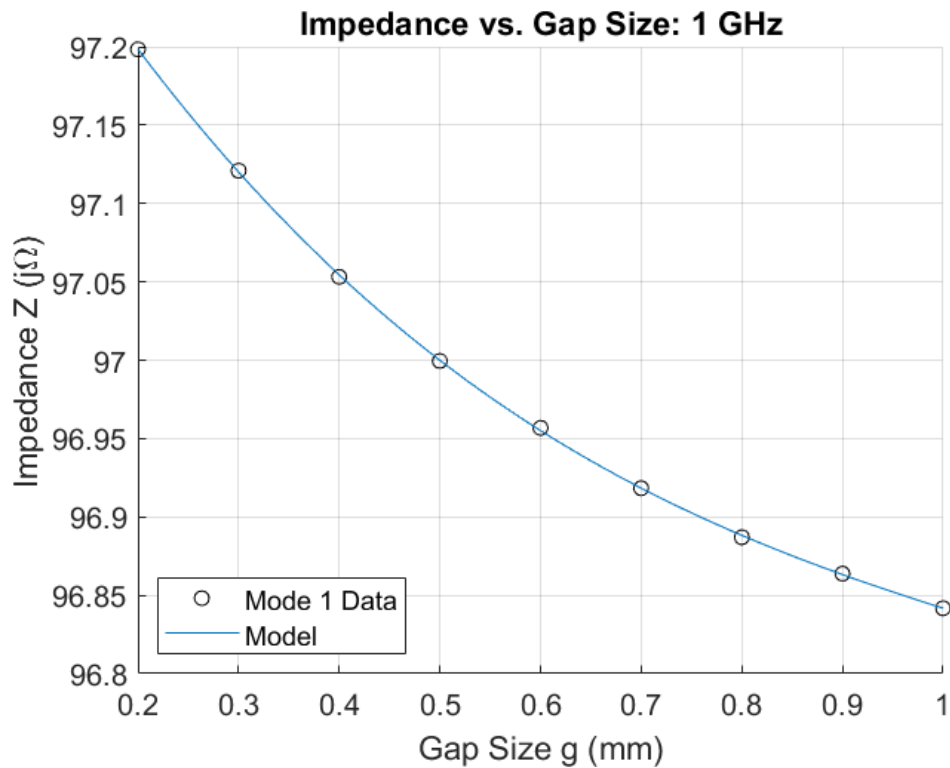


Figure 471: Circle Rogers 3010: Impedance vs. Gap Size, 1 GHz

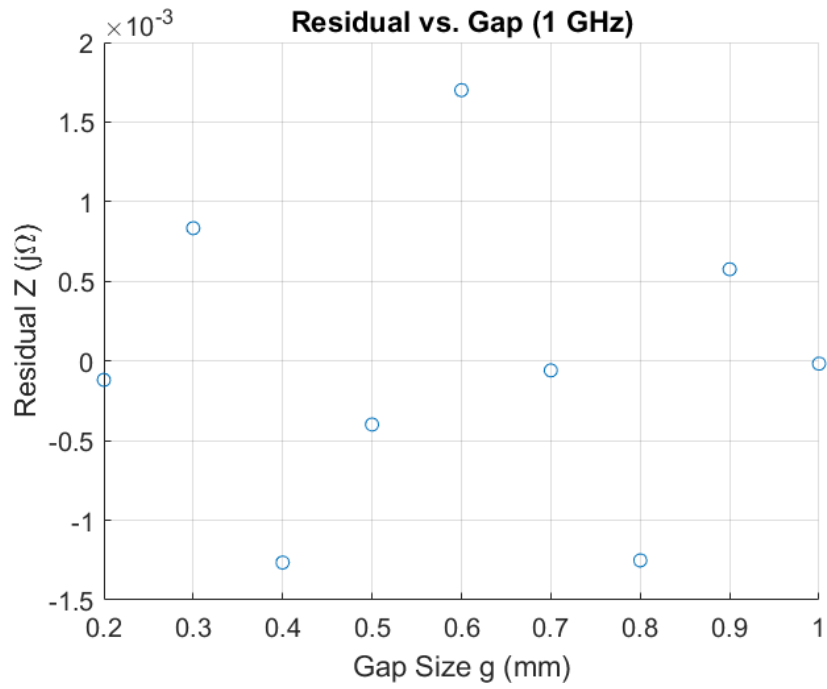


Figure 472: Circle Rogers 3010: Residuals, 1 GHz

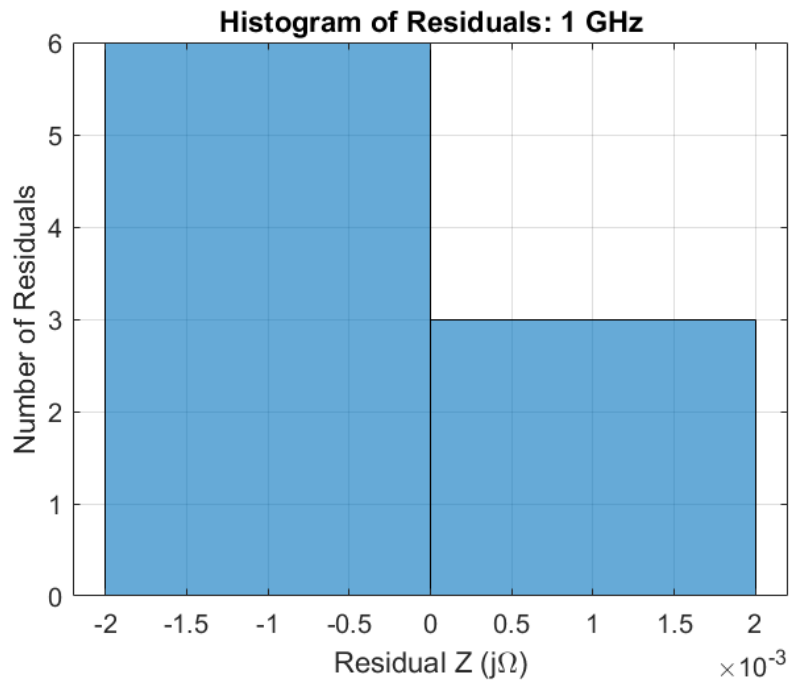


Figure 473: Circle Rogers 3010: Histogram of Residuals, 1 GHz

Model: 2 GHz

Equation form: $y = c_0 + c_1 \frac{1}{x^1} + c_2 \frac{1}{x^2}$

	<u>Coefficient</u>	<u>SE</u>	<u>tStat</u>	<u>pValue</u>
c_0 (intercept)	97.109	0.0098303	9878.6	7.2634×10^{-23}
c_1	0.60261	0.0083238	72.396	4.6742×10^{-10}
c_2	-0.051399	0.0013962	-36.813	2.681×10^{-8}

Table 88: Model Coefficients: 2 GHz

Model Statistics

Error Degrees of Freedom: 6
 Root Mean Squared Error (RMSE): 0.00602
 R-squared: 1
 Adjusted R-Squared: 1
 F-statistic vs. constant model: 1.78×10^4
 p-value = 4.76×10^{-12}

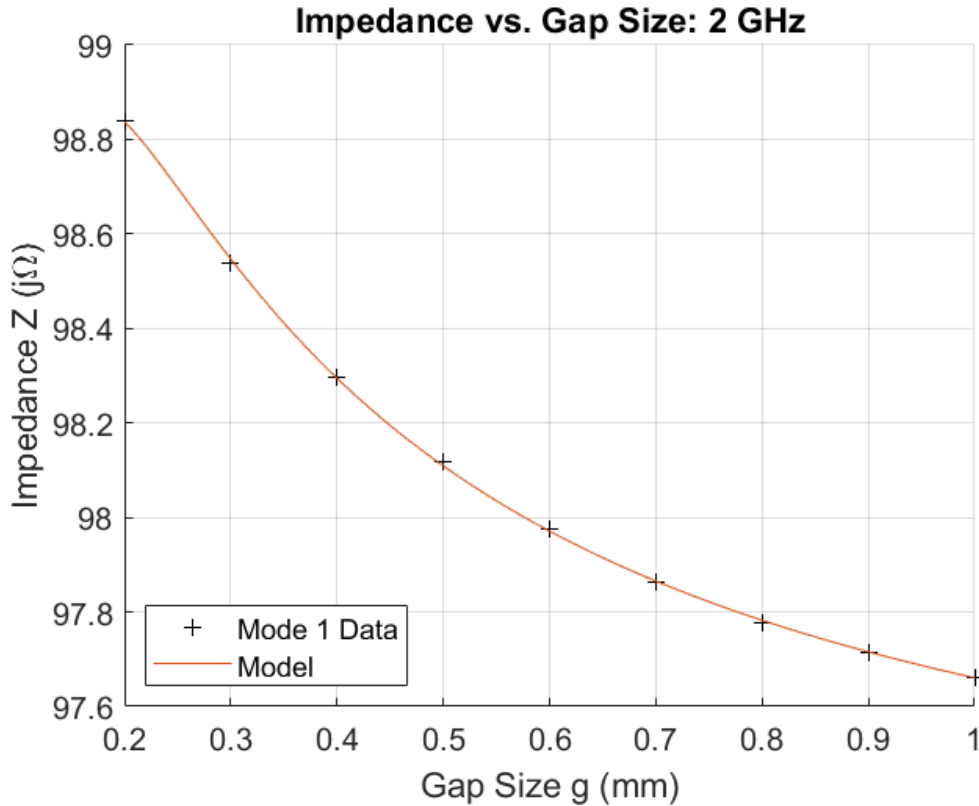


Figure 474: Circle Rogers 3010: Impedance vs. Gap Size, 2 GHz

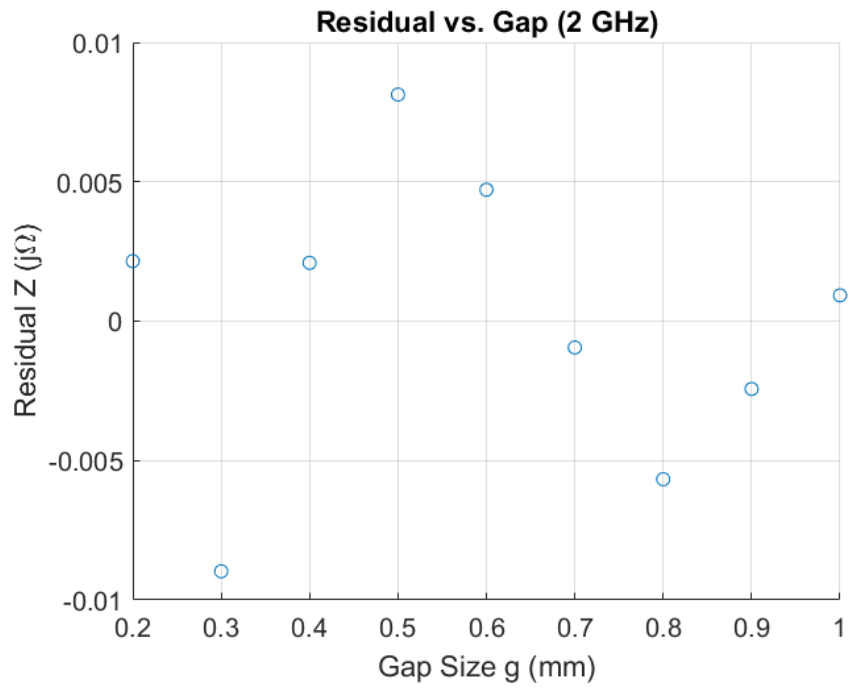


Figure 475: Circle Rogers 3010: Residuals, 2 GHz

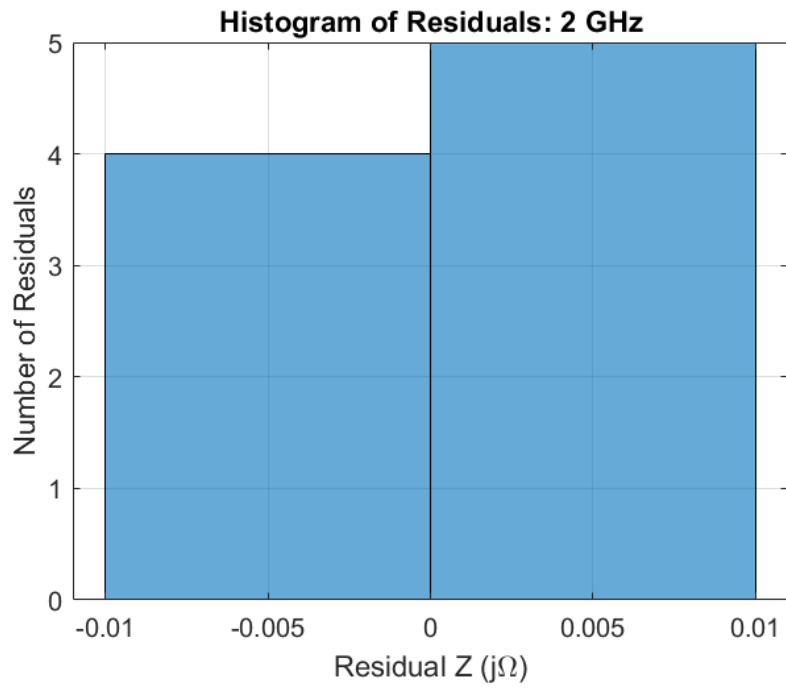


Figure 476: Circle Rogers 3010: Histogram of Residuals, 2 GHz

Model: 3 GHz

Equation form: $y = c_0 + c_1x^1 + c_2x^2$

	Coefficient	SE	tStat	pValue
c_0 (intercept)	103.2	0.10944	942.98	9.6004×10^{-17}
c_1	-8.3131	0.40677	-20.437	8.9243×10^{-7}
c_2	4.2457	0.33309	12.746	1.431×10^{-5}

Table 89: Model Coefficients: 3 GHz

Model Statistics

Error Degrees of Freedom: 6
 Root Mean Squared Error (RMSE): 0.0585
 R-squared: 0.997
 Adjusted R-Squared: 0.996
 F-statistic vs. constant model: 990
 p-value = 2.75×10^{-8}

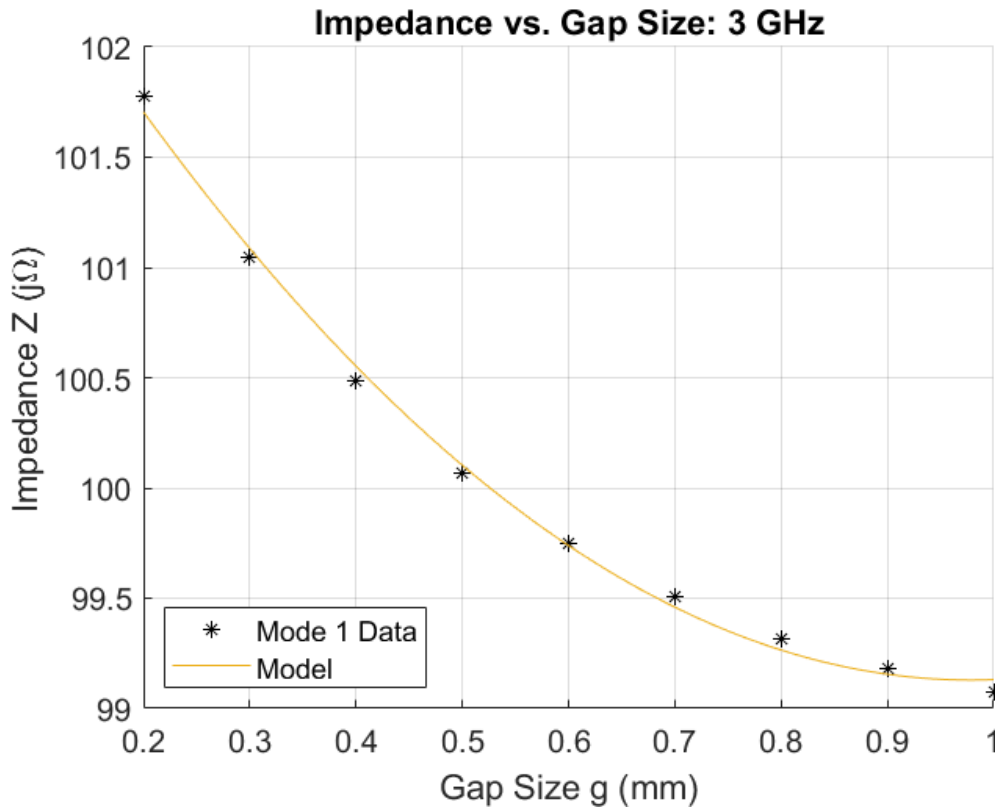


Figure 477: Circle Rogers 3010: Impedance vs. Gap Size, 3 GHz

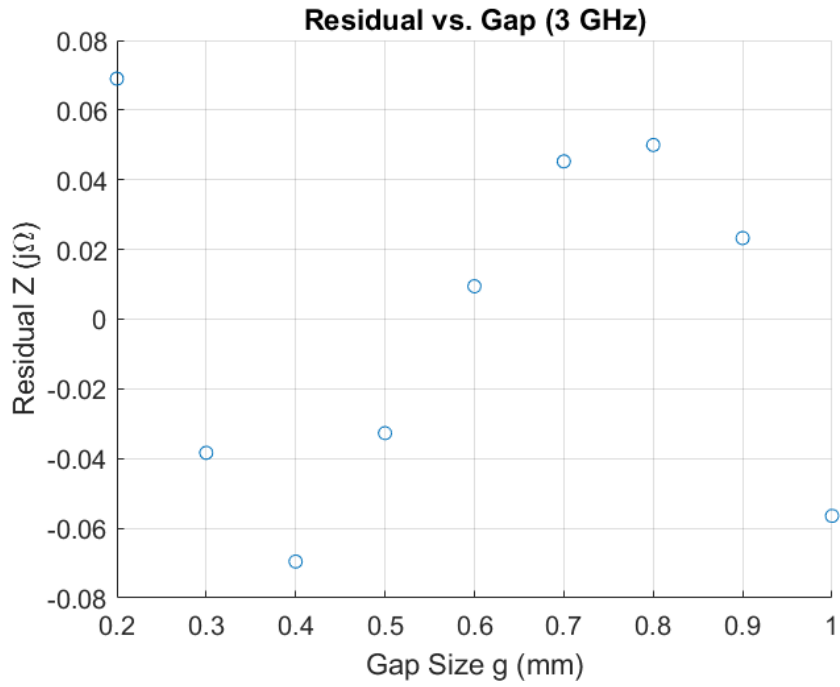


Figure 478: Circle Rogers 3010: Residuals, 3 GHz

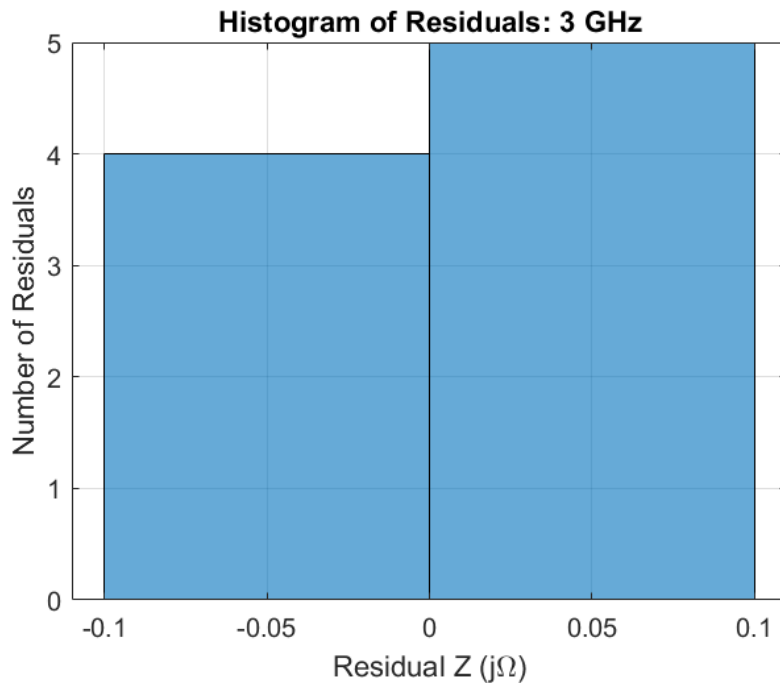


Figure 479: Circle Rogers 3010: Histogram of Residuals, 3 GHz

Model: 4 GHz

Equation form: $y = c_0 + c_1 \frac{1}{x^1} + c_2 \frac{1}{x^2}$

	<u>Coefficient</u>	<u>SE</u>	<u>tStat</u>	<u>pValue</u>
c_0 (intercept)	98.859	0.039669	2492.1	2.8181×10^{-19}
c_1	2.4464	0.03359	72.831	4.5094×10^{-10}
c_2	-0.18867	0.0056344	-33.485	4.722×10^{-8}

Table 90: Model Coefficients: 4 GHz

Model Statistics

Error Degrees of Freedom: 6
 Root Mean Squared Error (RMSE): 0.0243
 R-squared: 1
 Adjusted R-Squared: 1
 F-statistic vs. constant model: 2.14×10^4
 p-value = 2.76×10^{-12}

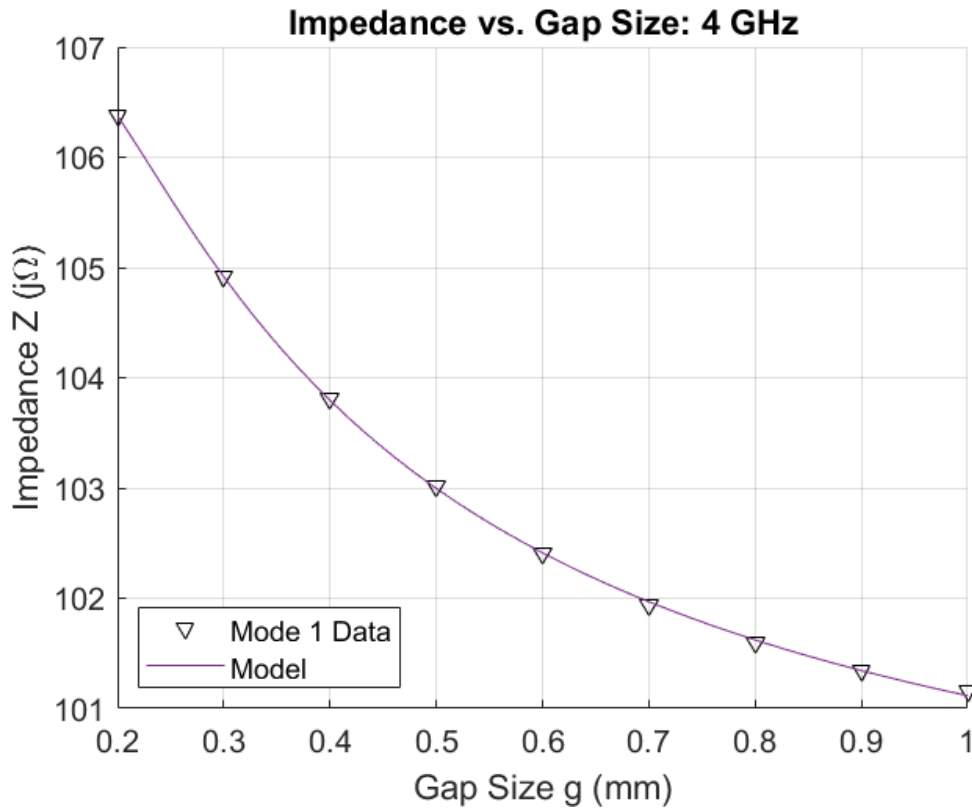


Figure 480: Circle Rogers 3010: Impedance vs. Gap Size, 4 GHz

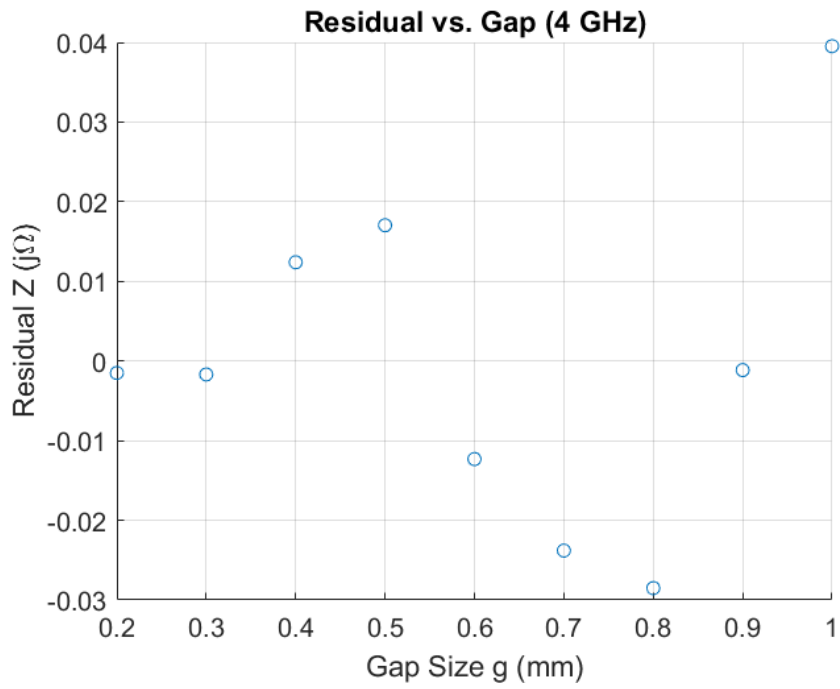


Figure 481: Circle Rogers 3010: Residuals, 4 GHz

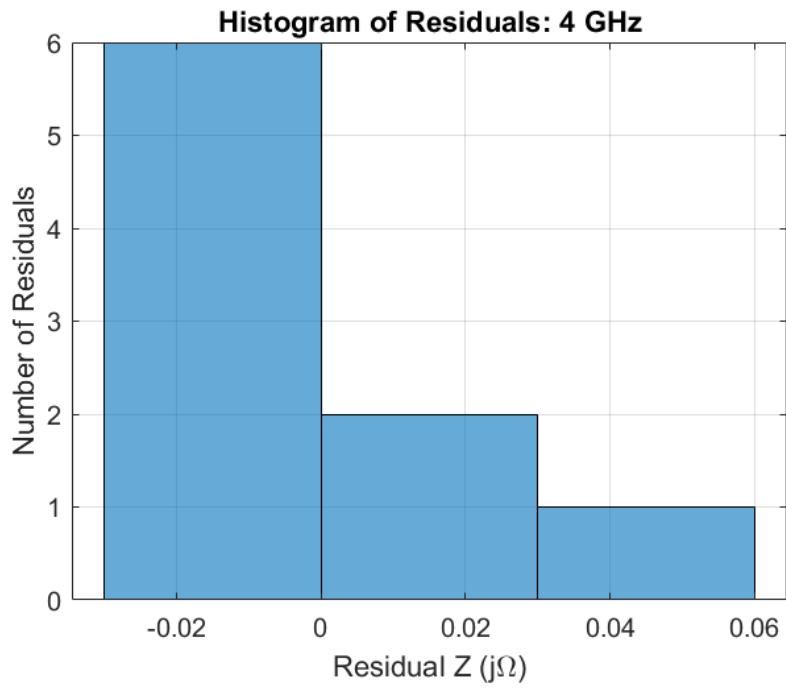


Figure 482: Circle Rogers 3010: Histogram of Residuals, 4 GHz

Model: 5 GHz

Equation form: $y = c_0 + c_1 \frac{1}{x^1} + c_2 \frac{1}{x^2}$

	Coefficient	SE	tStat	pValue
c_0 (intercept)	100.08	0.082851	1208	2.1722×10^{-17}
c_1	4.1577	0.070154	59.265	1.5508×10^{-9}
c_2	-0.30141	0.011768	-25.613	2.3341×10^{-7}

Table 91: Model Coefficients: 5 GHz

Model Statistics

Error Degrees of Freedom: 6
 Root Mean Squared Error (RMSE): 0.0508
 R-squared: 1
 Adjusted R-Squared: 1
 F-statistic vs. constant model: 1.55×10^4
 p-value = 7.23×10^{-12}

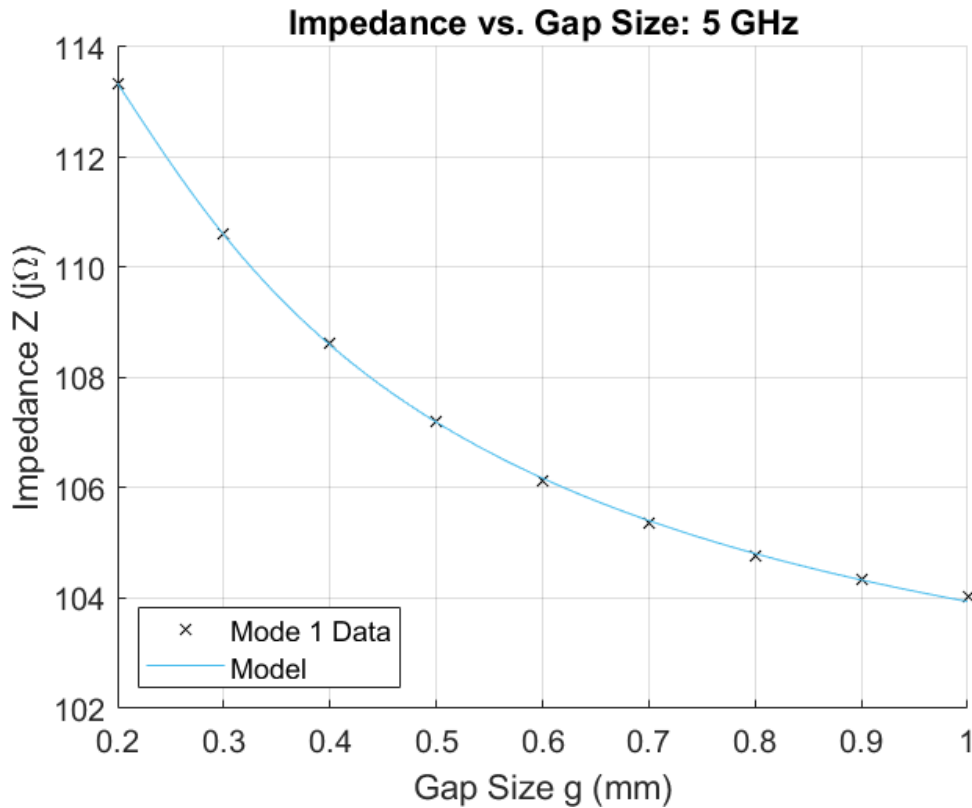


Figure 483: Circle Rogers 3010: Impedance vs. Gap Size, 5 GHz

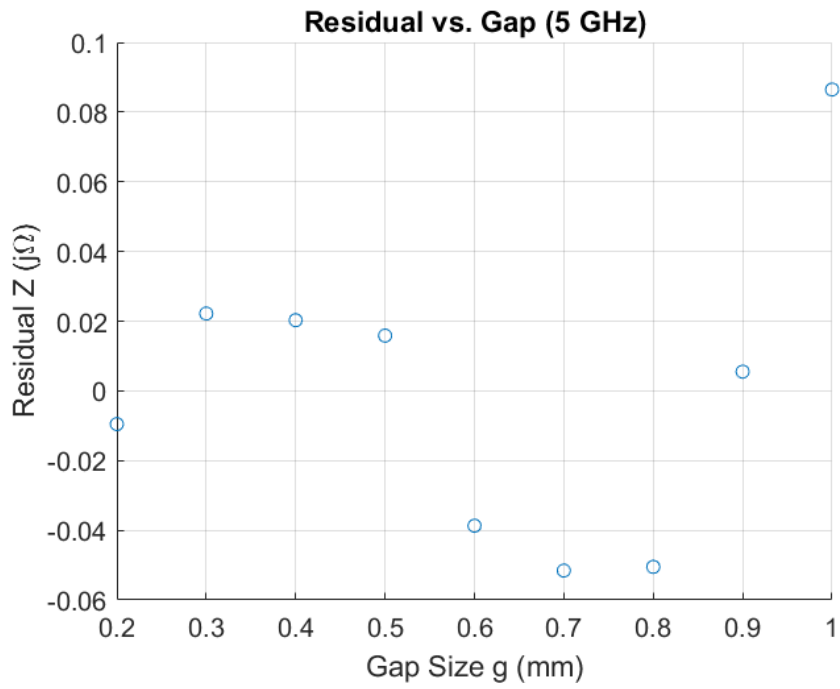


Figure 484: Circle Rogers 3010: Residuals, 5 GHz

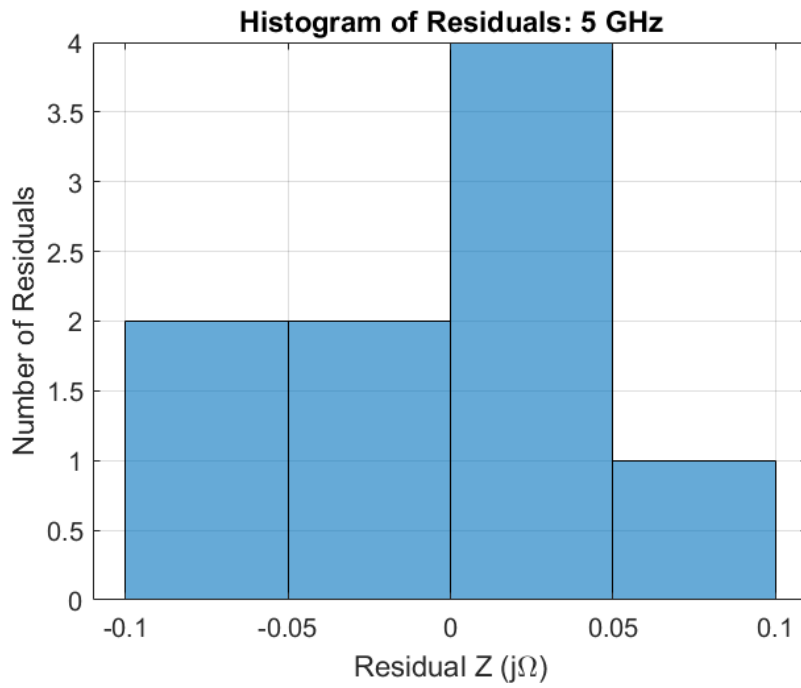


Figure 485: Circle Rogers 3010: Histogram of Residuals, 5 GHz

Model: 6 GHz

Equation form: $y = c_0 + c_1 \frac{1}{x^1} + c_2 \frac{1}{x^2} + c_3 \frac{1}{x^3} + c_4 \frac{1}{x^4}$

	<u>Coefficient</u>	<u>SE</u>	<u>tStat</u>	<u>pValue</u>
c_0 (intercept)	104.4	0.69374	150.49	1.1696×10^{-8}
c_1	1.4086	1.3106	1.0748	0.34298
c_2	2.7275	0.84467	3.2291	0.032002
c_3	-0.76108	0.22025	-3.4555	0.025923
c_4	0.063212	0.019662	3.215	0.032434

Table 92: Model Coefficients: 6 GHz

Model Statistics

Error Degrees of Freedom: 4

Root Mean Squared Error (RMSE): 0.045

R-squared: 1

Adjusted R-Squared: 1

F-statistic vs. constant model: 2.95×10^4

p-value = 3.44×10^{-9}

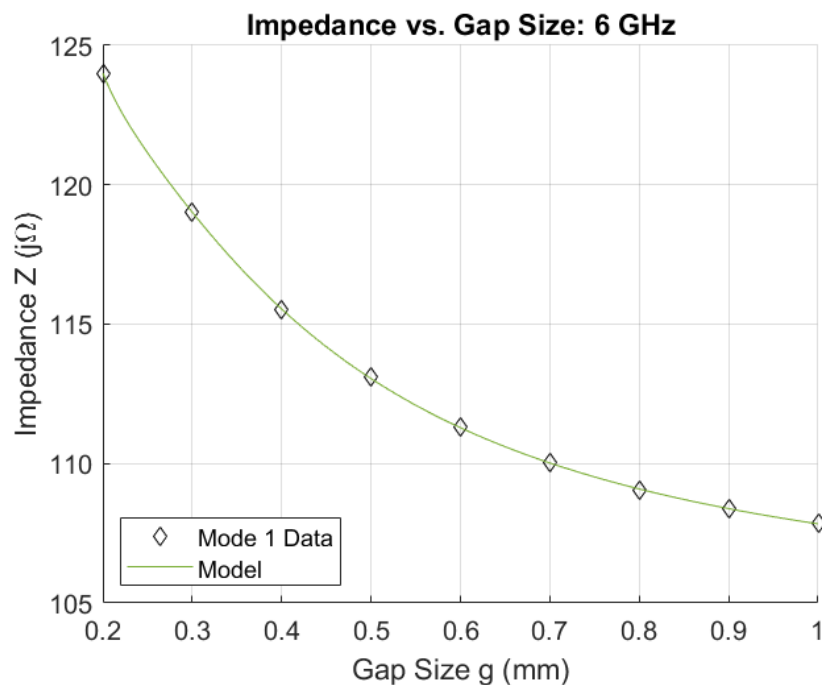


Figure 486: Circle Rogers 3010: Impedance vs. Gap Size, 6 GHz

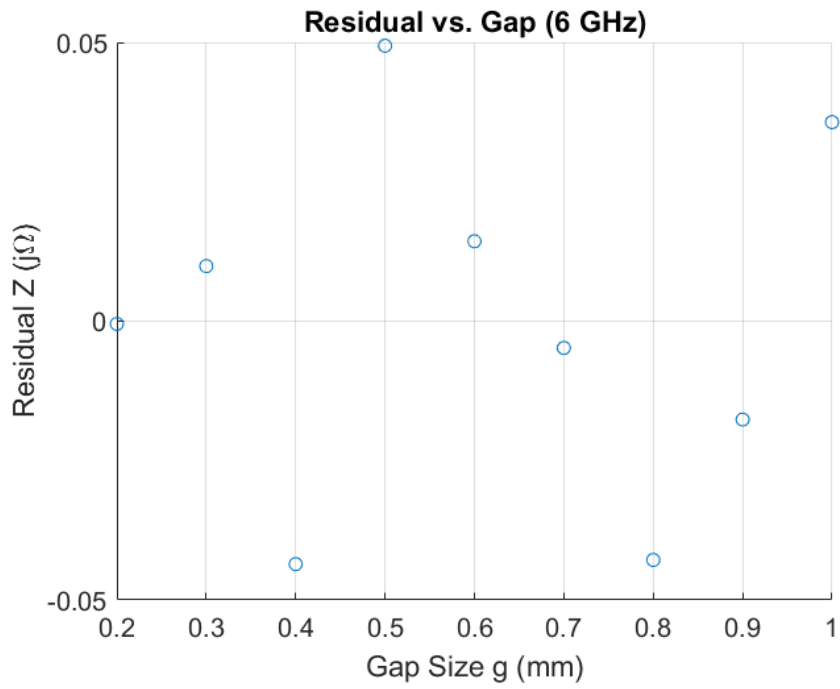


Figure 487: Circle Rogers 3010: Residuals, 6 GHz

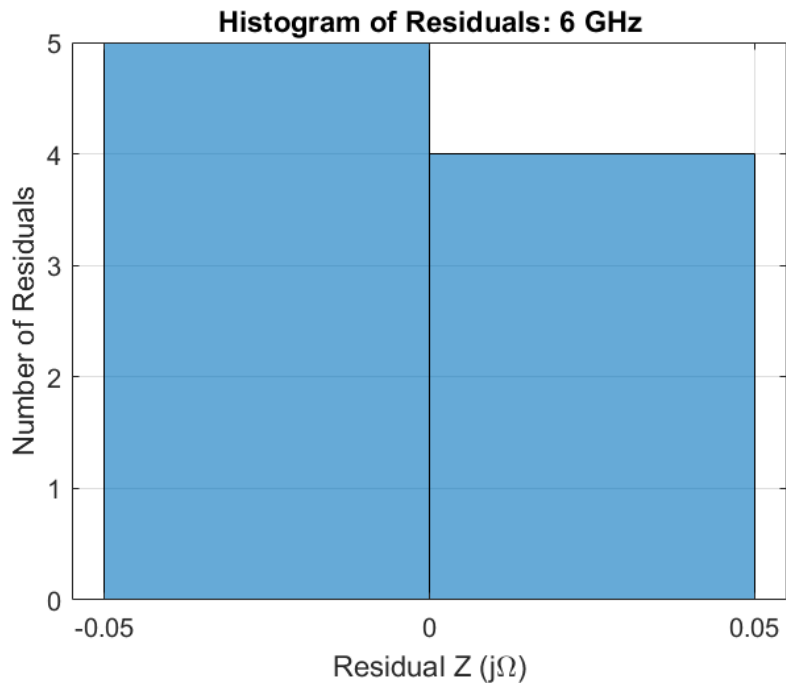


Figure 488: Circle Rogers 3010: Histogram of Residuals, 6 GHz

Model: 7 GHz

Equation form: $y = c_0 + c_1 \frac{1}{x^1} + c_2 \frac{1}{x^2}$

	Coefficient	SE	tStat	pValue
c_0 (intercept)	102.16	0.48354	211.28	7.5868×10^{-13}
c_1	11.091	0.40944	27.09	1.6719×10^{-7}
c_2	-0.69131	0.068679	-10.066	5.5792×10^{-5}

Table 93: Model Coefficients: 7 GHz

Model Statistics

Error Degrees of Freedom: 6
 Root Mean Squared Error (RMSE): 0.296
 R-squared: 0.999
 Adjusted R-Squared: 0.999
 F-statistic vs. constant model: 3.91×10^3
 p-value = 4.5×10^{-10}

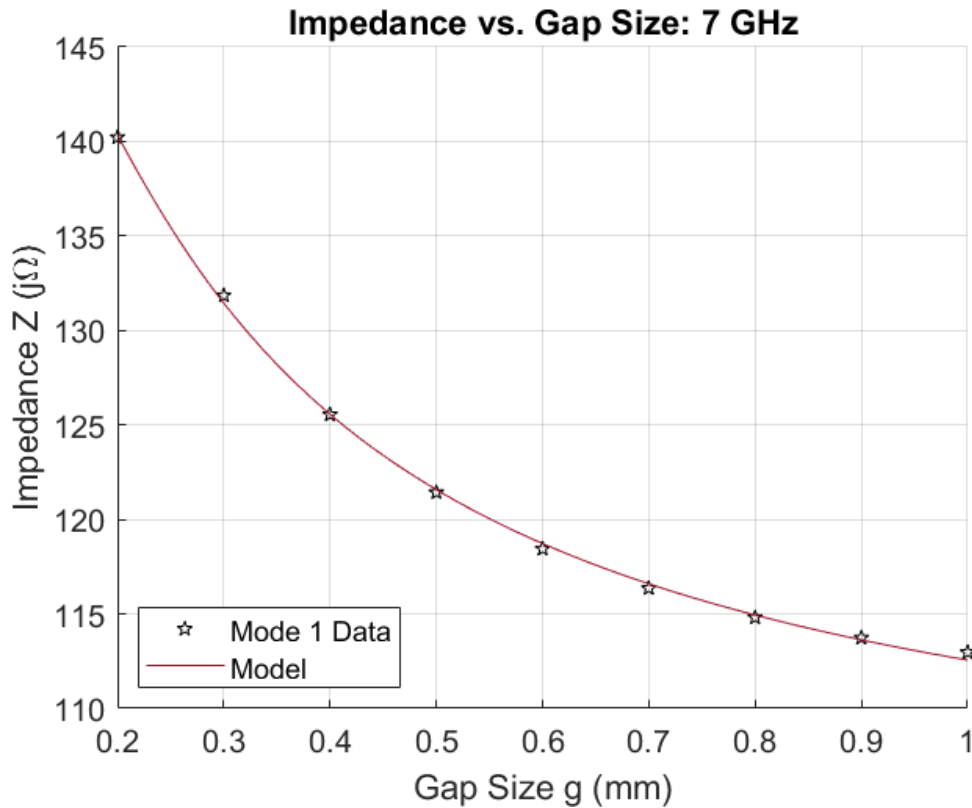


Figure 489: Circle Rogers 3010: Impedance vs. Gap Size, 7 GHz

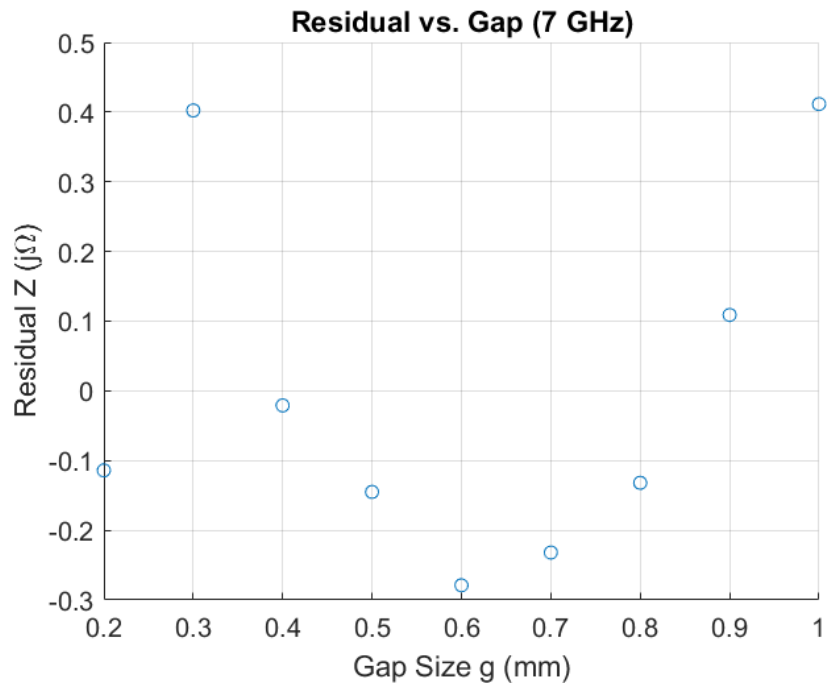


Figure 490: Circle Rogers 3010: Residuals, 7 GHz

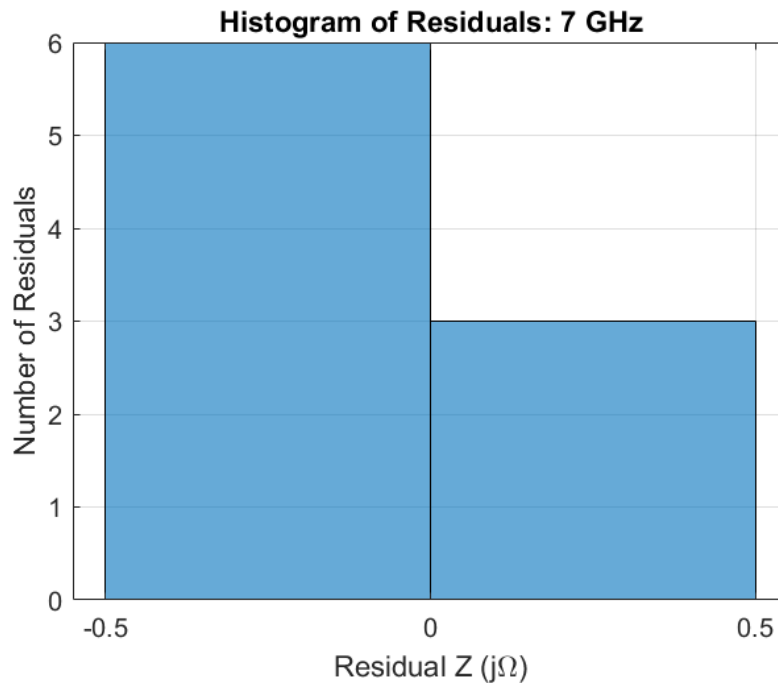


Figure 491: Circle Rogers 3010: Histogram of Residuals, 7 GHz

Model: 8 GHz

Equation form: $y = c_0 + c_1 \frac{1}{x^1} + c_2 \frac{1}{x^2}$

	<u>Coefficient</u>	<u>SE</u>	<u>tStat</u>	<u>pValue</u>
c_0 (intercept)	102.46	1.0616	96.516	8.3361×10^{-11}
c_1	17.192	0.89892	19.125	1.3218×10^{-6}
c_2	-0.71299	0.15078	-4.7285	0.0032294

Table 94: Model Coefficients: 8 GHz

Model Statistics

Error Degrees of Freedom: 6
 Root Mean Squared Error (RMSE): 0.65
 R-squared: 0.999
 Adjusted R-Squared: 0.999
 F-statistic vs. constant model: 2.74×10^3
 p-value = 1.3×10^{-9}

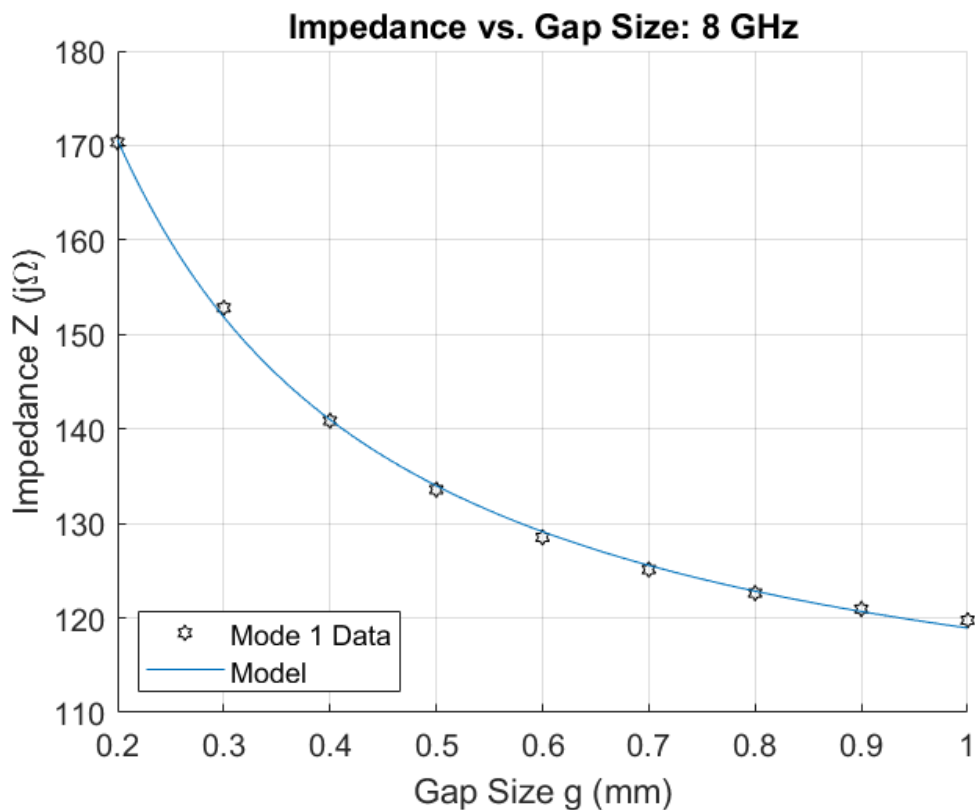


Figure 492: Circle Rogers 3010: Impedance vs. Gap Size, 8 GHz

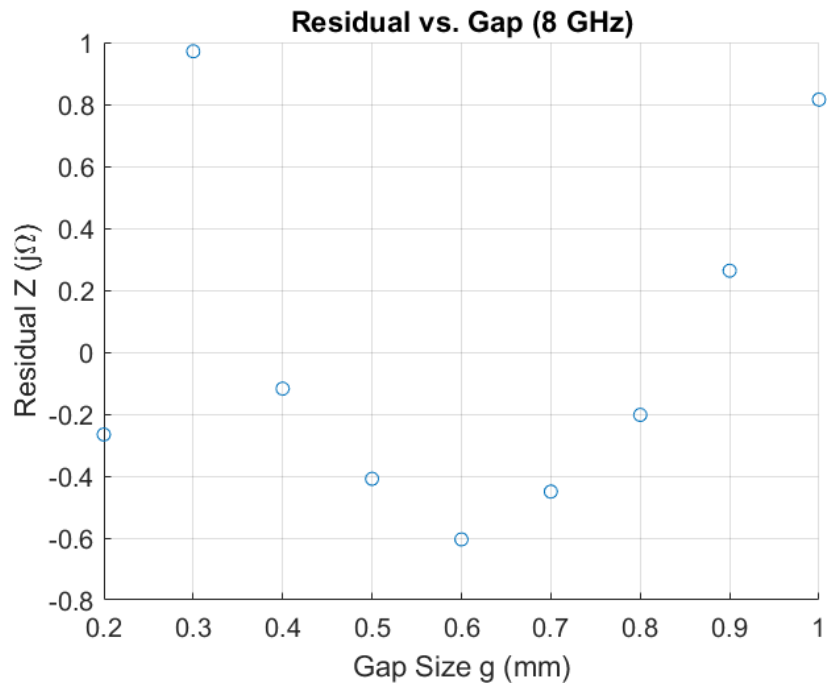


Figure 493: Circle Rogers 3010: Residuals, 8 GHz

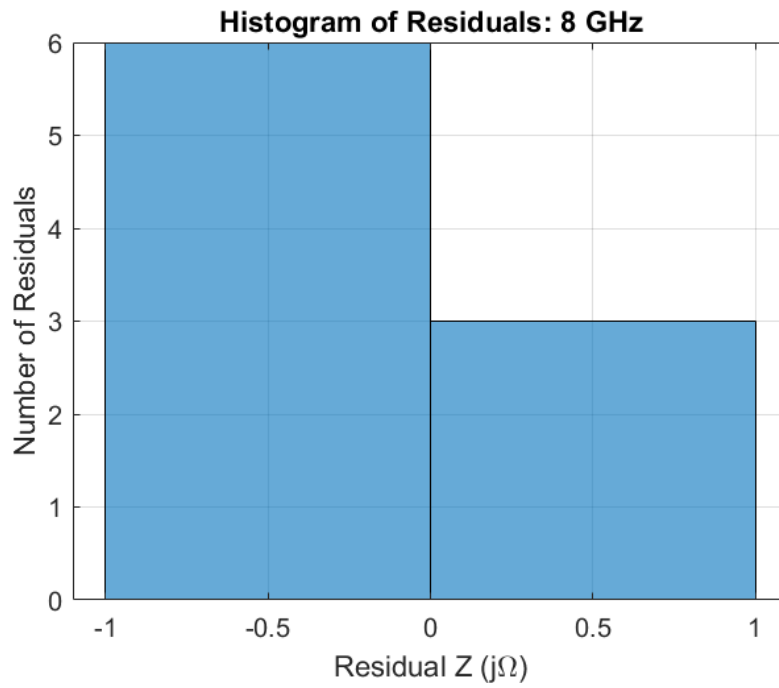


Figure 494: Circle Rogers 3010: Histogram of Residuals, 8 GHz

Model: 9 GHz

Equation form: $y = c_0 + c_1 \frac{1}{x^1} + c_2 \frac{1}{x^2}$

	<u>Coefficient</u>	<u>SE</u>	<u>tStat</u>	<u>pValue</u>
c_0 (intercept)	107.47	2.6609	40.388	1.7547×10^{-7}
c_1	20.069	2.166	9.2656	0.00024615
c_2	0.97563	0.35696	2.7331	0.041127

Table 95: Model Coefficients: 9 GHz

Model Statistics

Error Degrees of Freedom: 5

Root Mean Squared Error (RMSE): 1.47

R-squared: 0.999

Adjusted R-Squared: 0.998

F-statistic vs. constant model: 1.93×10^3

p-value = 6×10^{-8}

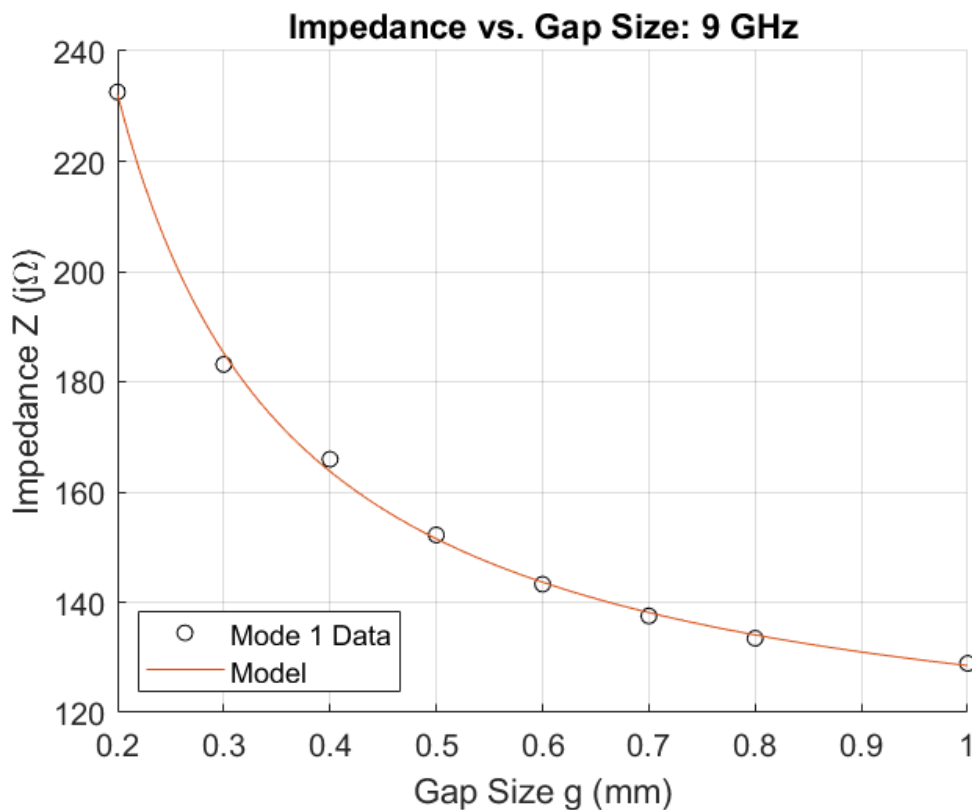


Figure 495: Circle Rogers 3010: Impedance vs. Gap Size, 9 GHz

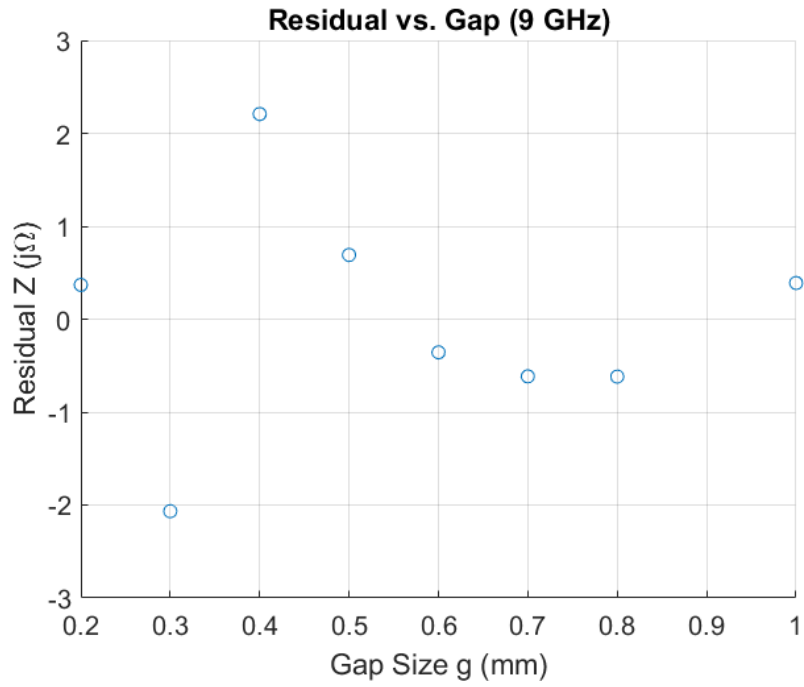


Figure 496: Circle Rogers 3010: Residuals, 9 GHz

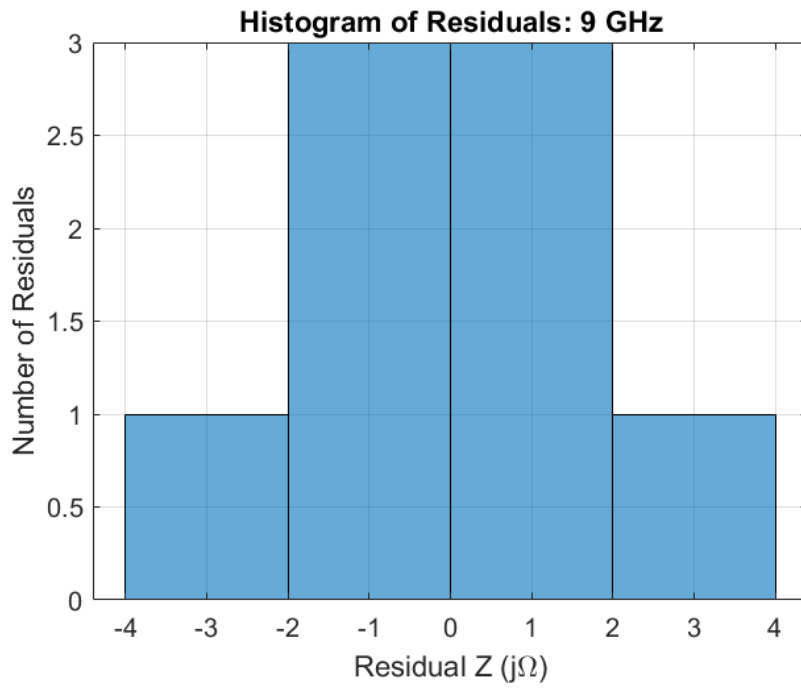


Figure 497: Circle Rogers 3010: Histogram of Residuals, 9 GHz

Model: 10 GHz

Equation form: $y = c_0 + c_1 \frac{1}{x^1} + c_2 \frac{1}{x^2} + c_3 \frac{1}{x^3}$

	<u>Coefficient</u>	<u>SE</u>	<u>tStat</u>	<u>pValue</u>
c_0 (intercept)	124.77	3.1907	39.104	2.0614×10^{-7}
c_1	-0.023797	4.2784	-0.0055622	0.99578
c_2	17.82	1.6584	10.745	0.00012098
c_3	-1.6996	0.18815	-9.0331	0.00027779

Table 96: Model Coefficients: 10 GHz

Model Statistics

Error Degrees of Freedom: 5
 Root Mean Squared Error (RMSE): 0.688
 R-squared: 1
 Adjusted R-Squared: 1
 F-statistic vs. constant model: 2.88×10^4
 p-value = 5.19×10^{-11}

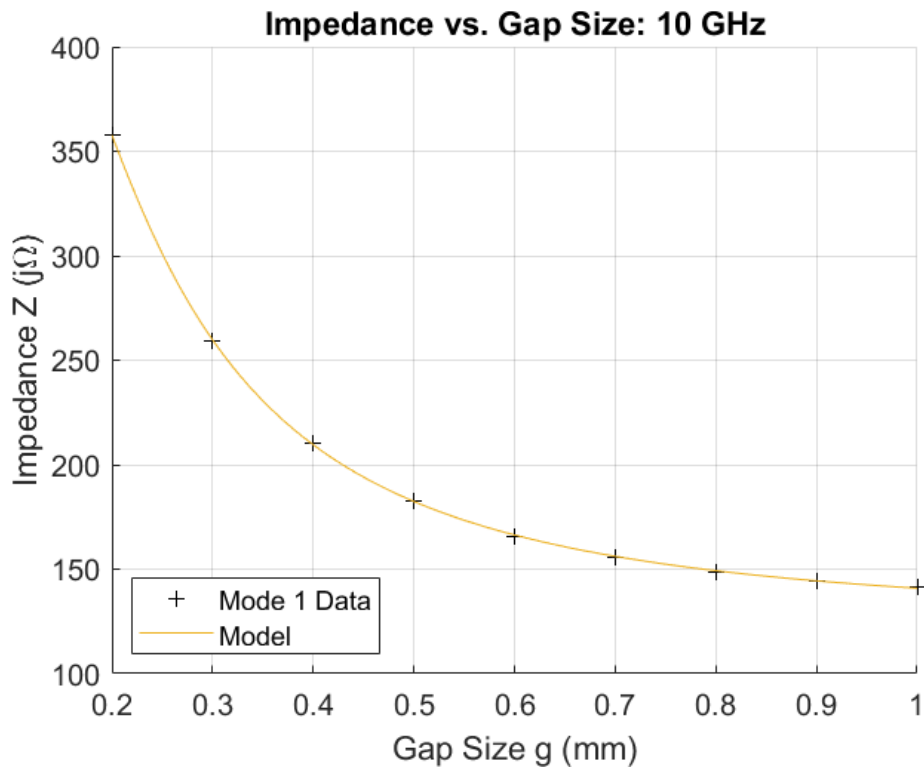


Figure 498: Circle Rogers 3010: Impedance vs. Gap Size, 10 GHz

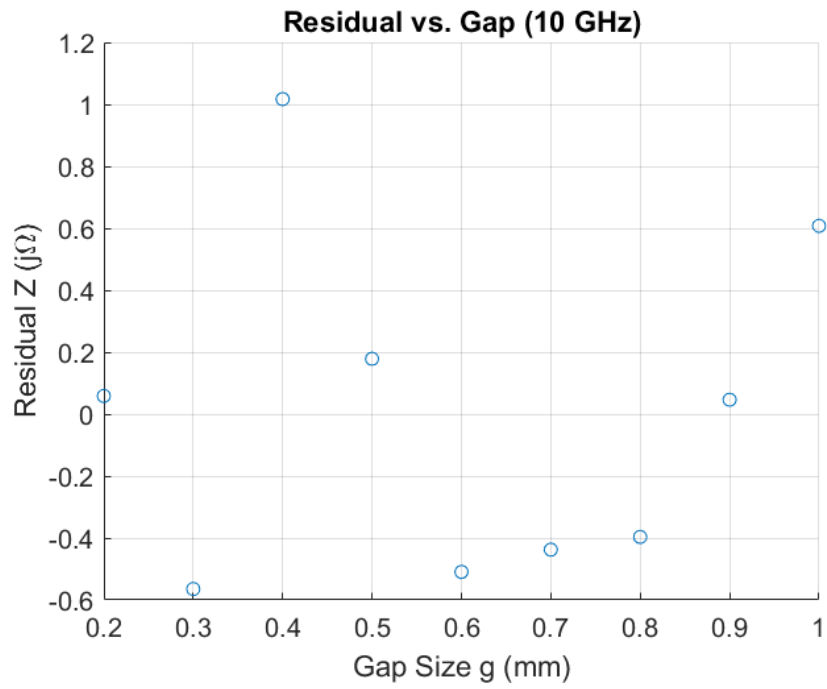


Figure 499: Circle Rogers 3010: Residuals, 10 GHz

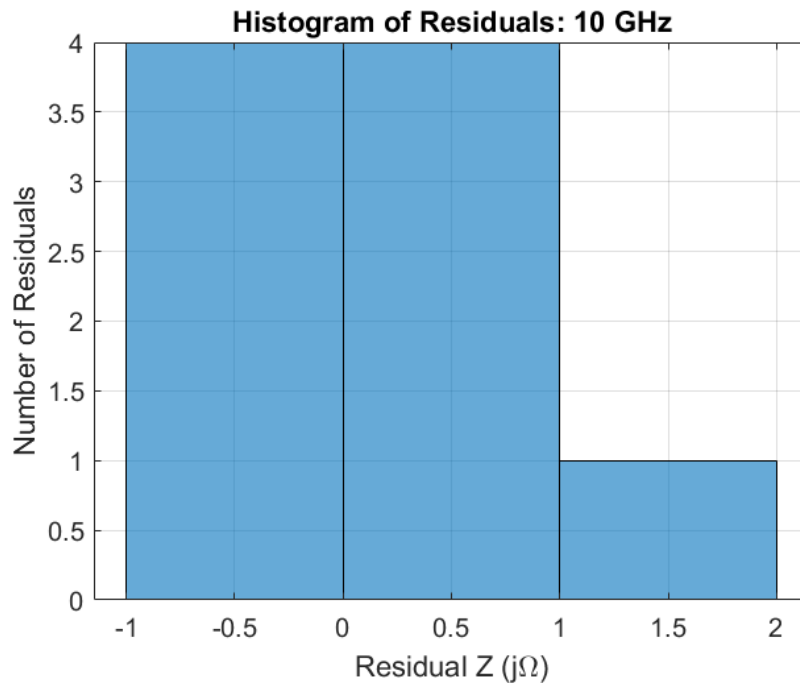


Figure 500: Circle Rogers 3010: Histogram of Residuals, 10 GHz

Model: 11 GHz

Equation form: $y = c_0 + c_1x^1 + c_2x^2 + c_3x^3 + c_4x^4$

	Coefficient	SE	tStat	pValue
c_0 (intercept)	1001.1	6.4123	156.12	1.0098×10^{-8}
c_1	-3291.7	55.496	-59.314	4.8383×10^{-7}
c_2	5076.8	161.6	31.417	6.1176×10^{-6}
c_3	-3604.4	191.79	-18.793	4.7205×10^{-5}
c_4	977.19	79.628	12.272	0.00025323

Table 97: Model Coefficients: 11 GHz

Model Statistics

Error Degrees of Freedom: 4

Root Mean Squared Error (RMSE): 0.611

R-squared: 1

Adjusted R-Squared: 1

F-statistic vs. constant model: 8×10^4

p-value = 4.68×10^{-10}

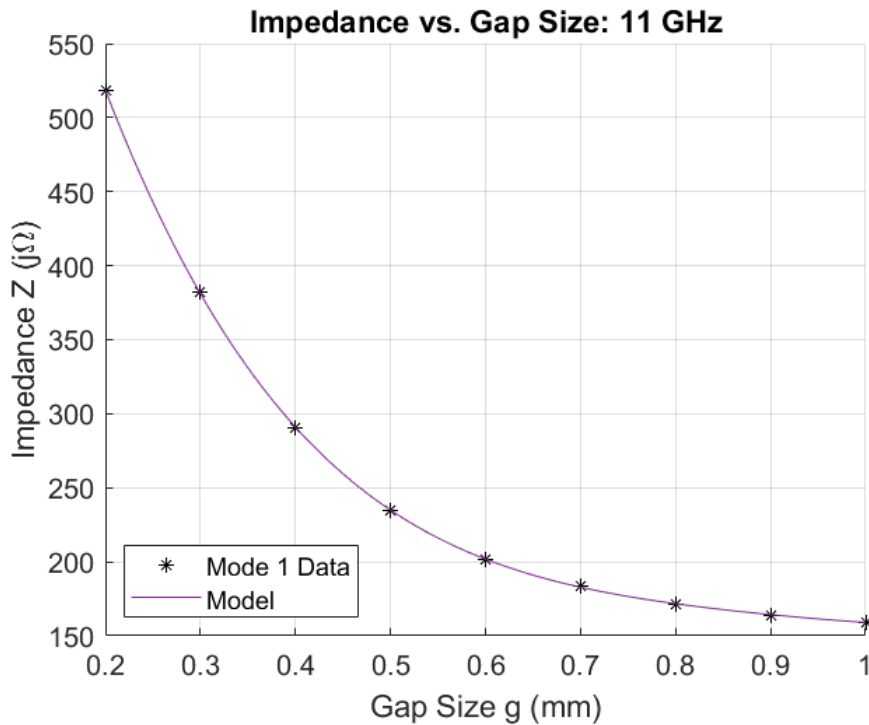


Figure 501: Circle Rogers 3010: Impedance vs. Gap Size, 11 GHz

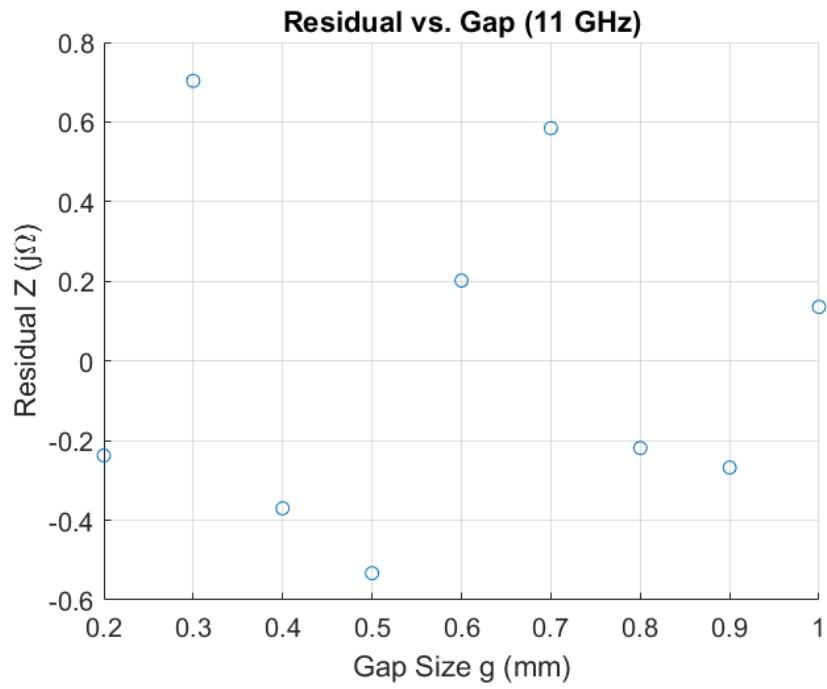


Figure 502: Circle Rogers 3010: Residuals, 11 GHz

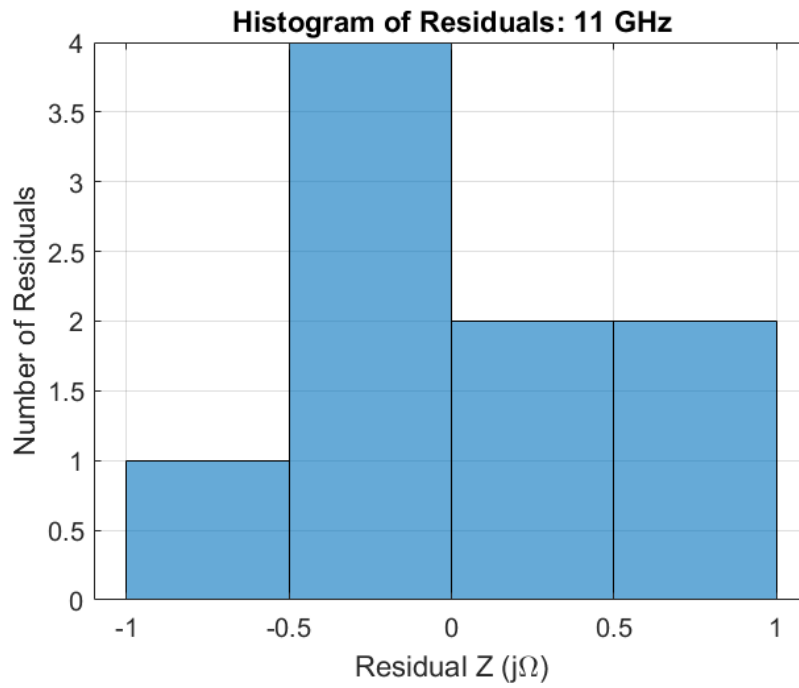


Figure 503: Circle Rogers 3010: Histogram of Residuals, 11 GHz

Model: 12 GHz

Equation form: $y = c_0 + c_1x^1 + c_2x^2 + c_3x^3$

	Coefficient	SE	tStat	pValue
c_0 (intercept)	1077.9	26.665	40.422	1.7474×10^{-7}
c_1	-2538.2	164.66	-15.414	2.0858×10^{-5}
c_2	2443.5	299.33	8.1631	0.00044835
c_3	797.35	165.12	-4.829	0.0047608

Table 98: Model Coefficients: 12 GHz

Model Statistics

Error Degrees of Freedom: 5
 Root Mean Squared Error (RMSE): 6.23
 R-squared: 0.999
 Adjusted R-Squared: 0.999
 F-statistic vs. constant model: 1.9×10^3
 p-value = 4.65×10^{-8}

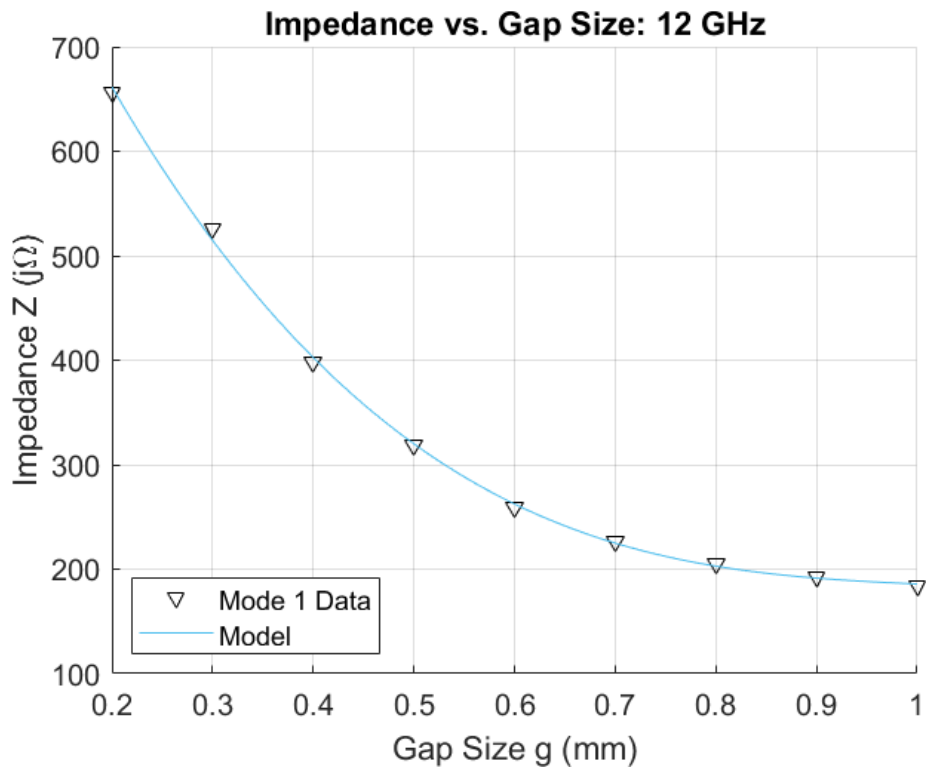


Figure 504: Circle Rogers 3010: Impedance vs. Gap Size, 12 GHz

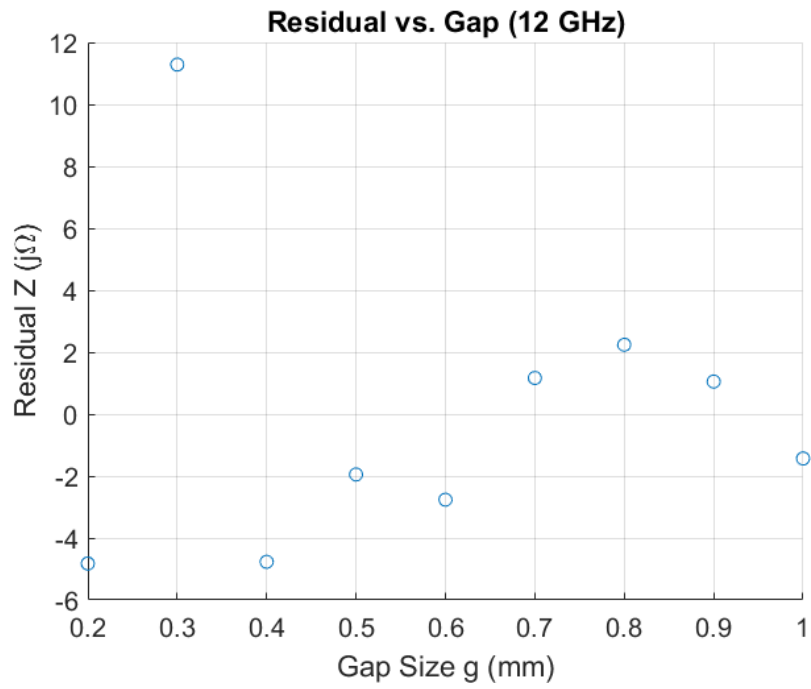


Figure 505: Circle Rogers 3010: Residuals, 12 GHz

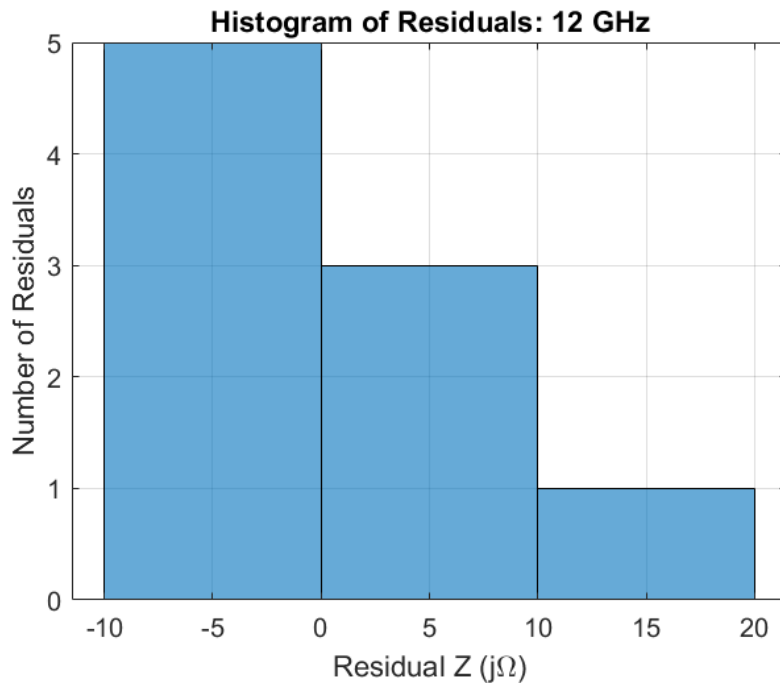


Figure 506: Circle Rogers 3010: Histogram of Residuals, 12 GHz

Model: 13 GHz

Equation form: $y = c_0 + c_1x^1 + c_2x^2$

	<u>Coefficient</u>	<u>SE</u>	<u>tStat</u>	<u>pValue</u>
c_0 (intercept)	1093.6	14.593	74.939	3.8005×10^{-10}
c_1	-1784.1	54.239	-32.894	5.252×10^{-8}
c_2	913.58	44.415	20.569	8.5887×10^{-7}

Table 99: Model Coefficients: 13 GHz

Model Statistics

Error Degrees of Freedom: 6

Root Mean Squared Error (RMSE): 7.79

R-squared: 0.999

Adjusted R-Squared: 0.998

F-statistic vs. constant model: 2.55×10^3

p-value = 1.63×10^{-9}

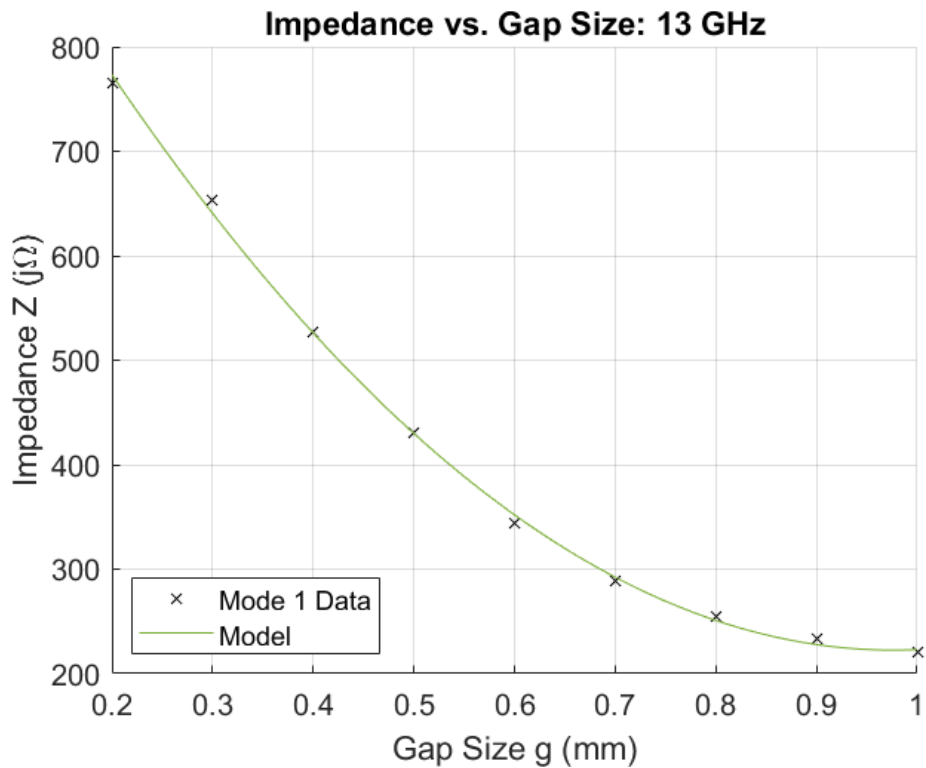


Figure 507: Circle Rogers 3010: Impedance vs. Gap Size, 13 GHz

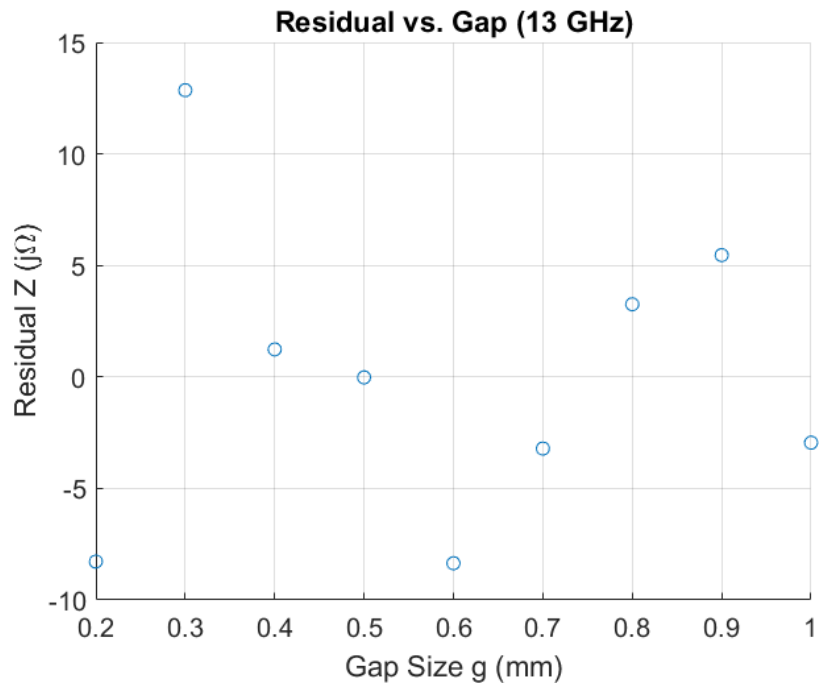


Figure 508: Circle Rogers 3010: Residuals, 13 GHz

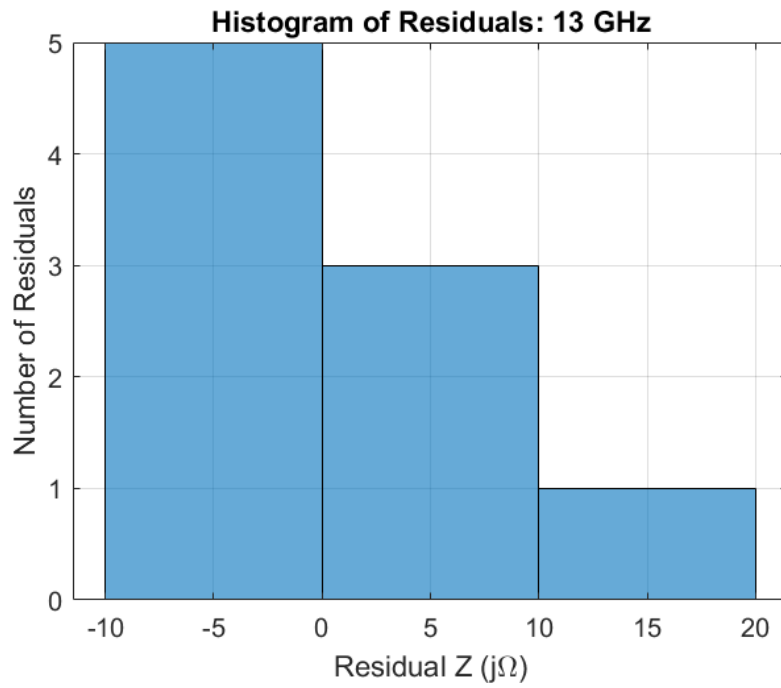


Figure 509: Circle Rogers 3010: Histogram of Residuals, 13 GHz

Model: 14 GHz

Equation form: $y = c_0 + c_1x^1 + c_2x^2 + c_3x^3$

	<u>Coefficient</u>
c_0 (intercept)	1052
c_1	-879.9
c_2	-638.5
c_3	739.4

Table 100: Model Coefficients: 14 GHz

Model Statistics

Error Degrees of Freedom: 5
Sum Squared Error (SSE): 210.5
Root Mean Squared Error (RMSE): 6.488
R-squared: 0.9994
Adjusted R-Squared: 0.9991

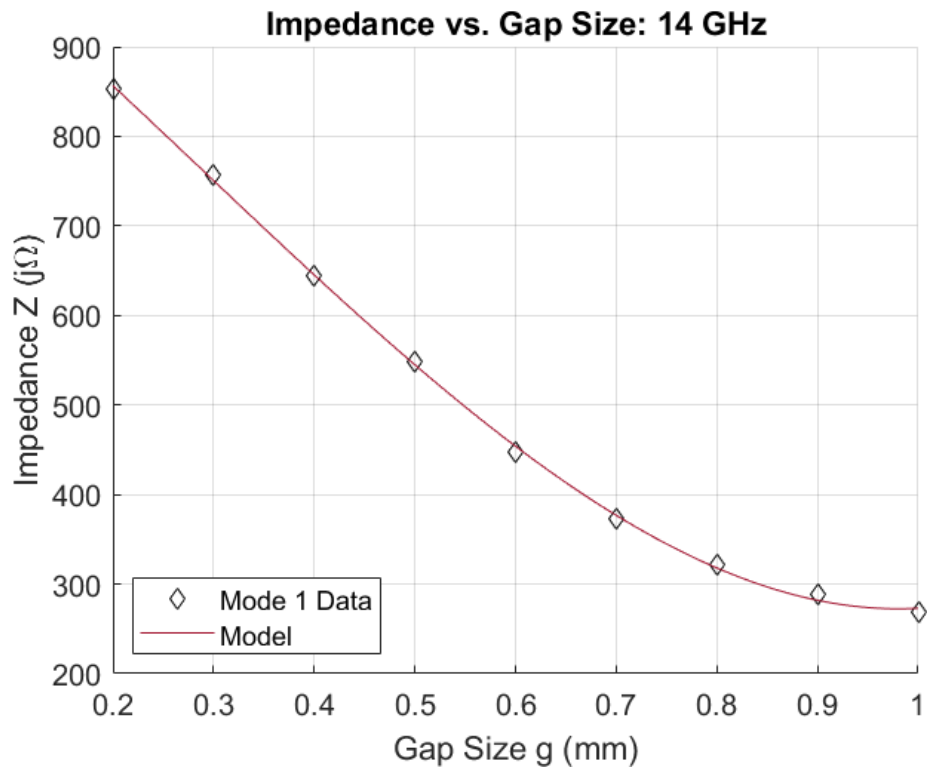


Figure 510: Circle Rogers 3010: Impedance vs. Gap Size, 14 GHz

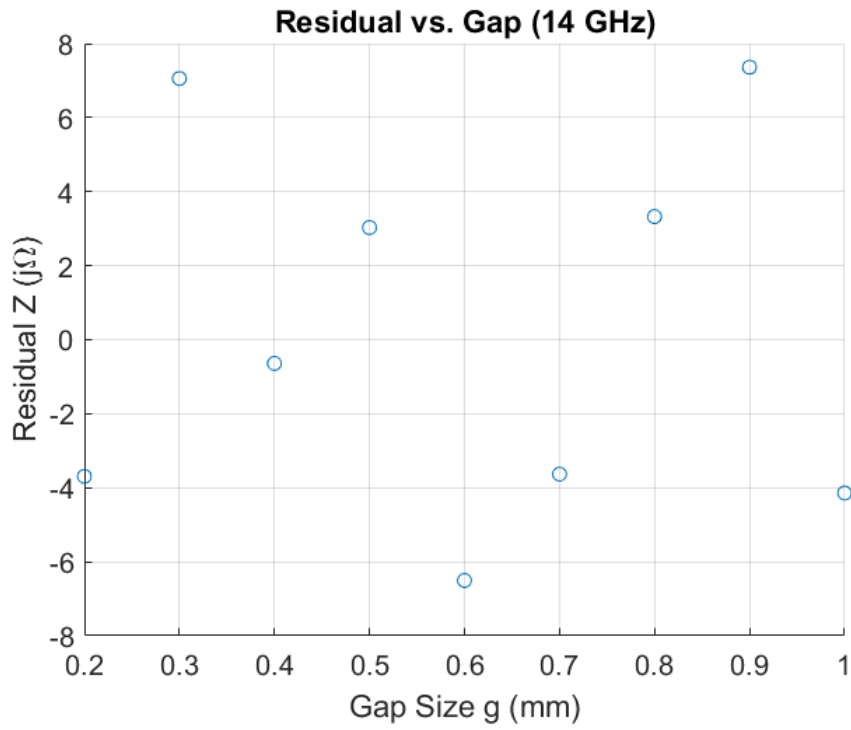


Figure 511: Circle Rogers 3010: Residuals, 14 GHz

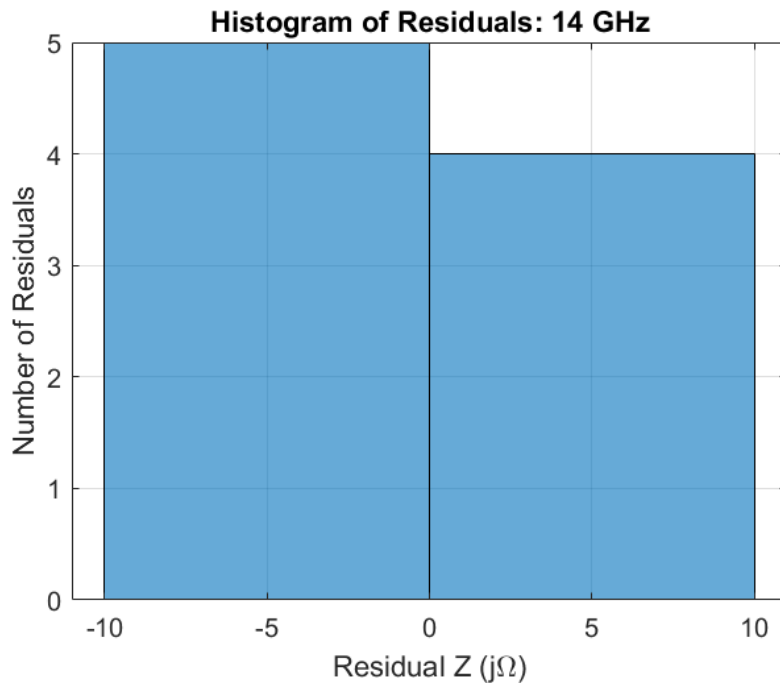


Figure 512: Circle Rogers 3010: Histogram of Residuals, 14 GHz

Model: 15 GHz

Equation form: $y = c_0 + c_1x^1 + c_2x^2 + c_3x^3$

	Coefficient	SE	tStat	pValue
c_0 (intercept)	1072.3	17.271	62.087	2.0515×10^{-8}
c_1	-499.42	106.65	-4.6827	0.0054202
c_2	-1142.6	193.87	-5.8937	0.0019996
c_3	903.94	106.95	8.4522	0.00038056

Table 101: Model Coefficients: 15 GHz

Model Statistics

Error Degrees of Freedom: 5
 Root Mean Squared Error (RMSE): 4.04
 R-squared: 1
 Adjusted R-Squared: 1
 F-statistic vs. constant model: 7.78×10^3
 p-value = 1.37×10^{-9}

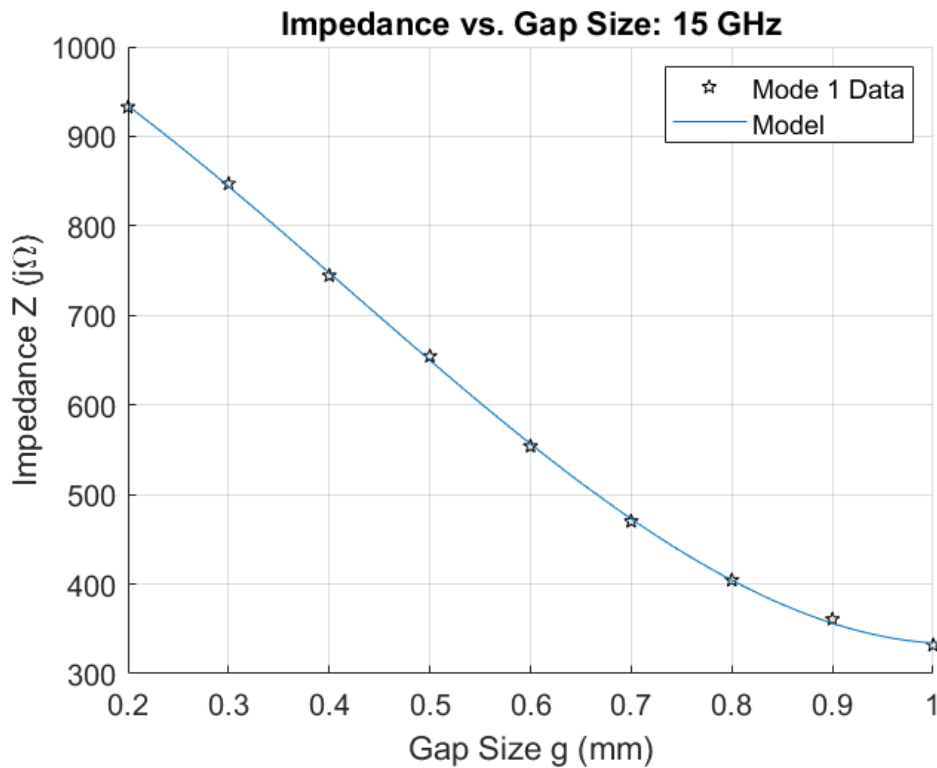


Figure 513: Circle Rogers 3010: Impedance vs. Gap Size, 15 GHz

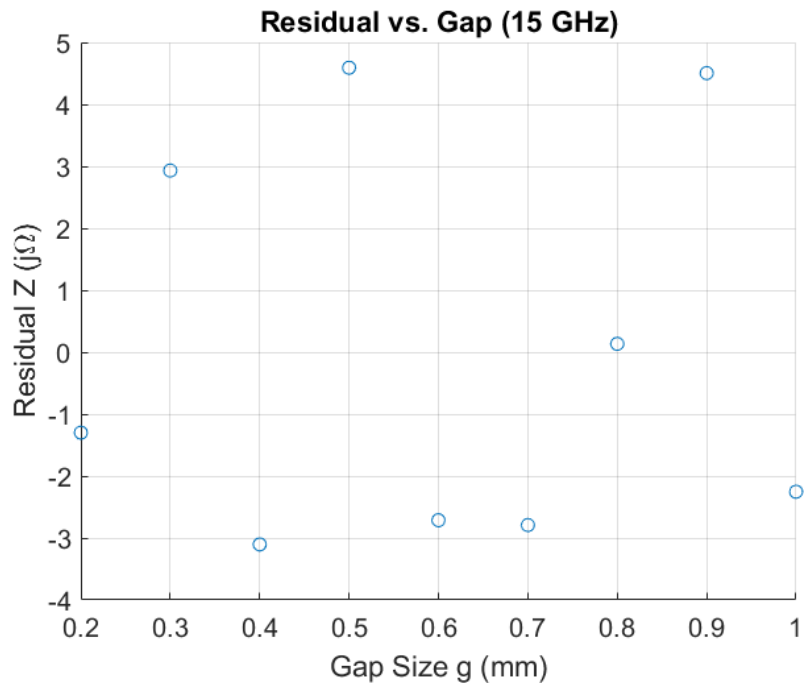


Figure 514: Circle Rogers 3010: Residuals, 15 GHz

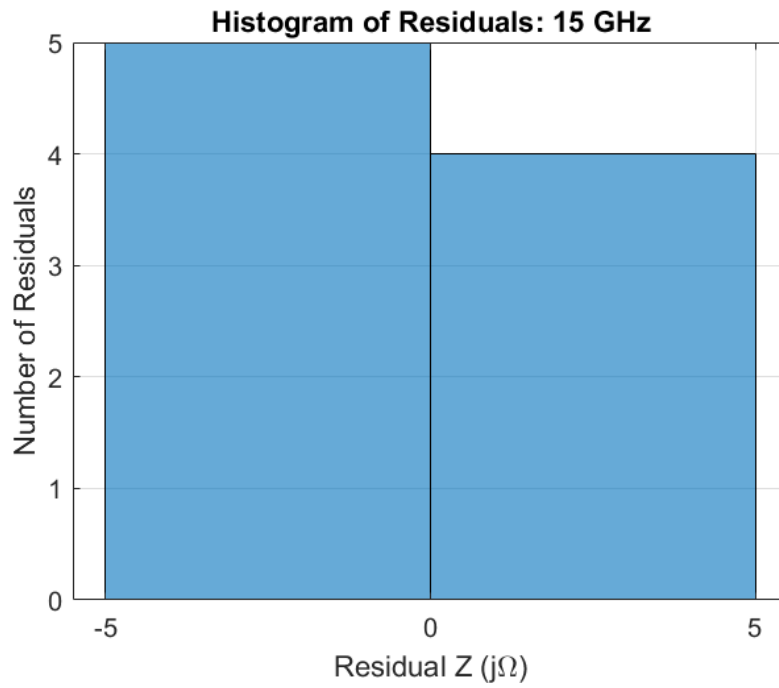


Figure 515: Circle Rogers 3010: Histogram of Residuals, 15 GHz

Model: 16 GHz

Equation form: $y = c_0 + c_1x^1 + c_2x^2 + c_3x^3$

	<u>Coefficient</u>	<u>SE</u>	<u>tStat</u>	<u>pValue</u>
c_0 (intercept)	1265.7	21.261	59.529	2.5312×10^{-8}
c_1	-1040.2	131.29	-7.9224	0.00051593
c_2	-219.57	238.67	-0.92	0.39979
c_3	399.95	131.66	3.0378	0.028823

Table 102: Model Coefficients: 16 GHz

Model Statistics

Error Degrees of Freedom: 5
 Root Mean Squared Error (RMSE): 4.97
 R-squared: 1
 Adjusted R-Squared: 1
 F-statistic vs. constant model: 5.61×10^3
 p-value = 3.1×10^{-9}

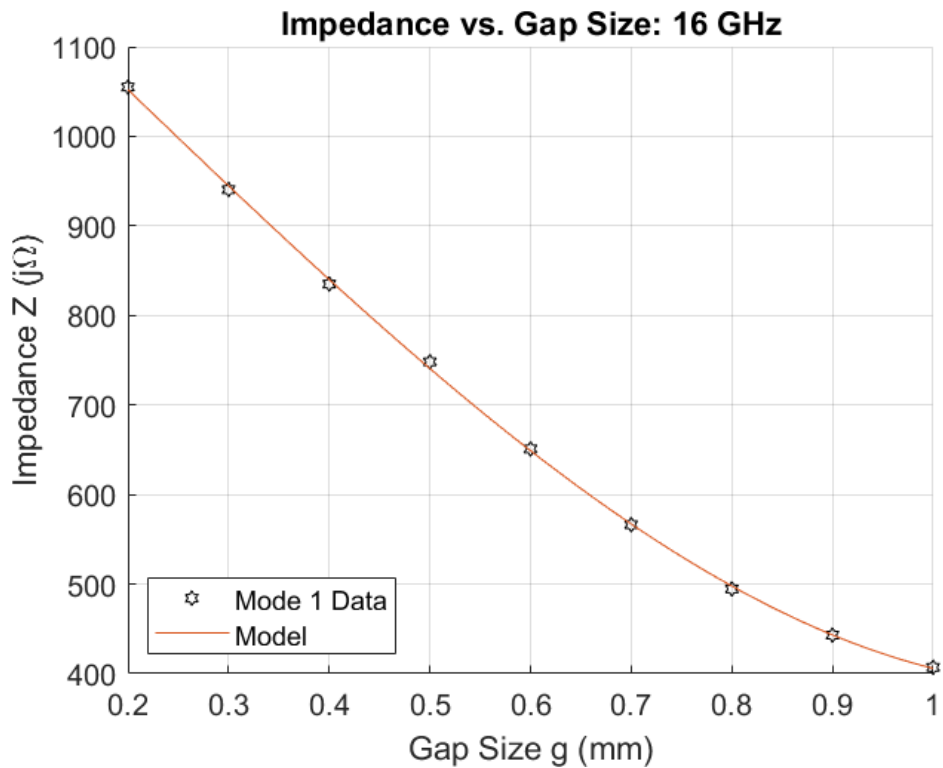


Figure 516: Circle Rogers 3010: Impedance vs. Gap Size, 16 GHz

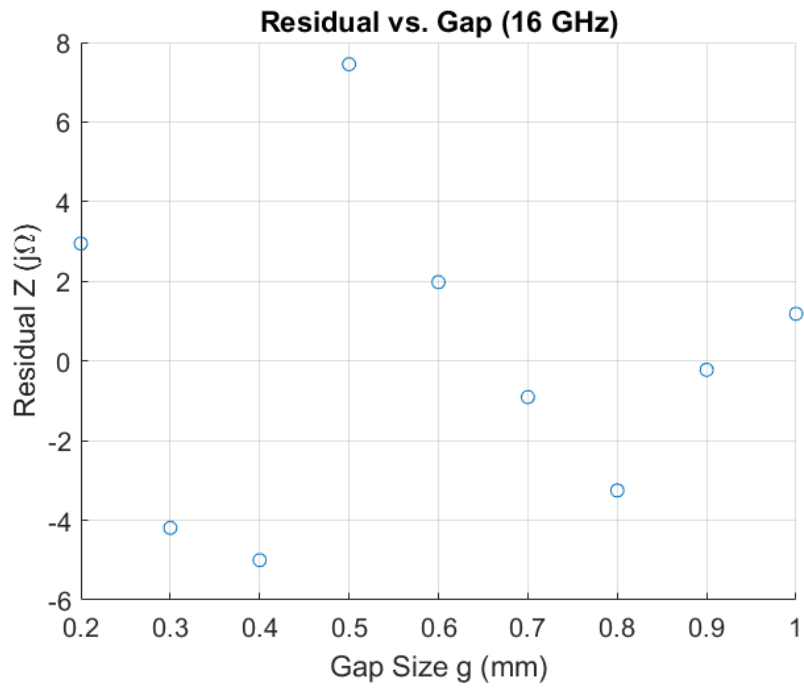


Figure 517: Circle Rogers 3010: Residuals, 16 GHz

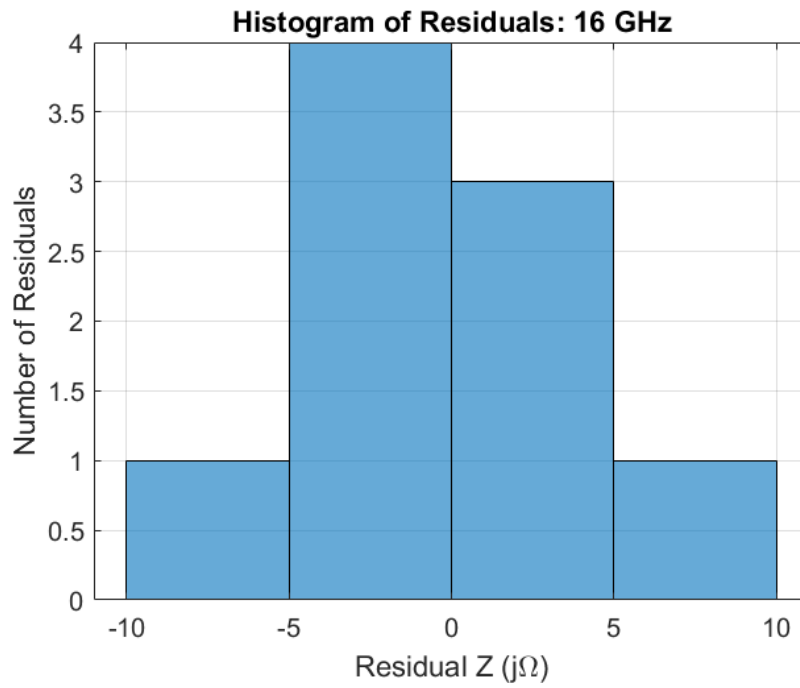


Figure 518: Circle Rogers 3010: Histogram of Residuals, 16 GHz

Model: 17 GHz

Equation form: $y = c_0 + c_1x^1 + c_2x^2$

	Coefficient	SE	tStat	pValue
c_0 (intercept)	1561.6	5.8685	266.09	1.1967×10^{-9}
c_1	-1818.8	17.714	-102.67	5.3956×10^{-8}
c_2	744.02	12.557	59.25	4.8593×10^{-7}

Table 103: Model Coefficients: 17 GHz

Model Statistics

Error Degrees of Freedom: 4
 Root Mean Squared Error (RMSE): 1.15
 R-squared: 1
 Adjusted R-Squared: 1
 F-statistic vs. constant model: 6.56×10^4
 p-value = 9.3×10^{-10}

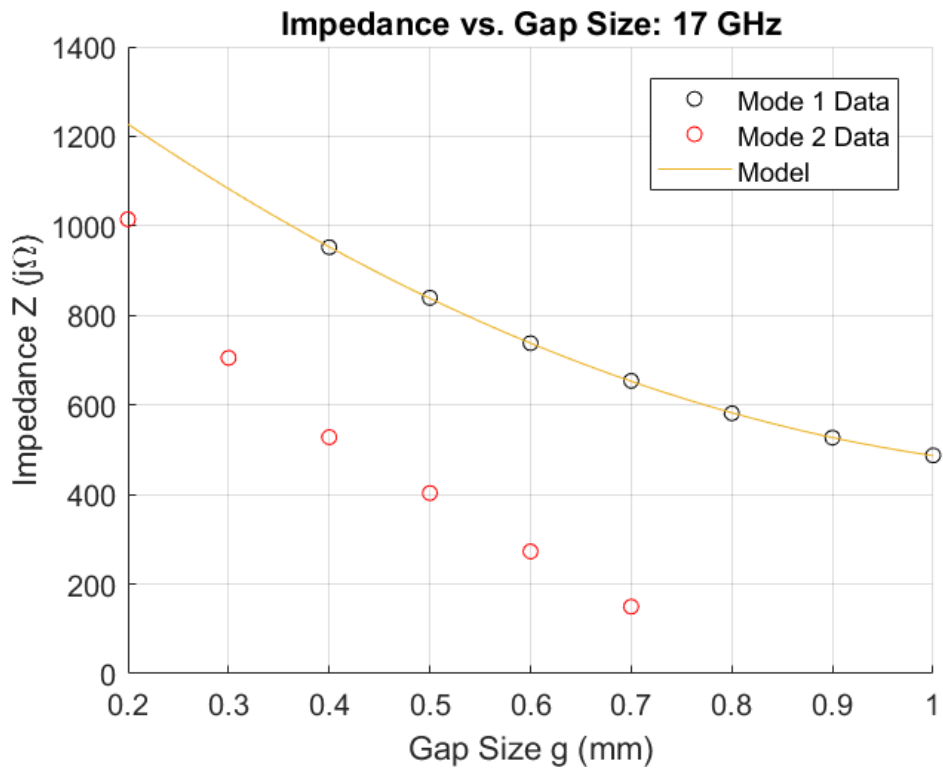


Figure 519: Circle Rogers 3010: Impedance vs. Gap Size, 17 GHz

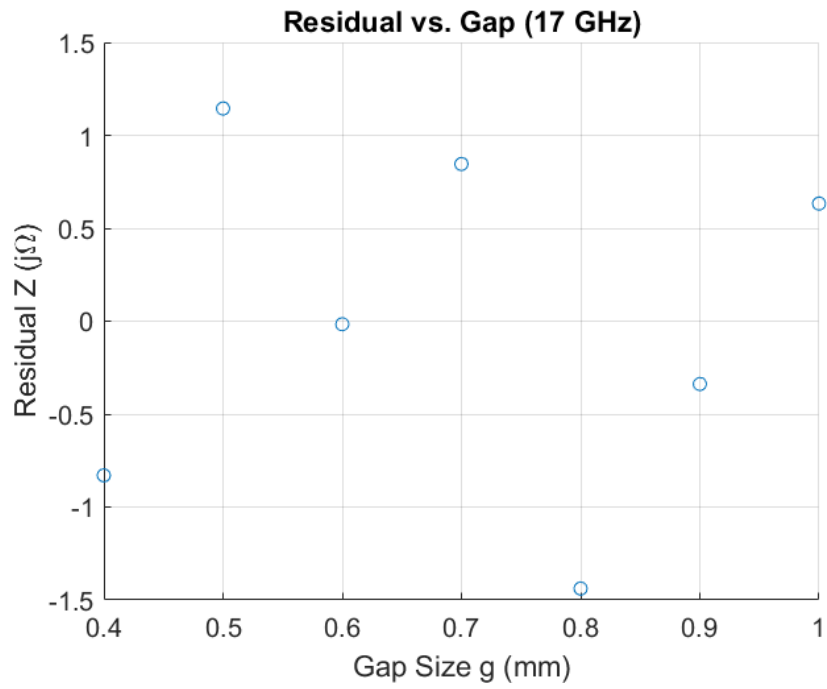


Figure 520: Circle Rogers 3010: Residuals, 17 GHz

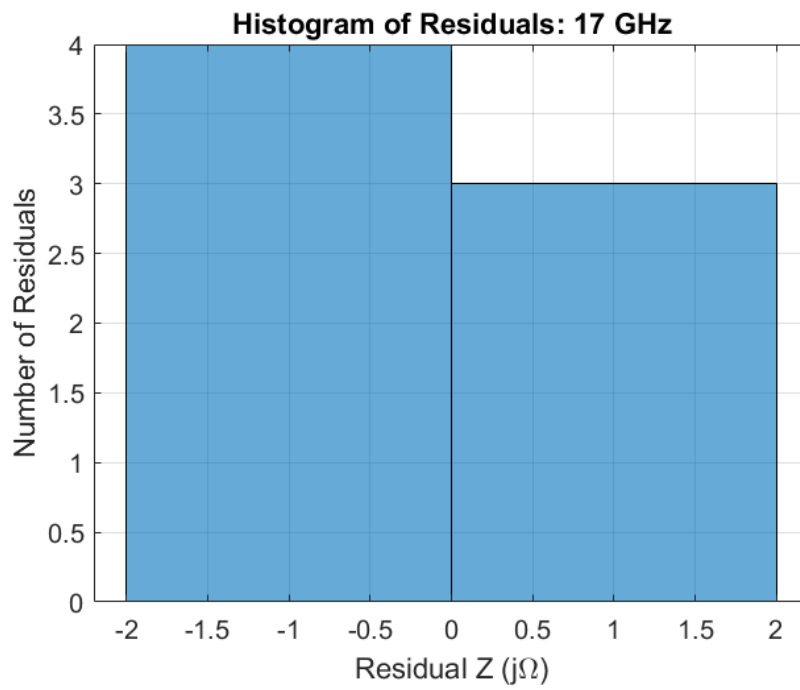


Figure 521: Circle Rogers 3010: Histogram of Residuals, 17 GHz

Model: 18 GHz

Equation form: $y = c_0 + c_1x^1 + c_2x^2$

	<u>Coefficient</u>	<u>SE</u>	<u>tStat</u>	<u>pValue</u>
c_0 (intercept)	1767.3	23.181	76.239	0.000172
c_1	-2113.9	59.277	-35.662	0.0007854
c_2	912.22	36.947	24.69	0.0016364

Table 104: Model Coefficients: 18 GHz

Model Statistics

Error Degrees of Freedom: 2

Root Mean Squared Error (RMSE): 1.38

R-squared: 1

Adjusted R-Squared: 1

F-statistic vs. constant model: 1.15×10^4

p-value = 8.69×10^{-5}

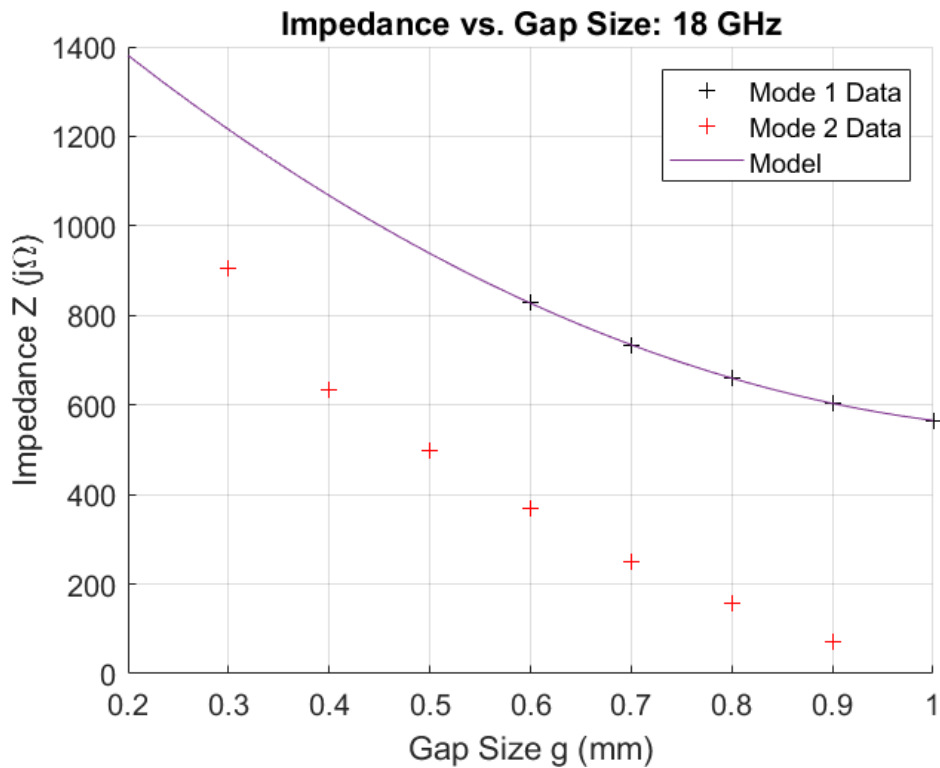


Figure 522: Circle Rogers 3010: Impedance vs. Gap Size, 18 GHz

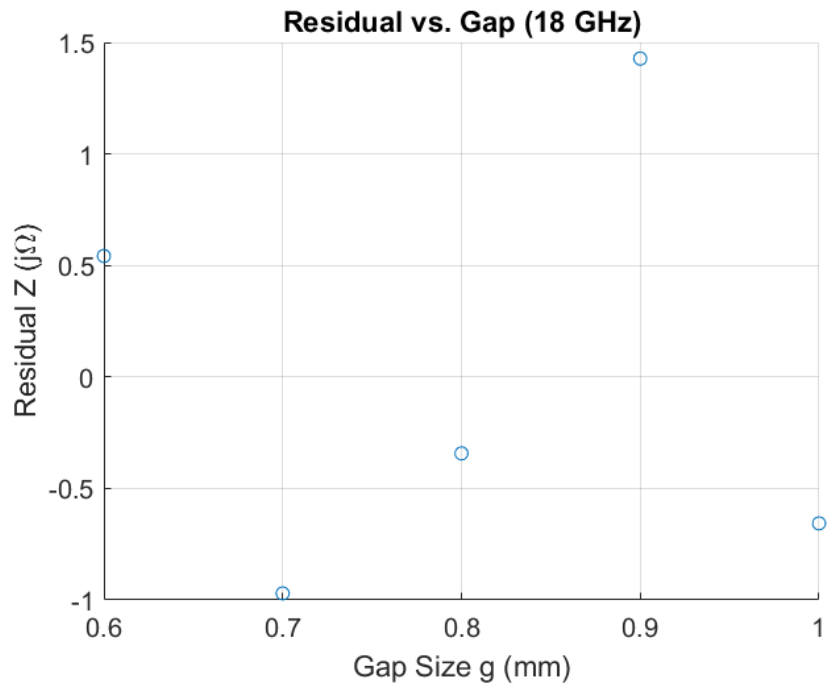


Figure 523: Circle Rogers 3010: Residuals, 18 GHz

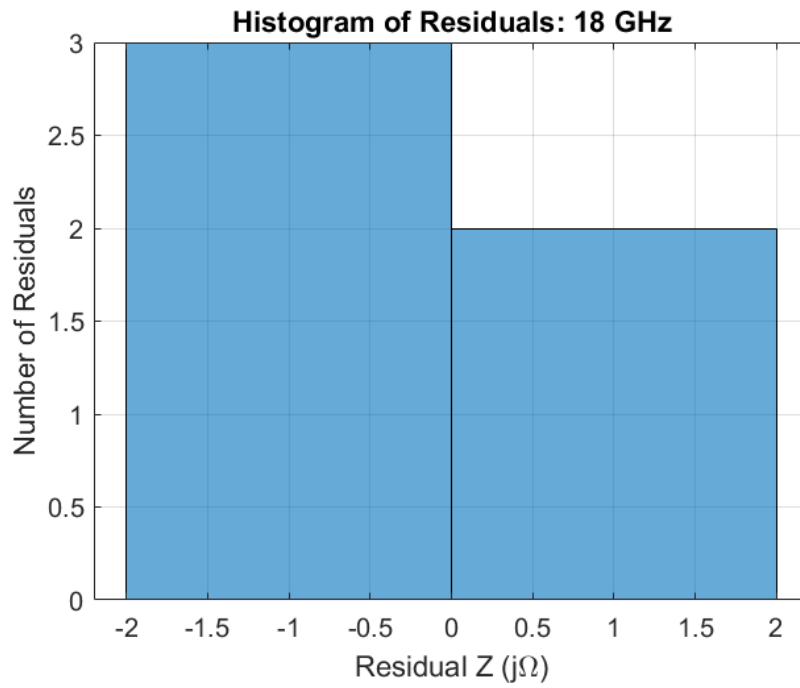


Figure 524: Circle Rogers 3010: Histogram of Residuals, 18 GHz

Model: 19 GHz

Equation form: $y = c_0 + c_1x^1 + c_2x^2$

	Coefficient	SE	tStat	pValue
c_0 (intercept)	2138.6	140.07	15.268	0.041637
c_1	-2768.3	333.91	-8.2905	0.07642
c_2	1265.6	196.15	6.4523	0.097887

Table 105: Model Coefficients: 19 GHz

Model Statistics

Error Degrees of Freedom: 1
 Root Mean Squared Error (RMSE): 3.92
 R-squared: 0.999
 Adjusted R-Squared: 0.998
 F-statistic vs. constant model: 639
 p-value = 0.028

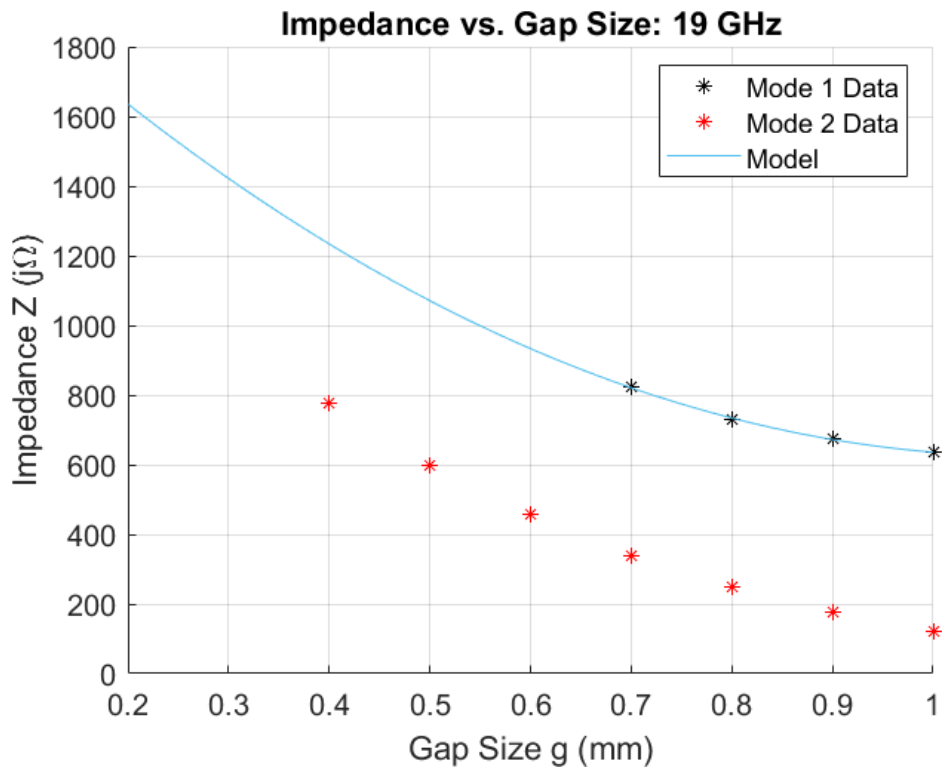


Figure 525: Circle Rogers 3010: Impedance vs. Gap Size, 19 GHz

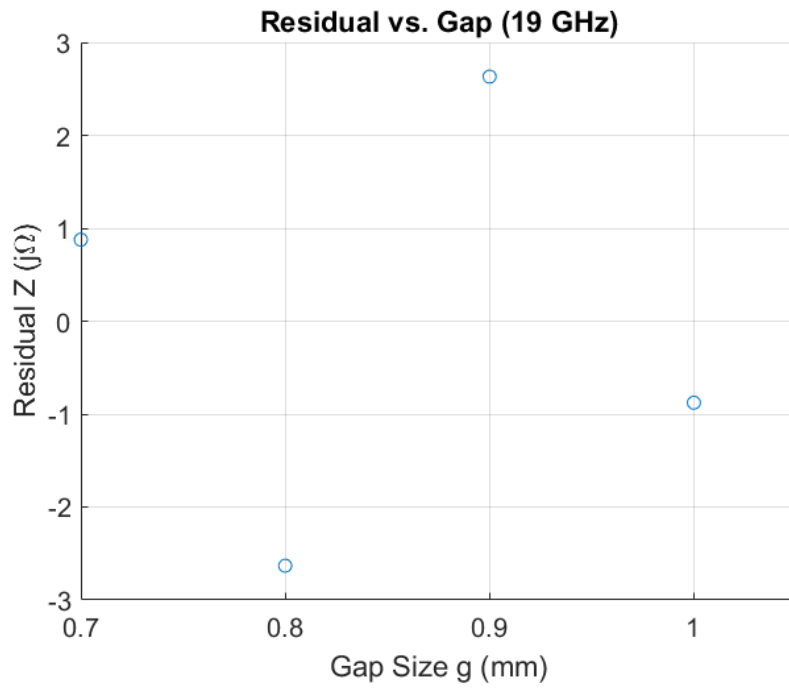


Figure 526: Circle Rogers 3010: Residuals, 19 GHz

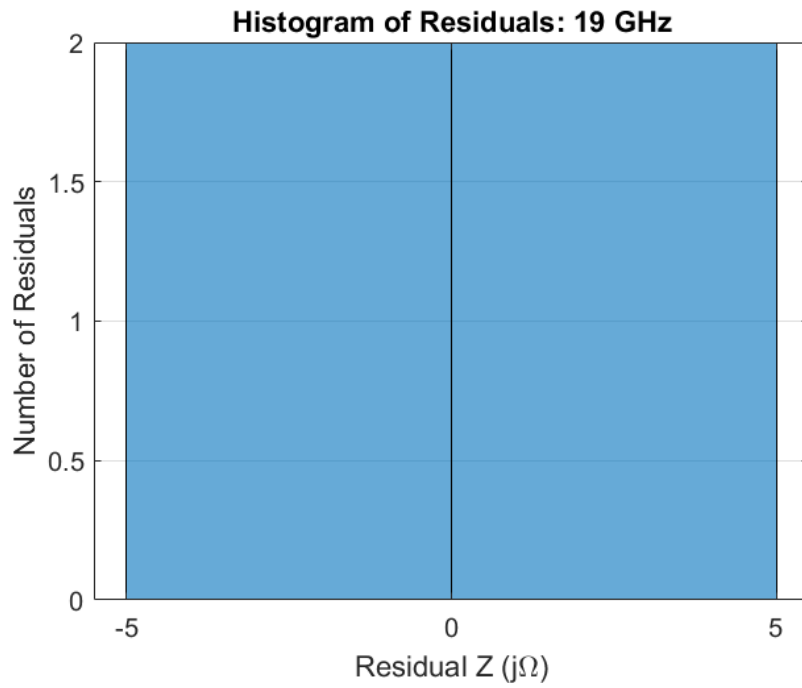


Figure 527: Circle Rogers 3010: Histogram of Residuals, 19 GHz

Appendix F. Fractal Rogers 3010 Unit Cell

Cell Parameters

Material: Rogers 3010

Dielectric Constant, ϵ_r : 11.2

Dissipation Constant, $\tan \delta$: 0.0022

Shape: circle

Dielectric Thickness: 1.27 mm

Copper Thickness: 0.035 mm

Cell Size, a : 4 mm

Subcell Size, $b = \frac{a-2g}{3}$

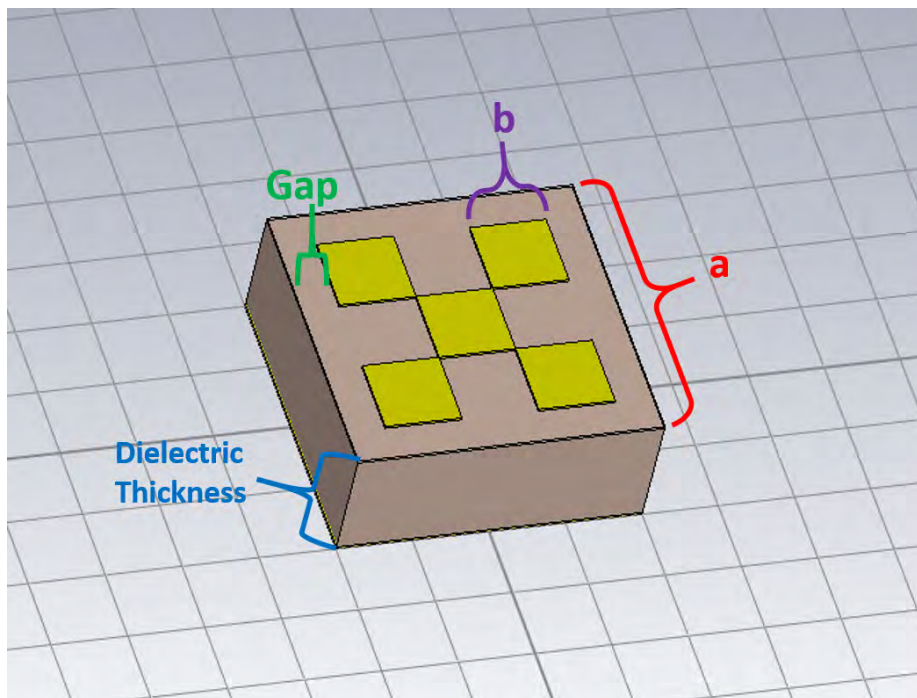


Figure 528: Circle Cell Geometry

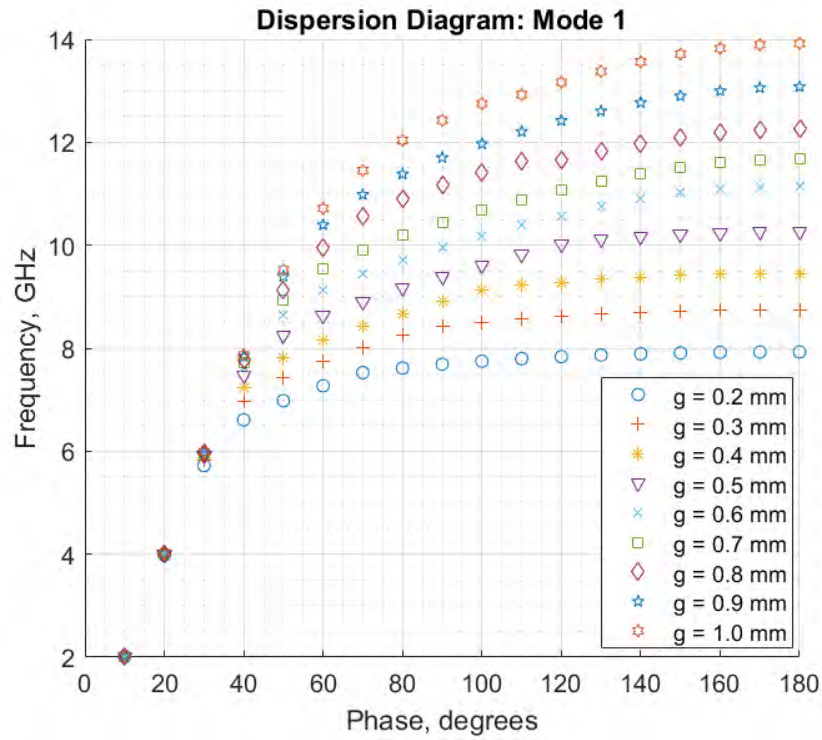


Figure 529: Fractal Rogers 3010: Dispersion Diagram, Mode 1

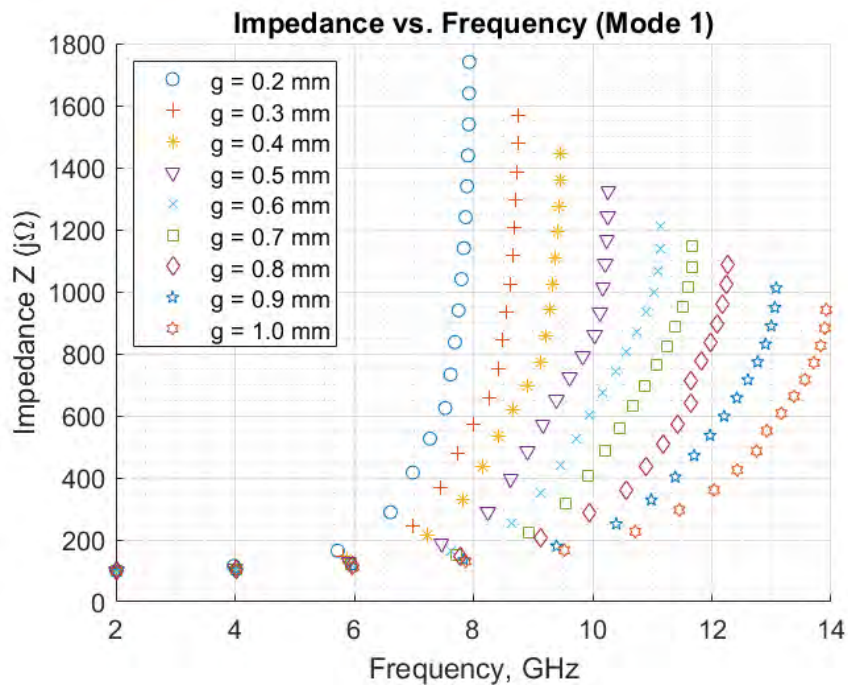


Figure 530: Fractal Rogers 3010: Impedance vs. Frequency, Mode 1

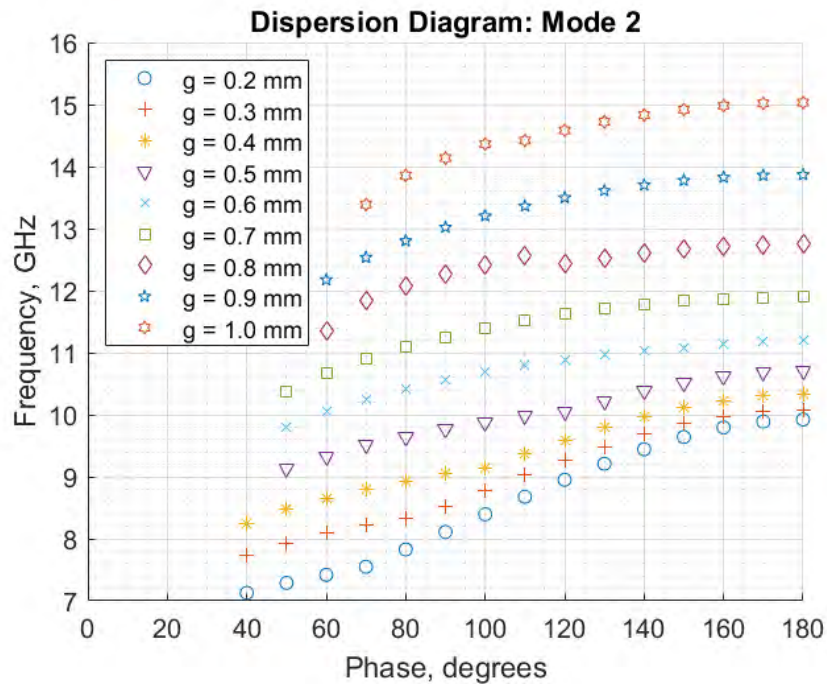


Figure 531: Fractal Rogers 3010: Dispersion Diagram, Mode 2

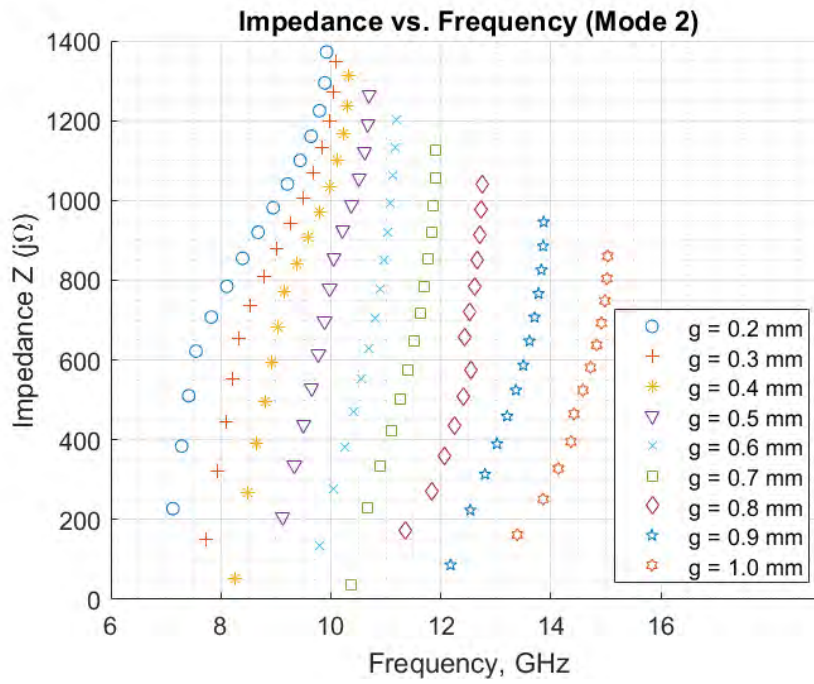


Figure 532: Fractal Rogers 3010: Impedance vs. Frequency, Mode 2

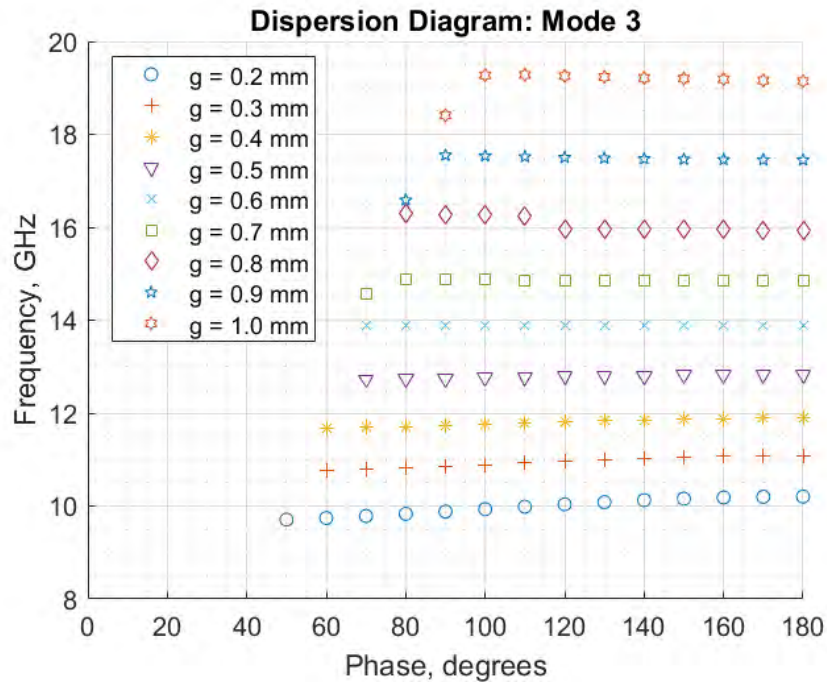


Figure 533: Fractal Rogers 3010: Dispersion Diagram, Mode 3

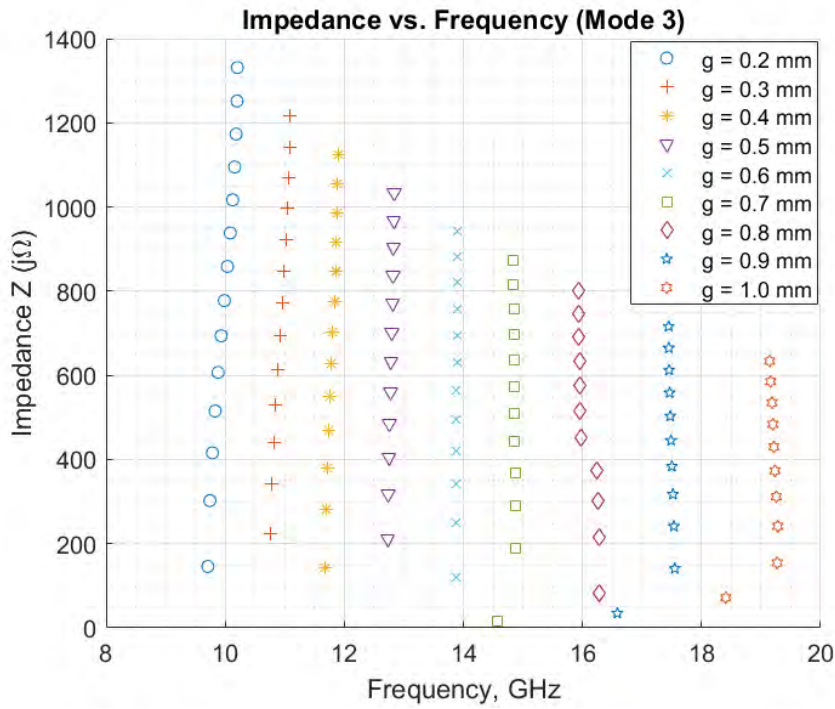


Figure 534: Fractal Rogers 3010: Impedance vs. Frequency, Mode 3

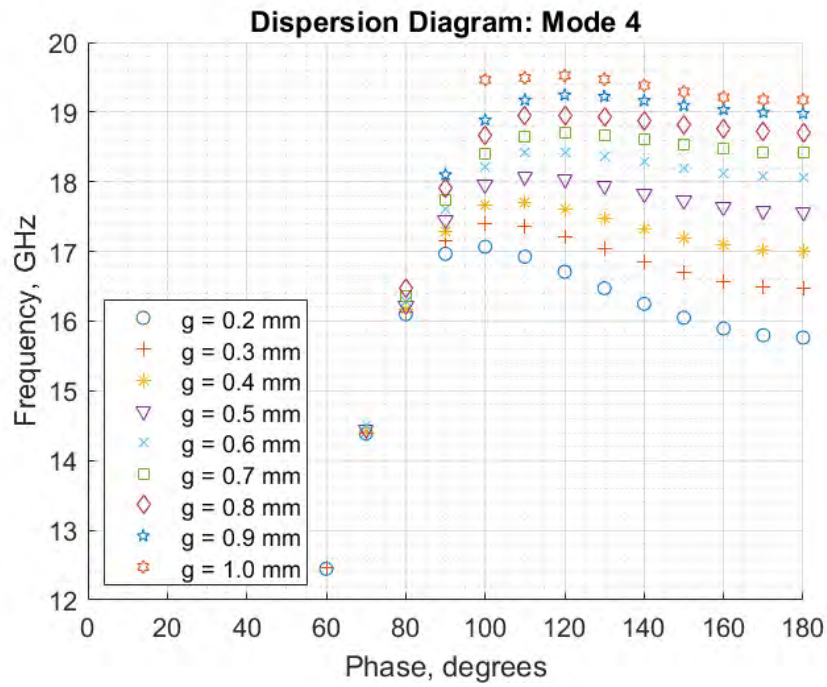


Figure 535: Fractal Rogers 3010: Dispersion Diagram, Mode 4

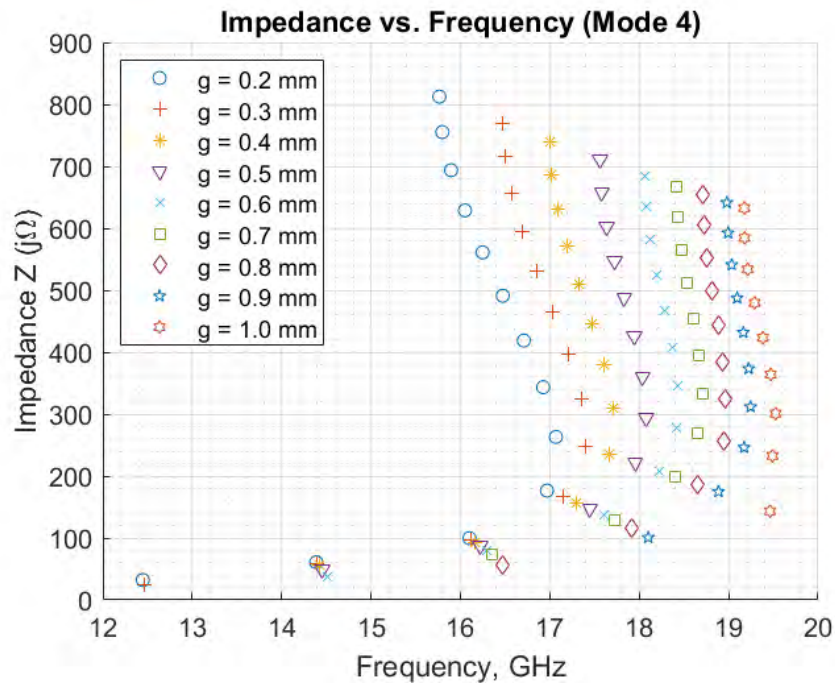


Figure 536: Fractal Rogers 3010: Impedance vs. Frequency, Mode 4

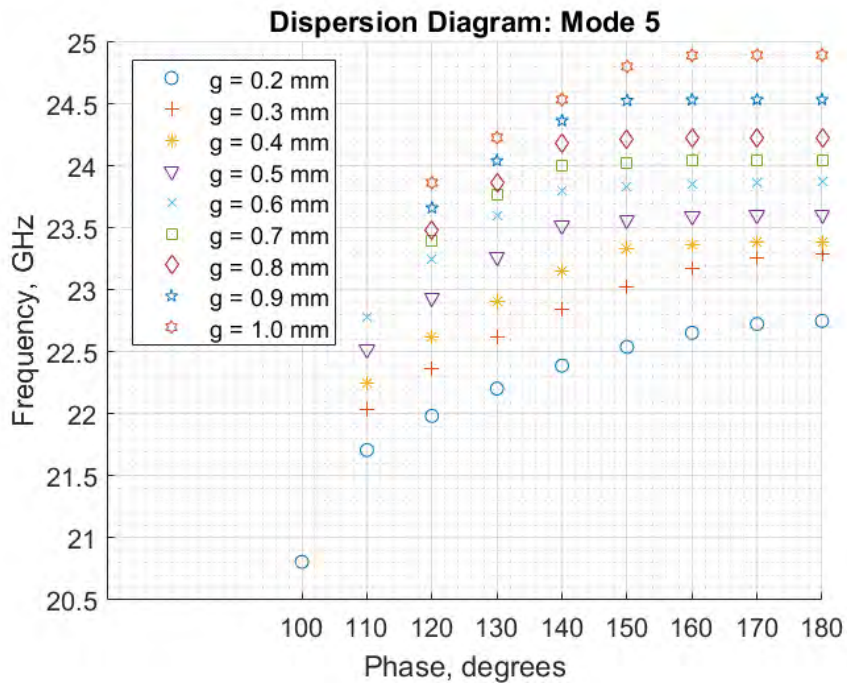


Figure 537: Fractal Rogers 3010: Dispersion Diagram, Mode 5

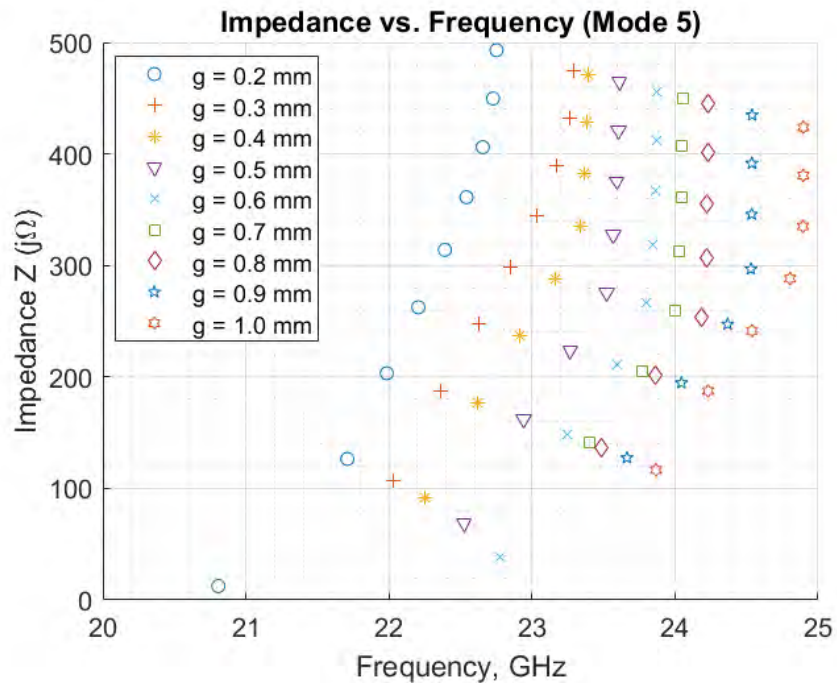


Figure 538: Fractal Rogers 3010: Impedance vs. Frequency, Mode 5

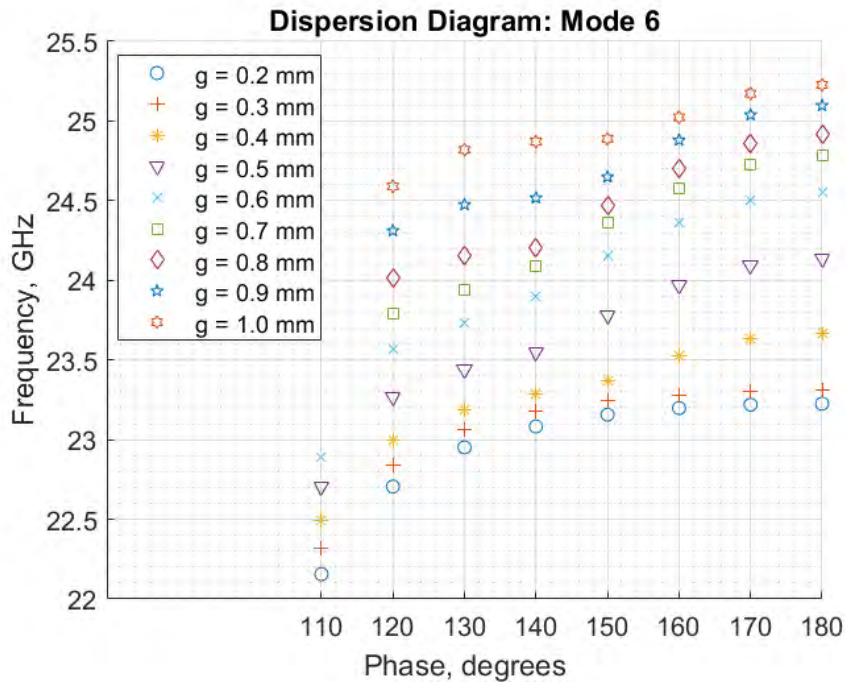


Figure 539: Fractal Rogers 3010: Dispersion Diagram, Mode 6

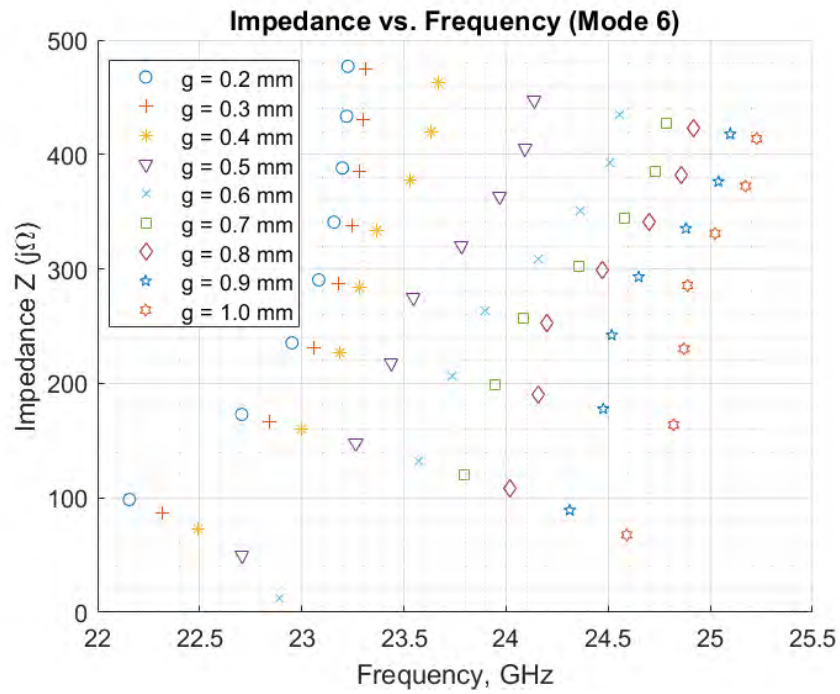


Figure 540: Fractal Rogers 3010: Impedance vs. Frequency, Mode 6

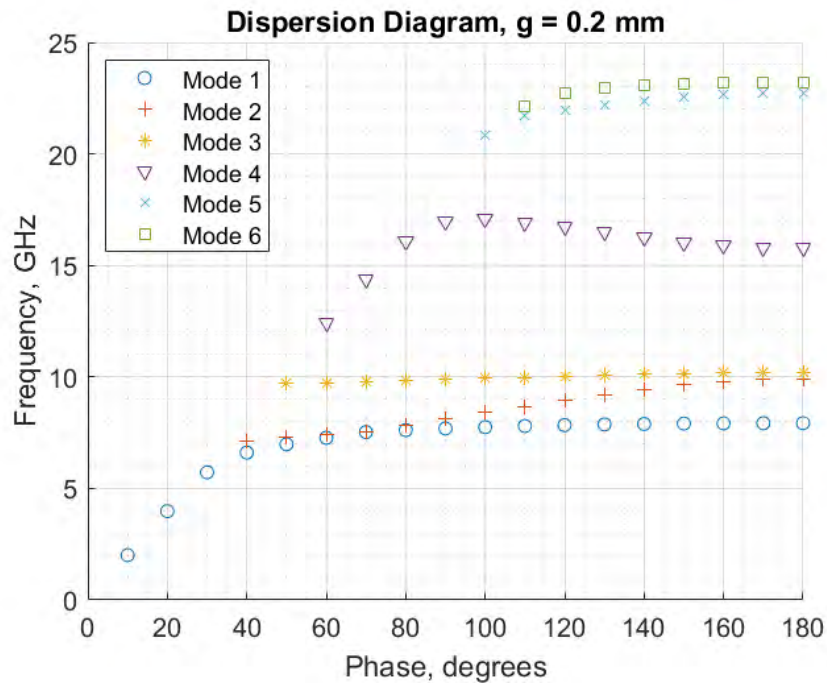


Figure 541: Fractal Rogers 3010: Dispersion Diagram, $g = 0.2$

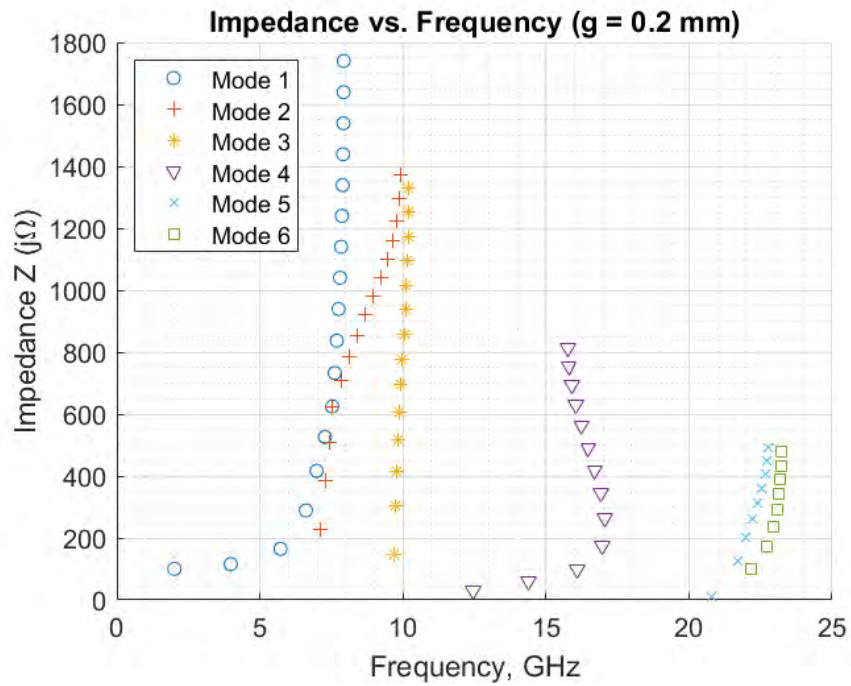


Figure 542: Fractal Rogers 3010: Impedance vs. Frequency, $g = 0.2$

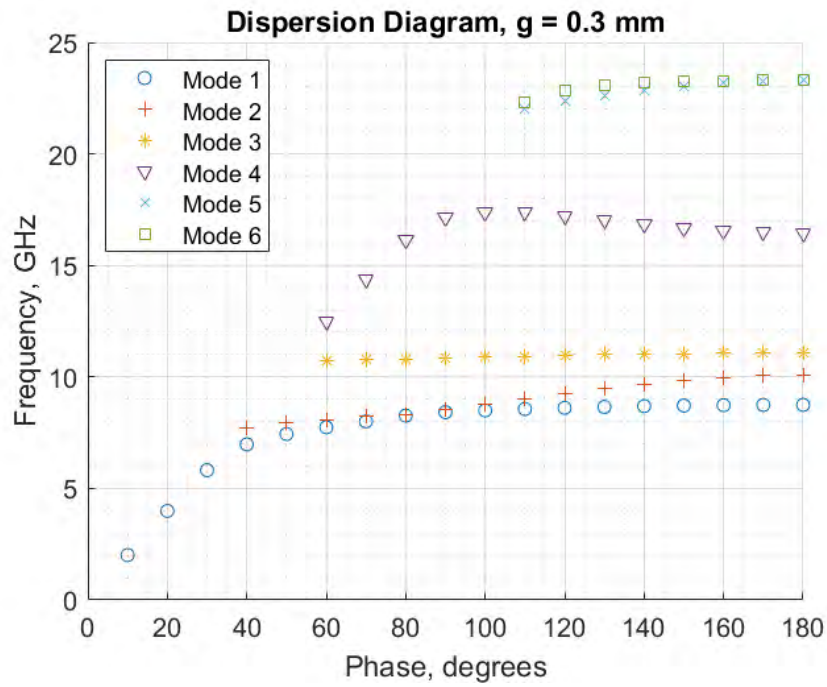


Figure 543: Fractal Rogers 3010: Dispersion Diagram, $g = 0.3$

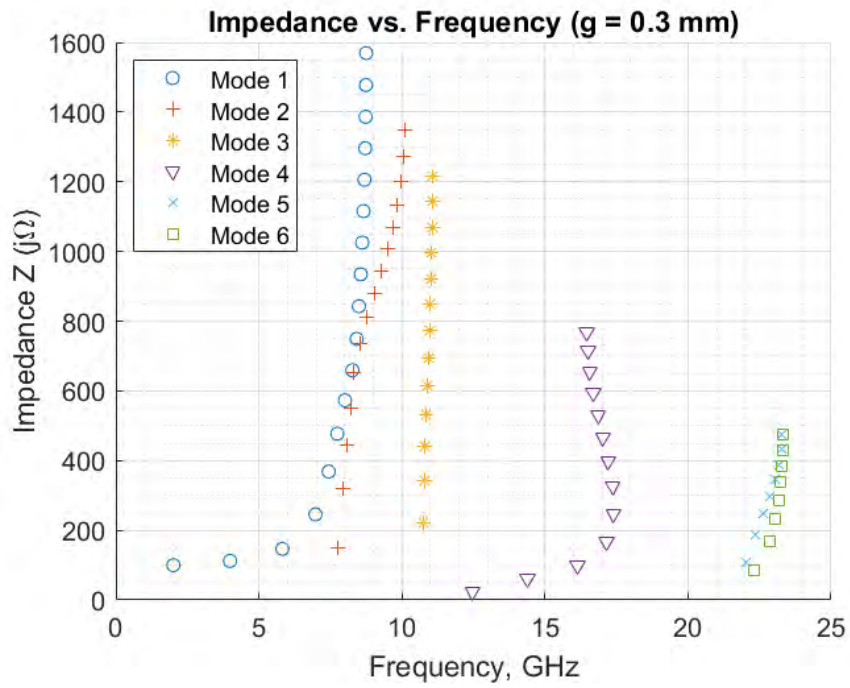


Figure 544: Fractal Rogers 3010: Impedance vs. Frequency, $g = 0.3$

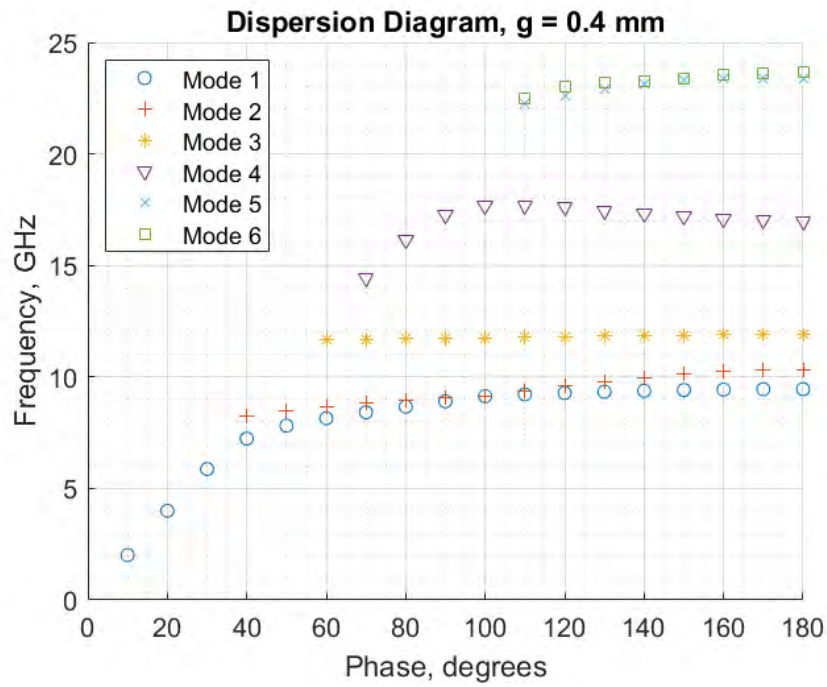


Figure 545: Fractal Rogers 3010: Dispersion Diagram, $g = 0.4$

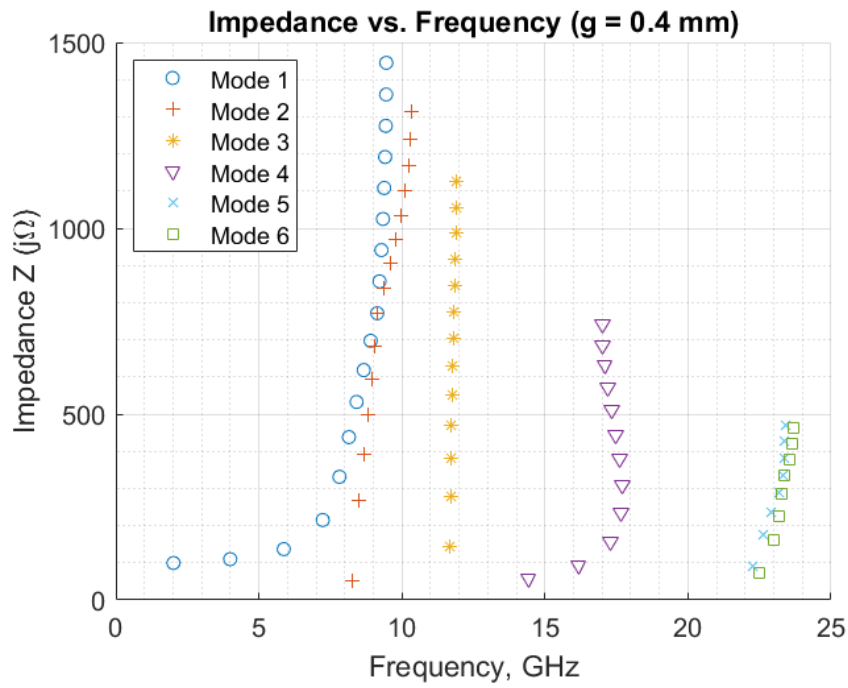


Figure 546: Fractal Rogers 3010: Impedance vs. Frequency, $g = 0.4$

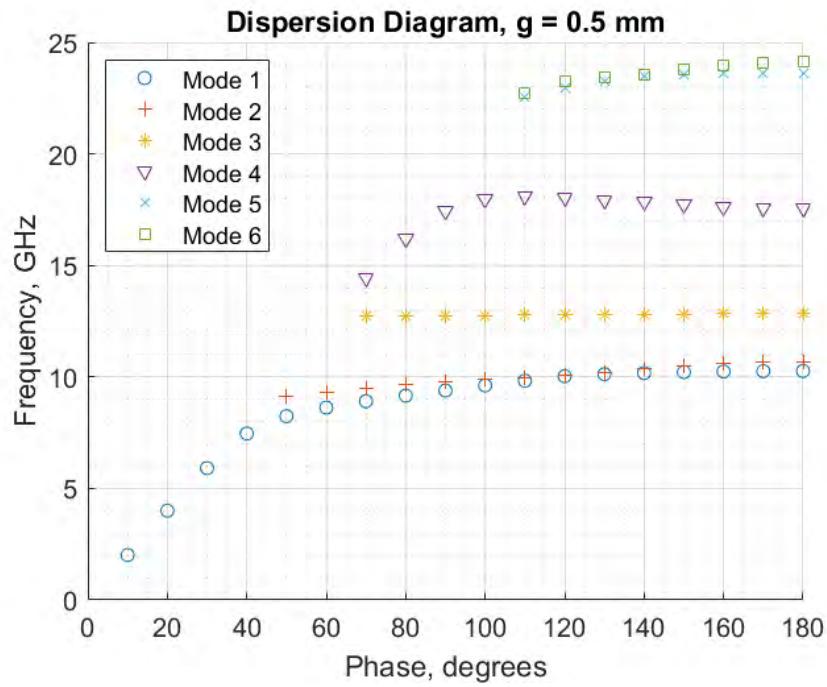


Figure 547: Fractal Rogers 3010: Dispersion Diagram, $g = 0.5$

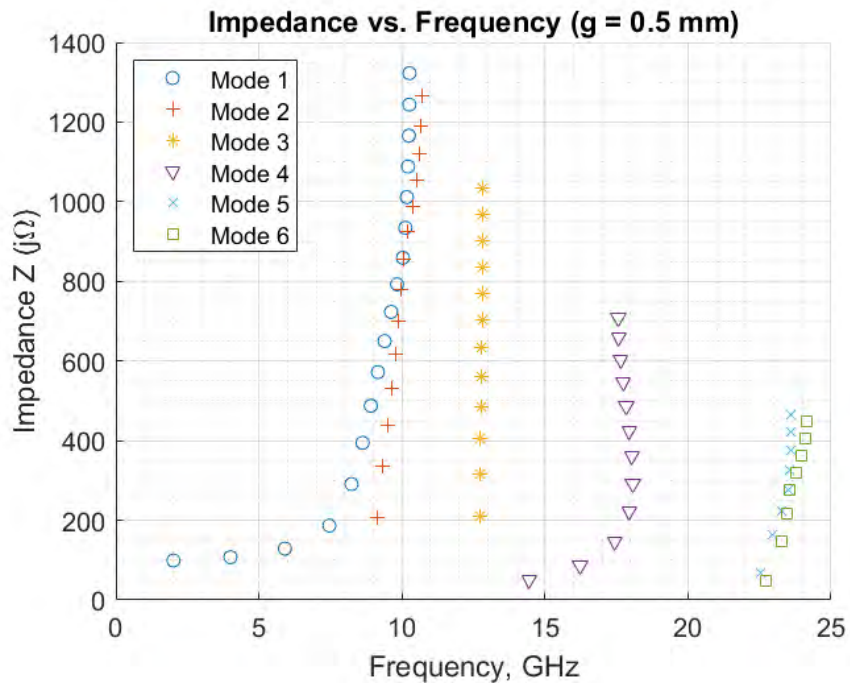


Figure 548: Fractal Rogers 3010: Impedance vs. Frequency, $g = 0.5$

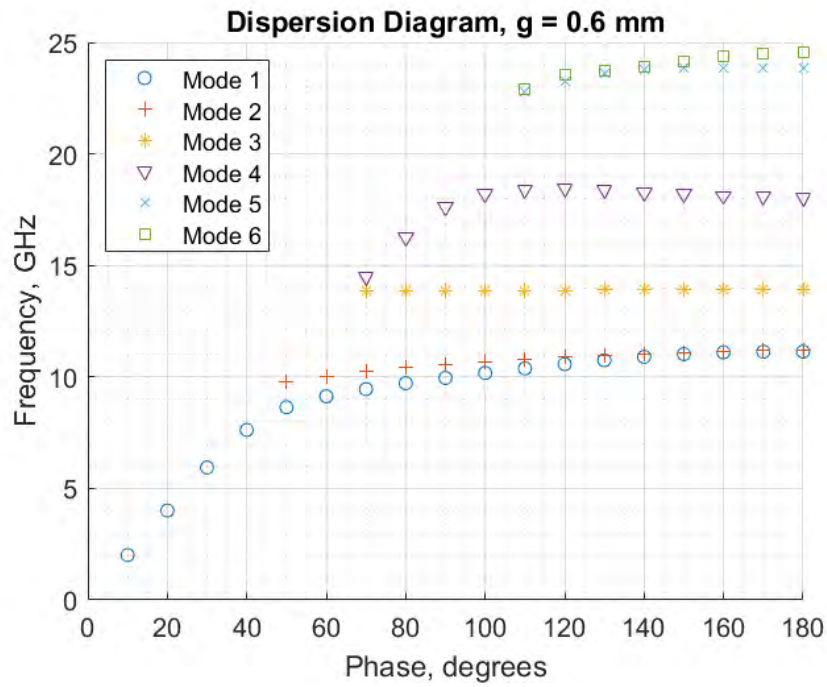


Figure 549: Fractal Rogers 3010: Dispersion Diagram, $g = 0.6$

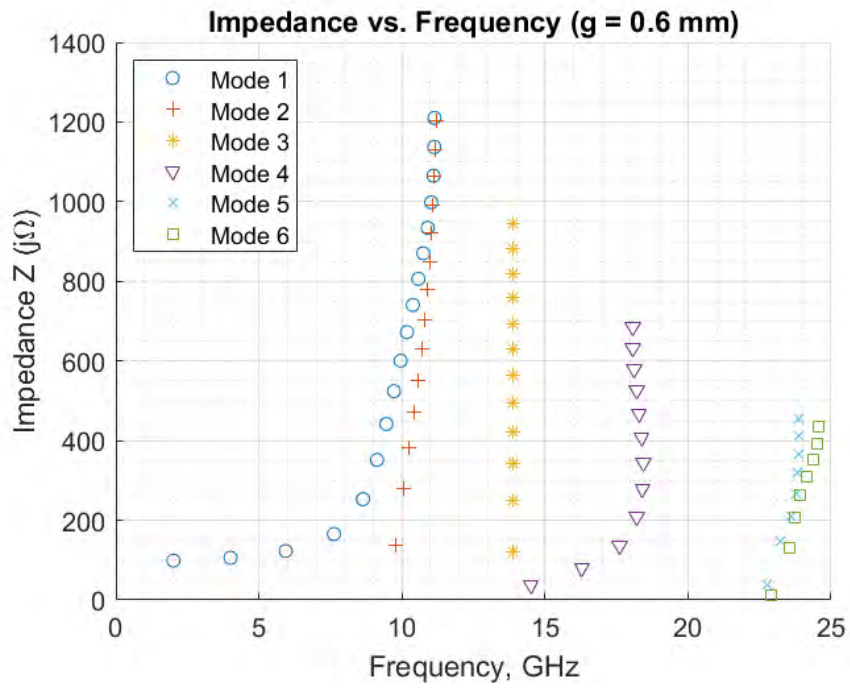


Figure 550: Fractal Rogers 3010: Impedance vs. Frequency, $g = 0.6$

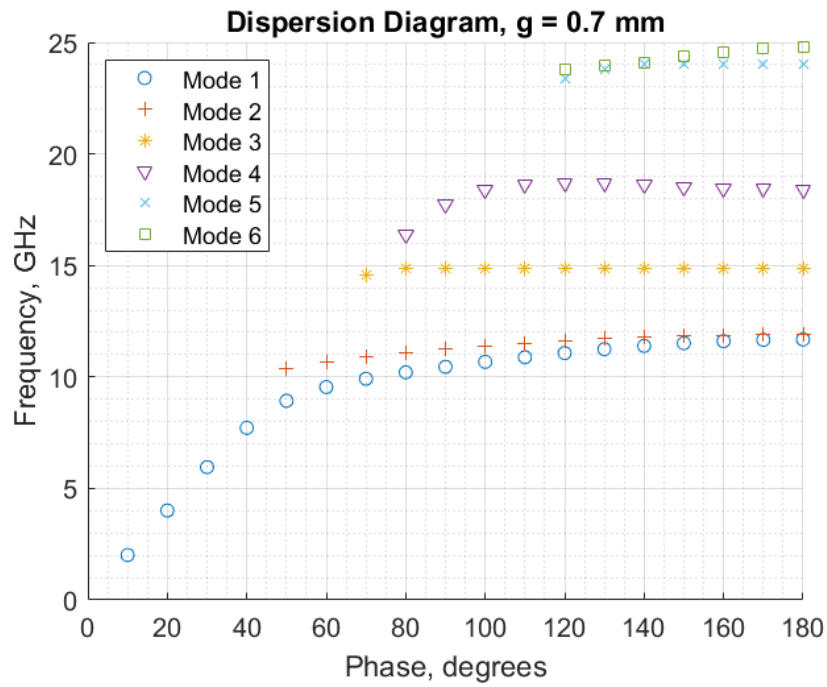


Figure 551: Fractal Rogers 3010: Dispersion Diagram, $g = 0.7$

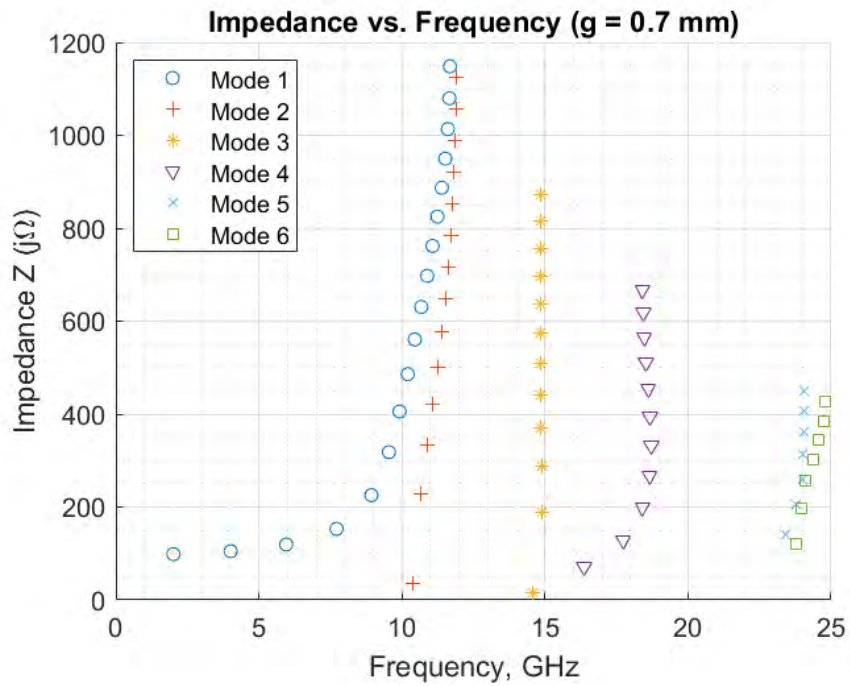


Figure 552: Fractal Rogers 3010: Impedance vs. Frequency, $g = 0.7$

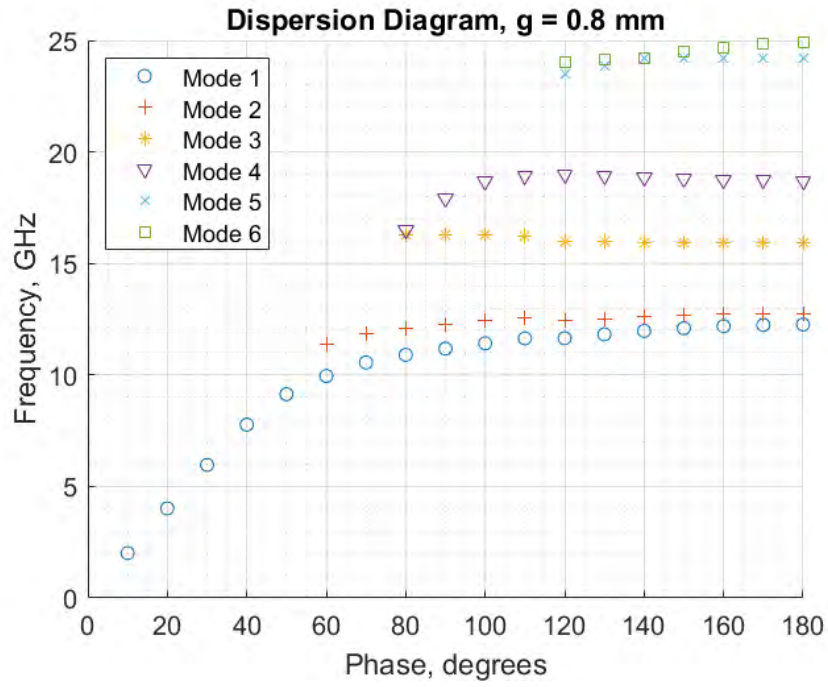


Figure 553: Fractal Rogers 3010: Dispersion Diagram, $g = 0.8$

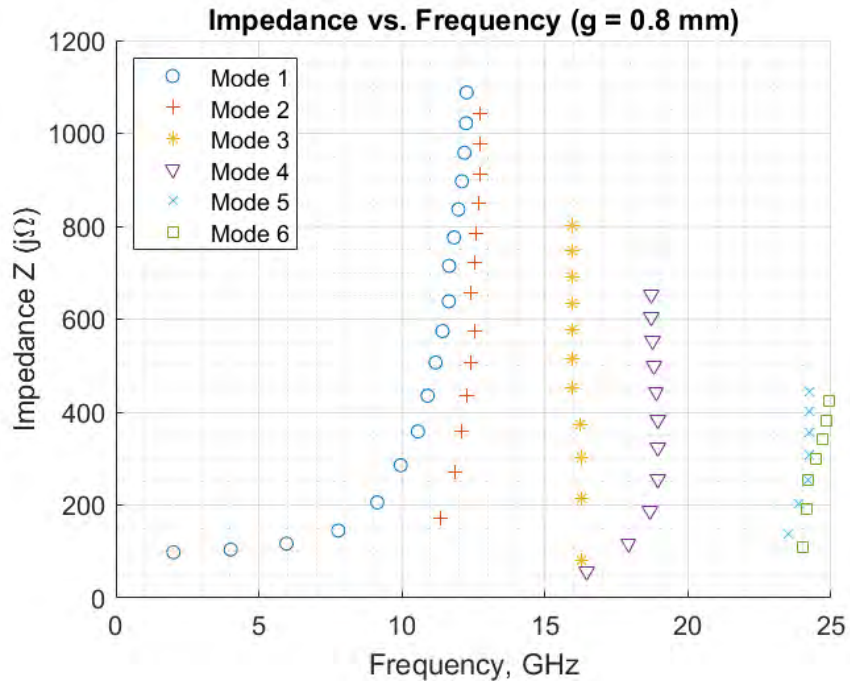


Figure 554: Fractal Rogers 3010: Impedance vs. Frequency, $g = 0.8$

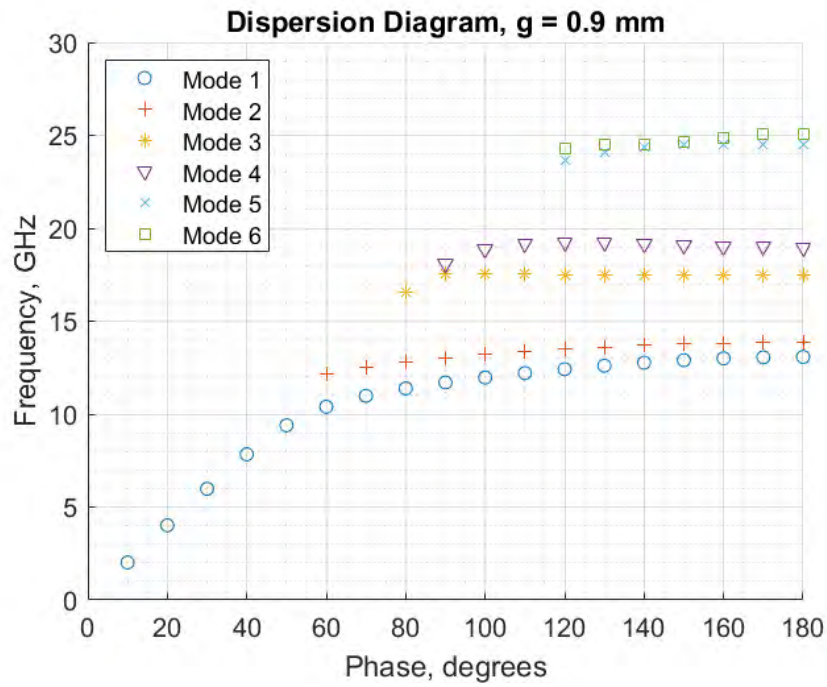


Figure 555: Fractal Rogers 3010: Dispersion Diagram, $g = 0.9$

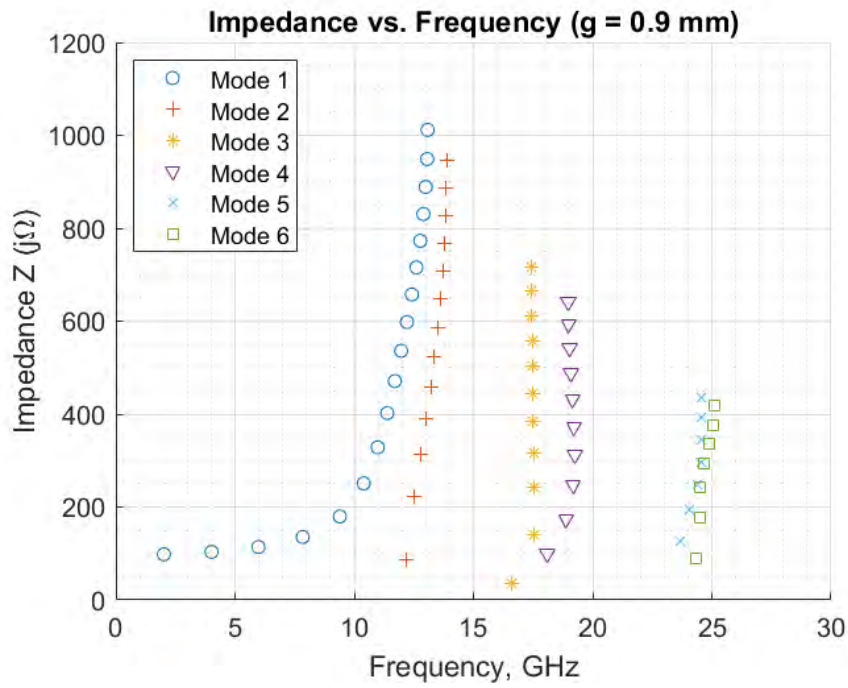


Figure 556: Fractal Rogers 3010: Impedance vs. Frequency, $g = 0.9$

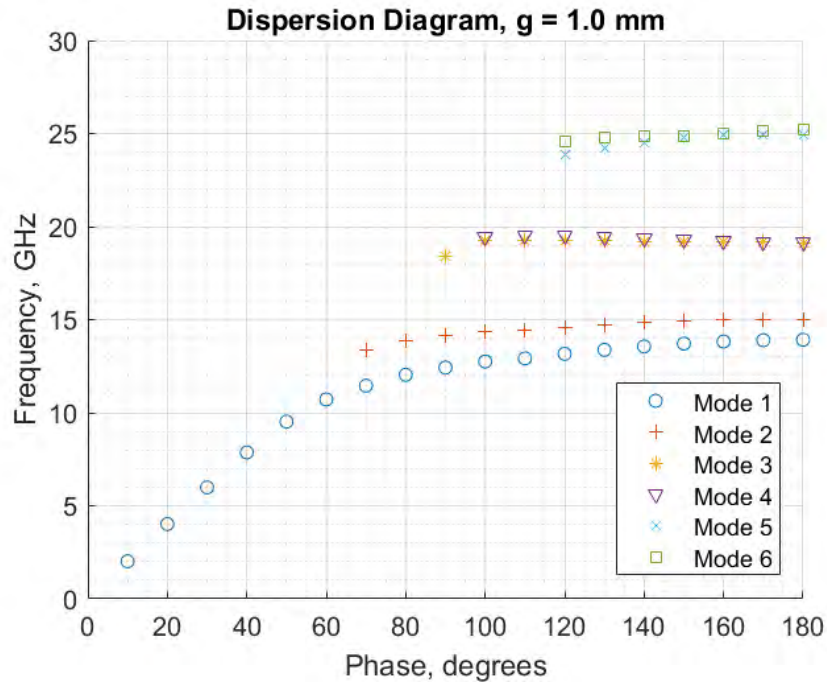


Figure 557: Fractal Rogers 3010: Dispersion Diagram, g = 1.0

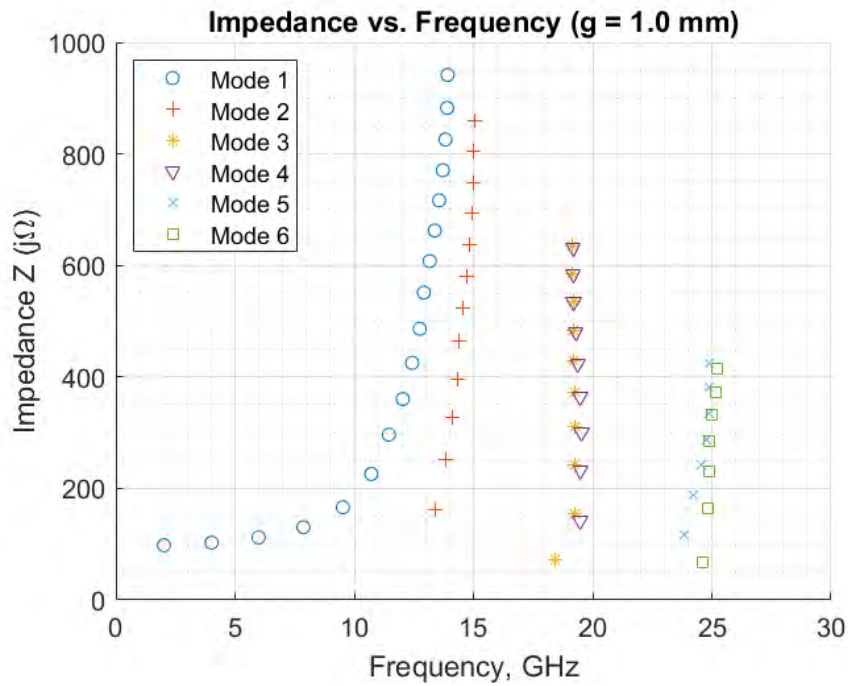


Figure 558: Fractal Rogers 3010: Impedance vs. Frequency, g = 1.0

Appendix G. 10" by 16" 17 GHz Duroid 5880 Antenna

Antenna Design Parameters	
Parameter	Value
Dimensions	16" by 10"
Material	Duroid 5880
Cell Shape	square
Cell Size, a	3 mm
Number of Cells	135 by 83 = 11,205
Design Frequency	17 GHz
ϕ	72°
θ_L	60°
X	164 j Ω
M	37.7 j Ω
Z_{min}	126.3 j Ω
Z_{max}	201.8 j Ω

Table 106: D5880 Antenna Design Parameters

Antenna Performance	
1.5:1 SWR Bandwidth	7.59 GHz (10.41 to 18 GHz)
2:1 SWR Bandwidth	8.47 GHz (9.53 to 18 GHz)
Resonant Frequency	15.36 GHz
Beamwidth at 15.36 GHz	5°
Gain at 15.36 GHz	15.5 dBi
Beamwidth at 17 GHz	8°
Gain at 17 GHz	18.1 dBi

Table 107: D5880 Antenna Performance

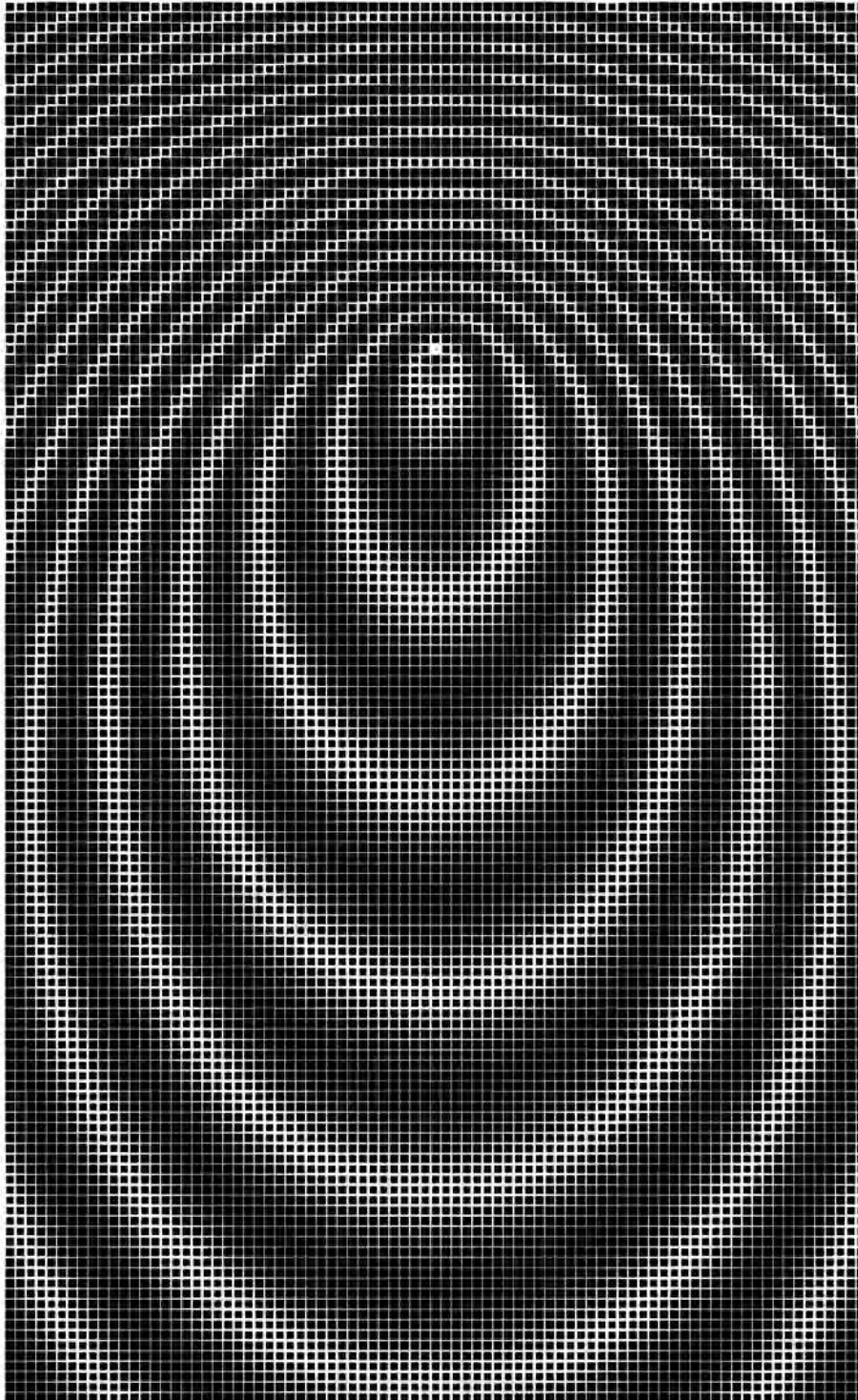


Figure 559: D5880 Antenna: Design Image (not to scale)

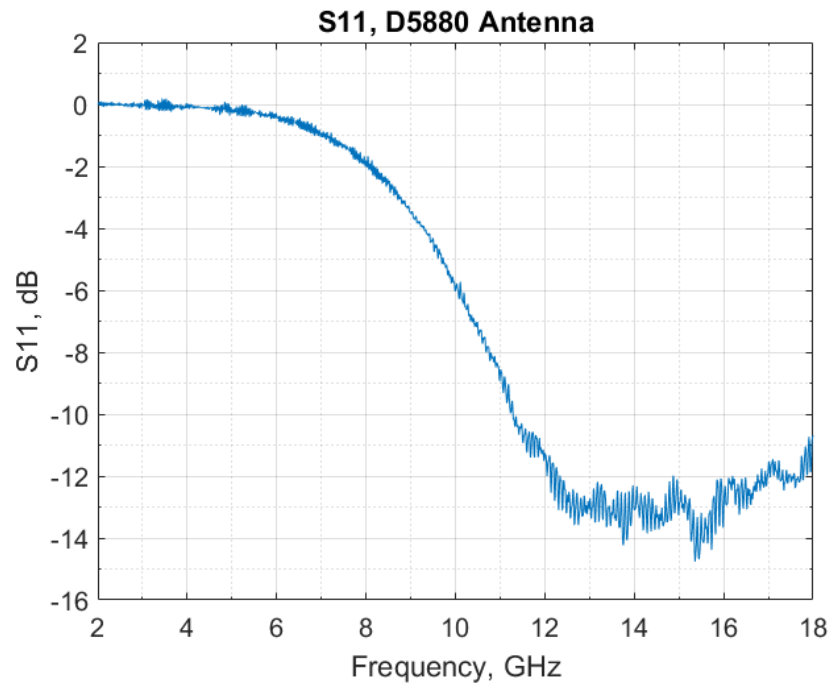


Figure 560: D5880 Antenna: S11, 2 to 18 GHz

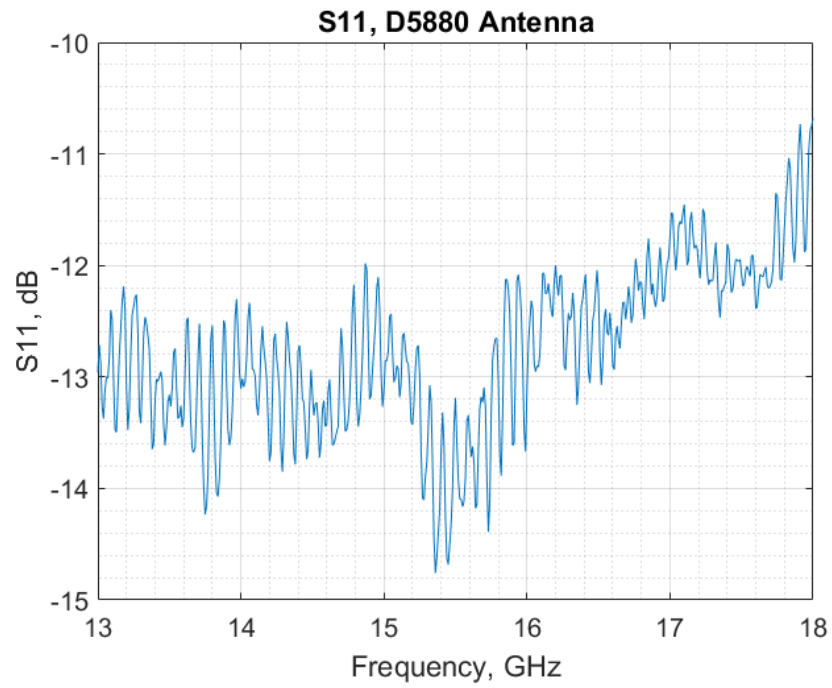


Figure 561: D5880 Antenna: S11, 13 to 18 GHz

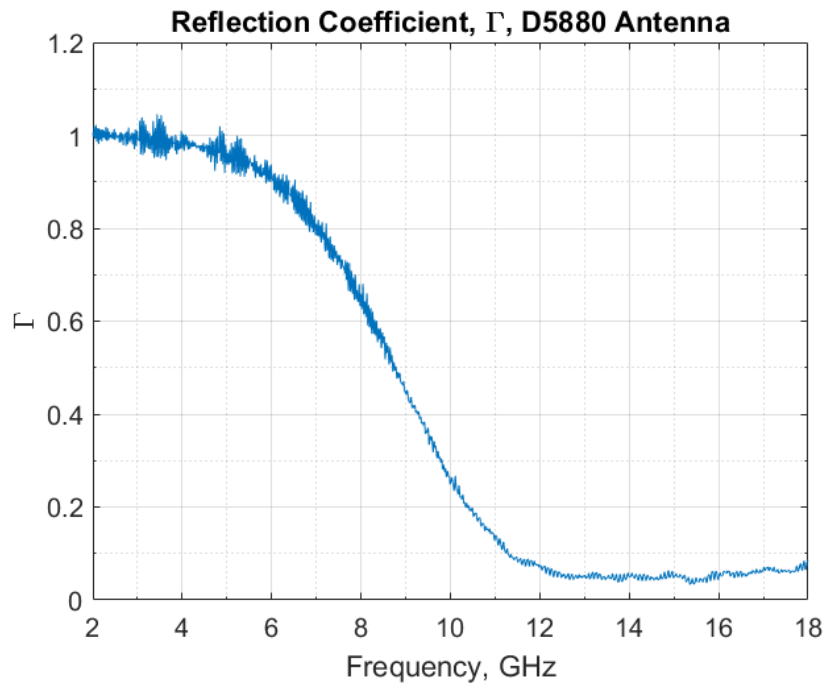


Figure 562: D5880 Antenna: Reflection Coefficient, Γ

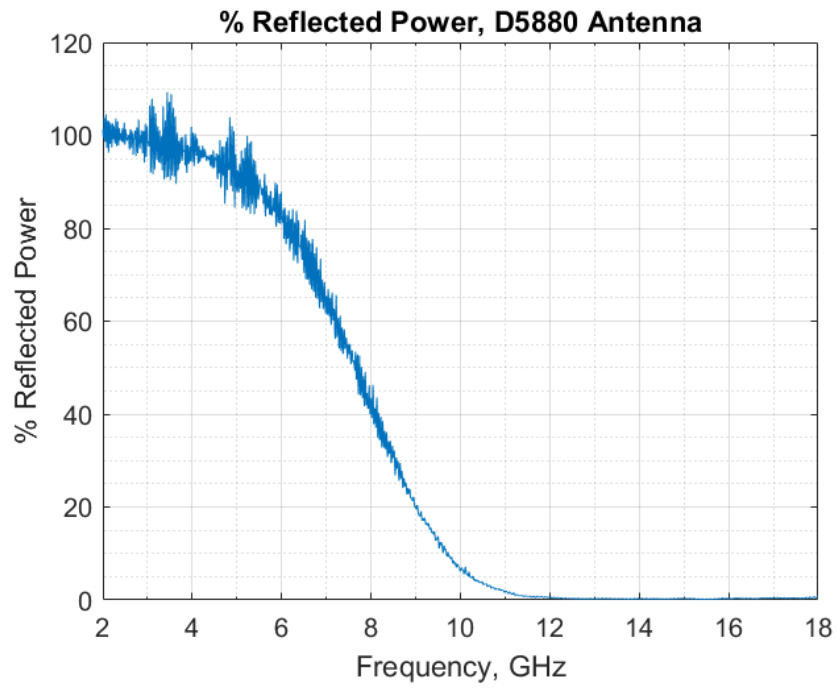


Figure 563: D5880 Antenna: Percent Reflected Power

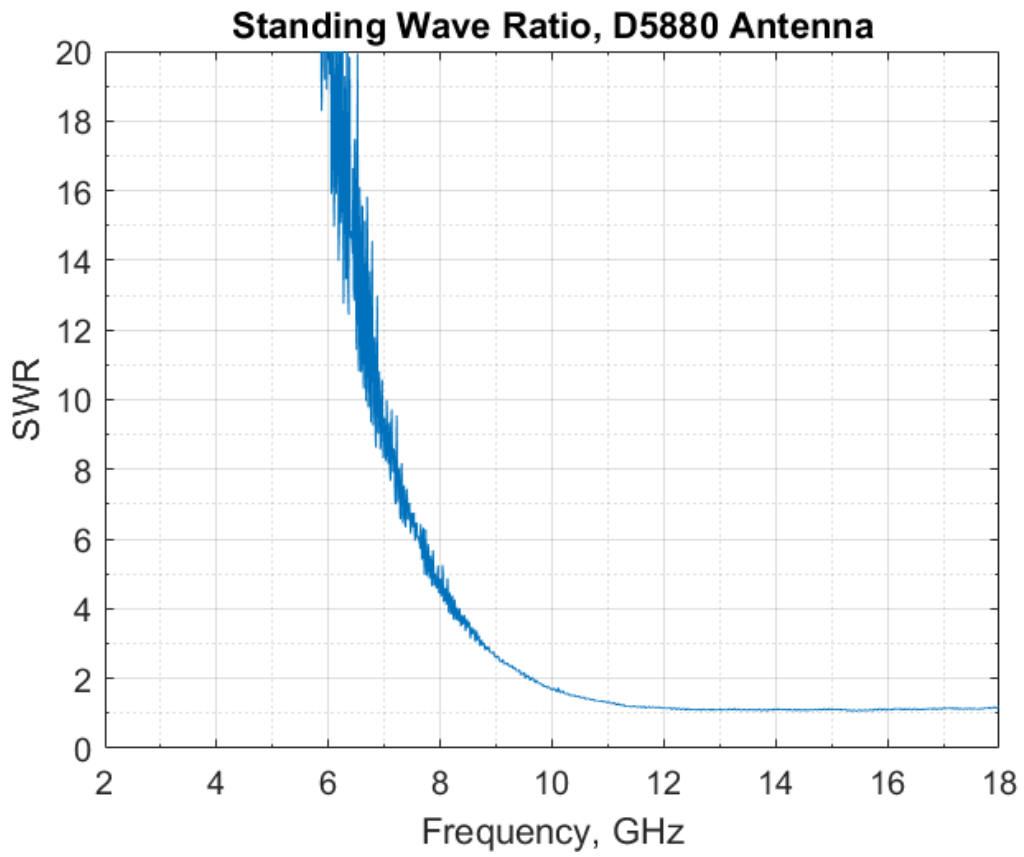


Figure 564: D5880 Antenna: Standing Wave Ratio (SWR)

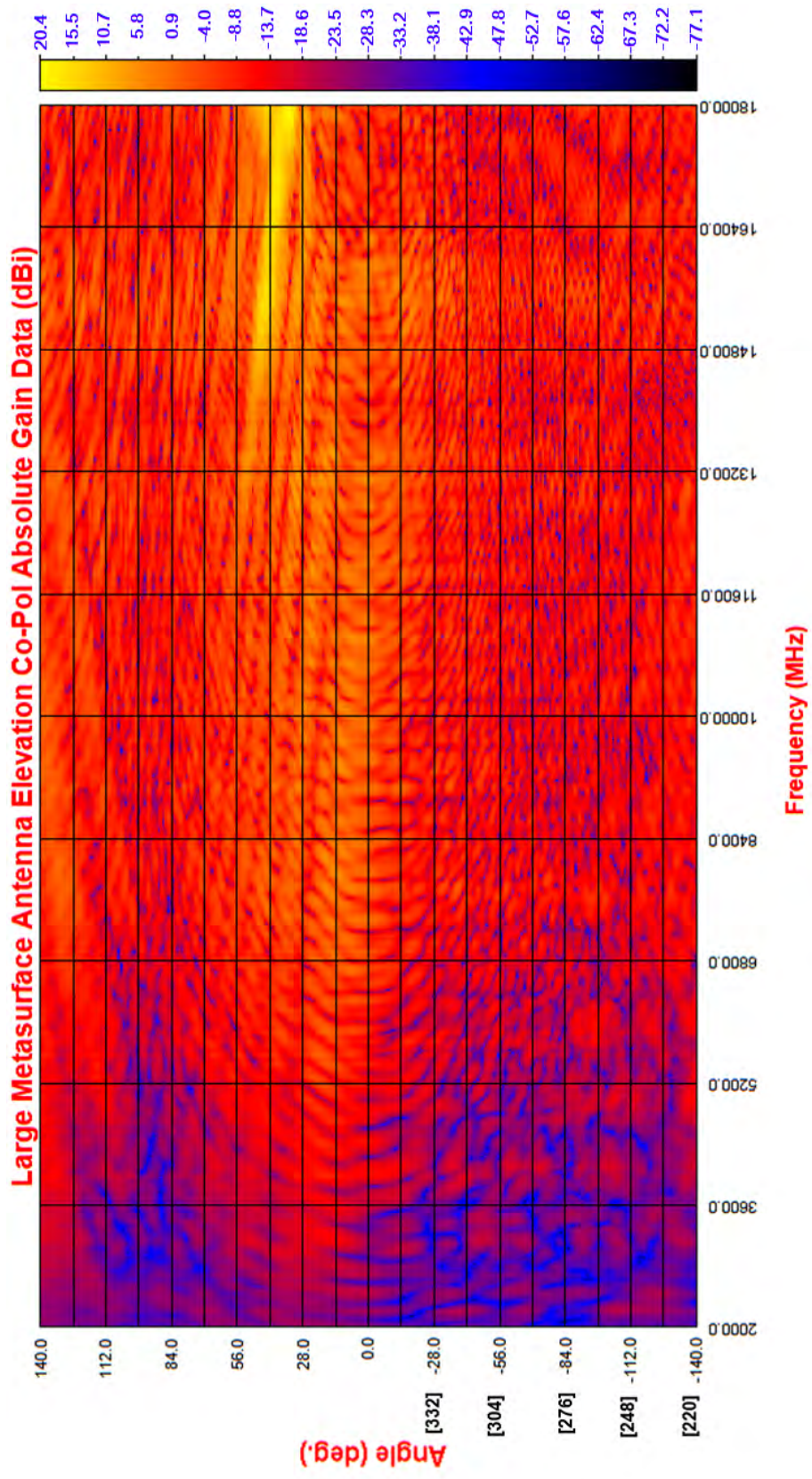


Figure 565: D5880 Antenna: Elevation Waterfall Gain Plot

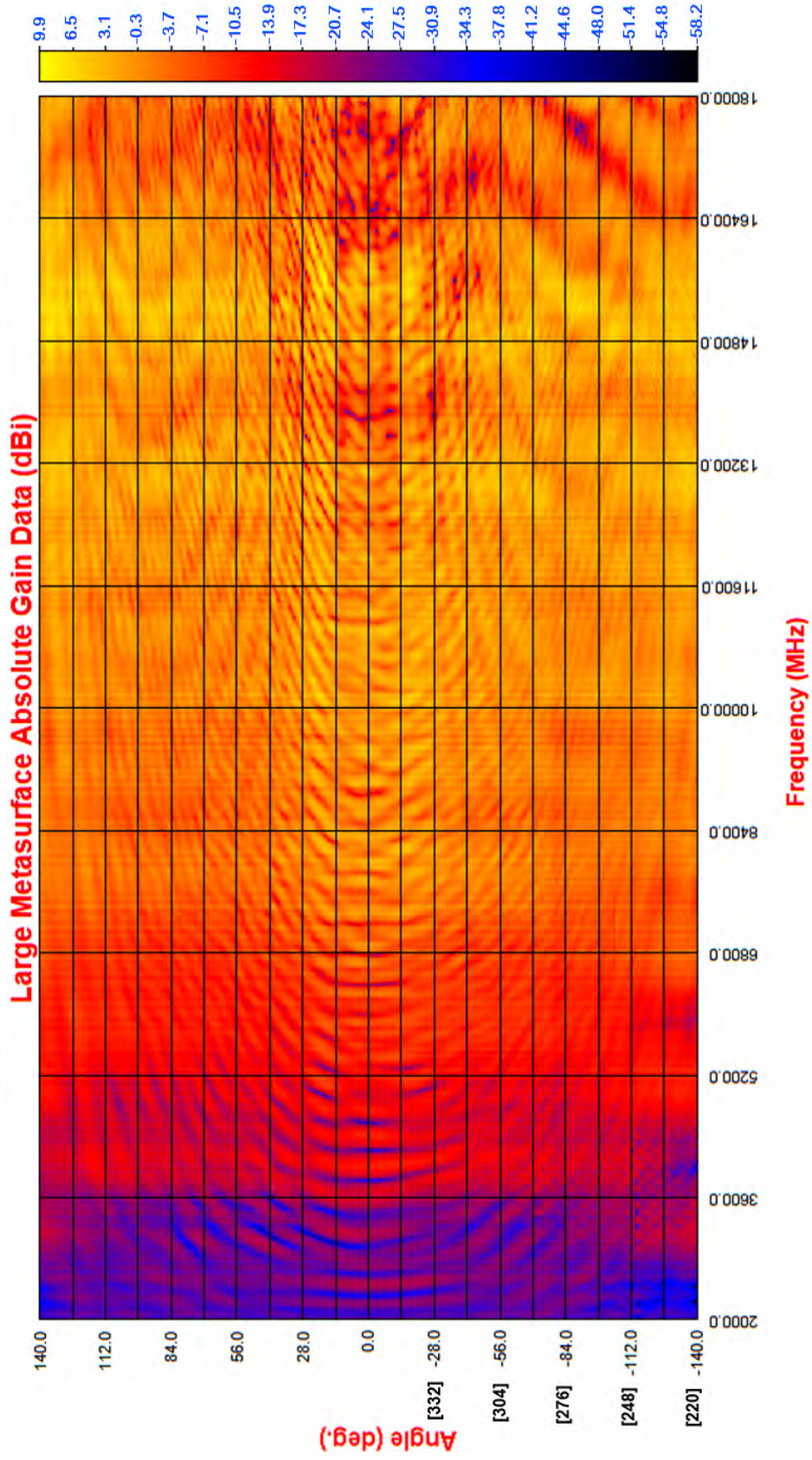


Figure 566: D5880 Antenna: Azimuth Waterfall Gain Plot

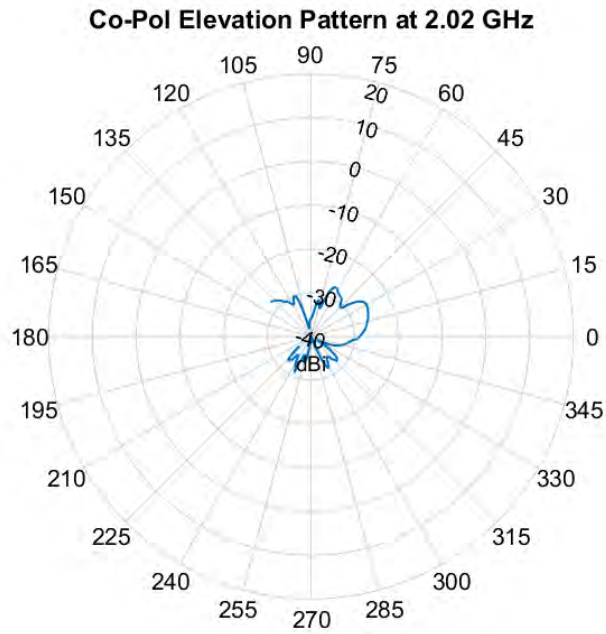


Figure 567: D5880 Antenna: Elevation Pattern, 2 GHz

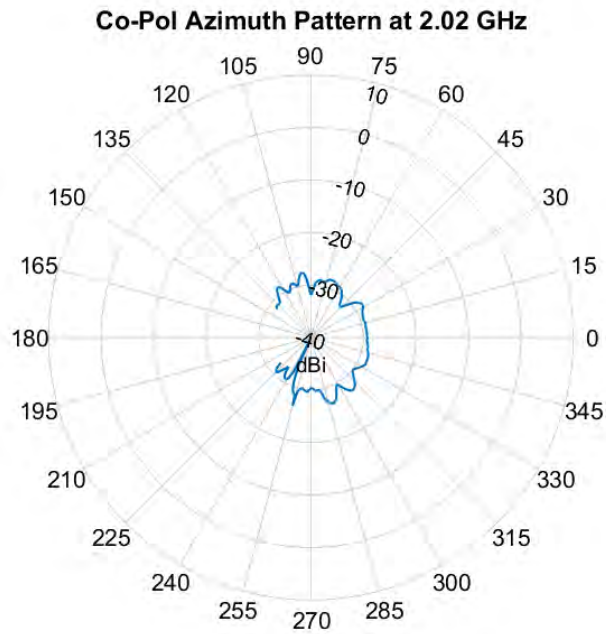


Figure 568: D5880 Antenna: Azimuth Pattern, 2 GHz

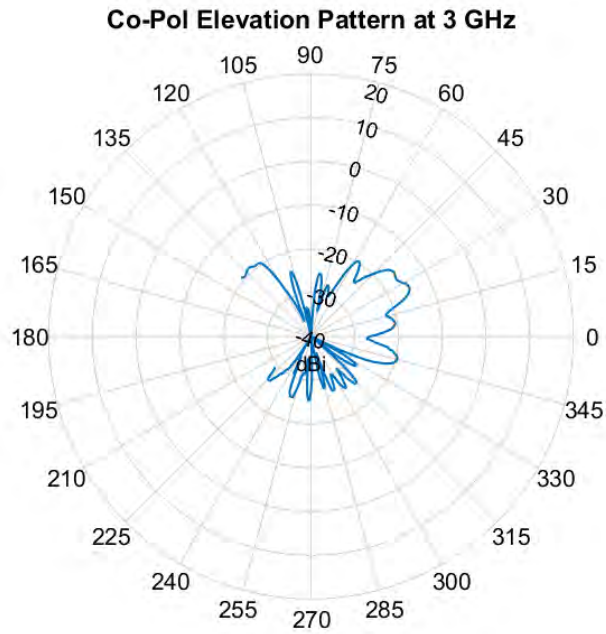


Figure 569: D5880 Antenna: Elevation Pattern, 3 GHz

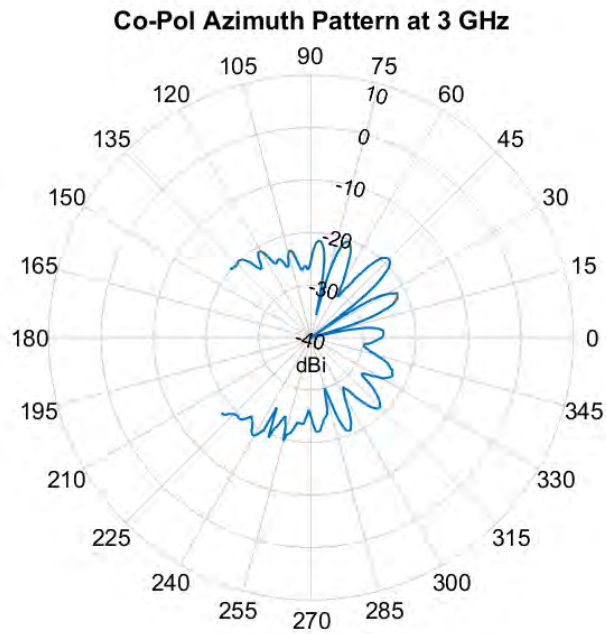


Figure 570: D5880 Antenna: Azimuth Pattern, 3 GHz

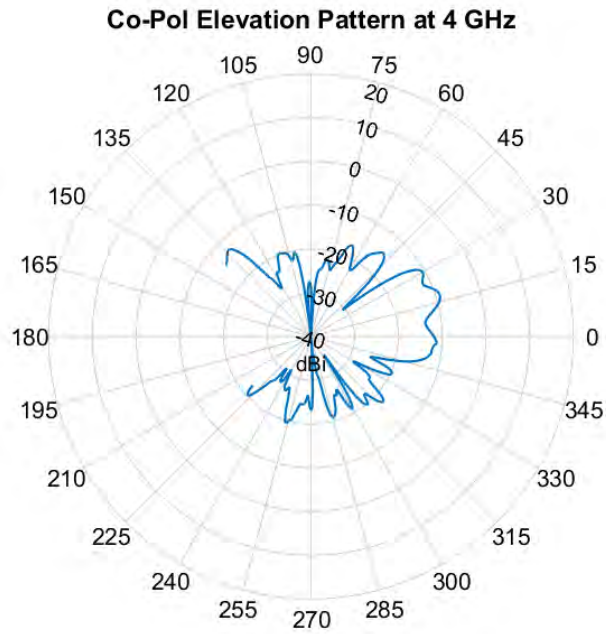


Figure 571: D5880 Antenna: Elevation Pattern, 4 GHz

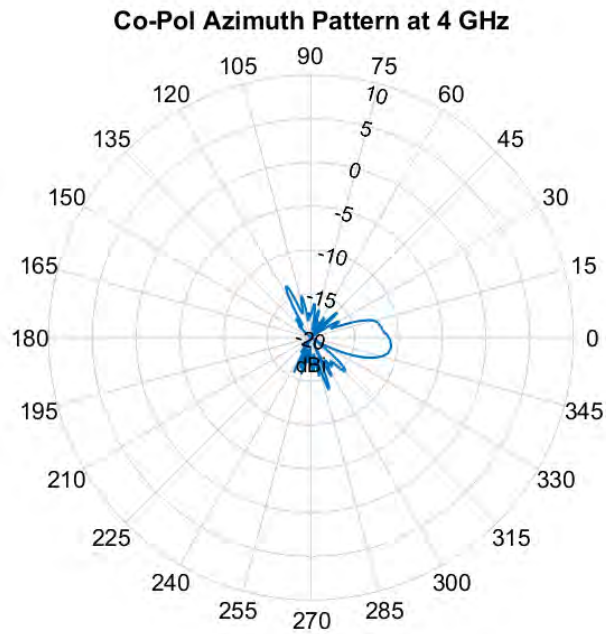


Figure 572: D5880 Antenna: Azimuth Pattern, 4 GHz

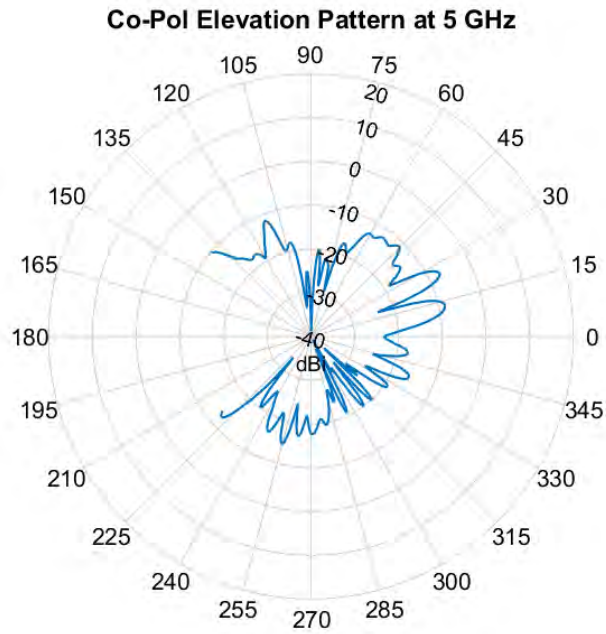


Figure 573: D5880 Antenna: Elevation Pattern, 5 GHz

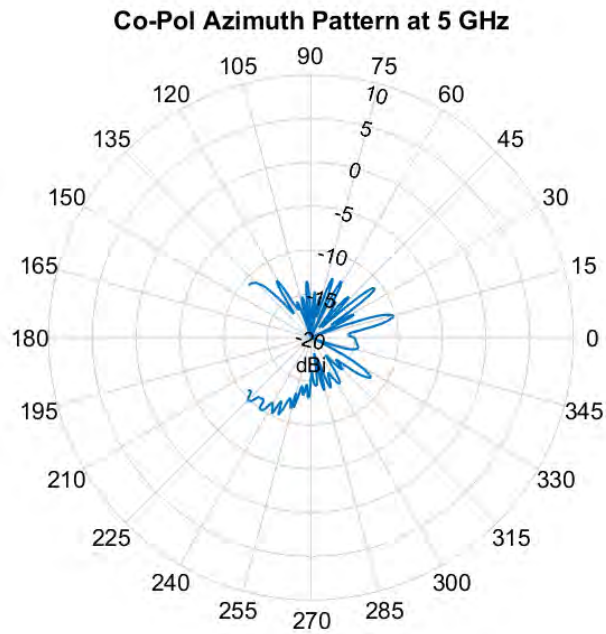


Figure 574: D5880 Antenna: Azimuth Pattern, 5 GHz

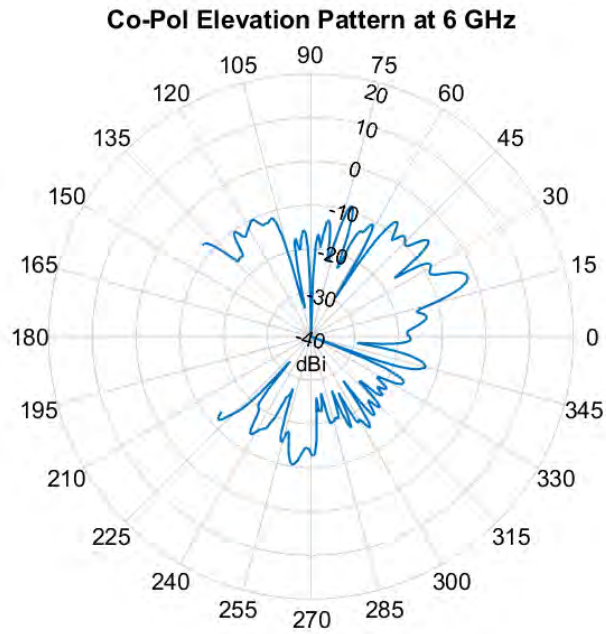


Figure 575: D5880 Antenna: Elevation Pattern, 6 GHz

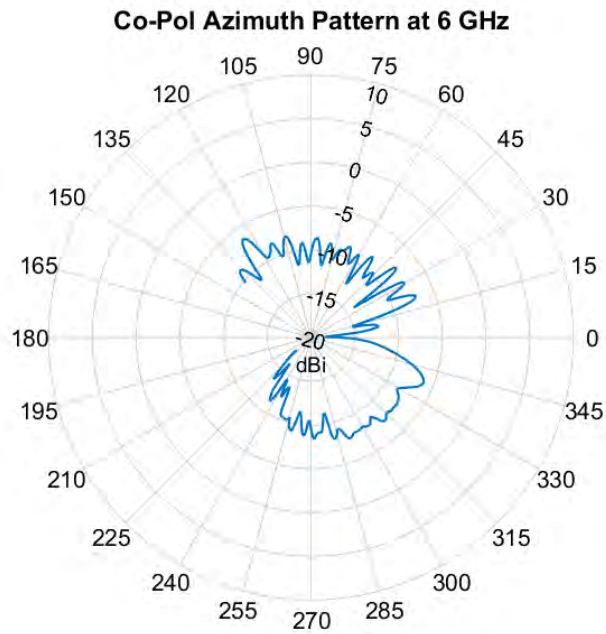


Figure 576: D5880 Antenna: Azimuth Pattern, 6 GHz

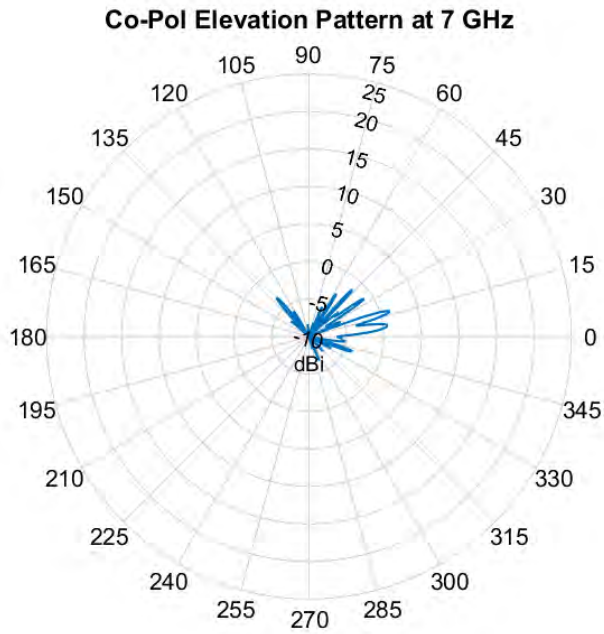


Figure 577: D5880 Antenna: Elevation Pattern, 7 GHz

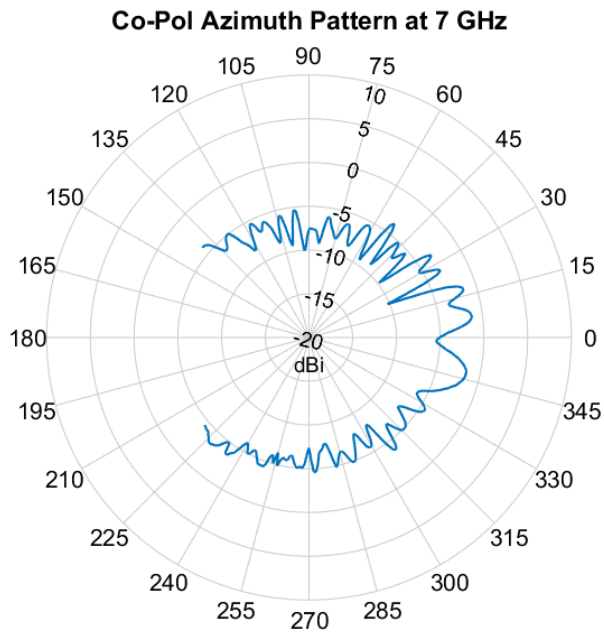


Figure 578: D5880 Antenna: Azimuth Pattern, 7 GHz

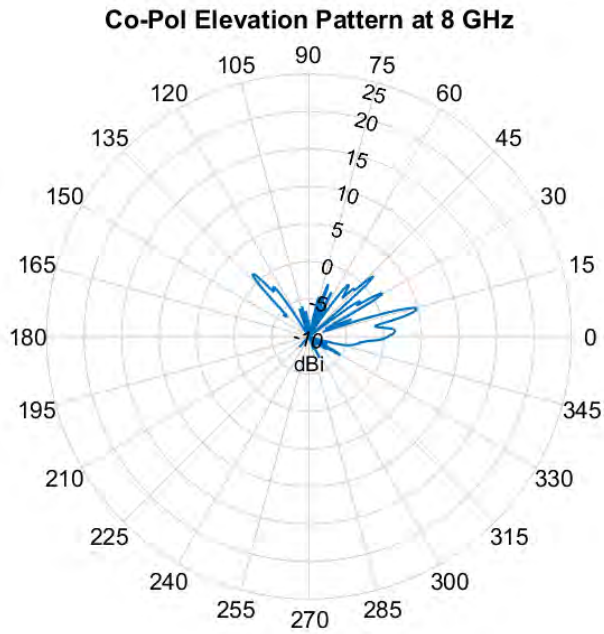


Figure 579: D5880 Antenna: Elevation Pattern, 8 GHz

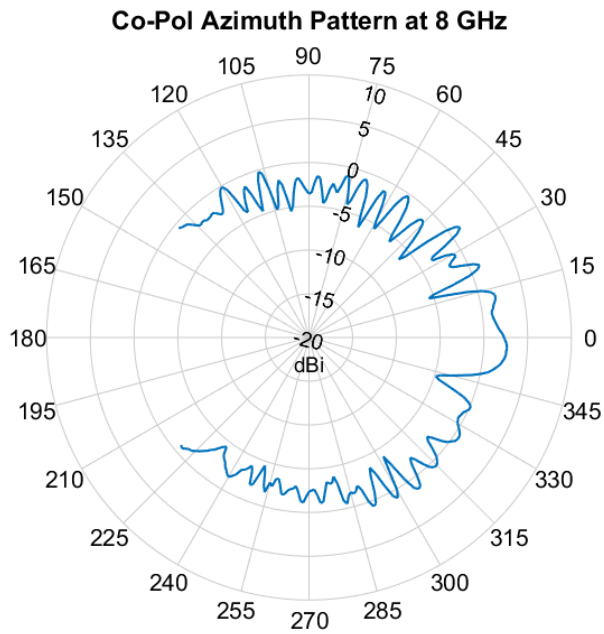


Figure 580: D5880 Antenna: Azimuth Pattern, 8 GHz

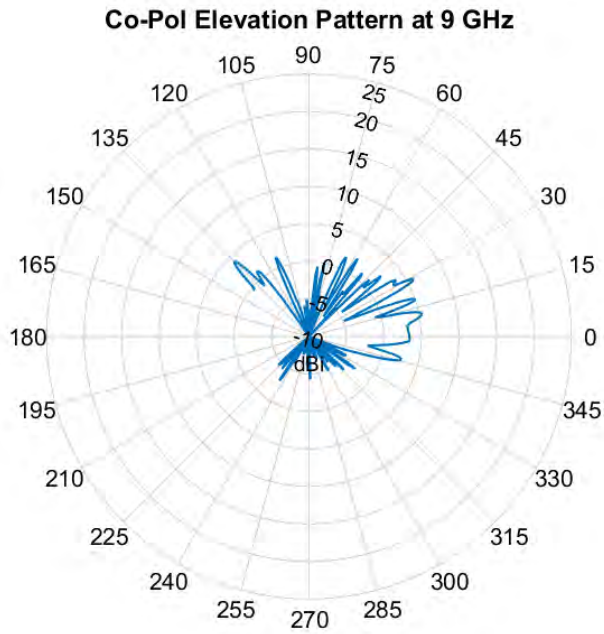


Figure 581: D5880 Antenna: Elevation Pattern, 9 GHz

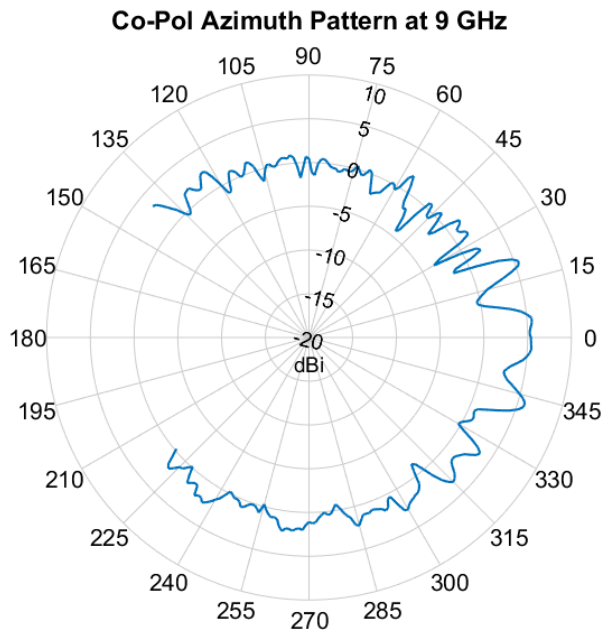


Figure 582: D5880 Antenna: Azimuth Pattern, 9 GHz

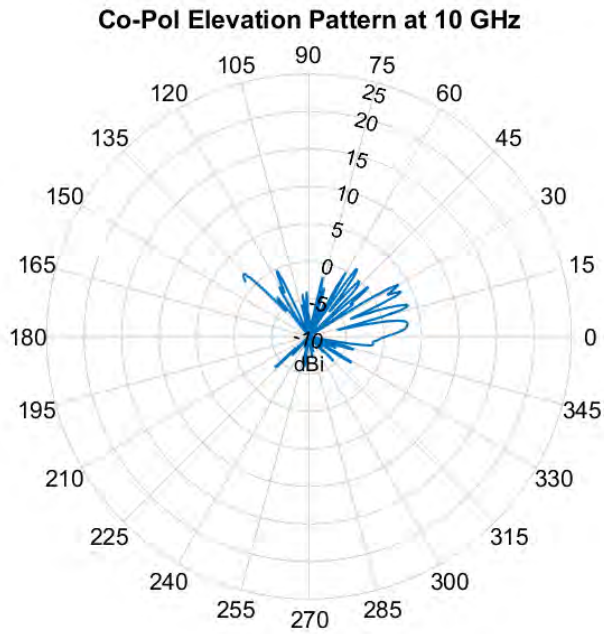


Figure 583: D5880 Antenna: Elevation Pattern, 10 GHz

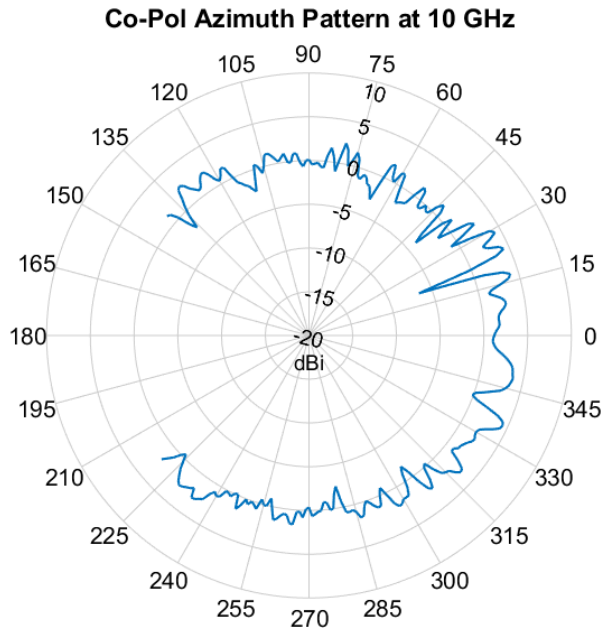


Figure 584: D5880 Antenna: Azimuth Pattern, 10 GHz

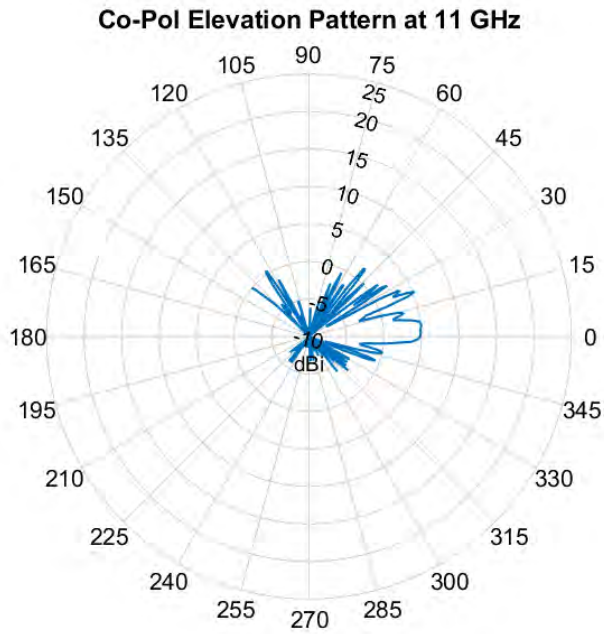


Figure 585: D5880 Antenna: Elevation Pattern, 11 GHz

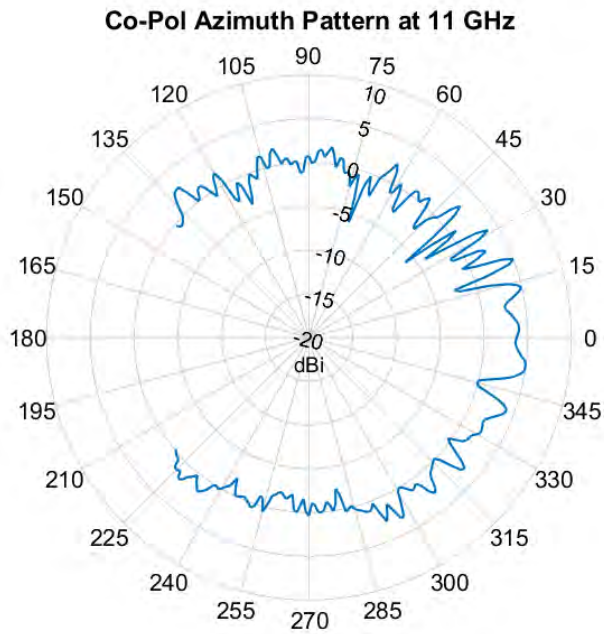


Figure 586: D5880 Antenna: Azimuth Pattern, 11 GHz

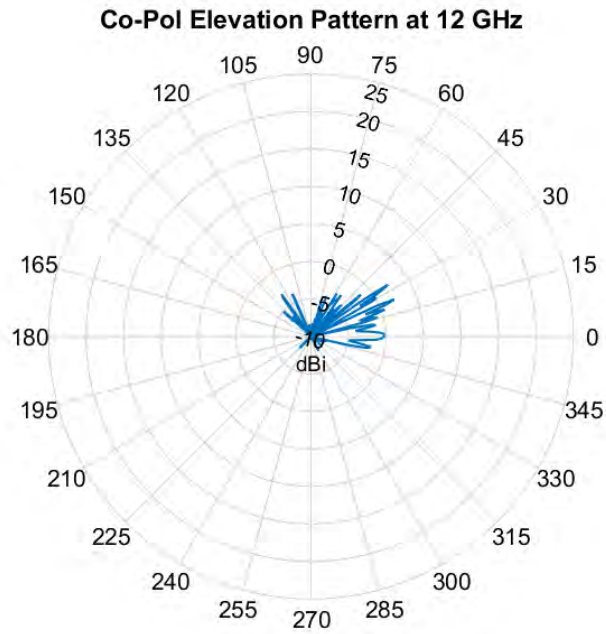


Figure 587: D5880 Antenna: Elevation Pattern, 12 GHz

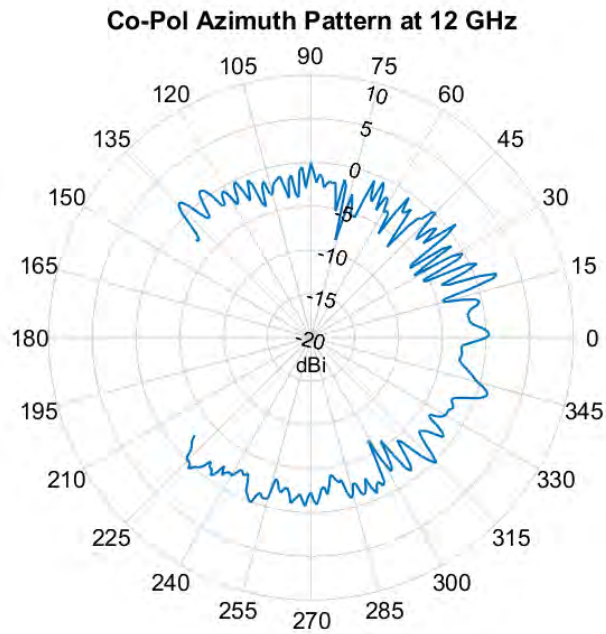


Figure 588: D5880 Antenna: Azimuth Pattern, 12 GHz

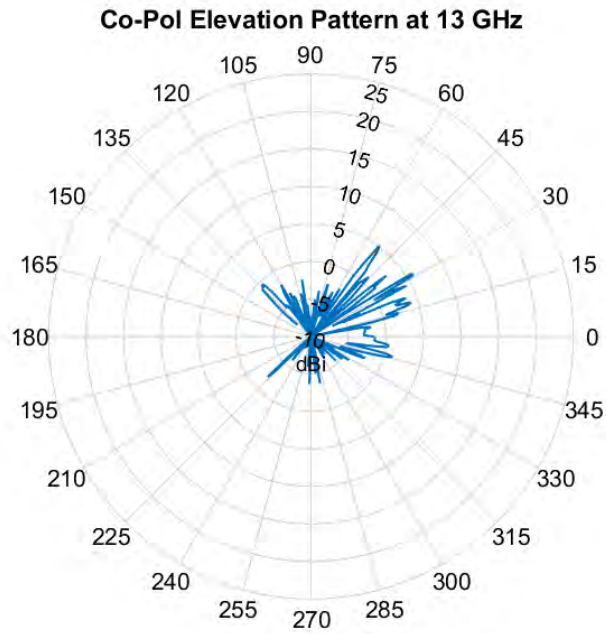


Figure 589: D5880 Antenna: Elevation Pattern, 13 GHz

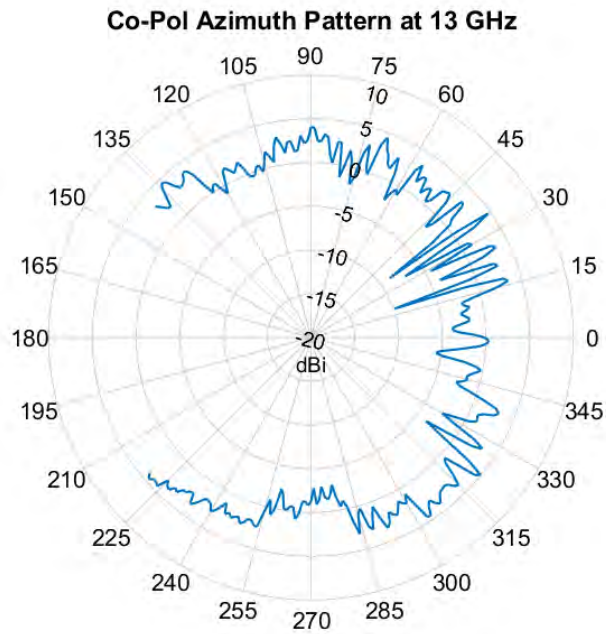


Figure 590: D5880 Antenna: Azimuth Pattern, 13 GHz

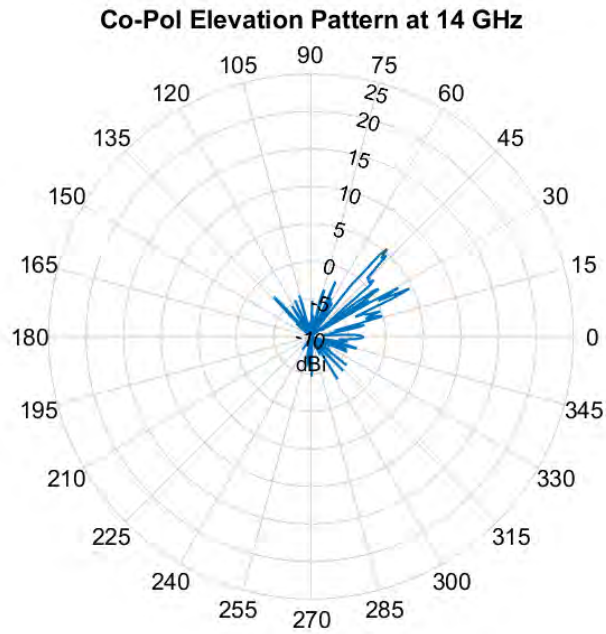


Figure 591: D5880 Antenna: Elevation Pattern, 14 GHz

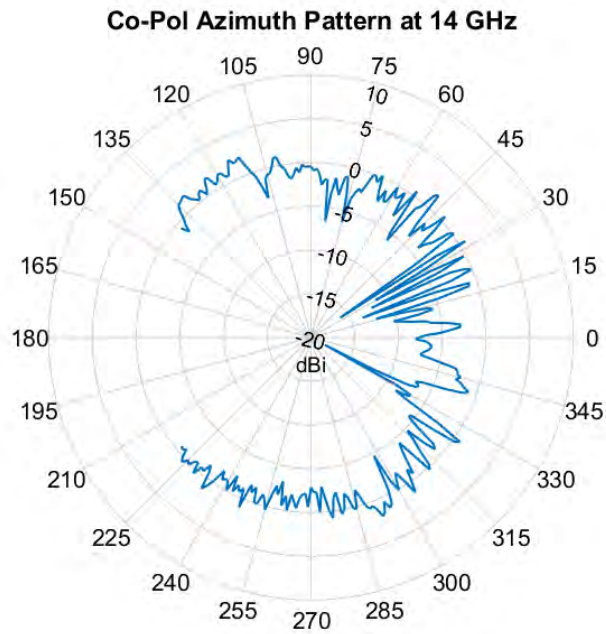


Figure 592: D5880 Antenna: Azimuth Pattern, 14 GHz

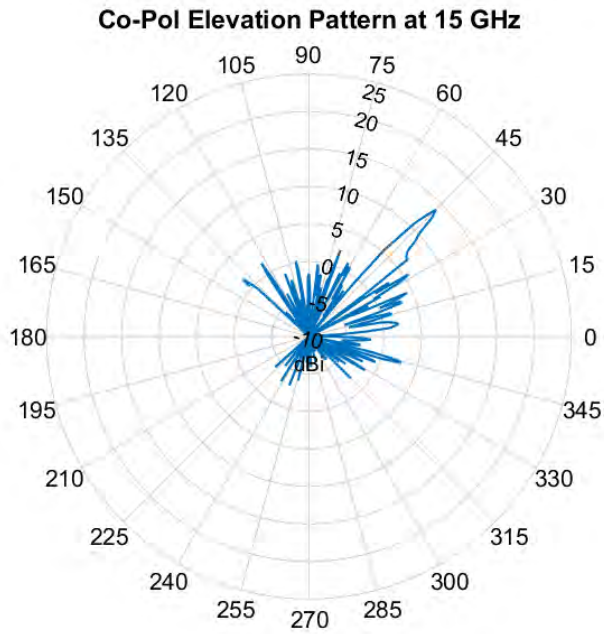


Figure 593: D5880 Antenna: Elevation Pattern, 15 GHz

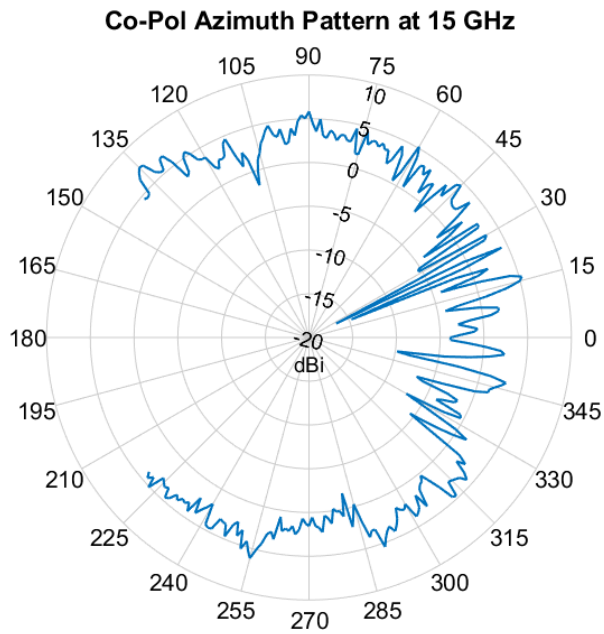


Figure 594: D5880 Antenna: Azimuth Pattern, 15 GHz

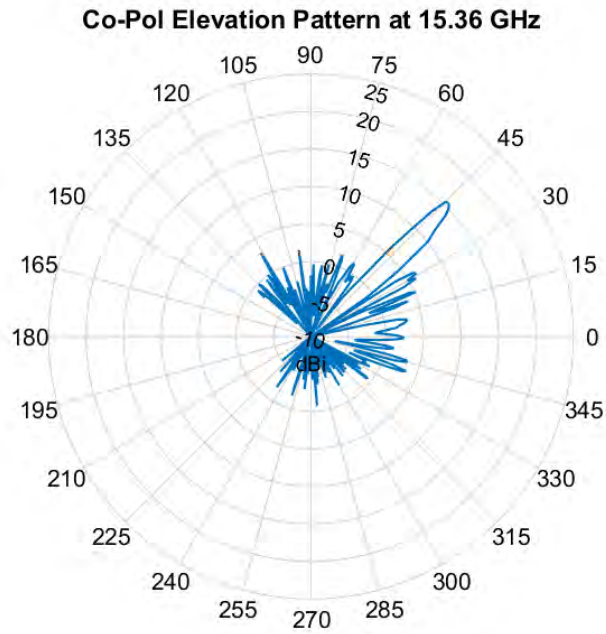


Figure 595: D5880 Antenna: Elevation Pattern, 15.360 GHz

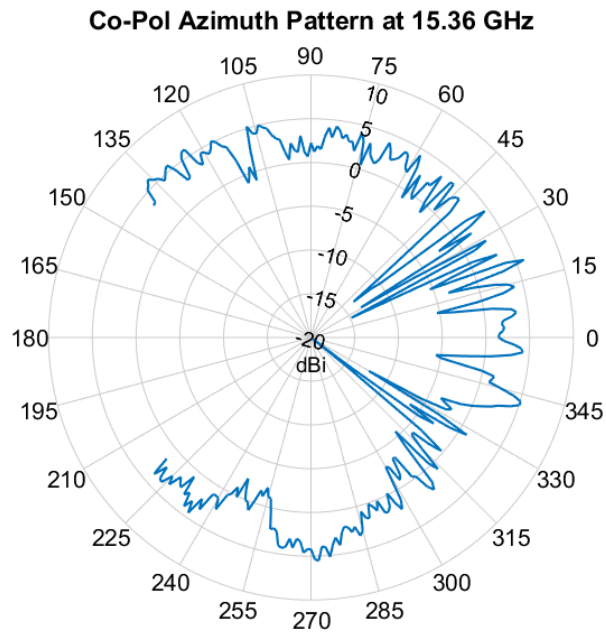


Figure 596: D5880 Antenna: Azimuth Pattern, 15.36 GHz

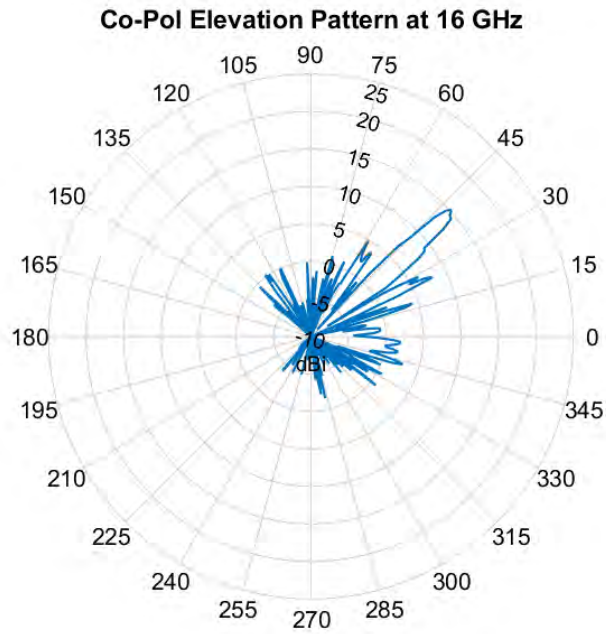


Figure 597: D5880 Antenna: Elevation Pattern, 16 GHz

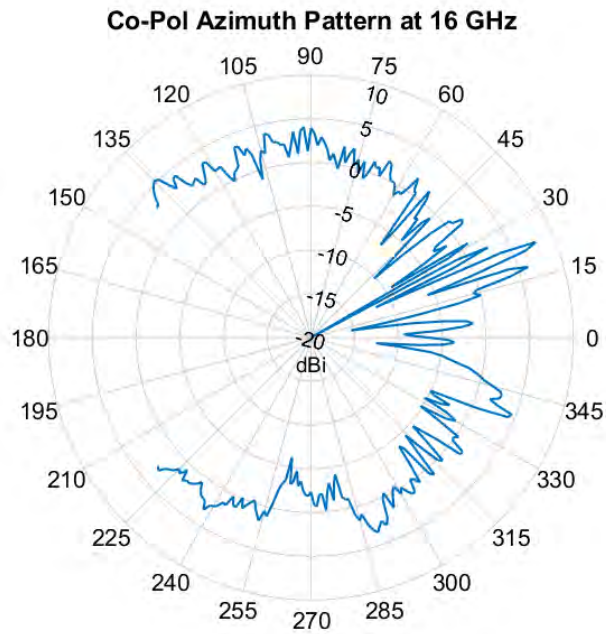


Figure 598: D5880 Antenna: Azimuth Pattern, 16 GHz

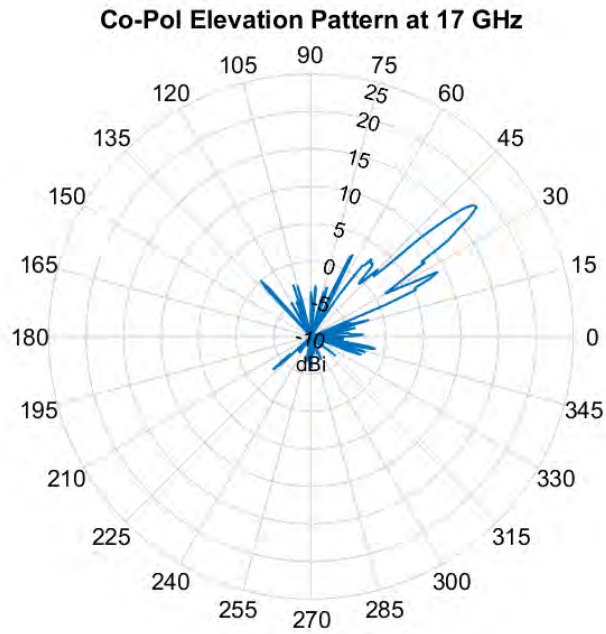


Figure 599: D5880 Antenna: Elevation Pattern, 17 GHz

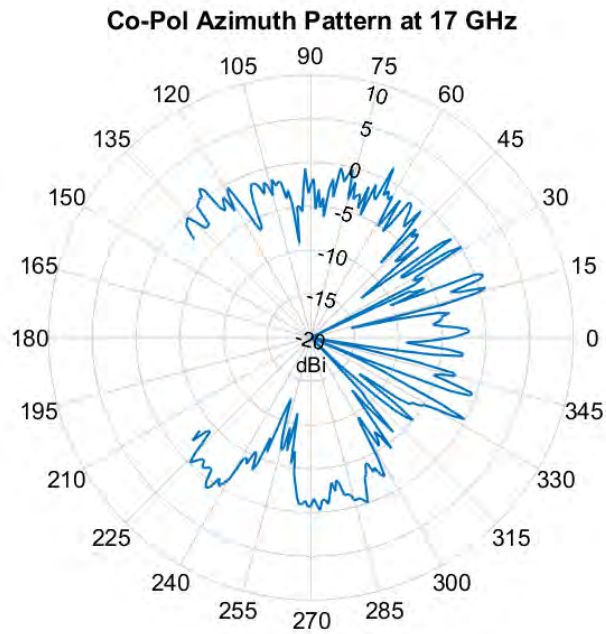


Figure 600: D5880 Antenna: Azimuth Pattern, 17 GHz

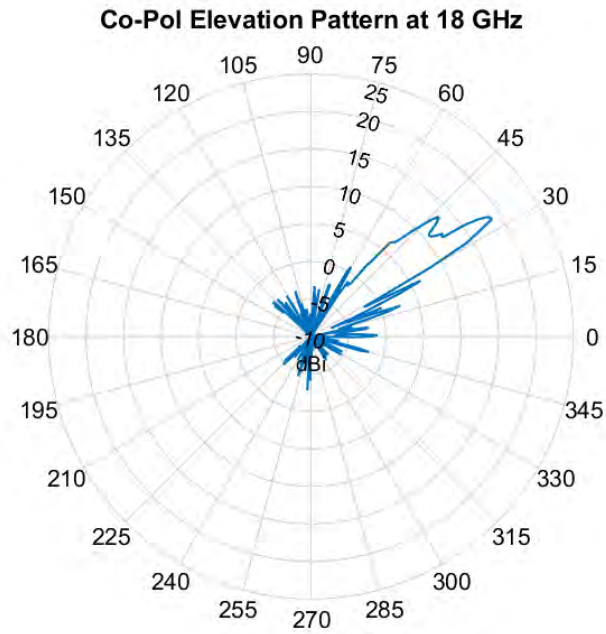


Figure 601: D5880 Antenna: Elevation Pattern, 18 GHz

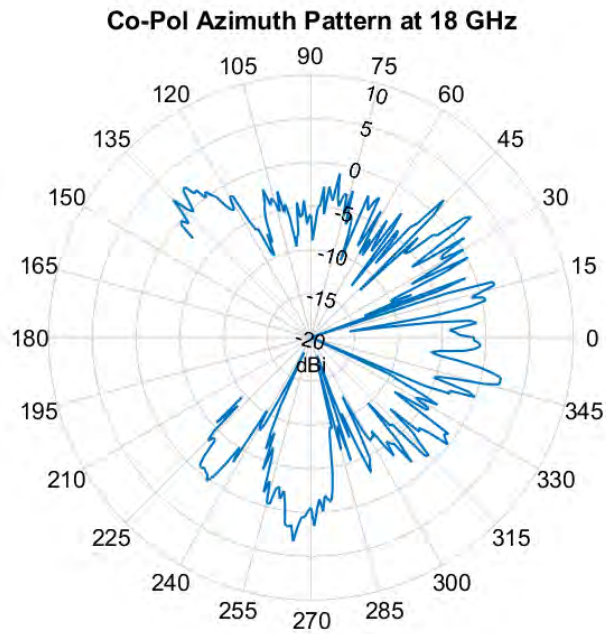


Figure 602: D5880 Antenna: Azimuth Pattern, 18 GHz

Appendix H. 10" by 16" FR4 Antenna

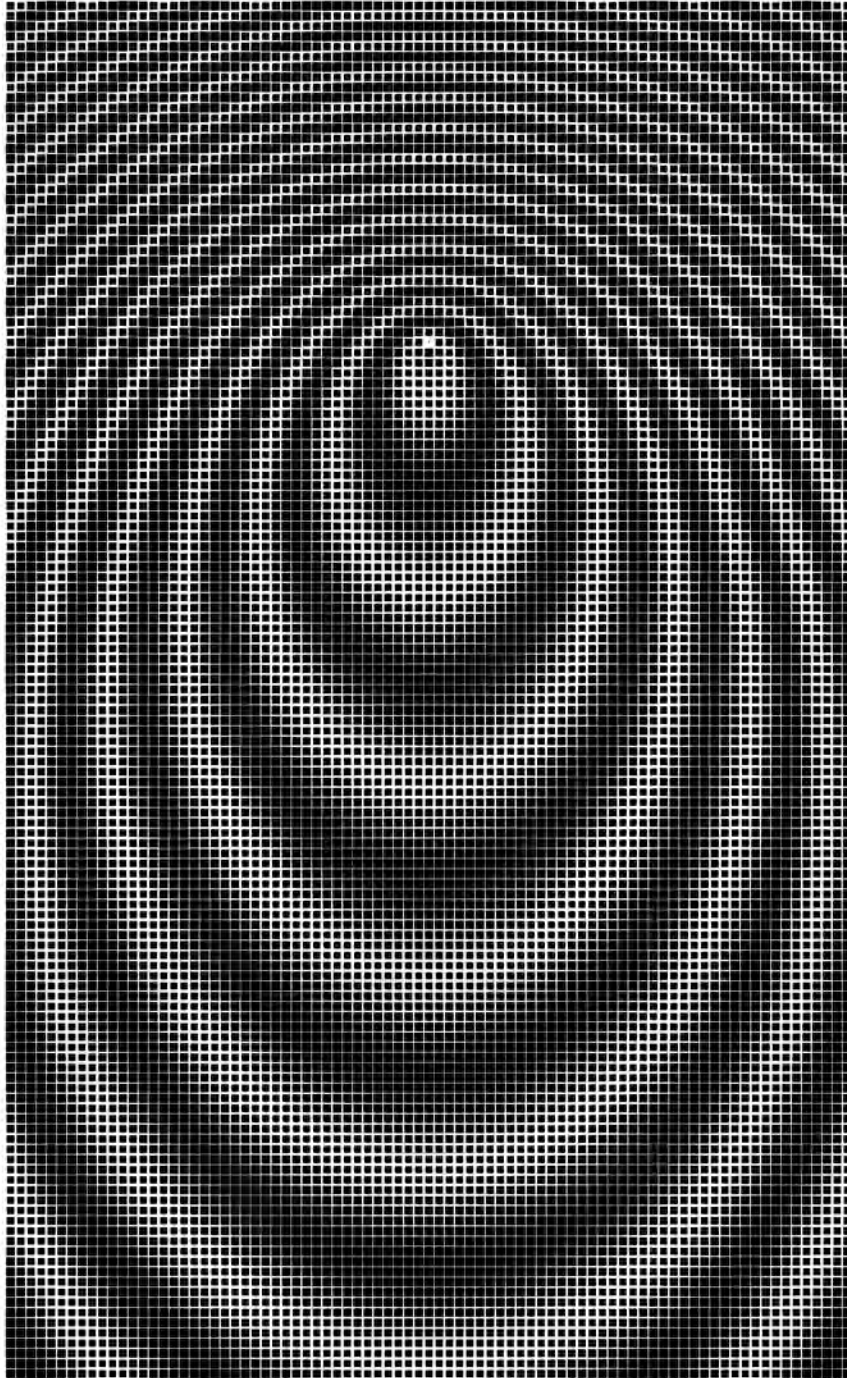


Figure 603: FR4 Antenna Design Image (not to scale)

Antenna Design Parameters	
<u>Parameter</u>	<u>Value</u>
Dimensions	16" by 10"
Thickness	0.7874 mm
Material	FR4
Cell Shape	square
Cell Size, a	3 mm
Number of Cells	135 by 83 = 11,205
Design Frequency	N/A
ϕ	72°
θ_L	60°
X	197.5
M	36.5 j Ω
Z_{min}	161
Z_{max}	234

Table 108: FR4 Antenna: Design Parameters

Antenna Performance		
<u>Parameter</u>	<u>Main beam #1</u>	<u>Main beam #2</u>
Beamwidth at 13 GHz	8°	N/A
Centerpoint at 13 GHz	51°	N/A
Gain at 13 GHz	5 dBi	N/A
Beamwidth at 14 GHz	17°	N/A
Centerpoint at 14 GHz	45°	N/A
Gain at 14 GHz	11 dBi	N/A
Beamwidth at 15 GHz	19°	N/A
Centerpoint at 15 GHz	42°	N/A
Gain at 15 GHz	14 dBi	N/A
Beamwidth at 16 GHz	30°	N/A
Centerpoint at 16 GHz	45°	N/A
Gain at 16 GHz	11 dBi	N/A
Beamwidth at 17 GHz	16°	26°
Centerpoint at 17 GHz	45°	20°
Gain at 17 GHz	9 dBi	9 dBi
Beamwidth at 18 GHz	16°	50°
Centerpoint at 18 GHz	54°	24°
Gain at 18 GHz	9 dBi	5 dBi

Table 109: FR4 Antenna Performance (Elevation)

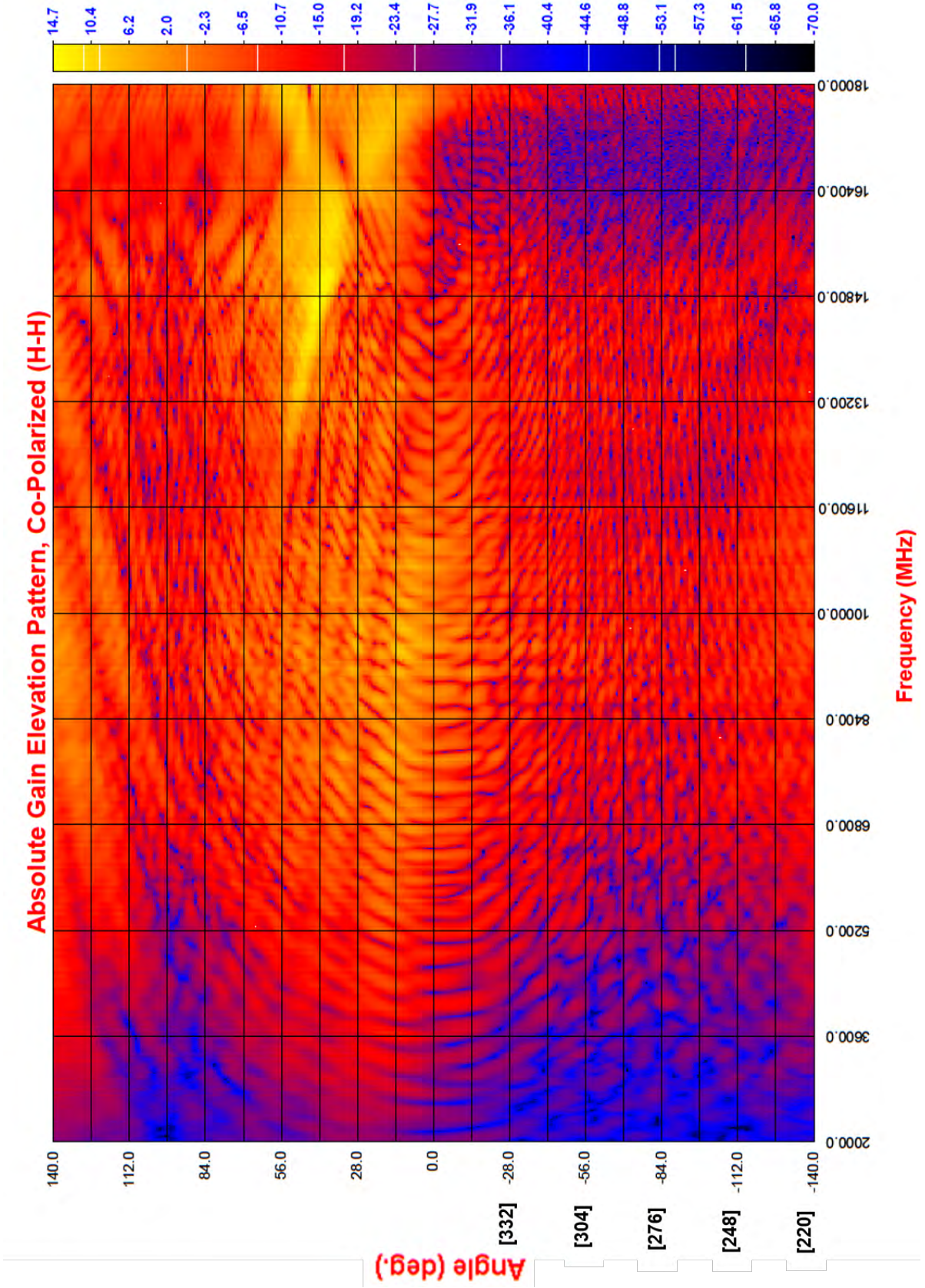


Figure 604: FR4 Antenna: Elevation Waterfall Gain Plot

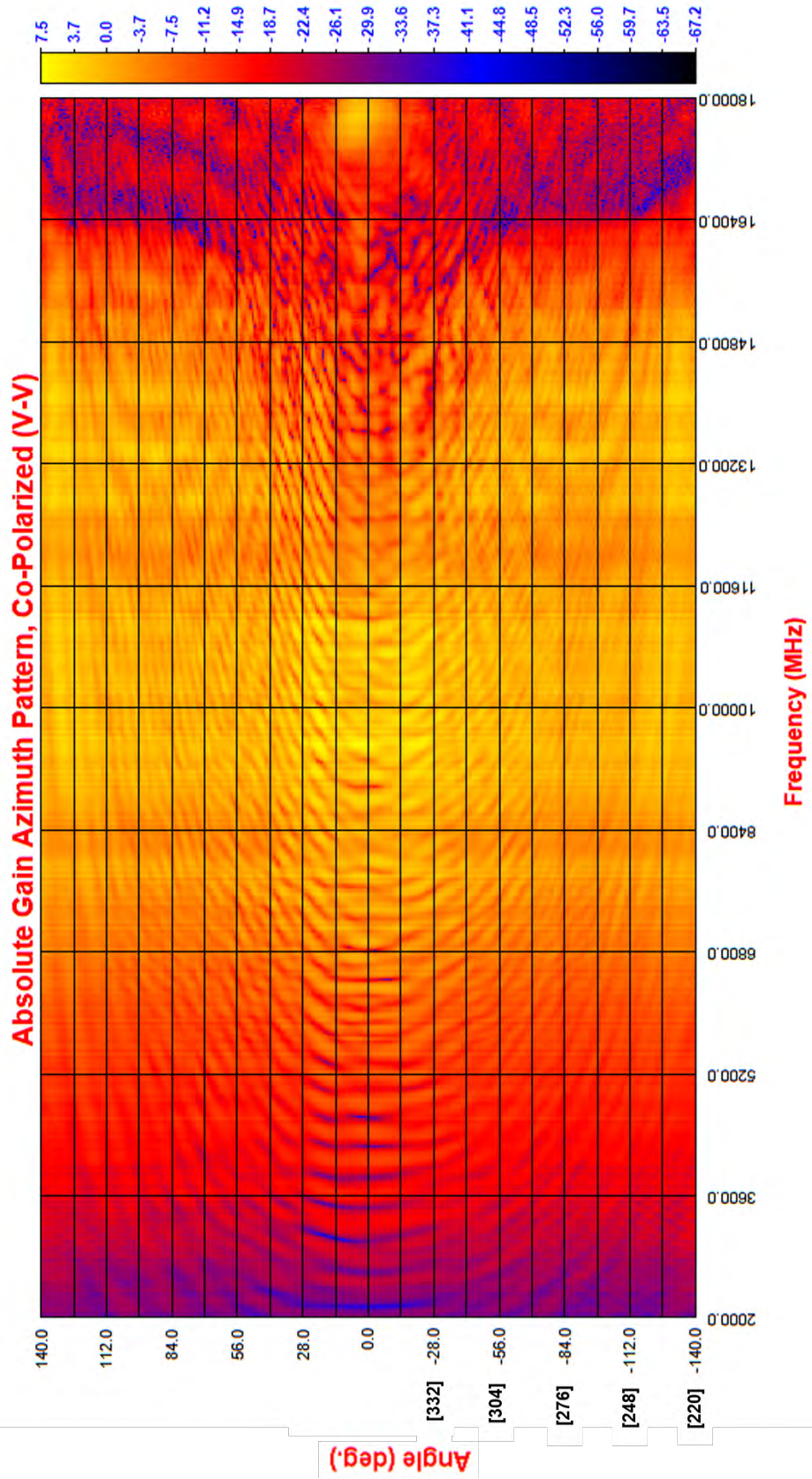


Figure 605: FR4 Antenna: Azimuth Waterfall Gain Plot

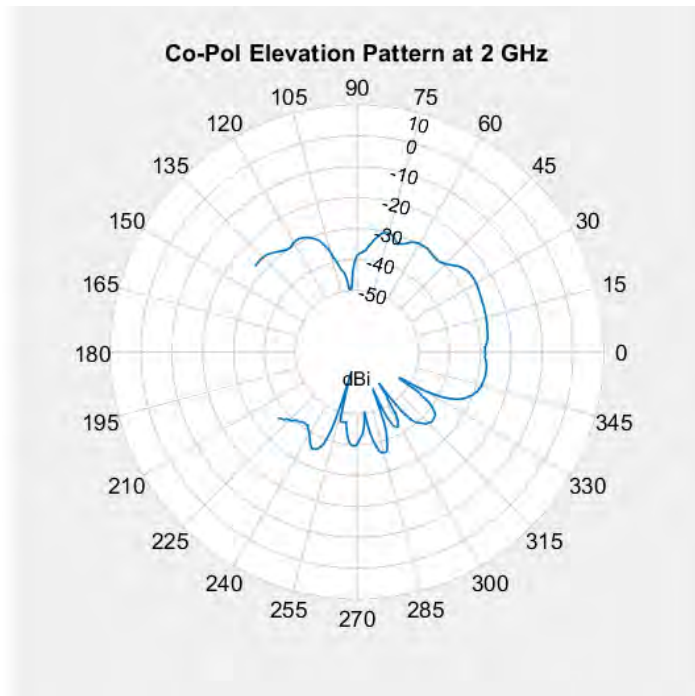


Figure 606: FR4 Antenna: Elevation Pattern, 2 GHz

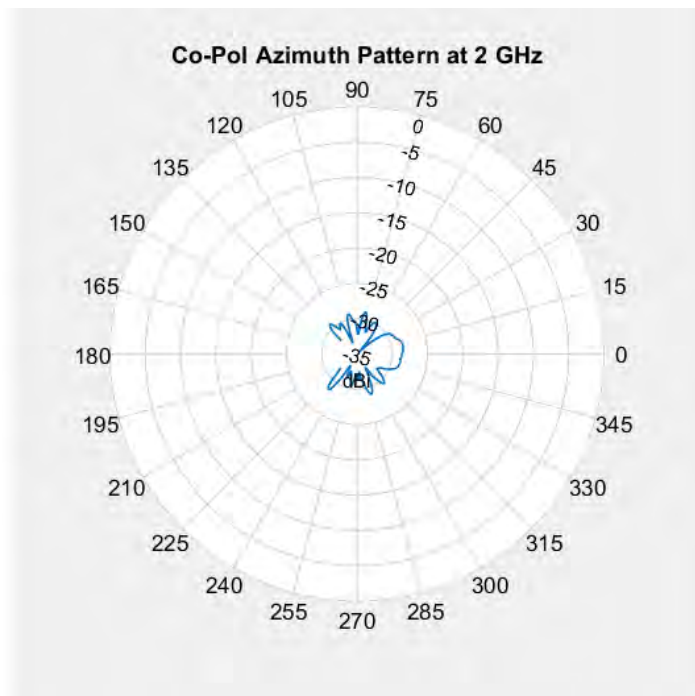


Figure 607: FR4 Antenna: Azimuth Pattern, 2 GHz

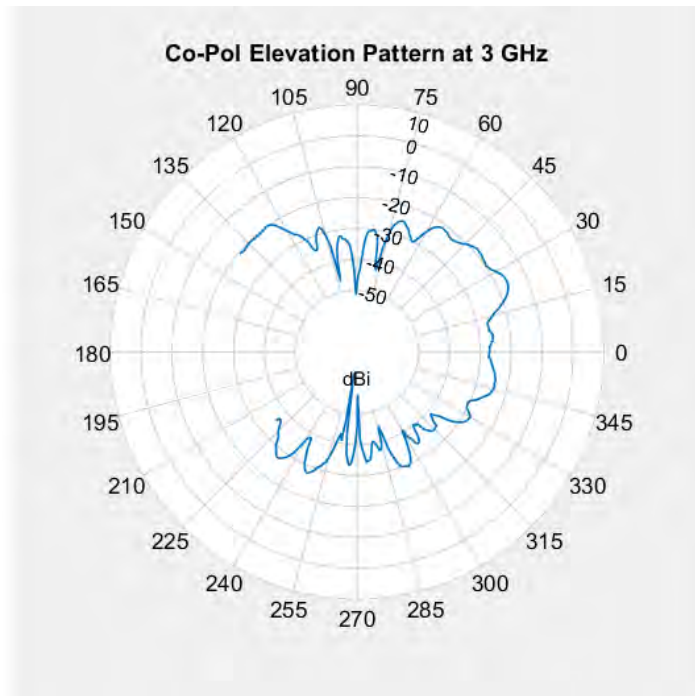


Figure 608: FR4 Antenna: Elevation Pattern, 3 GHz

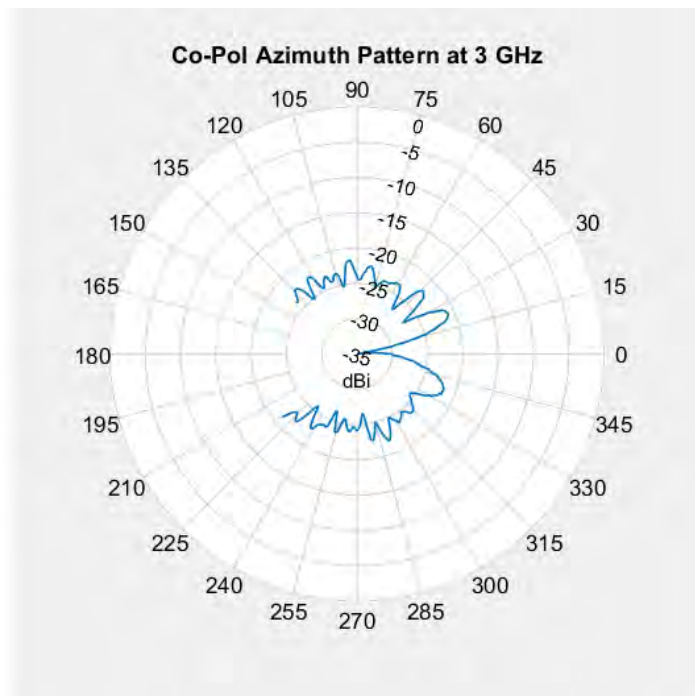


Figure 609: FR4 Antenna: Azimuth Pattern, 3 GHz

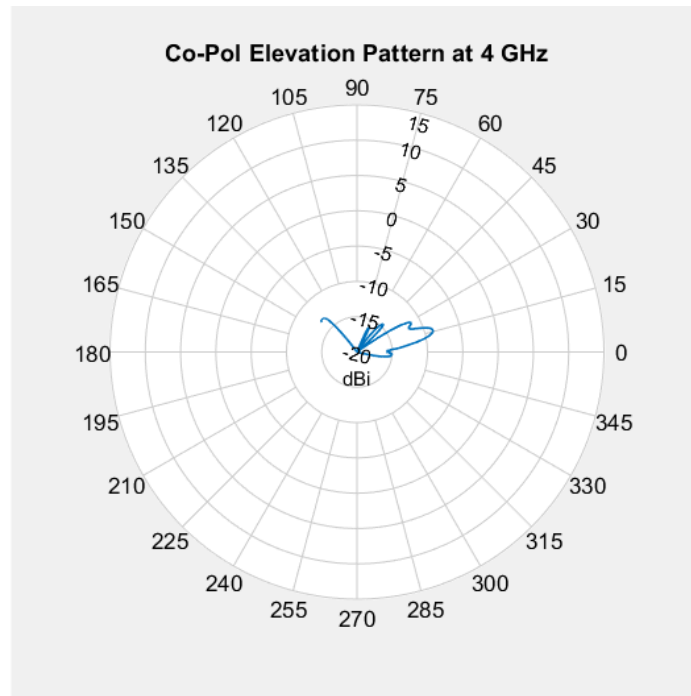


Figure 610: FR4 Antenna: Elevation Pattern, 4 GHz

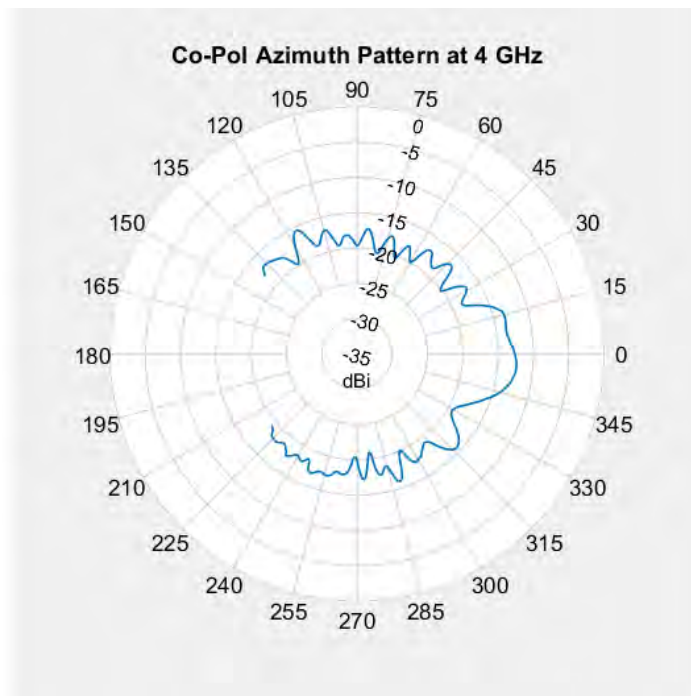


Figure 611: FR4 Antenna: Azimuth Pattern, 4 GHz

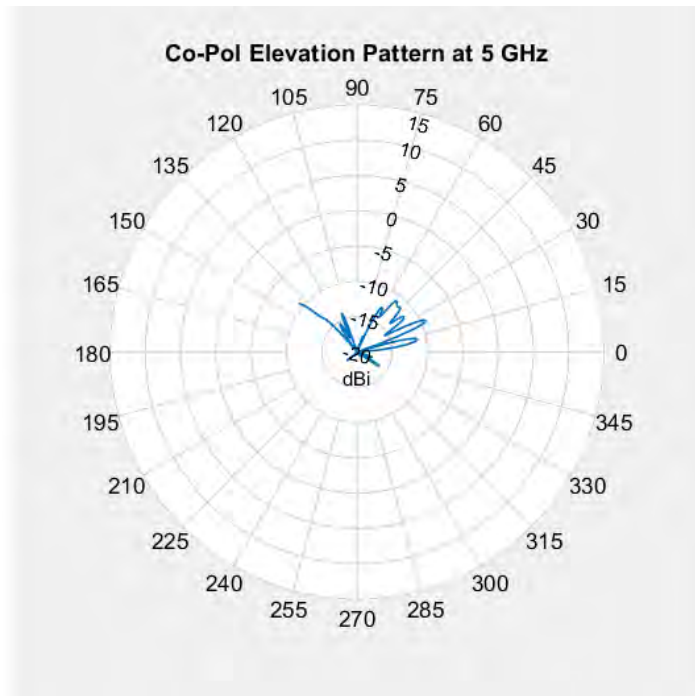


Figure 612: FR4 Antenna: Elevation Pattern, 5 GHz

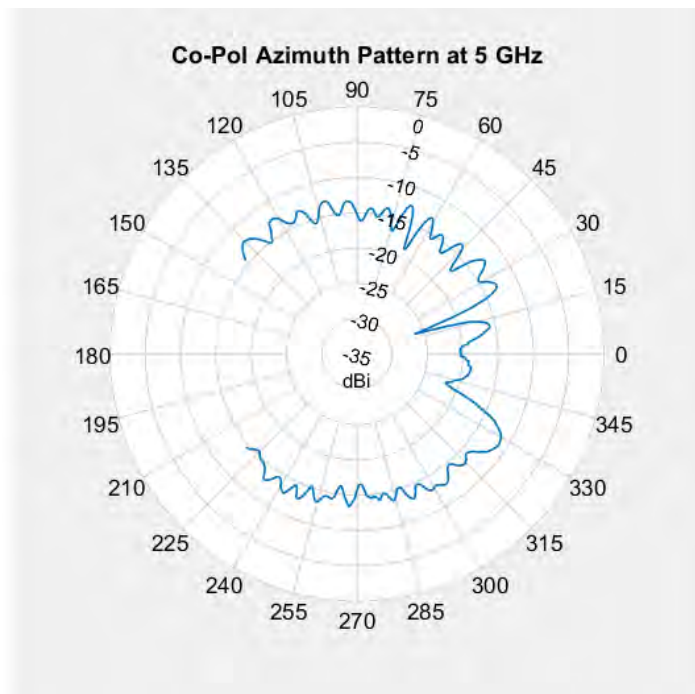


Figure 613: FR4 Antenna: Azimuth Pattern, 5 GHz

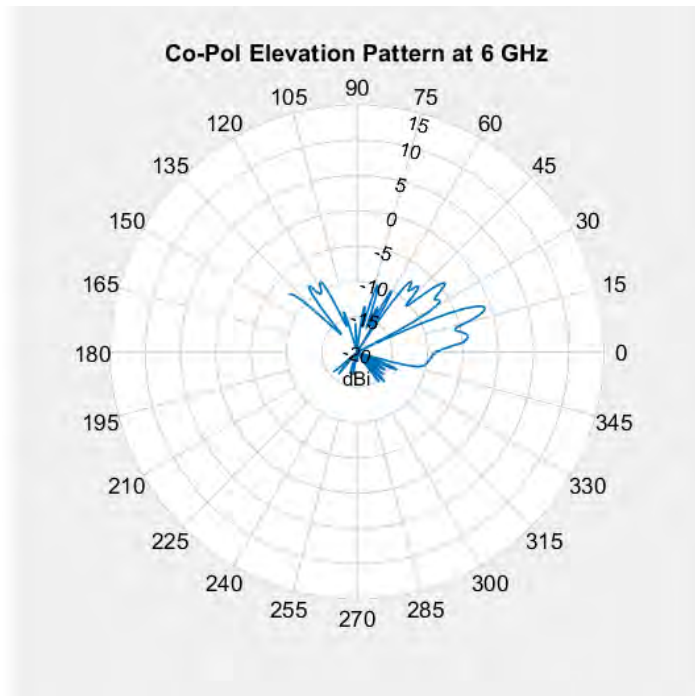


Figure 614: FR4 Antenna: Elevation Pattern, 6 GHz

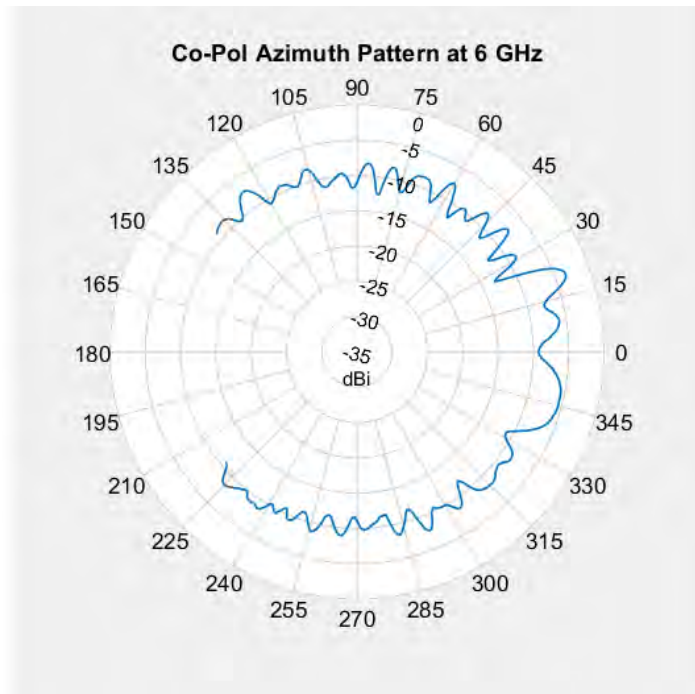


Figure 615: FR4 Antenna: Azimuth Pattern, 6 GHz

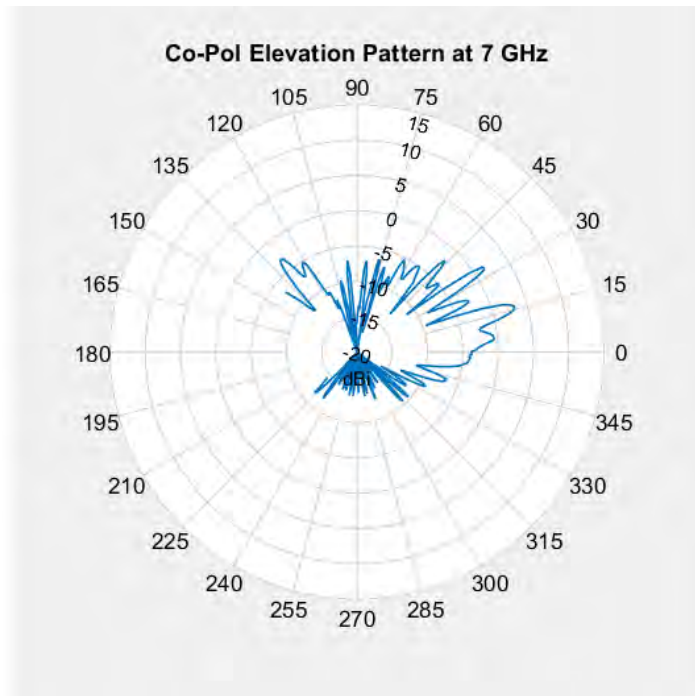


Figure 616: FR4 Antenna: Elevation Pattern, 7 GHz

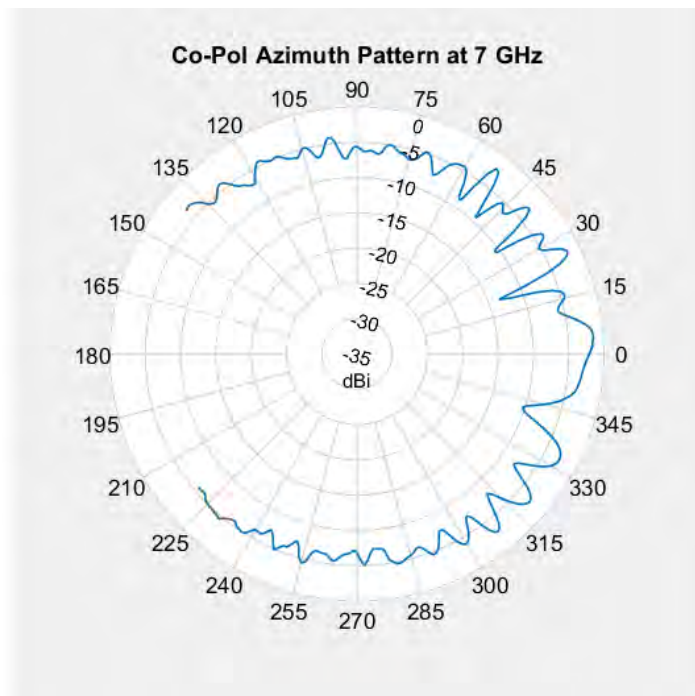


Figure 617: FR4 Antenna: Azimuth Pattern, 7 GHz

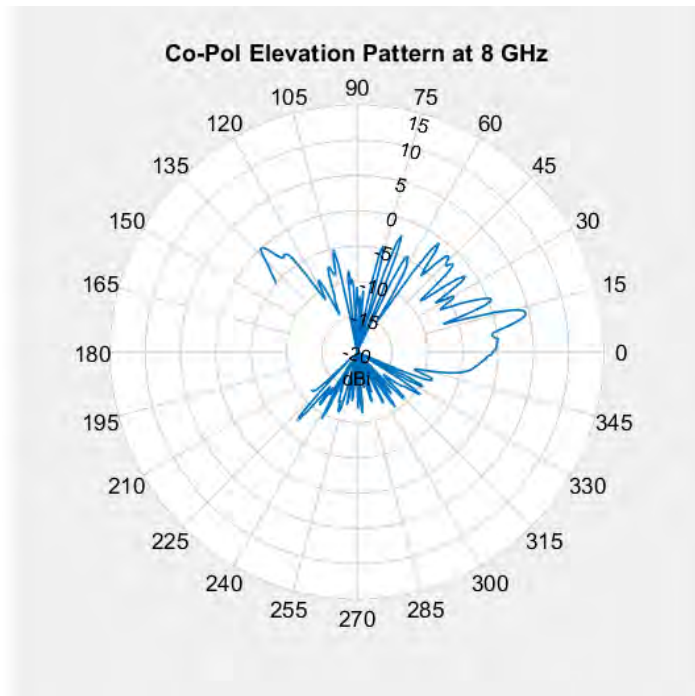


Figure 618: FR4 Antenna: Elevation Pattern, 8 GHz

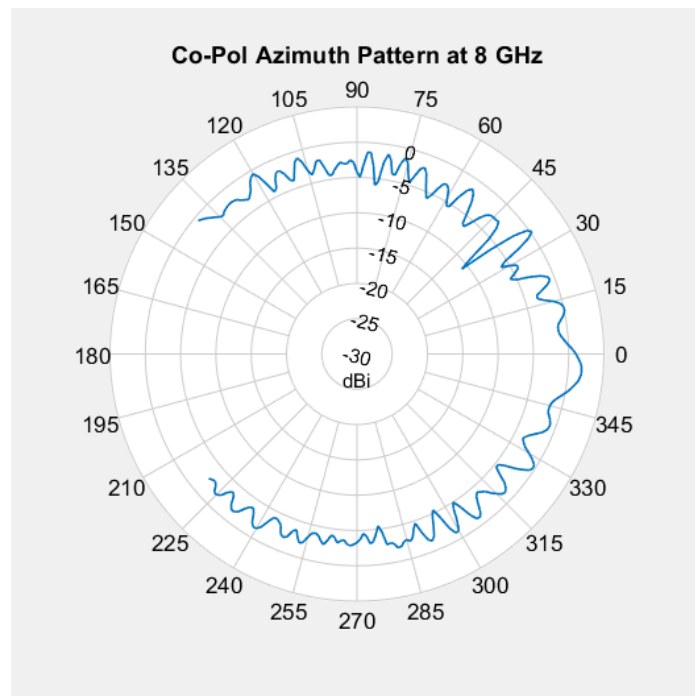


Figure 619: FR4 Antenna: Azimuth Pattern, 8 GHz

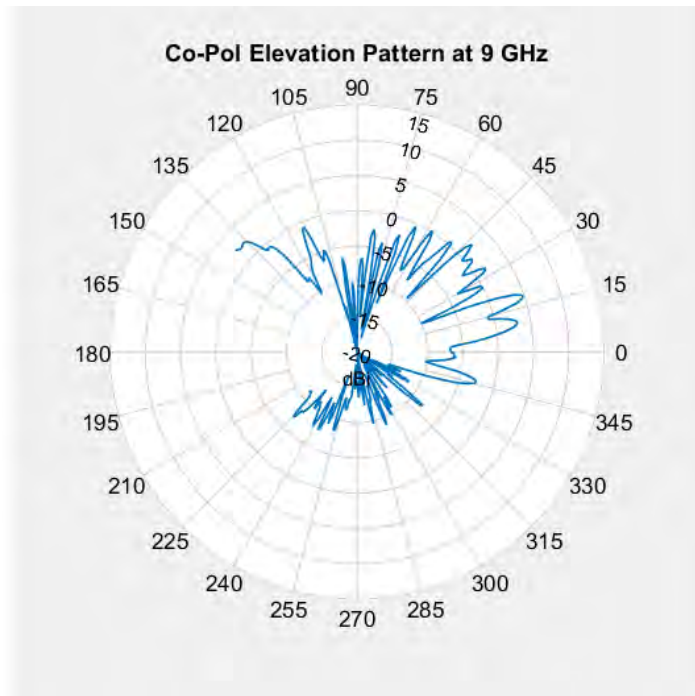


Figure 620: FR4 Antenna: Elevation Pattern, 9 GHz

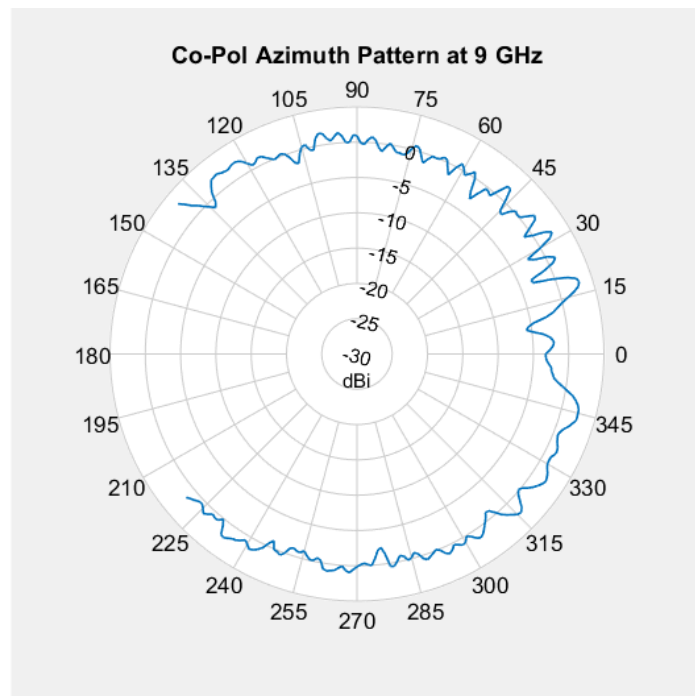


Figure 621: FR4 Antenna: Azimuth Pattern, 9 GHz

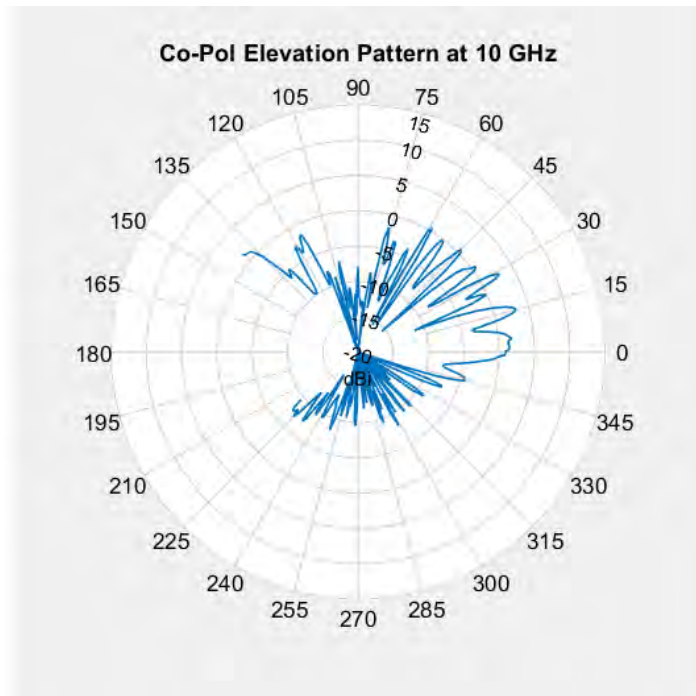


Figure 622: FR4 Antenna: Elevation Pattern, 10 GHz

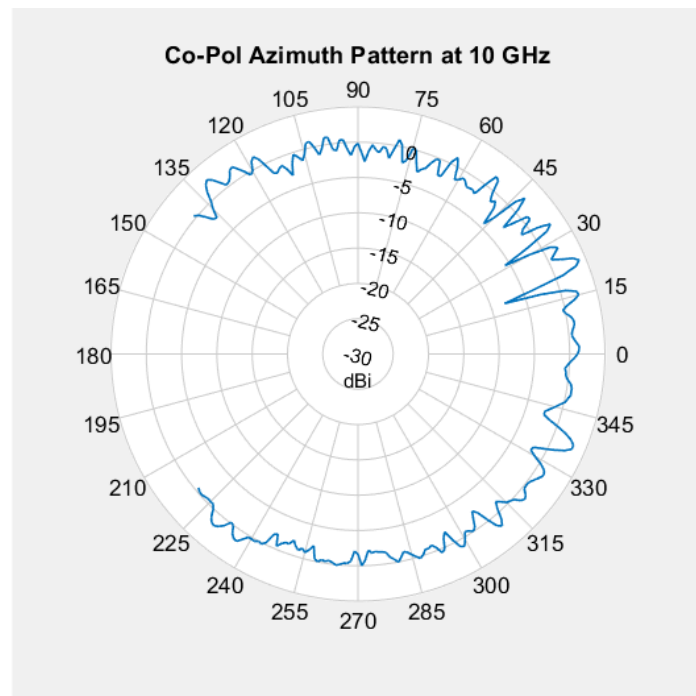


Figure 623: FR4 Antenna: Azimuth Pattern, 10 GHz

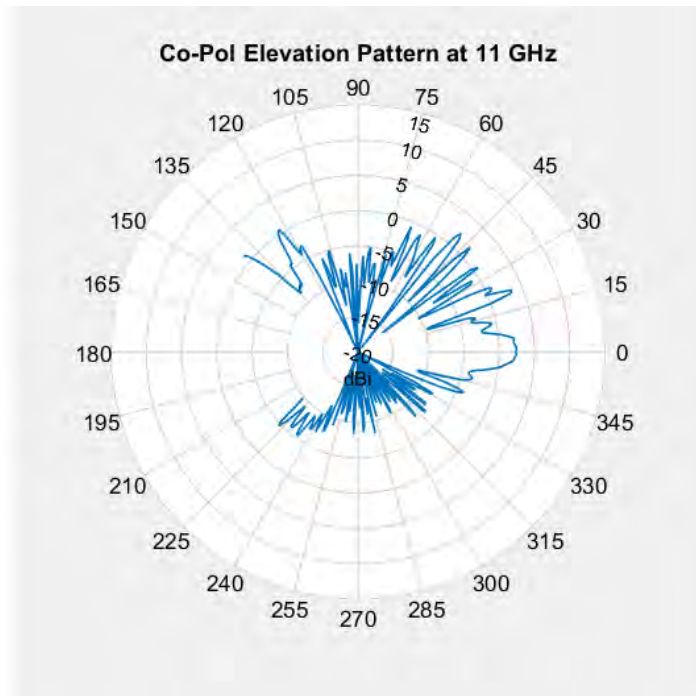


Figure 624: FR4 Antenna: Elevation Pattern, 11 GHz

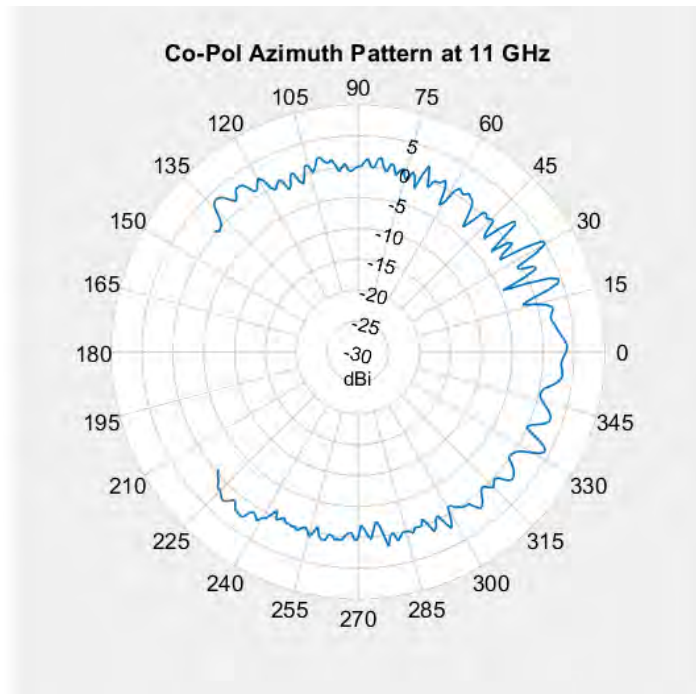


Figure 625: FR4 Antenna: Azimuth Pattern, 11 GHz

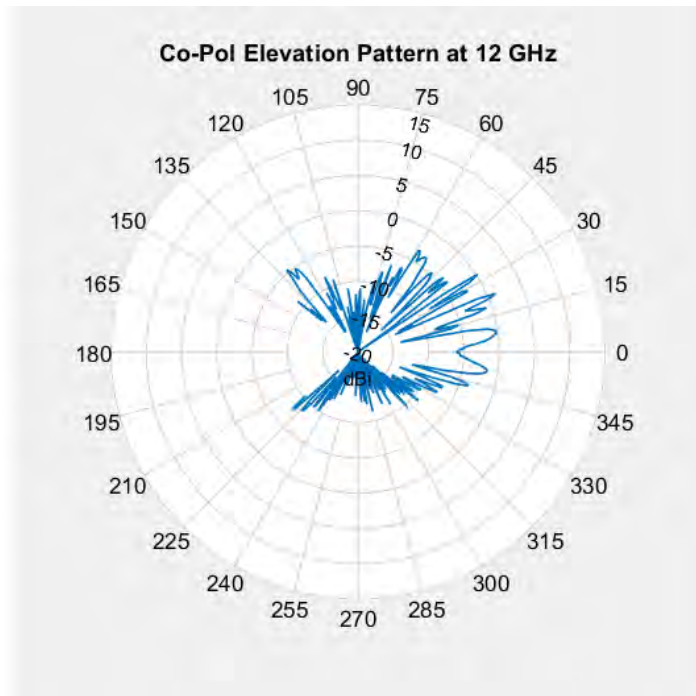


Figure 626: FR4 Antenna: Elevation Pattern, 12 GHz

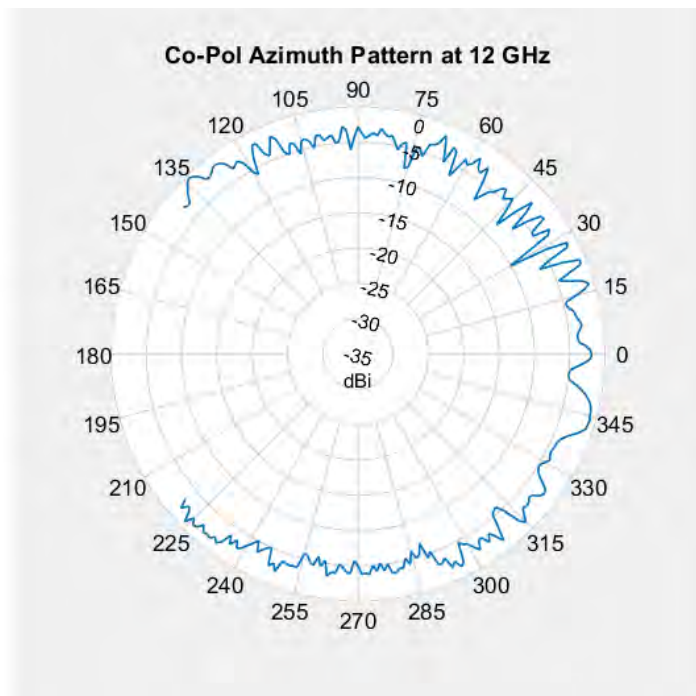


Figure 627: FR4 Antenna: Azimuth Pattern, 12 GHz

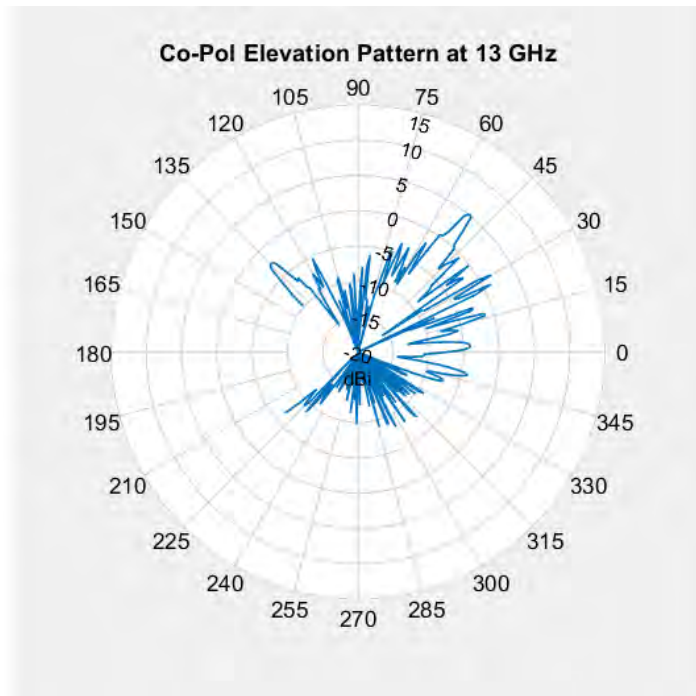


Figure 628: FR4 Antenna: Elevation Pattern, 13 GHz

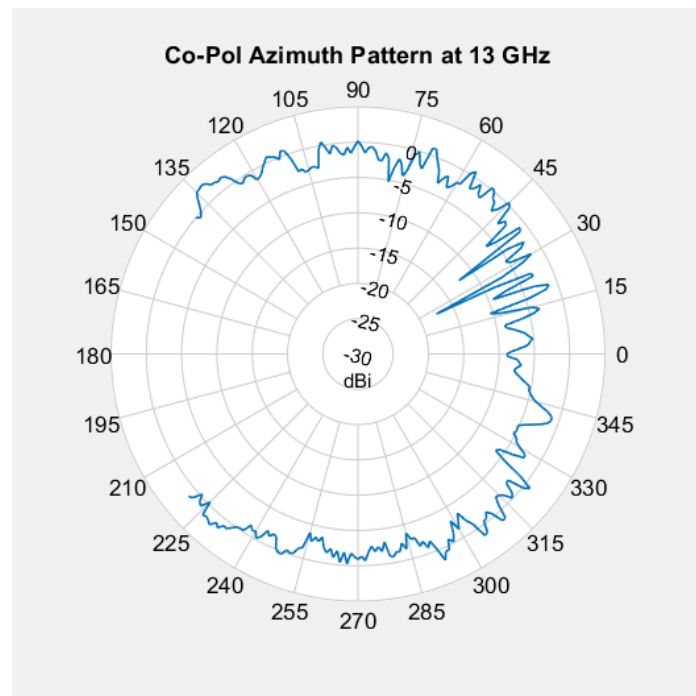


Figure 629: FR4 Antenna: Azimuth Pattern, 13 GHz

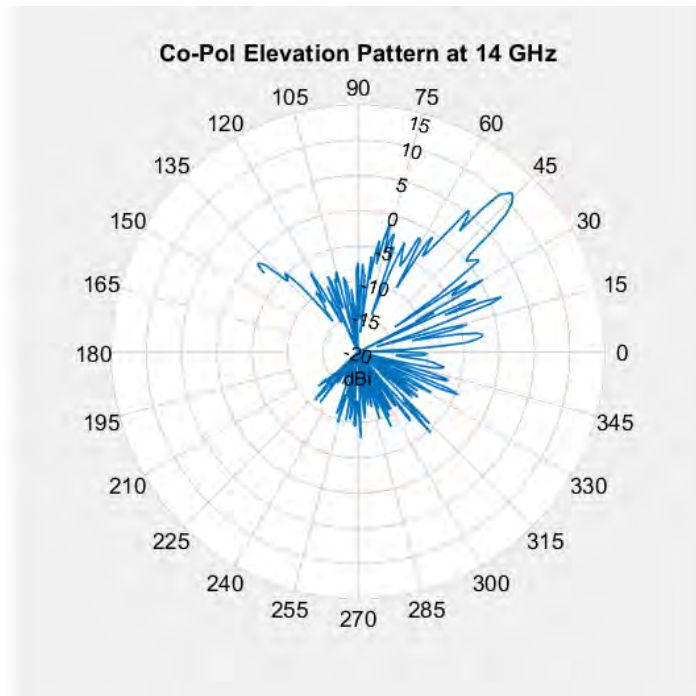


Figure 630: FR4 Antenna: Elevation Pattern, 14 GHz

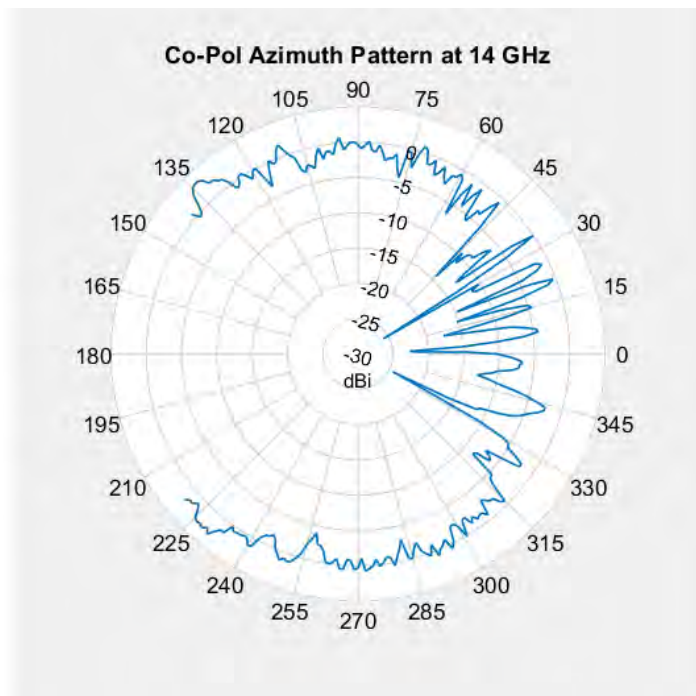


Figure 631: FR4 Antenna: Azimuth Pattern, 14 GHz

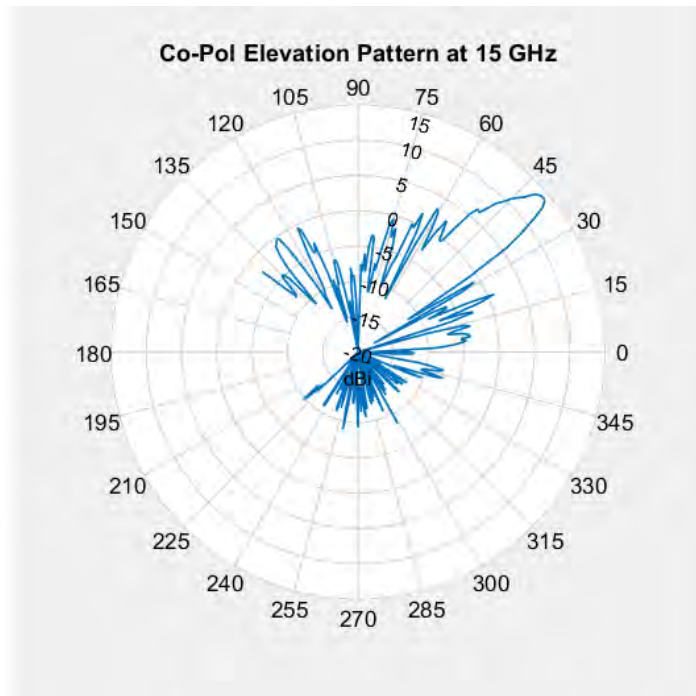


Figure 632: FR4 Antenna: Elevation Pattern, 15 GHz

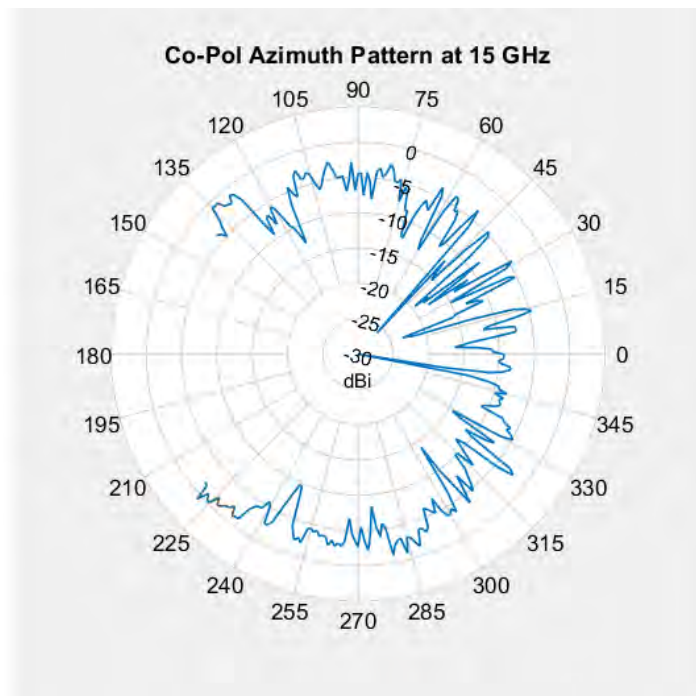


Figure 633: FR4 Antenna: Azimuth Pattern, 15 GHz

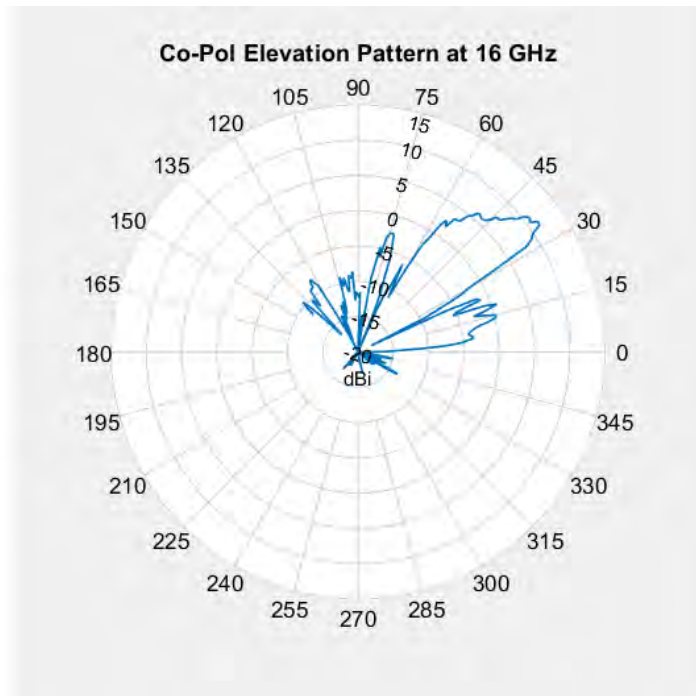


Figure 634: FR4 Antenna: Elevation Pattern, 16 GHz

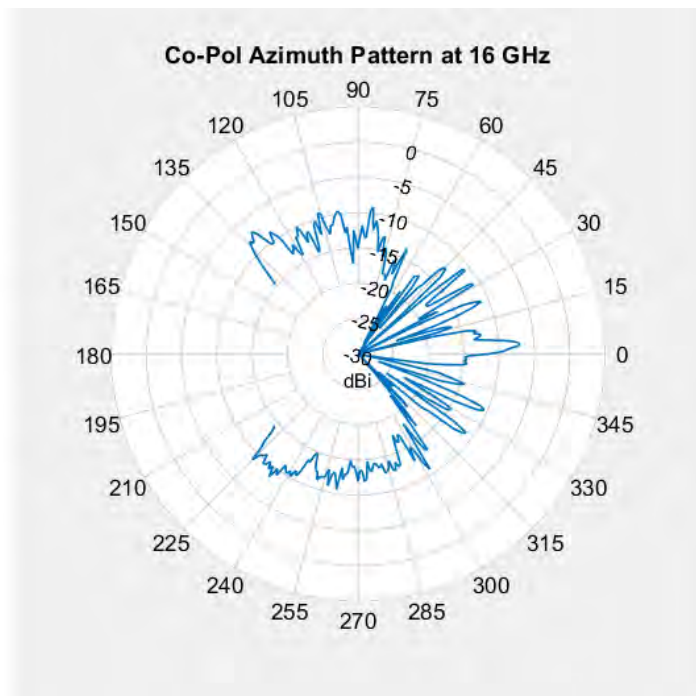


Figure 635: FR4 Antenna: Azimuth Pattern, 16 GHz

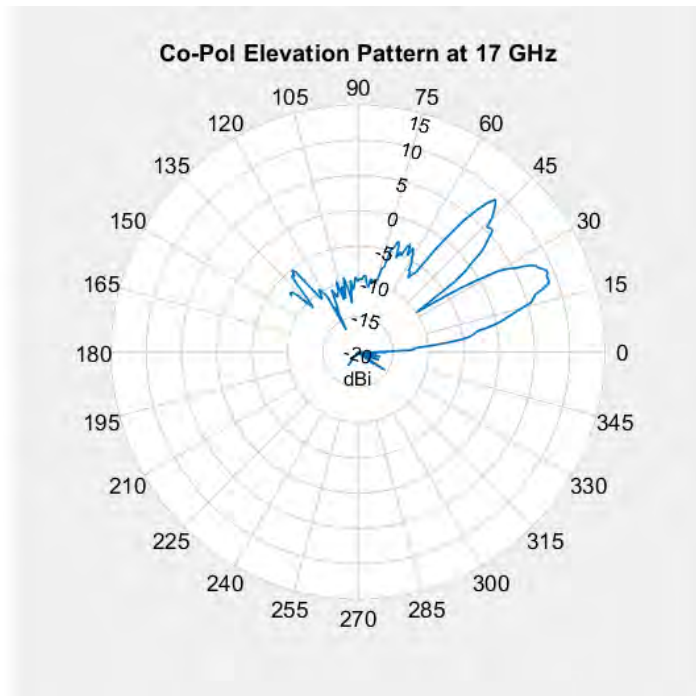


Figure 636: FR4 Antenna: Elevation Pattern, 17 GHz

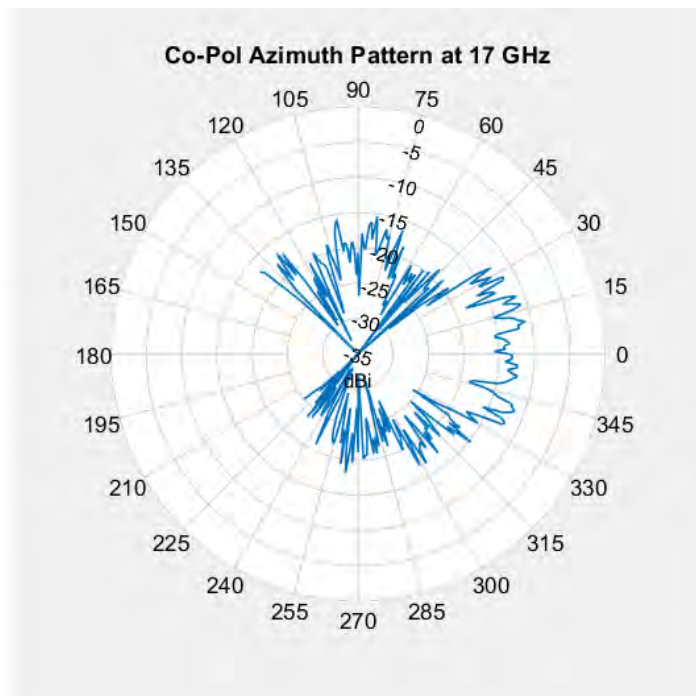


Figure 637: FR4 Antenna: Azimuth Pattern, 17 GHz

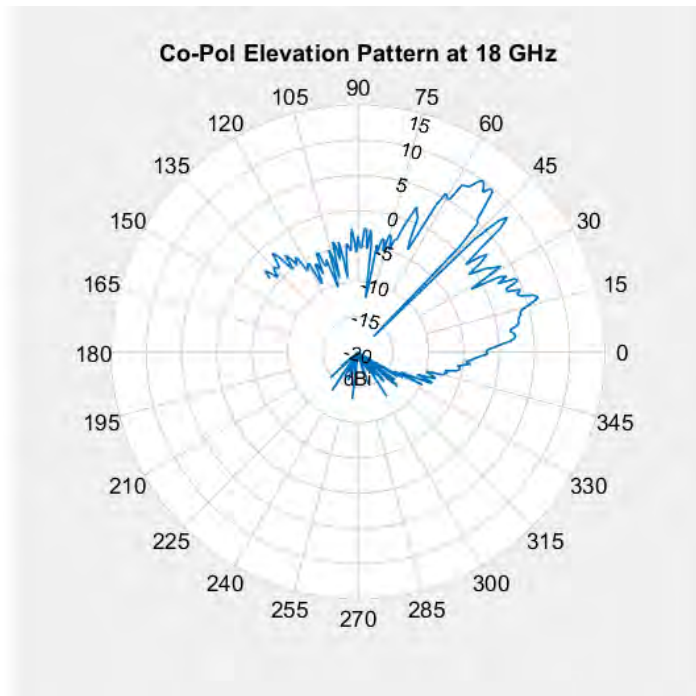


Figure 638: FR4 Antenna: Elevation Pattern, 18 GHz

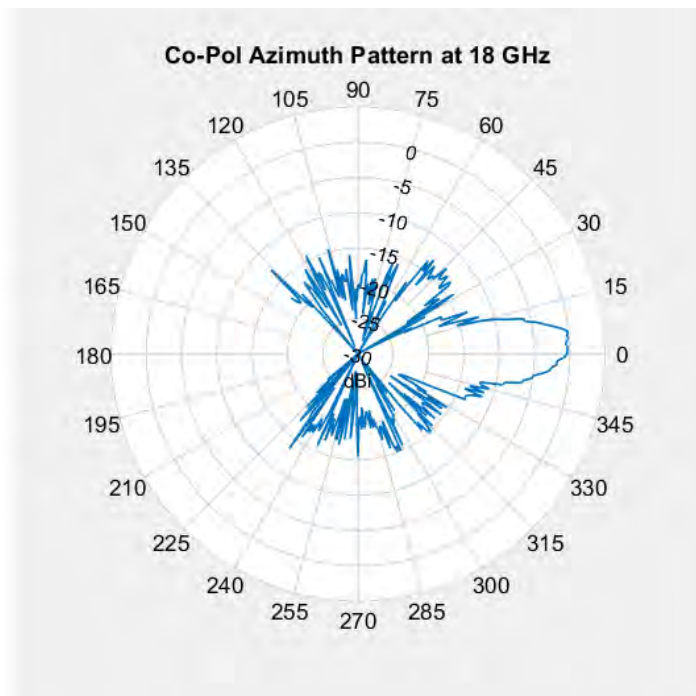


Figure 639: FR4 Antenna: Azimuth Pattern, 18 GHz

Appendix I. 8" by 8" 10 GHz Rogers 3010 Antenna

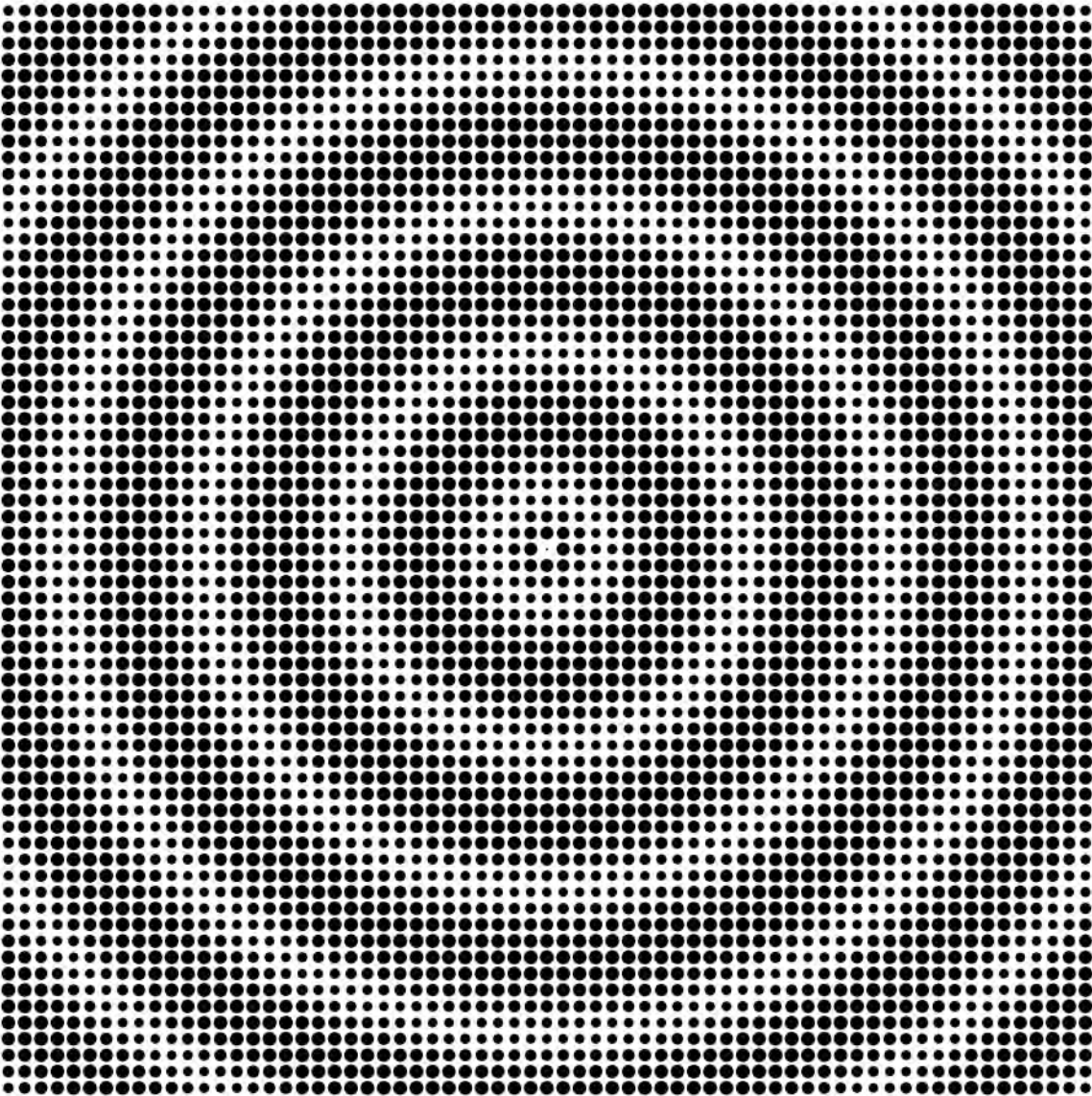


Figure 640: RO3010 Antenna Design Image (not to scale)

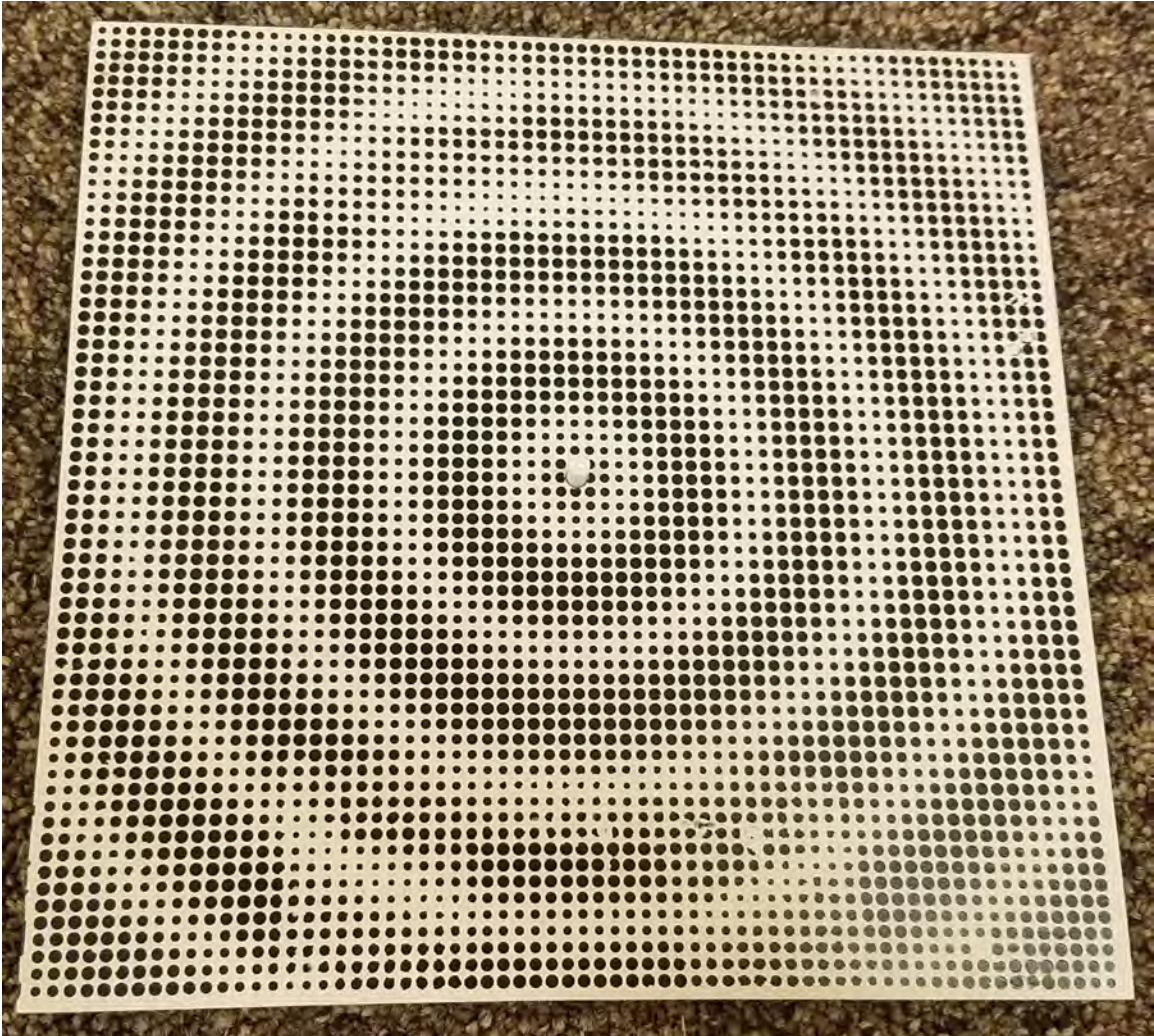


Figure 641: Completed RO3010 Antenna (top)



Figure 642: Completed RO3010 GHz Antenna (back)



Figure 643: 8" by 8" Copper Plate

Antenna Design Parameters	
Parameter	Value
Dimensions	8" by 8"
Thickness	1.27 mm
Material	Rogers 3010
Cell Shape	circular
Cell Size, a	3 mm
Number of Cells	67 by 67 = 4,489
Design Frequency	10 GHz
ϕ	0°
θ_L	40.984°
X	249.6
M	$0.8 \times 108.1 \text{ j}\Omega$ = 86.5 j Ω
Z_{min}	141.5 j Ω
Z_{max}	357.8 j Ω

Table 110: RO3010 Antenna Design Parameters

Antenna Performance		
	RO3010 Antenna	Copper Plate
1.5:1 SWR Bandwidth	8.06 GHz (6.47 to 14.53 GHz)	10.11 GHz (7.89-18 GHz)
2:1 SWR Bandwidth	12.09 GHz (5.91 to 18 GHz)	10.72 GHz (7.28-18 GHz)
Resonant Frequency	7.86 GHz	10.54 GHz
SWR at 7.86 GHz	1.07:1	1.58:1
SWR at 10 GHz	1.31:1	1.21:1
Gain at 10 GHz	1.8 dBi	3.4 dBi, 3.1 dBi
Beamwidth at 10 GHz	120°	100°, 90°
Beam Center at 10 GHz	0°	68°, 292°

Table 111: RO3010 Antenna Performance (Elevation)

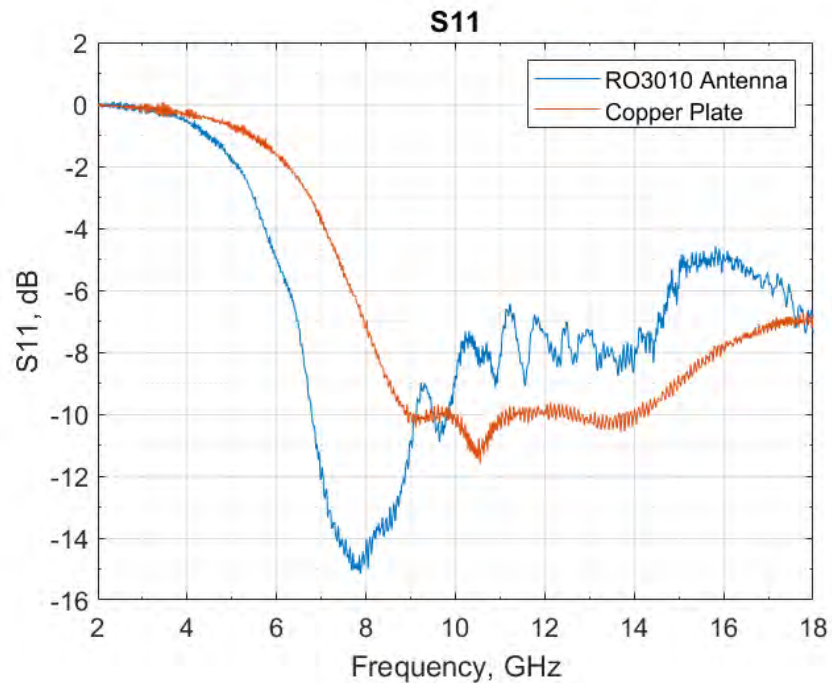


Figure 644: RO3010 Antenna: S11, 2 to 18 GHz

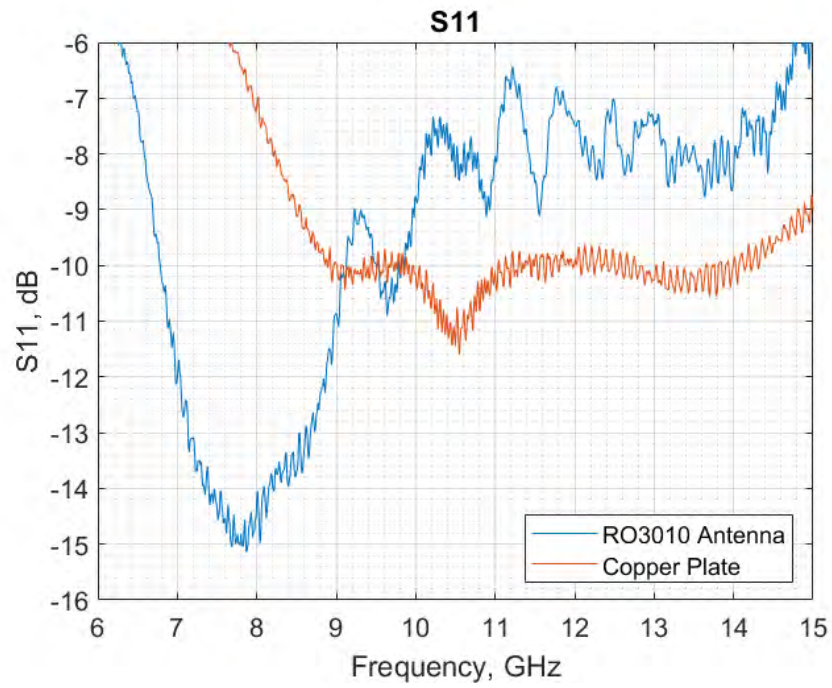


Figure 645: RO3010 Antenna: S11, 6 to 15 GHz

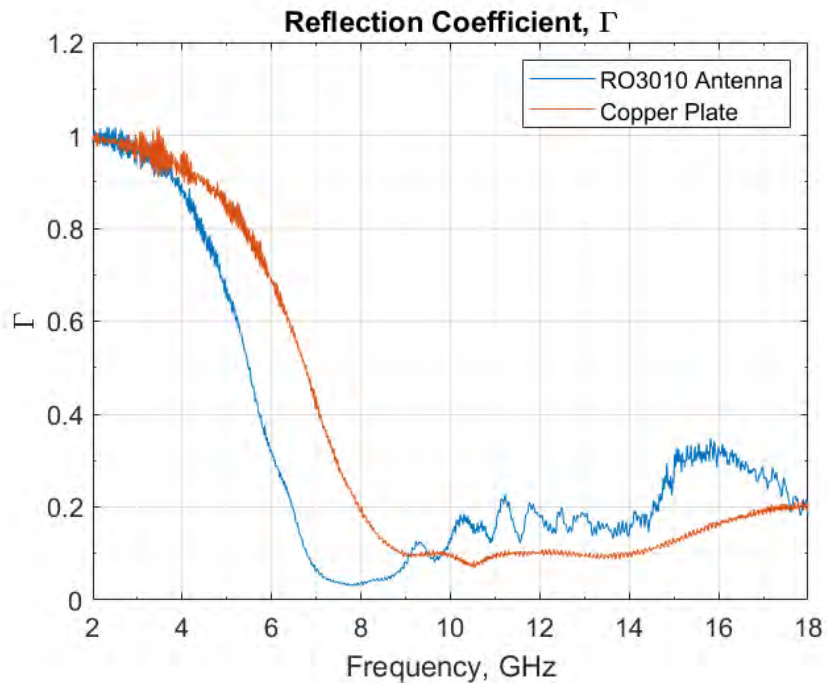


Figure 646: RO3010 Antenna: Reflection Coefficient, Γ

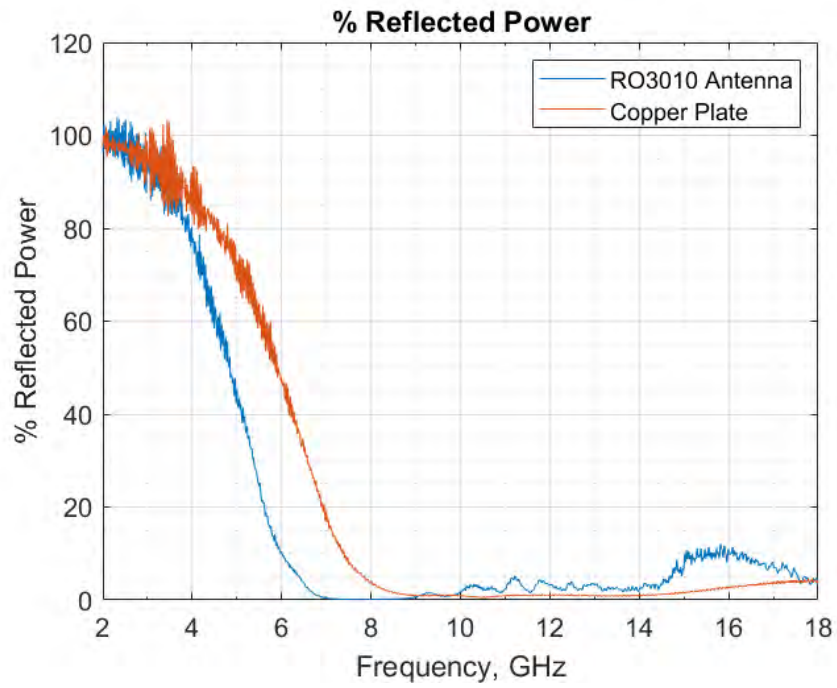


Figure 647: RO3010 Antenna: Percent Reflected Power

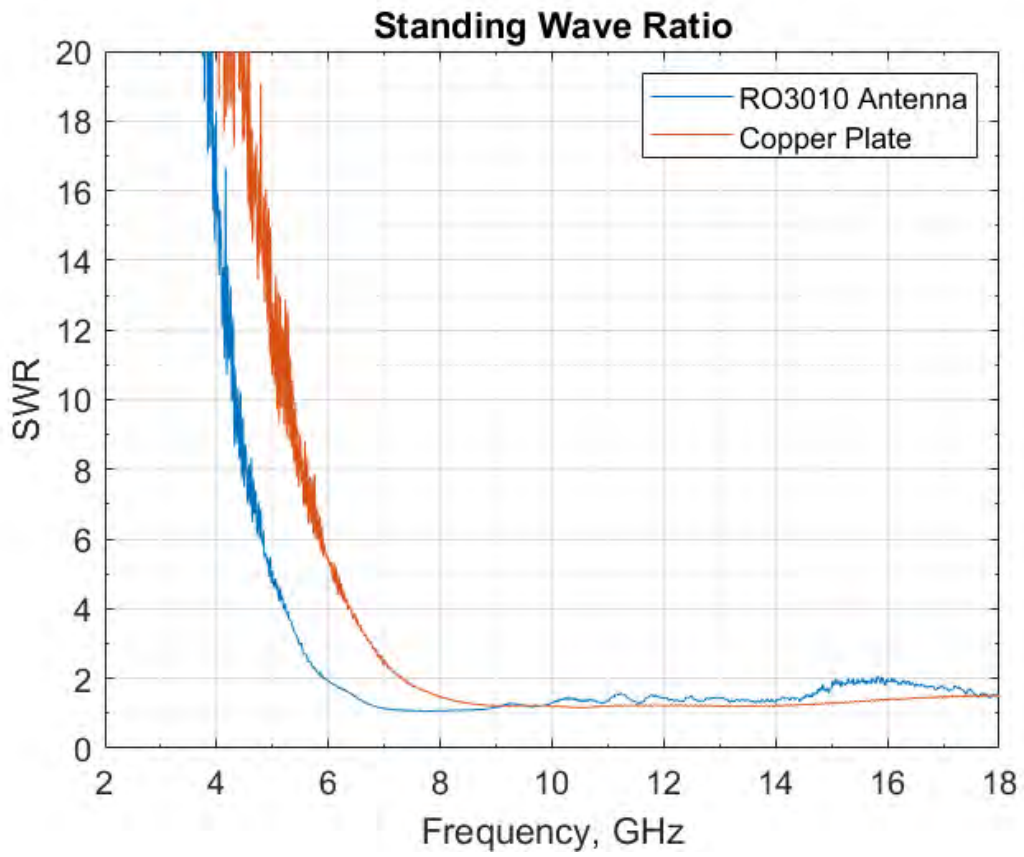


Figure 648: RO3010 Antenna: Standing Wave Ratio (SWR)

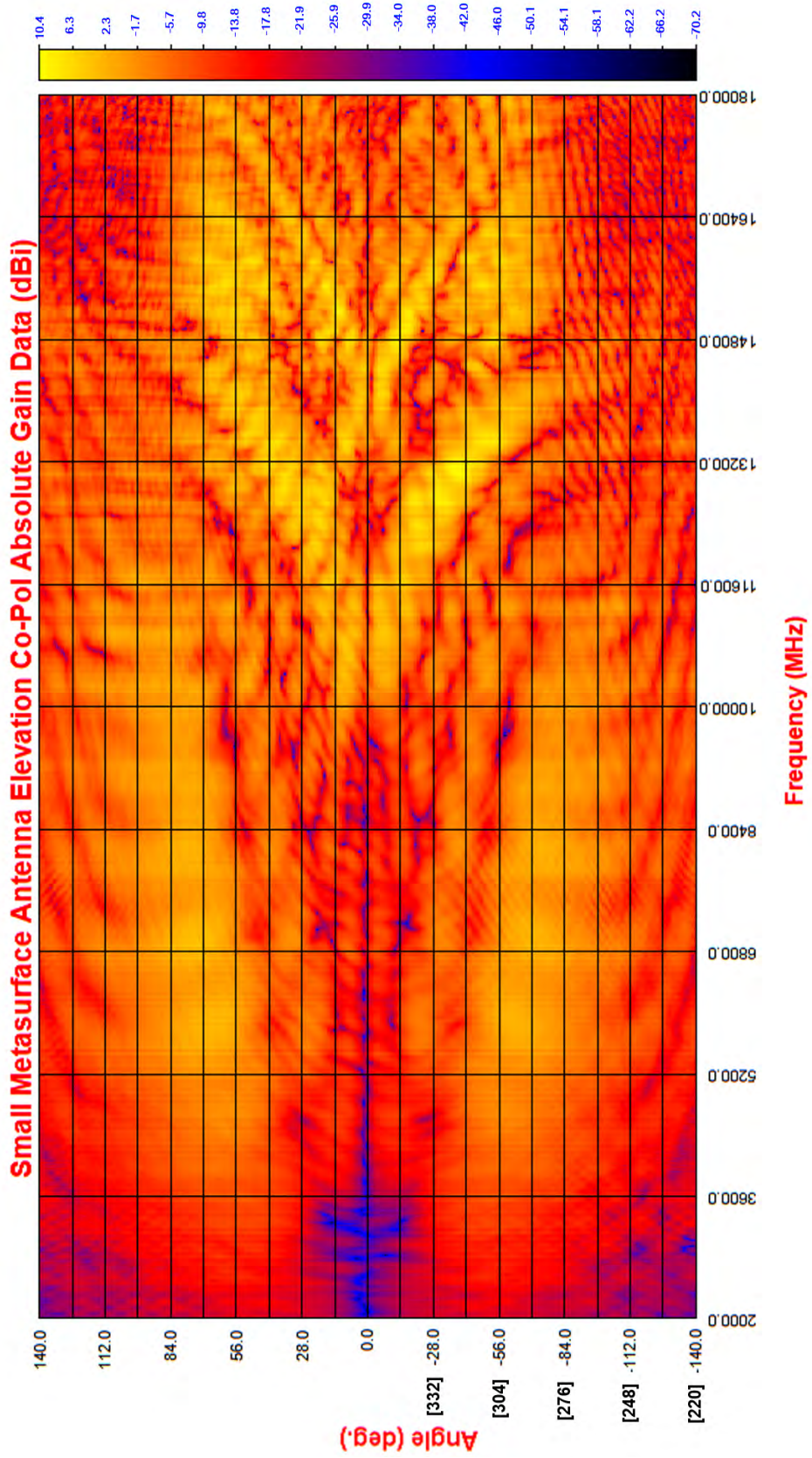


Figure 649: RO3010 Antenna: Elevation Waterfall Gain Plot

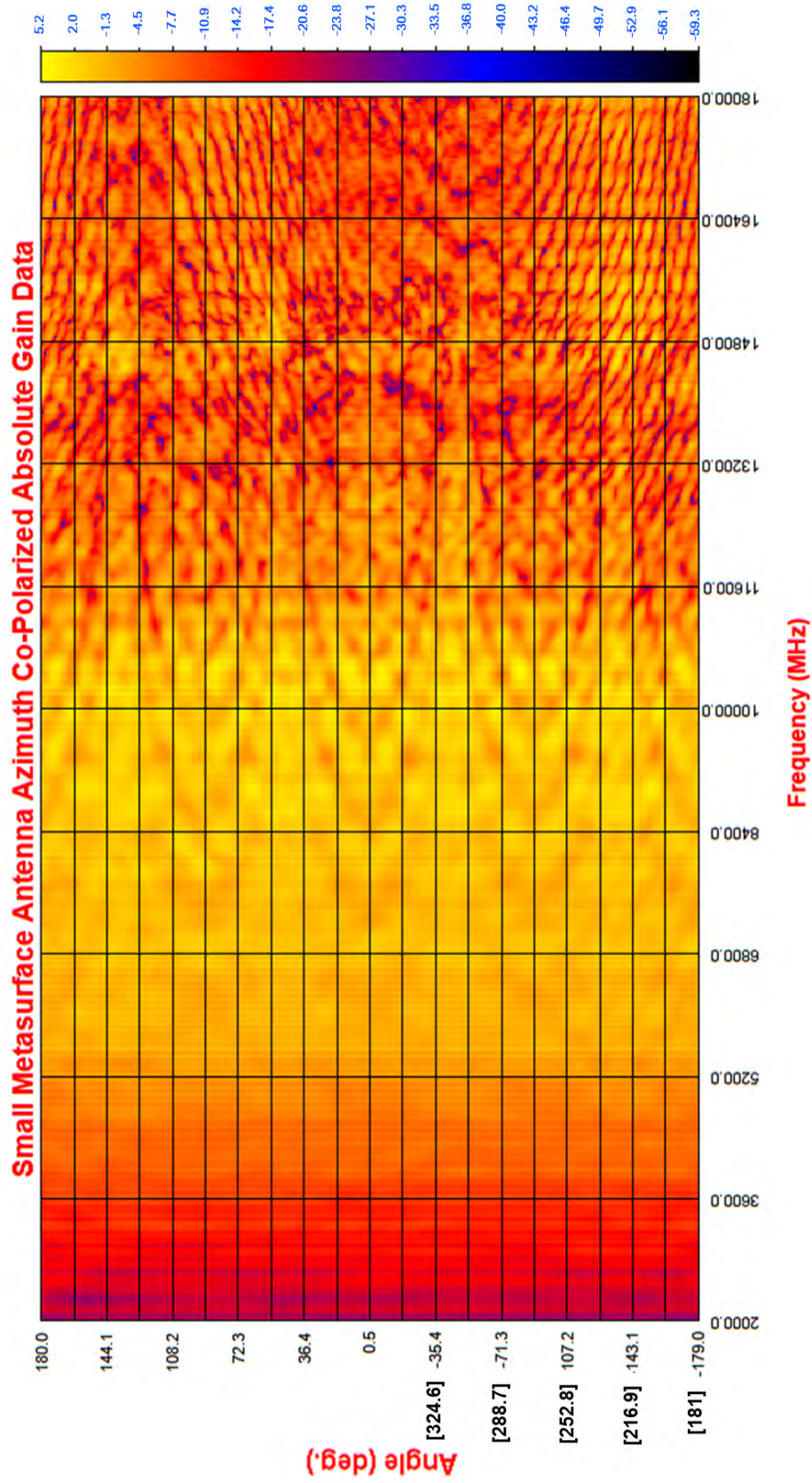


Figure 650: RO3010 Antenna: Azimuth Waterfall Gain Plot

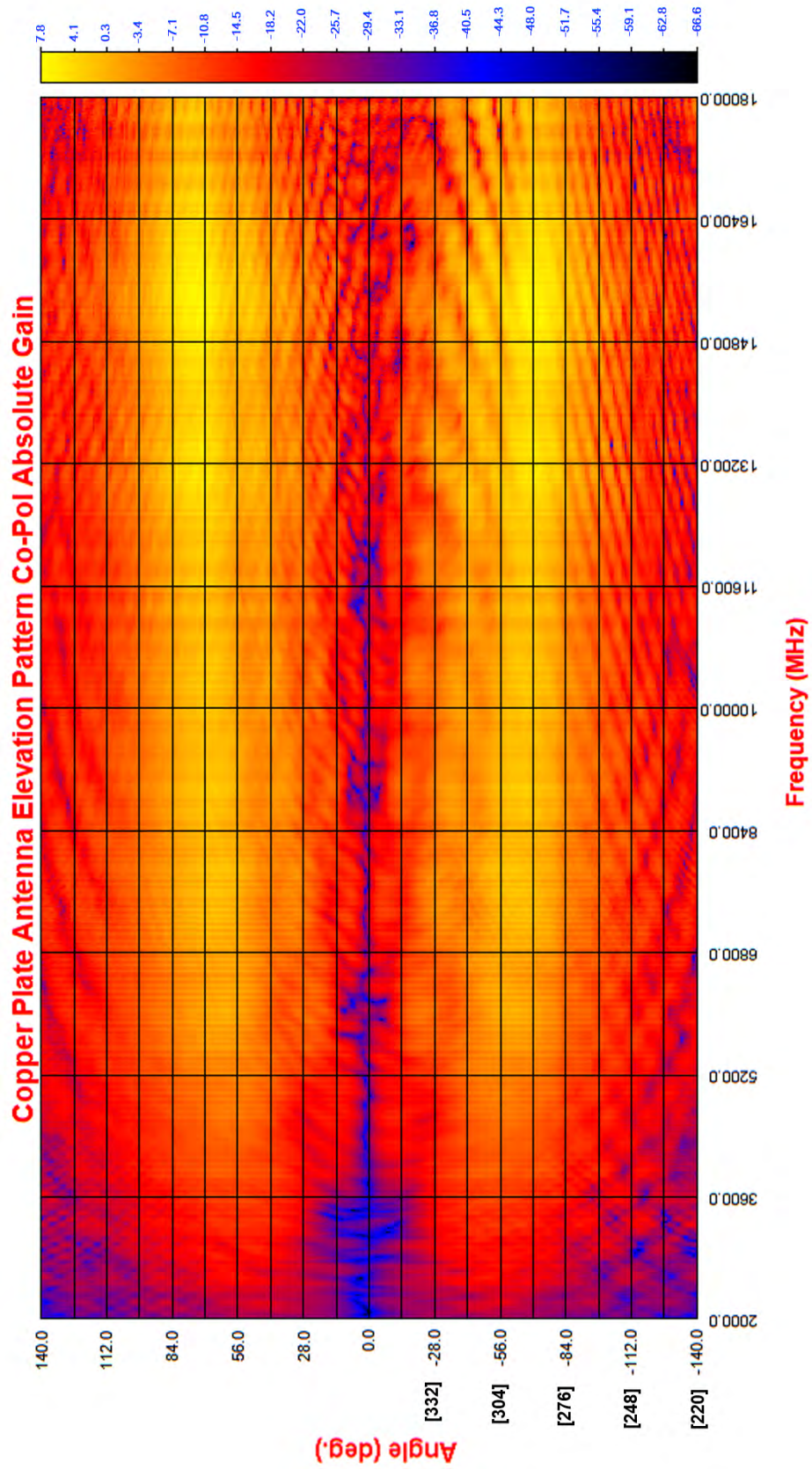


Figure 651: Copper Plate: Elevation Waterfall Gain Plot

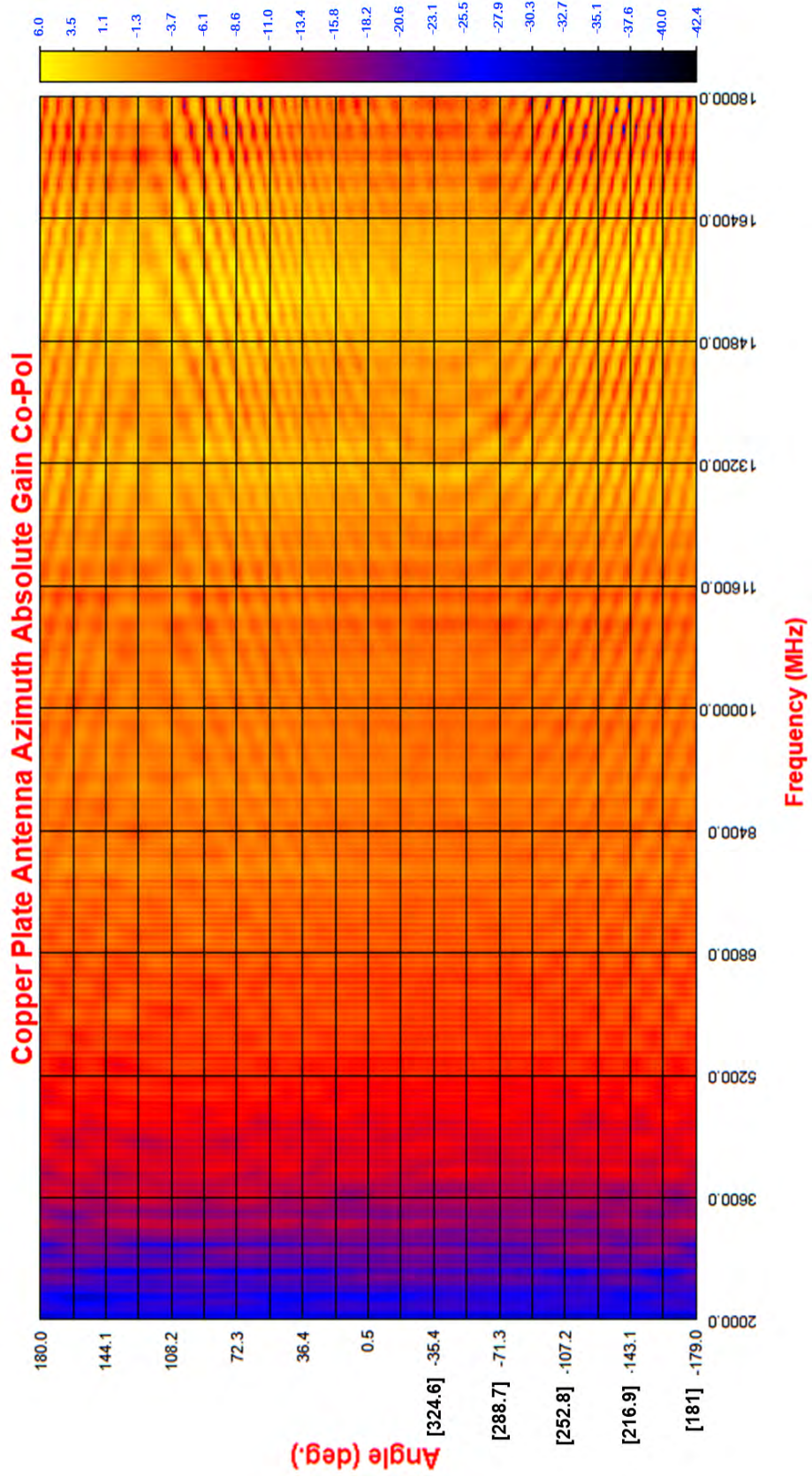


Figure 652: Copper Plate: Azimuth Waterfall Gain Plot

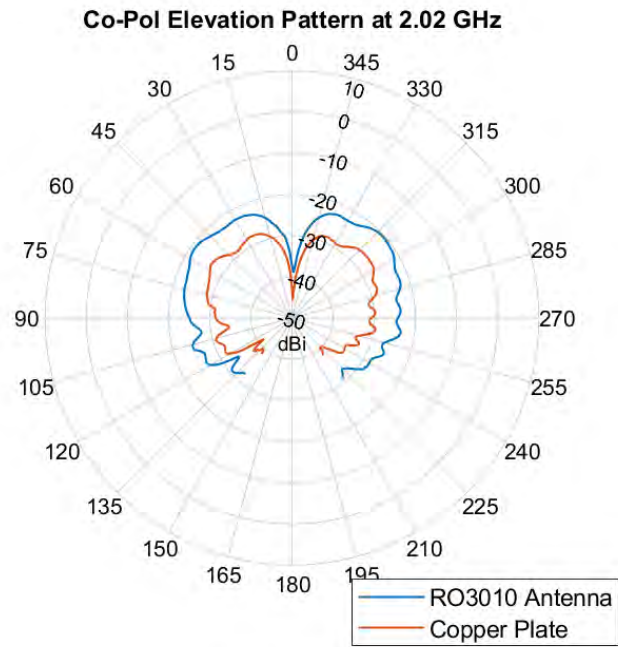


Figure 653: RO3010 Antenna: Elevation Pattern, 2 GHz

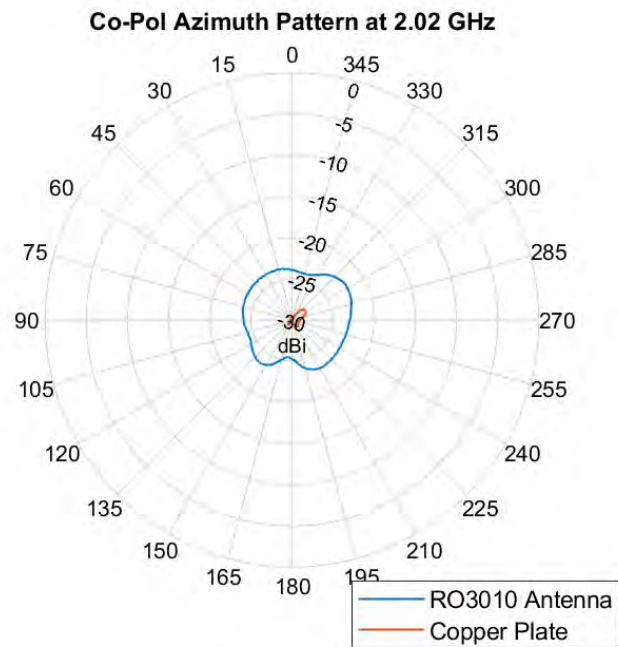


Figure 654: RO3010 Antenna: Azimuth Pattern, 2 GHz

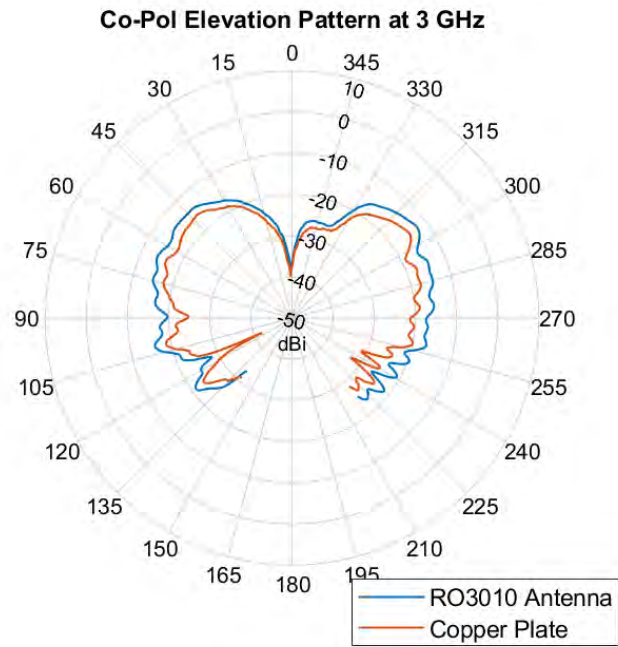


Figure 655: RO3010 Antenna: Elevation Pattern, 3 GHz

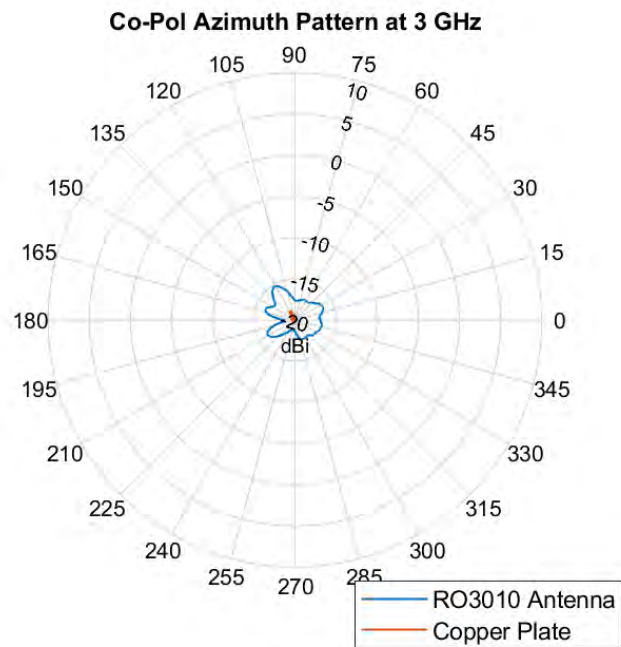


Figure 656: RO3010 Antenna: Azimuth Pattern, 3 GHz

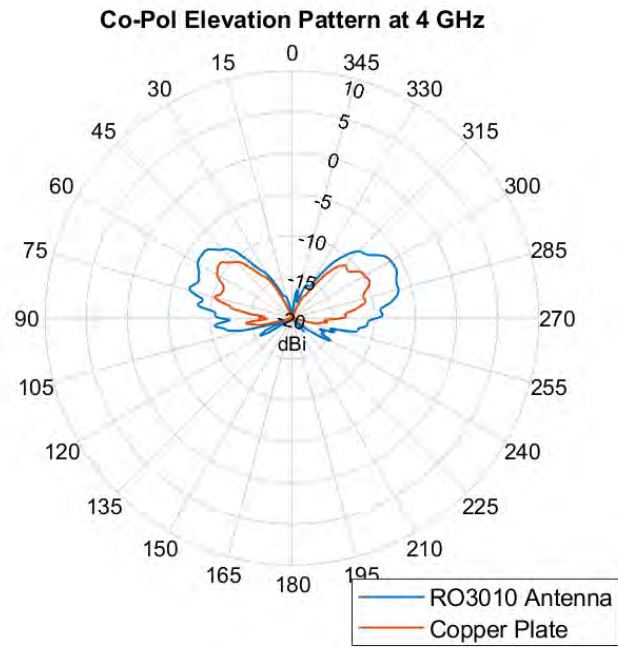


Figure 657: RO3010 Antenna: Elevation Pattern, 4 GHz

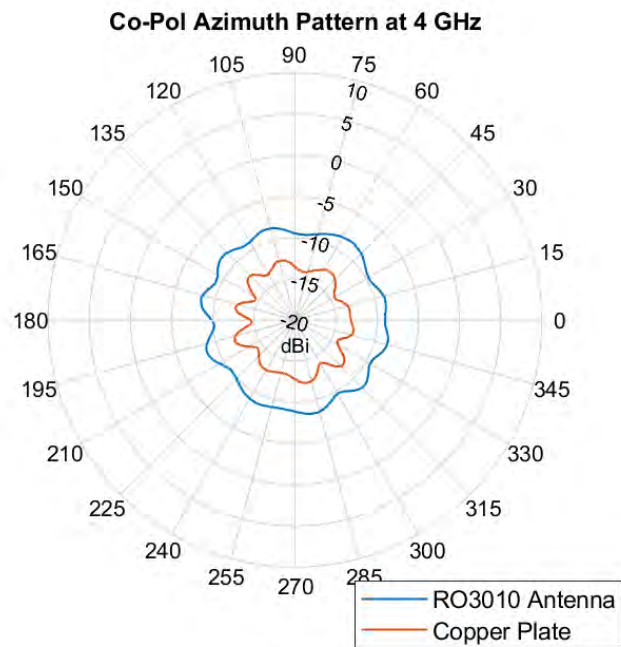


Figure 658: RO3010 Antenna: Azimuth Pattern, 4 GHz

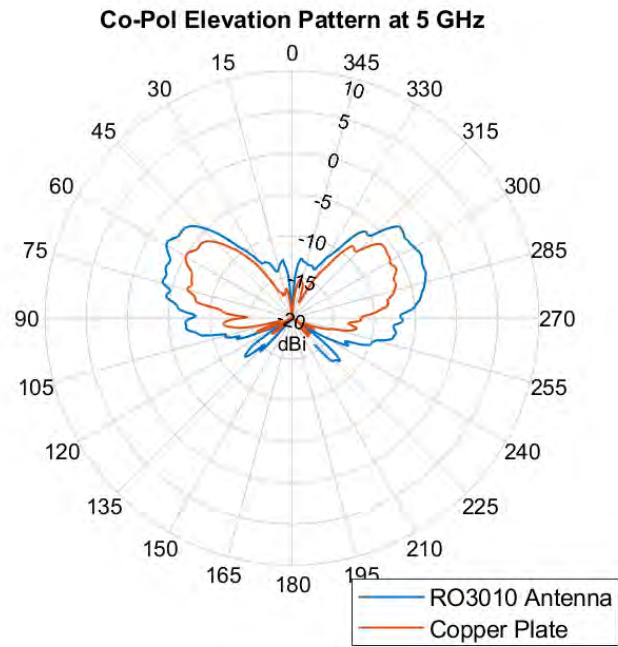


Figure 659: RO3010 Antenna: Elevation Pattern, 5 GHz

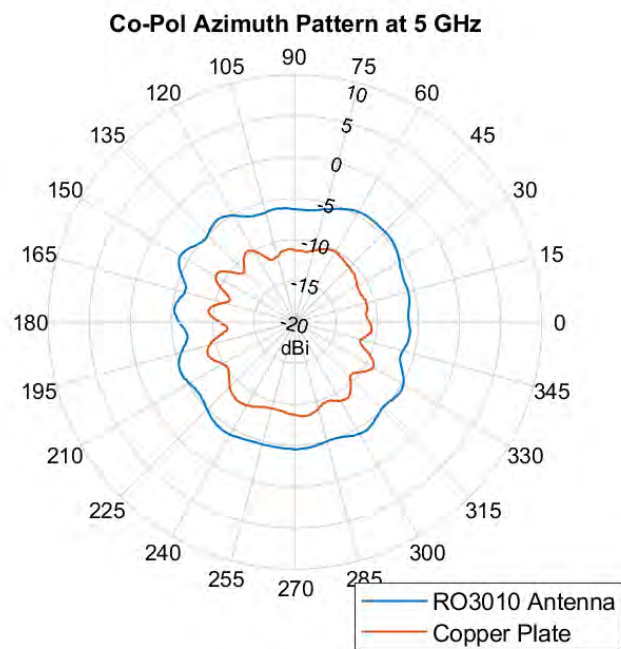


Figure 660: RO3010 Antenna: Azimuth Pattern, 5 GHz

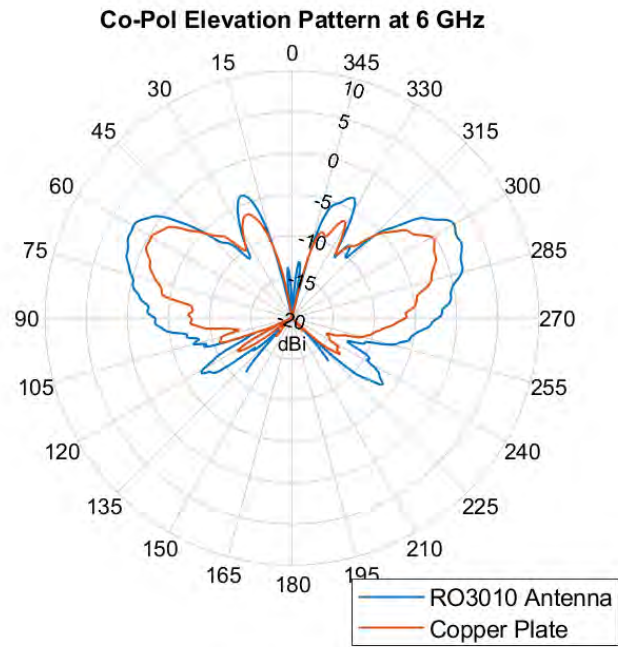


Figure 661: RO3010 Antenna: Elevation Pattern, 6 GHz

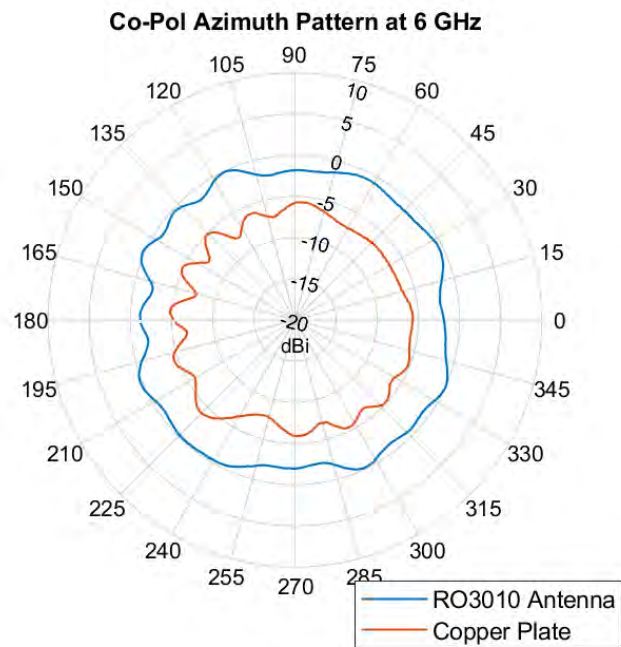


Figure 662: RO3010 Antenna: Azimuth Pattern, 6 GHz

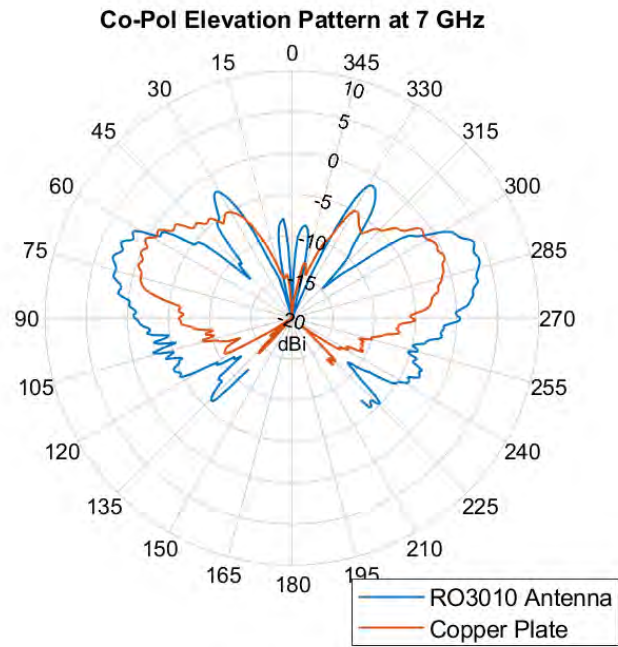


Figure 663: RO3010 Antenna: Elevation Pattern, 7 GHz

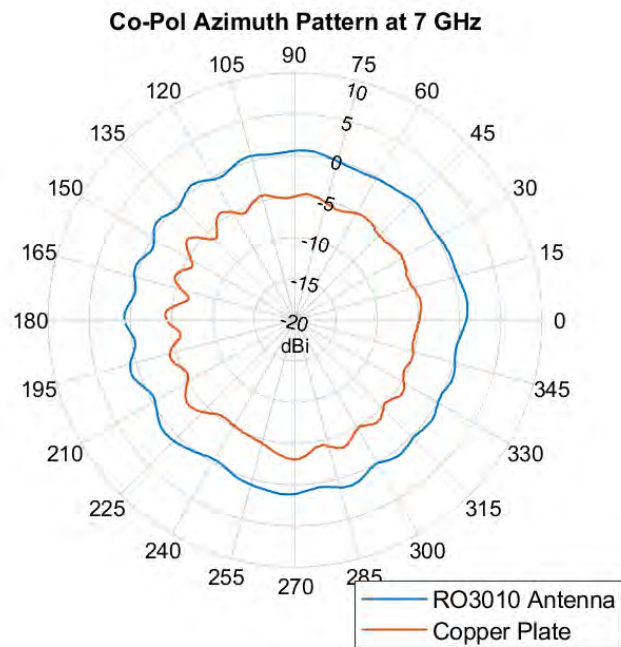


Figure 664: RO3010 Antenna: Azimuth Pattern, 7 GHz

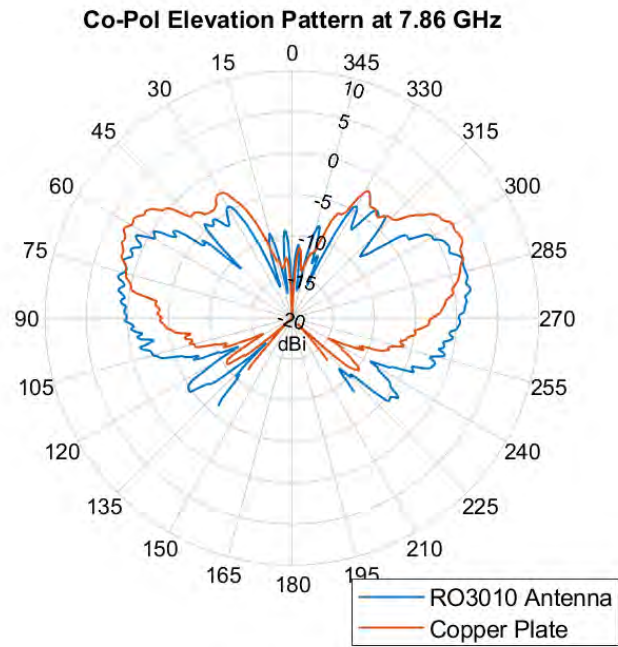


Figure 665: RO3010 Antenna: Elevation Pattern, 7.86 GHz

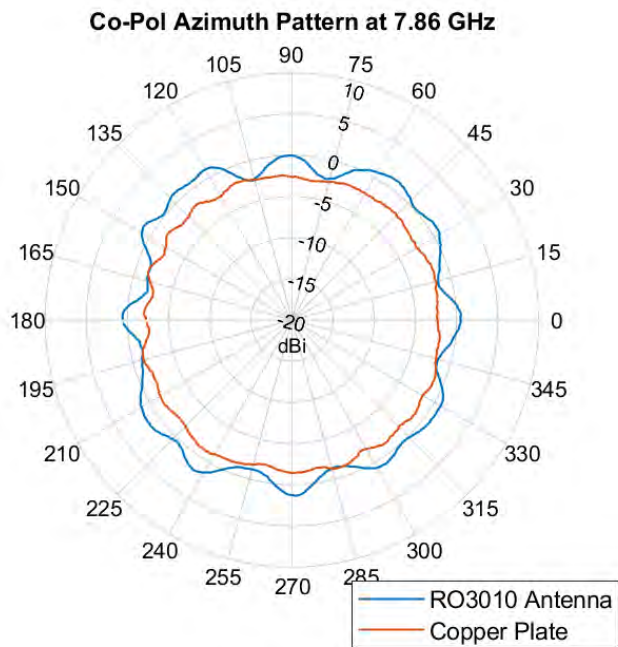


Figure 666: RO3010 Antenna: Azimuth Pattern, 7.86 GHz

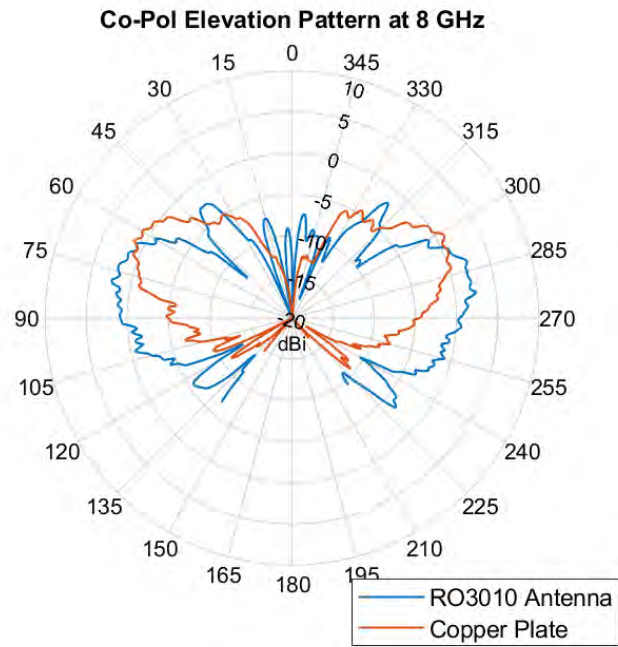


Figure 667: RO3010 Antenna: Elevation Pattern, 8 GHz

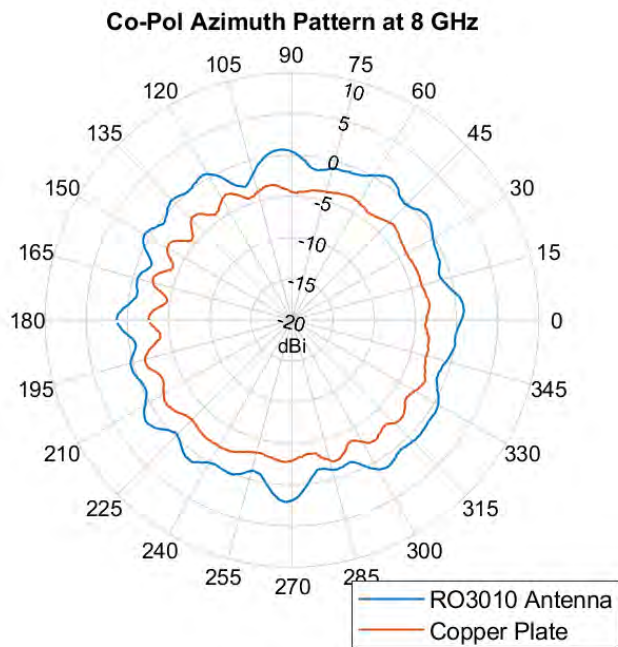


Figure 668: RO3010 Antenna: Azimuth Pattern, 8 GHz

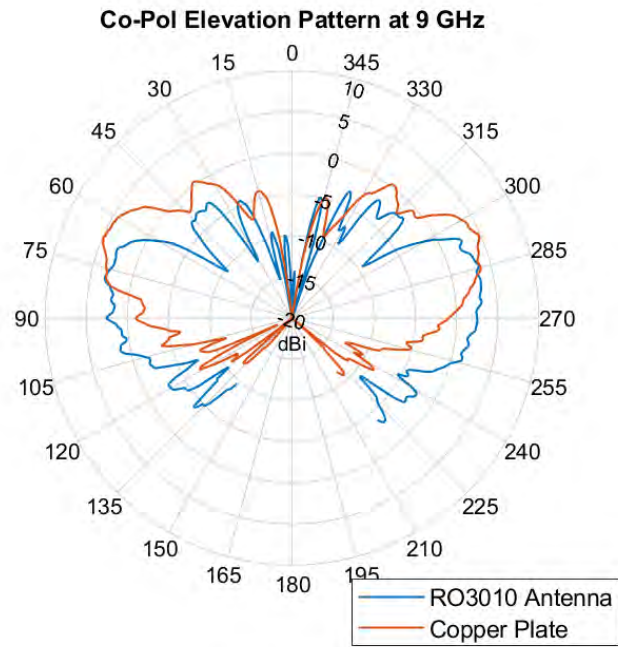


Figure 669: RO3010 Antenna: Elevation Pattern, 9 GHz

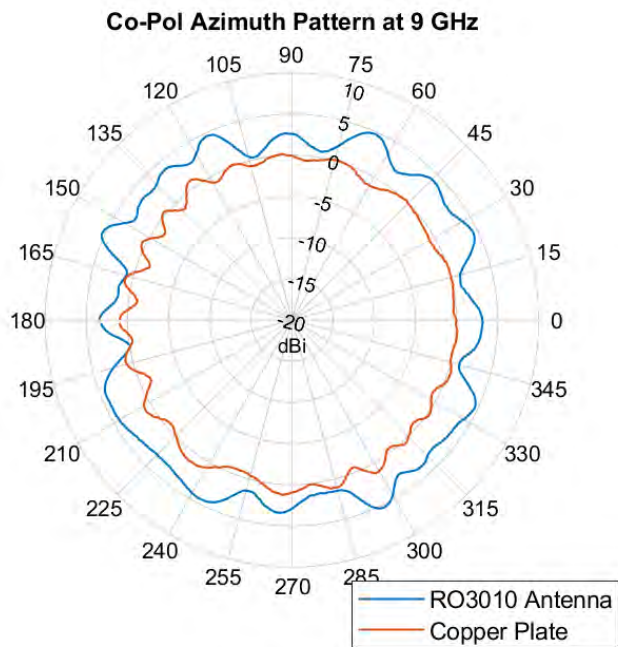


Figure 670: RO3010 Antenna: Azimuth Pattern, 9 GHz

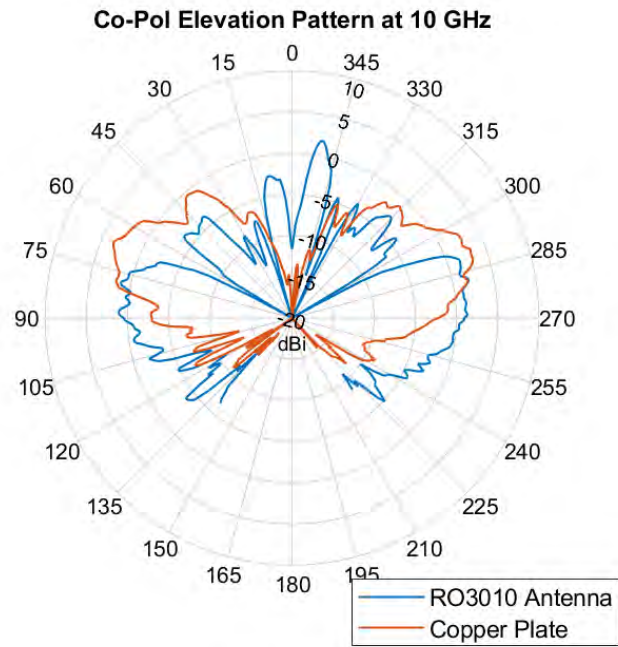


Figure 671: RO3010 Antenna: Elevation Pattern, 10 GHz

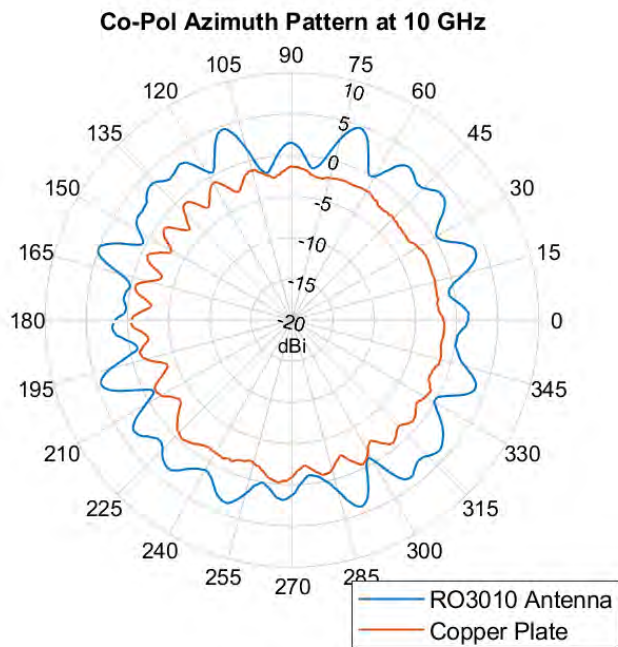


Figure 672: RO3010 Antenna: Azimuth Pattern, 10 GHz

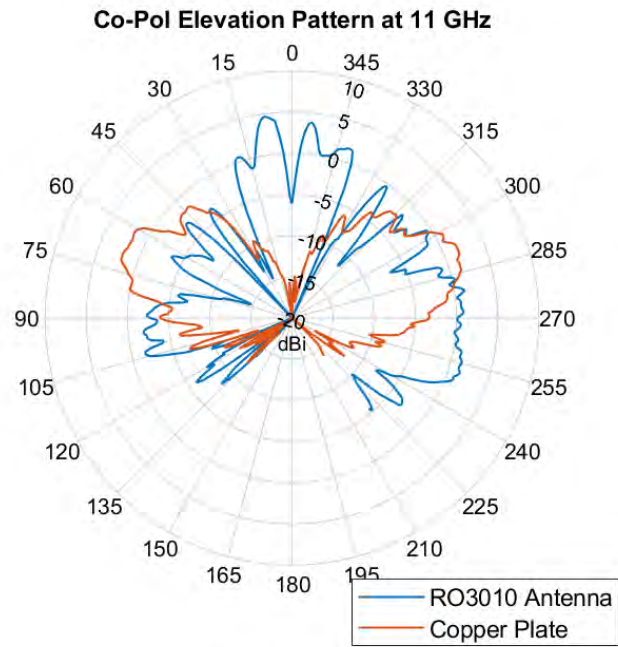


Figure 673: RO3010 Antenna: Elevation Pattern, 11 GHz

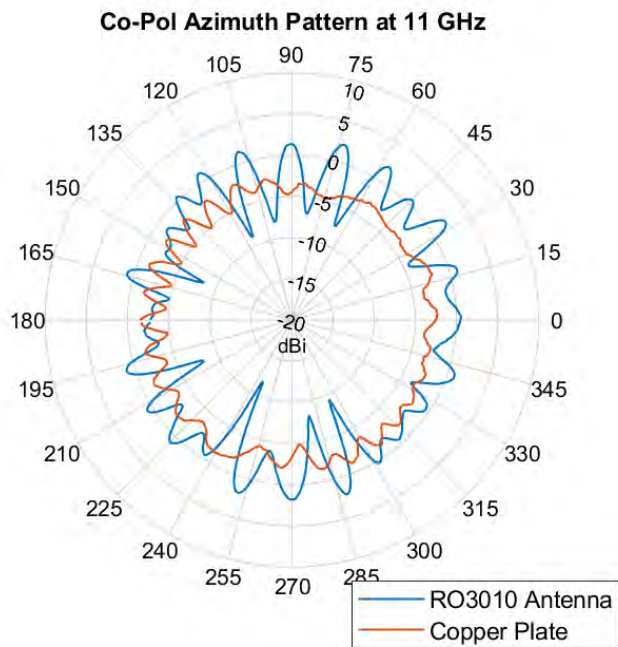


Figure 674: RO3010 Antenna: Azimuth Pattern, 11 GHz

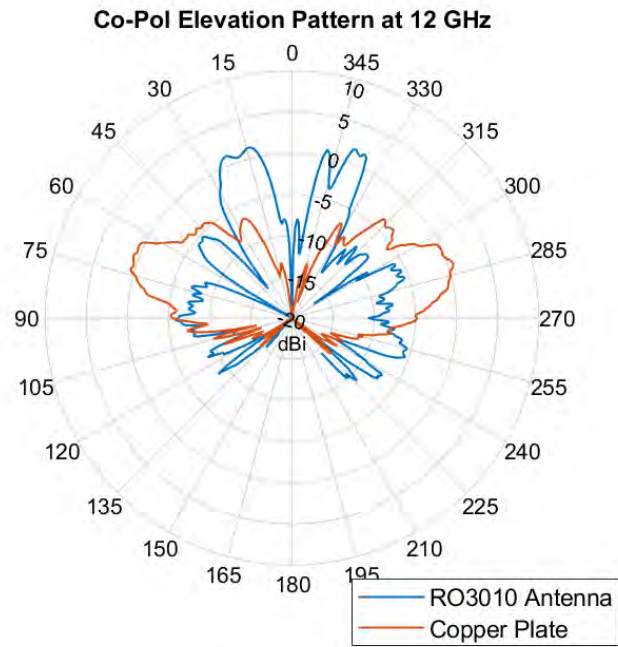


Figure 675: RO3010 Antenna: Elevation Pattern, 12 GHz

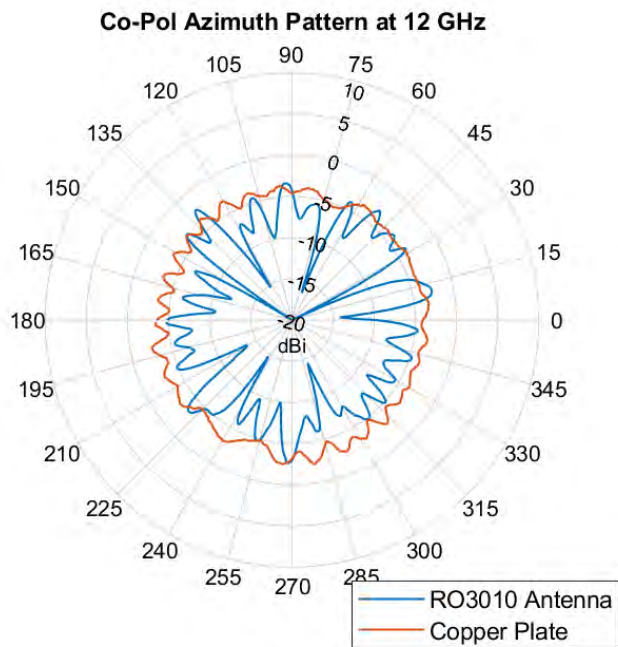


Figure 676: RO3010 Antenna: Azimuth Pattern, 12 GHz

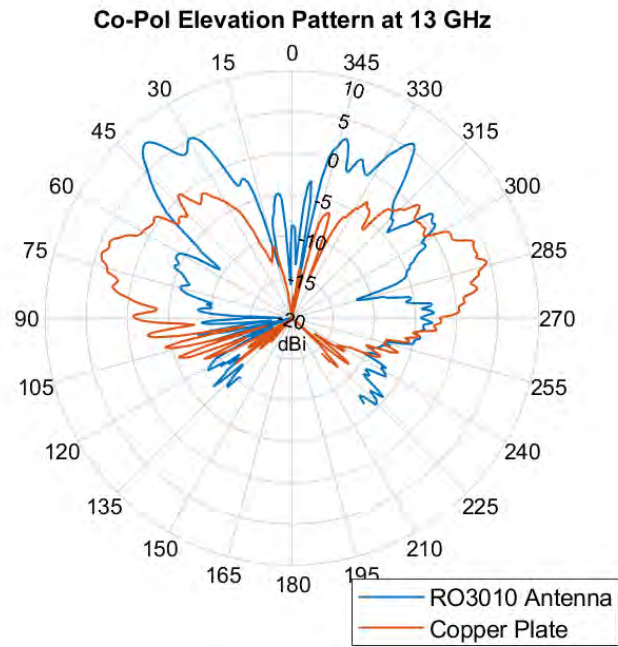


Figure 677: RO3010 Antenna: Elevation Pattern, 13 GHz

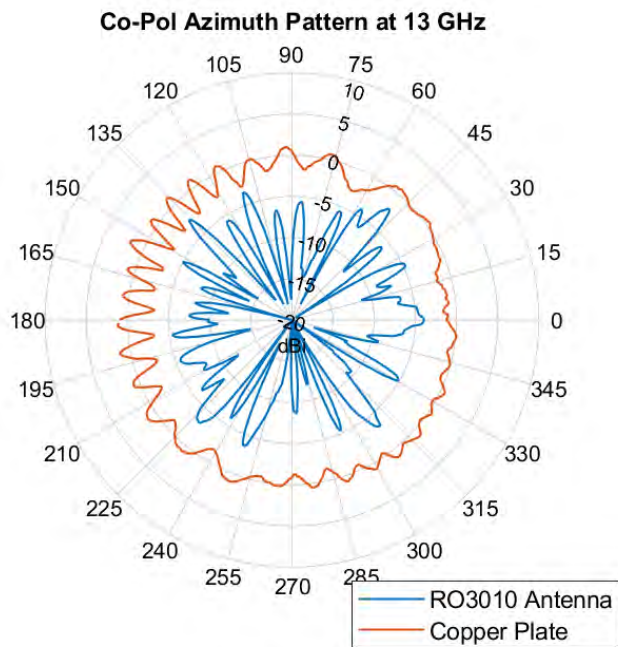


Figure 678: RO3010 Antenna: Azimuth Pattern, 13 GHz

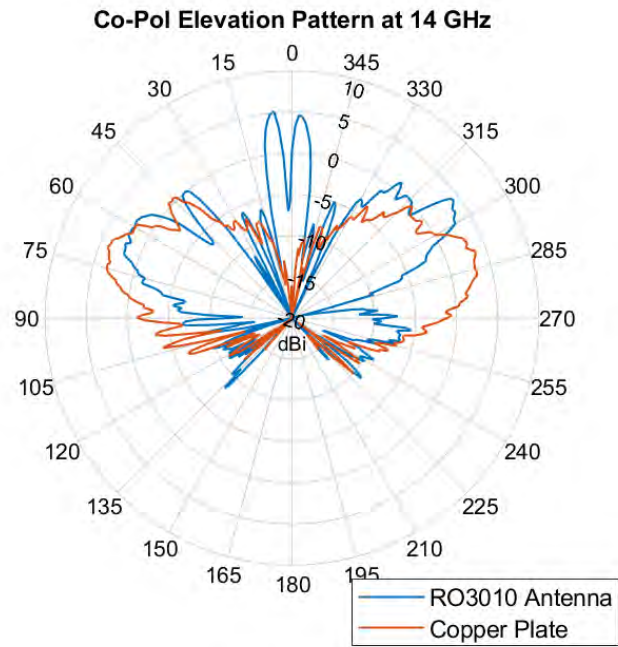


Figure 679: RO3010 Antenna: Elevation Pattern, 14 GHz

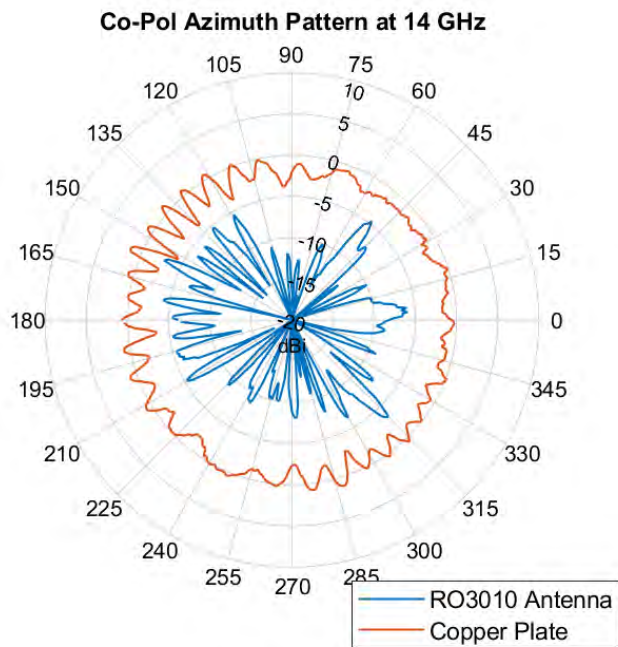


Figure 680: RO3010 Antenna: Azimuth Pattern, 14 GHz

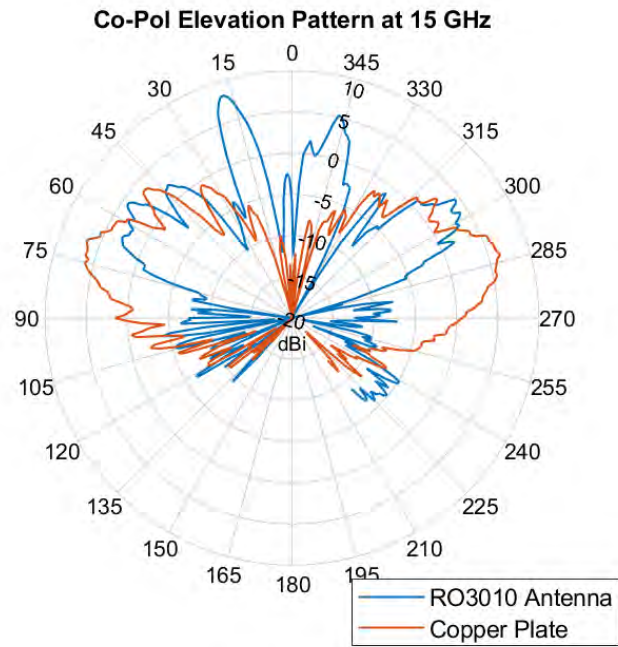


Figure 681: RO3010 Antenna: Elevation Pattern, 15 GHz

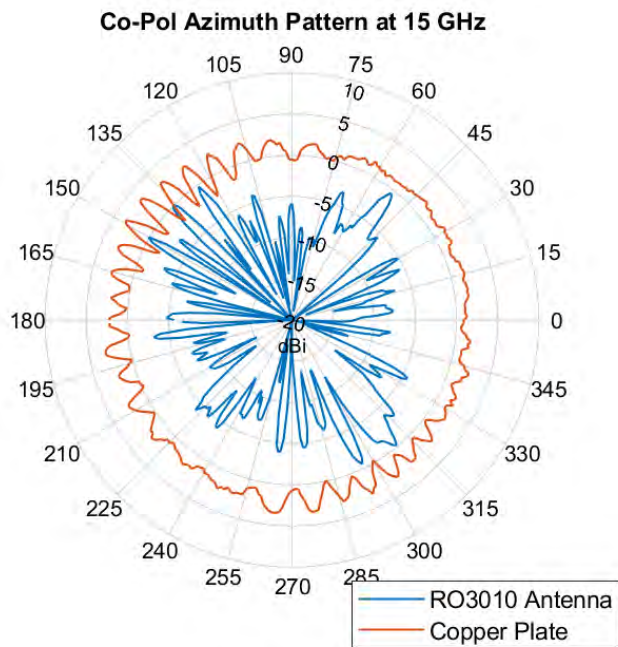


Figure 682: RO3010 Antenna: Azimuth Pattern, 15 GHz

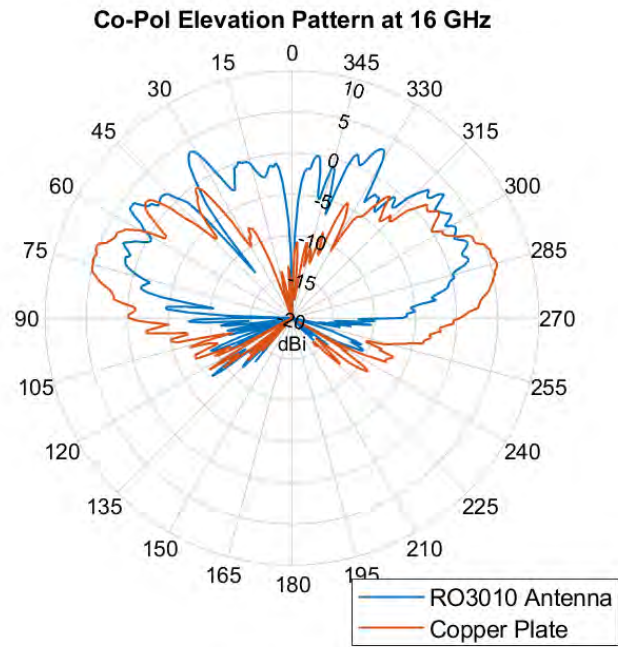


Figure 683: RO3010 Antenna: Elevation Pattern, 16 GHz

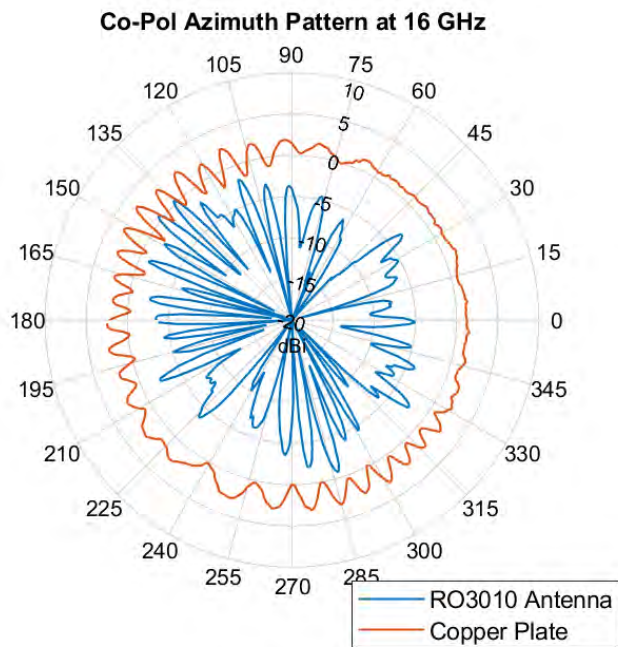


Figure 684: RO3010 Antenna: Azimuth Pattern, 16 GHz

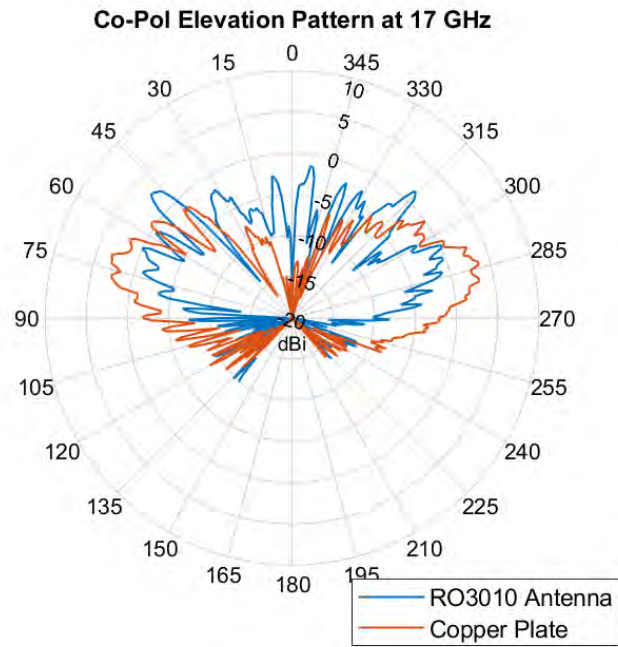


Figure 685: RO3010 Antenna: Elevation Pattern, 17 GHz

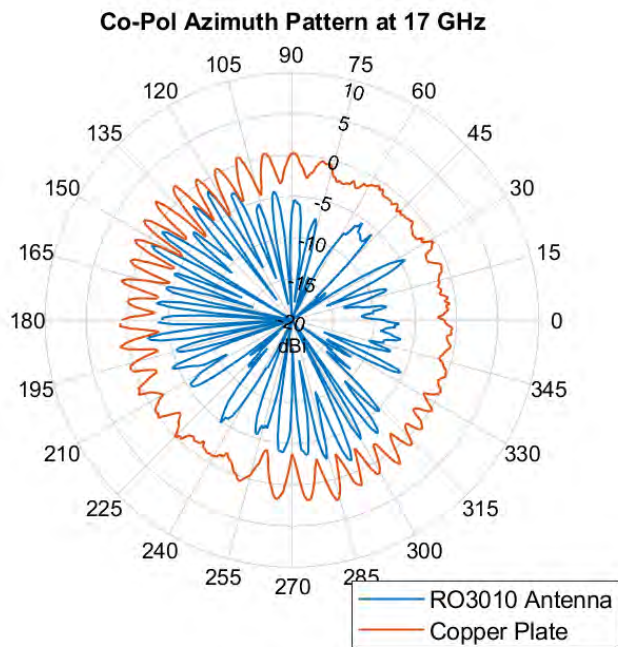


Figure 686: RO3010 Antenna: Azimuth Pattern, 17 GHz

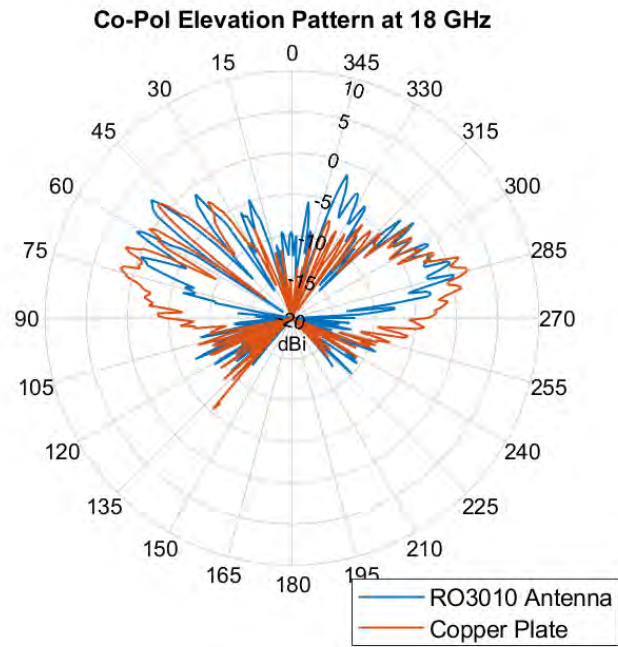


Figure 687: RO3010 Antenna: Elevation Pattern, 18 GHz

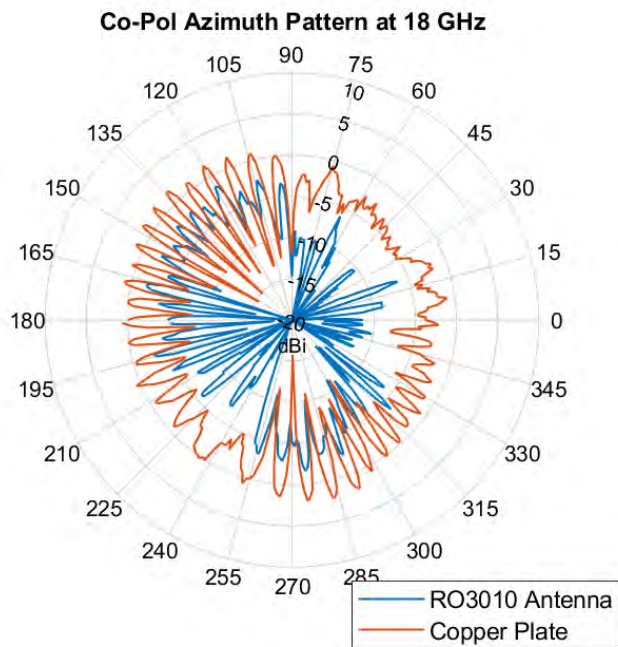


Figure 688: RO3010 Antenna: Azimuth Pattern, 18 GHz

Bibliography

1. A. Knisely. Design and development of a unique two-way field probe system using a shielded octocopter. Master's thesis, Air Force Institute of Technology, 2017.
2. C. Balanis. *Advanced Electromagnetics*. J. Wiley and Sons, Hoboken, NJ, 2012.
3. S. A. Tretyakov. Metasurfaces for general transformations of electromagnetic fields. *Philosophical Transactions of the Royal Society, Series A, Mathematical, Physical, and Engineering Sciences*, 373(2049), 2015.
4. M. Bute J. J. Barroso U. C. Hasar, A. Muratoglu and M. Ertugrul. Effective constitutive parameters retrieval method for bianisotropic metamaterials using waveguide measurements. *IEEE Transactions on Microwave Theory and Techniques*, 65(5):1488–1497, 2017.
5. S. N. Tsvetkova A. Daz-Rubio Y. RaDi V. S. Asadchy, M. Albooyeh and S. A. Tretyakov. Perfect control of reflection and refraction using spatially dispersive metasurfaces. *Physical Review B*, 94(7), 2016.
6. M. Mencagli E. Martini and S. Maci. Metasurface transformation for surface wave control. *Philosophical Transactions of the Royal Society, Series A, Mathematical, Physical, and Engineering Sciences*, 373(2049), 2015.
7. F. Bilotti D. Ramaccia, A. Toscano. A new accurate model of high-impedance surfaces consisting of circular patches. *Progress In Electromagnetics Research*, 21(8):1–17, 2011.
8. A. HESSEL A. A. OLINER. Guided waves on sinusoidally-modulated reactance surface. *IRE Transactions on Antennas and Propagation*, 7(12):201–208, 1959.

9. Joshua A. Gordon John OHara Jim Booth David R. Smith Christopher L. Holloway, Edward F. Kuester. An overview of the theory and applications of metasurfaces: The two-dimensional equivalents of metamaterials. *IEEE Transactions on Antennas and Propagation*, 54(2):10–35, 2012.
10. Romulo F. Nicholas G. Alexopolous Eli Yablonovitch Dan Sievenpiper, Lijun Zhang. High-impedance electromagnetic surfaces with a forbidden frequency band. *IEEE Transactions on Microwave Theory and Techniques*, 47(11):2059–2074, 1999.
11. J. J. Ottush J. L. Visher B. H. Fong, J. S. Colburn and D. F. Sievenpiper. Scalar and tensor holographic artificial impedance surfaces. *IEEE Transactions on Antennas and Propagation*, 58(10):3212–3221, 2010.
12. G. G. Vinning Douglas C. Montgomery, E. A. Peck. *Introduction to Linear Regression Analysis*. Wiley, Hoboken, New Jersey, 5th edition, 2012.
13. Boston University School of Public Health. Simple linear regression. World Wide Web Page. Available at
http://sphweb.bumc.bu.edu/otlt/MPH-Modules/BS/R/R5_Correlation_Regression/R5_Correlation_Regression4.html.
14. M. N. Hasan S. Symeonidis. Tensorbundle lab homepage. World Wide Web Page. Available at
<https://tensorbundle.wixsite.com/home>.
15. M. N. Hasan S. Symeonidis. Cst mws tutorial 23: Metamaterial srr unit cell - permittivity, permeability from s-parameters. World Wide Web Page. Available at
<https://www.youtube.com/watch?v=v8bPJ9kT-kY>.

16. Andre Rennings Christopher Caloz, Tatsuo Itoh. Crlh metamaterial leaky-wave and resonant antennas. *IEEE Transactions on Antennas and Propagation*, 50(5):25–39, 2008.

Acronyms

AFRL Air Force Research Laboratory. 4, 74

CST Computer Simulation Technology. iv, ix, 4, 12, 15, 19, 20, 23, 25, 27, 32, 36, 38, 40, 47, 59, 60, 66, 88, 113

DNG double negative. 6

EBG electromagnetic band-gap. 6

EM electromagnetic. 47, 60, 98, 110

HFSS High Frequency Simulation Software. 27, 113

NRTF National RCS Test Facility. 4

PBG photonic band-gap. 6

PEC Perfect Electric Conductor. 8, 16, 27, 47

RCS Radar Cross Section. 1, 3, 4, 46

SWR Standing Wave Ratio. iv, 74, 75, 94, 111

TM transverse magnetic. 10

USAF United States Air Force. 1

REPORT DOCUMENTATION PAGE

Form Approved
OMB No. 0704-0188

The public reporting burden for this collection of information is estimated to average 1 hour per response, including the time for reviewing instructions, searching existing data sources, gathering and maintaining the data needed, and completing and reviewing the collection of information. Send comments regarding this burden estimate or any other aspect of this collection of information, including suggestions for reducing this burden to Department of Defense, Washington Headquarters Services, Directorate for Information Operations and Reports (0704-0188), 1215 Jefferson Davis Highway, Suite 1204, Arlington, VA 22202-4302. Respondents should be aware that notwithstanding any other provision of law, no person shall be subject to any penalty for failing to comply with a collection of information if it does not display a currently valid OMB control number. **PLEASE DO NOT RETURN YOUR FORM TO THE ABOVE ADDRESS.**

1. REPORT DATE (DD-MM-YYYY) 26-03-2020		2. REPORT TYPE Master's Thesis		3. DATES COVERED (From — To) 1 Sept 2018 — 26 Mar 2020			
4. TITLE AND SUBTITLE Metasurface Antenna for Wideband Applications				5a. CONTRACT NUMBER			
				5b. GRANT NUMBER			
				5c. PROGRAM ELEMENT NUMBER			
				5d. PROJECT NUMBER			
				5e. TASK NUMBER			
6. AUTHOR(S) Lepley, Thomas A, Capt				5f. WORK UNIT NUMBER			
				7. PERFORMING ORGANIZATION NAME(S) AND ADDRESS(ES) Air Force Institute of Technology Graduate School of Engineering and Management (AFIT/EN) 2950 Hobson Way WPAFB OH 45433-7765			
				8. PERFORMING ORGANIZATION REPORT NUMBER AFIT-ENG-MS-20-M-036			
9. SPONSORING / MONITORING AGENCY NAME(S) AND ADDRESS(ES) National RCS Test Facility, 704 TG Det 1/TGRP Program Manager, Capt Nicole Feliciano 872 Dezonnia Drive Holloman AFB NM 88330 COMM 575-572-0734 Email: nicole.feliciano.2@us.af.mil				10. SPONSOR/MONITOR'S ACRONYM(S) NRTF			
				11. SPONSOR/MONITOR'S REPORT NUMBER(S)			
12. DISTRIBUTION / AVAILABILITY STATEMENT DISTRIBUTION STATEMENT A: APPROVED FOR PUBLIC RELEASE; DISTRIBUTION UNLIMITED.							
13. SUPPLEMENTARY NOTES							
14. ABSTRACT This effort explored design of metasurface antennas and evaluated their suitability for ultra-wideband applications (2 to 18 GHz). Six unit cell types were characterized. Eigenmode simulations produced frequency vs. phase data for the unit cells, from which impedance vs. gap size data was computed. A holographic design equation was used to generate the metasurface antenna designs. The unit cell simulations revealed that the assumption of single mode operation is a constraint for wideband designs. An 8" by 8" metasurface antenna with a Rogers 3010 dielectric and a design frequency of 10 GHz was fabricated and tested. It had a 1.5:1 SWR bandwidth of 8.06 GHz (6.47 to 14.53 GHz) and a 2:1 SWR bandwidth of 12.09 GHz (5.91 to 18 GHz). The main beam was 30° wide and had a peak gain of 1.8 dBi. The center of the main beam was $\theta_L = 0^\circ$ (+Z direction), which resulted in weaker gain as this is the endfire direction from the driven element. Despite that challenge, this antenna demonstrated that metasurface antennas show promise for ultra-wideband applications when high gain is not a requirement.							
15. SUBJECT TERMS antenna, wideband antenna, metasurface antenna, metamaterial, surface wave							
16. SECURITY CLASSIFICATION OF:			17. LIMITATION OF ABSTRACT	18. NUMBER OF PAGES	19a. NAME OF RESPONSIBLE PERSON		
a. REPORT	b. ABSTRACT	c. THIS PAGE			Dr. Peter J. Collins, AFIT/ENG		
U	U	U	UU	493	19b. TELEPHONE NUMBER (include area code) (937) 255-3636, ext 7256; Peter.Collins@afit.edu		